The *Streptomyces* cytoskeletal protein (Scy) is a key component of the Tip Organising Centre for polarized growth in *Streptomyces coelicolor*

Neil Andrew Holmes

w0450723

A thesis submitted for a Biomolecular sciences research degree of

Doctor of Philosphy.

School of Biological Sciences

University of East Anglia

Submitted September 2012

Abstract

The Gram-positive bacterium *Streptomyces coelicolor*, is one of the main genetic model organisms in the phylum of the Actinobacteria. *Streptomyces* bacteria are soil dwelling filamentous bacteria with a complex life cycle consisting of multigenomic hyphae that then form unicellular spores. Bacterial cell shape determination has been influenced heavily by the discovery that bacteria have a number of eukaryotic cytoskeletal homologues as well as a number of accessory proteins unique to prokaryotes. As cell shape determination is dependent on the sites of insertion of new cell wall material, this is characteristically organised and driven by cytoskeletal proteins.

***Streptomyces coelicolor* hyphal growth occurs through apical extension where new cell wall material is placed at the tips. This growth is driven in part by the cytoskeletal protein DivIVA. Here we characterise a novel *Streptomyces* cytoskeletal protein, Scy, encoded by the locus *sco5397*. Scy is a large protein with a novel coiled-coil 51-mer repeat structure. To study Scy, a *scy* knockout mutation was generated. The phenotype of the *scy* mutant suggests that it plays a significant role in cell shape, growth and chromosome positioning. Translational fluorescent protein fusions to *scy* were made and the subcellular localisation of Scy was determined to be strongly at growing hyphal tips. Further clarified here, Scy overexpression can recruit DivIVA protein and the cell wall synthesis machinery to new apical sites. The reciprocal is also shown whereby DivIVA overexpression can recruit Scy to new apical sites. Further to this *in vivo* and *in vitro* experiments were performed to determine that Scy and DivIVA interact, as well as the protein FilP encoded downstream of *scy*. The work here along with work in the field suggests that Scy forms part of a Tip Organising Centre (TIPOC) that alongside DivIVA, FilP, and numerous other proteins controls apical growth in the filamentous *Streptomyces*.**

Acknowledgments

I would firstly like to thank my primary superviser Dr Gabriella Kelemen for all her help with the project and for the many hours of fascinating scientific discussions that were necessary for this project to take shape. I would also like to thank the other members of my supervisory panel Dr Mette Mogensen, Dr Andrew Hemmings and Prof Keith Chater for their contributions. I would also like to thank my examiners Dr Michael McArthur and Dr Richard Daniel.

Many thanks to the other members of the Kelemen lab during my time there especially Dr Clare Winter, Dr Richard Leggett, Michael Gillespie, Nadezhda Gicheva, Lee Kellingrey and Ruchita Desai for all their technical help and commaradory. Also to undergraduate students that have contributed to the Scy story; Freyja Bjornson, Laura Parry, Lisa Goodman, Laura Kerry and Daniel Leonce. Thanks to John Walshaw for various discussions and inputs on coiled-coil proteins. Thanks to Dagmara Jakimowicz and Bartosz Ditkowski for the Scy:ParA collaboration. Dr Gay White for her help with Liposome manipulation. Thanks to Prof Klas Flärdh for various published constructs and strains. I would also like to thank all the friends and colleagues from the Biology department that have been there to help me along both socially and academically and made such a welcoming and enjoyable environment to work in.

I would like to thank the UEA Fell and Mountaineering club for various relaxing outdoor pursuits during my studies that have provided a great amount of reflection. Of course it wouldn’t be complete if I didn’t thank those who have been supporting me throughout the many many years of my education and life upto this point from my family; Louise Holmes, David Holmes, Carly Holmes, Peter Holmes, Gail Holmes, Barry Holmes, Stuart Freeland, Martin Freeland and Barbara Freeland.

Table of Contents

Abbreviations

AbpS	Avicel Binding Protein of *Streptomyces reticuli* (homologue of FilP of *S. coelicolor*)
ADP	Adenosine Diphosphate
ATP	Adenosine Triphosphate
APS	Ammonium Persulphate

Bld	Bald (Lacking Aerial Hyphae)
bp	Base Pairs
BSA	Bovine Serum Albumin
BTH	Bacterial Two-Hybrid
cAMP	Cyclic Adenosine Monophosphate
CAP	Catabolite Activator Protein
CC	Coiled-coil
CM	Complete Medium
C-terminal	Carboxyl Terminal
DMSO	Dimethyl Sulphoxide
DNA	Deoxyribonucleic Acid
dNTPs	Deoxynucleotide Triphosphates
DTBP	Dimethyl 3,3'-dithiobispropionimidate
DTT	Dithiothreitol
EGFP	Enhanced Green Fluorescent Protein
EDTA	Ethylenediaminetetraacetic Acid
FilP	Filamentous Protein P
FRT	FLP recognition target
GC	Guanine Cytosine
GDP	Guanosine Diphosphate
GFP	Green Fluorescent Protein
GTP	Guanosine Triphosphate
His	Histidine
IPTG	Isopropyl-β-D-thio-galactopyranoside
LB	Lennox Broth
MALDI-TOF	Matrix-Assisted Laser Desorption/Ionisation with Time of Flight analysers
mCherry	monomeric Cherry
mRNA	Messenger RNA
MCS	Multiple Cloning Site
MMG	Minimal Medium Glucose
MMM	Minimal Medium Mannitol
MW	Molecular Weight
N-terminal	Amino Terminal

nt	Nucleotides
OD	Optical Density
PAGE	Polyacrylamide Gel Electrophoresis
PBP	Penicillin Binding Protein
PCR	Polymerase Chain Reaction
PEG	Polyethylene Glycol
PSI-BLAST	Position-Specific Iterative Basic Local Alignment Search Tool
PVDF	Polyvinylidene Difluoride
RED	Red Recombinase (from phage lambda)
RNA	Ribonucleic Acid
SCO	Annotated gene from *Streptomyces coelicolor*
Scy	*Streptomyces* Cytoskeletal Protein
SDS	Sodium Dodecyl Sulphate
SFM	Soya Flour Mannitol Medium
SMC	Structural Maintainence of Chromosomes Protein
TAE	Tris Acetate EDTA
TEMED	Tetramethylethylenediamine
TBS	Tris Buffer Saline
TBST	Tris Buffer Saline Tween
Tris	2-Amino-2-(hydroxymethyl)-1,3-propanediol
tRNA	Transfer RNA
TSB	Tryptone Soya Broth
UV	Ultraviolet
Van-Fl	Fluorescently Labelled Vancomycin
v/v	Volume per Volume
WGA	Wheat Germ Agglutinin
WGA-Alexa488	Alexa Fluor® 488 WGA Conjugate
Whi	White (Lacking Correct Sporulation)
X-gal	5-bromo-4-chloro-indolyl-β-D-galactopyranoside

1 Inroduction

Streptomyces coelicolor is a Gram-positive bacterium that was originally isolated from the soil. The genus *Streptomyces* has received great attention due to its ability to produce secondary metabolites such as antibiotics whose antimicrobial activity is believed to confer a competitive advantage over other soil occupying bacteria (Bibb, 2005). The streptomycetes exhibit two mechanisms of growth; firstly they can grow and disperse by vegetative growth that does not exhibit fully completed cell division. The second form of growth leads to formation of specialised aerial hyphae that then divide to form large numbers of highly resistant spores (Anderson, and Wellington, 2001). The understanding of the developmental biology of *S. coelicolor* has progressed enormously in recent years, aided enormously because the *S. coelicolor* genome project was completed in 2002 (Bentley *et al.*, 2002). The completion of the genome project confirmed that *S. coelicolor* is more genetically complex with a larger genome and a higher number of regulatory genes in comparison to other bacteria. So far the study of morphologically defective mutants has provided fascinating insights into the complexity of signalling and regulation involved in the processes of aerial hyphae formation and sporulation (Flärdh, and Buttner, 2009). However, by comparison little is known about the most important factors involved with the formation of hyphae during vegetative growth.

Bacteria show a large diversity in terms of their cell shapes, with morphologies varying from spherical coccoid shaped bacteria, to rods, spiral shapes, stalked ends, crescents and filamentous shapes (Cabeen, and Jacobs-Wagner, 2005). Cell shape to a large extent is maintained by the tough peptidoglycan cell walls of bacteria. Peptidoglycan cell walls also characteristically protect bacterial cells from osmotic pressure created from differing osmolarities of the cytoplasm and the extracellular environment (Lederberg, 1956; Weidel, and Pelzer, 1964). A large number of the genes that have been shown to be important in the maintenance of cell shape have been found to be enzymes that are related to the function of cell wall synthesis (Spratt, 1975; Nelson, and Young, 2000; Blumberg, and Strominger, 1974). This includes the penicillin binding proteins (PBPs) that are involved in the final steps of peptidoglycan synthesis. However, it is emerging that the cell wall synthesis machinery depends upon cytoskeletal proteins that significantly contribute to cell shape and morphology primarily by directing sites of new cell wall insertion (Jones *et al.*, 2001; Ausmees *et al.*, 2003; Erickson *et al.*, 1996; Errington, 2003; Typas *et al.*, 2011; Mattei *et al.*, 2010).

Cytoskeletal proteins are defined as having the capacity to form filamentous polymers *in vivo* and *in vitro*, from only the original monomeric protein. The structure does not have to maintain stability as many cytoskeletal filaments exhibit dynamic assemblies and disassemblies in response to signals (Shih, and Rothfield, 2006). Eukaryotic cells have three different classes of cytoskeletal proteins that form filaments *in vivo* and *in vitro*; the actin filaments, the microtubules and the intermediate filaments (Goodson, and Hawse, 2002; Desai, and Mitchison, 1997; Steinert, and Roop, 1988). Prokaryotes have been shown to contain homologous proteins that are distantly related to each of the three classes of eukaryotic cytoskeletal proteins (Nogales *et al.*, 1998; van den Ent *et al.*, 2001; Ausmees *et al.*, 2003). Prokaryotes also seem to have novel cytoskeletal proteins that are not found in eukaryotes (Ingerson-Mahar, and Gitai, 2012), raising the possibility that there might be more unidentified cytoskeletal proteins in prokaryotes. The bacterial cytoskeletal proteins drive different factors in the form of cell shape determination, cell division and chromosome segregation (Michie, and Löwe, 2006). Bacteria are now regarded as being more than just "bags of enzymes" with complex cellular organisation in which cytoskeletal elements play a huge role.

In bacteria the tubulin homologue FtsZ is associated with cytokinesis. For example in *E. coli* polymerisation of FtsZ in symmetrical cell division leads to formation of a ring at the midpoint of the cell (the "Z ring") (Bi, and Lutkenhaus, 1991). The "Z ring" is the site where cell division is initiated, new cell wall insertion is triggered and invagination of the membrane occurs (Lutkenhaus, 1993). In many rod shaped bacteria the actin-like MreB family of proteins form helical filaments that facilitate lateral cell wall growth (Jones *et al.*, 2001). The use of fluorescent vancomycin to visualise sites of nascent peptidoglycan synthesis revealed that cell wall assembly in *B. subtilis* occurs in a helical pattern consistent with helices of an MreB-family protein (Daniel, and Errington, 2003). MreB is absent in coccoid shaped bacteria and therefore they do not exhibit lateral cell wall growth and use FtsZ to direct new cell wall insertion and to divide into equal sized daughter cells.

Due to its complex division cycle and filamentous growth *Streptomyces coelicolor* is a fitting model organism in which to study cytoskeletal proteins. Though much is still unknown, a rapidly increasing catalogue of *S. coelicolor* cytoskeletal proteins is being compiled (Table 1). Due to the complex morphological division of aerial hyphae of the *Streptomyces* into spores there is a large amount of interest in the process of sporulation and partitioning of chromosomes into separate spores. Most of the cytoskeletal proteins of *S. coelicolor* so far researched have been involved in these processes, to which a model of

their localisation patterns are shown in Figure 1. The *S. coelicolor* homologue of FtsZ seems to have a role in the division of the aerial hyphae into spores by positioning the sporulation septa (McCormick *et al.*, 1994). The *S. coelicolor* MreB homologues appear to play a role in spore maturation (Burger *et al.*, 2000; Mazza *et al.*, 2006; Heichlinger *et al.*, 2011). This is quite a different role of MreB in comparison to its function of driving lateral cell wall synthesis in rod shaped bacteria (Jones *et al.*, 2001). In *Streptomyces* the processes of chromosome segregation and condensation seem to be aided by homologues of the ParA, ParB, SMC and FtsK cell division proteins (Kim *et al.*, 2000; Dedrick *et al.*, 2009; Jakimowicz *et al.*, 2002; Jakimowicz *et al.*, 2005a; Jakimowicz *et al.*, 2007; Kois *et al.*, 2009; Wang *et al.*, 2007).

Table 1: Proteins with a possible cytoskeletal/cytoskeleton-associated role in *Streptomyces coelicolor*.

Protein Name	SCO Number	Possible Function	Reference(s)
FtsZ	SCO2082	Cell division, septum positioning	(McCormick *et al.*, 1994; Grantcharova *et al.*, 2003; Willemse *et al.*, 2011a)
SsgA	SCO3926	Cytoskeletal regulatory protein	(Kawamoto *et al.*, 1997; van Wezel *et al.*, 2000; Noens *et al.*, 2005)
SsgB	SCO1541	Cytoskeletal regulatory protein	(Kormanec, and Sevcikova, 2002; Keijser *et al.*, 2003; Sevcikova, and Kormanec, 2003; Noens *et al.*, 2005; Willemse *et al.*, 2011a; Xu *et al.*, 2009)
MreB	SCO2611	Spore maturation	(Burger *et al.*, 2000; Mazza *et al.*, 2006; Kleinschnitz *et al.*, 2011)
Mbl	SCO2451	Spore maturation	(Mazza *et al.*, 2006;

			Heichlinger *et al.*, 2011)
ParA	SCO3886	Chromosome condensation/ segregation	(Jakimowicz *et al.*, 2006; Jakimowicz *et al.*, 2007; Kim *et al.*, 2000)
ParB	SCO3887	Chromosome condensation/ segregation	(Jakimowicz *et al.*, 2002; Jakimowicz *et al.*, 2005a; Kim *et al.*, 2000)
DivIVA	SCO2077	Apical Growth	(Flärdh, 2003a)
SMC	SCO5577	Chromosome condensation/ segregation	(Dedrick *et al.*, 2009; Kois *et al.*, 2009)
ScpA	SCO1770	Chromosome condensation/ segregation	(Dedrick *et al.*, 2009; Kois *et al.*, 2009)
ScpB	SCO1769	Chromosome condensation/ segregation	(Dedrick *et al.*, 2009; Kois *et al.*, 2009)
FtsK	SCO5750	Chromsome segregation	(Wang *et al.*, 2007)
AbpS/FilP	SCO5396	Vegetative growth	(Bagchi *et al.*, 2008)
Streptomyces Cytoskeletal Protein (Scy)	SCO5397	Polarised growth and cell division	(Kelemen Lab, University of East Anglia)(Walshaw *et al.*, 2010), This Work

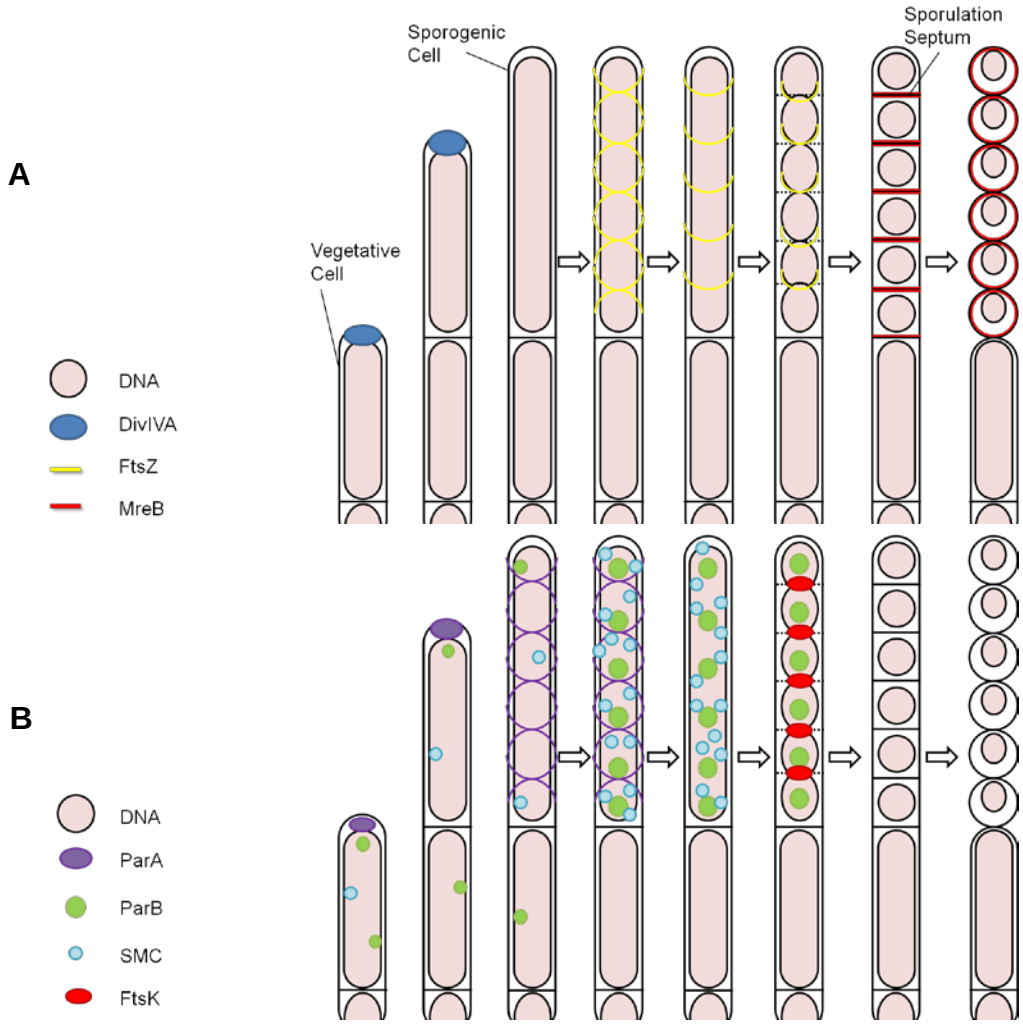

Figure 1: Positioning of a number of *S. coelicolor* cytoskeletal proteins in the process of extension and cell division where the aerial hyphae divide into spores (Adapted from Flärdh & Buttner, (2009), with information from Kois *et al.*, (2009), Jakimowicz *et al.*, (2005a). A) The cell shape determining factor DivIVA is involved in apical growth. In the aerial hyphae DivIVA disappears and FtsZ forms helices that then go on to mark the regular positions of sporulation septa. MreB later forms at sporulation sites and envelopes the spore wall and functions in spore maturation. B) ParA which can be associated with some hyphal tips, later in the aerial hyphae goes on to form helical filaments that place the nucleoid associated factor ParB at regular positions of one foci per spore forming compartment. SMC appears at a similar stage to ParB, which it does not localise as regularly as, and then disappears before ParB disappears. FtsK maybe involved in DNA transport across the separating sporulation compartments.

S. coelicolor features apical growth to which none of the already discussed proteins have been implicated. Apical growth is unusual in comparison to growth performed by most other bacteria , although bacterial examples of apical growth have been shown for even rod shaped bacteria including the actinomycete *Corynebacterium* (Letek *et al.*, 2009; Letek *et al.*, 2008) or *Mycobacterium* (Kang *et al.*, 2008), or recently, members of the Rhizobiales, such as *Agrobacterium tumefaciens* (Brown *et al.*, 2012). The filamentous growth of *Streptomyces* is more similar to growth featured by filamentous fungi. Cytoskeletal

proteins play an important role in growth of filamentous fungi normally by forming centres of organisation at the polar sites that drive elongation of the cells (Xiang, and Plamann, 2003; Harris, 2008); however, *Streptomyces* likely have evolved different mechanisms due to the large divergence between these groups of organisms, but it seems that cytoskeletal proteins also play a role in the developmental biology of *S. coelicolor* and its filamentous growth. Therefore, apical growth represents a relatively novel biological process in which to study. At the present, apical growth in *S. coelicolor* has been shown to be dependent on the bacterial cytoskeletal protein DivIVA (Flärdh, 2003b; Flärdh, 2003a). In *S. coelicolor divIVA* was found to be an essential gene and a knockout could not be achieved unless *divIVA* was provided *in trans*. Reduction of DivIVA to approximately 10% of normal levels, resulted in the phenotype of irregular curly shaped hyphae and apical branching. Whereas overexpression of DivIVA resulted in tip swelling and hyperbranching. A DivIVA-EGFP translational fusion localised to bright foci at hyphal tips to the same positions in which the cell wall is inserted. Time-lapse imaging showed that DivIVA-EGFP localised to future branch points significantly before new branch emergence (Hempel *et al.,* 2008). Collectively these observations suggest that DivIVA directs polar cell wall insertion in *Streptomyces*.

Located downstream of the *scy* gene characterised here, is a gene *filP* encoding another potential cytoskeletal protein, FilP, first identified and believed to resemble intermediate filament proteins from eukaryotes (Bagchi *et al.*, 2008). However, recently it has been predicted that FilP is not intermediate filament-like, but instead contains a novel type of coiled-coil repeat (Walshaw *et al.*, 2010). The *scy* gene upstream of *filP*, very likely encodes a novel *Streptomyces coelicolor* cytoskeletal protein (abbreviated to Scy).

Based on bioinformatics data (Walshaw *et al.*, 2010) Scy is an example of a novel cytoskeletal protein with a 51-mer repeat unit, which can also be found in FilP. Previously in the Kelemen lab it was found that a partial mutation (K110) in the *scy* gene resulted in defects with hyphal morphology and possibly growth at the tips of the hyphae. This mutant was seen to have short aerial hyphae and branching spore chains. DNA distribution was not even throughout the formation of the spores. Although the aerial hyphae are affected more, vegetative growth also showed a knotted phenotype showing Scy could be involved in general hyphae development.

Summarised in the following sections of this chapter is a current insight into firstly the understanding of the developmental biology of the *Streptomyces*, followed by a review of

cytoskeletal proteins in prokaryotic organisms and finally concluding with a review of cytoskeletal proteins and their role specifically in *Streptomyces*.

1.1 Streptomyces coelicolor, a model organism for bacterial development

1.1.1 The life cycle of Streptomyces coelicolor

While many bacteria divide by binary fission in a symmetric manner, *Streptomyces coelicolor* has a complex life cycle consisting of multiple stages of growth and sophisticated structures (Figure 2). The development of *S. coelicolor* beginning from a spore, starts with the emergence of either a single or two germ tubes (Jyothikumar *et al.*, 2008). The germ tubes grow out by extension in the tips, occasionally branching so that they form a complex mass of mycelium. New cell wall material is laid down at the tips and is similar to apical growth featured by filamentous fungi (Daniel, and Errington, 2003; Flärdh, 2003b). This growth is accompanied by and is proportional to the rate at which the DNA can be replicated and chromosomes doubled. The hyphae are essentially multigenomic, with relatively rare, widely spaced septa. Cell division does not occur in the vegetative hyphae, with tip extension and branching allowing expansion of the mycelia (Chater, 1993; Flärdh, 2003b). On an agar plate, growth occurs from the surface penetrating the substrate to form a vegetative mycelium. A number of factors including developmental signalling cascades, stress response and nutrient limitation in the substrate media, trigger the older parts of the vegetative mycelium to give rise to aerial hyphae. Aerial hyphae break through the surface tension of the aqueous environment of the substrate media to rise into the air (Kelemen, and Buttner, 1998). The aerial hyphae appear on an agar plate after 2-4 days as a fuzzy white surface. Initially aerial hyphae also grow as multigenomic structures. The aerial hyphae reach a point where they stop growing. They then lay down septa that divide the hyphae into prespore compartments, containing a single chromosome. The prespore compartments change shape and their wall thickens. At the same time as spores are formed, a grey polyketide pigment is produced. The production of spores at 4-6 days of growth on agar therefore coincides with a grey appearance on the surface of the colony (Kelemen *et al.*, 1998; Davis, and Chater, 1990; Chater *et al.*, 1989).

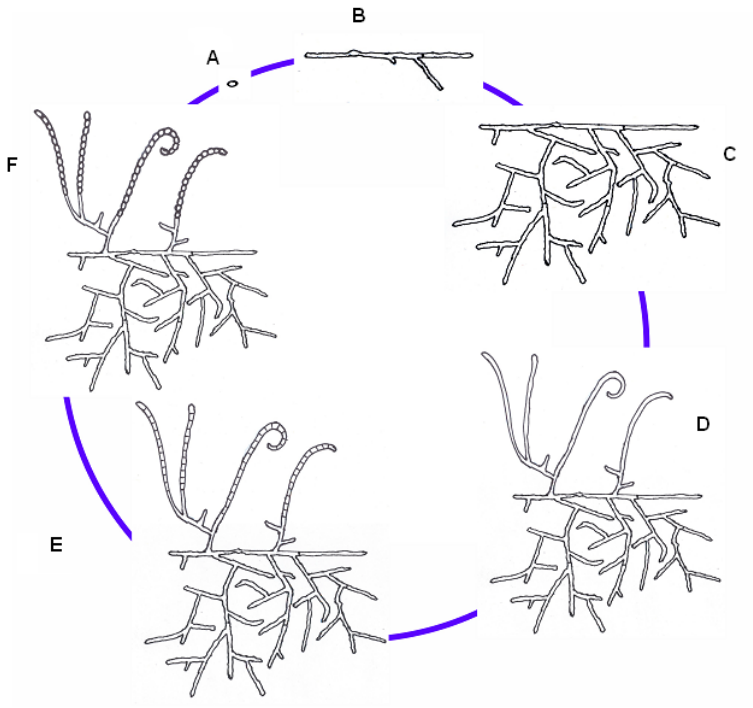

Figure 2: Life cycle of *Streptomyces coelicolor*. Unicellular spore (A), followed by germ tube emergence where tip extension and branching in the vegetative hyphae (B) leads to the development of a complex mass of mycelium (C). Aerial hyphae (D) form from older parts of the vegetative hyphae. Septation of the aerial hyphae (E), later leads to development of prespore compartments (F), that divide to form unicellular spores (A). Image courtesy of Gabriella Kelemen.

1.1.2 The S. coelicolor genome

The *S. coelicolor* genome is 8,677,507bps long, and consists of 7,825 predicted genes. The single chromosome is linear in structure, GC rich and contains a centrally located replication origin (*oriC*) with a conserved core of genes flanked by terminal inverted repeats (Bentley *et al.*, 2002). The genome was sequenced from a set of ordered Supercos-1 clones containing ~37.5kb fragments (Redenbach *et al.*, 1996). These cosmids have also been useful in creating gene knockouts by replacing genes with antibiotic resistance cassettes that can then be used for homologous recombination in *S. coelicolor*. The terminal ends of the chromosome show instability such that most of the essential genes of *S. coelicolor* are distributed in a central core (Bentley *et al.*, 2002; Volff, and Altenbuchner, 1998). The unstable ends contain non-essential genes such as those encoding secondary metabolite production. The central core shows synteny with other Actinomycetes such as *Mycobacterium tuberculosis* and *Corynebacterium diphtheriae* (Bentley *et al.*, 2002). Reinforcing suggestions that this part of the genome is conserved,

whereas the terminal regions have undergone more changes. There have been many potential gene duplications, leading to different isoforms of proteins that possibly could be involved in different stages of growth (Bentley *et al.*, 2002). It has been predicted that 12.3% of *S. coelicolor* genes encode regulatory proteins. This is reflected by *S. coelicolor* containing large numbers of putative sigma factors, sensor kinases, response regulators and DNA binding proteins (Bentley *et al.*, 2002). Having large numbers of regulatory genes helps to explain the high complexity of *S. coelicolor* development. Other prominent genes include those encoding for production of secondary metabolites, transporter proteins and secreted enzymes (Bentley *et al.*, 2002) consistent with *S. coelicolor's* competitive role in the soil. Sequencing of the *S. coelicolor* genome has been crucial for the understanding of its biology and for providing a more practical genetic platform to study this organism.

1.1.3 Important developmental genes

There are a number of important genes that play a significant role in *S. coelicolor* development and mutants of two sets of genes called *bld* and *whi* have been rigorously studied to understand *S. coelicolor* development. The consequence of a mutation in a *bld* gene results in colonies that do not form aerial hyphae so that they appear not to have the fuzzy morphology seen in the wild-type strain (Chater, 1993), therefore in part *bld* genes control the erection of aerial hyphae. A mutation in a *whi* gene results in colonies that do not complete sporulation, so they do not change to the grey colour of mature spores and hence appear white (Ryding *et al.*, 1999), therefore the *whi* genes act to control formation of spores from the aerial hyphae. Not surprisingly the majority of the *bld* and *whi* genes encode regulatory/signalling proteins. Some other important gene classes have also been identified; firstly the *ram* genes specify the production of a hydrophobic surfactant that allows the aerial hyphae to break the surface tension associated with air-water interfaces. The gene classes encoding the chaplins and the rodlins allow the formation of a hydrophobic surface structure that coats developing aerial hyphae enabling them to erect into a non-aqueous environment (Elliot *et al.*, 2003; Claessen *et al.*, 2003; Claessen *et al.*, 2002) .

1.1.4 A complex regulatory/signalling pathway controls aerial hyphae development

The *bld* genes are believed to act as a signalling cascade that leads to aerial hyphae formation (Figure 3). One of the overall effects of *bld* gene signalling is the release a

surfactant called SapB that allows the aerial hyphae to break the surface tension and erect into the air (Willey *et al.*, 1991). However, the phenotypic consequences of a *bld* mutation are in most cases dependent on the type of media in which a strain is grown on. Classical *bld* mutants lack aerial hyphae development when grown on a rich medium such as R2YE (For R2YE recipe visit Kieser *et al.*, (2000)), yet replacement of the carbon substrate from glucose to mannitol can in cases remove the bald phenotype (Chater, 1993). The *bld* genes could potentially form a signalling cascade as the mutants form a hierarchy where it is possible to complement an "earlier acting" *bld* gene mutant when grown adjacent to a "later acting" *bld* gene mutant. Whereas an "earlier acting" *bld* gene mutant cannot complement a "later acting" *bld* gene mutant. However, this model is not able to accommodate all the *bld* genes, omitting *bldB*, *bldI*, *bldL*, and *bldN*. It is therefore likely that the control of aerial hyphae initiation is more complex than the model shown in Figure 3. Yet based on the identities and functions known currently for the *bld* genes and a clear hierarchical progression there must be some form of integration of all the signals to then lead to aerial hyphae development.

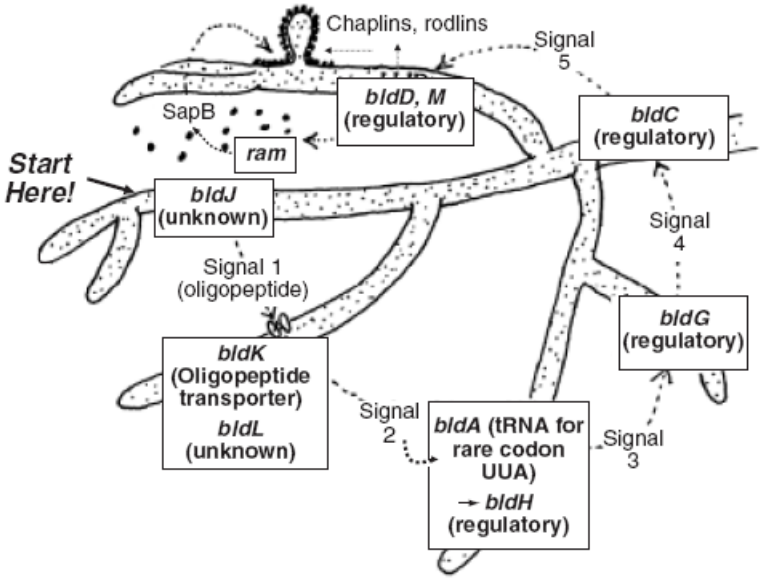

Figure 3: The *bld* genes form a signalling cascade that leads to production of surface proteins needed for erection of the aerial hyphae (taken from Chater & Chandra, (2006)). A large proportion of the *bld* genes form a hierarchy in which it is possible to complement earlier mutants with later mutants but not complement later with earlier.

The model of *bld* signalling begins with the transport of an extracellular signalling molecule to initiate aerial hyphae development. The oligopeptide importer function of *bldK* encoded proteins is believed to import an as yet unidentified extracellular signalling

molecule indirectly produced as a result of *bldJ* (Nodwell *et al.*, 1996; Nodwell, and Losick, 1998). Propagation of the signal from *bldK* dependent import of "signal 1" to *bldA* is currently unknown. However, the identity of *bldA* is a leucine tRNA that recognises the rare codon UUA (Lawlor *et al.*, 1987). The active form of the tRNA increases at the later stages of morphological differentiation allowing translation of proteins using this leucine codon (Leskiw *et al.*, 1993). Bioinformatic, transcriptomic and proteomic data suggest that *bldA* is a pleiotropic regulator affecting 2-3% of genes in the genome that contain the UUA codon (Li *et al.*, 2007a; Chater, and Chandra, 2008; Kim *et al.*, 2005; Hesketh *et al.*, 2007). However, the lack of aerial hyphae resulting from a mutation in *bldA* is mostly due to the loss of the transcriptional activator AdpA. The bald mutant *bldH* is actually a mutant of the gene encoding AdpA (Takano *et al.*, 2003). AdpA has been mostly studied in the closely related species *S. griseus* (Ohnishi *et al.*, 1999; Ohnishi *et al.*, 2005). The full regulon of AdpA in *S. griseus* or *S. coelicolor* has not been uncovered (Yamazaki *et al.*, 2004; Chater, and Chandra, 2008); however, some of the potential targets are genes for proteases (Kato *et al.*, 2005; Kato *et al.*, 2002; Tomono *et al.*, 2005), protease inhibitors (Kim *et al.*, 2005), a developmental sigma factor SsgA (Hirano *et al.*, 2006), the gene *ramR* (Yamazaki *et al.*, 2003; Ueda *et al.*, 2005; Xu *et al.*, 2010) and *bldN* (Yamazaki *et al.*, 2000).

The remaining *bld* genes not yet discussed, mostly play crucial roles in orchestrating transcriptional regulatory cascades that control developmental progression. The links between these *bld* gene functions, in order to establish a pathway are not clear despite the fact that a number of them fit into the hierarchal model discussed earlier and for example *bldB* and *bldI* can loosely be placed into an approximate complementation group (Willey *et al.*, 1993). The link between *bldH* and *bldG* is not clear. The *bldG* phenotype is caused by the absence of a protein showing sequence similarity to a family of anti-anti-sigma factors from *Bacillus* and *Staphylococcus* species (Bignell *et al.*, 2000). Downstream of *bldG* is a putative anti-sigma factor. However, there is no sigma factor ORF downstream or close by to *bldG*. Both *bldG* and the anti-sigma factor encoding gene are upregulated at the time of aerial hyphae formation and antibiotic production, consistent with a role in controlling aerial hyphae development (Bignell *et al.*, 2000). It seems that a sigma factor under regulation of BldG is the alternative stress response sigma factor, σ^H, how this affects aerial hyphae formation is uknown (Sevcikova *et al.*, 2010).

The genes *bldG* and *bldH* are both necessary to allow for the transcription of an extracytoplasmic RNA polymerase sigma encoded by *bldN* (Bibb *et al.*, 2000). However, despite working downstream in the signalling pathway from *bldG* and *bldH*, *bldN* did not

fit into a complementation group of *bld* mutants. Previously *bldN* had been defined as a *whi* mutant because certain point mutations lead to a lack of sporulation, whereas it was later found a null mutant was completely deficient in aerial hyphae formation. Hence differing point mutations can affect the degree of activity of σ^{BldN} (Bibb *et al.*, 2000). As *bldN* transcription is dependent on *bldG* there is likely another sigma factor that is controlled by *bldG* and therefore enabling expression of *bldN*. In *S. venezulae* it has recently been shown that *bldN* has a downstream anti-sigma factor, RsbN, that prevents premature sporulation (Bibb *et al.*, 2012). It was shown that the *bldM* gene is a direct target for σ^{BldN} (Bibb *et al.*, 2000). The *bldM* gene encodes a member of the FixJ subfamily of response regulators, but is unusual in that its putative phosphorylation site, aspartate-54 is not required for BldM function (Molle, and Buttner, 2000). A *bldM* mutant fits into the same complementation group as *bldD*. The *bldM* loci was originally classed as a *whi* gene, due to a number of mutant alleles that result in a lack of sporulation but normal production of aerial hyphae (Ryding *et al.*, 1999). As the null mutant is *bld*, this suggests that BldM is active in different stages of *S. coelicolor* growth. A sensor kinase for BldM has not yet been identified, along with the lack of importance of aspartate-54 it is currently not clear how BldM functions (Molle, and Buttner, 2000).

Mutants of the locus *bldC* are in a complementation group downstream of the *bldG* locus. The gene positioned at the *bldC* locus encodes for a member of the MerR family of DNA binding proteins. A *bldC* mutant is defective in aerial hyphae production and shows a reduction in the production of the antibiotics actinorhodin and undecylprodigiosin (Hunt *et al.*, 2005). To which it has been attributed to be needed for the normal transcription of activator genes required for production of these antibiotics. The transcription of *bldC* is constitutive, and no direct links to activation of other *bld* genes have been found, therefore its role in developmental morphogenesis is unclear.

The *bldD* gene along with *bldM* is in the final complementation group preceding production of SapB. The gene *bldD* encodes a transcription factor that is similar to the Helix-turn-helix-3 DNA binding proteins (Elliot *et al.*, 1998; Kelemen *et al.*, 2001), also including SinR that acts a repressor for genes essential for entry into sporulation in *B. subtilis* (Mandic-Mulec *et al.*, 1995). BldD was previously shown to act as a repressor for expression of the genes *whiG*, *bldN*, *bdtA* and *sigH* (Elliot *et al.*, 2001; Kelemen *et al.*, 2001). Searches based on a proposed BldD binding consensus sequence also suggested it binds upstream of *bldG* as well as a number of sigma factors (Touzain *et al.*, 2008). BldD was also shown to act as a repressor controlling its own expression (Elliot *et al.*, 1998).

Recently the BldD regulon was investigated using ChIP-chip and it was found that there were a potential of ~127 transcriptional units that are BldD targets (den Hengst *et al.*, 2010). These include the genes *bld*A, *bld*C, *bld*H/adpA, *bld*M, *bld*N, *ssg*A, *ssg*B, *fts*Z, *whi*B, *whi*G, *sme*A-*ssf*A, *nsd*A, *cvn*9 and *leu*A, showing that BldD affects a lot of different developmental process. 42 BldD targets encode regulatory proteins showing that BldD is a pleiotropic regulator in *S. coelicolor*. BldD is expressed at its highest levels during vegetative growth, as it represses a number of developmental genes it blocks aerial hyphae formation. BldD expression is reduced in the aerial hyphae hence releasing the repression on developmental genes needed to progress through the developmental cycle.

Mutants of *bldB* do not fit into the hierarchical model of complementation. Also, *bldB* mutants are special because they are bald and deficient in antibiotic production on both minimal media and rich media (Merrick, 1976). The protein encoded by *bldB* is likely a member of an actinomycete specific protein family (Eccleston *et al.*, 2006). The function of proteins in this family is currently unknown. It is likely that *whiJ* is also in this family of proteins. BldB could include a helix-turn-helix DNA binding motif suggesting it could potentially be a transcription factor (Pope *et al.*, 1998). It is also likely that BldB forms oligomers, most likely dimers (Eccleston *et al.*, 2002). Overexpression of BldB results in a block in sporulation (Eccleston *et al.*, 2006), suggesting BldB plays a critical role in the regulation of morphogenesis in *Streptomyces* development.

Aerial hyphae formation is enabled due to the ability of *S. coelicolor* to release a hydrophobic surfactant SapB that lowers surface tension as well as being able to coat the hyphae in novel hydrophobic structures. As mentioned above classical *bld* mutants lack aerial hyphae development when grown on a rich medium such as R2YE, yet on a minimal medium many are no longer bald (Chater, 1993). As the *bld* cascade leads to production of SapB, there must be an alternative SapB-independent pathway to aerial hyphae formation on minimal medium (Figure 4). This alternative pathway is due to the action of a family of hydrophobic secreted proteins called the “Chaplins”. The chaplins form an aerial surface structure believed to consist of amyloid-like filaments (Elliot *et al.*, 2003; Claessen *et al.*, 2003). Loss of all the chaplin encoding genes results in a strain that on minimal medium is less able to form aerial hyphae as on rich medium (Capstick *et al.*, 2007). A mutant losing all chaplin encoding genes and SapB production is bald under all conditions (Capstick *et al.*, 2007). Along with the rodlin proteins, SapB and the chaplins form a hydrophobic sheath that enables the aerial hyphae to break the surface tension of water-air interfaces

and erect into the air (Claessen *et al.*, 2004; Claessen *et al.*, 2003; Capstick *et al.*, 2007; Kodani *et al.*, 2004).

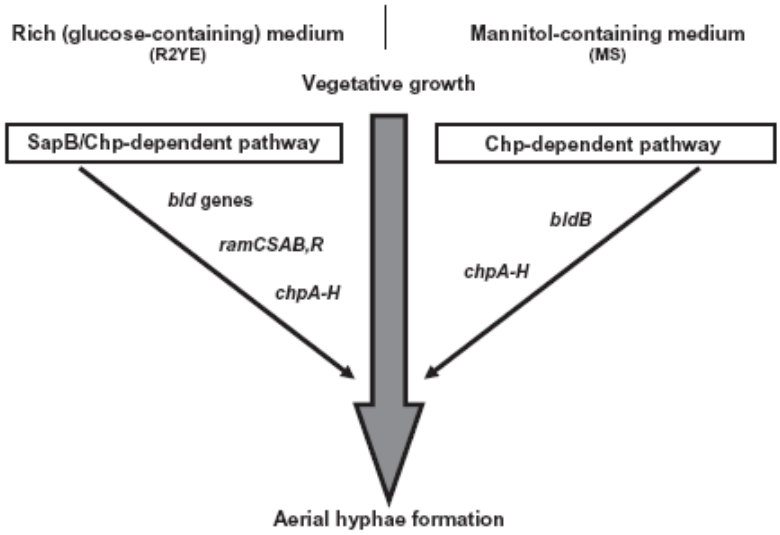

Figure 4: Model of the progression of developmental genes and their importance for aerial hyphae formation on either rich or minimal media (taken from Capstick *et al.*, (2007)).

Production of SapB coincides with the time in which aerial hyphae form (Willey *et al.*, 1991). It was then found that SapB was absent in *bld* mutants but present in *whi* mutants. Surprisingly purified SapB was able to restore aerial hyphae growth to *bld* mutants (Willey *et al.*, 1991). The rapid aerial mycelium (*ram*) gene cluster *ramCSAB* was shown to be responsible for the synthesis and modification of SapB (Kodani *et al.*, 2004). The *ram* genes in *S. coelicolor* were originally identified due to their ability to accelerate aerial hyphae formation when cloned into *Streptomyces lividans* (Ma, and Kendall, 1994; Keijser *et al.*, 2000). The gene *ramR* encodes a response regulator that activates expression of *ramCSAB* (Ma, and Kendall, 1994; Nguyen *et al.*, 2002; O'Connor *et al.*, 2002). RamC is similar to proteins involved in the maturation of lantibiotic peptides (Kodani *et al.*, 2004). The lantibiotic-like structure of SapB is believed to be produced firstly by production of a 42 amino acid peptide encoded by *ramS*, that is subsequently modified by RamC to form the mature SapB that acts a surfactant peptide (Kodani *et al.*, 2004). Sequence analysis of the *ramA* and *ramB* genes suggest that they could make up an ABC transporter protein, to which could function as a specific route for SapB export from the cell (Ma, and Kendall, 1994). It is currently believed that due to the ability of purified SapB to restore aerial hyphae growth to *bld* mutants (Willey *et al.*, 1991) that it is a surfactant that coats the hyphae and enables them to break the surface tension associated with air-water interfaces. If SapB is provided extracellularly then most *bld* mutants regain the ability to form aerial

hyphae. Yet these mutants still fail to form spores, suggesting that SapB only has a structural role and the intracellular signalling events needed to progress to the point of sporulation are not achieved (Willey *et al.*, 1991; Tillotson *et al.*, 1998). The intricate details of SapB formation and assembly on the hyphae are currently unknown.

Electron microscope images of the surface of *Streptomyces* spores and aerial hyphae showed that they appeared to have a 'basketwork' pattern of filaments that make up the hydrophobic surface (Hopwood, and Glauert, 1961). The layer of the surface consisting of these patterns is called the 'rodlet' layer and is dependent on the two groups of proteins, the chaplins and the rodlins (Claessen *et al.*, 2004). The chaplin proteins are a group of proteins all containing a conserved chaplin domain, as well as having a secretion signal. There are five short chaplins containing only one chaplin domain; ChpD, E, F, G and H. There are also three long chaplins containing two chaplin domains and a sorting signal; ChpA, B and C (Elliot *et al.*, 2003; Claessen *et al.*, 2003). The expression of the chaplin genes coincides with aerial hyphae and is restricted to aerial structures. The sorting signal on long chaplins enables covalent attachment to the cell wall. Whereas it is believed that the long chaplins anchor short chaplins to the cell wall (Claessen *et al.*, 2003; Elliot *et al.*, 2003). The long chaplains themselves are believed to be anchored to the cell wall by sortase enzymes (Duong *et al.*, 2012). Purified chaplin proteins self assemble into amyloid-like filaments, whereas their absence from *S. coelicolor* depletes the aerial hyphae and spores of the same filament covered rodlet layer (Claessen *et al.*, 2003; Claessen *et al.*, 2004; Sawyer *et al.*, 2011). There are two homologous rodlin proteins in *S. coelicolor*, RdlA and RdlB (Claessen *et al.*, 2002). *S. coelicolor* lacking the Rodlin proteins, lacks the characteristic 'rodlin layer' of filaments and has only fine fibril structures on the aerial hyphae and spores (Claessen *et al.*, 2004; Claessen *et al.*, 2002). Whereas the lack of chaplins results in aerial hyphae defects, a lack of the rodlins does not affect aerial hyphae formation (Claessen *et al.*, 2004). Therefore, it is believed that the chaplins are the hydrophobic structure seen on electron microscope images. It is believed that the rodlins do not themselves form the rodlet layer but somehow assemble the chaplins into the characteristic rodlet surface structures (Claessen *et al.*, 2004).

Currently nothing is known about whether the chaplins and SapB interact with each other. However, as shown it is clear that both are vital in the formation of the aerial hyphae allowing them to break surface tension. Yet it seems that SapB is more important on rich media whilst the Chaplins are only required for aerial hyphae formation on minimal media (Capstick *et al.*, 2007).

1.1.5 Regulation of sporulation

Different *whi* mutations can block the process of sporulation at different developmental points. Mutations of early acting *whi* genes fail to achieve sporulation septa. The early *whi* genes are *whiA, B, G, H, I* and *J* (Chater, 1972)(Figure 5). Mentioned later, SsgA and SsgB also block septum formation in the aerial hyphae (Keijser *et al.*, 2003; van Wezel *et al.*, 2000). Whereas some later acting *whi* genes morphologically produce spores but are deficient in the grey spore pigment. All of the early *whi* genes are necessary for the production of a late spore specific sigma factor, σ^F, as well as *whiE* that encodes proteins that synthesize the grey spore polyketide pigment. Sporulation seems to be tightly regulated with a number of checkpoints that need to be passed, depending on the input of many different signals.

Experimental data places *whiG* as the earliest acting *whi* gene, with mutations in *whiG* showing no signs of development towards sporulation (Chater, 1972; Chater, 1975; Chater, 1993). As a progression *whiG* (Figure 5) comes before *whiH*, which comes before *whiA,B* that then come before *whiI* in terms of the early acting *whi* genes (Chater, 1975). The promoter of *whiG* is a target for BldD binding, however, the consequence of this is unknown as *whiG* mRNA is present at all times, suggesting that it is regulated post-transcriptionally (Elliot *et al.*, 2001; Kelemen *et al.*, 1996). The locus whiG encodes a sigma factor which is believed to play a pivotal role in the initiation of sporulation (Chater *et al.*, 1989). Three of the direct targets for WhiG regulation are the early acting sporulation genes *whiH, whiI* and *whiA* (Ryding *et al.*, 1998; Ainsa *et al.*, 1999; Kaiser, and Stoddard, 2011). A *whiH* mutant shows loosely coiled aerial hyphae that are slightly fragmented though fail to produce wild-type spores (Chater, 1972). The locus *whiH* encodes a transcription factor protein similar to the transcriptional repressor protein GntR in *B. subtilis* (Ryding *et al.*, 1998). This could suggest that it responds to metabolic conditions. WhiH is autoregulatory, repressing its own transcription, though no other targets have been identified as yet (Ryding *et al.*, 1998). It could be possible that WhiH senses a signal following aerial hyphae formation that allows it to relieve repression of genes or lead to activation of genes that mediate changes needed for sporulation. A *whiI* mutant is similar in phenotype to *whiH* and seemingly has fragmented aerial hyphae, though *whiI* mutants form abnormally widely spaced sporulation septa (Chater, 1972). The locus *whiI* encodes an atypical response regulator protein, lacking some of the conserved

residues in the phosphorylation pocket. It is not adjacent to a histidine kinase and as yet no cognate histidine kinase has been identified (Ainsa *et al.*, 1999). WhiI likely acts as a transcriptional repressor to its own promoter. Though transcription of *whiI* increases at the same time as sporulation suggesting that this repression is somehow relieved (Ainsa *et al.*, 1999). Though currently no direct targets of WhiI are known, transcriptome analysis of wild-type *S. coelicolor* in comparison to mutant variations of *whiI* revealed 45 genes whose transcriptional expression was altered (Tian *et al.*, 2007). A number of these genes were analysed and found to encode products that were involved in spore maturation.

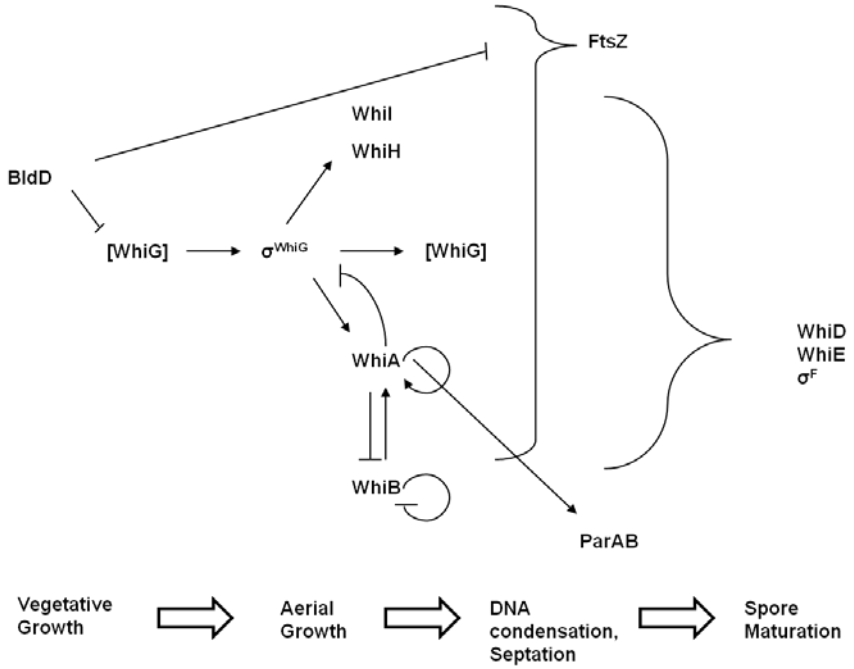

Figure 5: Regulation of sporulation in *Streptomyces*, adapted from Kaiser and Stoddard, (2011), with information from Chater, (2001), den Hengst *et al.*, (2010), Flärdh *et al.*, (2000). Inactive WhiG is in brackets, whereas active WhiG is represented as σ^{WhiG}. The early *whi* genes *whiA*, *B*, *G*, *H*, and *I* are responsible for transition from aerial growth to DNA condensation, septation and spore maturation (WhiJ not shown on diagram).

WhiA transcription is directly controlled by the sigma factor WhiG, WhiA then binds directly to WhiG and inhibits WhiG directed transcription (Kaiser, and Stoddard, 2011).WhiA and WhiB have been seen to effects each other's level of transcription in a currently unknown mechanism (Jakimowicz *et al.*, 2006). Both WhiA and WhiB represent a seemingly independent pathway to WhiH and WhiI, though they could possibly be providing the changes that signal allowing WhiI and WhiH to lose their autoregulatory functions and adopt activating functions (Chater, 2001). Mutants of the *whiA* locus have tightly coiled aerial hyphae that are longer than normal spore chains, there are no sporulation septa present (Chater, 1972; Chater, 1975). Mutants of the *whiB* locus are

similar to mutants of the *whiA* locus, with tightly coiled long aerial hyphae lack sporulation septa (Chater, 1972; Chater, 1975). These phenotypes are believed to result from uncontrolled growth, suggesting that WhiA and WhiB signal growth cessation that is needed before aerial hyphae can form septa and divide (Flärdh *et al.*, 1999; Ainsa *et al.*, 1999). The gene *whiA* encodes a protein whose function is likely as a transcription factor, as well as a direct inhibitor of WhiG (Kaiser, and Stoddard, 2011). *whiA* like genes are conserved across Gram-positive bacteria and are maintained in similar operons with other conserved genes of unknown function (Ainsa *et al.*, 2000). WhiA has two DNA binding domains that likely allow it to function as a transcription factor positively regulating its own promoter as well as binding to *parABp2* and it could possibly regulate other genes involved in sporulation (Ainsa *et al.*, 2000; Kaiser *et al.*, 2009; Kaiser, and Stoddard, 2011). The gene product of *whiB* is the founding member of a novel protein family that are conserved across the Actinobacteria, which have been named the WhiB-like (Wbl) family (Soliveri *et al.*, 2000). Also, included in this family is the product of the locus *whiD* (Molle *et al.*, 2000). The actual function of the Wbl proteins is currently unclear, they all contain four cysteine residues in an arrangement that are suggestive of metal binding and redox sensitivity (Soliveri *et al.*, 2000). In fact WhiD and other Wbl proteins have been shown to bind oxygen sensitive [4Fe-4S] clusters (Crack *et al.*, 2009; Jakimowicz *et al.*, 2005b; Alam *et al.*, 2007; Singh *et al.*, 2007). Two contrasting putative functions of Wbl proteins have been put forward, they could either be oxygen sensitive transcription factors based on their small size and positions of α-helical regions (Davis, and Chater, 1992; Soliveri *et al.*, 2000). The alternative and based on more recent data suggests that they may function as disulphide reductases based on their redox sensitive cluster (Alam *et al.*, 2007; den Hengst, and Buttner, 2008; Jakimowicz *et al.*, 2005b; Singh *et al.*, 2007). Mutations in *whiJ* can be white mutants, though oddly a full deletion of *whiJ* is able to sporulate (Chater, 1972; Gehring *et al.*, 2000; Chater, and Chandra, 2006; Ainsa *et al.*, 2010). It appears that whiJ with its flanking genes (*sco4542* and *sco4544*) could possibly form a regulatory system that is capable of repressing sporulation until an unknown signal is present (Ainsa *et al.*, 2010)

S. coelicolor has one FtsZ homologue which forms cytoskeletal structures that allow septum positioning and division of the aerial hyphae into spores (discussed in more detail later) (McCormick *et al.*, 1994; Schwedock *et al.*, 1997). FtsZ is a *whi* gene as knockouts fail to sporulate (McCormick *et al.*, 1994). The *ftsZ* gene has 3 promoters; however, the large increase in *ftsZ* transcription at the time of sporulation is associated with the *ftsZ2p*

promoter that is upregulated at the same time (Flärdh *et al.*, 2000). The upregulation of *ftsZ2p* is dependent on the presence of all of the early *whi* genes, *whiA, B, G, H, I* and *J* (Flärdh *et al.*, 2000). To which all of the early whi gene knockouts tested (all but *whiJ*) do not have the regular ladders of 'Z rings' associated with wild-type aerial hyphae (Grantcharova *et al.*, 2005). Due to the similarities in phenotypes of an *ftsZ2p* mutant and a *whiH* mutant, it has been suggested that WhiH may activate *ftsZ2p* (Chater, 2001; Flärdh *et al.*, 2000). If *ftsZ* is put under a constitutive promoter then it can be seen to complement *whiA, B, G, H, I* and *J* mutants to forming spores, albeit in some cases not wild-type-like spores (Willemse *et al.*, 2011b). Reinforcing an idea that these genes are crucial for correct temporal and spatial expression of *ftsZ*. Another family of genes that are important in the development of the aerial hyphae are the SsgA-like proteins (SALPs), this family of proteins occurs only in morphologically complex actinomycetes (Traag, and van Wezel, 2008). In fact SsgA and SsgB have been implicated in direct placement of FtsZ and therefore control a key step in cell division of the aerial hyphae (Willemse *et al.*, 2011a).

Following sporulation septation, there are three important late acting sporulation genes, being *whiD*, *whiE* and *sigF*. Whereas an early acting *whi* gene mutant fails to produce sporulation septa, *whiD* mutants do achieve formation of sporulation septa suggesting that *whiD* acts at a later stage. A *whiD* mutant can also form spores; however, these spores are abnormal, being irregular in size, having irregular spore wall deposition and the spores were prone to lysis and lacked the level of resistance of wild-type spores (Chater, 1972; Molle *et al.*, 2000). As mentioned above WhiD is a Wbl protein that has been shown to bind oxygen sensitive [4Fe-4S] clusters. This could mean the WhiD detects redox changes and result in a switch that allows the later stages of sporulation to occur (Chater, 1972; Jakimowicz *et al.*, 2005b; Molle *et al.*, 2000). Expression of *sigF*, encoding the late spore specific sigma factor, σF, depends on all of the early *whi* genes, *whiA, B, G, H, I* and *J* (Kelemen *et al.*, 1996). The mutant of the gene *sigF* produces a white phenotype where the spores are deformed in comparison to the wild-type. They exhibit smaller size, have thinner walls, have uncondensed chromosomes and lack some of the high resistance characteristics of wild-type spores (Potuckova *et al.*, 1995). σ^F encoded by *sigF* is similar to σ^B of *Bacillus subtilis*, which is involved in stationary phase gene expression and stress response (Boylan *et al.*, 1993; Potuckova *et al.*, 1995). σ^F seems to be only involved in morphological differentiation associated with spore formation in *S. coelicolor* (Potuckova *et al.*, 1995). No direct targets of σ^F are currently known; however, one of the two *whiE* promoters is indirectly activated by σ^F (Kelemen *et al.*, 1998), though it is anticipated that

there are more genes that are direct targets for σ^F. The locus *whiE* consists of eight genes, the removal of which gives a phenotype similar to the wild-type in its ability to form spores. However, the spores produced lack the grey colour, but in every other way are indistinguishable from the spores of the wild-type (Chater, 1972; McVittie, 1974). Six of the genes in the *whiE* locus show homology to genes involved with the synthesis of polyketide antibiotics, these genes are responsible for synthesising the grey polyketide spore pigment that gives spores a distinctive grey colour (Davis, and Chater, 1990).

1.1.6 Antibiotic/secondary metabolite production

The streptomycetes are noted for their production of a large proportion of commercially available antibiotics. These antibiotics are believed to be produced by the *Streptomyces* as a result of ecological pressures. Therefore, it is not surprising that the production of most antibiotics coincides with the growth of aerial hyphae and nutrient limitation. With antibiotics believed to play a competitive role, giving the streptomycetes an advantage over other microorganisms and acting as a defence mechanism (Chater, 2006). The aminoglycoside antibiotic, streptomycin was the first antibiotic to be discovered from *Streptomyces* species (Waksman *et al.*, 1946). This antibiotic produced by *S. griseus* was important in treating Tuberculosis infections and arguably led to the discovery of many more antibiotics from *Streptomyces* species. Notably *Streptomyces coelicolor* produces the antibiotics undecylprodigiosin and actinorhodin that are responsible for the red and blue pigmented colours that give the organism its name (Rudd, and Hopwood, 1979; Wright, and Hopwood, 1976; Feitelson *et al.*, 1985). *S. coelicolor* has been a valuable model for the study of antibiotics as they are produced coinciding with developmental stages and are linked to the developmental regulatory mechanisms. One of the notable mechanisms of regulation of antibiotic production is using the leucine tRNA encoded by *bldA*. This is most obvious due to the presence of TTA codons in many antibiotic regulatory and synthetic genes, as well as the notable lack of antibiotics in a *bldA* mutant (Bentley *et al.*, 2002; Chater, 2006; Merrick, 1976). Other than antibiotics, the *Streptomyces* produce notable secondary metabolites. These include, geosmin which is a chemical responsible for the smell of the soil (Cane *et al.*, 2006; Gerber, and Lechevalier, 1965). As well as the grey polyketide responsible for the grey colour of *Streptomyces* spores (Davis, and Chater, 1990). The current known antibiotics and secondary metabolites produced by the *Streptomyces* demonstrates the potential biological activities that these molecules can

perform and illustrates their importance in the potential production of compounds for pharmaceutical use.

1.2 Bacterial cytoskeletal proteins

1.2.1 Tubulin homologue-FtsZ

The bacterial cell division protein FtsZ shares homology with the eukaryotic cytoskeletal protein tubulin. This homology is not in the form of sequence similarity but is due to the two proteins sharing a 3D structure (Figure 6) (Nogales *et al.*, 1998; Erickson, 1998). Thus, suggesting that an FtsZ/tubulin cytoskeleton was present in the last common ancestor. FtsZ proteins are highly conserved across most bacteria and archaea (Erickson, 1997; Wang, and Lutkenhaus, 1996). They are also present in eukaryotic organelles, notably chloroplasts (Vitha *et al.*, 2001; Erickson, 1997). However, most mitochondria seem to have lost FtsZ and carry out cell division through the use of eukaryotic dynamin (Erickson, 2000).

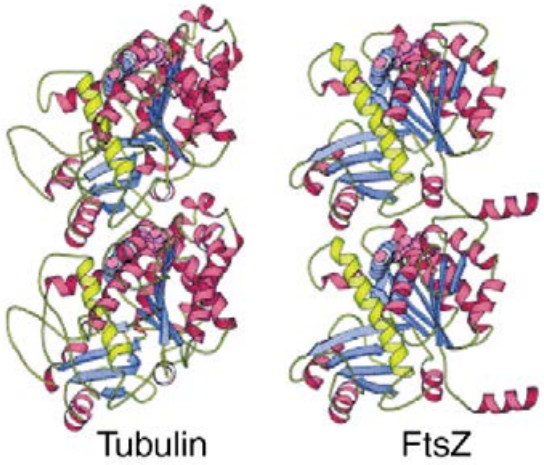

Figure 6: Alignment of the 3D structures of an α/β tubulin dimer and an FtsZ homodimer shows a conserved fold (taken from Carballido-Lopez & Errington, (2003)).

The polymerisation of FtsZ is similar to the way in which tubulin polymerises (Erickson *et al.*, 1996). Similarly to tubulin, FtsZ polymerisation depends on GTP binding and hydrolysis (Bramhill, and Thompson, 1994). FtsZ acts as a GTPase, whereby bound to GTP forms filaments but as GTP is hydrolysed to GDP, FtsZ polymers can disassemble. Thus, in an intracellular environment rich in GTP, FtsZ is able to assemble into filaments (Romberg, and Levin, 2003; Mukherjee, and Lutkenhaus, 1998). In most bacteria FtsZ polymerisation is associated with cytokinesis. For example in *E. coli* polymerisation of FtsZ in symmetrical cell division leads to formation of a ring, the "Z ring", at the midpoint of the cell (Stricker *et al.*, 2002). The "Z ring" is the site where cell division is initiated and

invagination of the membrane occurs (Lutkenhaus, 1993). The positioning of the Z ring classically can be determined by two factors: the positioning of the DNA in the cell, as well as the Min system (Harry, 2001; Raskin, and de Boer, 1997). The nucleoid occlusion model consists of the idea that the position of the replicated nucleoids and the association determines the position of the "Z ring", in some cases this involves Noc proteins that associate with the nucleoid and inhibit Z ring formation nearby (Wu *et al.*, 2009). After DNA replication, segregation of the DNA leads to the mid cell position of the cell being unoccupied by DNA and thus the position that FtsZ forms (Margolin, 2000). The Min system consists of a number of extraordinary oscillatory proteins that form concentration gradients that determine Z ring placement at the middle of the cell (discussed in more detail later) (Yu, and Margolin, 1999). There is increasing evidence that FtsZ rings are produced by spiral-like intermediate structures (Ben-Yehuda, and Losick, 2002; Michie *et al.*, 2006; Sun, and Margolin, 1998). These spirals are generally distributed as helices around the long axis, condensation of the helice could then lead to the formation of the ring structure seen at cell division sites. FtsZ itself may generate some of the force needed to constrict the cell at the division site, as FtsZ was found to be able to constrict liposomes *in vitro* (Osawa *et al.*, 2008). The properties of FtsZ to form at the division site and generate a constrictive force are also dependent on GTP hydrolysis (Li *et al.*, 2007b; Jimenez *et al.*, 2011).

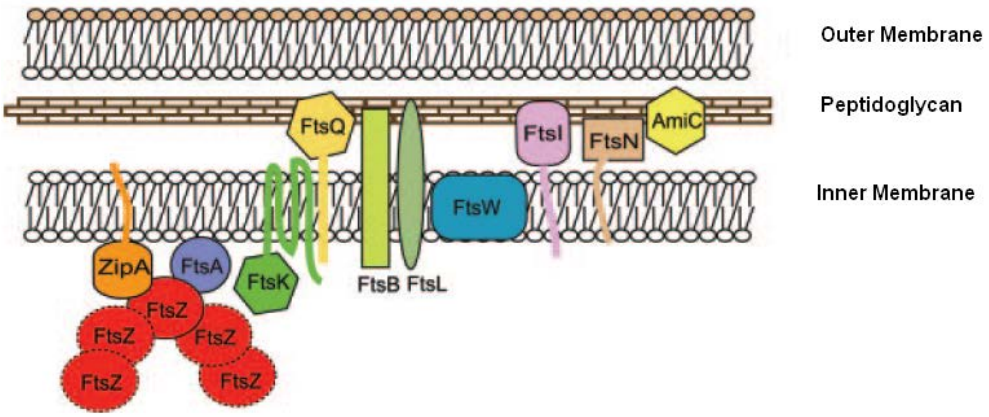

Figure 7: FtsZ rings and associated cell division proteins in *E. coli* (taken from Shih & Rothfield, (2006)). The macromolecular complex is important in driving the associated membrane and cell wall changes needed for the process of cell division.

In *E. coli*, FtsZ as well as a number of other proteins are needed to form the divisome (Figure 7) that actually leads to cell division and invagination. Formation of the Z-ring itself needs two other proteins, FtsA and ZipA to stabilise filament formation and tether

FtsZ to the membrane (Pichoff, and Lutkenhaus, 2002). ZipA has an N-terminal membrane embedded domain that could act as an anchor to the C-terminal FtsZ interacting domain, therefore reinforcing FtsZ ring placement at the membrane (Ohashi *et al.*, 2002; Pichoff, and Lutkenhaus, 2002; Hale *et al.*, 2000; Liu *et al.*, 1999). FtsA is considered to be within the MreB family of proteins and is capable of forming filaments (Szwedziak *et al.*, 2012). The exact mechanism of FtsA contribution to the divisome is unclear; however, its ability to polymerise into filaments is needed for normal function. The formation of a Z-ring then recruits proteins such as FtsI, FtsW, FtsK, FtsN, FtsL/DivIC, FtsQ/DivIB and AmiC (Errington *et al.*, 2003). The action of this multi-molecular complex then drives the changes associated with membrane constriction and cell wall synthesis associated with cell division. The FtsI protein is a penicillin binding protein that is involved in peptidoglycan synthesis at the cell division site creating the cell wall at future poles (Spratt, 1977). The function of the FtsW protein is as a transporter across the cytoplasm of lipid-linked precursors for peptidoglycan synthesis such as lipid II (Mohammadi *et al.*, 2011). FtsK is believed to function in ATP-dependent translocation of DNA through a closing septum to aid chromosome segregation (Aussel *et al.*, 2002; Bath *et al.*, 2000). FtsN has been shown to interact with the peptidoglycan synthase PBP1B as well as being able to stimulate the murein synthesis activity of PBP1B (Muller *et al.*, 2007; Ursinus *et al.*, 2004). Therefore, it is likely that FtsN's role is to modify or control murein synthesis at the cell division site. FtsL and FtsL like DivIC are transmembrane proteins, however, the exact function of these proteins is unknown other than that they are important to cell division and may contribute importantly to protein-protein interactions at the division site (Guzman *et al.*, 1992; Levin, and Losick, 1994). The function of FtsQ and FtsQ like DivIB is unknown, though crystal structure data has revealed that the α-domain of FtsQ has similarity to polypeptide transport-associated domains (van den Ent *et al.*, 2008; Beall, and Lutkenhaus, 1989). It is likely that the role of FtsQ is to assist in the assembly of the outer membrane proteins needed for cell division. AmiC is an enzyme involved in the cleaving of murein crosslinks (Heidrich *et al.*, 2001). Unlike other amidases it is localised to the septal ring (Bernhardt, and de Boer, 2003), showing that murein remodelling is necessary to allow cell division to occur. Other important components of the divisome that may help in FtsZ bundling are ZapA (Gueiros-Filho, and Losick, 2002; Low *et al.*, 2004) and ZapC (Hale *et al.*, 2011), as well as ZapA interacting ZapB (Galli, and Gerdes, 2012). The divisome components across bacterial species appears to vary, with several other important proteins, for example

EzrA (Levin *et al.*, 1999) and SepF (Hamoen *et al.*, 2006) in *B.subtilis*, underlying that the divisome has been adapted across bacterial species.

In addition to FtsZ there are other FtsZ-like proteins in bacteria that are diverse across bacteria and archaea and are putatively speculated to have a role in membrane remodelling (Makarova, and Koonin, 2010). There are also plasmid encoded FtsZ homologs involved in plasmid segregation, the most studied being TubZ (Larsen *et al.*, 2007). TubZ has an accessory protein TubR that helps it mediate interaction with plasmid DNA (Ni *et al.*, 2010). TubZ forms double helical filaments that resemble ParM filaments more than FtsZ filaments (Aylett *et al.*, 2010), suggesting that TubZ was able to evolve a different filament structure to FtsZ as well as a quite different function.

1.2.2 Actin homologues and MreB

A number of cytoskeletal proteins have been discovered in bacteria that are homologs of the eukarytotic cytoskeletal protein actin. These proteins share a conserved actin fold with eukaryotic actin in which the 3D structure is highly similar (van den Ent *et al.*, 2001; van den Ent *et al.*, 2002; Roeben *et al.*, 2006). The actin-like cytoskeletal proteins in bacteria that have been most studied include; the cell-shape determining protein MreB (Jones *et al.*, 2001), the plasmid partitioning protein ParM (Jensen, and Gerdes, 1997) and a recently discovered magnetosome-postioning protein MamK (Komeili *et al.*, 2006). A comparison of the 3D structures of actin and prokaryotic actin homologues MreB and ParM is shown in Figure 8. The ATPase domain is the most conserved characteristic of prokaryotic actin to eukaryotic actin (Bork *et al.*, 1992). Prokaryotic actin homologues MreB, ParM and MamK have all been shown to polymerise into filamentous structures similar to F-actin (van den Ent *et al.*, 2001; van den Ent *et al.*, 2002; Komeili *et al.*, 2006; Jones *et al.*, 2001). Similarly filament assembly and disassembly is controlled by ATP binding and hydrolysis. There are also a number of non-cytoskeletal proteins in bacteria that are considered in the actin family, including the cell division protein FtsA and the heat shock protein DnaK (van den Ent, and Löwe, 2000; Bork *et al.*, 1992). Recently a bioinformatic study found 35 actin-like protein families in bacterial genomes that have conserved 5 signature motifs, though they are not considered to be actin or MreB (Derman *et al.*, 2009). This suggests that actin-like proteins maybe more diverse and spread across bacterial groups than first realised. Discussed below are the filamentous, cytoskeletal actin homologues MreB and ParM and their role in bacterial cell biology.

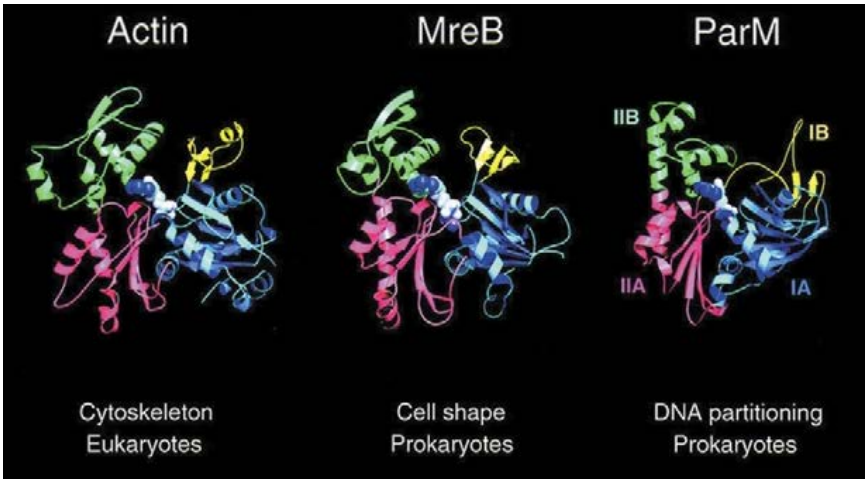

Figure 8: Alignment of the conserved 3D structures of actin, MreB and ParM. Taken from Carballido-Lopez & Errington, (2003). I and II represent the two domains, whereas A and B represent the separation into two subdomains.

One of the most common family of actin-like proteins in bacteria are the MreB family of proteins (Carballido-Lopez, 2006a). MreB proteins were originally defined as a cell shape-determining factor leading to acquisition of a rod shape or other more complex cell shapes other than spherical shaped cells (Daniel, and Errington, 2003). As such MreB is absent in coccoid shaped bacteria. In the rod shaped Gram-positive bacterium, *Bacillus subtilis*, the two MreB family proteins; MreB and Mbl are both important in cell shape determination (Varley, and Stewart, 1992; Abhayawardhane, and Stewart, 1995; Jones *et al.*, 2001). The MreB and Mbl proteins have been shown to localise as helical cords that follow the cell membrane and extend from the septum to the cell poles (Figure 9)(Jones *et al.*, 2001). The pitch of Mbl helices is slightly longer than for MreB suggesting that they form separate and distinct patterns of localisation. The differing results on cell shape from mutants of both MreB and Mbl and their differing localisation patterns suggests that they contribute to different aspects of the cell shape of *Bacillus subtilis* (Abhayawardhane, and Stewart, 1995; Jones *et al.*, 2001). The use of fluorescent vancomycin that stains sites of nascent peptidoglycan synthesis, revealed that cell wall assembly in *B. subtilis* occurs in a helical pattern (Daniel, and Errington, 2003). This is dependent on the Mbl protein, whereby the formation of the Mbl helices is dynamic with the cell cycle and elongates in parallel with cell growth (Figure 9)(Daniel, and Errington, 2003). Due to the insertion of new material in the cell wall, the cell wall then undergoes continuous helical twisting in the opposite direction to helical growth by Mbl, therefore relieving torsional stress (Figure 9). The nature of MreB formation and localisation has been called into question as Cryo-electron Tomography was applied on rod shaped cells and long helical filaments were not visible

(Swulius *et al.*, 2011), suggesting a rethink about the precise structure of MreB is needed. Instead it is now believed that MreB forms shorter discontinuous structures that are moved around the cell circumference by being closely coupled with the cell wall synthetic machinery that acts like a motor (van Teeffelen *et al.*, 2011; Garner *et al.*, 2011; Dominguez-Escobar *et al.*, 2011).

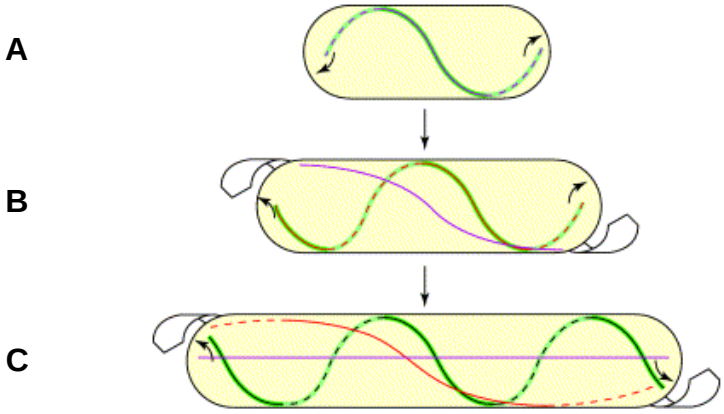

Figure 9: Mbl localisation as helices and formation of the cell wall. Taken from Carballido-Lopez & Errington, (2003). A) Helcial path of Mbl (Green) and insertion of new wall material (Purple). B) To avoid torsional stress the cell wall twists as it elongates (Broad Arrows). New cell wall is inserted with Mbl (Red), older cell wall from A) is now moved due to the cell wall twisting (Purple). C) New cell wall is continually added in the helical path of Mbl (Black), and older cell wall material further unwinds (Red)(Purple). Small arrows indicate Mbl growth.

The *mreB* genes of both *B. subtilis* and *E. coli* are organised such that they are positioned adjacent to two other genes *mreC* and *mreD* (Doi *et al.*, 1988; Levin *et al.*, 1992; Varley, and Stewart, 1992). This organisation is similarly conserved across most bacteria such that *mreB* is in a clustered operon with *mreCD* (Carballido-Lopez, and Errington, 2003). *E. coli* MreB forms helical localisation patterns similar to that of MreB and Mbl of *B. subtilis* and there is increasing evidence that MreB in *E. coli* controls cell wall material insertion (Kruse *et al.*, 2005; Kruse *et al.*, 2003; De Pedro *et al.*, 2003). MreC and MreD are also coupled to MreB function in *E. coli* and the depletion of either prevents correct MreB localisation *in vivo* (Kruse *et al.*, 2005). It is also likely that MreB, MreC and MreD form a complex based on interactions between MreC with both MreB and MreD *in vitro* (Kruse *et al.*, 2005). Similarly to *E. coli*, in *C. crescentus* it is the MreB protein encoded from an *mreBCD* operon that contributes to cell wall synthesis (Figge *et al.*, 2004; Dye *et al.*, 2005). It seems likely that cell wall synthesis is coordinated through MreB cytoskeletons by atleast the established interactions of MreC with cell wall synthetic enzymes such as penicillin-binding protein 2 (Kruse *et al.*, 2005; Leaver, and Errington, 2005; Dye *et al.*,

2005; De Pedro *et al.*, 2003). In addition to a potential complex is another protein that is important with regard to MreB and lateral cell wall insertion/shape determination, which is the co-localizing protein RodZ (Shiomi *et al.*, 2008; Bendezu *et al.*, 2009; Alyahya *et al.*, 2009). Rodz spans the membrane and reaches into the periplasm, the cytoplasmic end of RodZ can interact with MreB (van den Ent *et al.*, 2010). Components of the complex are expanding and also include murein biosynthetic enzymes, to which MurG makes a strong interaction with MreD (White *et al.*, 2010). This expanding evidence shows that MreB proteins play an important role in cell shape determination in bacteria through a complex in a similar way as FtsZ forms a complex. However, MreB proteins have also been linked with other possible functions, for example they have been shown to have a possible role in cell polarity localising certain proteins to the cell poles (Gitai *et al.*, 2004; Jyothikumar *et al.*, 2008; Shapiro *et al.*, 2002). There is also substantial evidence that MreB homologues have a role in chromosome segregation (Gitai *et al.*, 2004; Kruse *et al.*, 2003).

In typeII plasmid partitioning systems, partitioning of the plasmids are carried out by actin-like ATPases, to which ParM is the most understood (Jensen, and Gerdes, 1997; Jensen, and Gerdes, 1999). There are three components in the plasmid partitioning system of plasmid R1. There is *parM* encoding the actin-like protein ParM that acts as an assembling filament and physically moving the plasmid DNA (Moller-Jensen *et al.*, 2003; Moller-Jensen *et al.*, 2002). There is *parC* which is a cis-acting centromeric site needed for protein attachment to the plasmid. There is also *parR* which encodes a protein that binds *parC* and links the ParM protein to the plasmid DNA (Jensen, and Gerdes, 1997). Newly replicated plasmid DNA close to midcell positions is forced to opposite sides of the cell by the force of ParM assembly (Figure 10). To which, ParM assembles at a cap with an ATP-bound ParM monomer. Insertion of a new monomer is dependent on the cap monomer hydrolysing ATP to ADP, therefore all the ParM monomers in the filament are bound to ADP besides the terminal monomer (Garner *et al.*, 2004). Correct ParM formation depends on a process of dynamic instability where terminal ParM is stabilised by interaction with ParR bound to plasmid R1 DNA, only ParM filaments with a cap on each end will stably polymerise and thus push the two plasmids to opposite sides of the cell (Garner *et al.*, 2004; Garner *et al.*, 2007). Following ParM assembly and plasmid partitioning to daughter cells, ParM filaments disassemble

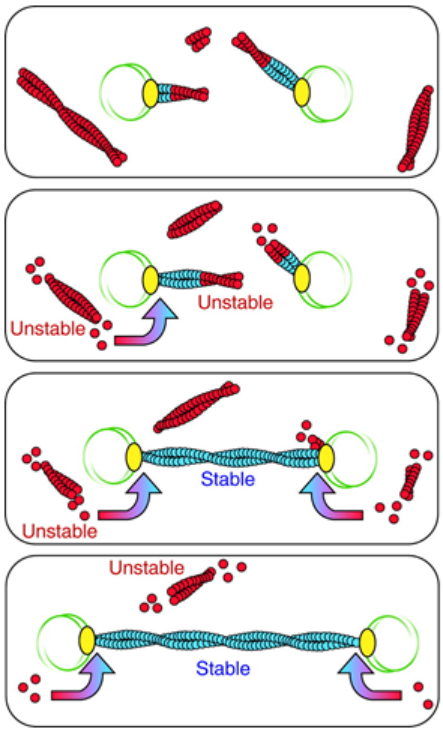

Figure 10: Showing the plasmid R1 partitioning system involving the actin-like protein ParM which pushes apart newly replicated plasmids. Taken from Shaevitz & Gitai, (2010). Unstable ParM filaments form (red). These are stabilised (blue) by ParR (yellow) bound to R1 plasmid DNA (green). A ParM filament stabilised at both ends can elongate and push the replicated plasmid DNA to opposite ends of the cell.

1.2.3 Intermediate filament-like protein CreS

The Gram-negative bacterium *Caulobacter crescentus* is a model of bacterial development and cellular differentiation. There are two differing cell types that are generated by a combination of asymmetrical division and subsequent cellular differentiation. A motile "swarmer" cell possessing a single polar flagellum allows dispersal of *C. crescentus* in an aquatic environment. However, it cannot initiate DNA replication and cell division. Cellular differentiation results in the production of a non-motile "stalked" cell, consisting of a single polar stalk. This cell acts as a predivisional cell, allowing DNA replication and cell division. Asymmetrical cell division of the stalked cell produces two compartments that result in the production of a new swarmer cell and a new stalked cell (Wheeler *et al.*, 1998).

C. crescentus during stationary phase growth is also capable of producing extended helical spiral shaped cells. The gene required for the determination of the crescent or helical cell shape characteristic of a wild-type *C. crescentus* cell is *creS* (Ausmees *et al.*, 2003). Knockouts of the gene *creS*, resulted in a straight rod shaped cell. The protein encoded by *creS*, crescentin, was localised in vibroid shaped cells to form a pole to pole filament along the concave side of the cell. Similarly in the helical cells crescentin formed a helical filament that ran alongside the inner curvature of the spiral (Ausmees *et al.*, 2003).

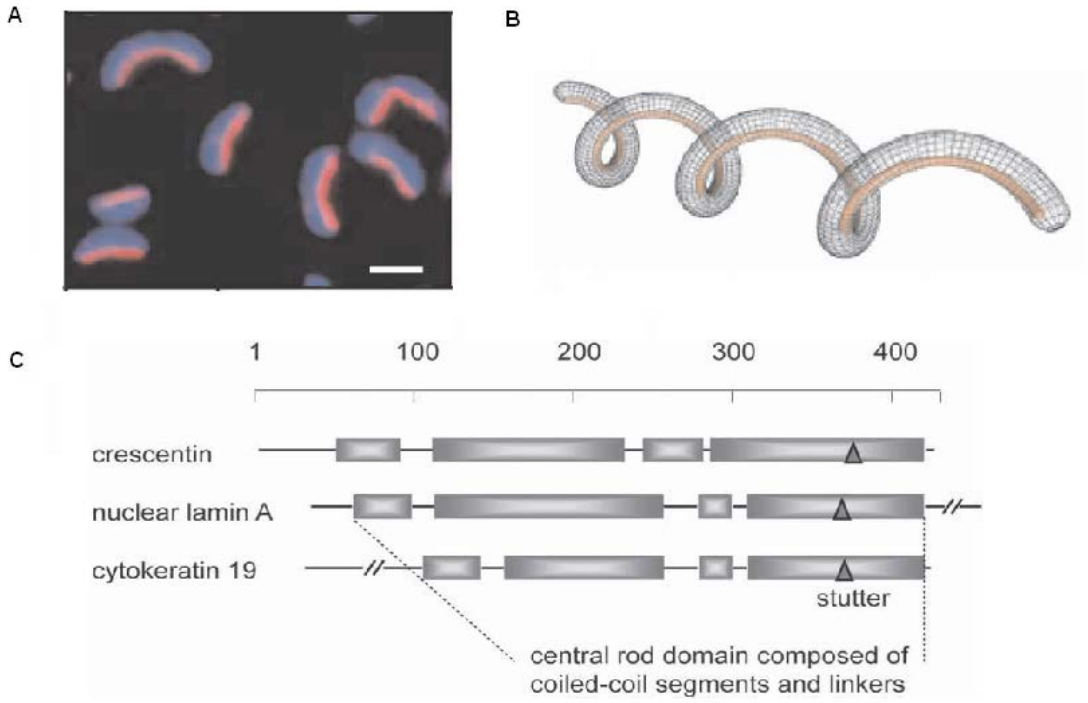

Figure 11: Crescentin the *Caulobacter crescentus* cytoskeletal protein. Adapted from Taken from Ausmees *et al.,* (2003). A) Immunolocalisation of crescentin in a crescent shaped cell. B) A representation of the helical localisation of crescentin to the inner curvature of a vibriod shaped *C. crescentus* cell. C) Comparison of domain organisation of predicted coiled-coils (grey rectangles) of crescentin to human intermediate filament proteins nuclear lamin A and cytokeratin 19.

Localisation of crescentin and its necessity for generation of a vibroid or helical cell shape, strongly suggests that crescentin has some form of structural role as a cytoskeletal protein. Sequence analysis and *in vitro* analysis suggests that crescentin is a bacterial equivalent to the intermediate filament proteins of eukaryotes (Ausmees *et al.,* 2003). Intermediate filaments have a characteristic domain organisation. They consist of four central heptad repeat coiled-coil domains surrounded by non-coiled-coil "head" and "tail" domains (Strelkov *et al.,* 2003). Crescentin has a similar domain organisation of the four central heptad repeat coiled-coil regions. There is also sequence similarity of between 25% identity and 45% similarity of crescentin with the eukaryotic intermediate filament protein cytokeratin 19, as well as 24% identity and 40% similarity with the eukaryotic intermediate filament protein nuclear lamin A (Ausmees *et al.,* 2003). In eukaryotic intermediate filament proteins the so called "head" and "tail" domains do not generally show high sequence conservation so these regions are not detected in crescentin (Strelkov *et al.*, 2003; Ausmees *et al.,* 2003). Crescentin does share similarities in terms of the biochemical properties of the intermediate filament proteins. Purified histidine-tagged crescentin spontaneously assembled into filaments without the addition of nucleotides or co-factors,

this being characteristic of intermediate filaments as opposed to actin and microtubules which require additional factors for assembly (Desai, and Mitchison, 1997; Ausmees *et al.*, 2003; Korn *et al.*, 1987). Crescentin's ability to result in a curved cell shape appears to be facilitated by its *in vivo* ability to form filaments that are connected to the membrane, that when detached compress into helical shapes. It is believed that the pressure applied from its mechanical compressive properties to one side of the cell result in a local release of strain that produces a gradient of elongation rates favouring higher elongation on the opposite cell. Therefore, the cell inserts peptidoglycan at different rates and this results in a maintained curvature (Cabeen *et al.*, 2009). Crescentin does not act alone in a *Caulobacter* cell and one of the proteins that may affect crescentin is MreB, possibly providing a connection to the cell envelope (Charbon *et al.*, 2009). Crescentin is also affected by an enzyme called Ctp synthase (CtpS) which may negatively regulate the ability of crescentin to cause curvature in the cell (Ingerson-Mahar *et al.*, 2010).

Quite recently the coiled-coil domain architecture of crescentin and eukaryotic intermediate filaments has served as a basis for searching for other possible intermediate filament-like proteins in bacteria (Bagchi *et al.*, 2008). These searches have produced potential candidates across widely spanning phylogenetic groups, suggesting that the intermediate filament-like rod domain architecture could be conserved across bacteria. Analysis of a small number of candidates from a possibly more conserved family of actinomycete intermediate filament-like proteins, suggest that these proteins have biochemical properties similar to intermediate filament proteins and crescentin. Three actinomycete intermediate filament-like proteins formed filamentous structures *in vitro* in a similar fashion to crescentin and intermediate filament proteins (Bagchi *et al.*, 2008). Differences, however, in the properties of the filaments could suggest that coiled-coil proteins in different bacteria can differ in a manner tailored to the function *in vivo*. Further analysis of the *Streptomyces coelicolor* intermediate filament-like protein AbpS/FilP suggest that this protein could be a cytoskeletal protein; however, its function is as yet unclear (AbpS/FilP discussed in more detail later) (Bagchi *et al.*, 2008). The candidate cytoskeletal proteins identified by Bagchi *et al.*, (2008) as well as the identification of crescentin, suggest that prokaryotes have a cytoskeletal system similar to eukaryotes that was probably inherited from the last common ancestor.

1.2.4 ParA/MinD family of proteins

The ParA/MinD superfamily of cytoskeletal proteins are a family only present in prokaryotes with no known homologs in the eukaryotes. They very often show properties of cytoskeletal proteins by their ability to self-assemble into long polymeric filamentous structures *in vitro* and in many cases have been shown to form filaments *in vivo* (Shih *et al.*, 2003; Ebersbach, and Gerdes, 2004). They are characterized by a deviant Walker A-type ATPase motif consisting of the amino acids residues GXGGXHKTS (Koonin, 1993). This motif is generally located within the nucleotide-binding P-loop, located near the N-terminus of the protein. The deviant Walker A-type motif separates them from a large number of the non-cytoskeletal Walker-type ATPases, though a very small number of non-cytoskeletal proteins also have this motif (Shih, and Rothfield, 2006; Koonin, 1993). The ParA/MinD superfamily can be divided into the MinD and ParA subgroups. Where the MinD subgroup of proteins has been found to be involved in the placement of cell division sites within various bacterial models (Shih *et al.*, 2003). The ParA subgroup has been found to be involved in the segregation of either plasmid DNA or chromosomal DNA (Ebersbach, and Gerdes, 2004; Sharpe, and Errington, 1996; Figge *et al.*, 2003).

In *E. coli* mutants of the Min system give rise to a minicell phenotype, with cells lacking normal DNA levels (Adler *et al.*, 1967). The proteins in this system; MinC, MinD and MinE control division site placement (Margolin, 2001). This is manifested by placement of the MinD cytoskeleton. To which this protein is spatially and temporally organised into helical oscillations (Raskin, and de Boer, 1999; Shih *et al.*, 2003). It assembles at cell poles and oscillates from one pole to the other. This is partly regulated by MinE, which helps prevent MinD formation at the mid-cell position (Hale *et al.*, 2001). The oscillations of MinD shown in Figure 12, create a concentration gradient where MinD is low in the midcell position. MinC mediates an inhibition of FtsZ polymerisation where MinD is positioned therefore preventing septum position at the cell poles and in the midcell where MinD is deficient, cell division can occur (Dajkovic *et al.*, 2008). *C. crescentus* has a protein MipZ that is a member of the ParA superfamily that functions in a manner similar to the min system, inhibiting polymerization of FtsZ and affecting the site of cell division (Thanbichler, and Shapiro, 2006). Whereas MinC does not affect the GTPase activity of FtsZ, MipZ stimulates the GTPase of FtsZ leading to excessive GDP bound FtsZ and depolymerisation. MipZ in a similar way to MinD, forms a polar gradient, where it is

highest in concentration at the cell poles and the concentration is lower towards the mid-cell position (Kiekebusch *et al.*, 2012).

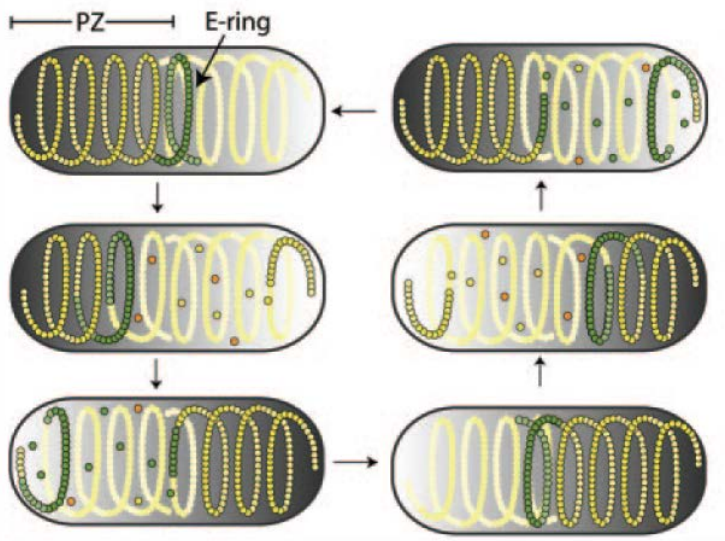

Figure 12: Dynamic helical MinD and MinE filaments showing cyclical assembly and disassembly. Taken from Shih & Rothfield, (2006). MinD-ATP subunits are coloured yellow, MinD-ADP subunits are coloured orange and MinE subunits are coloured green.

The Type I plasmid partitioning systems such as plasmid F, plasmid P1 and pB171 that have been studied in *E. coli* generally consist of a partitioning locus consisting of a ParA protein, a ParB protein and *cis*-acting DNA sites *parS*/*parC* (Mori *et al.*, 1989; Davis *et al.*, 1992; Ebersbach, and Gerdes, 2001). Depending on the plasmid segregation system, the Walker-type ATPase, ParA, can also go by alternative names SopA or ParF (Mori *et al.*, 1989; Barilla *et al.*, 2005). The centromere binding protein, ParB, can also go by the other names of SopB or ParG depending on the system (Mori *et al.*, 1989; Barilla *et al.*, 2005). The ParB proteins link the ParA proteins to the *parS/parC* sites. The ParA proteins involved in plasmid segregation have been shown to form cytoskeletal filaments as well as showing oscillatory localisation patterns similar to those observed for MinD proteins (Ebersbach, and Gerdes, 2004). The cytoskeletal filaments and dynamic nature of the ParA proteins are believed to mediate plasmid partitioning, yet at the moment there is no single clear model that describes how ParA proteins mediate plasmid translocation. Though possibilities are that oscillations set up concentration gradients for ParB binding at alternative poles of the cell, a similar pushing mechanism as to that performed by ParM in typeII plasmid partitioning systems or perhaps by ParA association with the nucleoid and piggy-backing chromosomal segregation (Shih, and Rothfield, 2006; Szardenings *et al.*, 2011).

ParA and ParB proteins have been shown to have a role in the segregation of chromosomal DNA within the model organisms *Bacillus subtilis*, *Caulobacter crescentus* and *Streptomyces coelicolor* (Sharpe, and Errington, 1996; Figge *et al.*, 2003; Jakimowicz *et al.*, 2007). In *Bacillus subtilis* the genome encoded ParA is named Soj and ParB is named SpoOJ. The precise roles of these proteins were for a time unclear, however, more recently a mechanism has been proposed in which SpoOJ and Soj are capable of controlling both DNA segregation and initiation of chromosomal replication (Figure 13)(Gruber, and Errington, 2009). SpoOJ has been shown to bind to a number of *parS* sites located close to the origin (Lin, and Grossman, 1998). SpoOJ has also been shown to be needed for the correct segregation of a nucleoid into the prespore compartment prior to sporulation (Wu, and Errington, 2003). Soj, however, does not control chromosome segregation, instead it can control DnaA; therefore, it controls chromosome replication and sporulation (Lee, and Grossman, 2006; Murray, and Errington, 2008). SpoOJ binds to parS sites and then spreads laterally for multiple kilobases, binding to DNA in a non-specific manner (Breier, and Grossman, 2007). SpoOJ is able to recruit SMC and the other condensing components to the replication origin (Gruber, and Errington, 2009), forming a nucleoprotein complex therefore facilitating its role in chromosome segregation. SpoOJ also believed to increase the ATPase activity of Soj (Leonard *et al.*, 2005), therefore also plays a role in controlling Soj and chromosome replication initiation as well.

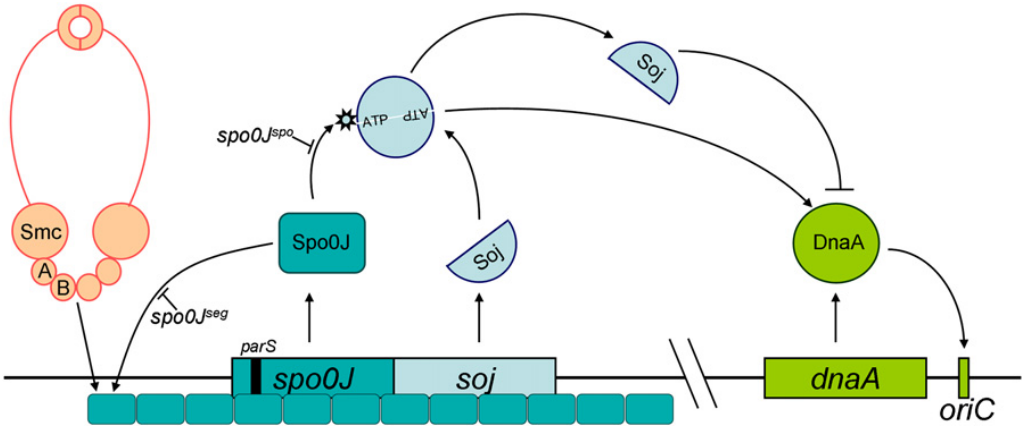

Figure 13: Role of SpoOJ and Soj in controlling Chromosome segregation and replication. Taken from Gruber & Errington, (2009). SpoOJ is able to trigger smc/condensin mediated chromosome segregation through binding to *parS* sites around the replication origin. Soj can control initiation of DNA replication through DnaA, where dimeric Soj activates DnaA and replication, whereas monomeric Soj inhibits DnaA. SpoOJ is able to stimulate Soj ATPase activity. *spoOJ*^{spo} and *spoOJ*^{seg} mutants that uncouple the two roles of SpoOJ.

1.2.5 DivIVA

DivIVA proteins are novel bacterial cytoskeletal proteins that have been shown to play differing roles in cell shape determination in a number of morphologically different bacteria. Members of the DivIVA protein family are conserved across Gram-positive bacteria (Oliva *et al.,* 2010), but are not present in Gram-negative bacteria, notably this includes the model organism *E. coli*. DivIVA has so far been most heavily studied in *Bacillus subtilis,* but also has been looked at in *Corynebacterium glutamicum*, *Streptomyces coelicolor*, *Streptococcus pneumoniae,* and *Mycobacterium* species. DivIVA from *B. subtilis* has been shown to form higher order oligomeric structures (Stahlberg *et al.,* 2004), this together with association of DivIVA with cell wall synthetic machinery (Mukherjee *et al.*, 2009) suggest that it is an important bacterial cytoskeletal protein.

The *divIVA* locus in *Bacillus subtilis* was first identified as a knockout, which causes a minicell phenotype similar to that seen in a *minC* or *minD* knockout (Cha, and Stewart, 1997; Lee, and Price, 1993). Overproduction of DivIVA resulted in long filamentous cells (Cha, and Stewart, 1997). DivIVA localises to newly emerging cell division sites, as well as sites at the cell poles where it remains even after cell division (Edwards, and Errington, 1997; Edwards *et al.*, 2000). The current model of DivIVA activity suggests that it sequesters the cell division inhibitors MinCD to the cell poles allowing cell division to occur at central sites (Cha, and Stewart, 1997; Edwards, and Errington, 1997). DivIVA itself has not been shown to bind either MinC or MinD, however there is another component MinJ which bridges DivIVA and MinD (Bramkamp *et al.*, 2008; Patrick, and Kearns, 2008). Only after establishment of the cell division site at midcell (and establishment of the new daughter cell pole) does DivIVA localise to the cell division site. DivIVA also has a second role, whereby it acts in the process of chromosome segregation. In sporulating cells, DivIVA interacts with the chromosome segregation machinery to help position the *oriC* region of the chromosome at the future cell pole that is to become the spore compartment (Perry, and Edwards, 2004; Thomaides *et al.*, 2001).

In actinomycetes, DivIVA proteins have been shown to have a somewhat different role in cell shape determination than to the role in *Bacillus subtilis*. In the organisms *Mycobacterium smegmatis*, *Mycobacterium tuberculosis*, *Streptomyces coelicolor,* and *Corynebacterium glutamicum,* DivIVA homologs appear to play a role in apical growth associated with long non-spherical cell shapes that are not dependent on MreB (Flärdh, 2003a; Hempel *et al.,* 2008; Letek *et al.,* 2008; Nguyen *et al.*, 2007; Ramos *et al.,* 2003).

Fluorescent vancomycin stains nascent sites of peptidoglycan insertion into the cell wall of gram-positive bacteria (Daniel, and Errington, 2003). Staining of the cell walls of *Mycobacterium smegmatis*, *Streptomyces coelicolor* and *Corynebacterium glutamicum* with fluorescent vancomycin suggests that these organisms insert new cell wall material at the tips (Daniel, and Errington, 2003; Flärdh, 2003b; Chauhan *et al.*, 2006). Current research suggests that DivIVA in these organisms affects cell wall assembly at apical growth sites, this could be by possible interaction with penicillin-binding proteins and/or other cell wall synthetic machinery (Letek *et al.*, 2008; Flärdh, 2003a; Hempel *et al.*, 2008; Nguyen *et al.*, 2007; Xu *et al.*, 2008). In *Mycobacterium*, the DivIVA homologue Wag31 has been shown to make direct contact with penicillin-binding protein 3 (PBP3) (Mukherjee *et al.*, 2009). Therefore, making the connection between DivIVA polar localisation and its effect on polarised growth in actinomycetes.

The DivIVA protein from *Streptococcus pneumoniae* has a somewhat similar localisation pattern as that in *Bacillus subtilis* of localisation to cell division sites and to cell poles (Fadda *et al.*, 2007). DivIVA of *Streptococcus pneumoniae* was also shown to have potential interactions with members of the cell division machinery and so is believed to play a role in maturation of cell poles (Fadda *et al.*, 2007). However, interestingly *Streptococcus pneumoniae* lacks a Min system suggesting its DivIVA and *B. subtilis* DivIVA could have independently evolved a similar function (Fadda *et al.*, 2007).

It is emerging that DivIVA may be partly regulated by posttranslational modifications such as phosphorylation. It was shown that Wag31 in *Mycobacteria* is post-translationally modified by phosphorylation (Kang *et al.*, 2005; Kang *et al.*, 2008). The phosphorylation state of Wag31 was shown to influence an effect on actively growing cells; however, the precise mechanism is currently uknown. Recently it has been found that *S. coelicolor* DivIVA is also phosphorylated (Manteca *et al.*, 2011; Hempel *et al.*, 2012). Interestingly DivIVA from spherical shaped *Streptococcus pneumoniae* is also phosphorylated, and cells carrying a non-phosphorylatable copy of DivIVA featured an extended cell shape (Fleurie *et al.*, 2012; Beilharz *et al.*, 2012).

Structural studies of DivIVA proteins have currently been limited to only the *Bacillus subtilis* DivIVA protein where the 3D structure has been solved (Oliva *et al.*, 2010). *Bacillus subtilis* DivIVA is 19.5kDa and according to sequence data forms coiled-coil structures possibly similar to tropomyosin (Edwards *et al.*, 2000). Analytical ultracentrifuge data suggests that DivIVA forms oligomers of 6-8 molecules (Stahlberg *et al.*, 2004). Transmission electron microscopy was used to visualised oligomeric structures

of DivIVA (Figure 14) (Stahlberg *et al.*, 2004). A 6-8-mer of DivIVA forms a characteristic ‘doggy bone’ shaped structure. These ‘doggy bone’ structures form end to end dimers that then assemble into higher order long thin wires of ‘doggy bones’. Individual wires can then associate with other wires to form 2-D structures, where individual ‘doggy bones’ can replace other ‘doggy bones’. Currently the implications of oligomerisation of DivIVA on the function of the protein are not very well understood; however, DivIVA structures contribute towards its role in cell division placement (Muchova *et al.*, 2002).

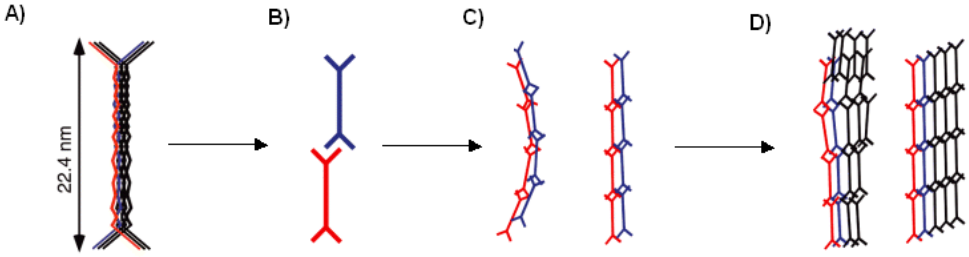

Figure 14: Assembly of DivIVA into higher order structures. DivIVA proteins form 6-8-mers that make a ‘doggy bone’ shaped structure (A). Individual ‘doggy bones’ form dimers (B) that then oligomerise to form long thin wires (C) and two dimensional networks (D). Adapted from Stahlberg *et al.*, (2004).

One idea for the ability of DivIVA to localise to polar positions is that the localisation is dependent on the geometrical cue of negative membrane curvature (Ramamurthi, and Losick, 2009; Lenarcic *et al.*, 2009) such as that found at the ends and the dividing mid-cell positions of a *B. subtilis* cell. Although unlikely that a single protein of DivIVA could sense membrane curvature it is more likely that the multimers of DivIVA are able to bridge the curvature of a membrane. Recently the crystal structure of *B. subtilis* DivIVA has been solved (Oliva *et al.*, 2010). The full length protein could not be solved. However, a crystal structure of the N-terminus and a low resolution crystal of the C-terminus were merged to make a model of the full length protein (Figure 15). The N-terminal domain was able to form a dimer. It was also shown to be important for membrane binding, whereby hydrophobic and positively charged residues allow binding. A Phenylalanine residue (F17) is considered essential for membrane binding allowing insertion into the membrane. The C-terminal crystal structure could only be solved to a lower resolution than the N-terminal, but confirmed that the C-terminal forms a coiled-coil, of which a dimer of two coiled-coils makes a tetramer with another dimer, this tetramer adds some curvature into the DivIVA molecule. Possibly suggesting that it could bend DivIVA proteins so that they could contact the membrane several times.

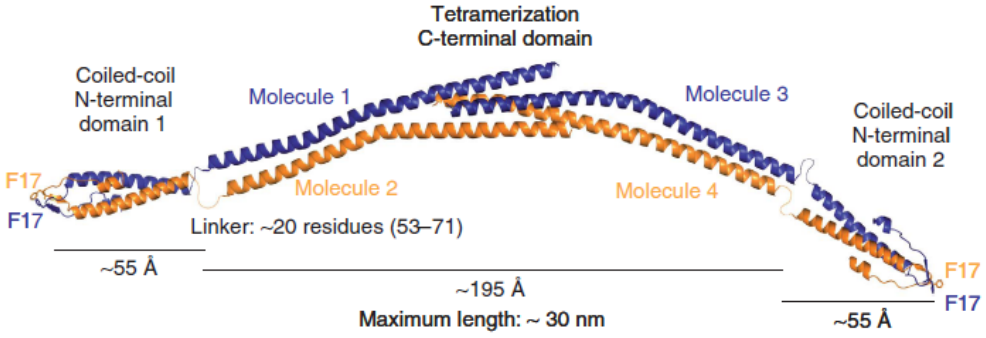

Figure 15: A composite model of the structure of a DivIVA tetramer formed from the crystal structures of the N-terminal and C-terminal domains. Taken from Oliva *et al.*, (2010). The N-terminal domain facilitates formation of a parallel dimer, the C-terminal domains can then form an anti-parallel tetramet.

There is a second DivIVA-like protein in *B. subtilis* called GpsB, which contains the N-terminal domain of DivIVA and has a different C-terminal (Claessen *et al.*, 2008). It has been shown that in cooperation with the cell division protein EzrA, GpsB coordinates localisation of PBP1 for control of new cell wall incorporation in the processes of both cell elongation and cell division. GpsB is also present in the genomes of other Gram-positive such as *Streptococcus pneumoniae*, *Staphylococcus aureus* and *Listeria monocytogenes*.

1.2.6 The Structural Maintenance of Chromosomes and MukB proteins

The Structural Maintenance of Chromosomes (SMC) proteins are a family present across all eukaryotes, as well as being found in all Gram-positive bacteria and archaea, but are found in less than half of the Gram-negative bacteria (Soppa, 2001). In eukaryotes, SMC proteins have been shown to have roles in multiple functions including chromosome condensation and cohesion, there is also evidence that they may be involved in DNA recombination and repair (eukaryotic SMC functions reviewed in (Ball Jr, and Yokomori, 2001; Strunnikov, and Jessberger, 1999)). In prokaryotes SMC proteins are involved in the processes of chromosome condensation and partitioning (Lindow *et al.*, 2002a; Jensen, and Shapiro, 1999). Gram-negative bacteria such as *E. coli* have a closely related protein to SMC proteins, called MukB (Niki *et al.*, 1991). MukB's structural similarity to SMC, as well as knockout phenotype suggest that MukB and SMC proteins are functionally analogous in bacteria (Melby *et al.*, 1998; Yamanaka *et al.*, 1994). Strictly speaking SMC and MukB proteins in bacteria aren't cytoskeletal proteins as they do not form filaments. However, when first discovered MukB was compared to myosin and kinesin in eukaryotes due to its coiled-coil structure with Walker A and B sites in terminal globular heads (Niki

et al., 1991). SMC and MukB proteins are the closest currently known bacterial proteins to having a motor-like function similar to the motor proteins associated with eukaryotic cytoskeletal filaments (Soppa, 2001).The functional role of SMC and MukB proteins in chromosome condensation and partitioning in the development of bacteria also makes SMC and MukB proteins of worth mentioning within this document.

The structure of SMC and MukB proteins (Figure 16) from the N-terminus begins with a globular domain containing a Walker A nucleotide binding motif. This then leads to two coiled-coil domains that are separated by a small globular hinge domain. Following the second coiled-coil domain is the C-terminal globular domain that contains a Walker B nucleotide binding motif. SMC and MukB proteins form anti-parallel homodimers whereby the coiled-coils form anti-parallel dimers and adjacent C and N terminal globular heads come together to form the proposed DNA binding molecular motor (Melby *et al.*, 1998). The hinge domain allows movement of the coiled-coil domains allowing the shape to be either an "open-V" or to lock the two globular heads and form a "folded rod". This flexibility of the hinge region could allow the two globular heads to bind to two separate DNA sites and provide movement. Studies with *Bacillus subtilis* SMC show that it preferentially binds single stranded DNA over double stranded DNA (Hirano, and Hirano, 1998). It has also been shown that in the presence of ATP it leads to the aggregation of single stranded DNA. The implications of this finding are currently unknown, though it could be that it somehow introduces writhe into DNA molecules through single-stranded DNA. In *B. subtilis*, SMC localises to the edge of the chromosomal DNA and particularly at replication forks (Graumann *et al.*, 1998; Lindow *et al.*, 2002b). In addition null mutants in *smc* in *B. subtilis* are more prone to producing anucleate elongated cells, and are lethal when grown at 37˚C (Moriya *et al.*, 1998). Therefore, reflecting that SMC must play a crucial role in organising the DNA. In *E. coli* MukB localised at the same position as *oriC* throughout the cell cycle (Danilova *et al.*, 2007). In *E. coli mukB* mutants are lethal at higher temperature and at lower temperatures have defects in chromosome partitioning (Niki *et al.*, 1991). Studies into the eukaryotic SMC complex condensin provide insights into SMC function, as condension may work by the coiled-coil arms of the protein looping to form a circle around strands of DNA, linking multiple strands that allow chromosome condensing and adding a certain amount of rigidity into the condensing chromosome (Cuylen *et al.*, 2011). It has also been reported that MukB associates with topoisomerase IV in *E. coli*, the decatanase activity of topoisomerase IV may help unlink segregating sister chromatids (Hayama, and Marians, 2010; Li *et al.*, 2010).

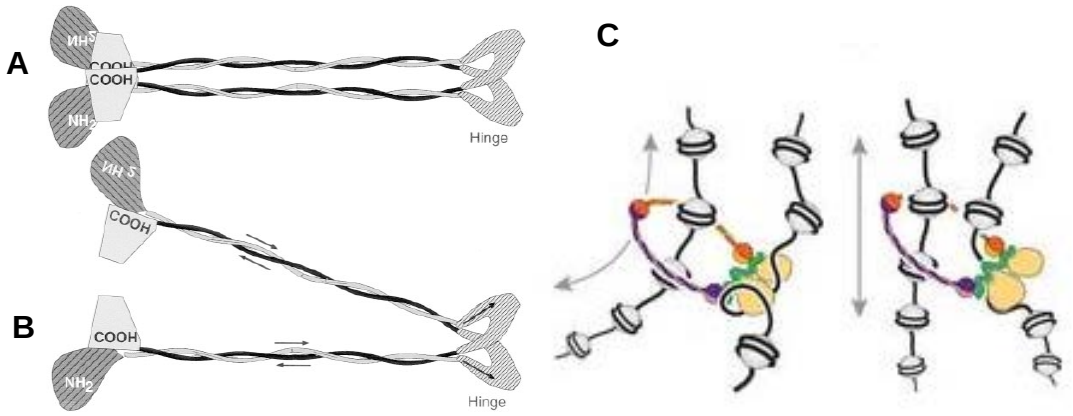

Figure 16: SMC structure and function. (A & B)The model of prokaryotic SMC structure based on Electron Micrograph images (taken from Melby *et al.*, (1998). Arrows indicate the N→C direction of the polypeptide, with SMC forming antiparallel coiled-coils. Associated terminal domains lock the molecule into a "folded-rod" (A) or unassociated leads to an "open-V" conformation (B). C) SMC in the eukaryotic condensin complex (taken from Cuylen *et al.*, (2011)). An SMC dimer, one monomer purple the other monomer orange, is the major component of condensing, the SMC coiled-coil arms are able to loop around strands of DNA (DNA is black, with Histone complexes attached in grey), enabling linking of DNA strands.

1.3 Polarisation in bacteria

Polarisation is important in bacteria for control of cell shape and also designating the ends of the cells. Cell shape determination in the standard rod shaped bacterium *E. coli* or *B. subtilis* depends on lateral cell wall synthesis where the positioning is directed by MreB homologs (Daniel, and Errington, 2003; Wachi *et al.*, 1987) and cell wall remodelling at cell division sites is dependent on FtsZ homologs (Lutkenhaus, 1993; Lutkenhaus, and Addinall, 1997). Fitting in with this idea spherical bacteria such as *S. pneumoniae* lack MreB and mediate cell division into identical daughters cells solely by cell wall synthesis directed by FtsZ (Koch, 2000). Cell division can be dependent on a Min system, which in turn is dependent on polarisation of the Min proteins (Shih *et al.*, 2003). In *B. subtilis* DivIVA plays a role in controlling the Min system and exhibits a polar localisation (Cha, and Stewart, 1997; Edwards, and Errington, 1997). Therefore, it is also of relevant note that in the actinomycetes where MreB is dispensable for cell shape determination, that a mechanism of polarised cell wall extension exists that appears to be heavily dependent on DivIVA (Flärdh, 2003a; Hempel *et al.*, 2008; Letek *et al.*, 2008; Nguyen *et al.*, 2007; Ramos *et al.*, 2003).

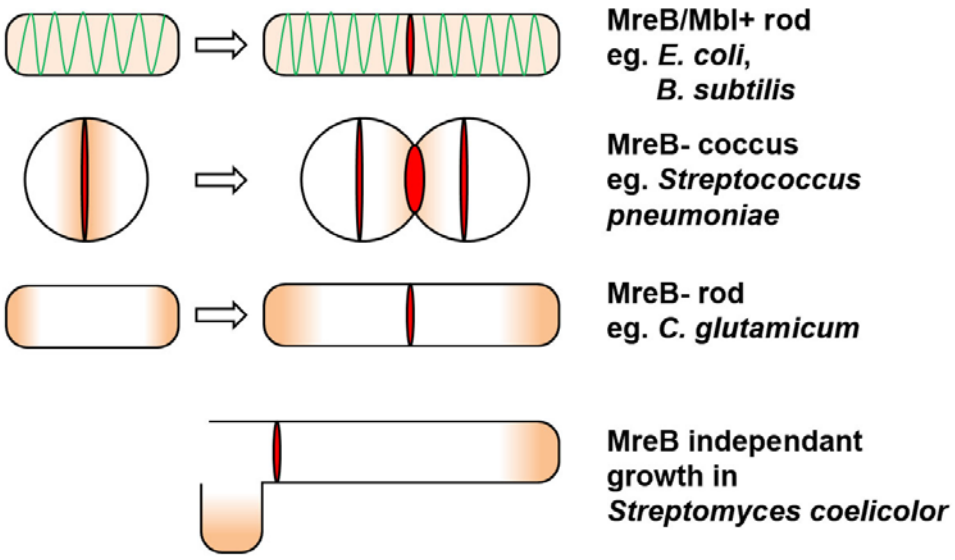

Figure 17: Cell Shape Determination and the role of Cytoskeletal Proteins. Adapted from Margolin, (2003). MreB (Green) is associated with rod shaped bacteria by means of a helical pattern of cell wall remodeling, FtsZ (red) facilitates cell wall remodeling at the cell division site. In spherical shaped bacteria cell shape is driven primarily by FtsZ (cell wall extension shown in orange). In Acinomycetes, the rod-shaped *C. glutamicum* lacks MreB and polar growth (orange) is governed by DivIVA, as well as in *S. coelicolor* where DivIVA controls apical growth and branching.

However, as such as these hard and fast rules (Figure 17) regarding bacterial cell shape are important in our understanding of bacterial cell shape determination it really comes as little surprise that there is more complexity involved, as well as an increasing list of other proteins that may be specific to bacterial groups, that also contribute to cell shape determination and/or cell polarity. Interestingly in the actinomycete *Corynebacterium glutamicum* a novel protein has also been identified, RsmP (Fiuza *et al.*, 2010), that is overexpressed when DivIVA is depleted. This protein forms cytoskeletal like filaments *in vivo* and *in vitro*, and was shown to be essential to maintenance of a rod shape. It was also demonstrated that RsmP is phosphorylated and a phosphomimetic copy of RsmP primarily localised to the cell poles. The precise mechanism in which RsmP contributes to cell shape determination, however, remains to be elucidated.

There are also other examples of bacteria more distantly related than the Gram-positive actinomycetes that demonstrate polarisation, Such as the Gram-negative *Caulobacter crescentus* which features a dimorphic life cycle where cell division generates two different cell types in the form of a motile swarmer cell and an immotile stalked cell. A single flagellum forms on the pole of the predivisional swarmer cell and on the opposite side of the predivisional cell a single stalk forms. Therefore, polarity is an important

determinate in being able to form quite different structures on the opposite sides of the pre-divisional cell. Polarity which appears to contribute to the cell cycle in *Caulobacter crescentus* is determined by a complex series of events involving a few novel polarity determining proteins TipN and PopZ (Schofield *et al.*, 2010; Lam *et al.*, 2006; Bowman *et al.*, 2010; Bowman *et al.*, 2008; Ebersbach *et al.*, 2008). These proteins appear to be important in determining the localisation of replication origins in the segregating chromosome in a ParAB system which they help localise to opposite cell poles. Also, important in this system is a protein MipZ, which interacts with ParB and therefore the origin of the nucleoid (Kiekebusch *et al.*, 2012; Thanbichler, and Shapiro, 2006). A cellular gradient of MipZ is established whereby it is most concentrated at the cell poles, as it is seen that MipZ interferes with FtsZ polymerisation this forms a system reminiscent of nucleoid occlusion. Where the site of cell division is established away from the cell poles and the nucleoid and is established in the mid-cell position. Interestingly prior to FtsZ positioning to the mid pole it may contribute as well as MreB to peptidoglycan at the cell pole associated with stalk synthesis (Divakaruni *et al.*, 2007; Wagner *et al.*, 2005).

As well as polarisation being important to *Caulobacter crescentus*, it is also important to other members of the alphaproteobacteria such as the Rhizobiales, which grow by budding that has an element of polarised growth to it (Hirsch, 1974; Brown *et al.*, 2012). However, this represents a relatively unknown mechanism. There are other bacteria for which polarised growth may be important for which there is not space to consider here, for a particularly good review look at (Brown *et al.*, 2011).

A possible important factor in cell biology and the formation of polarity is the organisation of the membrane. To which there is complexity emerging in terms of the pattern and distribution of lipids in the membrane (Owen *et al.*, 2012). Leading to the idea of lipid rafts where different types of lipids (such as cholesterol, saturated sphingolipids and phospholipids) may accumulate in different parts of the membrane, thereby changing the packing densities and affecting membrane protein positioning. Curvature of the membrane, such as cell poles, implemented by the bacterial cell wall maybe a mechanism by which lipids can separate into different phases (Huang *et al.*, 2006). Possibly important in this mechanism is the anionic phospholipid cardiolipin. The use of the stain 10-*N*-nonyl-3,6-bis(dimethylamino)acridine (or nonyl-acrydine-orange (NAO)), has been found to preferentially mark the position of cardiolipin in the membrane (Petit *et al.*, 1992). When used to stain *E. coli* (Mileykovskaya, and Dowhan, 2000) or *B. subtilis* (Kawai *et al.*, 2004) it was found that cardiolipin was more abundantly localised to the septum and poles

(the places of more extreme curvature). Cardiolipin was also found to be in abundance at the hyphal tips, branch points and anucleate regions of *S. coelicolor* (Jyothikumar *et al.*, 2012). Changes in levels of cardiolipin resulted in morphological defects in *S. coelicolor*, some of which are associated with the hyphal tip. If *E. coli* are forced by chambers into an altered cell shape (Renner, and Weibel, 2011), the parts of extreme negative curvature are those with the highest abundance of cardiolipin, as well as the pole localising protein MinD, suggesting a mechanism by which negative membrane curvature can relocalise lipids and proteins. However, the extent to how much lipid rafts affect protein localisation has yet to be validated. Be it by lipid distribution or by the actual membrane curvature (Lenarcic *et al.*, 2009; Ramamurthi, and Losick, 2009) the poles are important for protein localisation. Another mechanism of polarisation is nucleoid occlusion (Wu, and Errington, 2011; Wu *et al.*, 2009), whereby polar proteins may localise to the poles via the poles being DNA free, as seen for the protein PopZ from *C. crescentus* (Ebersbach *et al.*, 2008).

1.4 Bacterial cytoskeletal proteins in *Streptomyces*

1.4.1 FtsZ in Streptomyces

Cell division in bacteria requires FtsZ, the bacterial homologue of the eukaryotic cytoskeletal protein tubulin. Cell division in coccoid or rod shaped bacteria relies on the positioning of FtsZ into a ring around the mid cell. However, *S. coelicolor* is a filamentous bacterium in which binary fission does not occur, making the study of FtsZ of interest. The current research into the role of FtsZ in *Streptomyces* biology is summarised below.

It has been found that *S. coelicolor* has a single 399 amino acid long homologue of the cell division protein FtsZ. The FtsZ protein in *S. coelicolor* is highly similar to FtsZ in other bacteria, showing 48% sequence conservation to *E. coli* FtsZ with a further 22% sequence similarity (McCormick *et al.*, 1994). FtsZ knockouts are often lethal in bacteria as FtsZ is essential for cell division. However, in *S. coelicolor* surprisingly, an FtsZ mutant is viable. Though is lacking the vegetative crosswalls and the sporulation septa, the latter meaning it is unable to form spores. This data suggested that FtsZ is directly involved in the formation of vegetative crosswalls as well as the sporulation septa (McCormick *et al.*, 1994). An FtsZ mutant is viable as growth and transfer of the vegetative hyphae can somehow tolerate the absence of vegetative crosswalls.

The localisation pattern of FtsZ in *S. coelicolor* was first observed through immunofluorescence (Schwedock *et al.*, 1997). Within the vegetative hyphae only occasional widely spaced FtsZ "Z rings" were present. However, in the aerial hyphae FtsZ forms into FtsZ rings in a regularly spaced, ladder-like array with the average spacing of 1.3µm. The formation of the rings is extremely transient and is believed to happen prior to late nucleoid condensation, laying down the positioning for future sporulation septa. Having marked the position for septal formation and cytokinesis the FtsZ rings then seem to disappear (Schwedock *et al.*, 1997).Visualisations of FtsZ through EGFP translational fusions revealed that the rings begin with formations of spiral intermediates (Grantcharova *et al.*, 2005). The construction of Z rings visualised over time points suggested that FtsZ rings were constructed in a multi-step process. The stages of a proposed model of FtsZ assembly are shown in Figure 18. The upregulation of FtsZ associated shortly after aerial hyphae formation (Flärdh *et al.*, 2000) leads to formation of helical filaments in step B. These then give rise to a regular array of FtsZ rings (step C). Shortly after the rings have formed septation occurs (step D & E) leading to formation of unigenomic spores (step F) (Grantcharova *et al.*, 2005).

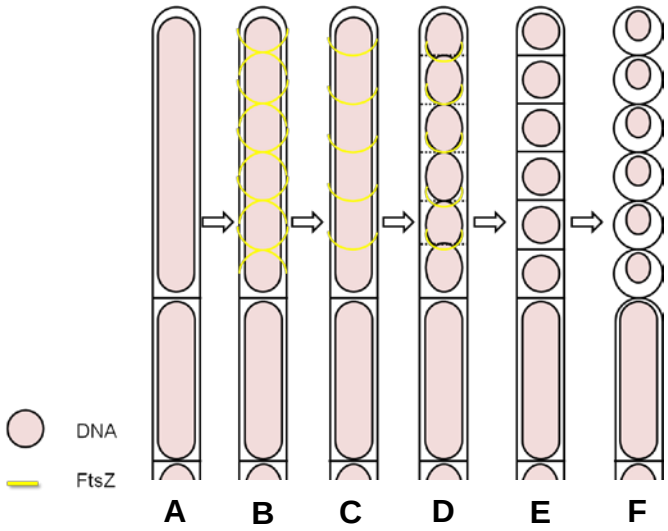

Figure 18: A dynamic model of FtsZ assembly through aerial hyphae septation and sporulation. Adapted from Flärdh & Buttner, (2009), with information from Grantcharova *et al.*, (2005). Progression occurs in the order of A→F during development.

Time-lapse imaging experiments have shown that FtsZ rings form in the vegetative hyphae at variable widely spaced distances, yet ring placement behind the hyphal tip progresses at a similar rate at which tip growth occurs (Jyothikumar *et al.*, 2008). The live images also suggest that vegetative hyphae Z rings form through spiral intermediates (Jyothikumar *et al.*, 2008), yet probably lacking the longer helical filaments observed in the aerial hyphae. The placement of the Z ring in *S. coelicolor* is a complex task and is believed to happen in

a positive manner whereby instead of inhibition by a min system, FtsZ must instead be recruited. In part this mechanism is unfolding and the two proteins SsgA and SsgB have been shown to positively recruit FtsZ (Figure 19)(Willemse *et al.*, 2011a). Whereby SsgA localisation in the aerial hyphae precedes SsgB to which SsgB localisation is dependent on SsgA. SsgB localisation precedes the localisation of FtsZ in the aerial hyphae, and formation of Z rings is dependent on SsgB. Therefore, forming a hierarchical system where SsgA recruits SsgB and SsgB recruits FtsZ.

Imaging of FtsZ has revealed that it is dynamic and has a cytoskeletal role in forming Z rings which are important for septum/cross wall formation and constriction of sporulation septum. This is crucial for cell division in the *Streptomyces*; however, this process is also dispensable due to the ability of the *Streptomyces* to grow vegetatively.

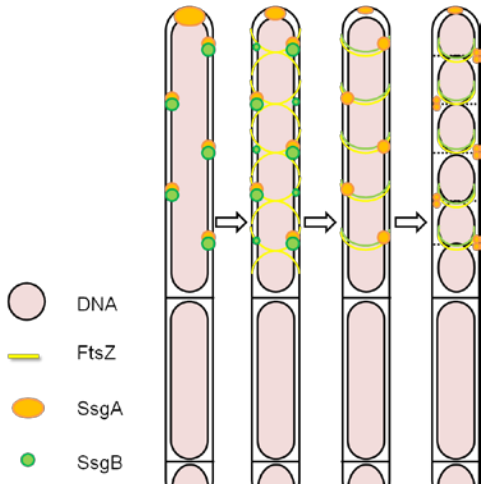

Figure 19: Placement of FtsZ by a positive mechanism involving SsgA and SsgB. SsgA recruits SsgB. SsgB recruits FtsZ and helps tether FtsZ to the membrane. SsgB continues to localise with FtsZ, whereas SsgA is removed and eventually comes to mark the positions of the future germinations sites. Adapted from Flärdh & Buttner, (2009), Jakimowicz & van Wezel, (2012).

1.4.2 MreB in Streptomyces

Actin homologous MreB proteins are notably present as cell shape determining factors in rod-shaped and other complex bacteria. Despite most actinomycetes lacking MreB proteins, *S. coelicolor* and other members of the genus *Streptomyces* possess MreB homologues (Burger *et al.*, 2000). *S. coelicolor* has 2 MreB homologues, one $MreB_{Sc}$ that is encoded in the gene cluster of *mreBCD*, the other Mbl_{Sc} (Burger *et al.*, 2000; Mazza *et al.*, 2006). There is also another MreB like protein encoded by *sco6166* which lacks the IB and IIB subdomains of actin (Heichlinger *et al.*, 2011). A cytoskeletal function involved in sporulation and spore wall formation are the current hypothesis for the function of the *Streptomyces* MreB proteins.

In many bacteria containing MreB proteins including *E. coli* and *B. subtilis*, the *mreB* gene is located as part of an operon also including *mreC* and *mreD* (Kruse *et al.*, 2005; Leaver,

and Errington, 2005). In *B. subtilis* the *mreBCD* cluster is near to *valS* encoding a valyl-tRNA-synthetase and *folC* encoding a folylpolyglutamate synthetase (Margolis *et al.*, 1993). In *S. coelicolor mreB* was found to be downstream of *valS* and *folC* in an operon of similar architecture containing *mreC* and *mreD* (Burger *et al.*, 2000). The MreC and MreD proteins of *Streptomyces coelicolor* are similar to those found in *E. coli* and *B. subtilis*, which have been shown to form a complex with MreB and attach it to the cell wall synthetic machinery (Kruse *et al.*, 2005; Leaver, and Errington, 2005; Burger *et al.*, 2000). The *mreBCD* operon is regulated by three promoters, one of which is developmentally upregulated at the time at which sporulation occurs (Burger *et al.*, 2000). Knockout mutants of the *mreB* gene found in the *mreBCD* cluster confirmed that the MreB protein was not vital for formation of vegetative hyphae. However, the aerial hyphae of *mreB* mutants swelled and lysed. Transmission electron microscopy showed that the aerial hyphae appeared deformed, with a characteristic bloated appearance. Also, the spores formed from an *mreB* mutant were large, had thinner spore walls and had lost their high resistance characteristic (Mazza *et al.*, 2006). Strains were generated for overexpression of MreB from a thiostrepton inducible *tipA* promoter. These strains were unable to grow on solid media containing thiostrepton. Whereas in liquid culture, with thiostrepton induction after 8 hours of normal growth, this lead to swelling and lysis of the hyphae (Mazza *et al.*, 2006).

Using an MreB-EGFP fusion protein driven from the endogenous promoter region, the knockout of endogenous MreB was complemented. MreB-EGFP was shown to localise at the septa in aerial hyphae, followed by a later localisation of MreB at the poles of the prespore chains. In more mature spores MreB then went on to completely surround the intracellular side of the spore wall forming a ring. Immunogold labelling of MreB and electron microscopy showed that MreB is present just underneath, internal to the spore wall (Mazza *et al.*, 2006). A comparison of FtsZ and MreB localisation patterns during development of the aerial hyphae and sporulation is shown in Figure 20. FtsZ directed septal positioning and septum formation occurs before MreB rings form, then FtsZ dismantles, whereas MreB localises to poles of prespores and as a ring internal to the sporewall.

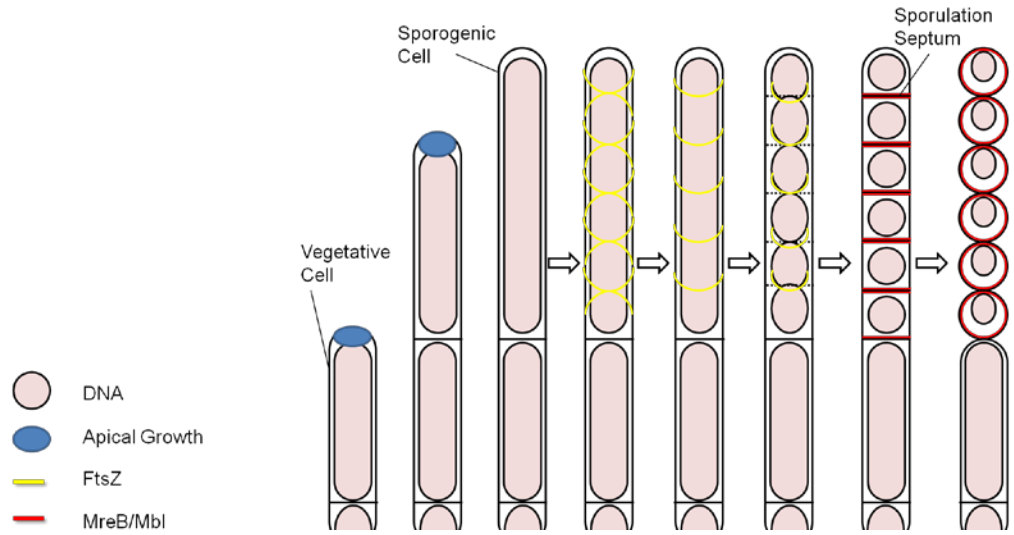

Figure 20: Positons of the cytoskeletal proteins MreB or Mbl and FtsZ through the development of the aerial hyphae into spores, neither MreB or FtsZ are involved in apical growth. Adapted from Flärdh & Buttner, (2009), Carballido-Lopez, (2006b), with information from Mazza *et al.*, (2006), Heichlinger *et al.*, (2011).

The Knockout mutants and localisation of MreB showed that it is not essential to vegetative growth in *S. coelicolor*, but is more important in the development of the aerial hyphae and in sporulation (Mazza *et al.*, 2006). The effect of overexpression suggests that the regulation of *mreB* has to be tightly controlled during development. In addition it was found that MreC and MreD also played a role in formation of the spores, as well as some of the other genes adjacent to the *mreBCD* cluster (Kleinschnitz *et al.*, 2011). The role of the second MreB protein of *S. coelicolor*, Mbl, is similar to the role of MreB, mutants of *mbl* exhibit a phenotype of swollen and prematurely germinating spores (Heichlinger *et al.*, 2011). It is believed that this is a non-redundant function in which Mbl cannot compensate for a lack of MreB. However, Mbl also localises in a similar pattern to MreB (Figure 20) and is dependant on MreB for localisation, whereas MreB is not dependent on Mbl for correct localisation (Heichlinger *et al.*, 2011). The MreB like protein encoded by *sco6166*, is expressed in the vegetative hyphae which is in contrast to the expression of *mreB* and *mbl* which occurs in the aerial hyphae. However, the effect of Sco6166 on the vegetative hyphae is not clear as a *sco6166* mutant had a wild-type phenotype (Heichlinger *et al.*, 2011). Based on the data gathered on MreB and Mbl, MreB and Mbl must perform a different function in *S. coelicolor* than in other bacteria. The fluorescent translational fusions suggest that MreB and Mbl does not form helical filaments similar to the way in which MreB does in *E. coli* and *B. subtilis* (Jones *et al.*, 2001; Kruse *et al.*, 2003). However, the effect on aerial hyphae and spores, as well as the localisation data suggest

that MreB and Mbl probably play a role in governing cell wall changes, it could possibly interact with PBPs or other cell wall synthetic machinery. However, in the vegetative hyphae these processes must be governed by a different mechanism.

1.4.3 ParA-ParB of Streptomyces

ParA in *Streptomyces coelicolor* is of note as a cytoskeletal filament. ParA along with ParB are important in chromosome segregation along sporulating aerial hyphae. The study of chromosome partitioning is of interest in *S. coelicolor* as unlike most bacteria studied, *S. coelicolor* has a linear chromosome. This along with the complex division of the aerial hyphae suggests that *S. coelicolor* would need a more complex method of chromosome segregation than for example *B. subtilis* or *C. crescentus*.

Regularly in bacteria the origin of replication is located downstream of *dnaA*, then located upstream of *dnaA* are the partitioning genes *parA* and *parB*. Not surprisingly in *S. coelicolor* the *parA* and *parB* genes are organised in an upstream location to *dnaA* (Kim *et al.*, 2000). ParA of *S. coelicolor* shows 55% similarity to Soj of *B. subtilis* and 49% similarity to ParA of *C. crescentus*. ParB of *S. coelicolor* shows 41% similarity to SpoOJ of *B. subtilis* (Kim *et al.*, 2000). The *S. coelicolor* chromosome also contains 24, 16bp *parS* sites, with a large majority of them located close to *oriC* (Kim *et al.*, 2000; Jakimowicz *et al.*, 2002). A partial mutant of *parB* was found to have problems in DNA segregation with 13% anucleate spores. The same phenotype was observed with a deletion removing a segment of DNA from both *parA* and *parB*. Transcription from one of the *parAB* promoters is upregulated at the time when the aerial hyphae emerge (Kim *et al.*, 2000).

In vitro and *in vivo* data suggest that ParB binds to sites closest to *oriC*, with the highest level of conservation to the predicted *parS* sequence. *In vitro* data suggests that ParB itself only binds to *parS* sites weakly, suggesting perhaps additional factors are needed. Due to the high density of *parS* sites close to the origin it is believed that ParB forms high-order nuclear protein complexes (Jakimowicz *et al.*, 2002). Using a ParB-EGFP translational fusion ParB localisation was visualised both in the vegetative hyphae and the aerial hyphae (Jakimowicz *et al.*, 2005a). In vegetative hyphae ParB-EGFP was either associated with the hyphal tip at an average distance of 1.4μm away from the tip, or was seen as relatively weakly visible irregularly placed foci. However, in aerial hyphae ParB-EGFP formed brighter foci that were regularly positioned. These foci are believed to coincide with the

position of *oriC* on each chromosome and corresponding with the time when DNA is condensing prior to spore septation. The foci are maintained until after septum formation and DNA condensation at which point they disappear (Jakimowicz *et al.*, 2005a).

A strain of *S. coelicolor* harbouring a knockout mutation of *parA* shows abnormal chromosome segregation and sporulation septum positioning compared to the wild-type (Jakimowicz *et al.*, 2007). It was quantified that 26.1% of spores were anucleate in a *parA* mutant. Surprisingly this is higher than the percentage observed for *ΔparB* and *ΔparAB* by Kim *et al*., (2000). The significance of differing observations are questionable when considering the likely difficulty in quantifying anucleate spores as well as possible varying culture conditions. Jakimowicz *et al.*, (2007) visualised immunostained ParA and found ParA to either be found at hyphal tips or extending from the tips as helical filaments. These helical filaments had a pitch of ~1.4μm, which interestingly corresponds to about the same length as prespore compartments. Based on their results they predicted a model in which ParA initially accumulated at the tips of new aerial hyphae, to then spread along growing aerial hyphae as a pair of helical filaments. Visualisation of immunostained ParA in either a ParB-EGFP strain or an FtsZ-EGFP strain at different developmental time points allowed the context of these helical ParA filaments to be formed (Jakimowicz *et al.*, 2007). A model for the proposed formation of ParA filaments during sporulation and chromosome segregation is shown in Figure 21. Spreading of ParA helices from the tips preceded formation of FtsZ spirals. By the time Z-rings had assembled, ParA structures had disappeared. ParA helices preceded regular ParB foci assembly and disassembled before ParB foci disassembled. ParA filaments did not overlap with ParB foci. However, the study of ParB foci in a ParA knockout showed that the usual regular assembly of ParB foci along the aerial hyphae was dependent on ParA (Jakimowicz *et al.*, 2007), suggesting that ParA could somehow position ParB complexes into the regular pattern observed for ParB-EGFP. It was also shown through *in vitro* studies that ParA positively increased the binding of ParB to *parS* sites. It was found that the ATPase activity of ParA increases ParB affinity for *parS* sites. Removal of the ATPase activity did not effect formation of ParA helices; however, there were still the chromosome segregation defects present that are associated with a *parA* knockout mutant. Bacterial two-hybrid data suggested that ParA and ParB interact and that this interaction is dependent on the ATPase activity of ParA (Jakimowicz *et al.*, 2007). Thus, it seems that ParA has a vital function in controlling the activity and assembly of ParB and thus ParA's absence manifests itself in chromosome segregation defects.

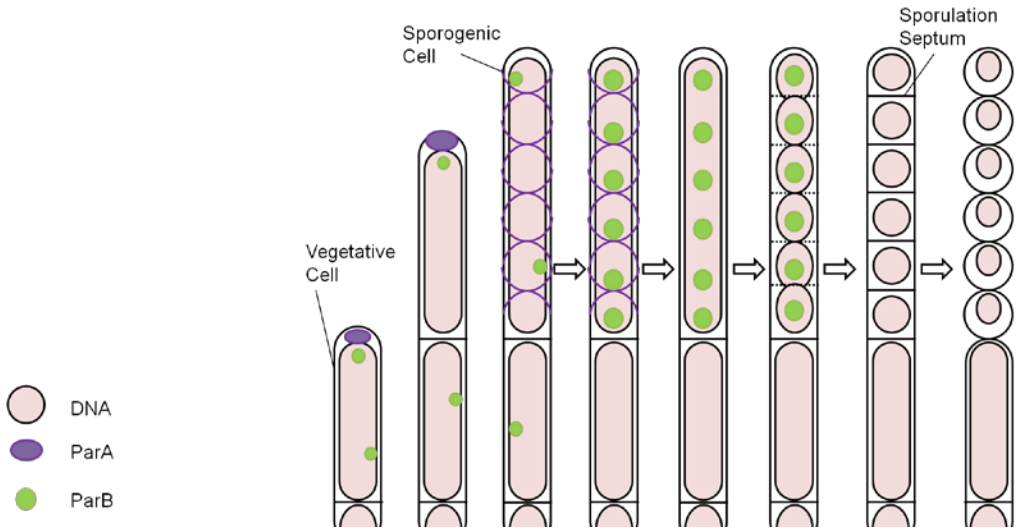

Figure 21: Developmental formation of ParA filaments and ParB foci in *S. coelicolor*. Adapted from Flärdh & Buttner, (2009), Jakimowicz *et al.*, (2007), with information from Jakimowicz *et al.*, (2005a). ParA can be seen in some vegetative cells associated with hyphal tips, whereas ParB was visualised at an average distance of 1.4µm from the tips or in an irregular faint pattern. ParA forms prior to regular ParB foci formation or FtsZ/septum formation, beginning from hyphal tips and spreading down the aerial hyphae. Once ParA filaments are formed the ATPase activity is believed to position ParB foci. As ParA is believed to form filaments with a regular structure it is believed that these filaments provide a positional cue for formation of ParB foci which form at regular positions that do not directly overlap with ParA filaments. In a *parA* mutant, regular ParB foci are absent suggesting that ParA helps coordinate ParB foci formation.ParA filaments disappear before FtsZ rings are formed and ParB foci remain after the disappearance of ParA filaments possibly by association with the chromosome.

Recently interest has gathered regarding the regulation of the ParAB system in *S. coelicolor*. An actinobacterial signature protein ParJ was identified, which likely contributes to regulation of ParA (Ditkowski *et al.*, 2010). ParJ was shown to interact with ParA and was able to depolymerise ParA filaments *in vitro*, leading to the possibility that ParJ helps regulate ParA directed chromosome segregation, possibly in a mechanism which triggers ParA to depolymerise after chromosomal segregation has reached a certain point. It was identified in *C. glutamicum* that the polarising protein DivIVA may help tether the replication origin to the cell pole via interaction with ParB, this was extended to show that *S. coelicolor* DivIVA also interacts with *S. coelicolor* ParB (Donovan *et al.*, 2012). Though this was not an extensive study it may suggest that DivIVA and the cell pole of *S. coelicolor* may contribute to regulation of the ParAB system. Alongside work presented here, it was found that the protein Scy the focus of this work, also interacts ParA and may be important in regulating ParA by preventing polymerisation of ParA in the vegetative and growing aerial hyphae (Ditkowski and Jakimowicz, unpublished). Not

surprisingly ParAB and chromosome segregation is regulated heavily in order to allow correct chromosome segregation of 1 chromosome per future spore in the aerial hyphae.

1.4.4 DivIVA of Streptomyces

The *Streptomyces coelicolor* genome contains a single DivIVA homologue with a potential cytoskeletal-like function. The DivIVA protein in *Bacillus subtilis* was localized to the cell poles, where it sequesters proteins in the Min system, this allows division to occur at central sites (Cha, and Stewart, 1997). However, *S. coelicolor* does not contain a Min system. $DivIVA_{SC}$ was localized to the sites of peptidoglycan synthesis and based on the effect of altered expression on tip formation, could have a role in hyphal tip growth (Flärdh, 2003a).

The DivIVA homologue in *S. coelicolor* shows high sequence conservation to DivIVA of the model organisms *Bacillus subtilis* and *Mycobacterium tuberculosis*. DivIVA-like proteins in the actinomycetes share a highly conserved N-terminus with *B. subtilis* and *M. tuberculosis*. In a similar manner they then have a less conserved coiled-coiled region, which is only highly conserved towards the C-terminal end of the coiled-coil region. All actinomycete DivIVA-like proteins analysed thus far, have an interrupted uncoiled variable stretch of sequence within the predicted coiled-coil region (Flärdh, 2003a). Similarly to other Gram-positive bacteria $divIVA_{Sc}$ is located closely downstream from *ftsZ*. However, unlike *ftsZ* in *S. coelicolor*, $divIVA_{Sc}$ was found to be an essential gene and knockouts could not be achieved. A $divIVA_{Sc}$ knockout could only be achieved when an additional copy of $divIVA_{Sc}$ was added *in trans*. By adding $divIVA_{Sc}$ *in trans* under a thiostrepton inducible promoter, in the absence of thiostrepton and due to the leaky nature of the promoter, the resulting strain K115 had 10% expression of wild-type levels of $DivIVA_{Sc}$. Reduction of $DivIVA_{Sc}$ to 10% resulted in the phenotype of irregular curly shaped hyphae. The branching pattern was severly disrupted with unusual apical branches forming close to the hyphal tips (Flärdh, 2003a). Thiostrepton induction of $DivIVA_{Sc}$ to 25 fold overexpression relative to wild-type levels, resulted in a phenotype in which the cells appeared swollen, with them being both shorter and thicker. They were still capable of branching, yet the tips appeared remarkably wider and rounder than the rest of the hyphae. Maintaining wild-type levels of $DivIVA_{Sc}$ till after the production of normal hyphae and then overexpressing $DivIVA_{Sc}$, resulted in tip swelling and hyperbranching. Thus, the $DivIVA_{SC}$ protein

probably plays a morphological role in tip formation and hyphal branching (Flärdh, 2003a).

A DivIVA$_{Sc}$-EGFP translational fusion strain driven by the endogenous promoter as well as encoding a wild-type copy of *divIVA$_{Sc}$* was used to visualise the localisation of DivIVA$_{Sc}$ (Strain K112). A strain only encoding DivIVA$_{Sc}$-EGFP with no wild-type copy of *divIVA$_{Sc}$* (Strain K117) was observed to have irregularities in branching and the shape of hyphal tips, suggesting an interference of EGFP on DivIVA$_{Sc}$ function. Both DivIVA$_{Sc}$-EGFP and endogenous DivIVA$_{Sc}$ together was considered wild-type in phenotype. In this strain DivIVA$_{Sc}$ was localised to bright foci at hyphal tips as well as newly emerging branch points (Figure 22A). DivIVA$_{Sc}$ could not be visualised in the spores; however, was present as a foci at the tips of emerging germ tubes (Flärdh, 2003a). This data is similar to the pattern observed in *S. coelicolor* with fluorescently labelled vancomycin staining newly forming cell walls (Figure 22C), suggesting a role for DivIVA$_{Sc}$ in positioning of apical growth regions (Daniel, and Errington, 2003; Flärdh, 2003b). The localisation of DivIVA$_{Sc}$-EGFP in strain K112 was visualised via time-lapse imaging allowing snap shot images to generate live cell imaging. This discovered that DivIVA$_{Sc}$ was localised to future branch sites significantly before branch emergence (Hempel *et al.*, 2008). A strain comprising of both DivIVA$_{Sc}$-EGFP driven from an endogenous promoter and endogenous DivIVA$_{Sc}$ overexpressed from *pTipA* allowed DivIVA$_{Sc}$ localisation when overepressed. Overexpression of DivIVA$_{Sc}$ leads to the assembly of multiple foci alongside the lateral wall where future branches will emerge (Hempel *et al.*, 2008). Thus, DivIVA$_{Sc}$ is a molecular marker of future branch sites and sites of polar growth.

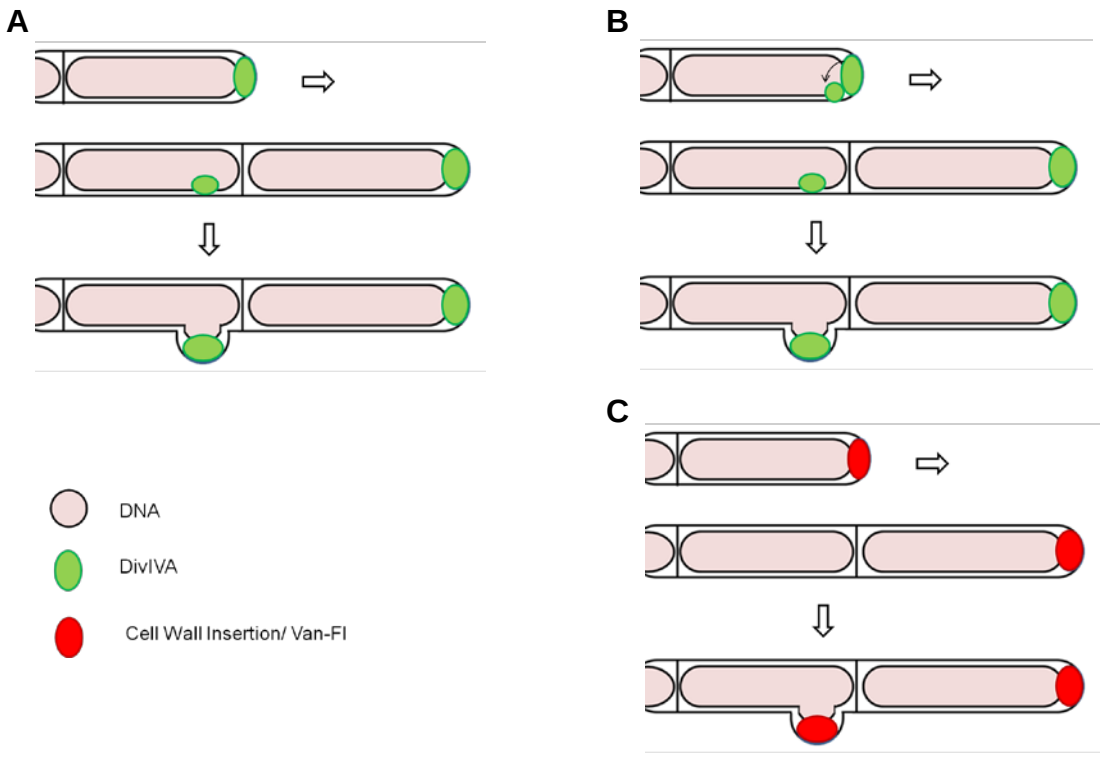

Figure 22: Localisation of DivIVA$_{Sc}$-EGFP and fluorescent vancomycin conjugate (Van-Fl) at apical tips. Information from Flärdh & Buttner, (2009), Richards *et al.*, (2012). DivIVA is positioned at growing tips and localises at future branch points (before cell wall extension) by two possible mechanisms; spontaneous nucleation (A) and Tip-focused splitting (B). Fluorescent vancomycin staining can only be seen once a new branch has committed to cell wall extension.

The mechanism by which DivIVA localises and establishes *de novo* tip formation is a subject of much interest. Of course one needs to remember that the *M. tuberculosis* DivIVA homologue Wag31 has already been shown to interact with a PBP protein, suggesting that DivIVA can recruit the cell wall synthesizing machinery (Mukherjee *et al.*, 2009). *Streptomyces* DivIVA as far as we know hasn't yet been shown to interact with a PBP; however, it was found to interact with an enzyme, CslA that catalyses the synthesis of cellulose like beta-glucan-containing polysaccharides at the hyphal tip (Xu *et al.*, 2008). A recent paper (Richards *et al.*, 2012) described a possible model of DivIVA foci formation and control of apical growth. This model describes a mechanism called Tip-focused splitting, where they observed that DivIVA foci break away from existing foci to establish new branch sites (Figure 22B). This could well be important for DivIVA foci propagation and hyphal branching. Also, this paper suggested a mechanism of *de novo* DivIVA foci formation and spontaneous branch formation (Figure 22A), incidentally needed for emergence of germ tubes from germinating spores. However, the interplay between these two possible mechanisms of DivIVA foci dynamics requires more

experimental biological insight to carefully determine how apical growth occurs in *S. coelicolor*. *S. coelicolor* DivIVA is also phosphorylated (Manteca *et al.*, 2011; Hempel *et al.*, 2012) similarly to DivIVAs from other organisms. It was shown that DivIVA phosphorylation resulted in disassembling of DivIVA from the tip and results in relocation of DivIVA foci and leads to branching at alternative sites. Alternatively lack of phosphorylation of DivIVA resulted in absence of branching. This provides a new dimension to DivIVA regulation and its involvement in controlling apical growth (Hempel *et al.*, 2012).

1.4.5 SMC in Streptomyces

The issue of chromosome condensation and segregation in *S. coelicolor* has thus far been described in reference to the ParA/B proteins. However, identification of a single homologue to the Structural Maintenance of Chromosomes (SMC) protein family has revealed a possible alternative and/or redundant pathway to the ParA/B system (Dedrick *et al.*, 2009; Kois *et al.*, 2009). Genetic and localisation studies likely suggest that *S. coelicolor* SMC plays a role somewhat similar to that of *B. subtilis* SMC or MukB of *E. coli*.

Analysis of the *S. coelicolor* genome identified a single SMC homologue (Bentley *et al.*, 2002). The *S. coelicolor* SMC protein has 47% sequence similarity to *B. subtilis* SMC and retains the same domain architecture (Kois *et al.*, 2009). An *smc* null mutant was observed to have no visible defects in growth or morphology. However, an *smc* null mutant exhibited a chromosome segregation defect with approximately 7-8% anucleate prespore compartments (Dedrick *et al.*, 2009; Kois *et al.*, 2009). It was also found that *S. coelicolor* has single homologues to the SMC associated proteins ScpA and ScpB in *Bacillus subtilis*, showing 47% and 44% sequence similarity respectively (Dedrick *et al.*, 2009; Kois *et al.*, 2009). Double knockouts of *scpAB* have been shown by two separate groups; however, the phenotypic consequence seen was slightly different. Whereas one group observed a chromosome segregation defect similar to that for the *smc* mutant, though with 6.3% anucleate prespores (Kois *et al.*, 2009). The other group observed no defects leading to anucleate prespores, but did observe a ‘bilobed’ DNA distribution in the spores where DNA was irregularly shaped in line with the contour of the spore (Dedrick *et al.*, 2009). Either observation suggests that ScpA and ScpB could be associated with SMC in a chromosome condensation/segregation function.

The *smc* gene has been subject to numerous combinations of double or even triple knockouts with varying genes involving chromosomal segregation or condensation. These including the *parA* and *parB* genes, as well as *ftsK* encoding a DNA motor protein that aids in movement of chromosomes to either side of an invaginating septum (Wang *et al.*, 2007). Quantification of the extent of chromosomal segregation defects was calculated by looking at the percentage of anucleate prespores. These knockout studies suggest that SMC and ParB possibly act in differing systems that to some extent could be redundant (Dedrick *et al.*, 2009; Kois *et al.*, 2009). A double knockout of *smc* and *parA* is equal to the phenotype of a *parA* knockout suggesting that *smc* does not contribute anything to a *parA* knockout strain (Kois *et al.*, 2009). A similar phenotype was seen for the double knockout of *ftsK* and *smc* (Dedrick *et al.*, 2009). Interestingly a triple knockout of *smc*, *parB* and *ftsK* had a lower percentage of anucleate prespores than a double knockout of *smc* and *parB* (Dedrick *et al.*, 2009). However, the viability of the spores from the triple knockout was significantly lower, possibly suggesting that each spore gets DNA, though not necessarily the correct allocation of DNA needed. This could make sense when considering FtsK's function in the moving of chromosome ends into the spore compartments just prior to septum closure, thus FtsK knockouts can guillotine separating chromosomes (Wang *et al.*, 2007).

Immunofluorescence and EGFP fusions have been used to visualise the localisation of the SMC protein during development in *S. coelicolor* (Kois *et al.*, 2009; Dedrick *et al.*, 2009). Both methods yielded a similar localisation pattern of SMC foci. In vegetative hyphae SMC only forms sporadic foci, suggesting that it does not have an important function in the development of the vegetative hyphae. SMC foci were more numerous in the aerial hyphae where they increased in number with the increasing length of the aerial hyphae. SMC foci were organised irregularly, though seemed to coincide with uncondensed chromosomes and as chromosomes condensed SMC foci disappeared. Immunolocalised SMC was then combined with fluorescent translational fusions of DnaN, FtsZ and ParB in order to determine any possible interaction and identify temporal patterns. The combination of immunolocalised SMC and the replisome marker, DnaN-EGFP, suggest that SMC foci do not co-localise with replisomes (Kois *et al.*, 2009). Thus, suggesting that DNA replication and SMC mediated chromosome condensation are likely to be spatially and temporally separated. SMC foci appear before assembly of FtsZ-EGFP into spirals, and both FtsZ rings and SMC disappeared quickly after septum formation. This suggests that they are both important at the same developmental time; however, no spatial pattern

between SMC foci and FtsZ rings was noted (Kois *et al.*, 2009). SMC foci first appear before regular ParB-EGFP foci (Figure 23). SMC foci reached their maximum number/intensity at the same time that ParB is organised into regularly spaced foci, suggesting that it is important that both processes happen in parallel at that developmental time point. Following septation, ParB foci remain assembled for longer than SMC foci. The organisation of SMC foci and ParB foci are not shared, as SMC is more irregular whereas ParB forms at regular places in the middle of the prespore compartment (Kois *et al.*, 2009). ParB foci assembly could be affected by the presence of SMC, as in an *smc* knockout ParB foci appear to be significantly weaker (Kois *et al.*, 2009).

Overall it seems that SMC in *S. coelicolor* is active in the process of sporulation from dividing aerial hyphae. Probably by playing a role in chromosome condensation and/or segregation. However, the combinations of knockout mutations of chromosome segregation proteins suggests that there are even more possible mechanisms for chromosome segregation in sporulating aerial hyphae. Localisation of SMC in relation to other developmental proteins suggests that it is involved in chromosome segregation and condensation; however, the exact role in combination with other proteins in cell division cannot yet be easily described.

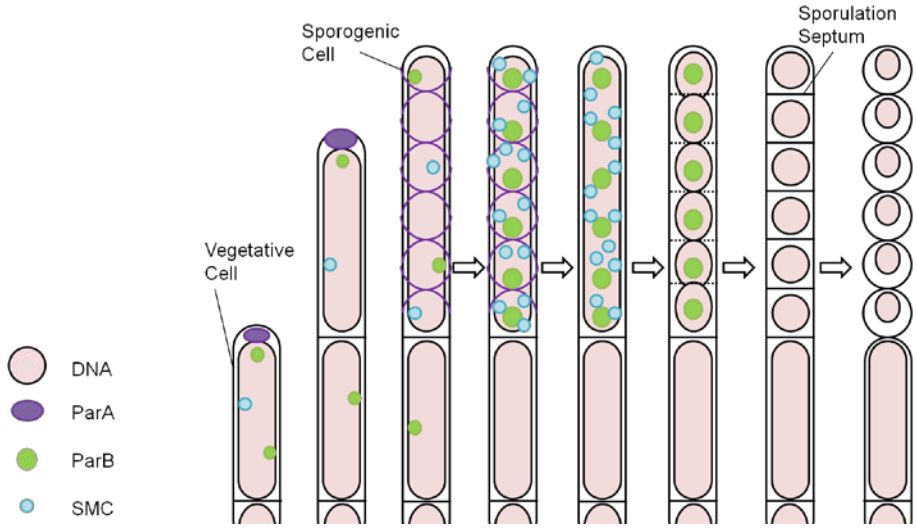

Figure 23: Model of localisation of SMC, ParB and ParA during aerial hyphae development. Adapted from Flärdh & Buttner, (2009), Kois *et al.*, (2009). SMC foci are most visible during stages of DNA condensation occurring at the same stage when regular ParB foci are visible performing chromosome segregation, that lasts for longer than SMC is present.

1.4.6 FilP/AbpS of Streptomyces

The search performed by Bagchi *et al.,* (2008) for proteins containing domain architecture similar to that of crescentin and intermediate filaments yielded three proteins from *S. coelicolor*. These included a protein encoded by *sco5396,* the homologue of this protein in *Streptomyces reticuli* had previously been shown to bind avicel and had therefore previously been named the Avicel Binding Protein (AbpS) in *S. reticuli* (Walter *et al.*, 1998). Also, identified was a protein encoded by *sco3114*, which has a similar sequence to AbpS. The search also identified a protein encoded by *sco5397* that has been a feature of research carried out by the Kelemen lab (University of East Anglia) and is a focus of the research to which this literature review is intended for (therefore is described in greater detail later). AbpS was shown by Bagchi *et al.,* (2008) to form filamentous structures *in vitro* and *in vivo* indicating that it possibly plays a cytoskeletal role in *S. coelicolor*. Therefore, they renamed AbpS to FilP (for Filament-forming protein).

AbpS was first identified in *S. reticuli* by its high affinity to avicel meaning that it could easily be co-purified alongside avicel (Walter *et al.*, 1998). Avicel is the crystalline form of cellulose. The *Streptomyces* strain *S. reticuli* is able to grow on medium containing avicel as the sole carbon source (Schlochtermeier *et al.*, 1992a). Avicel is the only known inducing carbon source for the production of a cellulase that is solely capable of degrading avicel, soluble cellulose, cellodextrins and p-nitrophenylcellobioside (Schlochtermeier *et al.*, 1992a; Schlochtermeier *et al.*, 1992b). The identification of AbpS implicated this protein as having a possible avicel/cellulose receptor function possibly associated with the production of the avicelase (Walter *et al.*, 1999; Walter, and Schrempf, 2003; Walter *et al.*, 1998). The sequence of AbpS was predicted to have a putative C-terminally located transmembrane segment. It was shown through FITC labelling and proteinase K experiments that AbpS is anchored to the cell wall and protrudes from the hyphae (Walter *et al.*, 1998). This was backed up by the use of immunolabelling and microscopic studies which suggested that the N-terminal portion of AbpS protrudes from the cell wall where the C-terminus is embedded (Walter *et al.*, 1999). The N-terminal section containing the avicel binding properties was shown to form α-helical coiled-coils. Crosslinking experiments suggested that AbpS oligomerizes into homotetramers that could make the functional ‘avicel receptor’ (Walter, and Schrempf, 2003). SCO5396 in *S. coelicolor* shows high sequence conservation to AbpS of *S. reticuli*, though thus far it remains to be

seen how relevant the studies of AbpS in *S. reticuli* are to its function in *S. coelicolor* to which Bagchi *et al.,* (2008) suggest a somewhat different role for FilP.

FilP was identified from a wide search of bacterial genomes looking for intermediate filament-like rod domains along with the proteins encoded by genes *sco5397* and *sco3116*. Further searches were carried out and Bagchi *et al.,* (2008) suggested that FilP was a member of a conserved rod-domain protein family in the actinomycetes. From sequence analysis, this group of proteins contained a pair of conserved sequence motifs at the N-terminal borders of the two first coiled-coil segments. Surprisingly SCO3114 and SCO5397 proteins were not members of this family of actinomycete rod-domain proteins (Bagchi *et al.*, 2008). In support of this family of actinomycete rod-domain proteins, 3 candidate proteins, including FilP from *S. coelicolor*, as well as a protein from *Mycobacterium bovis* and a protein from *Janibacter sp*, were shown to be able to all form filaments *in vitro* (Bagchi *et al.,* 2008). Purified histidine-tagged forms of the proteins spontaneously assembled into filaments without the addition of nucleotides or co-factors, this being a similar characteristic of intermediate filaments and crescentin (Ausmees *et al.*, 2003; Bagchi *et al.*, 2008).

A C-terminal EGFP fusion to FilP revealed that it appears to form filaments *in vivo* as well as *in vitro* (Bagchi *et al.,* 2008)(Figure 24). A strain only encoding FilP-EGFP and no wild-type copy of FilP was observed to have slight morphological defects. Whereas a strain containing both FilP-EGFP and endogenous FilP was considered wild-type in phenotype. Not surprisingly then FilP-EGFP with endogenous FilP appeared to form longer filamentous structures than FilP-EGFP alone. A description of FilP localisation is difficult as it appeared to form filaments at emerged germ tubes as well as in seemingly random places along the hyphae. Also, filaments were usually located at apical tip regions. Where FilP alone did not form at apical tip regions, only hybrid FilP-EGFP/FilP formed here. FilP localisation was present in vegetative hyphae as well as immature aerial hyphae, but not much in spore chains. It remains unclear as to how much EGFP interferes with the ability of FilP to assemble into higher order structures.

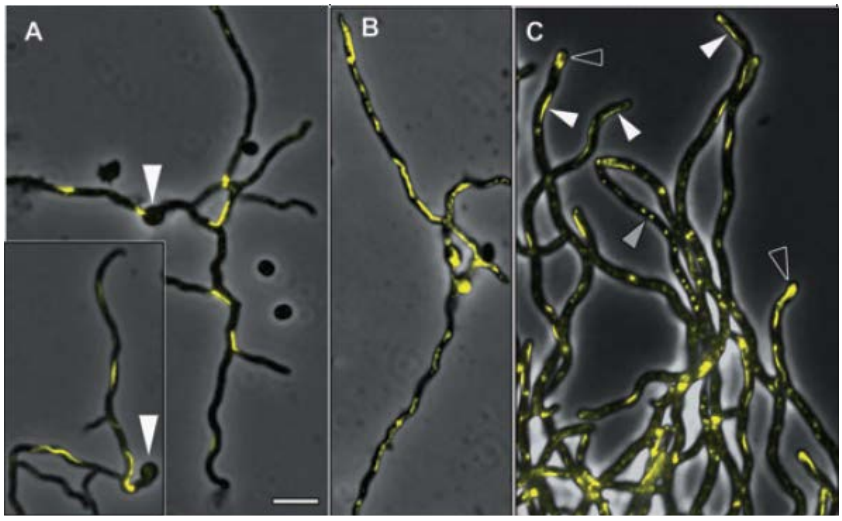

Figure 24: Localisation of FilP-EGFP C-Terminal translational fusion protein. Taken from Bagchi *et al.*, (2008). Strain M145 *filP*:: pNA432 (*filP-egfp*), contains only *filP-egfp*, inoculated on solid media (A). Strain M145 *filP*:: pNA859[Φ(*filP-egfp*)Hyb], contains both *filP* and *filP-egfp*, inoculated on solid media (B). M145 *filP*:: pNA859[Φ(*filP-egfp*)Hyb], contains both *filP* and *filP-egfp*, inoculated in liquid media (C).

A *filP* knockout was achievable and was described as having slight morphological defects associated with the vegetative hyphae, whereas the aerial hyphae appeared wild-type (Bagchi *et al.*, 2008). The *filP* mutant was suggested to be slightly delayed in terms of growth rate. Atomic force microscopy of vegetative hyphae of a *filP* knockout suggested that the rigidity of the structure was somewhat weaker than that observed in the wild-type (Bagchi *et al.*, 2008). Based on the information provided by Bagchi *et al.*, (2008), it could be that FilP seems to have a role in growing vegetative hyphae where it could either provide some form of structural support or play a role in apical growth. It is possible that FilP may have some form of interaction with DivIVA at hyphal tips. FilP is also known to be both phosphorylated (Manteca *et al.*, 2011) and acetylated (Hesketh *et al.*, 2002), but as far as we know it is unknown how post-translational modification affects FilP. A cytoskeletal role for FilP seems to dispute the finding that AbpS in *S. reticuli* is an avicel receptor/binding protein. It was suggested by Bagchi *et al.*, (2008) that FilP is intermediate filament-like, whereas AbpS is believed to have a transmembrane domain that is inconsistent with an intermediate filament-like protein (Walter *et al.*, 1998). Based on current information at the moment it is unclear the precise role of FilP in *S. coelicolor* and AbpS in *S. reticuli*. To add further confusion, recent bioinformatics has suggested that FilP is not an intermediate filament protein (and likely not a transmembrane protein) and instead has a novel coiled-coil periodicity that is similar to the protein Scy encoded by the

upstream gene *sco5397* (Walshaw *et al.*, 2010), this coiled-coil structure will be discussed in the next section.

1.4.7 The Streptomyces cytoskeletal protein (Scy)

The protein encoded by the locus *sco5397*, identified in searches for intermediate filaments by Bagchi *et al.*, (2008), in *S. coelicolor* is located upstream of *filP*. Current research by the Kelemen lab (University of East Anglia, Norwich), suggests that *sco5397* encodes a novel bacterial cytoskeletal protein that has thus been named Scy (for *Streptomyces* cytoskeletal protein). Based on bioinformatics data (Walshaw *et al.*, 2010), part of Scy consists of a novel repeat number unit not seen in the classical heptad Coiled-coil domains (Figure 25). Scy is 1326 amino acids long. The N-terminal end of Scy consists of a short 47 amino acid domain with the classical heptad repeat sequence (Figure 26A). A small "hinge" domain then separates the N-terminal coiled-coil domain from a longer coiled-coil domain of 1226 amino acids (Figure 26A). It is this domain that contains the novel form of non-heptad coiled coil sequences, whereby there is a periodicity of 3.643 (Walshaw *et al.*, 2010), higher than that of 3.5 of the heptad coiled-coil. This periodicity results in a repeat unit of 11-11-11-11-7. This alternate repeat unit results because of the differences between the repeat numbers of solvent exposed and non-polar buried residues that make up the proposed helical structure. A 51-residue coiled-coil repeat is expected to have spacings between the hydrophobic residues of 3, 4, (3, 4, 4) x 4 positions, made of one ''heptad" unit and four ''hendecad" units. This domain shows the non-heptad repeat sequence; however, the repeats contain 6 possible interruptions to which the consequence is currently unknown. It is likely that the novel repeat unit might have implications in the binding between Scy and it's *in vivo* interacting proteins. Thus, Scy is not an intermediate filament or crescentin like protein as these proteins are based on classical heptad repeat coiled-coil structures. FilP has a similar domain architecture to Scy with a 51-mer coiled coil (Figure 26B). Interestingly as well, the coiled-coil protein DivIVA has two coiled-coil segments (Figure 26C & D), with the CC2 domain possibly bearing some similarity to a non-heptad coiled coil, though it is also a short domain so it is uncertain if the periodicity of the hydrophobic residues has as much effect on the pitch of the repeat unit (Walshaw *et al.*, 2010).

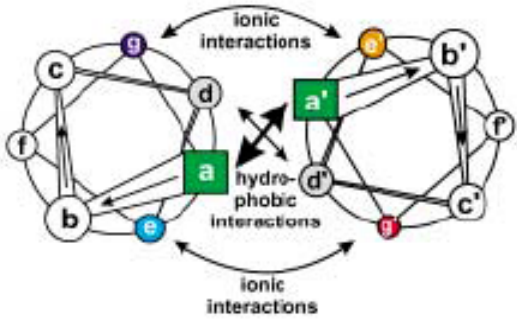

Figure 25: The classical Coiled-coil is a protein motif that forms two left handed helices with heptad amino acid repeats forming every two turns of the helices. The amino acids in the heptad repeat are labelled a, b, c, d, e, f, and g where a and d are nonpolar residues which allow dimerisation of two helices together. The amino acids e and g are normally polar and exposed to aqueous environments, they regularly dictate specificity between two helices binding together. Taken from Marson & Arndt, (2004).

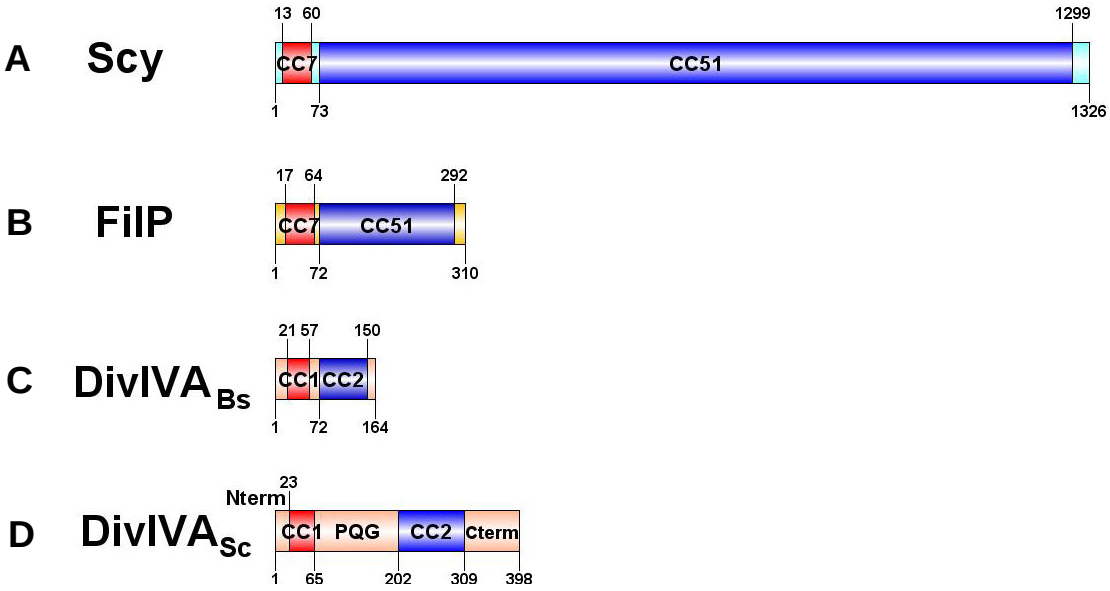

Figure 26: Domain architecture of Scy, FilP and DivIVA. Scy (A) and FilP (B) based on data from Walshaw *et al.*, (2010). CC7 (red) represents heptad coiled-coil domains. CC51 (blue) represents non-heptad coiled-coil domains. C) DivIVA of *B.subtilis* has two coiled-coil sections, CC1 (red) and CC2 (blue) (based on crystal structure data (Oliva *et al.*, 2010)). D) *S. coelicolor* DivIVA has an extended PQG linker separating the coiled-coils as well as an extended C-terminus (based on data from Wang *et al.*, (2009). Amino acid residues at borders are labelled.

It was found that a partial mutation in the *scy* gene resulted in defects with hyphal morphology and possibly growth at the tips of the hyphae. This mutant was seen to have short aerial hyphae and branching spore chains. DNA distribution was not even throughout the formation of the spores. Although the aerial hyphae are affected more, vegetative growth also showed a knotted phenotype showing Scy could be involved in general hyphae development. The precise function and interactions of this protein within the developmental model *Streptomyces coelicolor* should be a priority for future investigations.

1.4.8 Coiled-coil proteins in S. coelicolor

When looking at the complex organism *S. coelicolor* with a large bacterial genome, it was desired to know all the genes/proteins that consist of large stretches of coiled-coils (Table 2). The list provided by John Walshaw was used for Position-Specific Iterative Basic Local Alignment Search Tool (PSI-BLAST) searches here. It was of interest to note the order of size. Not suprisingly Scy (SCO5397) was the protein consisting of the longest stretches of Coiled-coils. Not suprisingly this was followed by the *S. coelicolor* SMC (SCO5577) protein having been noted that the protein consists of long coiled-coil stretches facilitating dimerisation. Also, of significant note in this list are the proteins FilP (SCO5396) and DivIVA (SCO2077) which have been mentioned in the introduction as important morphogenes. The other genes/proteins in the list have some interest though none with any immediate striking significance to the study here. The protein SCO3114 is known to have been picked up in the search for intermediate filament like proteins by Bagchi *et al.*, (2008). However, it cannot be ruled out that many of these genes/proteins may have a significant role in the biology of *S. coelicolor*.

Table 2: Showing the genes/proteins that consist of large (≥90 amino acid residues) coiled-coil stretches based on searching for heptad periodicity by John Walshaw.

SCO Number	Identity	No. Coiled-coil Residues	Total Coiled coil Regions	Notes
5397	Scy	1090	13	Similarity to kinetoplast associated protein, kinesin, Neurofilament and Plectin
5577	SMC	494	7	SMC, Condensin
1407	Hypothetical	408	11	Similarity to Chromosome Segregation ATPase
2383	Putative Secreted	354	5	Carbohydrate-binding domain, similarity to large adhesin
4254	Hypothetical	350	7	Low similarity
1300	Putative Exonuclease	288	7	MAP7 (Microtubule binding domain), Similarity to Exonucleases and SMC
6593	Hypothetical	285	6	P-loop and ALF domain
5396	AbpS/FilP	215	5	Similarity to Cellulose Binding

				Protein
6198	Putative Secreted	209	6	Signal Peptide, ALF domain
3542	Integral membrane protein with kinase activity	154	2	Thymidylate kinase domain
7327	Histidine Kinase	134	3	Putative two component Histidine Kinase
2136	Putative Secreted	134	2	Similarity to NLP_P60 Proteins
5748	Histidine Kinase	128	3	Putative Histidine Kinase
4202	Putative NLP/P60 Secreted Protein	127	2	NLP/P60-family secreted protein
4793	Putative NLP/P60 Secreted Protein	125	2	NLP/P60-family secreted protein
2077	DivIVA	123	2	DivIVA protein
2878	Hypothetical	119	2	Ala Rich, similarity to metolloprotease, adhesin, plectin and flotillin
2135	Putative Secreted	115	2	Similarity to NLP_P60 Proteins
2137	Hypothetical	114	2	DUF901 Superfamily
4796	Putative NLP/P60 Secreted Protein	113	3	NLP/P60-family secreted protein
606	Hypothetical	113	1	Low similarity
3114	Hypothetical	112	3	Similarity to Cellulose Binding Protein
4534	Transmembrane Protein	105	3	Membrane Spanning, Low Similarity
3534	Putative large ATP-binding protein	103	3	Similarity to RecN, SMC, Myosin Heavy Chain, etc
7021	Putative NLP/P60 Secreted Protein	102	2	NLP/P60-family secreted protein
2168	Hypothetical	98	2	Similarity to Phage Shock Protein and Transcriptional Regulators
3949	Secreted peptidase	96	3	Possible Metallopeptidase
5294	Putative NLP/P60 Secreted Protein	96	2	NLP/P60-family secreted protein

1511	Hypothetical	95	3	Similarity to DNA repair ATPase
3840	Hypothetical	91	3	Similarity to Heat Shock Protein DnaJ
3286	Putative Secreted	91	3	Similarity to Band_7 Protein, flotillin
3285	Large glycine/alanine rich protein	90	3	Similarity to AAA ATPase, DNA repair ATPase
6405	Putative DNA recombinase	90	2	Similarity to DNA recombinases, resolvases and integrases

1.5 Experimental aims

1.5.1 General aims

In this study we aimed to investigate the role of *scy* in the biology of the Actinomycete *Streptomyces coelicolor* and to determine any possible role of the novel coiled-coil in the functioning of the protein. To achieve this aim the objectives were the following;

- To generate a null mutant of the *scy* gene.
- To study any potential link between *scy* and the downstream gene *filP* by making a *filP* mutant and a *scy-filP* double mutant.
- To assess the phenotypes of these mutants both macroscopically and microscopically.
- To determine any dependence of any other cytoskeletal proteins, ie DivIVA, ParB or FtsZ on Scy by monitoring these proteins in the *scy* mutant.
- To further test the role of Scy *in vivo* by making translational fusions of *scy* to *egfp* or *mCherry* as reporters of subcellular localisation.
- It was also of interest to compare these localisation patterns with that of FilP and DivIVA.
- To look at the effect of Scy overexpression on the morphology of the hyphae, localisation of proteins and/or cell processes.
- To further characterise any interactions between Scy, FilP and DivIVA using the *in vivo* bacterial two-hybrid system along with the tip localised cytoskeletal protein ParA.

- To purify Scy, FilP and DivIVA from *E. coli* and perform biochemical experiments to test their pair-wise interactions *in vitro*.
- To purify Scy from *S. coelicolor* and to pull down other proteins that might be involved in apical growth.

2 Phenotypes of knockouts of the cytoskeletal protein encoding genes *scy* and *filP*

2.1.1 Introduction

In order to analyse the function of a gene, the first genetic experiment to perform is to make mutants in the gene of interest. We wished to study the gene encoding the protein Scy and so it was sought to generate a null mutant of the *scy* gene. As the gene *filP*, encoding the filamentous protein FilP, sits downstream to *scy* then we also wanted to knock this gene out. Also in order to test if there was any potential link between *scy* and the downstream gene *filP* we wanted to make a *scy-filP* double mutant. This would also allow us to determine if the two genes are redundant and if a double mutant has an additive effect. The mutants were made (10.1.42) by using the REDIRECT© PCR-targeting system (Gust *et al.*, 2002). The phenotypes of these mutants were studied both macroscopically and microscopically.

2.1.2 scy and scy-filP mutants were delayed in growth and development on SFM

For the resulting spore stocks of each of the unmarked mutant strains and the M145 strain, the spore titer was determined by making serial dilutions and counting the colony forming units on LB plates. The spore concentration of the stocks were the following: the M145 sporeprep contained approximately $2.7x10^{10}$ spores/ml, the *filP* sporeprep contained approximately $9.9x10^{9}$ spores/ml, the *scy* sporeprep contained approximately $3.2x10^{9}$ spores/ml and the *scy-filP* sporeprep contained approximately $4.1x10^{9}$ spores/ml.

When comparing macroscopic phenotypic characteristics of different *Streptomyces* strains on agar medium it is generally important to control the viable colony density, as both development and antibiotic production are effected by colony density. Therefore, to minimise density dependent effects we plated equal numbers of spores to the same area of the solid medium. For M145 and each of the mutant strains, 10^{6} spores were spread to an approximate area of a 3cm equilateral triangle of SFM media. The plates were then incubated at 30˚C for up to 6 days and two time points that showed interesting differences are presented in Figure 27. Both time points suggest that M145 and the *filP* mutant develop similarly, whereas the *scy* and *scy-filP* mutants are more similar to one another than from M145 and *filP*. After 1.5 days growth the M145 and *filP* strains are white and have

produced aerial hyphae, whereas the *scy* and *scy-filP* mutants are bald and lack the sign of aerial hyphae production. After 3 days growth all four strains sporulated as indicated by the dark grey colour that is associated with the grey spore pigment (Davis, and Chater, 1990). Though there is a significant developmental delay associated with the *scy* and *scy-filP* strains in comparison to M145 and *filP*. There was no discernable difference between M145 and *filP* or between *scy* and *scy-filP*.

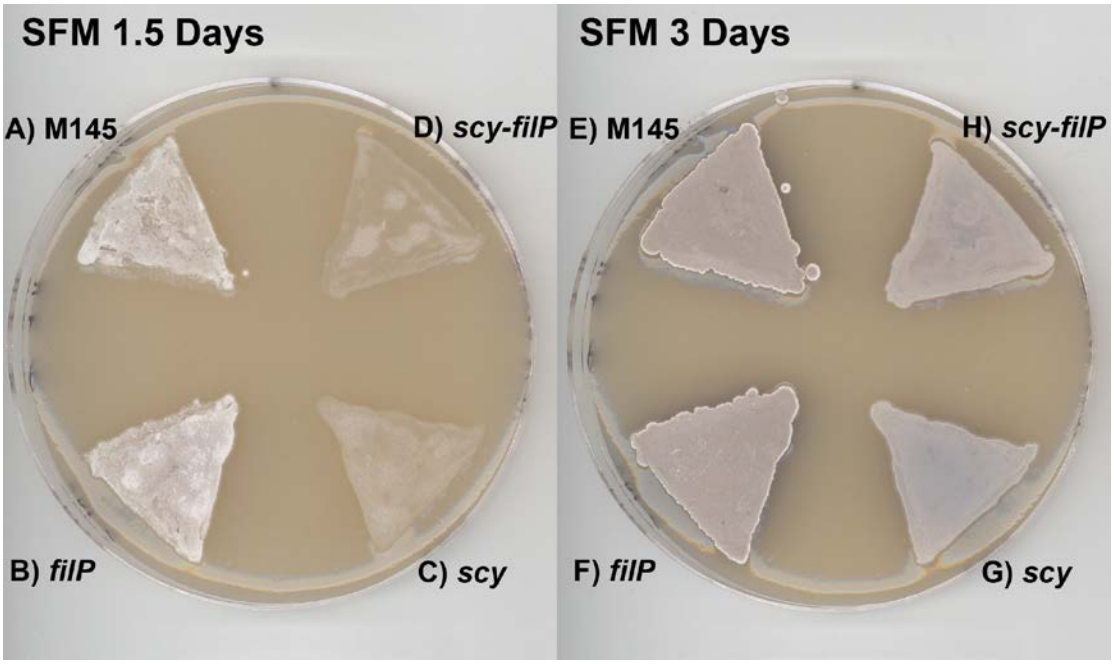

Figure 27: Macroscopic observations of the mutant strains reveals *scy* and *scy-filP* are delayed where as *filP* was similar to wildtype. 10^6 spores were inoculated in a confluent triangle area on SFM medium and growth was monitored after 1.5 days and 3 days at 30˚C. Confluent growth triangles consist of strains M145 wild type (A+E), *filP* (B+F), *scy* (C+G) and *scy-filP* (D+H) mutants.

To further characterise the macroscopic phenotypic differences between the different strains it was important to look at growth at lower colony densities, specifically at the level of single colonies. For M145 and each of the mutant strains, dilutions were made so that approximately 100 viable spores were spread evenly onto SFM medium over the area of a petri dish. To keep consistent experimental conditions the volume of media in each petri dish was maintained at approximately 30ml. The plates were incubated at 30˚C for 6 Days. We spread two plates for each strain, and the colony counts for the two different sets of plates are shown in Table 3.

Table 3: Colony counts of the theoretical ~100 colony plates for each of the strains. The numbers in bold represent the plates shown in Figure 28 and Figure 29. Whereas the numbers in regular format represent the plates used to observe single colonies in Figure 30.

Strain	Colonies on Plates
M145	34, **98**
filP	49, **79**
Scy	45, **72**
scy-filP	106, **109**

The colony morphology of the wild-type and the mutant strains was monitored after 3 and 5 days (Figure 28 and Figure 29). After 3 days growth the wild-type and the *filP* mutant strain were indistinguishable and they both show the powdery appearance that is characteristic of the aerial hyphae and the light grey colour indicates sporulation. The *scy* and *scy-filP* mutants have much less developed colonies that show the "bald" phenotype with no aerial hyphal development (Figure 28).

After 6 days growth the wildtype and *filP* mutant strain developed into mature sporulating colonies with a dark grey, powdery appearance. Whilst the *scy* and *scy-filP* mutants generated much smaller colonies with a lighter grey colouration after 6 days incubation (Figure 29).

The single colonies of the strains tested were also visualised using low magnification microscope (Figure 30). M145 and *filP* show colonies that are more advanced than *scy* and *scy-filP*. With M145 and the *filP* mutant, appearing as mature grey colonies, to which it is obvious that there are masses of aerial hyphae producing spores. The *scy* and *scy-filP* mutant colonies appear smaller in size. Though the images for Figure 30C and Figure 30D may be interpreted as looking different, it is obvious by appearance that they have both produced aerial hyphae, yet they lack the grey spore pigment, suggesting that they have not produced large numbers of spores. Therefore any difference between Figure 30C and Figure 30D we assume is not significant and may only result due to differences in light and that both strains were cultured on different plates.

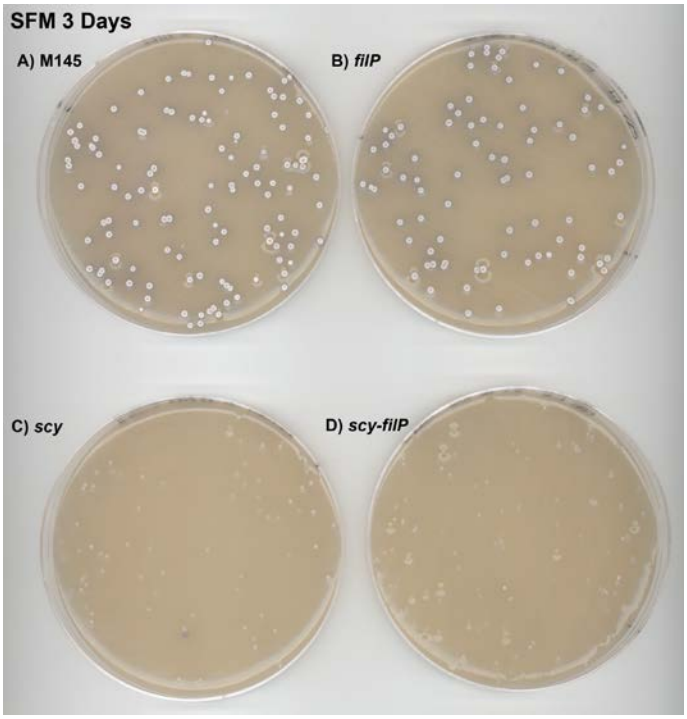

Figure 28: Single colonies of the mutant strains reveals *scy* and *scy-filP* are delayed where as *filP* was similar to wildtype. Single colonies grown at 30ºC for 3 Days, on SFM medium. Separate plates shown are A) 98 M145 colonies, B) 79 *filP* colonies, C) 72 *scy* colonies and D) 109 *scy-filP* colonies.

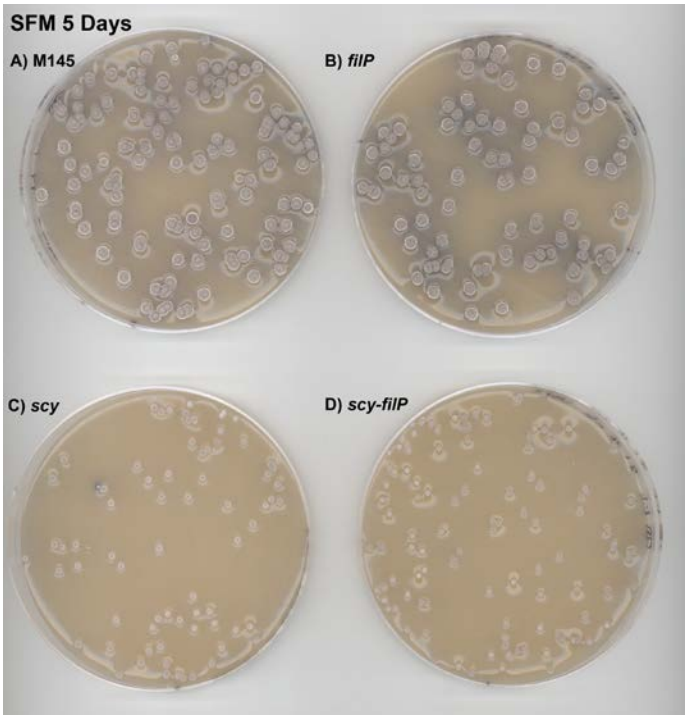

Figure 29: Single colonies of the mutant strains reveals *scy* and *scy-filP* are delayed where as *filP* was similar to wildtype. Single colonies grown at 30ºC for 5 Days, on SFM medium. Separate plates shown are A) 98 M145 colonies, B) 79 *filP* colonies, C) 72 *scy* colonies and D) 109 *scy-filP* colonies.

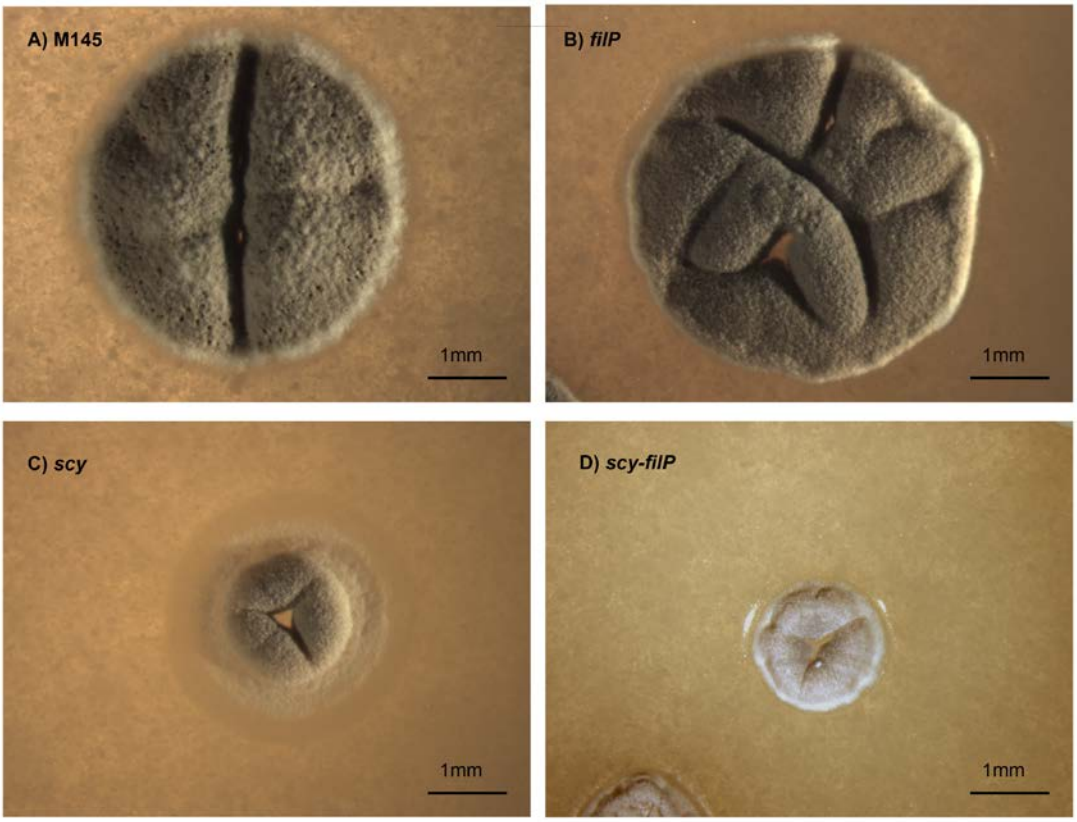

Figure 30: Colony morphology of the mutant strains reveals *scy* and *scy-filP* are delayed where as *filP* was similar to wildtype. Single colonies grown at 30ºC for 6 Days, on SFM medium, visualised with a lower magnification microscope. (A) an M145 colony, (B) a *filP* colony, (C) a *scy* colony and (D) a *scy-filP* colony. Scale bars are shown.

2.1.3 scy and scy-filP mutants were delayed in growth and development on different media

As apparent from the literature review, the study of *Streptomyces* development has been heavily catalogued by monitoring the phenotypes of different genetic mutants on varying types of media. To characterise the mutant phenotypes we monitored colony morphology on different media. SFM media is undefined as it contains hydrolysed soya flour. To include media with well defined components we used minimal media supplemented with glucose (MMG) or mannitol (MMM) as carbon sources. To test the colony morphology on a rich medium we tested growth on a complete media (CM). For M145 and each of the mutant strains, dilutions were made so that approximately 100 viable spores were spread onto CM, MMM and MMG. As before, to keep consistent experimental conditions the volume of media in each petri dish was maintained at approximately 30ml. The plates were incubated at 30˚C and observed over a period in excess of 10 days (Figure 31, Figure 32 and Figure 33). CM is an example of a rich medium. To which classical *bld* mutants lack

aerial hyphae development when grown on (Chater, 1993). As shown in Figure 31, *scy* and *scy-filP* are delayed in comparison to M145 and *filP* in the formation of aerial hyphae on CM. However, they do in fact produce aerial hyphae suggesting that they do not share the

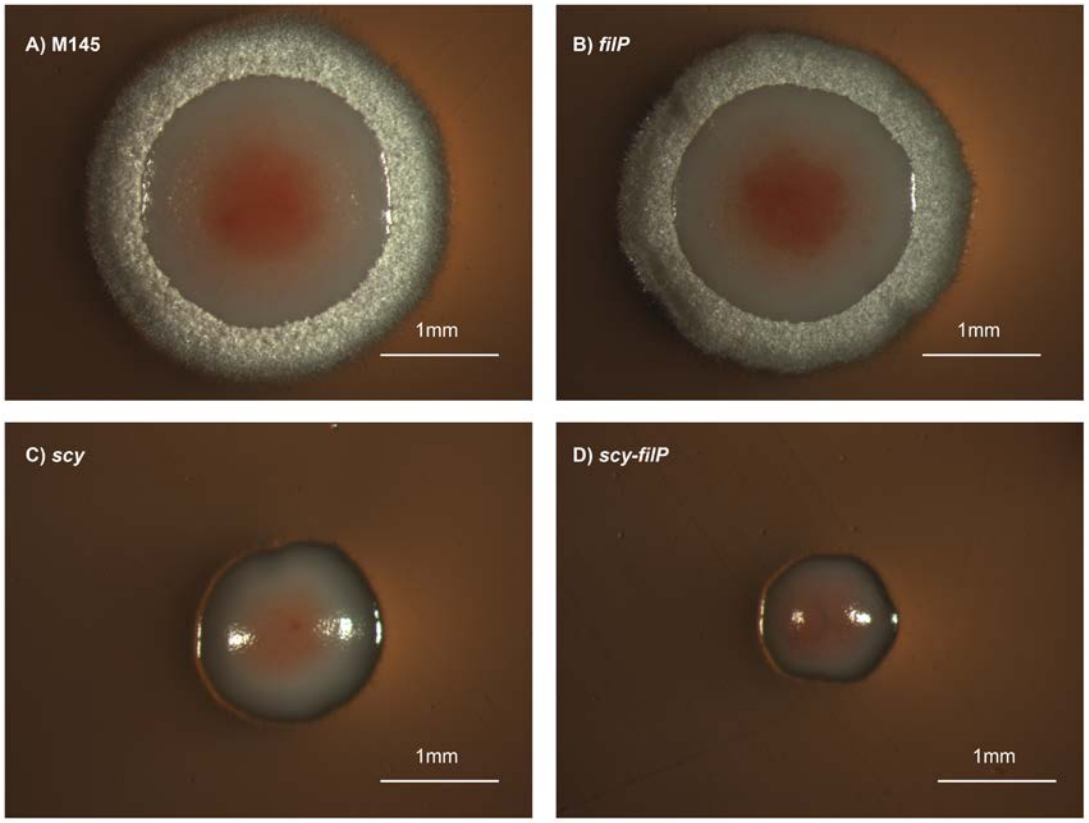

Figure 31: : Colony morphology of the mutant strains on CM reveals *scy* and *scy-filP* are also delayed on other media, where as *filP* was similar to wildtype. Single colonies grown at 30ºC for 4 Days, on CM medium, visualised with a lower magnification microscope. A) an example of an M145 colony from a 52 colony plate B) an example of a *filP* colony from a 66 colony plate C) an example of a *scy* colony from a 26 colony plate and D) an example of *scy-filP* colony from a 35 colony plate. Scale bars are shown.

properties of classical *bld* mutants. As seen on SFM there is a clear difference between growth of M145 or *filP* to that seen for *scy* or *scy-filP*. However, it is not obvious if there is a difference between M145 and *filP* or if there is a difference between *scy* or *scy-filP*. However, this media could potentially be an interesting media to investigate the phenotypes on further.

Morphogenesis of the aerial hyphae on minimal media containing mannitol (MMM) as opposed to that on rich media is controlled slightly differently (Chater, 1993), chaplin mutants are more associated with defects in terms of growth of aerial hyphae on minimal mannitol containing media (Capstick *et al.*, 2007). As shown in Figure 32, *scy* and *scy-filP* are delayed in the formation of the aerial hyphae, whereby at this time point they are only

just beginning to form aerial hyphae over the surface of the colony. As seen on SFM there is a clear difference between growth of M145 or *filP* to that seen for *scy* or *scy-filP*. Whereas both M145 and *filP* were similar and *scy* or *scy-filP* were similar. Based on the colour difference of the background of the M145 and *filP* colonies, they may be secreting different levels of antibiotics.

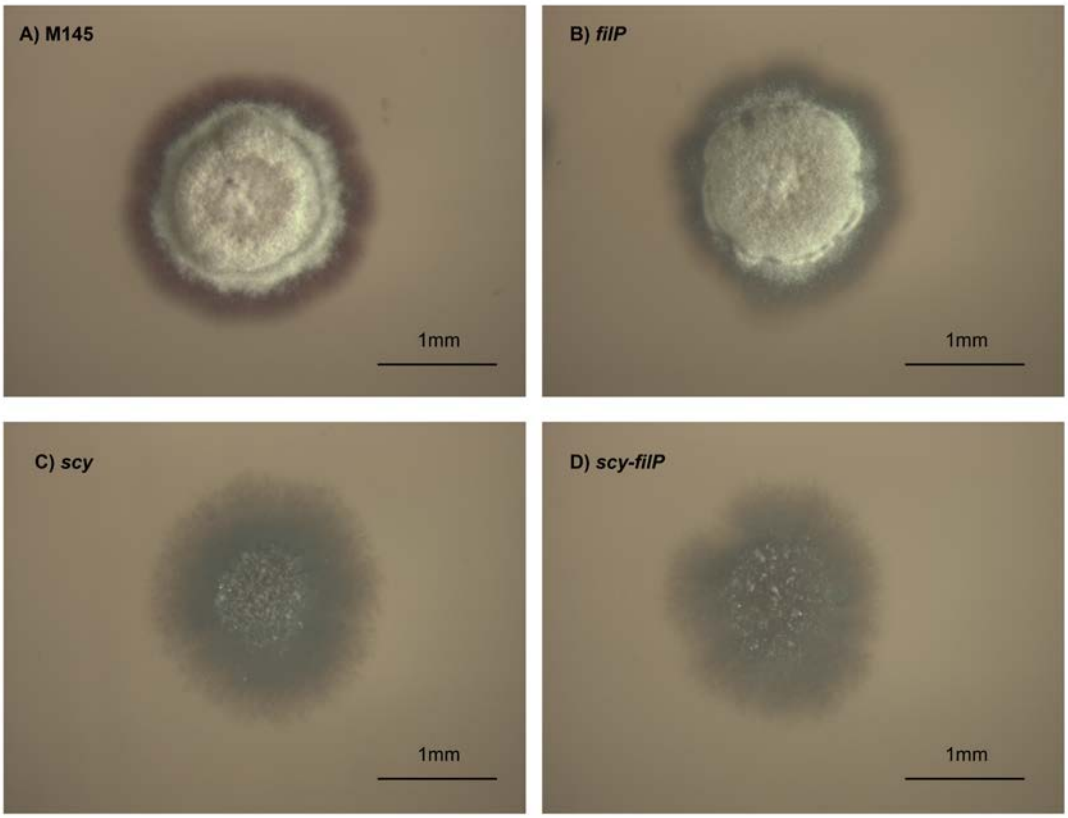

Figure 32: Colony morphology of the mutant strains on MMM reveals *scy* and *scy-filP* are also delayed on other media, where as *filP* was similar to wildtype. Single colonies grown at 30°C for 6 Days, on MMM medium, visualised with a lower magnification microscope. (A) an M145 colony from a 25 colony plate, (B) a *filP* colony from a 23 colony plate, (C) of a *scy* colony from a 32 colony plate and (D) a *scy-filP* colony from an 18 colony plate. Scale bars are shown.

Similarly to other media the observations of the growth of the strains on minimal medium containing glucose (MMG) showed that *scy* and *scy-filP* are delayed in the formation of the aerial hyphae (Figure 33), which form at a later point. As seen on SFM there is a clear difference between growth of M145 or *filP* to that seen for *scy* or *scy-filP*. Whereas any difference between M145 and *filP* is not obvious. In Figure 33 *scy* appears to show clearer hints that the aerial hyphae have begun forming whereas *scy-filP* is not as obvious, however, it is not clear if this actually represents a real difference as these changes can occur quite rapidly. Because of the way much delayed development of the *scy* and *scy-filP* mutants on MMG medium it could be interesting to pursue further in terms of monitoring the developmental progression of the different strains.

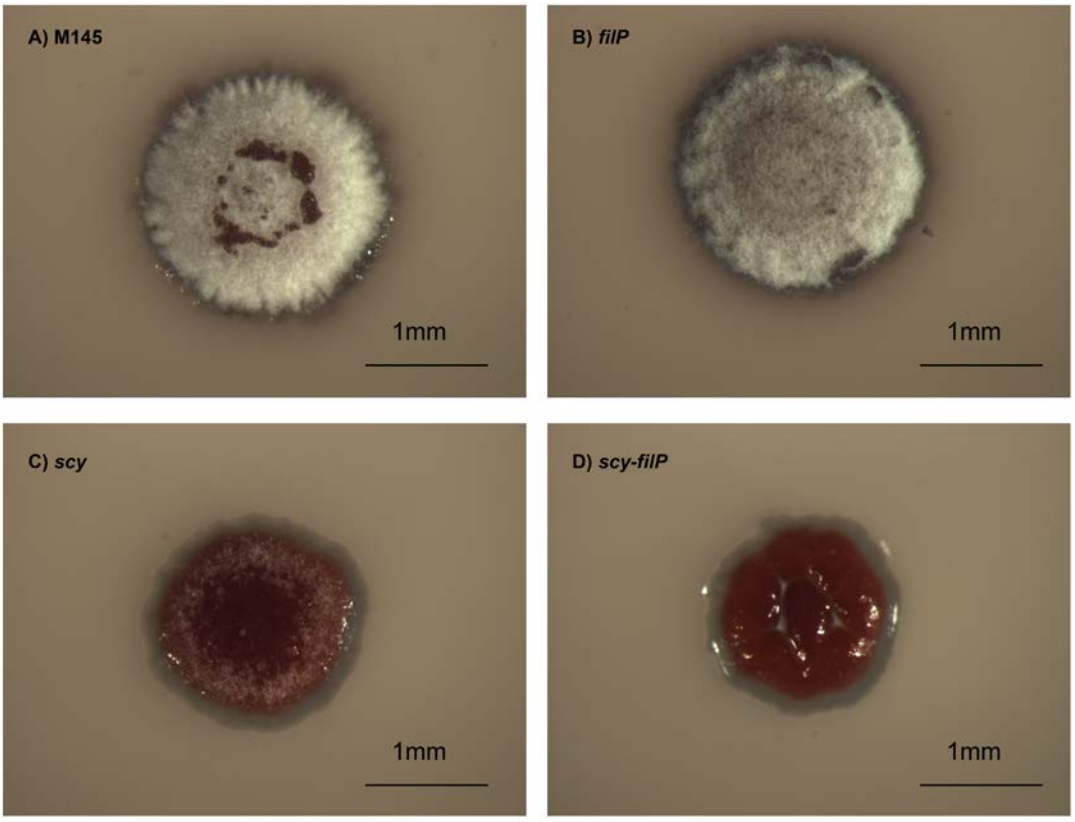

Figure 33: Colony morphology of the mutant strains on MMG reveals *scy* and *scy-filP* are also delayed on other media, where as *filP* was similar to wildtype. Single colonies grown at 30ºC for 6 Days, on MMG medium, visualised with a lower magnification microscope. (A) an M145 colony from a 30 colony plate, (B) a *filP* colony from a 19 colony plate, (C) a *scy* colony from an 11 colony plate and (D) a *scy-filP* colony from a 23 colony plate. Scale bars are shown.

2.1.4 scy and scy-filP mutants microscopically showed defects in polarised growth and cell division

In order to visualise the phenotypes of the hyphae formed by M145, *scy*, *filP* and *scy-filP* at a greater resolution optical microscopy using a confocal or epi-fluorescent microscope was performed. *S. coelicolor* has a complex life style generating a three dimensional network of branching filaments and spores. In order to visualise a younger stage of vegetative growth and to assess the filaments in two dimensions *Streptomyces* can be inoculated onto a surface of a cellophane disc lying on top of an agar medium. This method is excellent for monitoring germination and for young branching hyphal networks. However, the cellophane can quickly become overgrown and therefore this is not a good method for visualising later stages of growth.

Alternatively *Streptomyces* can be grown between the angle of an inserted coverslip and the supporting agar medium. This is associated with the ability to monitor more advanced vegetative growth and the development of the aerial mycelium. Part of the coverslip is submerged in the substrate material and the other part at the medium/air interface with the remainder exposed to the air. Here we used both two strategies to visualise the developmental life cycle of the *Streptomyces* strains analysed here. In addition, we also used the nucleic acid stain, propidium iodide (sigma) and the cell wall stain, wheat germ agglutinin (WGA) Alexa Fluor® 488 conjugate. Propidium iodide binds to nucleic acids by intercalating between bases (Waring, 1965). Once bound to DNA the fluorescence profile of propidium iodide changes and the fluorescence increases 20-30 fold (Arndt-Jovin, and Jovin, 1989), making it a particularly useful DNA stain. The Alexa Fluor® 488 WGA conjugate binds to sialic acid and N-acetylglucosaminyl residues (Wright, 1984). WGA conjugates have been documented to bind to cell wall and septa in Gram-positive bacteria (Pogliano *et al.*, 1997). In *S. coelicolor* WGA conjugate was able to mark the position of ladders of sporulation septa in lysozyme treated hyphae (Schwedock *et al.*, 1997). They also showed that in hyphae that were not treated with lysozyme the stronger signal was associated with growing hyphal tips or autolysis. It is believed that WGA binds better to smaller oligomers of cell wall but less to fully polymerized cell wall (Allen *et al.*, 1973). In the experiments here methanol was used as a fixative, which could allow more staining with WGA-Alexa488 by damaging the cell wall. Methanol fixation is necessary for propidium iodide staining because intact membrance is impermeable to propidium iodide.

Microscopic analysis of different strains on a cellophane surface involved *S. coelicolor* spores of the desired strain being diluted to ~4x 10^5 spores per plate, induced for germination at 50˚C for 10 minutes and sonicated 2 x 15 seconds in order to disperse spores. The dilution was then spread across the surface of a cellophane membrane positioned onto the SFM medium (as shown in Figure 124). After incubation at 30˚C for 12-16 hours, 1cm^2 squares of cellophane were cut with a razor blade and stained.

For microscopy of strains grown alongside a glass coverslip, coverslips were inserted into streaks of *Streptomyces* on SFM medium and the plates were incubated at 30˚C (as shown in Figure 123). Coverslips were removed at different time points between 2-4 days in order to cover the spectrum of the developmental cycle. The hyphae attached to the coverslips were then using in a staining procedure. For each of the different types of samples they

were first fixed with methanol, washed with water and stained with WGA-Alexa488 and propidium iodide. Finally, samples were washed again with water to remove unbound dye. The wild-type strain of *S. coelicolor* M145 was analysed first (Figure 34). Distinct stages of *S. coelicolor* development as depicted in cartoon form were matched with microscopic data observed. The life cycle begins from a single spore (Figure 34A&B). Spores of *S. coelicolor* do not stain well with WGA-Alexa488 and so samples from all the following figures with spores and later stages of spore development are not shown with the WGA-

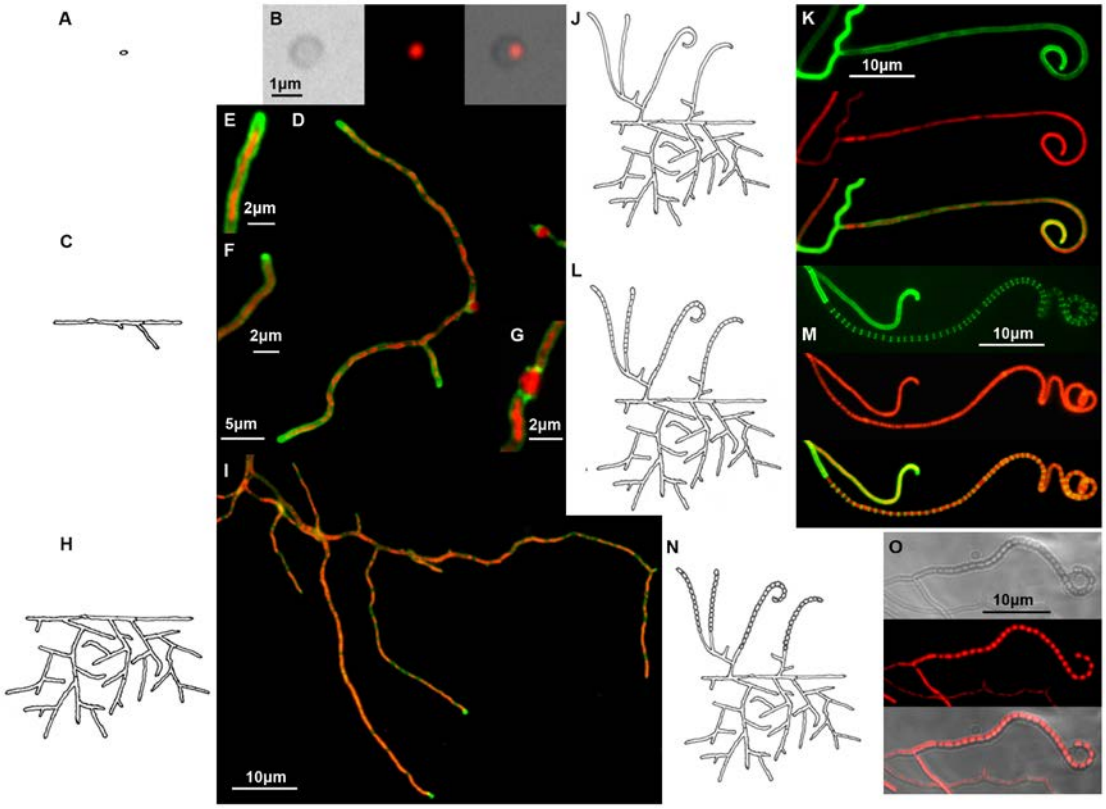

Figure 34: Microscopy of the developmental of wild-type *S. coelicolor* M145 using WGA-Alexa488 and propidium iodide shows multiple distinct stages. A single spore (A) and an image from coverslip samples (B). Germ tube (C) and a images of germtubes and early hyphae from cellophane grown samples (D-G). Branching leads to complex vegetative hyphae (H) taken from coverslip samples (I). Aerial hyphae forms from vegetative hyphae (J) and undergo various stages from the formation of sporulation septa (L) to the maturation of spores (N). Images taken from coverslip samples of pre-divisional aerial hyphae (K), aerial hyphae showing sporulation septation (M) and maturing spores (O). Samples were grown on SFM at 30˚C for 12-16 hours for cellophane samples and 2-4 says for coverslip samples. Samples then stained with WGA-Alexa488 and propidium iodide. (B) Brightfield left, propidium iodide (Red) middle, brightfield/propidium iodide overlay right. (D,E,F,G,I) Overlayed WGA-Alexa488 (Green)/propidium iodide (Red). (K,M) WGA-Alexa488 (Green) top, propidium iodide (Red) middle, Overlayed WGA-Alexa488 (Green)/propidium iodide (Red) bottom. (O) Brightfield top, propidium iodide (Red) middle, brightfield/propidium iodide overlay bottom. Scale bars are shown.

Alexa488 staining. Figure 34C-G shows the stage of germination where germ tubes have emerged and the first initial branches of the hyphae filaments begin to form. Note that it is also possible for multiple germ tubes to form from a single spore. Typically the hyphal tips have a more prominent staining with the WGA conjugate and are generally lacking in DNA (Figure 34D-F). Suggesting that the peptidoglycan at the growing hyphal tips are different, likely to be less crosslinked, than at the lateral hyphal wall that is more inert. However, the tip staining did vary greatly among samples.

Increasing numbers of branching points lead to an ever increasing complexity of the hyphal network (Figure 34H and I). The hyphal distribution and geometry exhibited by the wild-type M145 hyphae are generally quite straight with smooth bends or turns. Branch points occur occasionally, however, in agreement with Jyothikumar *et al.*, (2008), branch-to-branch distances show great variability.

Often curved aerial hyphae of M145 (Figure 34J) undergo synchronous sporulation septation along a tip proximal stretch of the hyphae (Figure 34L), that then later divide and form mature spores (Figure 34N). A number of images of different developmental stages are shown in Figure 34K,M and O. Hyphae destined to be spore chains show a smooth surface that can quite often exhibit a complex curl (Figure 34K). Sporulation septa develop synchronously at regular positions along the length of the hyphae (Figure 34M). After septation, the DNA becomes more compact in each individual spore compartment and the spores undergo a maturation period to form thick walled, highly resistant spores. In Figure 34O the DNA has condensed and more completely segregated in comparison to Figure 34M where the septa are visible using the WGA-Alexa488 stain.

As seen by macroscopic analysis the *scy* mutant is capable of forming aerial hyphae and spores. That means that it is capable of progressing through the stages of the *S. coelicolor* life cycle. However, macroscopical observation suggested that development of the *scy* mutant was delayed, possibly reflecting slower growth or a reduced ability to spread and form large scale colony structures. The young vegetative hyphae observed of cellophane grown samples do show a number of aberrations associated with an effect on polarised growth and hyphal characteristics (Figure 35A-F). One of these aberrations is the frequent apical branching or tip splitting (Figure 35B and E) which was rarely seen in the wild-type, M145 samples. It appears that the *scy* mutant may have more abundant branching, which matches statistical data recorded in the Kelemen lab (Richard Leggett (Holmes *et al.*, 2013)), that may in part be due to apical branching or tip splitting or may result from branches formed further behind the tip. The tip staining with WGA-Alexa488 is variable,

which may or may not be due to the staining procedure rather than the phenotype. However, it is noticeable that the tip architecture of the s*cy* mutant is very different from the wild-type, M145 which usually has a smooth tip shape, whereas the tips of the *scy* mutant appear more prone to variation and in some examples (Figure 35C) can appear more club shaped. The variation in tip shape is probably what accounts for an uneven hyphal diameter seen at positions behind the hyphal tip, as hyphal width must be determined by the tip diameter at the time in which new cell wall was incorporated in that position. As can be seen at later stages of vegetative growth alongside coverslips, (Figure 35H) the *scy* mutant appears less straight and smooth than those seen of the wild-type. With sharp turns which is consistent with a tip growth defect. The *scy* mutant has a characteristic "wriggly" appearance that can then manifest itself in the form of complex knots (Figure 35G and H). The knots can often occur at branch points when the *scy* mutant is grown alongside coverslips. These knots are the likely result of aborted branching attempts, which presumably have implications on the overall hyphal dynamics of a developing colony.

The observation above that branches form complex knots of hyphae, could explain the reduction in total number as well as a delay in the production of aerial hyphae. However, the *scy* mutant is not "bald", it was possible to observe occasional yet seemingly rarer aerial hyphae that undergo differentiation to form spore chains as can be seen across different developmental stages in Figure 35I,J,K and L. Over-branching was not only characteristic of the vegetative hyphae but also of the aerial filaments, a trait not normally observed for the wild-type. The aerial hyphae could later metamorphose into spore chains (Figure 35J,K and L) despite branching generating branching spore chains with defects of shape, DNA content and size. Figure 35I, is an example of a structure that is believed to be an aerial hyphae prior to sporulation that is a *scy* equivalent to the M145 structure seen in Figure 34K. This could be the case as the WGA-Alexa488 staining is reduced and the hyphae have not yet formed septa or segregated the DNA. However, as *scy* has not been subjected to time-lapse imaging it is not known whether the hyphal structures such as the one in Figure 35I actually develop into sporechains. The *scy* mutant is able to form sporulation septa in an array of ladders (Figure 35J), but these are not as ordered as the wild-type and appear to generate irregularly sized prespore compartments. This could be due to the irregular septum positioning as well as the physical constraints to which the abnormal shaped hyphae then exert on the prespore compartments. In more mature sporulating hyphae (Figure 35K and L) the spores are unusual in shape and have irregular

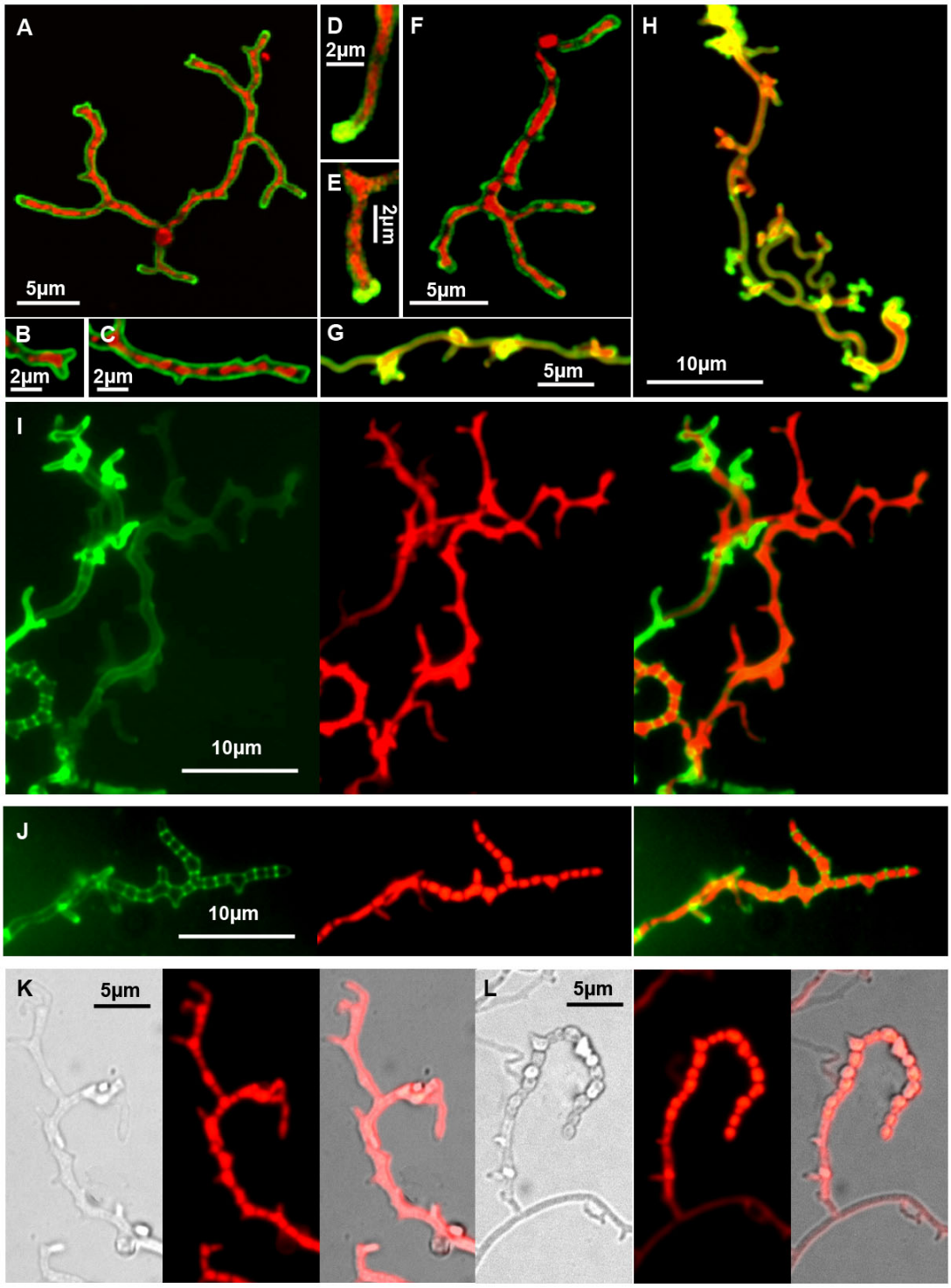

Figure 35: Microscopy of the *scy* mutant reveals an effect on polarised growth and cell division. Images of early vegetative hyphae from cellophane grown samples (A-F) with abnormal branching and hyphal defects. Irregular defects seen in vegetative hyphae of coverslip samples (G,H) with knotted hyphae and branches. Coverslip samples of pre-divisional branching aerial hyphae (I), branching aerial hyphae showing sporulation septa (J) and irregularly shapped maturing spores (K,L). Samples were grown on SFM at 30˚C for 12-16 hours for cellophane samples and 2-4 days for coverslip samples. Samples then stained with WGA-Alexa488 and propidium iodide. (A-H) Overlayed WGA-Alexa488 (Green)/propidium iodide (Red). (I,J) WGA-Alexa488 (Green) left, propidium iodide (Red) middle, Overlayed WGA-Alexa488 (Green)/propidium iodide (Red) right. (K,L) Brightfield left, propidium iodide (Red) middle, brightfield/propidium iodide overlay right. Scale bars are shown.

chromosome distribution, where Figure 35K appears to be less developed than Figure 35L based on Figure 35K having less condensed chromosomal DNA. The latter could be the result of a DNA segregation defect or a DNA condensation defect. The spore chains of the *scy* mutant are also shorter in comparison to the wild-type, which generally has long smooth prespore structures. Despite the branching effect, this could result in sporechains that produce fewer spores. There is also a likely reduced production of the aerial hyphae that develop into spores due to morphological defects and/or aborted branches which could also reduce the number of actual spores that are produced. The microscopic observations made in this study suggest that *scy* is morphologically affected in growth and this is likely associated with aberrant tip growth. Also, the *scy* mutant is affected in the process of cell division during sporulation of the aerial hyphae.

The *filP* mutant macroscopically did not differ from the wild-type. However, microscopic observations made by Bagchi *et al.,* (2008) suggest that *filP* displays a different phenotype to the wild-type. The microscopic observations made here also suggest that *filP* differs from M145, although with more subtle differences possibly explaining why these differences are not manifested at the macroscopic level.

The young vegetative hyphae observed by microscopy of cellophane grown samples (Figure 36A-E) appear to be more similar to the wild-type than the equivalent *scy* images. It does not appear as though there is an affect on the tip architecture of the *filP* mutant or an effect on tip splitting. However, Figure 36D and E show a common hyphal anomaly seen in *filP* mutant where there is a sudden change in direction of the extending hyphae and it grows back towards the hyphae it originated from. Samples of later time points of the *filP* mutant grown alongside coverslips exhibit abnormal growth resulting from change of direction or “wriggly” looking hyphae with some similar properties to the phenotype seen for *scy* (Figure 36F and G). Perhaps suggesting possibly some form of functional overlap between the two proteins encoded by the genes *scy* and *filP*. The *filP* “wriggly” phenotype is possibly manifested due to the same reasons that hyphal rigidity are decreased in *filP* as shown by Bagchi *et al.,* (2008).

The aerial hyphae of a *filP* mutant was reported by Bagchi *et al.,* (2008), “did not display any striking morphological defects”. The aerial hyphae of the *filP* mutant observed in our experiment not surprisingly showed all the similar developmental stages to M145. However, it is unclear if the aerial hyphae of a *filP* mutant have subtle phenotypic differences to M145, albeit clearly not as extreme phenotypic differences as those seen for *scy*. An example of a *filP* aerial hyphae is shown in Figure 36H. Figure 36I shows an

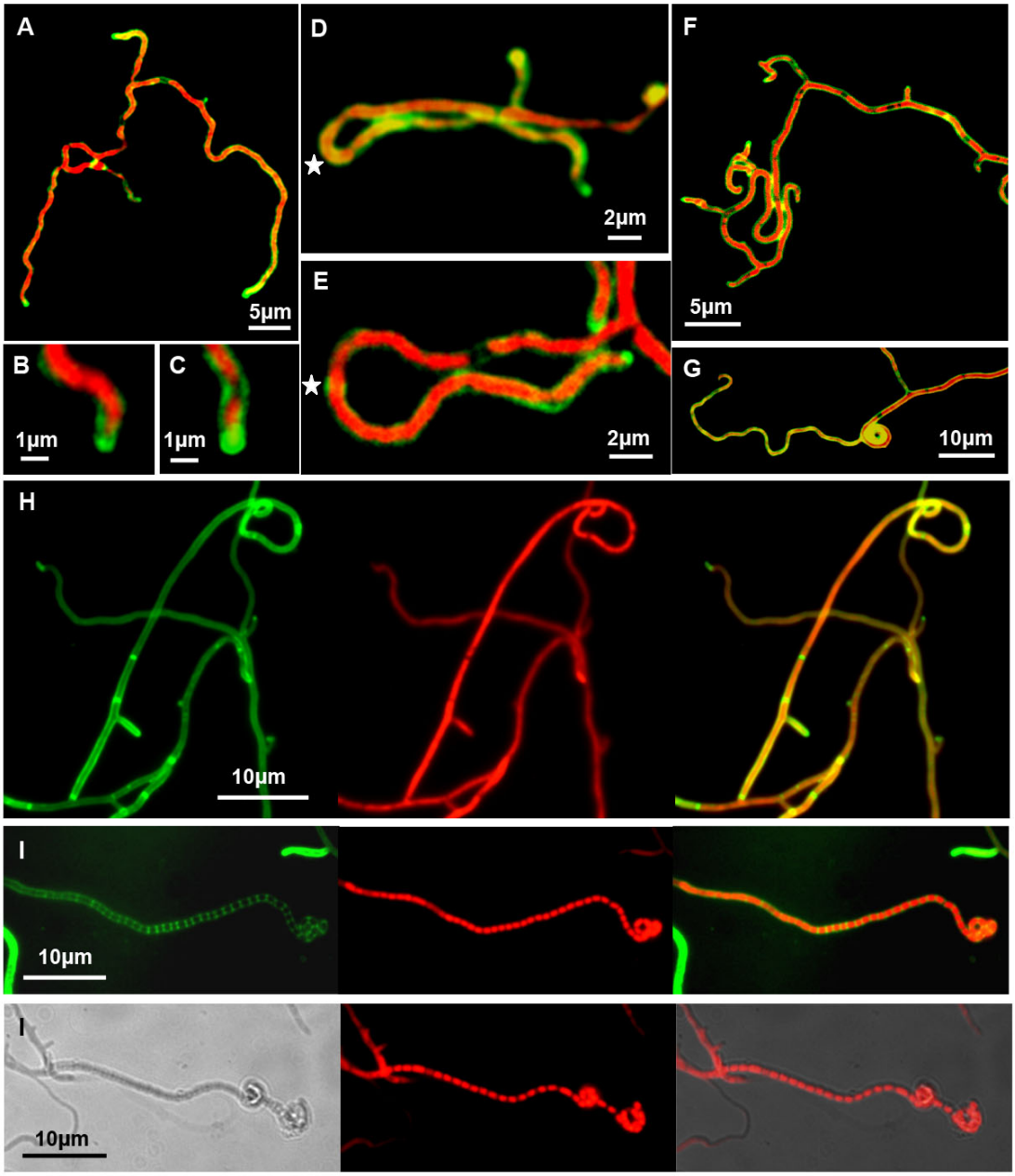

Figure 36: Microscopy of the *filP* mutant reveals a subtle phenotype associated with vegetative growth. Images of early vegetative hyphae from cellophane samples (A-E). (D-E) with * marking the positions of irregular turning seen in the *filP* mutant. Irregular defects seen in vegetative hyphae shown from coverslip samples (F,G) with turning defects and "wrigglyness". Images taken from coverslip samples of pre-divisional aerial hyphae (H), aerial hyphae showing sporulation septation (I) and maturing spores (J). Samples were grown on SFM at 30˚C for 12-16 hours for cellophane samples and 2-4 days for coverslip samples. Samples then stained with WGA-Alexa488 and propidium iodide. (A-G) Overlayed WGA-Alexa488 (Green)/propidium iodide (Red). (H,I) WGA-Alexa488 (Green) left, propidium iodide (Red) middle, Overlayed WGA-Alexa488 (Green)/propidium iodide (Red) right. (J) Brightfield left, propidium iodide (Red) middle, brightfield/propidium iodide overlay right. Scale bars are shown.

example of a *filP* prespore chain with sporulation septation, suggesting that synchronous cell division is not affected. The aerial hyphae of the *filP* mutant did not exhibit a

branching phenotype like that shown by the *scy* mutant. The example of a more mature prespore chain of *filP* (Figure 36J) shows a more wild-type phenotype than the equivalent stage in the *scy* mutant. Suggesting that DNA segregation and distribution is not affected. If there is any difference then it would be a subtle difference in hyphal shape, while it appears that the shape of prespores and spores that are formed are wild-type. It appears that our *filP* mutant displays the same microscopic phenotype as that seen for the *filP* mutant in Bagchi *et al.*, (2008) for both vegetative growth and aerial growth.

Macroscopically the *scy-filP* double mutant appeared the same as the *scy* mutant. However, microscopy could still detect some discernible differences. The young vegetative hyphae of cellophane grown samples of the *scy-filP* double mutant (Figure 37A-E) do show a number of aberrations associated with an effect on polarised growth and hyphal characteristics similar to those seen for the *scy* mutant. Tip splitting and abnormal tip architecture with hyphal width differences are also present in the *scy-filP* double mutant (Figure 37A, C and E). Later stages of vegetative growth alongside coverslips exhibited defects in terms of knots and aborted branches similar to that observed in the *scy* mutant(Figure 37F).

The *scy-filP* mutant was capable of producing aerial hyphae and spores (Figure 37G, H and I); however, as seen for the *scy* mutant, there were fewer aerial hyphae that were more delayed in formation. In Figure 37G, is an example of a structure that is believed to be an aerial hyphae prior to sporulation that is a *scy-filP* equivalent to the *scy* structure seen in Figure 35J, where the developmental fate of this type of hyphae is not yet clear. In Figure 37H the aerial hyphae features prominent branches. There are also irregularly placed sporulation septa and irregularly shaped prespore compartments in the *scy-filP* double mutant similar to those seen in the *scy* mutant (Figure 35J). The spore shapes and DNA distribution in the spore compartments of the *scy-filP* double mutant are irregular (Figure 37I), similar to the equivalent samples of the *scy* mutant (Figure 35K and L).

The microscopy data suggests that there is no significant difference between the *scy-filP* and the *scy* mutants. The *scy-filP* mutant exhibits the characteristic branches that form complex knots and a “wriggly” appearance, together with uneven hyphal width originating from abnormal tip architecture. The aerial hyphae are also much shorter than the wild-type, a similar feature to that observed for the *scy* mutant, as well as the other aerial hyphae abnormalities such as branching and uneven septum positioning.

It is interesting to note that the *scy-filP* mutant is phenotypically more similar to *scy* rather than *filP*, therefore suggesting that *scy* is the more dominant gene in terms of phenotypic effects. If there is a difference between *scy-filP* and *scy* then it is likely far too subtle to

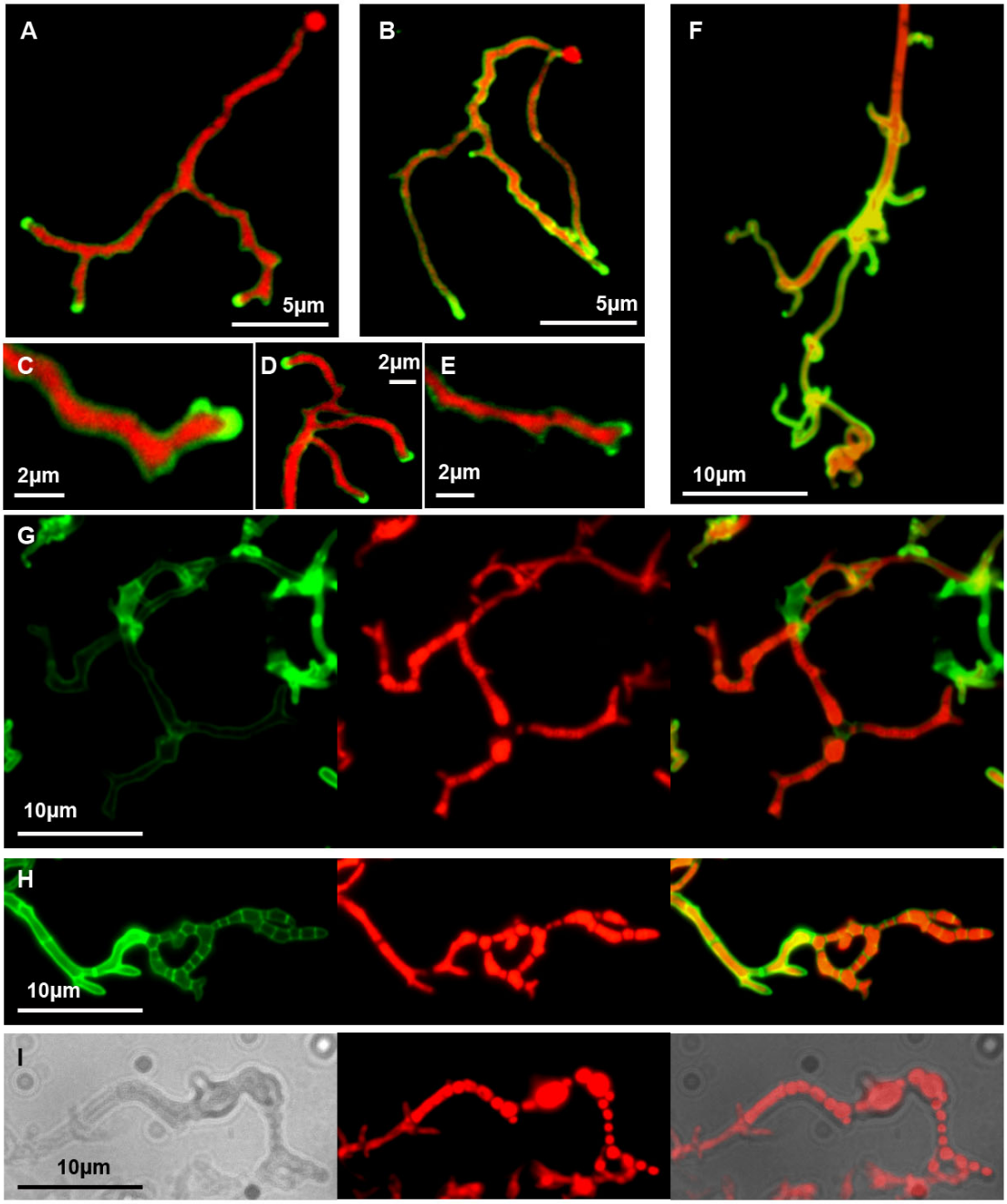

Figure 37: Microscopy of the *scy-filP* mutant reveals an effect on polarised growth and cell division similar to the *scy* mutant. Images of early vegetative hyphae from cellophane samples (A-E) with abnormal branching and hyphal defects. Irregular defects seen in vegetative hyphae shown from coverslip samples (F) with knotted hyphae and branches. Images taken from coverslip samples of pre-divisional branching aerial hyphae (G), branching aerial hyphae showing sporulation septation (H) and irregularly shapped mature spores (I). Samples were grown on SFM at 30˚C for 12-16 hours for cellophanes and 2-4 days for coverslip samples. Samples then stained with WGA-Alexa488 and propidium iodide. (A-F) Overlayed WGA-Alexa488 (Green)/propidium iodide (Red). (G,H) WGA-Alexa488 (Green) left, propidium iodide (Red) middle, Overlayed WGA-Alexa488 (Green)/propidium iodide (Red) right. (I) Brightfield left, propidium iodide (Red) middle, brightfield/propidium iodide overlay right. Scale bars are shown.

manifest as a discernable difference. There is also the possibility that perhaps *scy* and *filP* function in the same pathway, with there being a potential overlap in the single phenotypes, with *scy* being the more detrimental to the same pathway, therefore in this case it is expected that the double knockout would show more of a *scy* phenotype.

2.1.5 Measuring septum length reveals scy and scy-filP septum positioning is disturbed

As the *scy* and *scy-filP* mutants displayed irregularly placed sporulation septa and irregularly shaped prespore compartments, we decided to to quantify this effect by measuring the distance between the sporulation septa in the strains *scy*, *scy-filP* and *filP*. The wild-type strain M145 was also quantified as a control strain. This was done using the Ziess Axiovision software Rel 4.8 which has a measuring function. The data was collected and placed into groups and plotted onto histograms (Figure 38). As can be seen from the graphical representation it appears as though the *scy* and the *scy-filP* mutants display a phenotype with more dispersed sizes of sporulation septa. Statistical analysis of the measurements can be seen in (Table 4 & Table 5). There was no significant difference between M145 and *filP* means by T-Test. Nor was there a difference between *scy* and *scy-filP* means. However, *scy* and *scy-filP* means were significantly different to M145 or *filP*. Proving that these two strains are affected in the placement of the sporulation septa, whereby there was also a greater variation and standard deviation. Therefore, these strains are affected in the process of cell division. The separate mutations in *scy* and *filP* do not appear to be additive as the *scy* mutation appears dominant to the *filP* mutation that separately did not have an effect and the *scy-filP* mutant is identical to the *scy* mutant.

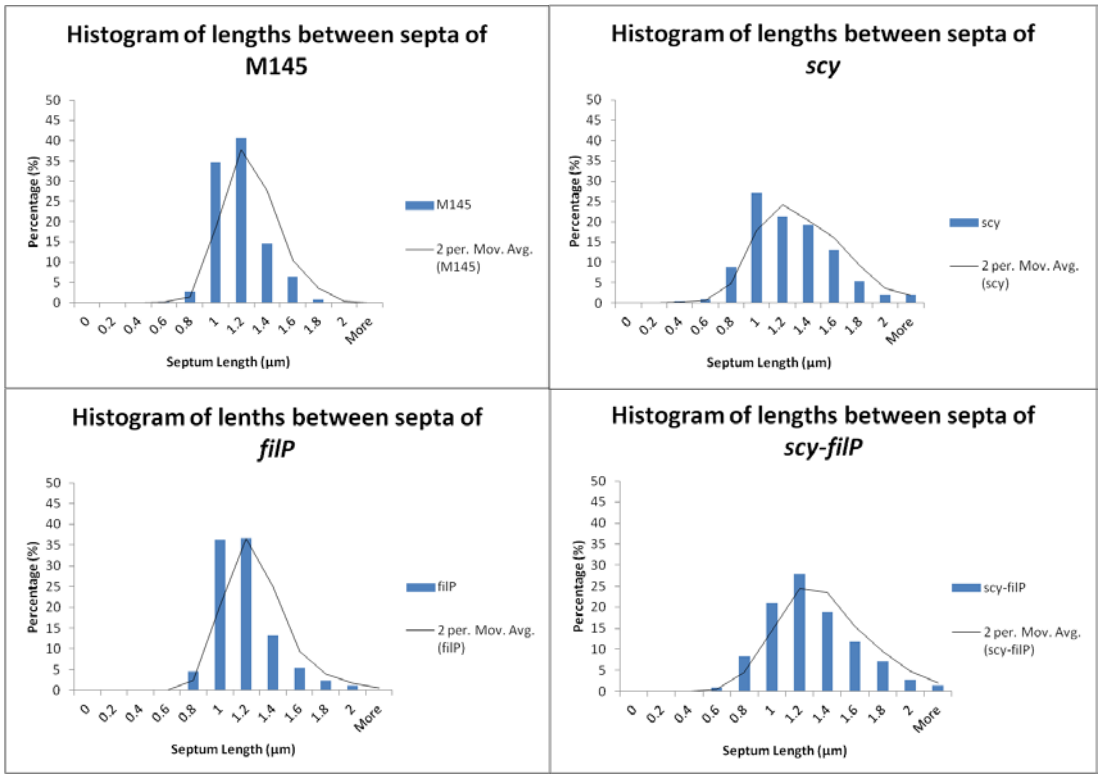

Figure 38: Histograms of measured distances between sporulation septa in the strains M145, *scy*, *filP* and *scy-filP* shows that scy and scy-filP have a greater variation in septum placement.

Table 4: Analysis of Measurements between Sporulation Septa of M145, *scy*, *filP* and *scy-filP*.

	M145	*scy*	*filP*	*scy-filP*
Sample numbers (n)	420.00	421.00	437.00	438.00
Total Septum Measurements (µm)	453.78	489.01	472.91	521.19
Mean Septum Measurements (µm)	1.080	1.162	1.082	1.190
Variance (μm^2)	0.034	0.109	0.050	0.111
Standard Deviation (µm)	0.185	0.330	0.224	0.333
Minimum (µm)	0.570	0.340	0.570	0.480
Maximum (µm)	1.690	2.700	2.000	3.470

Table 5: Statistical Test Analysis of Measurements between Sporulation Septa of M145, *scy*, *filP* and *scy-filP*. First One-tailed F-Tests were performed to test samples for variances. Then, depending on the outcome either Two-tailed T-Tests for evaluating sample means were performed assuming Equal or Unequal Variances. In this case only *scy* against *scy-filP* were deemed to have equal variances. P values of less than 0.05 led to rejecting a null hypothesis of equal samples variances (F-Test) or means (T-Test).

	M145	*Scy*	*filP*	*scy-filP*	
M145		1.255E-05	0.901	3.601E-09	T-Test Two-tail P values
scy	0.000E+00		4.427E-05	0.210	
filP	3.914E-05	1.501E-15		2.825E-08	
scy-filP	0.000E+00	0.406	1.110E-16		
F-Test One-tail P values					

2.1.6 The scy mutant produces fewer spores than M145

Both the macroscopic and microscopic observations suggested that the *scy* mutant produces significantly less spores than M145. The following section details a crude analysis to attempt to quantify the production of spores in the *scy* mutant in comparison to M145.

For M145 and *scy*, dilutions were made so that approximately a similar number of viable spores were spread on SFM medium. To keep consistent experimental conditions the volume of medium in each petri dish was maintained at approximately 30ml and plates were incubated at 30˚C for 7 Days. After the incubation period the number of colonies on each plate was counted and recorded. To each plate 2.5ml of H_2O was added and the spores rubbed off with a sterile cotton bud. The liquid was collected from these plates. After centrifuging this spore mix the pellet consisting of the spores was resuspended in 1ml of 20% glycerol for both. For the resulting spore stocks of each, a series of dilutions were made. Dilutions of the factors $5x10^{-6}$, $5x10^{-7}$,$5x10^{-8}$ and $5x10^{-9}$ were spread with 3 replicas for each dilution, onto LB agar plates and incubated at 30˚C for 2 days. Those plates that had a countable number of colonies were then quantified. For M145 only the dilutions at $5x10^{-7}$and $5x10^{-8}$ dilutions were used, whereas for *scy* only the dilutions at $5x10^{-6}$ and $5x10^{-7}$ were used for spore counts. A representative plate from the $5x10^{-7}$ dilution range is shown in Figure 39. The average spores per ml as calculated by the analysis in 3 separate experiments are shown in Table 6A. The number of colonies to which the spores originated from was factored into calculating a ratio of the number of M145 spores produced to *scy*, in an attempt to compare the spore production by both strains. According to this analysis M145 produces in a scale of 5-10 times as many spores as *scy*. This is a crude method of

analysis but the large difference detected likely represents an actual difference. As the *scy* mutant is delayed in growth forming less biomass in the incubation period and developing less biomass to aerial hyphae and spores, this could account for a decrease in the production of spores, as well as a aberrations visualised by microscopy in the process of cell division.

Table 6: Calculating the relative number of spores produced by M145 in comparison to the *scy* mutant.

A) Repeat 1	Strain	Average (Spores/ml)	Number of colonies spores were collected from	Average Spores/Colony	Ratio M145/*scy*
	M145	1.4E+09	380	3.9E+06	5.9
	scy	1.8E+08	280	6.6E+05	
B) Repeat 2	Strain	Average (Spores/ml)	Number of colonies spores were collected from	Average Spores/Colony	Ratio M145/*scy*
	M145	2.8E+09	543	5.2E+06	9.9
	scy	2.9E+08	550	5.3E+05	
C) Repeat 3	Strain	Average (Spores/ml)	Number of colonies spores were collected from	Average Spores/Colony	Ratio M145/*scy*
	M145	3.2E+09	979	3.3E+06	4.8
	scy	7.1E+08	1029	6.9E+05	

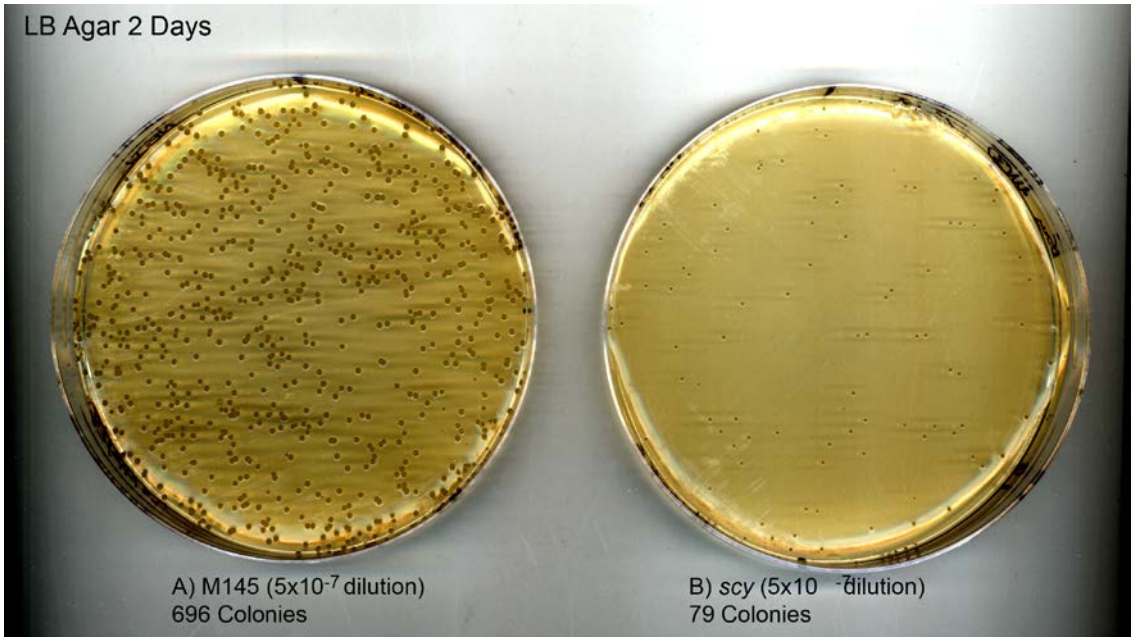

Figure 39: The *scy* mutant produced fewer viable spores than the wildtype. Viable spores of the 5x10^{-7} dilution on LB Agar, after 2 days incubation at 30˚C. Shown is M145 696 colonies (A) and *scy* 79 colonies (B).

2.1.7 Adding scy in trans complements the scy mutant phenotype

An important step in establishing if a phenotypic effect is due to the actual absence of the gene is to add a copy of the gene *in trans* back into the mutant strain. Therefore, if the phenotype reverts back to the wild-type then the phenotype is due to a knockout of that particular gene. The Kelemen lab had previously constructed a plasmid pIJ8660-Pscy-scy. This plasmid is descended from the vector pIJ8660 (Sun *et al.*, 1999) which is able to replicate in *E. coli*, as well as having the property of being able to be conjugated into *Streptomyces* species via containing *oriT* from RK2 (Pansegrau *et al.*, 1994). This vector also has the temperate phage *Φ*C31 *int* gene and *attP* site, allowing integration of the plasmid at the chromosomal *Φ*C31 attachment site in *S. coelicolor*. The plasmid pIJ8660 also contains a selectable marker in the form of *aac(3)IV*, conferring apramycin resistance. The plasmid pIJ8660-Pscy-scy contains the *scy* promoter fragment generated here (10.1.46) with a fragment containing the whole of *scy* sitting upstream. Due to the construction of the plasmid the *scy* gene has an altered ATG codon instead of a GTG at the start codon, as well as an additional adenine as the base prior to the open reading frame. These alterations to the endogenous sequences are likely to have a negligible effect on *scy* expression and the functioning of the resulting protein. Therefore, *scy* should be able to be

expressed from its own promoter, however, upon introduction into *S. coelicolor* located chromosomally as a single copy from the *Φ*C31 attachment site.

Introduction of the plasmids was through the non-methylating *E. coli* strain *E. coli* ET12567 containing the plasmid pUZ8002 that facilitates conjugation with *S. coelicolor* (MacNeil *et al.*, 1992). The 1µl of each plasmid stock of pIJ8660-*Pscy-scy* and the empty pIJ8660 vector were electroporated into *E. coli* ET12567/pUZ8002 cells. Transformants were grown on LB with the antibiotics kanamycin and chloramphenicol for ET12567/pUZ8002 and apramycin for selection of pIJ8660-Pscy-scy or pIJ8660 plasmids.

E. coli ET12567 carrying either pIJ8660-Pscy-scy or pIJ8660 were used for conjugation into either spores of M145 or *scy*. Apramycin was used to select for the integration of the pIJ8660 vectors into the chromosome. As success of this conjugation is dependent on integration as opposed to homologous recombination, successful conjugants were achieved with high frequency than the mutant generation experiments. Replica plating wasn't necessary as the pIJ8660 vector can only be maintained stably in the presence of apramycin in *Streptomyces* by insertion into the chromosome. Therefore, this successfully generated the strains M145/pIJ8660, *scy*/pIJ8660, M145/pIJ8660-Pscy-scy and *scy*/pIJ8660-Pscy-scy. Each strain was used for preparation and storage in the form of spore preps.

By the same method as mentioned above the spore preparations of the strains M145/pIJ8660, *scy*/pIJ8660, M145/pIJ8660-Pscy-scy and *scy*/pIJ8660-Pscy-scy were titrated and tested for viable spores on LB. To which the M145/pIJ8660 sporeprep contained $1.6x10^{10}$ spores per ml. The *scy*/pIJ8660 sporeprep contained $1.6x10^{9}$ spores per ml. The M145/pIJ8660-Pscy-scy sporeprep contained $1.0x10^{10}$ spores per ml. The *scy*/pIJ8660-Pscy-scy sporeprep contained $9.0x10^{9}$ spores per ml.

To actually test complementation, the pIJ8660-*Pscy-scy* strains were tested in comparison to the pIJ8660 strains in order to rule out any differences being due to the properties of the effect of the pIJ8660 vector on *Streptomyces*. In the same controlled manner as above, for each of the strains dilutions were made so that 10^{6} spores were spread in 15µl of liquid on SFM medium. This was to an approximate area of a 3cm equilateral triangle and spread with a sterile toothpick. The plates were then incubated at 30˚C for up to 6 Days, two time points that were informative are shown in Figure 40. Both time points suggest that M145/pIJ8660, M145/pIJ8660-*Pscy-scy* and *scy*/pIJ8660-Pscy-scy are similar in macroscopic phenotype. Whereas *scy*/pIJ8660 appears to be clearly different to the other strains. After 2 days growth M145/pIJ8660, M145/pIJ8660-*Pscy-scy* and *scy*/pIJ8660-

Pscy-scy appear to have formed aerial hyphae and may be on the verge of producing spores. Whereas *scy*/pIJ8660 could just be initiating aerial hyphae production. After 3 days growth M145/pIJ8660, M145/pIJ8660-*Pscy*-*scy* and *scy*/pIJ8660-Pscy-scy appear to have formed spores as indicated by the grey spore colour. Whereas *scy*/pIJ8660 appears to be at the stage of aerial hyphae formation without the production of spores. These macroscopic observations are already suggestive that the *scy* phenotype has been complemented.

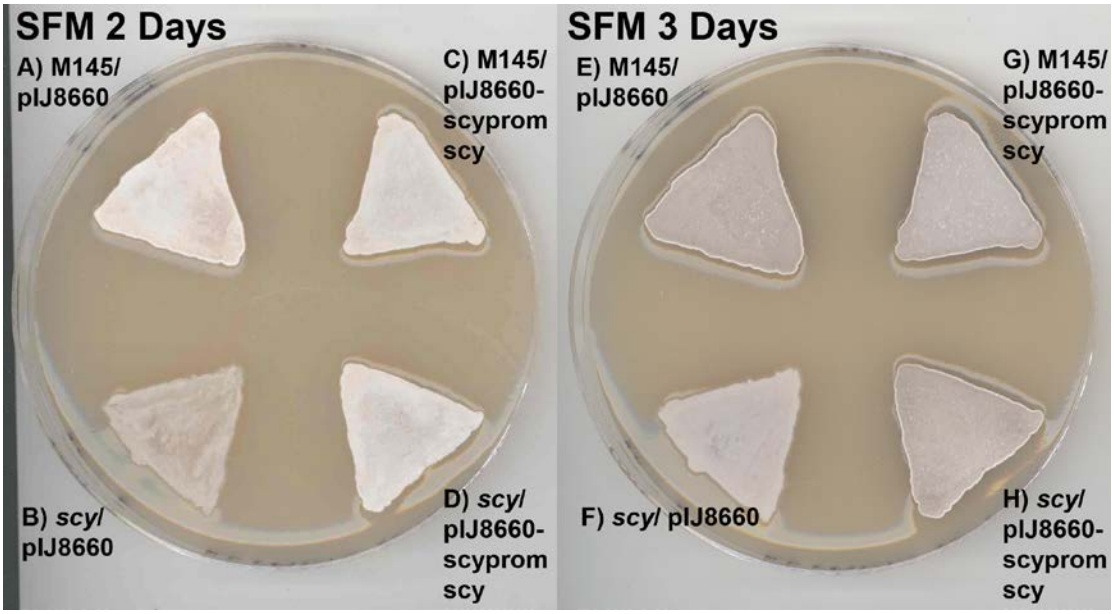

Figure 40: Macroscopic observations of the complementing strains shows that adding *scy in trans* can revert the scy mutant to wildtype. 10^6 spores were inoculated in a confluent triangle area on SFM medium and growth was monited after 2 days and 3 days at 30˚C. Confluent growth triangles consist of strains M145/pIJ8660 (A+E), scy/pIJ8660 (B+F), M145/pIJ8660-*Pscy*-*scy* (C+G) and scy/pIJ8660-*Pscy*-*scy* (D+H).

In order to assess if all the attributes to which were earlier associated with a *scy* phenotype have been complemented the DNA stain propidium iodide and the cell wall stain WGA-Alexa488 were used in combination with microscopy. This was performed in a similar way to the M145 and *scy* mutant strains as mentioned above, where strains were grown on SFM alongside coverslips. Time points were observed between 2-4 days in order to cover the spectrum of the developmental cycle. However, only a few examples of images are shown as the objective is only to assess if the phenotype has been complemented. To which examples of both vegetative hyphae and aerial hyphae for each strain are shown Figure 41. M145/pIJ8660 appears similar to M145 with nominal differences introduced by the pIJ8660 vector and the use of apramycin as a selectable marker. Figure 41A,B and Figure 41C display examples of M145/pIJ8660 vegetative hyphae and aerial hyphae, respectively.

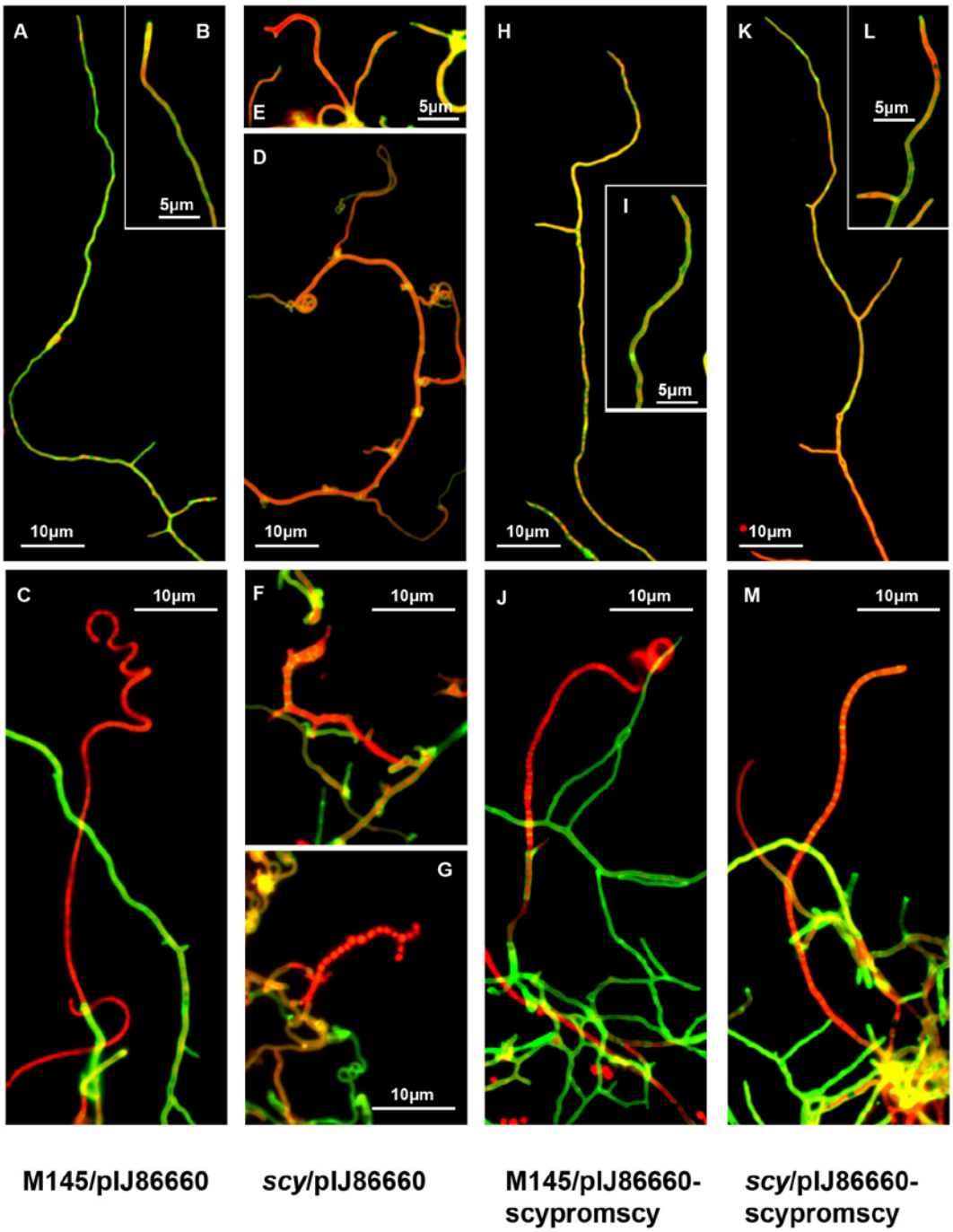

Figure 41: Microscopic observations of the complementing strains shows that adding *scy in trans* can revert the scy mutant to wildtype. Images of M145/pIJ8660 vegetative hyphae (A,B) and aerial hyphae (C) shown from coverslip samples displaying a wild-type phenotype. Images of *scy*/pIJ8660 vegetative hyphae (D,E) and aerial hyphae (F,G) shown from coverslip samples displaying a *scy* mutant phenotype. Images of M145/pIJ8660-scypromscy vegetative hyphae (H,I) and aerial hyphae (J) shown from coverslip samples with a wild-type-like phenotype despite dosage issues. Images of *scy*/pIJ8660-scypromscy vegetative hyphae (K,L) and aerial hyphae (M) shown from coverslip samples with a wild-type-like phenotype suggesting complementation of the *scy* mutation. Samples were grown for 2-4 days on agar plates alongside coverslips. Samples then stained with WGA-Alexa488 and propidium iodide. All images are overlayed with the two channels from WGA-Alexa488 (Green)/propidium iodide (Red). Scale bars are shown.

There was no apparent difference between *scy*/pIJ8660 and *scy*. To which Figure 41D and E display examples of *scy*/pIJ8660 vegetative hyphae with the characteristics documented above for *scy*. Figure 41F and G show *scy*/pIJ8660 aerial hyphae with the abnormal characteristics of *scy* aerial hyphae. The strain M145/pIJ8660-Pscy-scy encodes two copies of the *scy* gene. To which it may be expected that there could be issues due to dosage of *scy*. However, there were no striking differences of this strain to M145/pIJ8660. Examples of M145/pIJ8660-Pscy-scy vegetative hyphae can be seen in Figure 41H and I, showing no obvious defects. An example of an M145/pIJ8660-Pscy-scy aerial hyphae in Figure 41J shows normal septum positioning and prespore chain shape. Therefore, it would seem that a second copy of *scy* in this experiment has a negligible effect. It was observed that *scy*/pIJ8660-Pscy-scy was wild-type-like and the attributes of a *scy*-like phenotype were not apparent. Figure 41K and L show examples of *scy*/pIJ8660-Pscy-scy aerial hyphae, showing a smooth shape that is generally seen in the wild-type. Figure 41M shows an example of a *scy*/pIJ8660-Pscy-scy prespore chain with sporulation septa already marked and regularly spaced compartments. It also shows a non-branching phenotype. Therefore, it seems that the *scy* strain was complemented by the addition of pIJ8660-Pscy-scy, which suggests that the absence of *scy* is responsible for the phenotypic effects observed in this study. Although the *scy* mutant has had the apramycin resistance gene removed generating an in frame scar, it is also possible that the mutant phenotype is caused by a polar effect on other genes, for example if a promoter sequence was present in the *scy* open reading frame. However the complementation in this experiment by *scy* provided in trans would suggest that the phenotype is caused by deletion of the *scy* gene rather than a polar effect on downstream genes.

2.1.8 Summary

It was observed that the phenotype of the *scy* and the *scy-filP* mutant were different to M145 and *filP* macroscopically. This was seen across varying types of media. Microscopy revealed that the *scy* mutant had a phenotype with effects related to apical growth and branching. As well as in the process of cell division in relation to DNA segregation, irregular sporulation septation and reduced formation of spores. This same phenotype was seen in the *scy-filP* mutant. However the *filP* mutant did not have the same properties and displayed a more subtle phenotype. Therefore we conclude that the *scy-filP* mutant

phenotype results from a dominant effect of the *scy* mutation and it is not possible to determine if *filP* mutation has an additive effect.

3 Fluorescent Localisation Studies of Scy

3.1.1 Introduction

In order to determine the function of Scy *in vivo*, we fused *scy* to either *egfp* or *mCherry* to generate constructs expressing translational fusion proteins to the fluorescent proteins EGFP (Zhang *et al.*, 1996) or mCherry (Campbell *et al.*, 2002), respectively (for additional information see Appendix 11.1). This would allow us to monitor the subcellular localisation patterns of the protein. In order to confirm the localisation pattern of Scy, the fusion protein was fused to either terminus of Scy and also to different domains in order to probe the function of each domain.

3.2 Localisation of Scy using N-terminal fluorescent fusions

3.2.1 EGFP-Scy localises to hyphal tips

The plasmid pIJ8660-Pscy-egfp-scy (pK56; 10.1.46) enables expression of an EGFP-Scy fusion protein under the control of the native *scy* promoter sequence. The vector pIJ8660 (Sun *et al.*, 1999), enabled the introduction of this plasmid into *Streptomyces*. In order to introduce this plasmid to *Streptomyces* first we passaged the plasmid through the non-methylating *E. coli* strain *E. coli* ET12567 containing the plasmid pUZ8002 that facilitates conjugation into *S. coelicolor*. Plasmid pIJ8660 carries the *attP* site and an integrase which facilitates integration of a single copy of a *Pscy-egfp-scy* fragment at the *Φ*C31 attachment site into the *S. coelicolor* chromosome. The plasmid pIJ8660 also contains *aac(3)IV* allowing selection through apramycin resistance. When introduced into the strain M145 this generates a merodiploid strain carrying *scy* and *egfp-scy*. Conjugation efficiencies achieved with plasmid pIJ8660-Pscy-egfp-scy were very high. However, 2 representative colonies were chosen and propagated further so that spore preparations were generated. These 2 colonies were later found to be identical so the results of only 1 colony are shown here.

Spores of M145 carrying pIJ8660-Pscy-egfp-scy were grown on cellophane on top of SFM medium (as shown in Figure 124) for 12-16 hours and then visualised using fluorescence microscopy (Figure 42). EGFP-Scy localised primarily to the hyphal tips forming bright foci. Together with at other positions along the hyphal wall that could correspond to the

establishment of new sites for polar cell wall insertion and formation of new branch positions. The foci were not always the same size or intensity and occasionally extended further behind the tip, for reasons that cannot be explained at this point. Scy is positioned at the hyphal tip which is the location of active growth and cell wall extension. However, in this experiment samples were removed from their substrate medium, placed onto a microscope slide and snapshot images were taken in order to determine if EGFP-Scy was associated with growing tips. Live imaging and time lapse microscopy could not be used in this experimental setup as transferring the cellophane to a microscope slide and sealing with a coverslip depletes the hyphae of substrate medium, air and glycerol as well as nail varnish that are used in the mounting procedure would also disturb the growth. Time-lapse imaging has been attempted in the Kelemen lab with cellophanes, however, only limited videos could be captured due to technical problems such as sample drying out. In the field, other laboratories have had more success with live imaging when sandwiching mycelium between agar plugs and an oxygen permeable plastic dish, whilst incubating samples in a 30°C chamber and visualising with an inverted microscope (Jyothikumar *et al.*, 2008).

Creating a merodiploid strain of *S. coelicolor* did not disturb hyphal growth. However, there were present some minor disturbances such as curling hyphal branches that may deem this fusion only partially functional. However, this behaviour could be caused by introducing a second copy of *scy* or by introducing an artificial protein with an EGFP tag that may not behave exactly as in the native scenario. To assess whether the EGFP-Scy fusion protein was fully functional, pIJ8660-Pscy-egfp-scy was moved into the *scy* non-marked mutant strain. To test whether EGFP-Scy could complement the *scy* mutation we spread identical numbers of spores (10^6 in 15µl volume spread) of the strains; M145/pIJ8660, M145/pIJ8660-Pscy-egfp-scy, *scy*/pIJ8660 and *scy*/pIJ8660-Pscy-egfp-scy. This was to an approximate area of a 3cm equilateral triangle and spread with a sterile toothpick. The plates were then incubated at 30˚C and imaged after two day and three day time points (Figure 43). The strain *scy*/pIJ8660-Pscy-egfp-scy was more like the M145/pIJ8660 strain than the *scy*/pIJ8660 strain so EGFP-Scy did result in a significant reversion of the phenotypic effects of a *scy* mutant back into the phenotype observed for the wild-type. This would suggest that the EGFP-Scy fusion protein was able to function in a similar manner to the native Scy protein. However, there was a minor delay with strains M145/pIJ8660-Pscy-egfp-scy and *scy*/pIJ8660-Pscy-egfp-scy in comparison to M145/pIJ8660. This could be representative of a partial complementation. As the M145

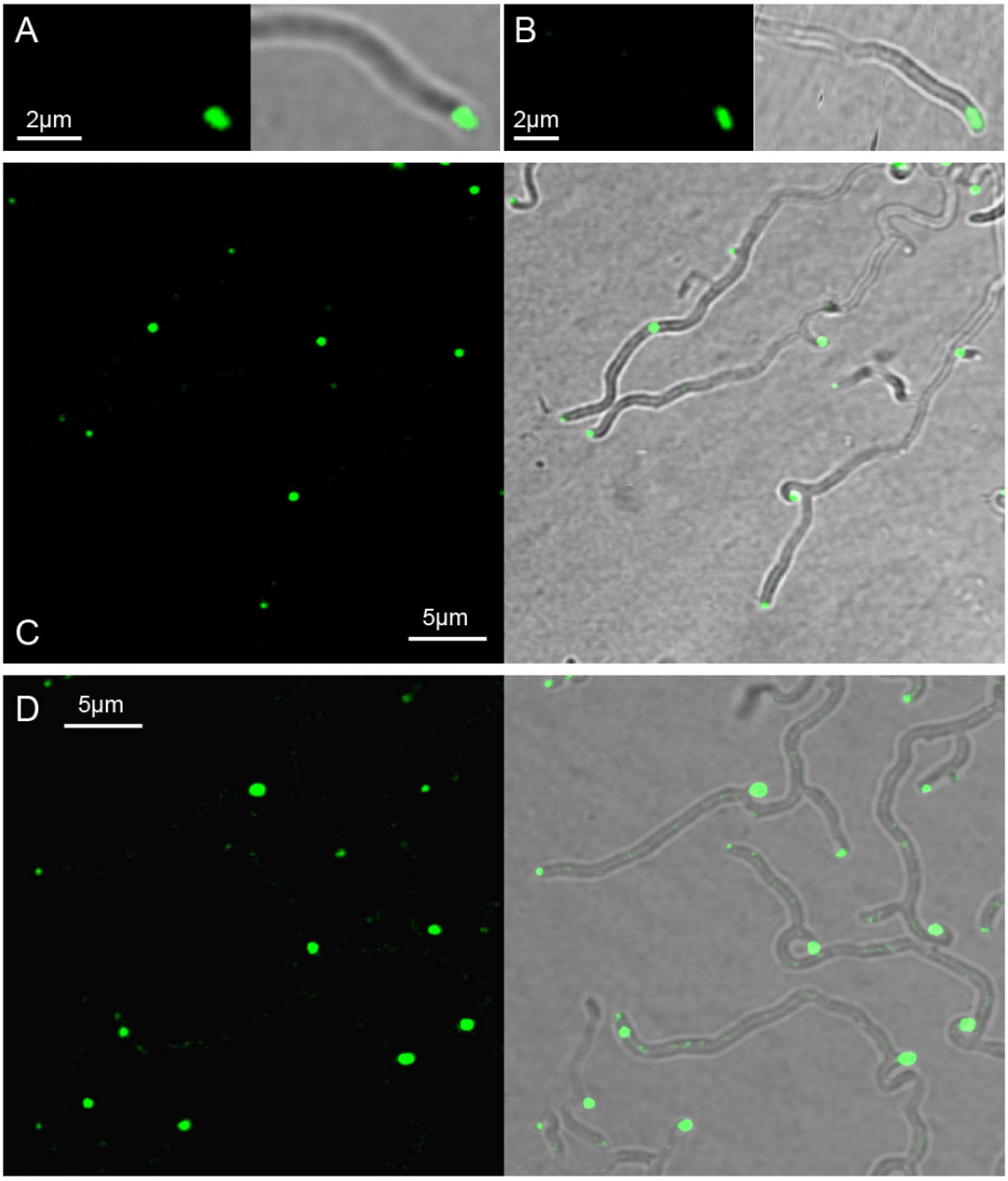

Figure 42: Localisation of EGFP-Scy was to foci at hyphal tips and along the hyphal walls. *S. coelicolor* M145 carrying pIJ8660-Pscy-egfp-scy, was grown for 16 hours on solid SFM medium supplemented with apramycin and the samples were viewed by laser-scanning confocal microscopy (A-D). Corresponding fluorescence images are left of the respective merged fluorescent and brightfield image. Scale bars are shown.

and *scy* backgrounds carrying pIJ8660-Pscy-egfp-scy look similar this would rule out a copy number effect and suggest that the partial complementation effect is due to the EGFP fusion protein not acting exactly like the native protein.

To test whether EGFP-Scy could complement the *scy* mutation and if all the attributes to which were earlier associated with a *scy* phenotype have been complemented the DNA stain propidium iodide and the cell wall stain WGA conjugated to Alexa-488 were used in

combination with microscopy. The strains M145/pIJ8660-Pscy-egfp-scy and *scy*/pIJ8660-Pscy-egfp-scy were grown on SFM alongside coverslips (as shown in Figure 123). Time points were observed between 2-4 days in order to cover the spectrum of the developmental cycle. However, only a few examples of images are shown as the objective is only to assess if the phenotype has been complemented. To which examples of both vegetative hyphae and aerial hyphae for each strain are shown Figure 44. There were no apparent differences of M145/pIJ8660-Pscy-egfp-scy and *scy*/pIJ8660-Pscy-egfp-scy in relation to M145/pIJ8660 (Figure 41) in terms of either vegetative growth or aerial growth. Therefore, suggesting that EGFP-Scy functions similarly to Scy in the vegetative hyphae grown alongside coverslips or in the development of aerial hyphae and the development of spore chains. Also, of note there were seemingly no dosage effects of the copy of *egfp-scy* in addition to the copy of *scy* in the wild-type.

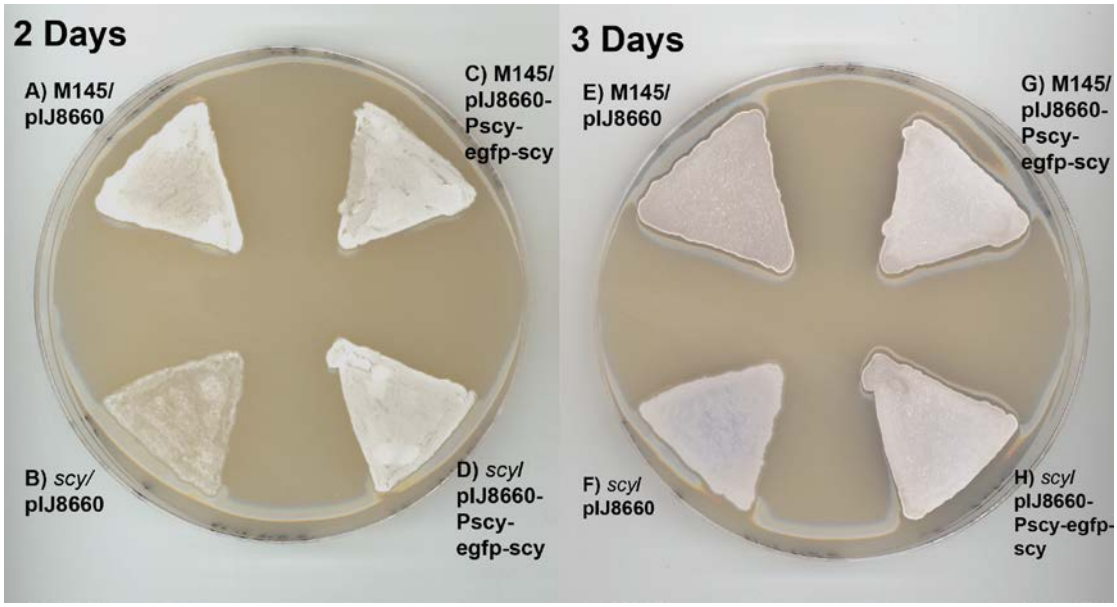

Figure 43: Complementation studies using strains expressing EGFP-Scy shows that adding *egfp-scy in trans* can revert the scy mutant to wildtype. 10^6 spores were inoculated in a confluent triangle area on SFM medium and growth was monitored after 2 and 3 days at 30˚C. Confluent growth of strains M145/pIJ8660 (A+E), *scy*/pIJ8660 (B+F), M145/pIJ8660-Pscy-egfp-scy (C+G) and *scy*/pIJ8660-Pscy-scy (D+H).

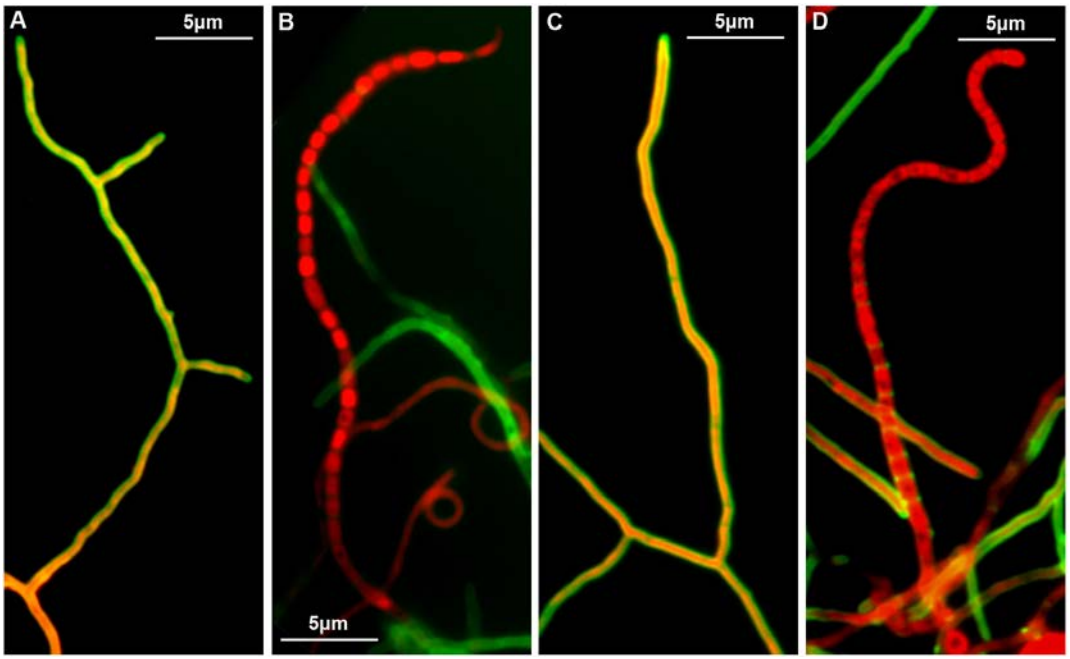

Figure 44: Microscopic observations show that adding *egfp-scy in trans* can revert the scy mutant to wildtype. Microscopy of the *scy* mutant complementation with pIJ8660-Pscy-egfp-scy. Images of M145/pIJ8660-Pscy-egfp-scy vegetative hyphae (A) and aerial hyphae (B) shown from coverslip samples displaying a wild-type phenotype. Images of *scy*/pIJ8660-Pscy-egfp-scy vegetative hyphae (C) and aerial hyphae (D) shown from coverslip samples also displaying a wild-type phenotype. Samples were grown for 2-4 days on agar plates alongside coverslips. Samples then stained with WGA-Alexa488 and propidium iodide. All images are overlayed with the two channels from WGA-Alexa488 (Green)/propidium iodide (Red). Scale bars are shown.

3.2.2 mCherry-Scy localises to hyphal tips

To establish the localisation of Scy with an mCherry fusion tag, partly in order to increase the flexibility of genetic tools available and also to determine if the protein functioned differently (and to perform co-localisation studies) the plasmid pIJ8660-Pscy-mCherry-scy (pK57 (Holmes *et al.*, 2013)) was constructed (10.1.47). The plasmid pIJ8660-Pscy-mCherry-scy is similar to pIJ8660-Pscy-egfp-scy except that it generates an mCherry-Scy fusion protein instead of an EGFP-Scy fusion protein. The vector pIJ8660-Pscy-mCherry-

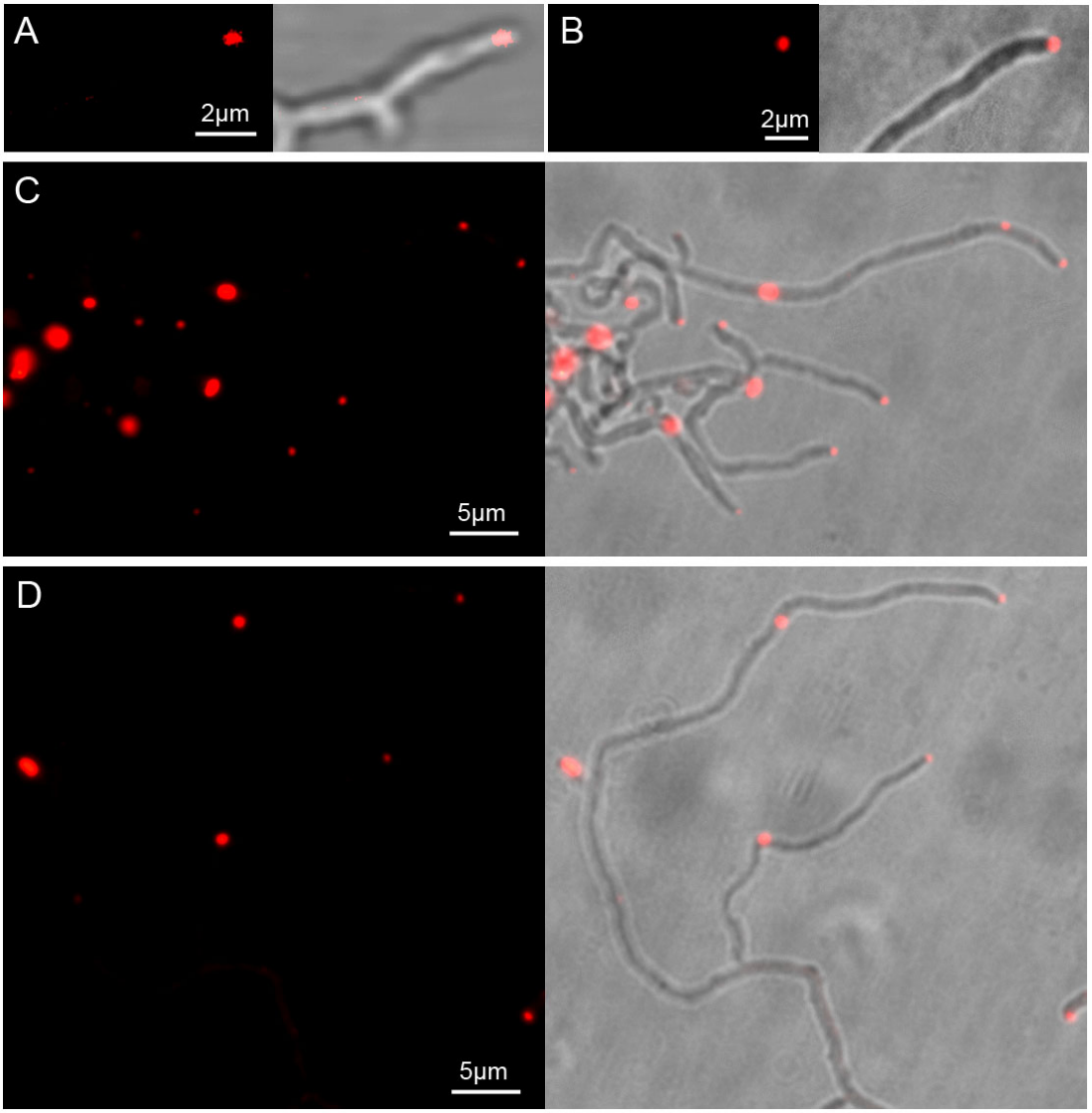

Figure 45: Localisation of mCherry-Scy was to foci at hyphal tips and along the hyphal walls. *S. coelicolor* M145/pIJ8660-Pscy-mCherry-scy, was grown for 16 hours on solid SFM medium and the samples were viewed by laser-scanning confocal microscopy (A-D). Corresponding fluorescence images are left of the respective merged fluorescent/brightfield image. Scale bars are shown.

scy was passaged into *Streptomyces* via conjugation with *E. coli* ET12567. When introduced into the strain M145 this generates a merodiploid strain carrying Scy and mCherry-Scy. Conjugation efficiencies achieved were very high, yet only 2 representative colonies were chosen and propagated further so that spore stocks were generated. These 2 colonies were later found to be identical so the results of only 1 colony are shown here.

Spores of M145 carrying pIJ8660-Pscy-mCherry-scy were similarly grown on cellophane on top of SFM medium for 12-16 hours and then visualised through fluorescence microscopy (Figure 45). Interestingly mCherry-Scy similarly to EGFP-Scy, localised primarily to the hyphal tips and at other lateral positions along the hyphal wall that could

correspond to future branch points. Similarly to EGFP, the foci were not always the same size or intensity and occasionally extended further behind the tip, for reasons that cannot be explained at this point. The mCherry-Scy foci were less bright than the EGFP-Scy foci and sometimes suffered problems of photobleaching, accountable to the physical properties of mCherry fluorescence in comparison to EGFP. This however, is not recognizable in the fluorescent images as the exposure was often set higher to obtain a visible signal. Similarly to the hyphae carrying EGFP-Scy there were present some minor disturbances associated with hyphal branching that are assumed to result in a similar fashion to the possible partial functioning of EGFP-Scy. M145 carrying pIJ8660-Pscy-mCherry-scy were wild-type-like and similar in phenotype to M145 carrying pIJ8660-Pscy-egfp-scy which we found was still functional despite minor phenotypic effects (Figure 43 and Figure 44).

3.3 Localisation of Scy using C-terminal fluorescent fusions

3.3.1 Scy-EGFP localises to hyphal tips

EGFP fusion proteins represent an important tool in studying protein localisation, though it is known in studies of eukaryotic cytoskeletal systems such as the microfilament protein actin that EGFP fusions can affect protein function (Westphal *et al.*, 1997; Deibler *et al.*, 2011; Ballestrem *et al.*, 1998). EGFP fusions can be used to discern *in vivo* behaviours of proteins regardless and in fact the behaviour of different EGFP fusions to complex proteins can be used as a dissection tool. Therefore, to verify localisation of Scy in *Streptomyces* and to further dissect the behaviour of this protein *in vivo* we aimed to generate a C-terminal fusion of EGFP to Scy (10.1.48). The plasmid pIJ8660-Pscy-scy-egfp enables expression of a Scy-EGFP fusion protein. The plasmid pIJ8660-Pscy-scy-egfp was mobilised into *Streptomyces coelicolor* M145. When introduced into the strain M145 this generates a merodiploid strain expressing the proteins

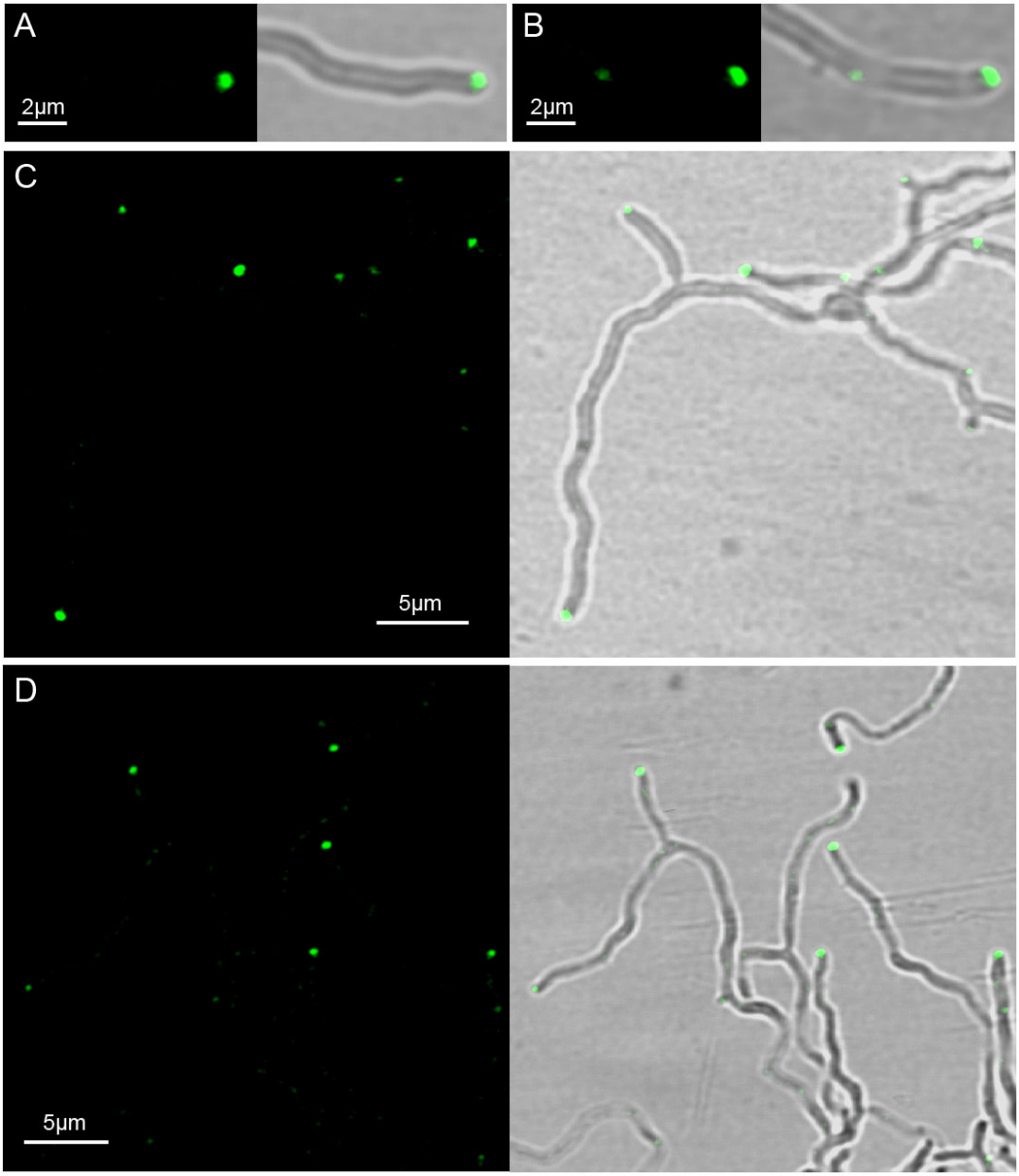

Figure 46: Localisation of Scy-EGFP was to foci at hyphal tips and along the hyphal walls. *S. coelicolor* M145/pIJ8660-Pscy-scy-EGFP, was grown for 16 hours on solid SFM medium supplemented with apramycin and the samples were viewed by laser-scanning confocal microscopy (A-D). Corresponding fluorescence images are left of the respective merged fluorescent/brightfield image. Scale bars are shown.

Scy and Scy-EGFP. Spores of M145 carrying pIJ8660-Pscy-scy-egfp were inoculated onto cellophane covering SFM medium and were incubated for 12-16 hours and then visualised through fluorescence microscopy (Figure 46). Scy-EGFP, similarly to EGFP-Scy, primarily localised to the hyphal tips and at other positions along the hyphal wall that likely correspond to future branch points. Consistent with the idea that changing the

positioning of the EGFP tag may change the *in vivo* dynamics of the protein behaviour, Scy-EGFP foci were less bright and suffered from photobleaching. For the sake of clarity, however, the signal is shown in Figure 46 prior to photobleaching. This could result due to less uptake of Scy-EGFP with native Scy or possibly less aggregation in comparision to EGFP-Scy and therefore Scy-EGFP could form less artificial structures. Scy-EGFP foci appear to follow the shape of the hyphal tip more than EGFP-Scy, however this could be caused by EGFP-Scy foci being brighter and therefore not resolving the shape of EGFP-Scy localisation as precisely. A microscopic difference between Scy-EGFP and EGFP-Scy is the less present minor disturbances associated with hyphal branching as seen in the microscopy (Figure 46), which could be due to less incorporation of Scy-EGFP into native structures or a possible more wild-type functioning Scy-EGFP than EGFP-Scy. Scy-EGFP was found to complement the phenotype associated with the aerial hyphae of a *scy* mutant in the same was as EGFP-Scy (11.2), so we assume that it is able to function somewhat like the native protein.

3.3.2 Fixing and propidium iodide staining of EGFP Scy fusions reveal a difference in N-terminal and C-terminal

It has long been suggested that polar localisation of proteins may in part depend on the positioning of the nucleoid which often does not find itself at the extremes of the cell or the at the midcell position (Wu, and Errington, 2011). In order to compare the localisation patterns of the EGFP fusions of Scy with DNA, we aimed to compare Scy localisation with the DNA stain propidium iodide. Whilst attempting this it was noticed that there were differences between M145 strains carrying pIJ8660-Pscy-egfp-scy and pIJ8660-Pscy-scy-egfp and their ability to withstand downstream treatments. Spores of each strain were similarly grown on cellophane on top of SFM medium for 12-16 hours. After which $1cm^2$ squares of cellophane were cut with a razor blade and stained as was done for the mutant analysis on cellophane. That is they were first fixed with methanol. Following this they were washed and stained with propidium iodide. They were washed again to remove unbound dye and then visualised through fluorescence microscopy (Figure 47).

It was observed that EGFP-Scy foci were able to withstand the chemical treatment associated with fixing and then staining, whereas Scy-EGFP foci were not visible after methanol fixation and PI staining. This could be due to the same reason that Scy-EGFP foci were less bright and suffered from photobleaching, perhaps representing a lower

abundance of this fusion protein at the hyphal tip complexes. It may also represent the dynamic distribution that might be needed with a protein perhaps associated with hyphal tip growth when the cells are no longer viable and the tips aren't growing. Whereas EGFP-Scy might form aggregates and the dynamics less susceptible to environmental conditions or cessation of growth. It is also of note that EGFP-Scy can be found in regions of less DNA staining in the cell, consistent with the observations above that the tips are absent of DNA. Scy localisation might by influenced by a system analogous to nucleoid occlusion; however, EGFP-Scy foci cannot be seen at all hyphal segments that are less staining with PI.

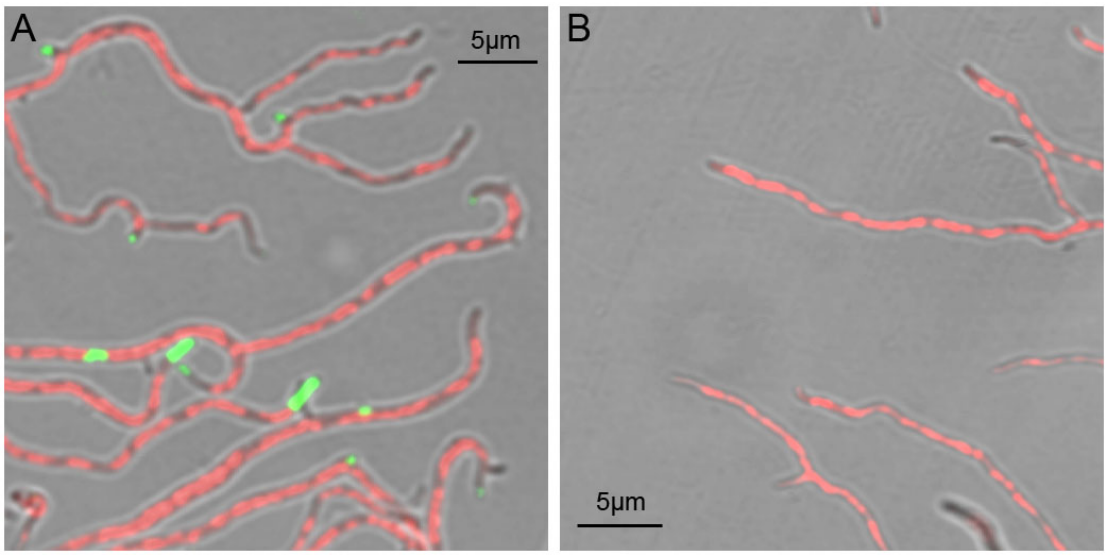

Figure 47: Localisation of EGFP-Scy and Scy-EGFP with staining and fixing reveal differences in the fusion proteins ability to withstand treatment. Localisation of EGFP-Scy (A) in green can be seen to form foci at hyphal tips and along the hyphal walls. Green signal of Scy-EGFP (B) cannot be visualised in these hyphae. *S. coelicolor* M145/pIJ8660-Pscy-EGFP-scy and M145/pIJ8660-Pscy-scy-EGFP, were grown for 16 hours on solid SFM medium, samples then fixed with methanol and stained with propidium iodide. The samples were viewed by laser-scanning confocal microscopy. All images are overlayed with the two channels green (protein) and propidium iodide (Red) then fluorescencent images are merged with the brightfield image. Scale bars are shown.

3.3.3 Scy-mCherry localisation was not discernable in the plasmid pIJ8660-Pscy-scy-mCherry

To further assess the localisation of Scy with a C-terminal fluorescent fusion/increase the genetic toolbox for study (and to perform co-localisation studies), a Scy-mCherry C-terminal fusion was constructed (10.1.49). The plasmid pIJ8660-Pscy-scy-mCherry encodes a Scy-mCherry fusion protein. Being a pIJ8660 derivative the plasmid was

mobilised into *Streptomyces* via *E. coli* ET 12567/pUZ8002. M145 carrying pIJ8660-Pscy-scy-mCherry was inoculated onto cellophane covering SFM medium and then visualised using fluorescence microscopy (Figure 48). Surprisingly, we could not detect strong foci at tip positions (although occasional weak tip signals could be seen) or at sites along the hyphal wall. Instead it was observed that there was a weak diffuse mCherry signal throughout the hyphae. Introduction of pIJ8660-Pscy-scy-mCherry into the *scy* mutant resulted in a complementation of the *scy* mutant phenotype suggesting that there might be free Scy protein in the hyphae. The lack of tip-localised Scy-mCherry foci in the strain carrying pIJ8660-Pscy-scy-mCherry was likely to be the result of the absence of Scy-mCherry produced. We confirmed the plasmid is correct and that the strain tested contained the correct plasmid. Linkers can affect fusion proteins and they might be target sites for proteolytic enzymes. Alternatively a linker site might then favour optional sequences for an alternative translational start site, which would enable translation of mCherry independently of Scy.

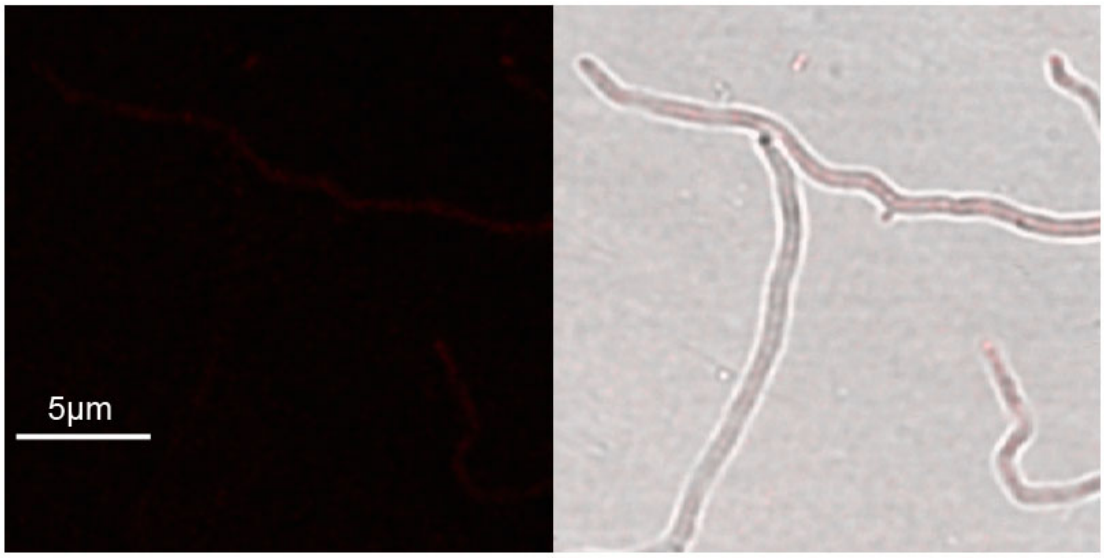

Figure 48: Scy-mCherry was not detectable at hyphal tips. The Scy-mCherry fusion had a weak diffuse signal, red channel (left); with brightfield merged with red channel (right). *S. coelicolor* M145/pIJ8660-Pscy-mCherry-scy, was grown for 16 hours on solid SFM medium and the samples were viewed by laser-scanning confocal microscopy. Scale bars are shown.

3.3.4 Scy-Δlink-mCherry localised to hyphal tips

As the plasmid pIJ8660-Pscy-scy-mCherry did not generate a signal, we wanted to test the fusion by removing the His-Met-Gly-Gly-Gly-Gly-Gly linker to assess the localisation of Scy with a C-terminal functioning mCherry fluorescent fusion. The plasmid pIJ8660-Pscy-scy-Δlink-mCherry was constructed (10.1.50) which encodes a fusion to the C-terminus of Scy generating a Scy-mCherry fusion protein where Scy is joined to mCherry without a glycine linker for spacing as was done previously for the other fusions. Being a pIJ8660 derivative the plasmid was mobilised into *Streptomyces* via conjugation with *E. coli* ET12567/pUZ8002. M145 carrying pIJ8660-Pscy-scy-Δlink-mCherry was grown on cellophane on top of SFM medium and then visualised using fluorescence microscopy (Figure 49). We could clearly identify Scy-mCherry at hyphal tips and at some additional lateral positions. This was consistent with the localisation that observed when expressing Scy-EGFP, EGFP-Scy or mCherry-Scy. In addition to the strong tip foci we could visualise some dispersed red fluorescence throughout the hyphae. Introduction of pIJ8660-Pscy-scy-mCherry into the *scy* mutant resulted in a complementation of the *scy* mutant phenotype, suggesting the Scy-mCherry fusion protein was functional. The reasons for the difference between constructs carrying a linker or no linker are not clear. It is possible that the linker is more prone to proteolysis in certain cases or that alternative translational starts sites are used.

3.4 Detection of Scy fluorescent fusion proteins

In order to confirm the successful expression of fusion proteins of Scy to the respective fluorescent proteins, cell extracts of *S. coelicolor* were analysed on SDS-PAGE gels under semi-denaturing conditions that allow the folding of the fluorescent proteins and visualised using a phosphoimager with settings that could detect the fluorophores. This method of fluorescence scanning has been used previously to successfully analyse the expression of a ParB-EGFP fusion protein in *S. coelicolor* (Jakimowicz *et al.*, 2005a). Spores of M145 carrying either pIJ8660-Pscy-egfp-scy, pIJ8660-Pscy-mCherry-scy, pIJ8660-Pscy-scy-egfp or pIJ8660-Pscy-scy-mCherry were inoculated onto cellophane on top of SFM medium for 18 hours. Cells were then collected from the cellophane surface and were resuspended in a Tris-Magnesium buffer. Cells were lysed using FastPrep treatment, which disrupts the cells

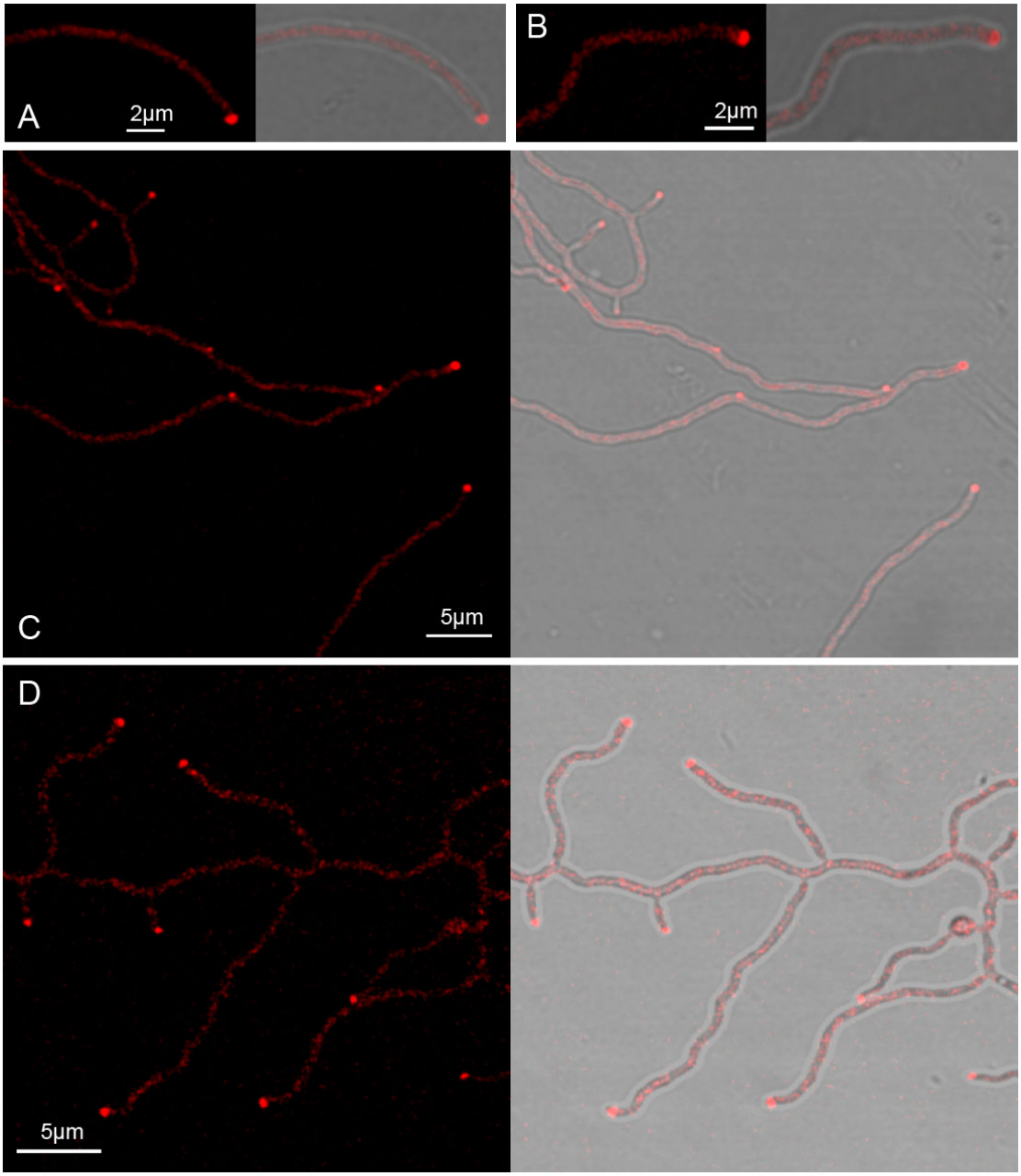

Figure 49: Localisation of Scy-Δlink-mCherry was to foci at hyphal tips as well as a more diffuse signal in other locations. *S. coelicolor* M145/pIJ8660-Pscy-scy-Δlink-mCherry, was grown for 16 hours on solid SFM medium and the samples were viewed by laser-scanning confocal microscopy (A-D). Corresponding fluorescence images are left of the respective merged fluorescent/brightfield image. Scale bars are shown.

by vigorous shaking in the presence of <106µm glass particles. The cell extracts were centrifuged to separate both pellet and supernatant, of which the pellet was re-suspended in the same buffer as before. The supernatants and pellets were then analysed on SDS-PAGE gels whereby the samples were not boiled prior to loading therefore preventing denaturation of the fluorescent tags and maintaining fluorescence activity (Figure 50).

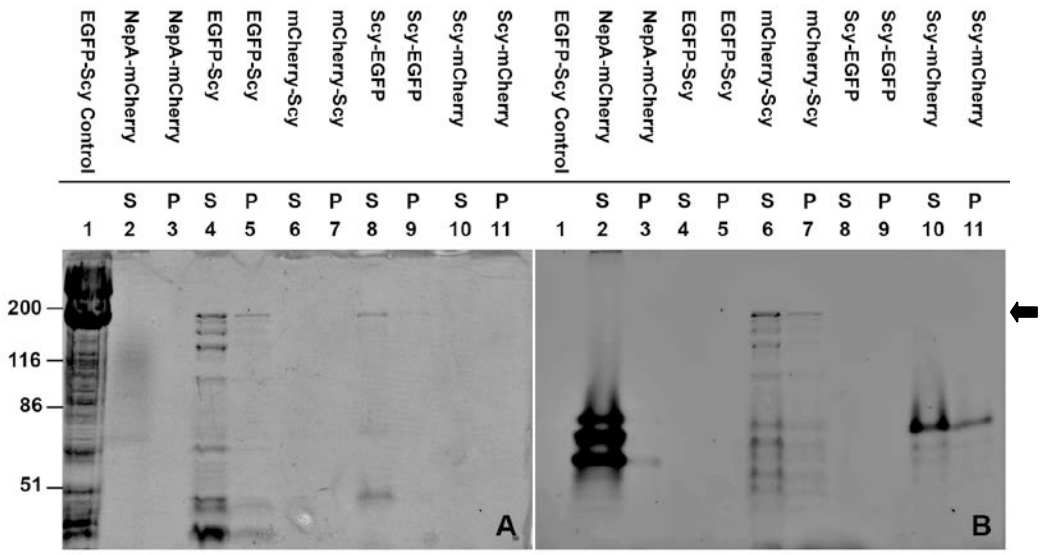

Figure 50: SDS-PAGE was used to detect the Scy fluorescent fusion proteins. For analysis of the EGFP fusions the gel was excited at 488nm and the emission read at 532nm (A). For analysis of the mCherry fusions the gel was excited at 532nm and the emission read at 555nm (B). A control of the Supernatant of a cell extract of *E.coli* expressing EGFP-Scy was used (Holmes and Kelemen, unpublished) (Lane 1). Also, a control of cell extracts of *S. coelicolor* expressing NepA-mCherry after 40 hours growth was used (Lane 2 & 3). A signal can be seen for cell extracts of M145/pIJ8660-Pscy-egfp-scy (Lane 4 & 5). A signal can be seen for cell extracts of M145/pIJ8660-Pscy-mCherry-scy (Lane 6 & 7). A signal can be seen for cell extracts of M145/pIJ8660-Pscy-scy-egfp (Lane 8 & 9). A high molecular weight signal could not be seen for cell extracts of M145/pIJ8660-Pscy-scy-mCherry (Lane 10 & 11). Samples were separated into both Supernatant fractions (S) and Pellet fractions (P). Shown on the left hand side are the positions and sizes of a protein MW marker (not visible on images shown) displayed in kDa.

The gel was visualised for EGFP activity by exciting at 488nm and the emission was then detected at 532nm (Figure 50A). Similarly to monitor mCherry activity the gel was excited at 532nm and the emission was then detected at 555nm (Figure 50B). The expected size for the EGFP-Scy fusion protein from pIJ8660-Pscy-egfp-scy was 173.8kDa, there was a higher molecular weight band that could correspond with this size. If a fusion protein wasn't present then free EGFP would run at 27.1kDa, which would migrate much further in the gel. It was also seen that there were similar high molecular weight bands for pIJ8660-Pscy-mCherry-scy (mCherry-Scy; 173.6kDa) and pIJ8660-Pscy-scy-egfp (Scy-EGFP; 174.1kDa), corresponding to the size of a Scy fluorescent protein fusion. Similarly a cell extract from *E. coli* overexpressing EGFP-Scy (Chapter 7) generated a band at a similar position. Therefore, it is reasonable to suggest that these bands are evidence that the fusion proteins were successfully being produced in *S. coelicolor*. It can also be seen that there are bands of smaller sizes, these could possibly be products of partial degradation of the protein. It is unclear if this reflects proteolytic activity in the hyphae and/or could be damaged/dead hyphae or partially proteolysed protein produced when lysing the cells. It is

interesting to note that the higher proportion of activity of the Scy fusion proteins is in the supernatant fractions suggesting that Scy is cytoplasmic or membrane bound. However, the activity in the pellet could correspond to insoluble Scy aggregates, cell wall bound Scy or Scy from unlysed cells. Strikingly the strain expected to express Scy-mCherry joined by a gly linker does not have a high molecular weight band. This could explain why there was no significant tip signal corresponding to the localisation of Scy. It would suggest that somehow an intact fusion of Scy to mCherry is not present. Perhaps an explanation for this could be that either this fusion for some reason is more susceptible to protein degradation or it could be that it is not expressed correctly perhaps with translation occurring at a methionine located within the linker or at the beginning of *mCherry*. These results do not exclude the possibility that degradation removing the *mCherry* tag could leave the wildtype protein intact and therefore explain why pIJ8660-Pscy-scy-mCherry can complement the *scy* mutant.

We could, however, detect Scy-mCherry at the tips of the strain expressing Scy-mCherry without the penta-glycine linker (Figure 49). Cell extracts from the strain of M145 carrying pIJ8660-Pscy-scy-Δlink-mCherry were also analysed on partially denaturing SDS Polyacrylamide gels (Figure 51). There was a visible faint higher molecular weight band corresponding to the size of a Scy-Δlink-mCherry (173.3kDa) fluorescent protein fusion, running at approximately the same size as an mCherry-Scy fusion protein. The Scy-mCherry fluorescent protein fusion was more visible in the supernatant fraction suggesting that it was cytoplasmic or membrane bound. Therefore, it is reasonable to suggest that the Scy-mCherry fusion protein was successfully being produced in *S. coelicolor* backing up the microscopy observations.

3.5 Localisation of the N-terminal and C-terminal domains of Scy

3.5.1 The C-terminal domain of Scy can localise to hyphal tips

Scy has two main domains, a small N-terminal heptad coiled-coil domain and a large non-heptad coiled-coil domain (Walshaw *et al.,* 2010). To test whether the N or C terminal domain alone are sufficient for tip localisation we generated *egfp* fusions to DNA encoding either the Scy-N domain or the Scy-C domain (10.1.51). The vectors pIJ8660-Pscy-egfp-scy-C and pIJ8660-Pscy-egfp-scy-N encode fusions of EGFP to the N-terminus of either the Scy-C or the Scy-N domains, respectively. These pIJ8660 derivatives were mobilised

into *Streptomyces* via conjugation with *E. coli* ET 12567/pUZ8002. Introduction of either pIJ8660-Pscy-egfp-scy-C and pIJ8660-Pscy-egfp-scy-N into the *scy* mutant failed to result

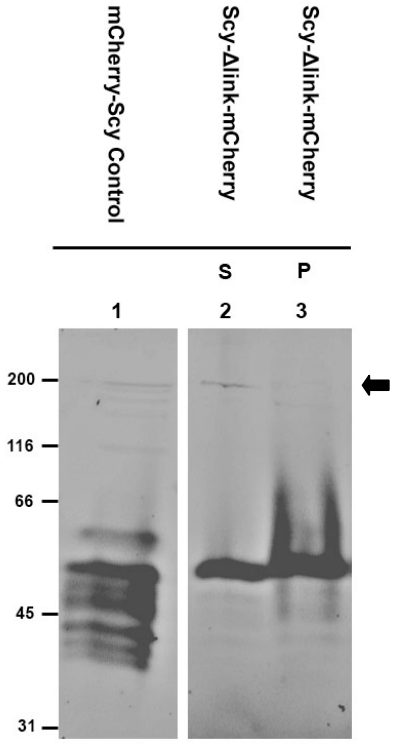

Figure 51: SDS-PAGE was used to detect the Scy-Δlink-mCherry fluorescent fusion protein. For analysis of the Scy-Δlink-mCherry fluorescent fusion the gel was excited at 532nm and the emission read at 555nm. A control of the Supernatant of a cell extract of M145/pIJ8660-Pscy-mCherry-scy was used (Lane 1). A signal can be seen for cell extracts of M145/pIJ8660-Pscy-scy-Δlink-mCherry (Lane 2 & 3). Samples were separated into both Supernatant fractions (S) and Pellet fractions (P). Shown on the left hand side are the positions and sizes of a protein MW marker (not visible on images shown) displayed in kDa. The arrow shows the size of the higher molecular weight band representing a fusion protein.

in complementation of the *scy* mutant phenotype (11.2). M145 carrying either pIJ8660-Pscy-egfp-scy-C or pIJ8660-Pscy-egfp-scy-N was grown on cellophane on top of SFM medium and then visualised using fluorescence microscopy (Figure 52). EGFP-Scy-C was able to form foci at the hyphal tip and foci along the hyphal wall in a manner similar to EGFP-Scy. This signal was also observed in a *scy* mutant carrying pIJ8660-Pscy-egfp-scy-C (data not shown) suggesting that the C-terminal domain of Scy is capable of localising without the native protein present. EGFP-Scy-N did not generate foci at tip positions or at sites along the hyphal wall (Figure 52B). Instead it was observed that there was a weak diffuse EGFP signal throughout the hyphae. Therefore, suggesting that EGFP-Scy-N cannot localise to apical growth sites even when the native protein is present. The expression of truncated EGFP fusions of Scy in cell extracts of *S. coelicolor* expressing EGFP-Scy-N or EGFP-Scy-C were assessed on SDS-PAGE gels under semi-denaturing conditions and the fluorophore activity was detected with a phosphoimager. Spores of M145 carrying either pIJ8660-Pscy-egfp-scy-N or pIJ8660-Pscy-egfp-scy-C were inoculated onto cellophane on top of SFM medium for 18 hours. Cells were collected

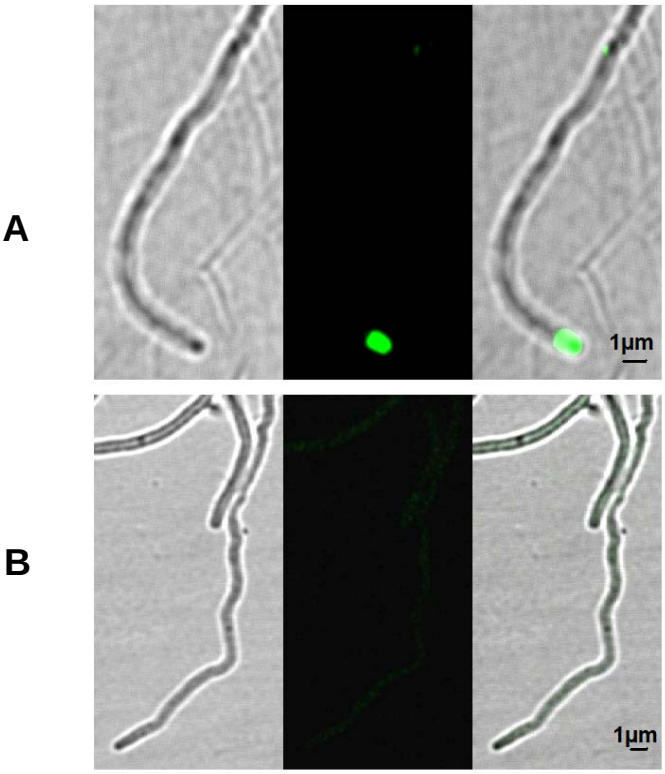

Figure 52: EGFP-Scy-C localised to hyphal tips whereas EGFP-Scy-N was not detectable at hyphal tips. Localisation of EGFP-Scy-C to the hyphal tips (A); with brightfield (left), EGFP fluorescence (middle) and a merged image (right). The EGFP-Scy-N fusion had a diffuse signal (B); with brightfield (left), EGFP fluorescence (middle) and a merged image (right). *S. coelicolor* M145 carrying either pIJ8660-Pscy-egfp-scy-C and pIJ8660 pIJ8660-Pscy-egfp-scy-N, were grown for 16 hours on solid SFM medium and the samples were viewed by laser-scanning confocal microscopy. Scale bars are shown.

from the cellophane surface, lysed and separated into supernatant and pellet fractions as described previously (3.4). The samples were then analysed on SDS-PAGE gels whereby the samples were not boiled prior to loading therefore preventing denaturation of the fluorescent tags and maintaining fluorescence activity. The gel was visualised for EGFP activity by exciting at 488nm and the emission was then detected at 532nm (Figure 53). The expected size for the EGFP-Scy-C fusion protein would be 165.8kDa, it was seen that there were high molecular weight bands for pIJ8660-Pscy-egfp-scy-C corresponding to a similar size. These also ran to a similar distance as for M145/pIJ8660-Pscy-egfp-scy as well as a cell extract from *E. coli* overexpressing EGFP-Scy-C which both generated a band at a similar position. It is unclear if there is a migration distance difference between full length and Scy-C fusions, as the N-terminal is only small and the difference is unlikely to be resolved. It can also be seen that there are bands of smaller sizes that could correspond to degradation products. For M145/pIJ8660-Pscy-egfp-scy-N, the expected size of the EGFP-Scy-N fusion is 36kDa, so not suprisingly there were no higher molecular weight bands visible. However, in comparison to the control of EGFP from *S. coelicolor* and EGFP-Scy-N from *E. coli*, as well as the matching to degradation products in EGFP-

Scy-C it cannot be concluded that the EGFP seen has the small sized Scy-N domain attached. In this case the free EGFP from *S.coelicolor* does not run to the expected size of 27.1kDa, which could be caused by oligomerisation of EGFP. Perhaps more detailed proteomic analysis would be of use to follow up this experiment. Signals for both samples can be seen in both Supernatant and Pellet fractions, this is not necessarily dissimilar to the full length Scy protein; however, the very highest band of EGFP-Scy-C is more present in the Pellet fraction, when it was more visible in the Supernatant fraction of the full length protein. Therefore, possibly suggesting that the full length protein needs to be intact for correct folding/positioning in the cytoplasm or the membrane.

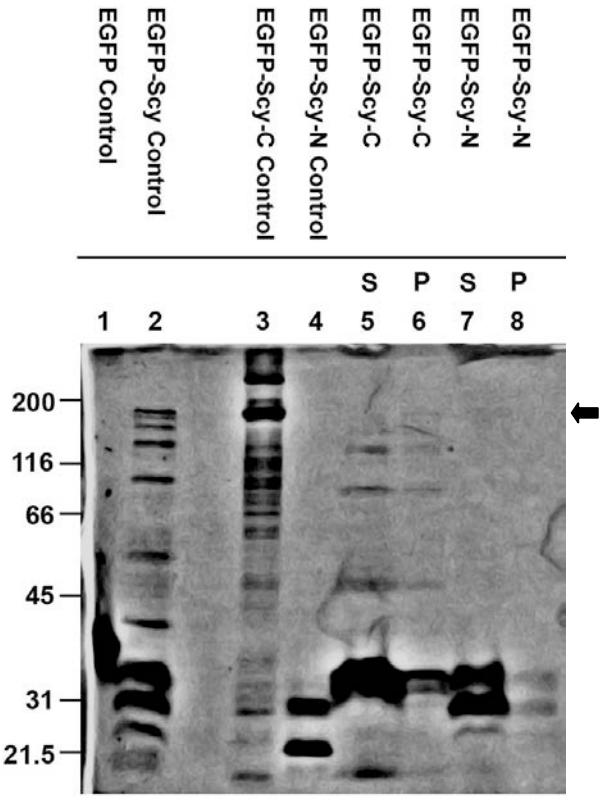

Figure 53: SDS-PAGE was used to detect EGFP-Scy-C and EGFP-Scy-N fluorescent fusion proteins. The gel was excited at 488nm and the emission read at 532nm for analysis of EGFP fusions. A control of the Supernatant of a cell extract of *S. coelicolor* expressing EGFP from Psco4002 (Holmes and Kelemen, unpublished) (Lane 1). A control of the Supernatant of a cell extract of M145/pIJ8660-Pscy-egfp-scy (Lane 2). Controls of Supernatants of cell extracts of *E.coli* expressing EGFP-Scy-C (Lane 3) and EGFP-Scy-N (Lane 4) (Holmes and Kelemen, unpublished). Supernatant (S) and Pellet (P) of a cell extract of M145/pIJ8660-Pscy-egfp-scy-C (Lane 5 & 6) shows a high molecular weight band corresponding to EGFP-Scy-C. Supernatant (S) and Pellet (P) of a cell extract of M145/pIJ8660-Pscy-egfp-scy-N (Lane 7 & 8) shows the abolition of a high molecular weight band, though EGFP-Scy-N runs to a similar height as EGFP (Lane 1).

Shown on the left hand side are the positions and sizes of a protein MW marker (not visible on images shown) displayed in kDa. The arrow shows the size of the higher molecular weight band representing an EGFP-Scy or EGFP-Scy-C fusion protein.

3.5.2 Scy-N-EGFP localisation was not discernable in the plasmid pIJ8660-Pscy-scy-N-egfp

To test whether the N-terminal domain of Scy is unable to localise in *S. coelicolor*, we aimed to generate an EGFP fusion to the C-terminal end of Scy-N. As *egfp* would be on

the C-terminal side of the sequence encoding the Scy-N domain, it would possibly rule out the event that EGFP-Scy-N does not localise because the N-terminal end of Scy-N is important for recruitment to a subcellular site. The reason why we thought that this might be relevant is that there have been previous reports for DivIVA that suggest that the N-terminal may significantly contribute to subcellular localisation (Lenarcic *et al.*, 2009; Oliva *et al.*, 2010). The plasmid pIJ8660-Pscy-scy-N-egfp was constructed (10.1.53), which encodes a fusion of EGFP to the C-terminus of the Scy-N domain expressing Scy-N-EGFP. The plasmid was mobilised into *Streptomyces* via *E. coli* ET 12567/pUZ8002. Introduction of pIJ8660-Pscy-scy-N-egfp into the *scy* mutant failed to result in complete complementation of the *scy* mutant phenotype (11.2). M145 carrying pIJ8660-Pscy-scy-N-egfp was grown on cellophane on top of SFM medium and then visualised using fluorescence microscopy (Figure 54). Scy-N-EGFP similarly to EGFP-Scy-N generated a weak diffuse EGFP signal throughout the hyphae. Therefore, ruling out the possibility that the failure of Scy-N to localise in the previous experiment was from an abnormality generated from the EGFP being positioned on the N-terminus, that is EGFP was not necessarily blocking something on the amino terminus of Scy-N.

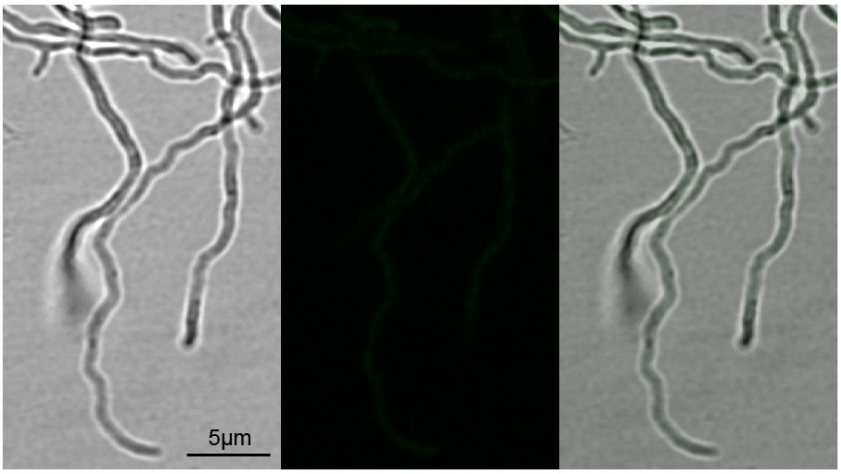

Figure 54: Scy-N-EGFP was not detectable at hyphal tips. The Scy-N-EGFP fusion had a diffuse signal; with brightfield (left), EGFP fluorescence (middle) and a merged image (right). *S. coelicolor* M145 carrying pIJ8660-Pscy-scy-N-egfp, was grown for 16 hours on solid SFM medium and the samples were viewed by laser-scanning confocal microscopy. Scale bars are shown.

3.5.3 Summary

It was observed that fluorescent fusion proteins of Scy localised to the hyphal tips and branch sites of *Streptomyces*. In combination with the phenotypic effects of the *scy* mutant this would suggest that Scy somehow in *vivo* functions at the hyphal tip possibly with a role in cell shape determination and cell extension. Placing of the fluorescent tag on different ends of the protein did not change the localisation of Scy to hyphal tips and branches, but did show slight differences in complentation and foci formation. Truncations of the Scy coiled-coil domains showed that the N-terminal domain is dispensible for localisation and that the C-terminal domain may drive Scy to polar sites.

4 Scy and its possible role during apical growth and cell division

4.1.1 Introduction

As the phenotype of the *scy* mutant and the Scy localisation data suggested that Scy was involved in apical growth, we wanted to explore this further by looking at the apical determinat DivIVA or by looking at active cell wall growth. Therefore we wanted to see if Scy colocalised at actively growing hyphal tips with DivIVA and/or cell wall synthesis. Further we wanted to monitor DivIVA or cell wall synthesis in the *scy* mutant. We also wanted to test the function of Scy further by overexpressing *scy* and finding the effect of overexpression on DivIVA or cell wall synthesis insertion and branching dynamics. As a comparison we also replicated DivIVA overexpression experiments from Flärdh (2003a) with the intent of combing Scy localisation. As a *scy* mutant also had defects in terms of cell division we also wanted to look at the localisation patterns of the cell division proteins FtsZ and ParB to reveal any new insight into this phenotype.

4.1.2 Scy co-localises with DivIVA and sites of new cell wall insertion

As initial analysis suggests that Scy localises at hyphal tips, this is also the location of new cell wall insertion as marked by fluorescent vancomycin (Van-Fl) staining (Daniel, and Errington, 2003) and localisation of the predicted PBP interacting protein DivIVA (Flärdh, 2003a).

Therefore, to determine if Scy is localised to actively growing hyphal tips it was sought to monitor Scy localisation in comparison to DivIVA-EGFP or Van-Fl. Because both DivIVA-EGFP and Van-Fl emit green fluorescence, for co-localisation studies we had to use the mCherry fusions to Scy. The construct pIJ8660-Pscy-mCherry-scy was introduced into M145 carrying pKF59 (Flärdh, 2003a), which itself generates a DivIVA-EGFP fusion. M145/pKF59/pIJ8660-Pscy-mCherry-scy expressing both mCherry-Scy and DivIVA-EGFP was grown on cellophane placed on top of SFM medium and after 12-18 hours growth the cellophane discs with the growing hyphal filaments were visualised using fluorescence microscopy. DivIVA-EGFP and mCherry-Scy co-localised not only at hyphal tips but also at sites along the lateral wall (Figure 56). As it has previously been shown that

DivIVA-EGFP localises to sites of future tip positions prior to branch formation (Hempel *et al.*, 2008) this also suggests that Scy localises to *de novo* sites of tip formation. To monitor new cell wall synthesis, M145/pIJ8660-Pscy-mCherry-scy was grown on cellophane placed on top of SFM medium and the growing hyphae were stained with a mixture of 1 µg/ml BODIPY FL vancomycin (Molecular Probes) and 1 µg/ml unlabelled vancomycin (Sigma) for 5 minutes prior to collection of the sample, which was visualised using fluorescence microscopy. mCherry-Scy co-localised with fluorescent vancomycin, therefore, Scy marks sites of new cell wall synthesis (Figure 56). Therefore, together with its co-localisation with DivIVA, these observations suggest that Scy as well as DivIVA are implicated in the placement of the cell wall synthetic machinery and hyphal tip growth.

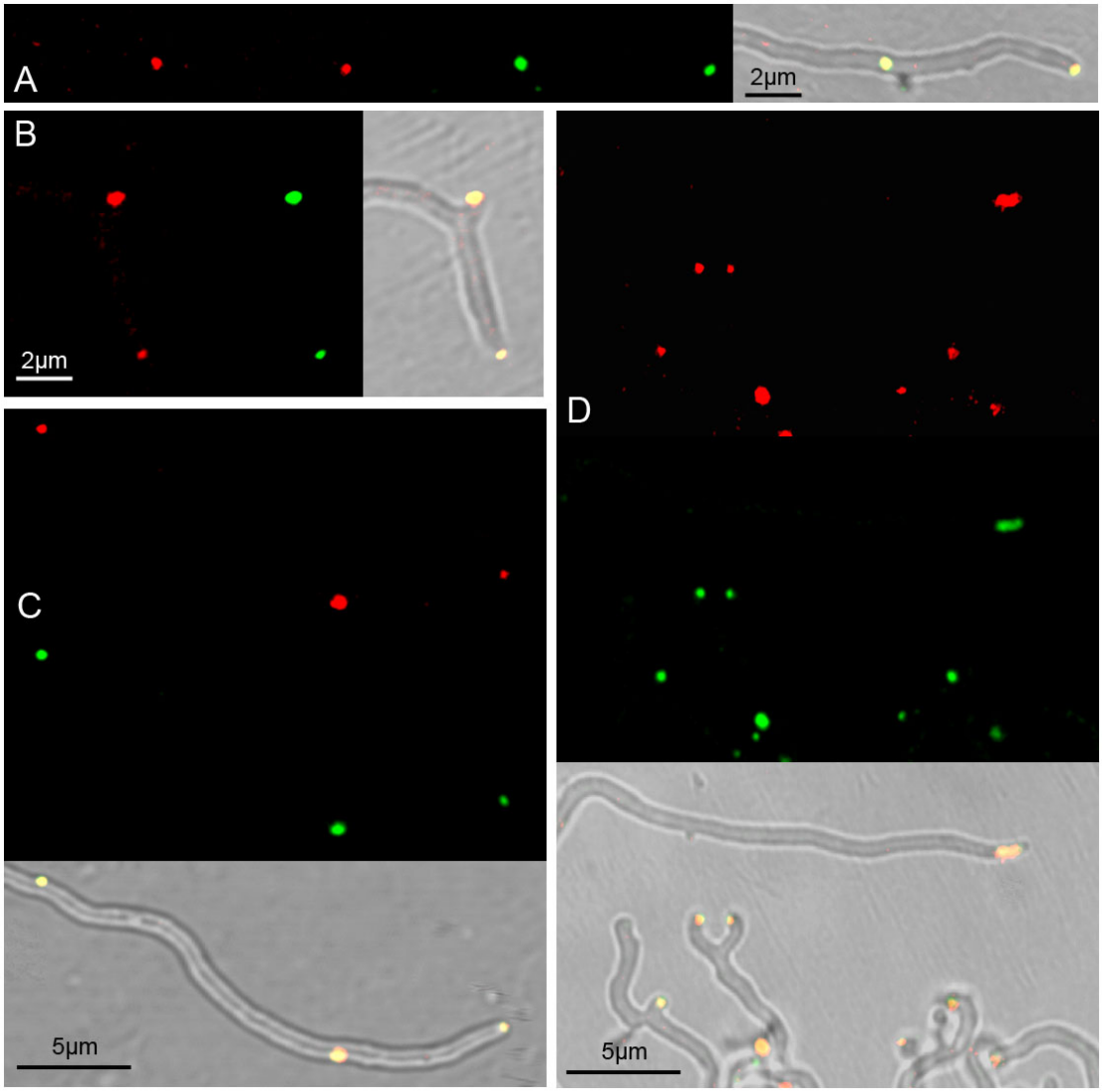

Figure 55: Scy co-localises with DivIVA. Localisation of mCherry-Scy foci (in red) overlaps with DivIVA-EGFP foci (in green). Co-localisation can be seen merged with the brightfield image, whereby both proteins localise to hyphal tips and future branch points (A-D). *S. coelicolor* M145/pKF59/pIJ8660-Pscy-mCherry-scy, was grown for 16 hours on solid SFM medium and the samples were viewed by laser-scanning confocal microscopy. Corresponding fluorescence images are next to one another and the respective overlayered image. Scale bars are shown.

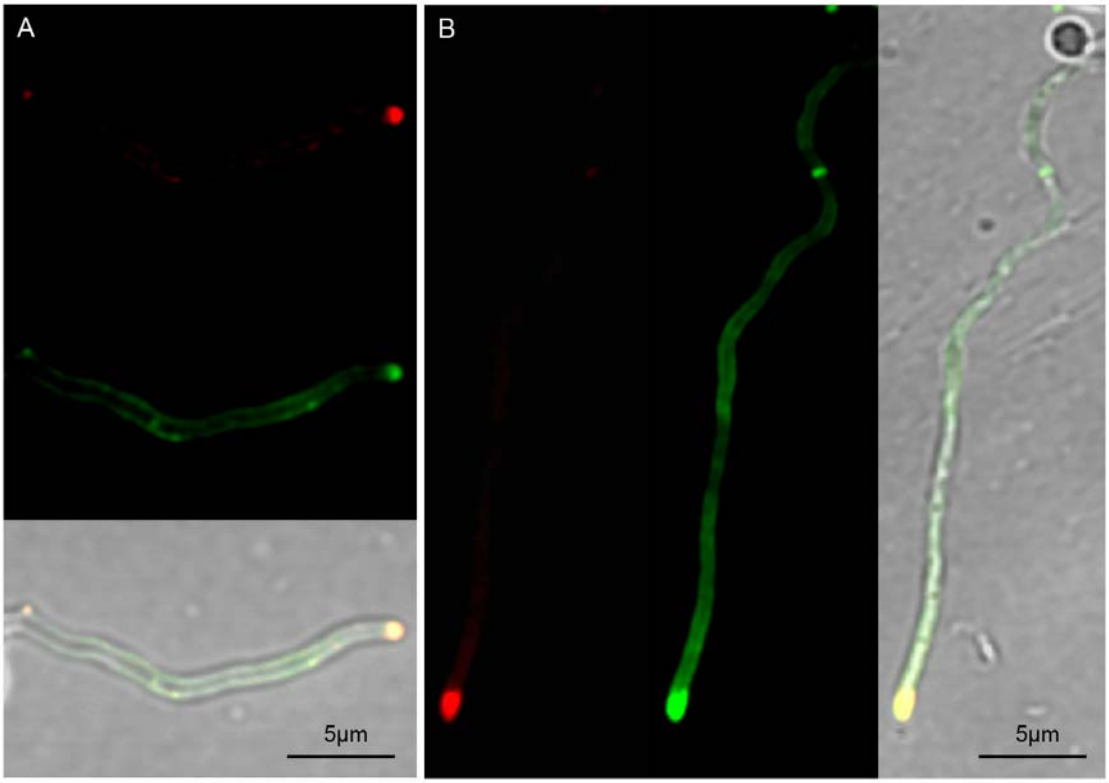

Figure 56: Scy co-localises with sites of cell wall insertion. mCherry-Scy (in red) overlaps with fluorescent vancomycin staining (in green). Co-localisation can be seen merged with the brightfield image whereby Scy and the cell wall machinery localise to hyphal tips (A&B). *S. coelicolor* M145/pIJ8660-Pscy-mCherry-scy, was grown for 16 hours on solid SFM medium prior to Van-Fl staining and the samples were viewed by laser-scanning confocal microscopy. Corresponding fluorescence images are next to one another and the respective overlayered image. Scale bars are shown.

To assess the localisation of Scy with a C-terminal fluorescent fusion in comparison to DivIVA-EGFP, the plasmid pIJ8660-Pscy-scy-Δlink-mCherry was used. The construct pIJ8660-Pscy-scy-Δlink-mCherry was introduced into M145 carrying pKF59 (Flärdh, 2003a), producing a strain that expresses both Scy-mCherry and DivIVA-EGFP. M145/pKF59/pIJ8660-Pscy-scy-Δlink-mCherry was grown on cellophane placed on top of SFM medium and then visualised using fluorescence microscopy. DivIVA-EGFP and Scy-mCherry co-localised at hyphal tips (Figure 57). However, at other locations for example along the lateral wall where new branch points may emerge, the co-localisation of DivIVA-EGFP and Scy-mCherry was not so obvious. This is likely because the construct of pIJ8660-Pscy-scy-Δlink-mCherry as shown in M145 (Figure 49) generates a diffuse background signal. The mCherry signal has less intensity than EGFP and the C-terminal fusion is also weaker than that seen using the N-terminal mCherry fusion. The weaker DivIVA signal associated with future branch sites is not matched by the Scy-mCherry

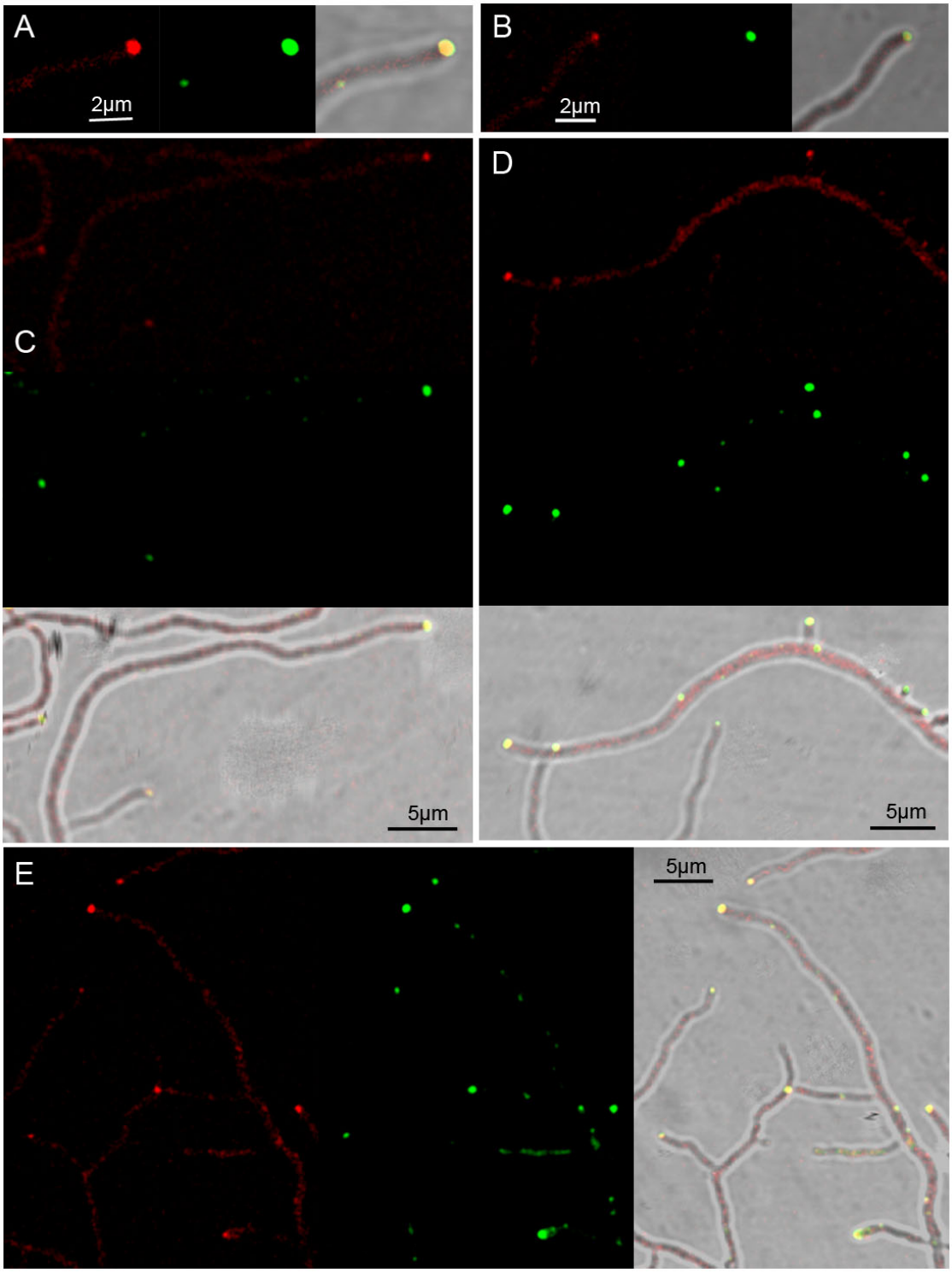

Figure 57: A Scy C-terminal fusion protein also co-localises with DivIVA. Localisation of Scy-mCherry foci (in red) overlaps with DivIVA-EGFP foci (in green). Co-localisation can be seen merged with the brightfield image, whereby both proteins localise to hyphal tips and future branch points (A-D). However Scy-mCherry has a weaker diffuse signal throughout the hyphae other than the intense foci at tip and branch positions. *S. coelicolor* M145/pKF59/pIJ8660-Pscy-scy-Δlink-mCherry, was grown for 16 hours on solid SFM medium and the samples were viewed by laser-scanning confocal microscopy. Corresponding fluorescence images are next to one another and the respective overlayered image. Scale bars are shown.

signal, although it is also of note that mCherry suffers from bleaching more than EGFP. Regardless, the co-localisation at brighter spots of existing apical sites, suggests the co-localisation of DivIVA and Scy at hyphal tips, consistent with the hypothesis that Scy functions at the growing hyphal tips.

4.1.3 DivIVA and sites of cell wall insertion are aberrant in the scy mutant

The *scy* mutant was shown to have various abnormalities associated with hyphal tip growth and branching. DivIVA and sites of new cell wall insertion marked by Van-Fl co-localise with mCherry-Scy suggesting that Scy has a function related to polarised growth and the probable complex organisation of proteins and metabolic precursors that are likely to be needed to sustain apical extension of the cell. Therefore, the *scy* mutation could have an affect on both DivIVA localisation and cell wall synthesis. To test this, we monitored either DivIVA-EGFP or Van-Fl in the *scy* mutant and compared this to the localisation patterns found in the wild-type. In order to monitor DivIVA localisation in the two strains, pKF59 carrying *divIVA-egfp* (Flärdh, 2003a) was moved into the wild-type M145 or a truncated *scy* mutant, K110 generated previously in the Kelemen lab. Both M145/pKF59 and K110/pKF59 were grown on cellophane placed on top of SFM medium and after 16 hours growth the hyphal network was then visualised by fluorescence microscopy. It was observed that in the wild-type, DivIVA-EGFP localised to the hyphal tip as a single focus that followed the smoothly defined curvature of the tip (Figure 58A-C). This is compatible with the proposed role of negative membrane curvature at the tip as a possible cue for localisation of DivIVA in other biological systems (Ramamurthi, and Losick, 2009; Lenarcic *et al.*, 2009). In comparison, in the *scy* mutant, the DivIVA-EGFP localisation pattern was different (Figure 58D-H). That is, DivIVA-EGFP appeared to be less compact at the hyphal tip with multiple foci often appearing. This aberrant localisation of DivIVA could result in asymmetrical tip curvature leading to more DivIVA mislocalisation. The multiple foci of DivIVA are also likely to give rise to the splitting tips often seen in a *scy* mutant. Multiple and irregular DivIVA foci are also presumably responsible for the uneven hyphal diameter seen in a *scy* mutant.

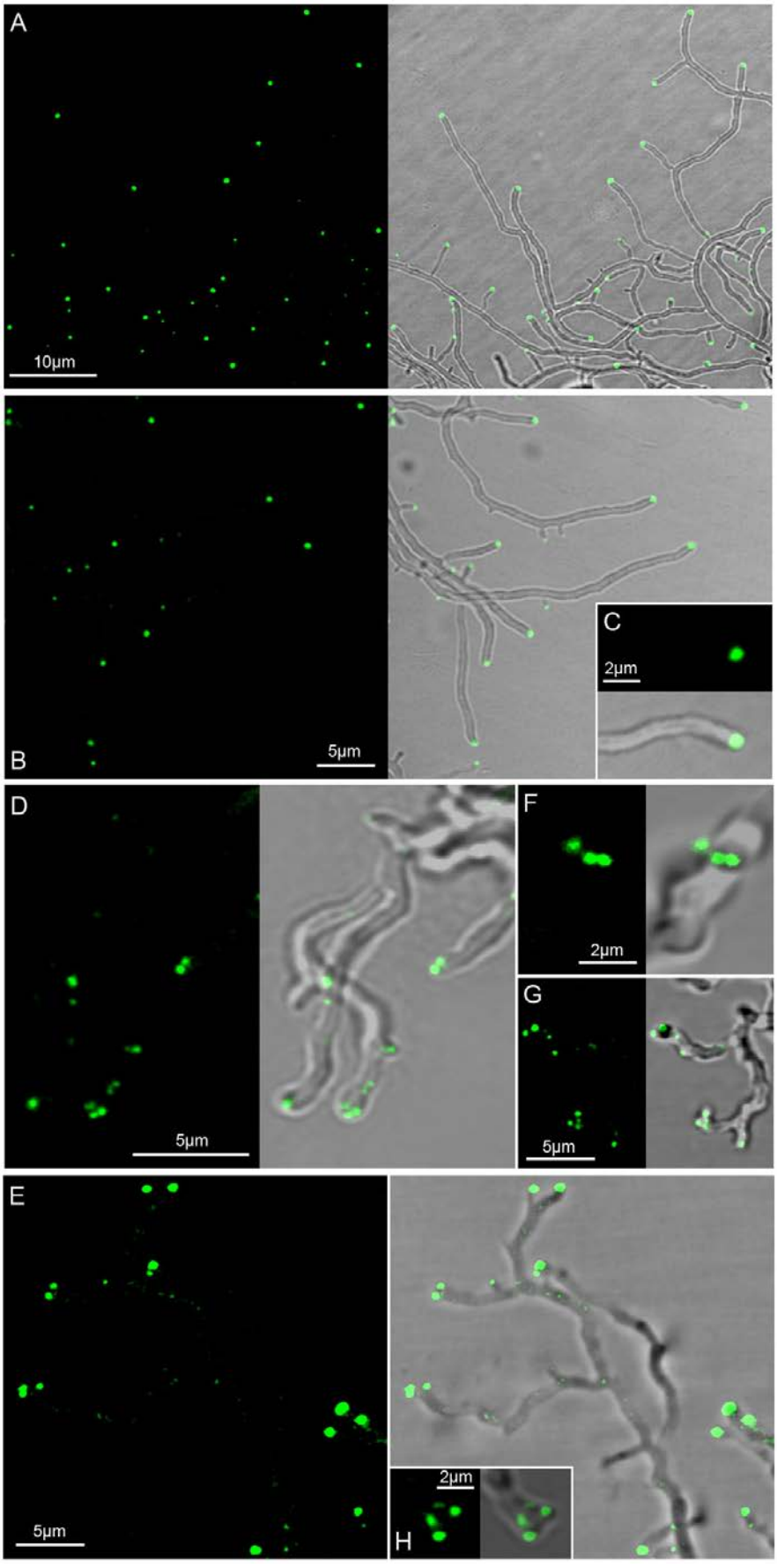

Figure 58:

DivIVA is mislocalised in a *scy* mutant. Localisation of DivIVA-EGFP foci (in green) normally positioned at hyphal tips in M145 (A-C). DivIVA-EGFP localisation is disturbed in a *scy* mutant (D-H), with numerous foci that could cause morphological difficulties and splitting tips. *S. coelicolor* M145/ pKF59 or scy/pKF59, was grown for 16 hours on solid SFM medium and the samples were viewed by laser-scanning confocal microscopy. Corresponding fluorescence images are next to the respective overlayered/merged brightfield image. Scale bars are shown.

To confirm that the DivIVA mislocalisation would also be consistent with aberrant cell wall insertion, both M145 and K110 were grown on SFM medium alongside a coverslip and hyphae were stained with Van-Fl and propidium iodide, samples were then visualised through fluorescence microscopy. It was observed that in M145 (Figure 59A&B), Van-Fl strongly stained a tip-proximal portion of the hyphal tip, similar in appearance to the foci observed previously for DivIVA-EGFP. However, in the *scy* mutant a more intense and extended Van-FL signal was often seen (Figure 59C-E). Consistent with the DivIVA localisation pattern a bulbous and bi-lobed Van-FL signal was often seen marking apical branching or tip splitting. It is worth noting that the aberrant staining pattern with Van-Fl could reflect either excessive or mislocalised cell wall insertion or could mark places of cell wall turnover of damage.

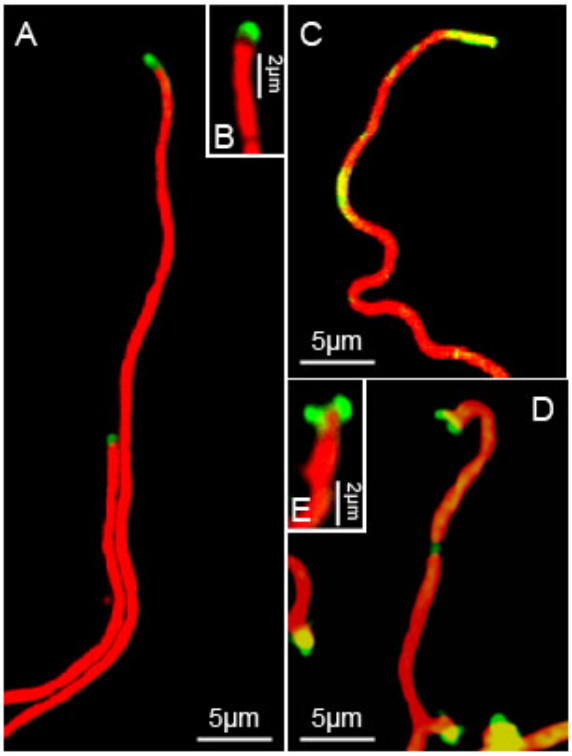

Figure 59: Cell wall insertion is altered in a *scy* mutant. Localisation of Van-Fl foci (in green) marking cell wall remodelling at hyphal tips in M145 (A&B). Localisation is disturbed in a *scy* mutant (C-E), with at times extended foci and foci at splitting tips. *S. coelicolor* M145 or *scy*, were grown for 2-4 days on agar plates alongside coverslips. Samples then stained with Van-Fl and propidium iodide. All images are overlayed with the two channels from Van-Fl (Green)/propidium iodide (Red). Scale bars are shown.

4.1.4 Overexpression of Scy generates new polarisation sites

In addition to the characterisation of the *scy* mutant phenotype, we were also interested to perform the opposite experiment, to express *scy* at a high level. For Scy overproduction in *Streptomyces*, the Kelemen lab had previously constructed a plasmid pCJW93-scy (pK48; Figure 204) This plasmid is descended from the vector pCJW93 (Wilkinson *et al.*, 2002), which is able to replicate in *E. coli*, and can be conjugated into *Streptomyces* species via *oriT* from RK2 (Pansegrau *et al.*, 1994). The vector pCJW93 also contains the replication

origin *oriV* from the vector pIJ6021 (Takano *et al.*, 1995) allowing high copy replication in *Streptomyces*, a selectable marker in the form of *aac(3)IV*, conferring apramycin resistance and the thiostrepton inducible *tipA* promoter (Murakami *et al.*, 1989), as well as the *tsr* gene encoding thiostrepton resistance. The multiple cloning site, downstream of *PtipA*, was where a fragment containing the whole of *scy* was cloned, in the resulting vector pCJW93-scy (pK48) (Figure 204). The *scy* gene has an altered ATG codon instead of a GTG at the start codon, unlikely to have an effect on Scy function based on the complementation experiment (2.1.7). Insertion of *scy* resulted in fusion of *scy* to an N-terminally encoded 6x His tag. Also, *scy* will be expressed from *PtipA* in a thiostrepton dependent manner.

Through conjugation pCJW93-scy (pK48) was introduced into M145 or M145/pKF59. Apramycin was maintained throughout to prevent loss of the vector which was at times experienced to be unstable across multiple generations. M145/pK48 was grown on cellophane on top of SFM medium for 16 hours, then the cellophane was transferred to a fresh SFM plate containing either thiostrepton (20μg/ml) or no thiostrepton at all (the control). Then after 3 hours, induced samples or uninduced samples were visualised through confocal microscopy. It can be seen that M145 carrying pK48 with no thiostrepton induction is comparable to a wild-type phenotype (Figure 60A), yet it is likely that carrying the pK48 vector does slow the growth, possibly by a metabolic price of carrying a high copy number vector. In comparison to the wild-type-like uninduced hyphae, microscopy performed on hyphae exposed to high levels of thiostrepton revealed quite distinctive effects with a large number of new tips emerging, generating numerous short and curved branches emerging from the parent hyphal fragment (Figure 60B&C).

When M145/pKF59/pK48 was grown and exposed to thiostrepton in a similar manner, it was possible to follow the localisation of DivIVA-EGFP in response to Scy overproduction (Figure 60E&F). As a control, in M145/pKF59/pK48 grown in the absence of thiostrepton, DivIVA-EGFP was positioned mostly at existing hyphal tips with a wild-type-like morphology (Figure 60D). However, after 1 hour exposure to thiostrepton, multiple DivIVA-EGFP foci were seen to localise along the length of the hyphae at ectopic locations other than the normal position at the hyphal tips (Figure 60E). This would suggest that the increased levels of Scy promoted the *de novo* formation of DivIVA assemblies at new locations, and as DivIVA is likely to promote the local incorporation of cell wall material, these DivIVA foci are believed to lead to the high numbers of short branches. These short branches formed after 3 hours were seen to have DivIVA-EGFP at

their ends (Figure 60F), confirming that the foci of DivIVA-EGFP seen after 1 hour are likely the sites of new branch formation.

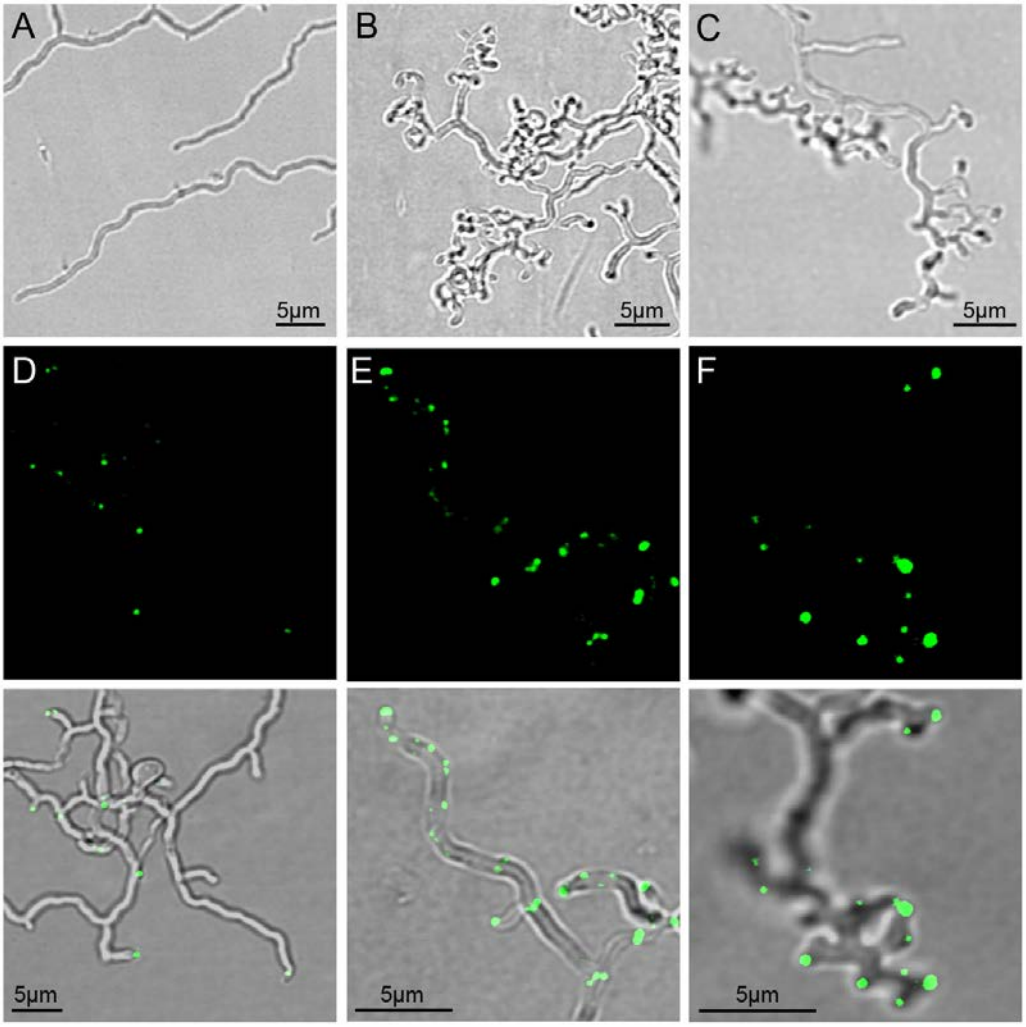

Figure 60: Overexpression of Scy was seen to result in over-branching possibly via recruitment of DivIVA to ectopic locations. Uninduced M145/pK48 had a wild-type phenotype (A); however, when induced for 3 hours was seen to form an overbranching phenotype (B&C). When carrying pKF59 uninduced samples (D) had normal DivIVA localisation. However after 1hr induction (E) DivIVA localised to many new sites down the hyphae and after 3 hours was likely to have resulted in the overbranching that resulted (F). *S. coelicolor* M145/pK48 or M145/pKF59/pK48, were grown for 16 hours on solid SFM medium, then either grown in the presence or absence or 20µg/ml thiostrepton. The samples were viewed by laser-scanning confocal microscopy. For A-C brightfield images are displayed, but for D-F corresponding fluorescence images are next to the respective overlayered/merged brightfield image. Scale bars are shown.

4.1.5 Detection of DivIVA-EGFP from cell extracts of the scy mutant and of the Scy overexpressing strain

It was very interesting that both in the case of the *scy* mutant (Figure 58D-H) and when Scy was overexpressed (Figure 60E&F), we found more DivIVA foci than in the wild-type. It was important to check the levels of DivIVA to see if the amount of DivIVA was still relatively constant or if there was a change in cellular levels of DivIVA in response to the changing levels of Scy. To do this, we analysed cell extracts from both the *scy* mutant and the *scy* overproducing strain using SDS-PAGE gels under semi-denaturing conditions and visualised DivIVA-EGFP using a phosphoimager with settings that could detect the EGFP fluorophore. Spores of M145 or *scy* (K110) carrying pKF59 were inoculated onto cellophane placed on top of SFM medium for 17 hours. Cells collected from the cellophane surface were resuspended in a Tris-Magnesium buffer and were lysed through FastPrep treatment by vigorous shaking in the presence of glass particles (<106μm). Following the crude cell extracts were quantified using a Bio-rad protein assay. The same amount of total protein from each sample was then run on an SDS-PAGE gel whereby the samples were not boiled prior to loading therefore preventing denaturation of the fluorescent tag and maintaining fluorescence activity. The gel was visualised for EGFP activity by exciting at 488nm and the emission was then read at 532nm (Figure 61A). There was a strong band between the 50 and 75 kDa molecular weight markers that corresponds to the size of a DivIVA-EGFP fusion protein. The relative intensity of the bands in Figure 61A are; lane 1 is 869.29 and lane 2 is 831.00. The intensity of the bands appears to be comparable between M145 and the *scy* mutant. Therefore, it appears at this early stage in the life cycle that the level of DivIVA is very similar in the *scy* mutant in comparison to the wild-type. The observed more DivIVA foci in the *scy* mutant therefore means that either each foci may contain less DivIVA, which is unlikely as the brightness appears comparable, or perhaps more DivIVA is drawn into foci from the free DivIVA pool in the cell. If in fact DivIVA foci break and disperse more easily from the existing tip then it is possible that the extending hyphal tip is then able to accommodate more addition of DivIVA into the tip foci from the DivIVA pool, than it may have done had the assembly not undergone a splitting event.

To test the DivIVA levels when Scy was overproduced, spores of M145/pKF59/pK48 were inoculated onto cellophanes placed on top of SFM medium for 22 hours. Then, the cellophanes were transferred to fresh SFM plates containing either thiostrepton (20μg/ml)

or no thiostrepton. Then after 1 or 3 hours, cell material was collected from the cellophane surface of all samples. Crude cell extracts were generated as above and were quantified using a Bio-rad protein assay. The same amount of total protein from each sample was then run on an SDS-PAGE gel with no boiling prior to loading, in order to maintain EGFP fluorescence. All samples contained a strong band with the predicted size of 68.4kDa, corresponding to DivIVA-EGFP (Figure 61B). The relative intensity of the bands in Figure 61B are; lane 1 is 785.89, lane 2 is 794.52, lane 3 is 773.93 and lane 4 is 799.43. The

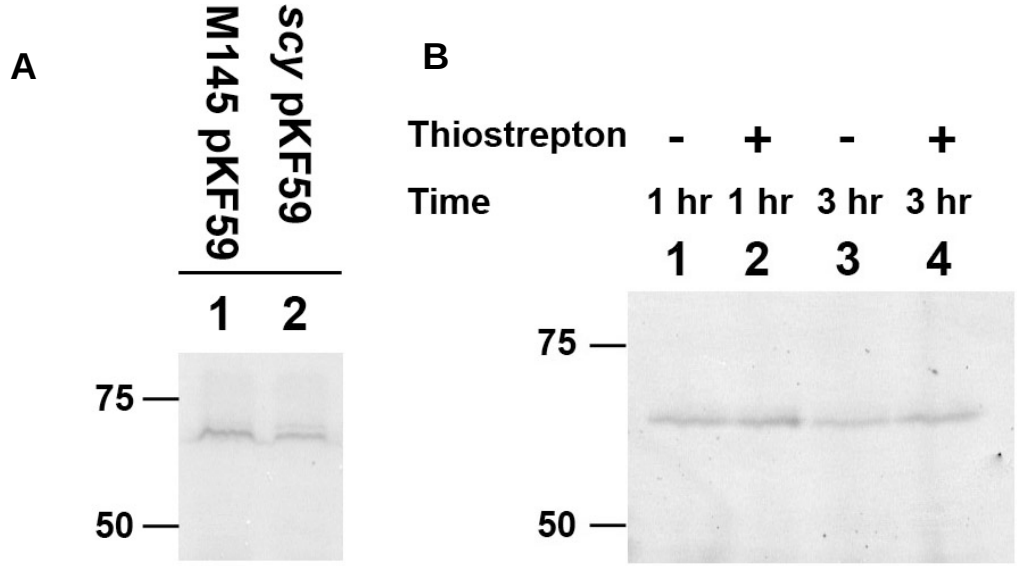

Figure 61: SDS-PAGE was used to detect the level of DivIVA-EGFP in a *scy* mutant and when Scy is overexpression. For analysis of DivIVA-EGFP the gel was excited at 488nm and the emission read at 532nm. Analysed on 8% acrylamide (A) are comparable signals for total cell extracts of either *S. coelicolor* M145 carrying pKF59 (Lane 1) or the *scy* mutant carrying pKF59 (Lane 2), samples were grown for 17 hours prior to collection. Analysed on 8% acrylamide (B) are comparable signals for total cell extracts of either *S. coelicolor* M145/pKF59/pIJ6902-scy (Lanes 1-4) grown in the absence (-) or presence (+) of 20µg/ml thiostrepton. All samples were grown initially for 22 hours, then either with or without 20µg/ml thiostrepton for either a further 1 or 3 hours. Shown on the left hand side are the positions and sizes of a protein MW marker (not visible on images shown) displayed in kDa.

intensity of the bands appears to be comparable between the uninduced and induced samples at 1 hour or 3 hour time points. Therefore, it appears that the level of DivIVA does not increase with overexpression of Scy and the generation of more DivIVA foci is not due to an increase in the amount of DivIVA. As there are more DivIVA-EGFP foci in the induced samples this could mean that each foci may contain less DivIVA or perhaps more DivIVA is drawn into foci from the free DivIVA pool in the cell. This latter would be consistent with the ability to form spontaneous sites for new branch formation instead of taking DivIVA from assemblies already present at the hyphal tips. DivIVA appears to

remain at a constant level when Scy is overexpressed, leading to the possibility that the effects of overbranching are not due to an increase in DivIVA.

4.1.6 Scy directly co-localises with de novo sites of cell wall insertion when Scy is overexpressed

The hyperbranching and ectopic DivIVA recruitment when *scy* is overexpressed, could of course be caused by Scy indirectly affecting DivIVA and/or the cell wall synthesis machinery by somehow relieving an inhibitory factor. Alternatively Scy could be acting as a positive factor, where overexpressed Scy could recruit factors needed for establishment of a new branching site. In order to test these two hypotheses, we aimed to visualise Scy localisation in a variety of alternative genetic backgrounds for various downstream applications. The routinely used pIJ8660 derivatives integrate into the *attP* attachment site in the chromosome and confer resistance to apramycin. In order to introduce a second construct into cells that carry a pIJ8660 derivative, we were looking for plasmids that carry different resistance markers and integrate at a different chromosomal site. The plasmid pMS82 (Gregory *et al.*, 2003) mediates integration into the *S. coelicolor* chromosome at the *Φ*BT1 attachment site, which differs to the *Φ*C31 attachment site found in most other *Streptomyces* integrative vectors. This attachment site, following the introduction of the plasmid through conjugation via the non-methylating *E. coli* strain *E. coli* ET12567, will stably integrate and result in a single copy of the plasmid DNA in the chromosome. The plasmid pMS82 also contains a hygromycin resistance cassette as opposed to the apramycin cassette commonly used as the marker of choice for *Streptomyces* manipulation. The vector pMS82-Pscy-mCherry-scy was constructed (10.1.54) carrying *Pscy-mCherry-scy* in pMS82. The plasmid pMS82-Pscy-mCherry-scy which carries hygromycin resistance, therefore allowing combination with strains carrying the pCJW93-scy (pK48) vector used for overexpression of Scy. The plasmid pMS82-Pscy-mCherry-scy was introduced through conjugation via the non-methylating *E. coli* strain *E. coli* ET12567 into M145/pK48 and selected apramycin and hygromycin resistant colonies were streaked for single colonies followed by spore preparation.

M145/pK48/pMS82-Pscy-mCherry-scy was grown on cellophane placed on top of SFM medium for 16 hours, then the cellophane was transferred to a fresh SFM plate containing either thiostrepton (20μg/ml) or no thiostrepton at all (the control). After 3 hours, all samples were stained with the mixture of 1 μg/ml BODIPY FL vancomycin (Molecular

Probes) and 1 µg/ml unlabelled vancomycin (Sigma) for 5 minutes prior to collection of the sample. Samples were visualised through confocal microscopy (Figure 62). M145/pK48/pMS82-Pscy-mCherry-scy in the absence of thiostrepton induction appears wild-type-like with mCherry-Scy and Van-Fl foci predominantly at hyphal tips and possible future branch sites (Figure 62A). After 1 hour exposure to thiostrepton, the samples had multiple mCherry-Scy and Van-Fl foci along the length of the hyphae (Figure 62B), in a fashion similar to the numerous DivIVA-EGFP foci seen when Scy was overproduced. Furthermore it was seen after 3 hours of induction that there were many new branches established (Figure 62C), which would suggest that the spontaneous recruitment of Scy and the cell wall synthetic machinery to new sites along the hyphae led to branching. Many of these newly formed branches had an mCherry-Scy foci as well as staining strongly with Van-Fl supporting this idea. However, some of the branches were left with only an mCherry-Scy foci and did not stain with Van-Fl, this suggests that some of the multiple branches that are formed when Scy is overexpressed may become abortive and not continue to actively grow. Overproduction of Scy, whilst other factors are limiting such as the cell wall synthesis machinery could be the cause of the abortive branching. Suggesting that there is then an uncoupling of Scy with actively growing zones. Therefore, we may conclude Scy is likely a polarity factor able to positively generate new sites for recruitment of DivIVA and/or cell wall synthesis machinery in an as so far unclear mechanism.

4.1.7 The effect of DivIVA depletion and overexpression on morphology and Scy localisation

The plasmid pMS82-Pscy-mCherry-scy allowed greater flexibility for combination with other marked strains and therefore we introduced it into the strains K114 (*divIVA*$_{SC}^{+}$/*tipAp-divIVA*$_{SC}^{+}$) and K115 (*ΔdivIVA*$_{SC}$/*tipAp-divIVA*$_{SC}^{+}$) (Flärdh, 2003a). Both of these strains carry a copy of *divIVA* driven by the thiostrepton inducible promoter *tipA*; however, K114 carries a native chromosomal copy of *divIVA* and K115 carries an apramycin resistance cassette in place of the *divIVA* gene.

As *divIVA* is an essential gene in *S. coelicolor*, therefore, Scy localisation cannot be studied in the complete absence of DivIVA. Instead K115 carrying pMS82-Pscy-mCherry-scy was grown on the surface of a cellophane placed on top of SFM medium with 0.1µg/ml thiostrepton. Following 14 hours of growth, the cellophane was transferred to an SFM

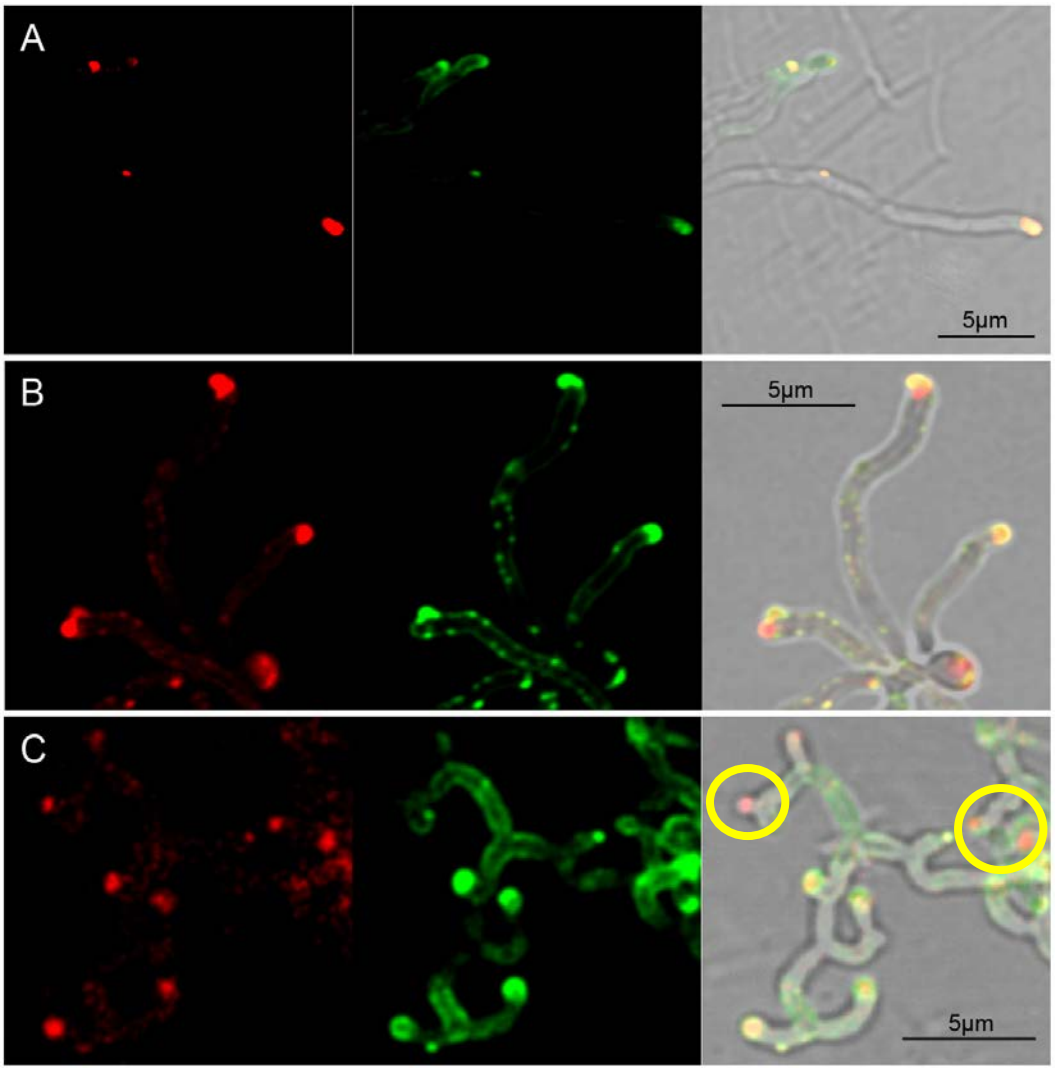

Figure 62: Overexpression of Scy can be seen to influence cell wall insertion directly at sites where mChery-Scy is recruited. Uninduced M145/pK48/pMS82-Pscy-mCherry-Scy had a wild-type phenotype with Van-Fl (Green) and mCherry (Red) foci at hyphal tips(A). However when induced for 1 hours was seen to form multiple new foci of Van-Fl and mCherry-Scy at ectopic locations (B). After 3 hours overbranching had resulted with mCherry-Scy foci established at tips and in cases Van-Fl staining of the same tips (C). *S. coelicolor* M145/pK48/pMS82-Pscy-mCherry-Scy, were grown for 16 hours on solid SFM medium, then either grown in the presence or absence of 20µg/ml thiostrepton. The samples were viewed by laser-scanning confocal microscopy. Yellow circle marks positions where Scy is detected without aVan-Fl signal. Corresponding fluorescence images are next to the respective overlayered/merged brightfield image. Scale bars are shown.

plate lacking thiostrepton and growth was continued for a further 5 hours. It was previously shown that K115 in the absence of thiostrepton produces DivIVA at a 10-fold lower amount than the wild-type strain M145. After 5 hours of DivIVA depletion (Figure 63B&C) the hyphae displayed the previously reported branching defects including curly hyphae and apical branching (Flärdh, 2003a). The control strain K114 carrying pMS82-Pscy-mCherry-scy grown in the absence of thiostrepton and therefore expressing close to

normal levels of DivIVA protein, did not display the same hyphal abnormalities as the DivIVA depletion strain (Figure 63A). However, it did display the phenotypic aberrations associated with the mCherry-Scy fusion protein. In the event of DivIVA depletion Scy localisation did not appear to be perturbed and Scy remained at polar sites. It was shown that DivIVA can be seen to disperse from the hyphal tip in a *scy* mutant, however, it seems that Scy does not exhibit similar behaviour when DivIVA is depleted.

To look at the effect of DivIVA overexpression on Scy localisation the strain K114 carrying pMS82-Pscy-mCherry-scy was studied. Firstly the hyphae were grown for 14 hours on a cellophane surface on SFM medium in the absence of the inducer. The hyphae displayed wild-type morphology (Figure 63A). Then, the cellophane was transferred to an SFM plate containing 20µg/ml thiostrepton and grown for a further 3-5 hours, and samples were visualised through confocal microscopy (Figure 63D&E). It was seen that the previously reported effects of DivIVA overexpression (Flärdh, 2003a) were reproduced: swollen hyphal tips forming bulbous structures and the formation of multiple small rounded outgrowths. It was seen that mCherry-Scy localised to these small outgrowths but the foci had lower intensities perhaps suggesting a titration of uninduced levels of the Scy protein. Although it was seen that DivIVA overexpression resulted in formation of new tips, comparatively this was a rarer event, by far the greater effect was the dominance of DivIVA dependent expansion of the existing hyphal tips resulting in the ballooning effect seen. At these swollen existing tips mCherry-Scy could be seen to localise to an aggregate that has been previously reported to be a DNA free space that also contains DivIVA (Flärdh, 2003a; Wang *et al.*, 2009). It is likely therefore that DivIVA recruits all of the machinery needed for tip growth to this aggregate.

It was previously shown that the effects of DivIVA overproduction can be blocked by treatment of the hyphae with the cell wall growth inhibitor bacitracin (Hempel *et al.*, 2008). The mode of action of bacitracin is to stop the export of lipid II (Stone, and Strominger, 1971), needed as a precursor for peptidoglycan synthesis. To analyse the effect of DivIVA overexpression on Scy localisation in comparison with cell wall insertion, the strain K114 carrying pMS82-Pscy-mCherry-scy was studied. Firstly the hyphae were grown for 14 hours on a cellophane surface on SFM medium in the absence of the inducer, then were stained with the mix of 1 µg/ml BODIPY FL vancomycin (Molecular Probes)

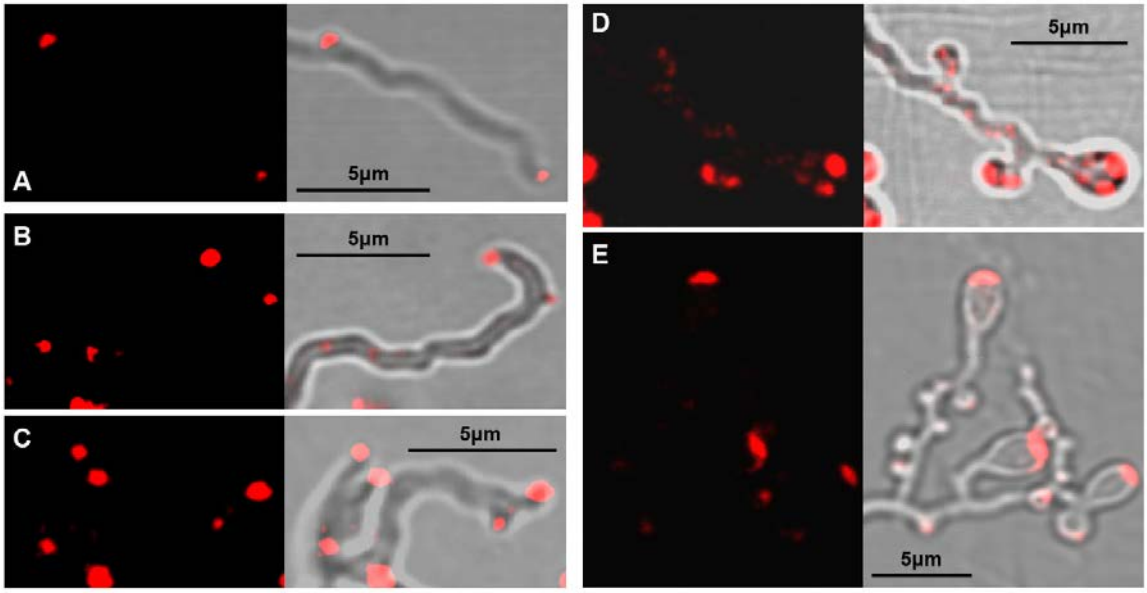

Figure 63: Localisation of Scy when DivIVA is depleted or overexpressed confirms that Scy is associated with Polar sites. Localisation of mCherry-Scy at apical sites in K114 carrying pMS82-Pscy-mCherry-scy grown in the absence of Thiostrepton and therefore control levels of DivIVA (A). When strain K115 carrying pMS82-Pscy-mCherry-scy is grown in the absence of Thiostrepton for 5 hours and is depleted of DivIVA expression Scy is not diminished from polar sites (B & C). When strain K114 carrying pMS82-Pscy-mCherry-scy is grown in the presence of Thiostrepton (20μg/ml) for 3 hours (D) and 5 hours (E) and DivIVA is overexpressed Scy forms in an aggregate at the hyphal tips and is recruited to overbranching positions. The samples were viewed by laser-scanning confocal microscopy. Fluorescence images of mCherry-Scy (red) are next to the respective overlayered/merged brightfield image. Scale bars are shown.

and 1 μg/ml unlabelled vancomycin (Sigma) for 5 minutes prior to collection of the sample. It can be seen that K114/pMS82-Pscy-mCherry-scy with no thiostrepton induction appears wild-type-like with mCherry-Scy and Van-Fl foci predominantly at hyphal tips and possible future branch sites (Figure 64A). When the cellophane was transferred to an SFM plate containing 20μg/ml thiostrepton and grown for a further 3 hours and stained with Van-Fl, Scy aggregates formed at the hyphal tips co-localising with Van-Fl (Figure 64B). Therefore, showing that the positioning of Scy aggregates overlaps with the sites of growth even at the bulbous form of the hyphal tip that occurs following DivIVA overexpression, consistent with the idea that DivIVA recruits all of the machinery needed for tip growth to aggregates. To test whether the block of cell wall synthesis had an effect on the phenotype observed during DivIVA overproduction, cellophane disks were transferred to SFM plates containing either 50μg/ml of bacitracin and no thiostrepton or 50μg/ml of bacitracin and 20μg/ml thiostrepton and incubated for a further 3 hours followed by Van-Fl staining. In the absence of thiostrepton, hyphae look wild-type (Figure 64C), albeit it is likely that they are not growing as samples left to grow in the incubator failed to grow to a confluent lawn. Consistent with this mCherry-Scy and Van-Fl did not

stain strongly in these hyphae; however, there was some signal present that may represent areas where the hyphae are attempting to grow but failing. It is possible that the block in cell wall synthesis also results in death via leaving a gap in the cell wall at previous sites of growth. Thiostrepton induced samples also failed to exhibit the effects of DivIVA

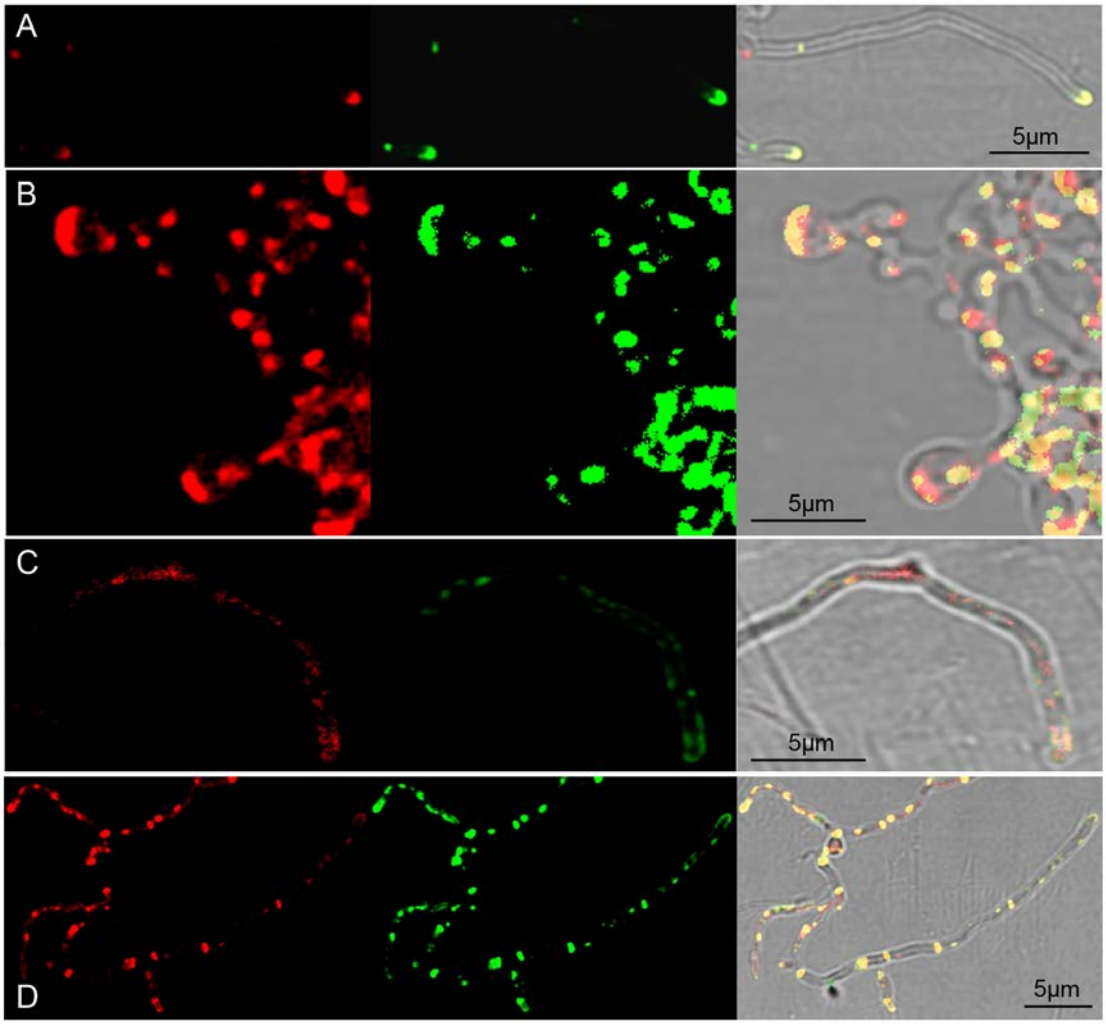

Figure 64: Scy and cell wall synthesis localisation is affected when DivIVA is overexpressed and/or hyphae are exposed to bacitracin. Localisation of mCherry-Scy (Red) or Van-Fl (Green) at apical sites in K114 carrying pMS82-Pscy-mCherry-scy grown in the absence of Thiostrepton and therefore control levels of DivIVA (A). When strain K114 carrying pMS82-Pscy-mCherry-scy is grown in the presence of thiostrepton (20µg/ml) for 3 hours (B) and DivIVA is overexpressed, Scy forms in an aggregate at the hyphal tips which co-localises with Van-Fl. Alternatively when grown in the presence of bacitracin (50µg/ml) for 3 hours (C) and cell wall growth stalls, mCherry-Scy and Van-Fl staining are dimmer and more dispersed. When grown in the presence of both thiostrepton and bacitracin for 3 hours (D), the effects of DivIVA overexpression cease, despite lack of growth Van-Fl and mCherry-Scy visibly mark various locations. The samples were viewed by laser-scanning confocal microscopy. Fluorescence images of mCherry-Scy (red), Van-Fl (green) are next to the respective overlayered/merged brightfield image. Scale bars are shown.

overproduction (Figure 64D), consistent with previous observations (Hempel *et al.*, 2008). There were no bulging hyphal tips or sites of multiple new branches suggesting that the effects of DivIVA overexpression are dependent on new cell wall synthesis. However,

there were quite prominent foci of mCherry-Scy and Van-Fl at both hyphal tips and in a manner along the length of the hyphae. However, presumably these do not represent actively growing zones, but probably represent where overproduced DivIVA would be directing new cell wall insertion sites, that then fail to grow due to bacitracin treatment. A possibility is that these sites are marked for cell wall growth, with the presumption that at any site of cell wall growth there must be mechanisms of breaking the existing wall to allow new synthesis, so may represent sites where cell material has been degraded. This could plausibly result in the strong Van-Fl foci seen. It is interesting to note that the mCherry-Scy foci are brighter at high levels of DivIVA even in the presence of bacitracin, unlike the weaker mCherry-Scy foci seen when bacitracin is present but DivIVA is at normal levels. This suggests that overexpressed DivIVA can recruit Scy without the need for active growth (this presumably holds true at sites of future outgrowths needed to form new branches).

When DivIVA was overproduced in K114/pMS82-Pscy-mCherry-Scy, there was presumably an active recruitment of Scy to the hyphal tips and to new branch sites. Therefore, it was important to establish whether the Scy levels changed during DivIVA induction. Spores of K114/pMS82-Pscy-mCherry-Scy were inoculated onto cellophanes placed on top of SFM medium for 16 hours. Then, the cellophanes were transferred to fresh SFM plates containing either thiostrepton (20μg/ml) or no thiostrepton. After 1 or 3 hours, cell material was then collected from the cellophane surface and cell extracts were generated and were quantified. Equal amount of total protein from each sample was then analysed on an SDS-PAGE gel with no boiling to maintain mCherry fluorescence. The gel was visualised for mCherry activity using phosphoimager and by exciting at 532nm and the emission was then read at 555nm (Figure 65). A strong band corresponding to the 173kDa mCherry-Scy fusion protein was detected in all samples. The relative intensity of the bands; in lane 3 is 152.60, lane 4 is 171.89, lane 5 is 199.07 and lane 6 is 217.79. These numbers appears to be comparable between the uninduced and induced samples, however we cannot rule out that there might be a slight increase in Scy in response to DivIVA overexpression. As there is not a ten-fold increase in the level of Scy with overexpression of DivIVA, it is likely that the increase of mCherry-Scy at bulging tips and the recruitment of Scy foci to new sites is not due to an indirect increase in the amount of Scy.

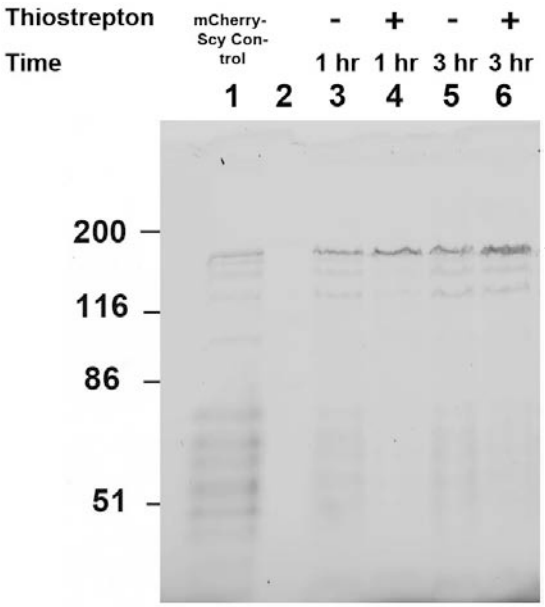

Figure 65: SDS-PAGE was used to detect the level of mCherry-Scy in samples when DivIVA overexpression is either induced on non-induced. For analysis of mCherry-Scy the 8% acrylamide gel was excited at 532nm and the emission read at 555nm. A control of the Supernatant of a cell extract of M145/pIJ8660-Pscy-mCherry-scy was used (Lane 1). Comparable signals are visible for total cell extracts of either *S. coelicolor* K114/pMS82-Pscy-mCherry-scy (Lanes 3-6) grown in the absence (-) or presence (+) of 20µg/ml thiostrepton. All samples were grown initially for 16 hours, then either with or without 20µg/ml thiostrepton for either a further 1 or 3 hours. Shown on the left hand side are the positions and sizes of a protein MW marker (Lane 2 (not visible on images shown)) displayed in kDa. The arrow shows the size of the higher molecular weight band representing an mCherry-Scy fusion protein.

4.1.8 FtsZ-EGFP mislocalises in a scy mutant

In addition to polarised growth, the *scy* mutant had a defect in cell division as it formed irregularly shaped spore compartments (Figure 35). Therefore, we wanted to monitor the cell division protein FtsZ in order to determine whether FtsZ localisation was Scy dependent. The plasmid pKF41 (Grantcharova *et al.*, 2005) enables expression of an FtsZ-EGFP fusion protein, so this plasmid was introduced into M145 and the *scy* mutant strains through conjugation facilitated by *E. coli* ET 12567/pUZ8002 and integration of a single copy at the *Φ*C31 attachment site. Spores of M145 and *scy* carrying pKF41 were grown between the angle of a coverslip and SFM medium and then visualised through fluorescence microscopy. Normal FtsZ rings were detected marking the sporulation septa along the length of the aerial hyphae in the wild-type strain (Figure 66). In the *scy* mutant there were fewer aerial hyphae that sporulated and therefore, not surprisingly, many aerial hyphae showed abnormal FtsZ localisation. Instead of the ladder like pattern less orderly FtsZ filaments were present, often positioned adjacent to the lateral walls of the hyphae. This could represent a direct effect of Scy on the localisation pattern of FtsZ or a by product of the morphological effects of the *scy* mutant effecting the hyphal cell wall defects.

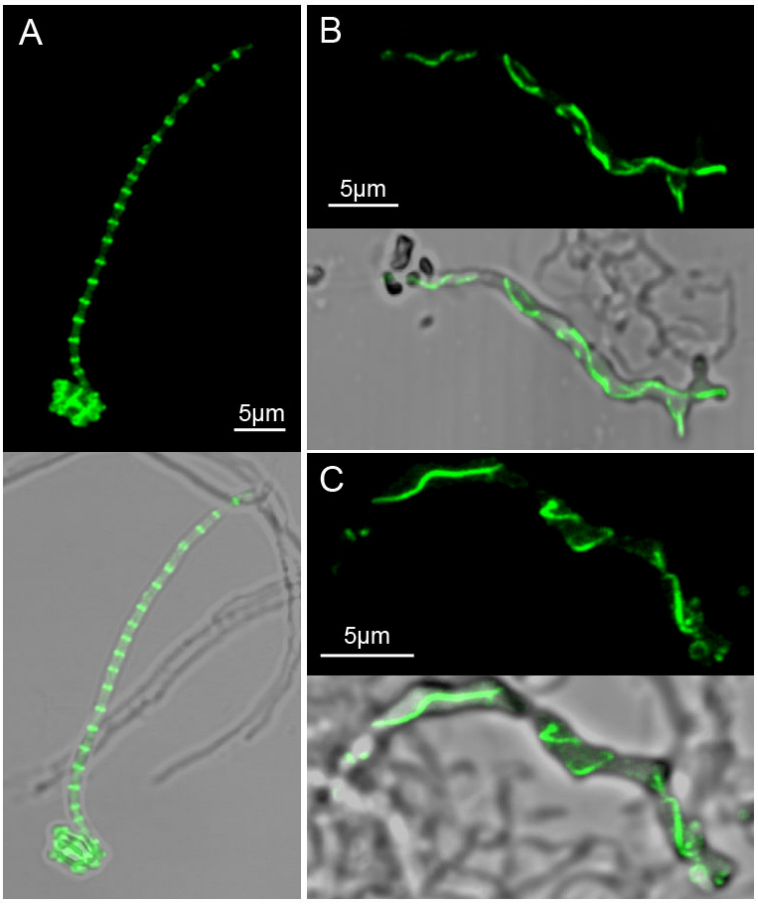

Figure 66: FtsZ localisation is affected in the *scy* mutant. Localisation of FtsZ-EGFP foci (in green) normally positioned as a ladder like array at crosswalls in M145 (A). FtsZ-EGFP localisation is disturbed in a *scy* mutant (B & C), with less ordered filaments that run adjacent to the hyphae instead of in rings at future septa. *S. coelicolor* M145/ pKF41 or *scy*/pKF41, were grown for 44 hours on solid SFM medium in the angle between a coverslip and the samples were viewed by laser-scanning confocal microscopy. Corresponding fluorescence images are next to the respective overlayered/merged brightfield image. Scale bars are shown.

4.1.9 ParB-EGFP mislocalises in a scy mutant

Another phenotype of the *scy* mutant related to cell division was the irregular distribution of DNA in the spore compartments. To test the effect of Scy on DNA segregation, we monitored a protein part of the DNA segregation machinery, in this case ParB as a reporter of the ParAB system. The strain J3310 (Jakimowicz *et al.*, 2005a) enables the expression of a ParB-EGFP fusion protein in M145 where the chromosomal *parB* allele was replaced by *parB-egfp*. We introduced the *scy* mutation into the J3310 strain using the knockout method described for the generation of the *scy* mutant. Using the Redirect technology, double crossover events were selected by identifying apramycin resistant and kanamycin sensitive colonies generating *scy::aac(3)IV/parB-egfp*. Spores of M145 and *scy* mutant

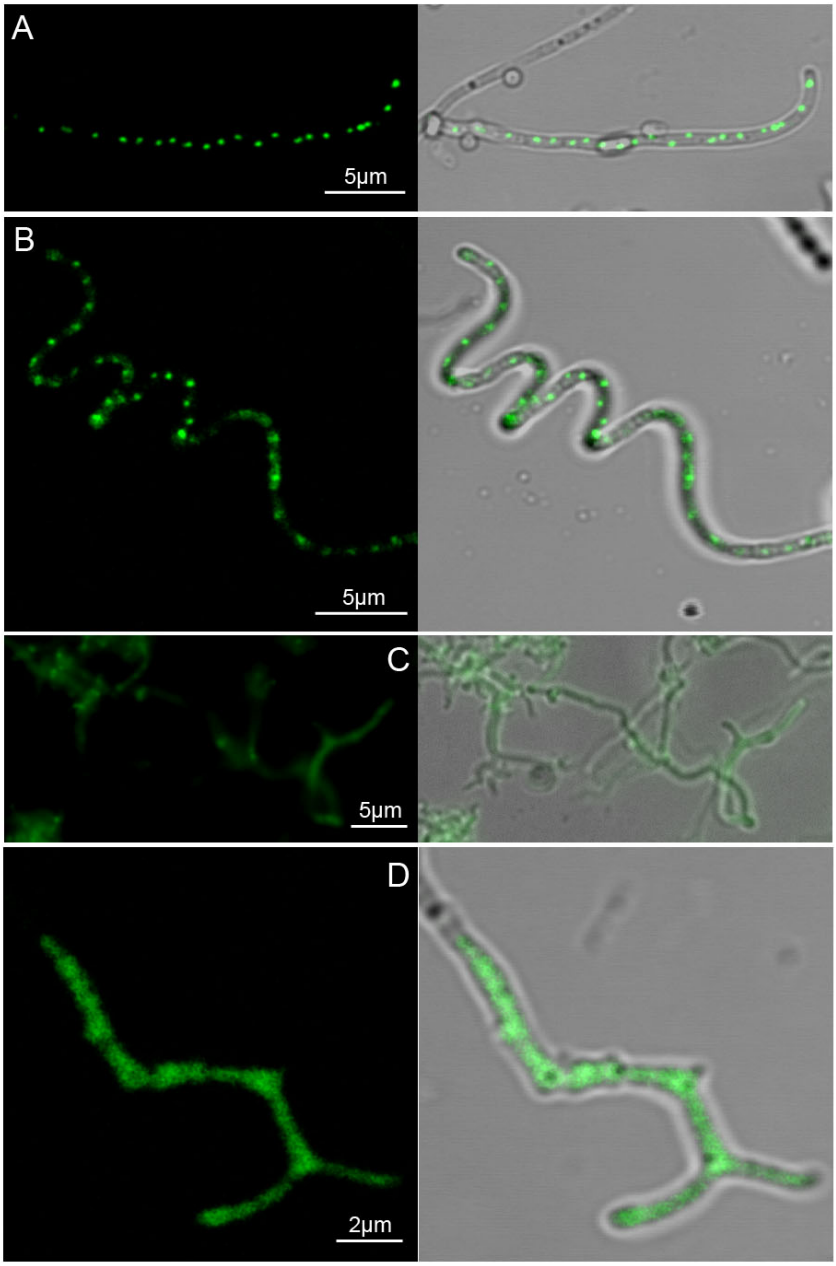

Figure 67: ParB localisation is affected in a *scy* mutant. Localisation of ParB-EGFP foci (in green) normally positioned as regular foci down sporulating aerial hyphae in M145 (A & B). ParB-EGFP localisation is disturbed in a *scy* mutant (C & D), with a dispersed signal in the aerial hyphae. *S. coelicolor* J3310 or J3310::scy*::aac(3)IV*, were grown for 44 hours on solid SFM medium in the angle between a coverslip and the samples were viewed by laser-scanning confocal microscopy. Corresponding fluorescence images are next to the respective overlayered/merged brightfield image. Scale bars are shown.

strains carrying *parB-egfp* were grown alongside a coverslip in SFM medium and after 2 days grothw at 30^{o}C, aerial hyphae were visualised through fluorescence microscopy. Regular ParB-EGFP foci were seen in the sporulating aerial hyphae of the wild-type strain, whereas in the *scy* mutant most of the aerial hyphae had a strong dispersed ParB-EGFP signal, lacking the bright discrete foci (Figure 67). This could help explain the aberrant

DNA segregation in the spore chains of a *scy* mutant suggesting that in the absence of Scy the segregation machinery was presumably not functioning correctly.

4.1.10 Summary

Monitoring Scy localisation in comparison to DivIVA or active cell wall insertion as marked by Van-Fl suggests that Scy colocalises with sites of active growth at hyphal tips and future branch points. Monitoring of DivIVA or Van-Fl in the *scy* mutant suggest that tip and branching defects seen in the *scy* mutant occur due aberrant or mislocalisation of DivIVA and the cell wall synthetic machinery. Overexpression of Scy resulted in *de novo* formation of multiple new branches confirming that Scy has a function related to control of tip growth and branching. Localisation of Scy in a DivIVA depletion or overexpression background suggested that DivIVA could recruit Scy to active sites but did not rule out that Scy could also localise independtly. Mislocalisation of FtsZ and ParB in a *scy* mutant background reveals cellular insights into the aberrations seen with cell division.

5 Localisation of FilP in *Streptomyces*

5.1.1 Introduction

As *filP* sits downstream of *scy*, it was of interest to be able to verify the localisation of *filP* and to be able to test the localisation of *filP* in our research. Therefore we constructed fusion proteins to FilP to test several combinations. We wanted to look at the localisation of FilP in a *scy* mutant background to determine if Scy affects FilP *in vivo*. As Scy and DivIVA were seen to colocalise at the hyphal tips (Chapter 4) then we wanted to colocalise FilP with either Scy or DivIVA.

5.1.2 FilP-EGFP forms filaments

For assessing the localisation of FilP we constructed a *filP-egfp* fusion (10.1.55). The plasmid pIJ8660-PfilP-filP-egfp (pK67) enables expression of a FilP-EGFP fusion protein under the control of the native *filP* promoter sequence. The vector was mobilised into *Streptomyces* via conjugation and integration in the same method as previously discussed for pIJ8660 vectors. It was impossible to assess the correct functioning of the FilP-EGFP fusion protein, as the *filP* mutant was so subtle that it wasn't clear if the fusion protein was able to complement the mutant. Spores of M145 carrying pIJ8660-PfilP-filP-egfp were grown on cellophane on top of SFM medium for 12-16 hours and then visualised through fluorescence microscopy (Figure 68). Similarly to (Bagchi *et al.*, 2008) it was seen that FilP-EGFP formed filaments down the hyphae. These were often seen at the sites of inner curvature. However not all sites of inner curvature were occupied with FilP-EGFP filaments so it is currently unknown what the determining factor for localisation of FilP filament formation is. FilP-EGFP signal was also often seen as foci at the hyphal tips. This is of course interesting as Scy and DivIVA also localise to the hyphal tips. Signal was also present at undefined locations as foci that we predict are aggregates of FilP-EGFP and could represent artefacts generated by the EGFP fusion and/or multiple copies of FilP.

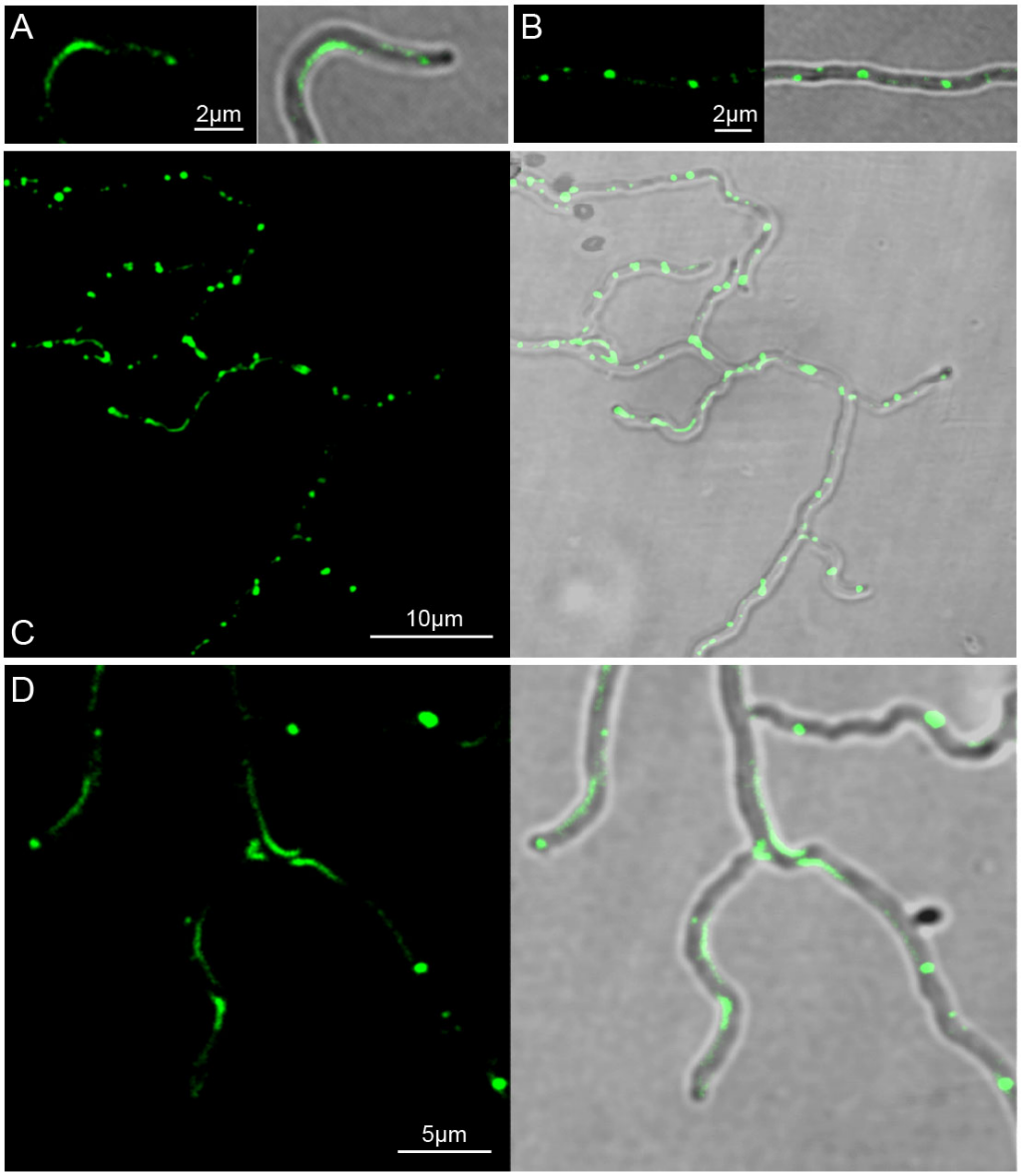

Figure 68: Localisation of FilP-EGFP was to foci and filaments at locations just behind the hyphal tips as well as at other undefined locations along the hyphae. Filaments may have a preference for forming on the inner curve of a hyphal bend. Large foci may resemble FilP aggregates. *S. coelicolor* M145/pIJ8660-PfilP-filP-EGFP, was grown for 16 hours on solid SFM medium and the samples were viewed by laser-scanning confocal microscopy (A-D). Corresponding fluorescence images are left of the respective merged fluorescent/brightfield image. Scale bars are shown.

5.1.3 FilP localisation was monitored in a scy mutant

We were interested to see the filamentation behaviour of FilP-EGFP in the *scy* mutant possibly hypothesizing that FilP-EGFP filaments would be abolished in the *scy* mutant. The plasmid pIJ8660-PfilP-filP-egfp (pK67) was passaged into the *scy* mutant strain through conjugation with *E. coli* ET 12567/pUZ8002. Spores of *scy* carrying pIJ8660-PfilP-filP-egfp were grown on cellophane on top of SFM medium for 12-16 hours and then

visualised through fluorescence microscopy (Figure 69). However, there were still FilP-EGFP filaments in the *scy* mutant, though we speculate that there may be less FilP-EGFP filaments. FilP-EGFP still forms aggregates in the *scy* mutant and perhaps aggregates more in the *scy* mutant than in the wild-type strain. If FilP-EGFP does form less filaments in the *scy* mutant then this may suggest that Scy helps to promote FilP filamentation. Alternatively the effects on cell shape that occur when *scy* is deleted could act as a secondary factor, whereby one of the cues for FilP filament formation is the physical structure presented by the cell membrane and cell wall.

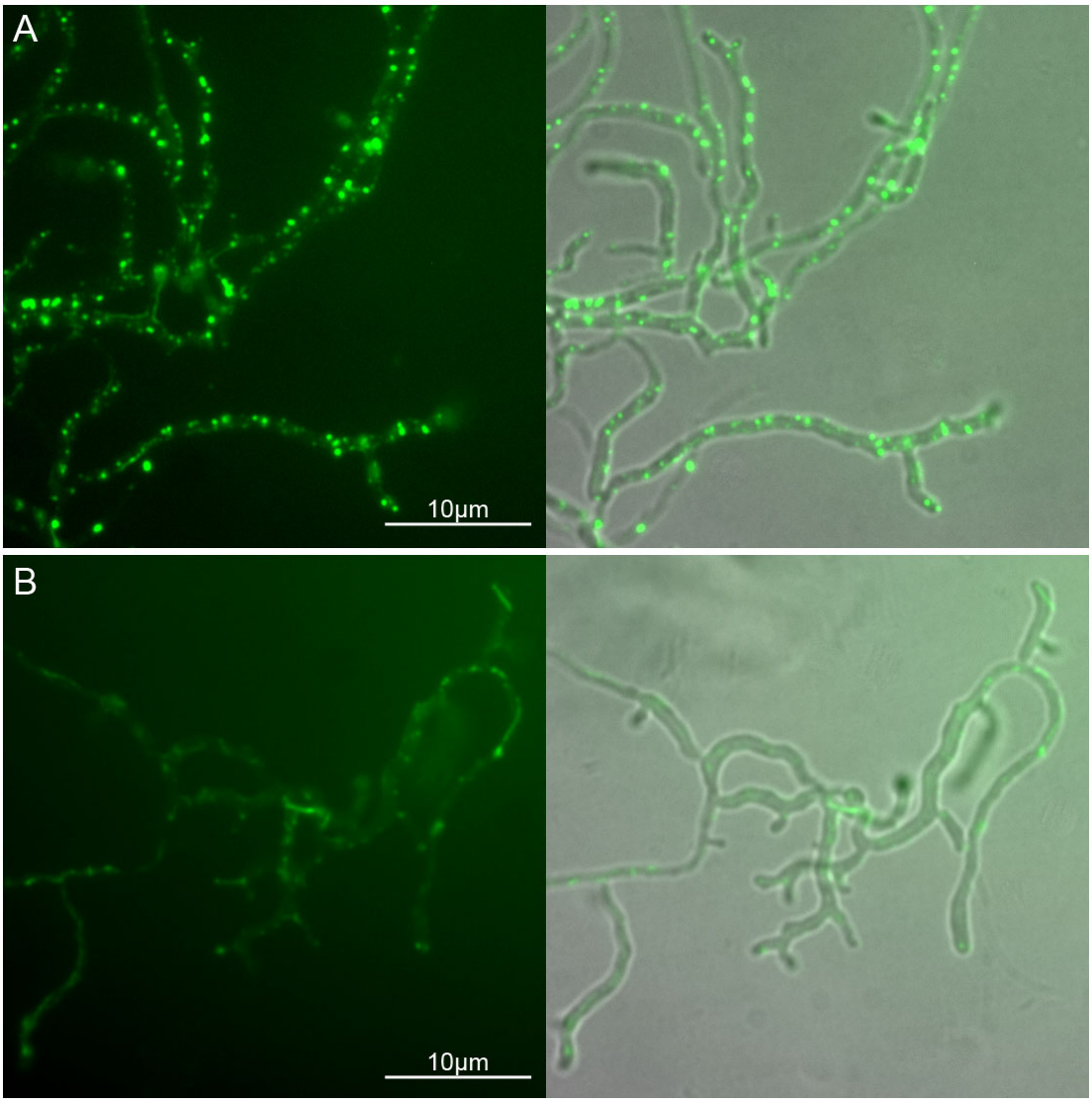

Figure 69: FilP-EGFP in a *scy* mutant formed filaments and aggregates at undefined locations along the hyphae. Filaments may have a preference for forming on the inner curve of a hyphal bend. The strain *scy* carrying pIJ8660-PfilP-filP-EGFP, was grown for 16 hours on solid SFM medium and the samples were viewed by laser-scanning confocal microscopy (A+B). Corresponding fluorescence images are left of the respective merged fluorescent/brightfield image. Scale bars are shown.

5.1.4 Co-localisation of FilP and Scy was observed in vegetative hyphae

To be able to co-localise FilP and Scy, the plasmid pIJ8660-PfilP-filP-egfp (pK67) was combined in the same M145 strain as already carrying pMS82-Pscy-mCherry-scy. Spores of M145 carrying pIJ8660-PfilP-filP-egfp and pMS82-Pscy-mCherry-scy were grown on

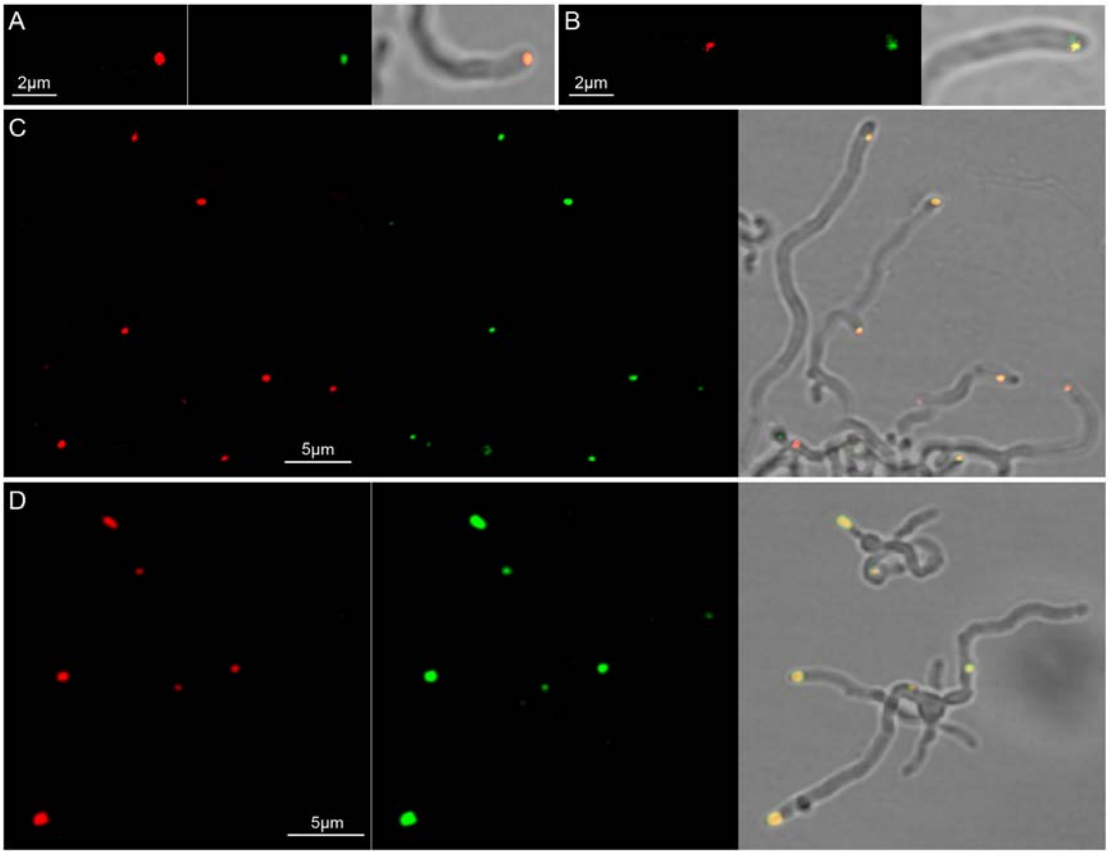

Figure 70: FilP co-localisates with Scy at apical sites. Localisation of mCherry-Scy foci (in red) overlaps with FilP-EGFP foci (in green). Co-localisation can be seen merged with the brightfield image, whereby both proteins localise to hyphal tips (A-D). However FilP-EGFP filaments were not visible. *S. coelicolor* M145/pMS82-Pscy-mCherry-scy/pIJ8660-PfilP-filP-egfp, was grown for 16 hours on solid SFM medium and the samples were viewed by laser-scanning confocal microscopy. Corresponding fluorescence images are next to one another and the respective overlayered image. Scale bars are shown.

cellophane on top of SFM medium for 12-16 hours and then visualised through fluorescence microscopy (Figure 70). There were often co-localising foci of FilP and Scy at the hyphal tips. However, FilP-EGFP filaments were not visible. The hyphae although resembling wild-type also displayed some of the phenotypic effects seen when the Scy N-terminal fusions were introduced. The effect of a Scy fusion as well as a FilP fusion and their respective native copies possibly leaves conditions that are too artificial and perhaps this is why there were no FilP-EGFP filaments visible. Possibly explaining why FilP-

EGFP shows a different localisation pattern when mCherry-Scy is present (Figure 70) in comparison to complete absence of Scy (Figure 69). However, the fact that Scy and FilP co-localised at hyphal tips would suggest that they somehow function cooperatively in the hyphal tips of *Streptomyces*.

5.1.5 FilP-mCherry localises differenty to FilP-EGFP

As localisation of FilP-EGFP perhaps generated many artefacts as a result of the fusion to EGFP, we sought to localise FilP with a different fluorescent fusion. The construct pKF59 used for assessing the localisation of DivIVA (Flärdh, 2003a) is of course an EGFP fusion so a different tag to FilP would also enable the combination of localisation of FilP and DivIVA as well. We constructed the plasmid pIJ8660-PfilP-filP-mCherry (10.1.56), which enables expression of a FilP-mCherry fusion protein under the control of the native *filP* promoter sequence. The vector was mobilised into *Streptomyces* via conjugation and integration in the same method as previously discussed for pIJ8660 vectors. Spores of M145 carrying pIJ8660-PfilP-filP-mCherry were grown on cellophane on top of SFM medium for 12-16 hours and then visualised through fluorescence microscopy (Figure 71). Less FilP filaments were seen with the mCherry fusion than with the EGFP fusion. Whereas many aggregates were still visible with the mCherry fusion. Perhaps suggesting that FilP-mCherry is aberrant at forming the native structures formed by untagged FilP or the filaments seen by FilP-EGFP. Although there were less filaments there were occasionally visible small basket like structures behind the hyphal tip (Figure 71B). These look somewhat different to the FilP-EGFP filaments, instead of forming predominantly on one side of the hyphae they seem to encase either side of the hyphal wall. They appeared to follow behind the hyphal tips, so pIJ8660-PfilP-filP-mCherry was also introduced into M145 already carrying pKF59 (Flärdh, 2003a). Consistent with the observation above, the FilP-mCherry baskets followed behind the apical signal seen with DivIVA-EGFP (Figure 71D&E). It may be that the complex of proteins at the hyphal tip in the form of either Scy, DivIVA or any other factors may make contact with FilP structures and promote their assembly. There appeared to be no obvious relationship between FilP-mCherry aggregates and the localisation of DivIVA-EGFP (Figure 71C,D&E).

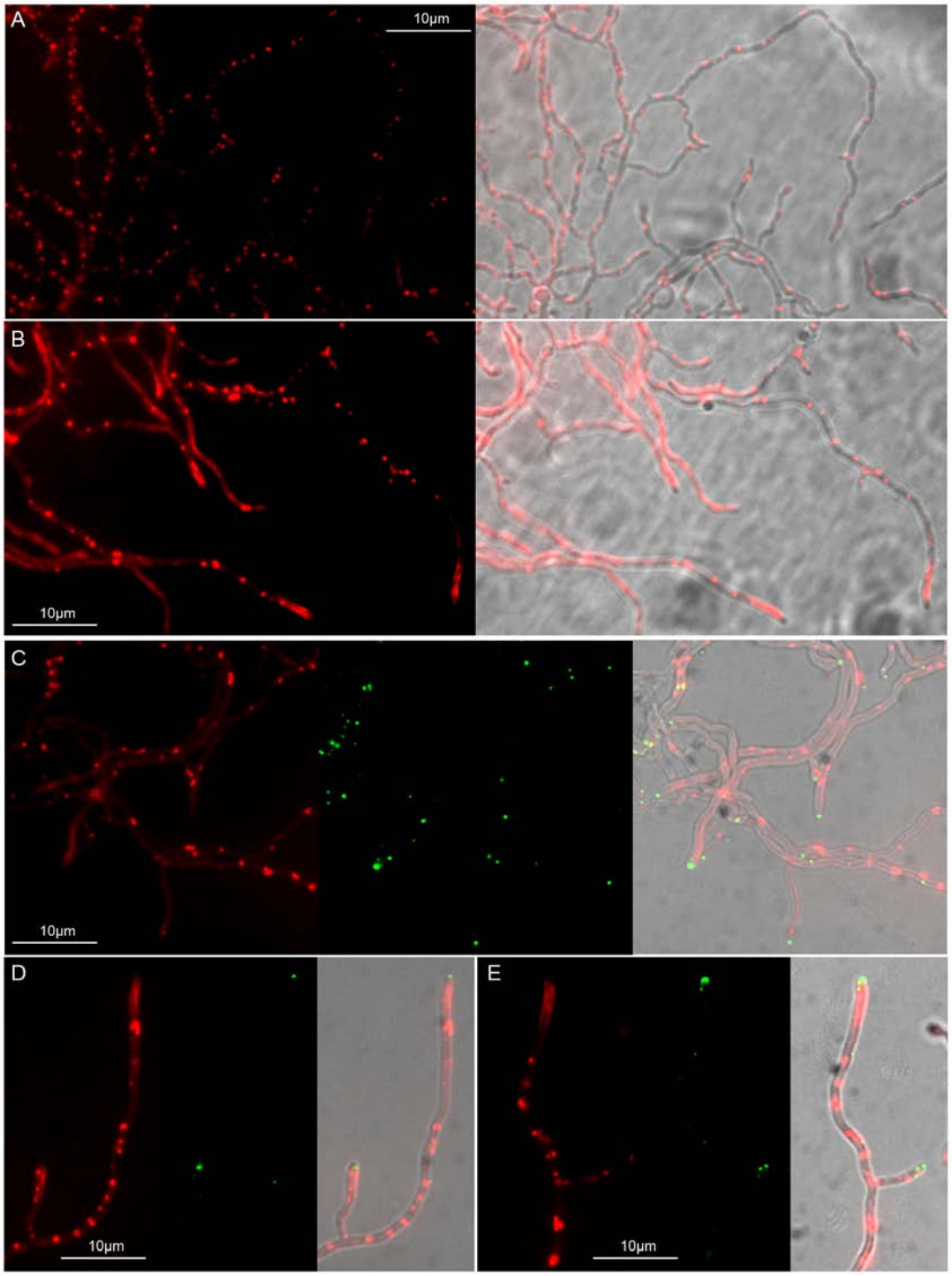

Figure 71: Localisation of FilP-mCherry was to foci at undefined locations along hyphae as well as a more diffuse signal in other locations (A&B). FilP-mCherry (in red) does not overlap with DivIVA-EGFP foci (in green) but could localise close to DivIVA-EGFP near the tips of some hyphae (C,D&E). Both signals can be seen merged with the brightfield image (right). Either *S. coelicolor* M145/pIJ8660-PfilP-filP-mCherry or M145/pKF59/pIJ8660-PfilP-filP-mCherry, was grown for 16 hours on solid SFM medium and the samples were viewed by laser-scanning confocal microscopy. Corresponding fluorescence images are next to one another and the respective overlayered image. Scale bars are shown.

5.1.6 FilP-Δlink-mCherry localises similarly to FilP-mCherry

As the generation of a Scy C-terminal fusion with mCherry resulted in a difference between having the presence or absence of a linker, we wanted to test a FilP-mCherry C-terminal fusion without the His-Met-Gly-Gly-Gly-Gly-Gly linker found in pIJ8660-PfilP-filP-mCherry. We constructed a pIJ8660 plasmid carrying a non-linkered *filP-mCherry* fusion. The plasmid pIJ8660-PfilP-filP-Δlink-mCherry (10.1.57) enables expression of a FilP-mCherry fusion protein lacking a glycine linker, driven by the native *filP* promoter sequence. The vector was passaged into *Streptomyces* via conjugation and integration in the same method as previously discussed for pIJ8660 vectors. Spores of M145 carrying pIJ8660-PfilP-filP-Δlink-mCherry were grown on cellophane on top of SFM medium for 12-16 hours and then visualised through fluorescence microscopy (Figure 72). Similarly to the FilP-mCherry fusion, less FilP filaments were seen with the Δlink-mCherry fusion than with the EGFP fusion. Whereas many aggregates were also still visible with the Δlink-mCherry fusion. Perhaps suggesting that FilP-Δlink-mCherry is also aberrant at forming the native structures formed by untagged FilP or the filaments seen by FilP-EGFP. Like FilP-mCherry, FilP-Δlink-mCherry had the small basket like structures behind the hyphal tip (Figure 72B). The plasmid pIJ8660-PfilP-filP-Δlink-mCherry was also introduced into M145 carrying pKF59 (Flärdh, 2003a). In the strain M145/pKF59/pIJ8660-PfilP-filP-Δlink-mCherry also formed FilP-Δlink-mCherry baskets just behind the DivIVA-EGFP foci (Figure 72D). Similarly there also appeared to be no obvious relationship between FilP-mCherry aggregates and the localisation of DivIVA-EGFP (Figure 72C&D). Therefore, instead of in the case of Scy, for FilP-mCherry fusions the non-linkered fusion and the linkered fusion show no apparent difference.

5.2 Detection of FilP fluorescent fusion proteins

In order to confirm the expression of fusion proteins of FilP to the respective fluorescent tags, cell extracts of *S. coelicolor* were analysed on SDS-PAGE gels under semi-denaturing conditions and visualised using a phosphoimager with settings that could detect the fluorophores. Spores of M145 carrying either pIJ8660-PfilP-filP-egfp, pIJ8660-PfilP-filP-mCherry or pIJ8660-Pscy-scy-Δlink-mCherry were inoculated onto cellophane placed on top of SFM medium for 18 hours. Cell material was then collected from the cellophane surface, cells were lysed through FastPrep treatment, by vigorous shaking in the presence

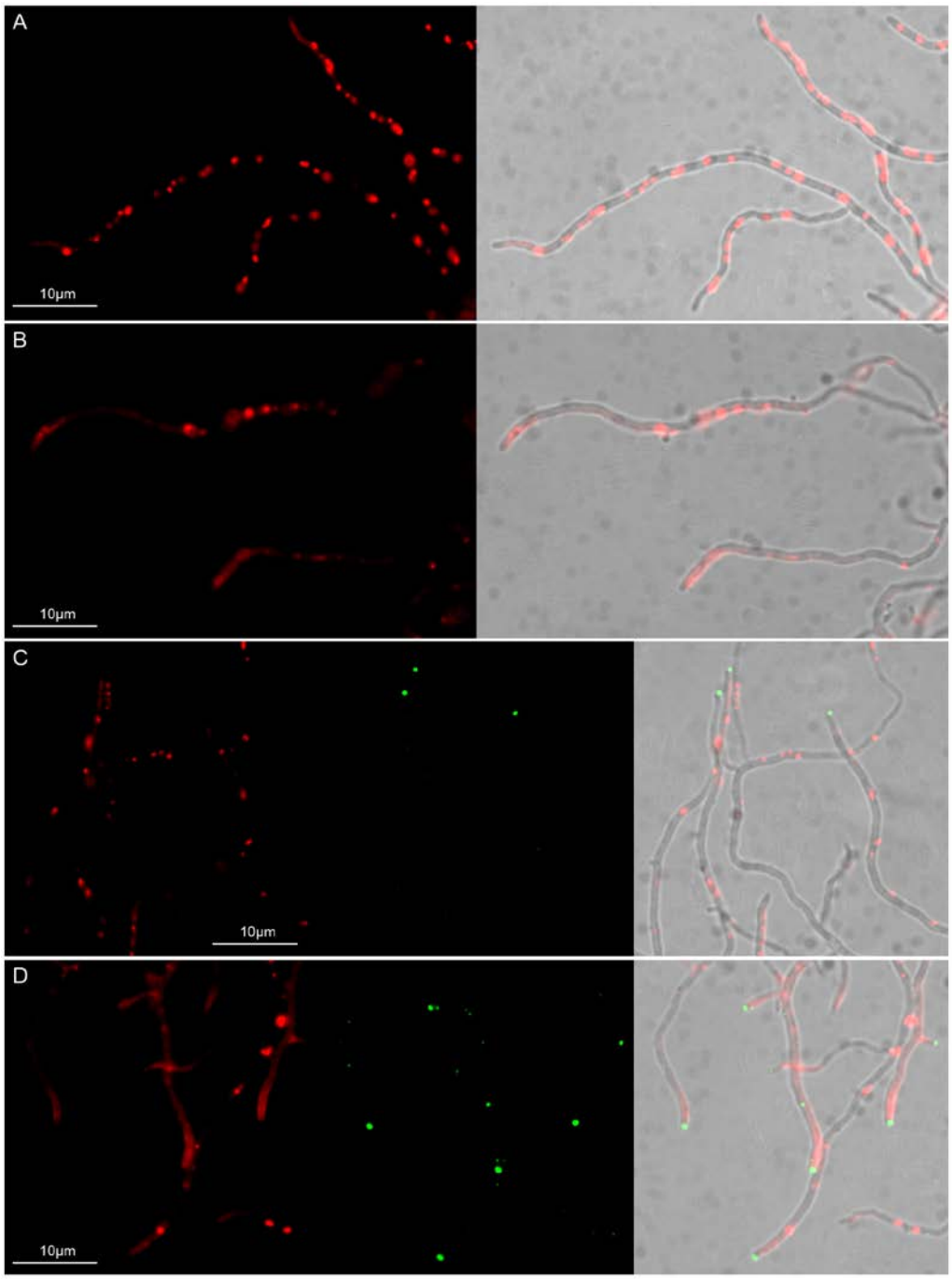

Figure 72: Localisation of FilP-Δlink-mCherry was to foci at undefined locations along hyphae as well as a more diffuse signal in other locations (A&B). FilP- Δlink-mCherry (in red) does not overlap with DivIVA-EGFP foci (in green) but could localise close to DivIVA-EGFP near the tips of some hyphae (C&D). Both signals can be seen merged with the brightfield image (right). Either *S. coelicolor* M145/pIJ8660-PfilP-filP-Δlink-mCherry or M145/pKF59/pIJ8660-PfilP-filP-Δlink-mCherry, were grown for 16 hours on solid SFM medium and the samples were viewed by laser-scanning confocal microscopy. Corresponding fluorescence images are next to one another and the respective overlayered image. Scale bars are shown.

of glass particles (<106μm). Following this, the samples were centrifuged, the supernatants were collected and the pellets were re-suspended in the same buffer as before. The samples were then analysed on SDS-PAGE gels whereby the samples were not boiled prior to loading therefore preventing denaturation of the fluorescent tags and maintaining fluorescence activity.

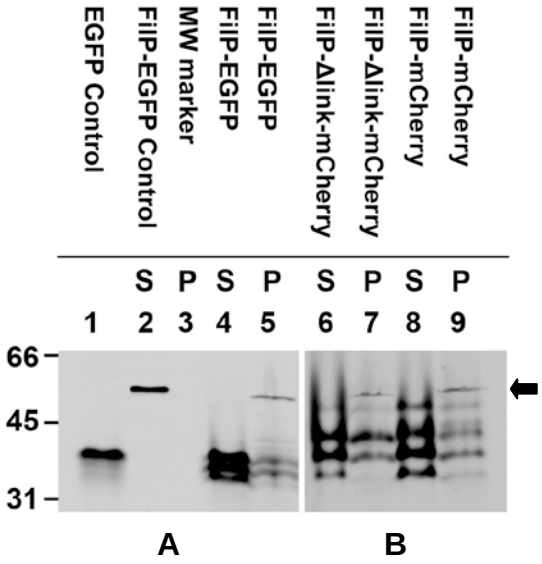

Figure 73: SDS-PAGE was used to detect the FilP fluorescent fusion proteins. For analysis of the EGFP fusions the gel was excited at 488nm and the emission read at 532nm (A). For analysis of the mCherry fusions the gel was excited at 532nm and the emission read at 555nm (B). A control of a cell extract of expressing EGFP from Psco4002 (Holmes and Kelemen, unpublished) after 40 hours growth was used (Lane 1). A control of purified FilP-EGFP from *E.coli* was used (Holmes, unpublished) (Lane 2). A signal can be seen for cell extracts of M145/pIJ8660-PfilP-filP-egfp (Lane 4 & 5). A signal can be seen for cell extracts of M145/pIJ8660-PfilP-filP-Δlink-mCherry (Lane 6 & 7). A signal can be seen for cell extracts of M145/pIJ8660-PfilP-filP-mCherry (Lane 8 & 9). Samples were separated into both Supernatant fractions (S) and Pellet fractions (P). Shown on the left hand side are the positions and sizes of a protein MW marker (Lane 3, not visible on images shown) displayed in kDa. The arrow shows the size of the higher molecular weight band representing a fusion protein.

The gel was visualised for EGFP activity by exciting at 488nm and the emission was then read at 532nm (Figure 73A). Similarly to monitor mCherry activity the gel was instead excited at 532nm and the emission was then read at 555nm (Figure 73B). The expected size for the FilP-EGFP fusion protein from pIJ8660-PfilP-filP-egfp was 62.3kDa, it was seen that there was a higher molecular weight band for M145 carrying pIJ8660-PfilP-filP-egfp that could correspond to the size of a FilP fluorescent protein fusion. A cell extract from *E. coli* overexpressing FilP-EGFP generated a band at a similar position. Therefore, it is reasonable to suggest that this is evidence that the FilP-EGFP fusion protein was successfully generated and expressed in *S. coelicolor*. It can also be seen that there are bands of smaller sizes, these could possibly be products of partial degradation of the protein. It is unclear if this resembles activity in the hyphae that we see microscopically, or could be damaged/dead hyphae or partially proteolysed protein produced when lysing the cells. The expected size for the FilP-mCherry fusion protein was 61.8kDa and for FilP-Δlink-mCherry was 61.5kDa, both the M145 strains carrying either pIJ8660-PfilP-filP-mCherry or pIJ8660-PfilP-filP-Δlink-mCherry have a higher molecular weight band that

likely represents expression of the fusion proteins. This would support the microscopic observations that there is little difference between the two constructs. Unlike Scy the presence of the Glycine linker on a C-terminal mCherry fusion did not make a difference for FilP. It is interesting to note that the higher proportion of activity of the FilP fusion proteins is in the pellet fractions suggesting that FilP is possibly insoluble/ forms higher order structures or makes contact with the cell wall.

5.2.1 Summary

Monitoring of FilP-EGFP confirmed that this fusion protein forms filaments down the hyphae of *Streptomyces* and occasionally at hyphal tips. We also noticed that FilP-EGFP forms aggregates. FilP-EGFP filaments were still present in a *scy* mutant, however filamentation was reduced, but the effects of *scy* mutation on FilP formation is unclear. Scy and FilP fusions colocalise but in an artificial manner due to the non-native scenario in the strain studied. FilP fluorescent fusion to mCherry formed structures behind the hyphal tip and DivIVA, as well as aggregations in other locations. The localisation pattern of FilP fusions suggests some role in apical growth, however the functionality of FilP fusions is currently in question.

6 Using a Bacterial Two-Hybrid System to Analyse Interactions of the *S. coelicolor* Hyphal Tip

6.1.1 Introduction

As Scy, DivIVA and FilP may all be associated with hyphal tips and all contain coiled-coil regions, we wanted to see if they might function together possibly by interaction. In order to test protein-protein interactions *in vivo* in a heterologous host we implemented the use of a bacterial two-hybrid system (Karimova *et al.*, 1998; Karimova *et al.*, 2000)(Figure 74). The system works by splitting the adenylate cyclase of *Bordetella pertussis* into two non-functional parts, T18 and T25. The fusing of these fragments to two separate proteins of interest results in a screen whereby if the bait proteins interact then it can allow reconstitution of the two fragments into an active adenylate cyclase. As adenylate cyclase catalyses the conversion of ATP to cAMP the coupling of this system in an adenylate cyclase-deficient strain of *E. coli* (*cya*) allows monitoring of a cAMP signal transduction. When produced, cAMP activates the cAMP dependent catabolite activator protein (CAP) which in turn switches on the *lac* promoter. The reporter gene *lacZ* encoding β-galactosidase can be monitored with a traditional Blue/White screen using X-gal as the substrate for LacZ.

To be able to test our genes of interest in this system and thus study protein-protein interactions, the BACTH vectors pUT18C and pKT25 were used (Karimova *et al.*, 2000)(Figure 205). These vectors both have a multiple cloning site (MCS) downstream of DNA encoding either T18 (pUT18C) or T25 (pKT25) domains allowing cloning in fusions to the C-terminal end of each CyaA domain. They also encode separate resistance markers of ampicillin and kanamycin for pUT18C and pKT25, respectively. The plasmid pUT18C is a derivative of the high copy number vector pUC19 (Yanisch-Perron *et al.*, 1985). Whereas pKT25 is a derivative of the low copy number vector pSU40 (Bartolome *et al.*, 1991). Both vectors have separate replicons making them compatible for cotransformation in the same host for screening of interactions via β-galactosidase activity.

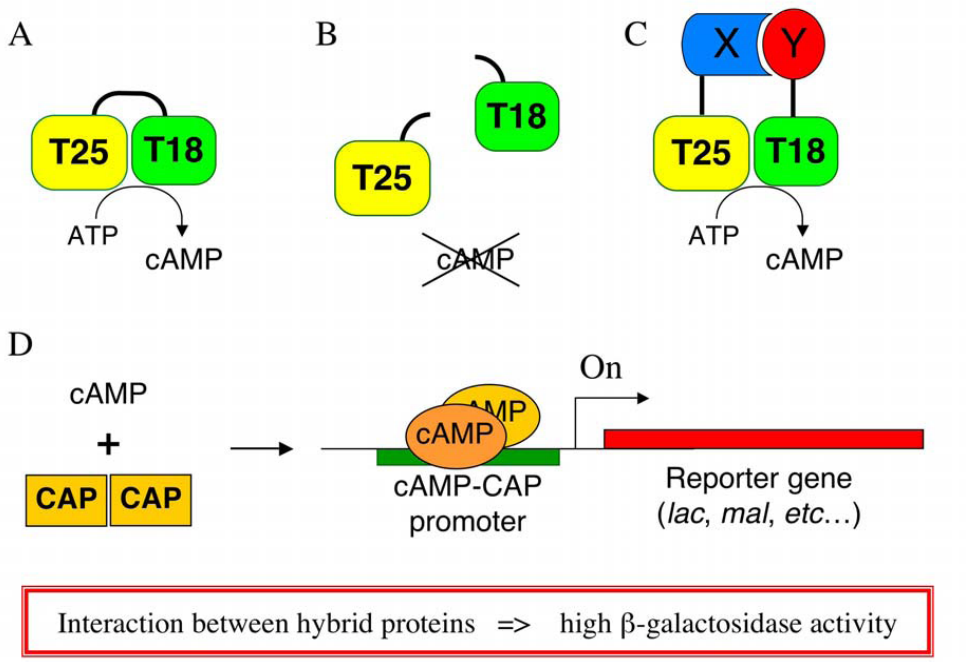

Figure 74: The BACTH Bacterial Two-Hybrid System. Taken from Karimova *et al.*, (2000). The *Bordetella pertussis* adenylate cyclase (CyaA) consists of two domains T25 and T18 both needed to catalyse the conversion of ATP into cAMP (A). When these are separate the enzymatic activity is lost (B). Heterodimerisation of the T25 and T18 domains through interaction of two fused proteins X and Y to either domain, restores the enzymatic activity (C). Increased cAMP produced by T25 and T18 binds to CAP. CAP bound to cAMP acts as a transcriptional regulator of genes including the *lac* or *mal* operons (D). This allows the *E.coli* to utilise lactose or maltose, thus enabling the screening of these genes, i.e., the activity of β-galactosidase on X-gal containing media.

6.1.2 Interactions between full length Scy, DivIVA and FilP in the BTH system

To investigate if the cytoskeletal proteins Scy, DivIVA and FilP interact *in vivo*, protein pairs were tested using the bacterial two-hybrid system. It has already been shown that T18-Scy and T25-Scy restored the adenylate cyclase function in a cAMP dependent β-galactosidase assay (Walshaw *et al.*, 2010) suggesting either parallel homo-dimerisation of Scy and/or interactions within a higher order assembly. Previously before in the Kelemen lab (unpublished) it has been shown that Scy and FilP interact in the bacterial two-hybrid system. We wanted to test the Scy and FilP interaction in this experiment in order to compare it to the tests between Scy and DivIVA. The FilP constructs (Holmes *et al.*, 2013) used in the experiment can be seen in Figure 209. In order to test the interactions of DivIVA we cloned *divIVA* into pUT18C and pKT25 to generate DNA encoding T18-DivIVA or T25-DivIVA with T18 or T25 at the N-terminal of DivIVA, respectively (10.1.58).

Displayed in Table 7 are the scores from interactions between T18-Scy against the partners of T25-Scy, T25-DivIVA and T25-FilP (Figure 75). T18-DivIVA against the partners of T25-Scy, T25-DivIVA and T25-FilP (Figure 76). T18-FilP against the partners of T25-Scy, T25-DivIVA and T25-FilP (Figure 77). Having tested all the homo- and hetero-pairs of proteins it appears that we were able to demonstrate *in vivo* pairwise interactions between all the tested pairs. Interestingly interactions between T25-DivIVA and T18-Scy or T18-FilP were reproducibly weaker than between T18-DivIVA and the corresponding T25 fusions. As mentioned before (6.1.1), pKT25 is a low copy number vector whereas pUT18C is a high copy vector, therefore we can speculate that for successful interactions DivIVA had to be supplied in a greater amount than either Scy or FilP. This could be explained by effects brought on by oligomerisation of the proteins and the effect that this has on the need to bring together the N-terminal domains of the adenylate cyclase in order to get a positive reaction. The interaction between T18-Scy and T25-DivIVA in Figure 75.4 is the same pairing as in Figure 82.3 (shown later), There appears to be a discrepancy between the interaction scores, this is likely reflective of repeat experiments where the bacterial two-hybrid system may not behave exactly the same way in terms of colour development. However, consistently when T18 is fused to DivIVA a greater reaction is seen with T25-Scy than the opposite pairings (Compare Figure 75.4 to Figure 76.3 and Figure 82.3 to Figure 79.3 where the colour indicates more quickly with a T18-DivIVA/T25-Scy pairing). A similar discrepancy can be seen with T25-FilP and T18-DivIVA in Figure 77.4 and Figure 88.3.

Table 7: Bacterial Two-Hyrid interactions and scores from full length Scy, DivIVA and FilP experiments.

Crossreference	pUT18C construct	pKT25 construct	Interaction Score
Figure 75.1	pUT18C-zip	pKT25-zip	+++
Figure 75.2	pUT18C	pKT25	
Figure 75.3	pUT18C-scy	pKT25-scy	+++
Figure 75.4	pUT18C-scy	pKT25-divIVA	
Figure 75.5	pUT18C-scy	pKT25-filP	++
Figure 76.3	pUT18C-divIVA	pKT25-scy	++
Figure 76.4	pUT18C-divIVA	pKT25-divIVA	++
Figure 76.5	pUT18C-divIVA	pKT25-filP	++
Figure 77.3	pUT18C-filP	pKT25-scy	++
Figure 77.4	pUT18C-filP	pKT25-divIVA	

Figure 77.5	pUT18C-filP	pKT25-filP	+++

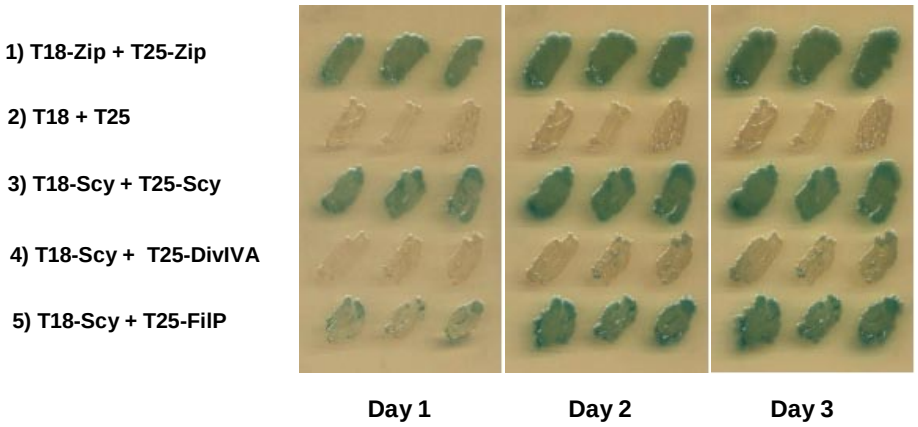

Figure 75: The bacterial two-hybrid system was used to analyse protein:protein interactions. Transformants of BTH101 was performed with the following plasmid pairs; 1) pUT18C-zip + pKT25-zip, 2) pUT18C + pKT25, 3) pUT18C-scy + pKT25-scy, 4) pUT18C-scy + pKT25-divIVA, 5) pUT18C-scy + pKT25-filP. Three colonies of each transformant were streaked on LB solid medium omitting glucose plus X-gal and IPTG. The plates were imaged at growth after 1, 2 and 3 days at 30ºC. Blue colour of colonies was indicative of interactions as seen in the positive control (1). Whereas colonies that remained pale were regarded to be negative as can be seen with the negative control (2).

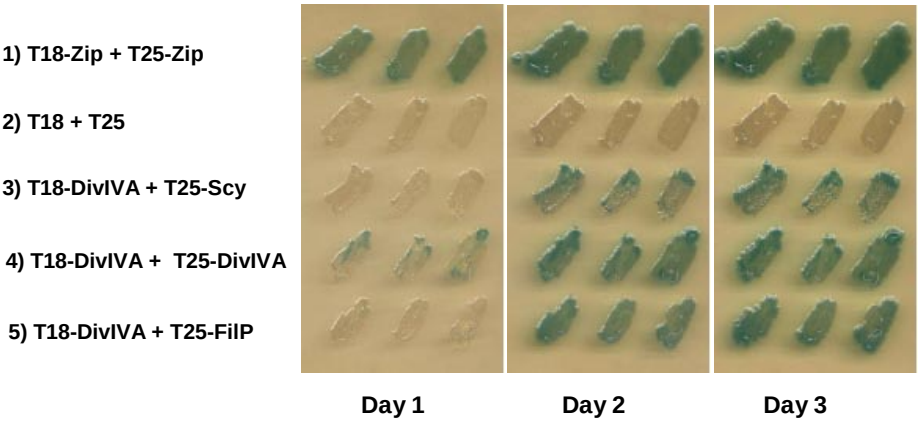

Figure 76: The bacterial two-hybrid system was used to analyse protein:protein interactions between Scy, DivIVA and FilP. Transformants of BTH101 was performed with the following plasmid pairs; 1) pUT18C-zip + pKT25-zip, 2) pUT18C + pKT25, 3) pUT18C-divIVA + pKT25-scy, 4) pUT18C-divIVA + pKT25-divIVA, 5) pUT18C-divIVA + pKT25-filP. Three colonies of each transformant were streaked on LB solid medium omitting glucose plus X-gal and IPTG. The plates were imaged at growth after 1, 2 and 3 days at 30ºC. Blue colour of colonies was indicative of interactions as seen in the positive control (1). Whereas colonies that remained pale were regarded to be negative as can be seen with the negative control (2).

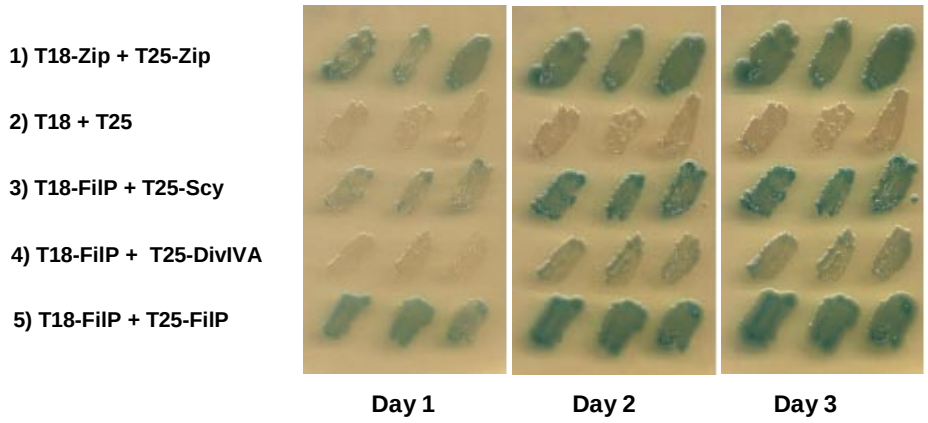

Figure 77: The bacterial two-hybrid system was used to analyse protein:protein interactions between Scy, DivIVA and FilP. Transformants of BTH101 was performed with the following plasmid pairs; 1) pUT18C-zip + pKT25-zip, 2) pUT18C + pKT25, 3) pUT18C-filP + pKT25-scy, 4) pUT18C-filP + pKT25-divIVA, 5) pUT18C-filP + pKT25-filP. Three colonies of each transformant were streaked on LB solid medium omitting glucose plus X-gal and IPTG. The plates were imaged at growth after 1, 2 and 3 days at 30ºC. Blue colour of colonies was indicative of interactions as seen in the positive control (1). Whereas colonies that remained pale were regarded to be negative as can be seen with the negative control (2).

6.1.3 Dissection of interactions between Scy and DivIVA domains in the BTH system

The protein DivIVA, from *B. subtilis* has been recently crystallised (Oliva *et al.*, 2010), there are two separate coiled-coil sections; CC1 and CC2 (Figure 78A). CC2 may or may not be a 51-mer non-heptad coiled coil similar to the CC51 region of Scy and FilP (Walshaw *et al.*, 2010). However, crystallisation was performed by separating DivIVA into two separately folding parts, an N-terminal domain and a C-terminal domain (Figure 78B). *S. coelicolor* DivIVA is similar to that of *B. subtilis* except that it has an extended PQG region and C-terminal tail (Figure 78C). For Bacterial two-hybrid studies we wanted to narrow down whether the N-terminal half of DivIVA was responsible for Scy interaction or the C-terminal half of DivIVA. Therefore, we aimed to separate DivIVA into DivIVA-N and DivIVA-C as marked in Figure 78D. Constructs were then generated for either *divIVA-N* (10.1.58) or *divIVA-C* (10.1.60) in pUT18C or pKT25.

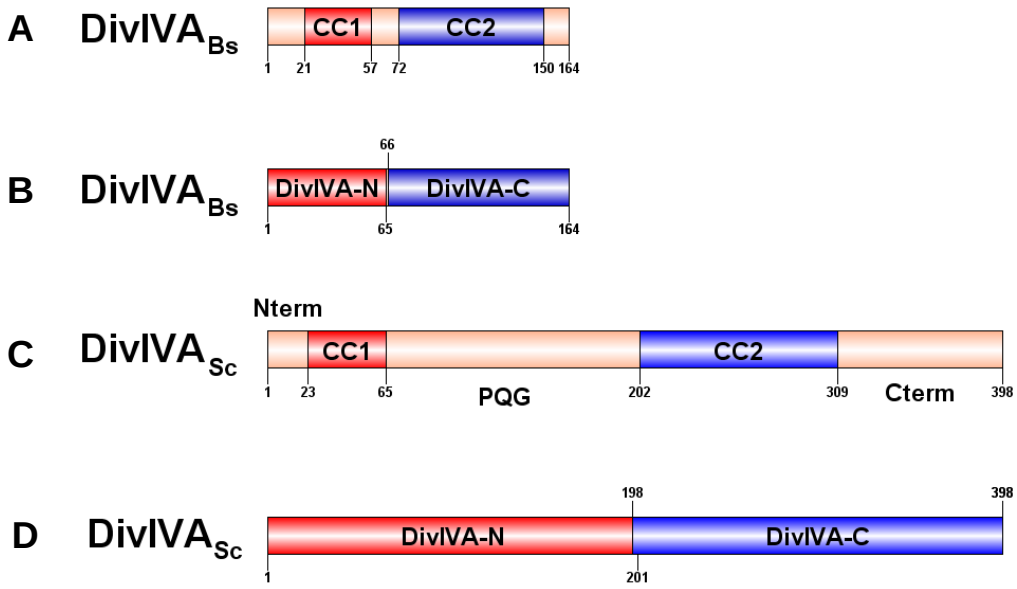

Figure 78: The architecture of DivIVA. A) DivIVA of *B. subtilis* has two coiled-coil sections, CC1 (red) and CC2 (blue) (based on crystal structure data (Oliva *et al.*, 2010)). B) For crystallising *B. subtilis* DivIVA was separated into two; the N-terminus (red) and the C-terminus (blue). C) *S. coelicolor* DivIVA has an extended PQG linker separating the coiled-coils as well as an extended C-terminus (based on data from Wang *et al.*, (2009)). D) For narrowing down DivIVA interactions we aimed to separate *S. coelicolor* DivIVA into two, so we separated; the N-terminus (red) containing the short Nterm segment, CC1 and PQG (amino acid residues 1-201), and the C-terminus (blue) containing CC2 and the extended Cterm (amino acid residues 198-398). Amino acid residues at borders are labelled.

To investigate the interaction between Scy and DivIVA *in vivo*, domain pairs were monitored in the bacterial two-hybrid system. Displayed in Table 8 are the scores from interactions between T18-DivIVA against the partners of T25-Scy, T25-Scy-N and T25-Scy-C (Figure 79). T18-DivIVA-N against the partners of T25-Scy, T25-Scy-N, T25-Scy-C and T25-DivIVA as a control (Figure 80). T18-DivIVA-C against the partners of T25-Scy, T25-Scy-N and T25-Scy-C (Figure 81). T25-DivIVA against the partners of T18-Scy, T18-Scy-N and T18-Scy-C (Figure 82). T25-DivIVA-N against the partners of T18-Scy, T18-Scy-N and T18-Scy-C (Figure 83). T25-DivIVA-C against the partners of T18-Scy, T18-Scy-N and T18-Scy-C (Figure 84). The overall effect seen was the more obvious interaction between Scy-C and DivIVA-C with full length versions of DivIVA and Scy, respectively, as well as their C domains. Less clear was the effect of DivIVA-N and Scy-N which were on the whole less reactive; however, in comparison to the negative control it cannot be ruled out that the N-terminal domains contribute towards an interaction. Consistently with (6.1.2) it seems that interactions were stronger and developed to a blue colour quicker when the T18 fusion was to DivIVA or DivIVA-C. From this experiment it seems likely that the C-terminal domain containing the 51-mer coiled-coils contributes

more strongly to the interaction between Scy and DivIVA than do the heptad coiled-coil N-terminal domains.

Table 8: Bacterial Two Hyrid Interactions and scores from Scy and DivIVA truncated domain experiments.

Crossreference	pUT18C construct	pKT25 construct	Interaction Score
Figure 79.1	pUT18C-zip	pKT25-zip	+++
Figure 79.2	pUT18C	pKT25	
Figure 79.3	pUT18C-divIVA	pKT25-scy	++
Figure 79.4	pUT18C-divIVA	pKT25-scy-N	
Figure 79.5	pUT18C-divIVA	pKT25-scy-C	++
Figure 80.3	pUT18C-divIVA-N	pKT25-scy	
Figure 80.4	pUT18C-divIVA-N	pKT25-scy-N	
Figure 80.5	pUT18C-divIVA-N	pKT25-scy-C	
Figure 80.6	pUT18C-divIVA-N	pKT25-divIVA	++
Figure 81.3	pUT18C-divIVA-C	pKT25-scy	+++
Figure 81.4	pUT18C-divIVA-C	pKT25-scy-N	
Figure 81.5	pUT18C-divIVA-C	pKT25-scy-C	++
Figure 82.3	pUT18C-scy	pKT25-divIVA	++
Figure 82.4	pUT18C-scy-N	pKT25-divIVA	
Figure 82.5	pUT18C-scy-C	pKT25-divIVA	++
Figure 83.3	pUT18C-scy	pKT25-divIVA-N	
Figure 83.4	pUT18C-scy-N	pKT25-divIVA-N	
Figure 83.5	pUT18C-scy-C	pKT25-divIVA-N	
Figure 84.3	pUT18C-scy	pKT25-divIVA-C	++
Figure 84.4	pUT18C-scy-N	pKT25-divIVA-C	
Figure 84.5	pUT18C-scy-C	pKT25-divIVA-C	++

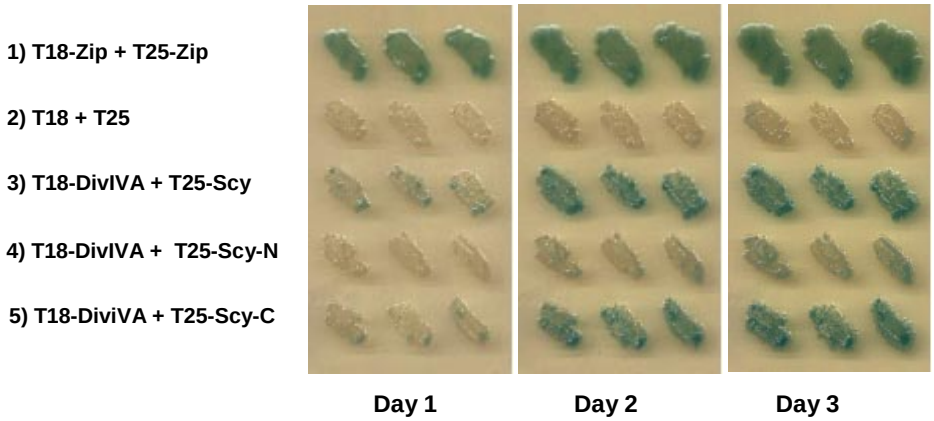

Figure 79: The bacterial two-hybrid system was used to analyse protein:protein interactions between DivIVA and the domains of Scy. Transformants of BTH101 was performed with the following plasmid pairs; 1) pUT18C-zip + pKT25-zip, 2) pUT18C + pKT25, 3) pUT18C-divIVA + pKT25-scy, 4) pUT18C-divIVA + pKT25-scy-N, 5) pUT18C-divIVA + pKT25-scy-C. Three colonies of each transformant were streaked on LB solid medium omitting glucose plus X-gal and IPTG. The plates were imaged at growth after 1, 2 and 3 days at 30ºC. Blue colour of colonies was indicative of interactions as seen in the positive control (1). Whereas colonies that remained pale were regarded to be negative as can be seen with the negative control (2).

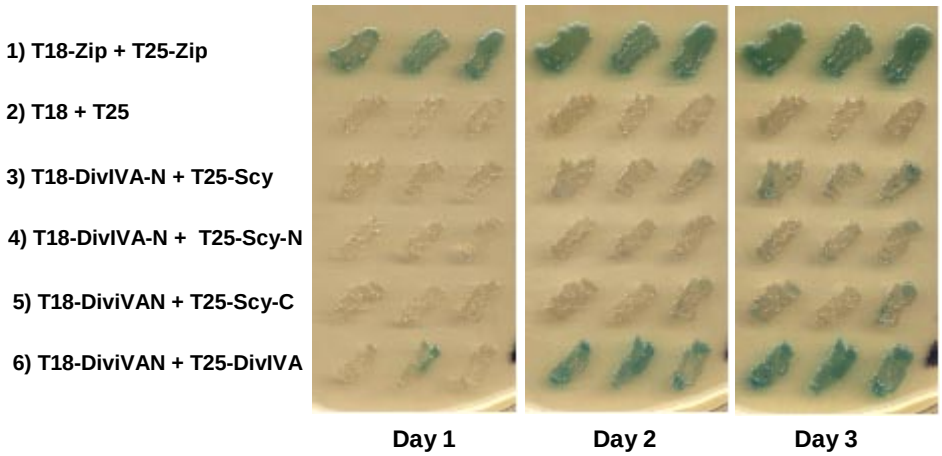

Figure 80: The bacterial two-hybrid system was used to analyse protein:protein interactions between DivIVA-N and the domains of Scy. Transformants of BTH101 was performed with the following plasmid pairs; 1) pUT18C-zip + pKT25-zip, 2) pUT18C + pKT25, 3) pUT18C-divIVA-N + pKT25-scy, 4) pUT18C-divIVA-N + pKT25-scy-N, 5) pUT18C-divIVA-N + pKT25-scy-C, 6) pUT18C-divIVA-N vs pKT25-divIVA. Three colonies of each transformant were streaked on LB solid medium omitting glucose plus X-gal and IPTG. The plates were imaged at growth after 1, 2 and 3 days at 30ºC. Blue colour of colonies was indicative of interactions as seen in the positive control (1). Whereas colonies that remained pale were regarded to be negative as can be seen with the negative control (2).

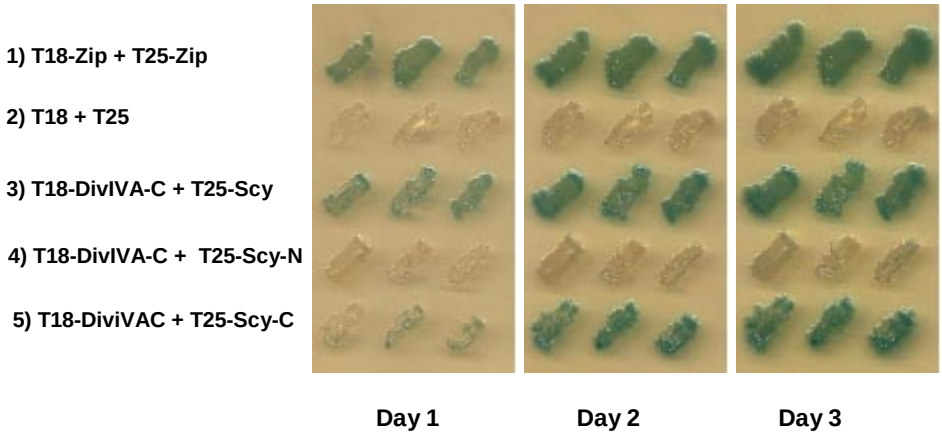

Figure 81: The bacterial two-hybrid system was used to analyse protein:protein interactions between DivIVA-C and the domains of Scy. Transformants of BTH101 was performed with the following plasmid pairs; 1) pUT18C-zip + pKT25-zip, 2) pUT18C + pKT25, 3) pUT18C-divIVA-C + pKT25-scy, 4) pUT18C-divIVA-C + pKT25-scy-N, 5) pUT18C-divIVA-C + pKT25-scy-C. Three colonies of each transformant were streaked on LB solid medium omitting glucose plus X-gal and IPTG. The plates were imaged at growth after 1, 2 and 3 days at 30ºC. Blue colour of colonies was indicative of interactions as seen in the positive control (1). Whereas colonies that remained pale were regarded to be negative as can be seen with the negative control (2).

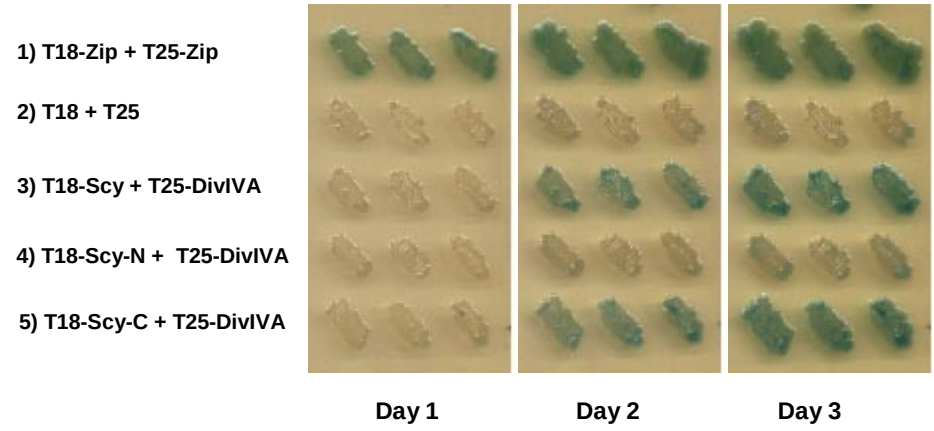

Figure 82: The bacterial two-hybrid system was used to analyse protein:protein interactions between DivIVA and the domains of Scy. Transformants of BTH101 was performed with the following plasmid pairs; 1) pUT18C-zip + pKT25-zip, 2) pUT18C + pKT25, 3) pUT18C-scy + pKT25-divIVA, 4) pUT18C-scy-N + pKT25-divIVA, 5) pUT18C-scy-C + pKT25-divIVA. Three colonies of each transformant were streaked on LB solid medium omitting glucose plus X-gal and IPTG. The plates were imaged at growth after 1, 2 and 3 days at 30ºC. Blue colour of colonies was indicative of interactions as seen in the positive control (1). Whereas colonies that remained pale were regarded to be negative as can be seen with the negative control (2).

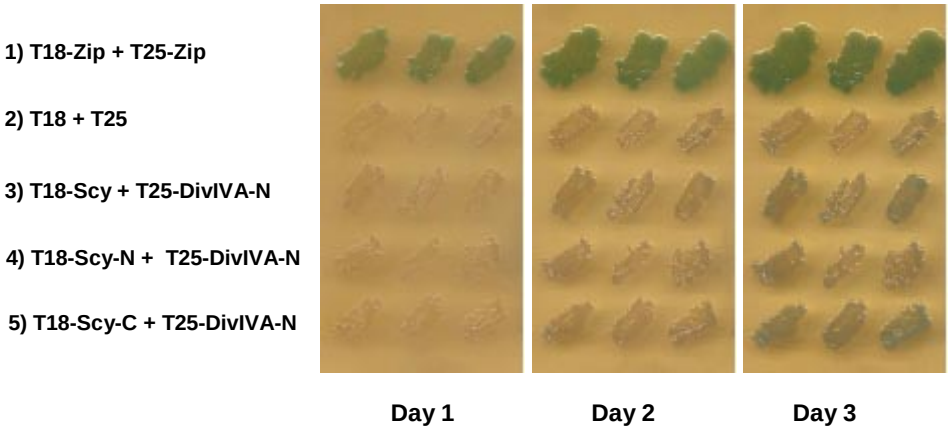

Figure 83: The bacterial two-hybrid system was used to analyse protein:protein interactions between DivIVA-N and the domains of Scy. Transformants of BTH101 was performed with the following plasmid pairs; 1) pUT18C-zip + pKT25-zip, 2) pUT18C + pKT25, 3) pUT18C-scy + pKT25-divIVA-N, 4) pUT18C-scy-N + pKT25-divIVA-N, 5) pUT18C-scy-C + pKT25-divIVA-N. Three colonies of each transformant were streaked on LB solid medium omitting glucose plus X-gal and IPTG. The plates were imaged at growth after 1, 2 and 3 days at 30ºC. Blue colour of colonies was indicative of interactions as seen in the positive control (1). Whereas colonies that remained pale were regarded to be negative as can be seen with the negative control (2).

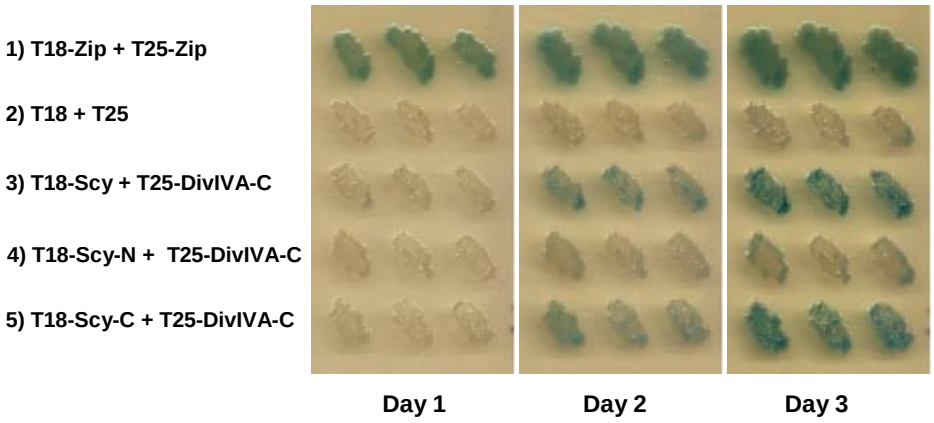

Figure 84: The bacterial two-hybrid system was used to analyse protein:protein interactions between DivIVA-C and the domains of Scy. Transformants of BTH101 was performed with the following plasmid pairs; 1) pUT18C-zip + pKT25-zip, 2) pUT18C + pKT25, 3) pUT18C-scy + pKT25-divIVA-C, 4) pUT18C-scy-N + pKT25-divIVA-C, 5) pUT18C-scy-C + pKT25-divIVA-C. Three colonies of each transformant were streaked on LB solid medium omitting glucose plus X-gal and IPTG. The plates were imaged at growth after 1, 2 and 3 days at 30ºC. Blue colour of colonies was indicative of interactions as seen in the positive control (1). Whereas colonies that remained pale were regarded to be negative as can be seen with the negative control (2).

6.1.4 Dissection of interactions between Scy domains and FilP in the BTH system

To compare the interaction between Scy and FilP *in vivo* with the Scy-DivIVA interaction, domains of Scy were monitored in the bacterial two-hybrid system with FilP. Displayed in Table 9 are the scores from interactions between T25-FilP against the partners of T18-Scy,

T18-Scy-N and T18-Scy-C (Figure 85). T18-FilP against the partners of T25-Scy, T25-Scy-N and T25-Scy-C (Figure 86). The overall effect seen was the more obvious interaction between Scy or Scy-C with full length FilP. Less clear was the effect of Scy-N and FilP which was less. There was no major difference between interactions depending on the arrangements of T18 or T25 domains with Scy domains or FilP. However, from this experiment it seems likely that the C-terminal 51-mer coiled-coil of Scy contributes more strongly to the interaction between Scy and FilP, similar to the effect seen for Scy and DivIVA. The obvious experiment that wasn't carried out here was the dissection of the domains in FilP and their contribution to the interaction with Scy.

Table 9: Bacterial Two Hyrid Interactions and scores from Scy truncated domains and full length FilP experiments.

Crossreference	pUT18C construct	pKT25 construct	Interaction Score
Figure 85.1	pUT18C-zip	pKT25-zip	+++
Figure 85.2	pUT18C	pKT25	
Figure 85.3	pUT18C-filP	pKT25-scy	+++
Figure 85.4	pUT18C-filP	pKT25-scy-N	
Figure 85.5	pUT18C-filP	pKT25-scy-C	++
Figure 86.3	pUT18C-scy	pKT25-filP	++
Figure 86.4	pUT18C-scy-N	pKT25-filP	
Figure 86.5	pUT18C-scy-C	pKT25-filP	++

6.1.5 Dissection of interactions between DivIVA domains and FilP in the BTH system

To test the interaction between DivIVA and FilP *in vivo,* domains of DivIVA were monitored in the bacterial two-hybrid system with FilP. Displayed in Table 10 are the scores from interactions between T25-FilP against the partners of T18-DivIVA, T18-DivIVA-N and T18-DivIVA-C (Figure 87). T18-FilP against the partners of T25-DivIVA, T25-DivIVA-N and T25-DivIVA-C (Figure 88). There was a difference in terms of the interactions when the arrangement of T18 and T25 domains was changed. With T18-DivIVA or T18-DivIVA-C an interaction was observable with full length FilP fused to T18.

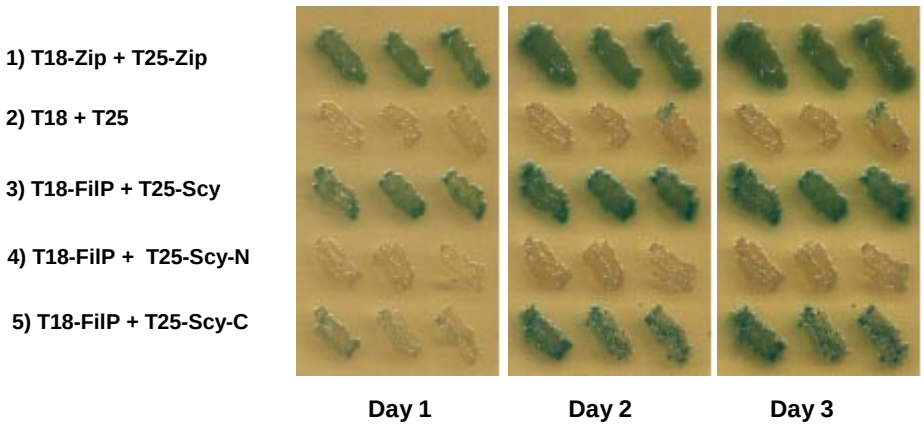

Figure 85: The bacterial two-hybrid system was used to analyse protein:protein interactions between FilP and the domains of Scy. Transformants of BTH101 was performed with the following plasmid pairs; 1) pUT18C-zip + pKT25-zip, 2) pUT18C + pKT25, 3) pUT18C-filP + pKT25-scy, 4) pUT18C-filP + pKT25-scy-N, 5) pUT18C-filP + pKT25-scy-C. Three colonies of each transformant were streaked on LB solid medium omitting glucose plus X-gal and IPTG. The plates were imaged at growth after 1, 2 and 3 days at 30ºC. Blue colour of colonies was indicative of interactions as seen in the positive control (1). Whereas colonies that remained pale were regarded to be negative as can be seen with the negative control (2).

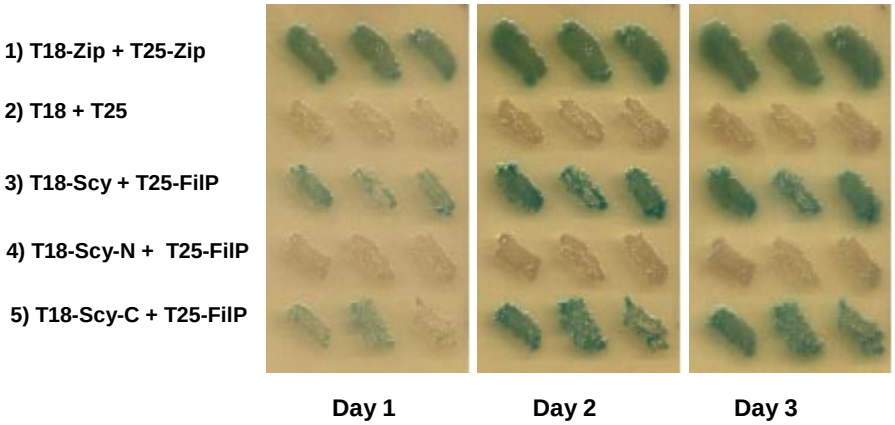

Figure 86: The bacterial two-hybrid system was used to analyse protein:protein interactions between FilP and the domains of Scy. Transformants of BTH101 was performed with the following plasmid pairs; 1) pUT18C-zip + pKT25-zip, 2) pUT18C + pKT25, 3) pUT18C-scy + pKT25-filP, 4) pUT18C-scy-N + pKT25-filP, 5) pUT18C-scy-C vs pKT25-filP. Three colonies of each transformant were streaked on LB solid medium omitting glucose plus X-gal and IPTG. The plates were imaged at growth after 1, 2 and 3 days at 30ºC. Blue colour of colonies was indicative of interactions as seen in the positive control (1). Whereas colonies that remained pale were regarded to be negative as can be seen with the negative control (2).

However, these reactions were slower to develop when the arrangement was T18-FilP and DivIVA or DivIVA-C were fused to T25. In fact T25-DivIVA-C appeared to be not much more than a possible interaction with T25-DivIVA-N and T18-FilP. Less clear was the potential interaction of T18-DivIVA-N and T25-FilP which was less than DivIVA or

DivIVA-C in this scenario. Thus, from this experiment it seems likely that DivIVA interacts with FilP, it is possible that the C-terminus of DivIVA contributes more to this interaction. Similarly to the test of Scy domains, the obvious experiment that wasn't carried out here was the dissection of the domains in FilP and their contribution to the interaction with DivIVA.

Table 10: Bacterial Two Hyrid Interactions and scores from DivIVA truncated domains and full length FilP experiments.

Crossreference	pUT18C construct	pKT25 construct	Interaction Score
Figure 87.1	pUT18C-zip	pKT25-zip	+++
Figure 87.2	pUT18C	pKT25	
Figure 87.3	pUT18C-divIVA	pKT25-filP	++
Figure 87.4	pUT18C-divIVA-N	pKT25-filP	
Figure 87.5	pUT18C-divIVA-C	pKT25-filP	++
Figure 88.3	pUT18C-filP	pKT25-divIVA	++
Figure 88.4	pUT18C-filP	pKT25-divIVA-N	
Figure 88.5	pUT18C-filP	pKT25-divIVA-C	+

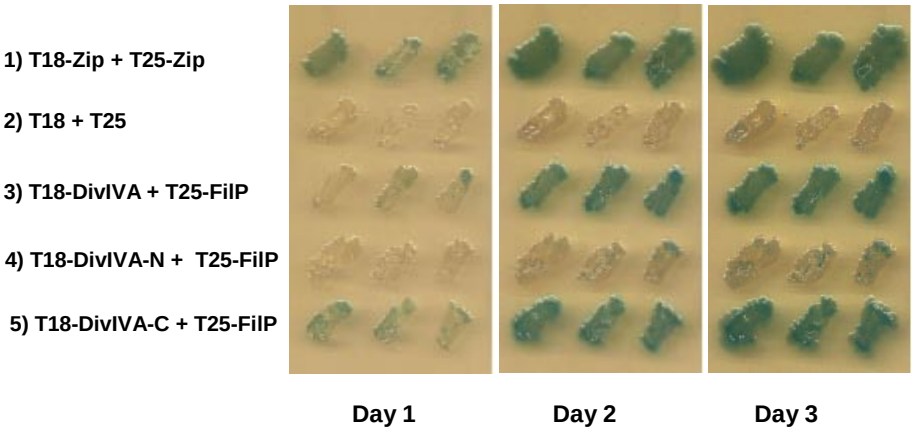

Figure 87: The bacterial two-hybrid system was used to analyse protein:protein interactions between FilP and the domains of DivIVA. Transformants of BTH101 was performed with the following plasmid pairs; 1) pUT18C-zip + pKT25-zip, 2) pUT18C + pKT25, 3) pUT18C-divIVA + pKT25-filP, 4) pUT18C-divIVA-N + pKT25-filP, 5) pUT18C-divIVA-C + pKT25-filP. Three colonies of each transformant were streaked on LB solid medium omitting glucose plus X-gal and IPTG. The plates were imaged at growth after 1, 2 and 3 days at 30ºC. Blue colour of colonies was indicative of interactions as seen in the positive control (1). Whereas colonies that remained pale were regarded to be negative as can be seen with the negative control (2).

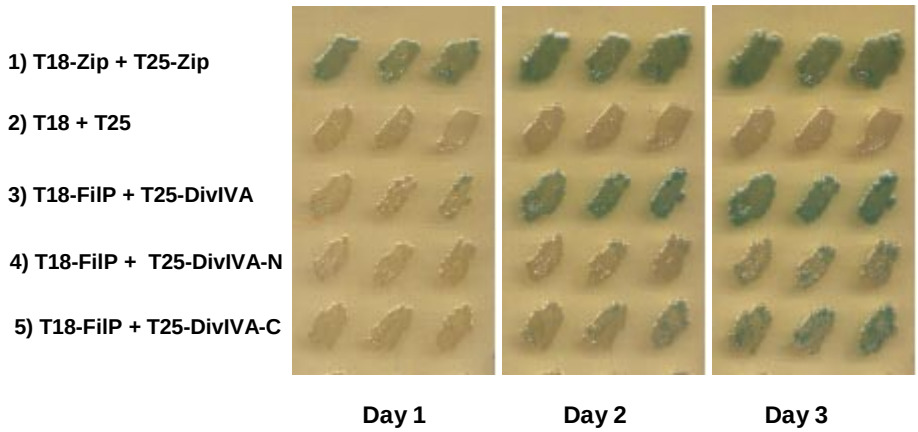

Figure 88: The bacterial two-hybrid system was used to analyse protein:protein interactions between FilP and the domains of DivIVA. Transformants of BTH101 was performed with the following plasmid pairs; 1) pUT18C-zip + pKT25-zip, 2) pUT18C + pKT25, 3) pUT18C-filP + pKT25-divIVA, 4) pUT18C-filP + pKT25-divIVA-N, 5) pUT18C-filP + pKT25-divIVA-C. Three colonies of each transformant were streaked on LB solid medium omitting glucose plus X-gal and IPTG. The plates were imaged at growth after 1, 2 and 3 days at 30ºC. Blue colour of colonies was indicative of interactions as seen in the positive control (1). Whereas colonies that remained pale were regarded to be negative as can be seen with the negative control (2).

6.1.6 Interactions between ParA and cytoskeletal proteins in the BTH system

We received a construct pKT25-parA that has been used in two-hybrid experiments by Jakimowicz *et al.*, (2007). ParA has been shown recently to interact with Scy (Jakimowicz unpublished). It has also been shown that DivIVA (Jakimowicz *et al.*, 2007) with ParA was found to be negative. To investigate if the different domains of DivIVA generated here showed an interaction with ParA *in vivo* protein/domain pairs were monitored using the bacterial two-hybrid system. To confirm any results the Scy, FilP and DivIVA experiments were all repeated here. Displayed in Table 11 are the scores from interactions between T25-ParA against the partners of T18-Scy, T18-Scy-N, T18-Scy-C and T18-FilP (Figure 89). T25-ParA against the partners of T18-DivIVA, T18-DivIVA-N and T18-DivIVA-C (Figure 90). Not surprisingly it was found that the interactions between Scy or Scy-C against ParA could be reproduced. Interactions between Scy-N, full length FilP and full length DivIVA were not readily detected in line with previous findings. The DivIVA-N and DivIVA-C combinations with ParA produced a change in colour perhaps suggesting that the individual domains were able to show a sign of a potential interaction not found with full length DivIVA. We were only supplied with a T25-ParA construct, whereas it may be interesting to test a T18-ParA with some of the constructs.

Table 11: Bacterial Two-Hyrid interactions and scores from ParA experiments.

Crossreference	pUT18C construct	pKT25 construct	Interaction Score
Figure 75.1	pUT18C-zip	pKT25-zip	+++
Figure 75.2	pUT18C	pKT25	
Figure 89.3	pUT18C-scy	pKT25-parA	+
Figure 89.4	pUT18C-scy-N	pKT25-parA	
Figure 89.5	pUT18C-scy-C	pKT25-parA	+
Figure 89.6	pUT18C-filP	pKT25-parA	
Figure 90.3	pUT18C-divIVA	pKT25-parA	
Figure 90.4	pUT18C-divIVA-N	pKT25-parA	+?
Figure 90.5	pUT18C-divIVA-C	pKT25-parA	+?

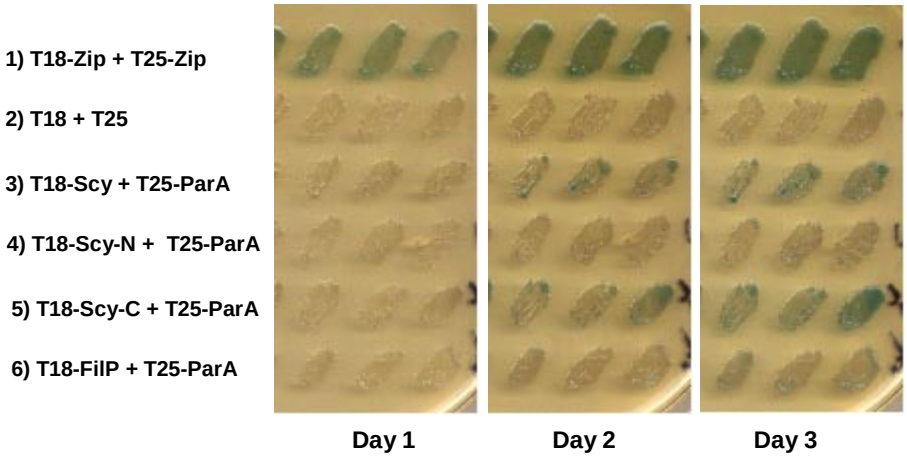

Figure 89: The bacterial two-hybrid system was used to analyse protein:protein interactions between Scy or FilP and ParA. Transformants of BTH101 was performed with the following plasmid pairs; 1) pUT18C-zip + pKT25-zip, 2) pUT18C + pKT25, 3) pUT18C-scy + pKT25-parA, 4) pUT18C-scy-N + pKT25-parA, 5) pUT18C-scy-C + pKT25-parA, 6) pUT18C-filP + pKT25-parA. Three colonies of each transformant were streaked on LB solid medium omitting glucose plus X-gal and IPTG. The plates were imaged at growth after 1, 2 and 3 days at 30ºC. Blue colour of colonies was indicative of interactions as seen in the positive control (1). Whereas colonies that remained pale were regarded to be negative as can be seen with the negative control (2).

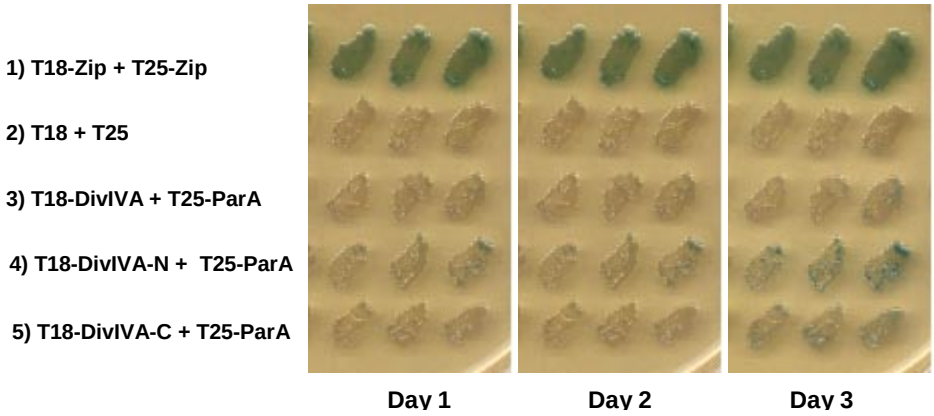

Figure 90: The bacterial two-hybrid system was used to analyse protein:protein interactions between ParA and the domains of DivIVA. Transformants of BTH101 was performed with the following plasmid pairs; 1) pUT18C-zip + pKT25-zip, 2) pUT18C + pKT25, 3) pUT18C-divIVA + pKT25-parA, 4) pUT18C-divIVA-N + pKT25-parA, 5) pUT18C-divIVA-C + pKT25-parA. Three colonies of each transformant were streaked on LB solid medium omitting glucose plus X-gal and IPTG. The plates were imaged at growth after 1, 2 and 3 days at 30ºC. Blue colour of colonies was indicative of interactions as seen in the positive control (1). Whereas colonies that remained pale were regarded to be negative as can be seen with the negative control (2).

6.1.7 Summary

Pairwise combinations of proteins in the bacterial two-hybrid system revealed interactions between the three coiled-coil proteins Scy, FilP and DivIVA *in vivo* in an *E.coli* cell. The Scy-DivIVA interaction was dissected further and it was shown that the interaction was likely due to the C-terminal domains of each proteins rather than the N-terminal domains that were more weakly reactive. The C-terminal domain of either Scy or DivIVA was responsible for each protein's interaction with FilP. It was also confirmed that Scy interacted with ParA, however a strong interaction could not be detected between ParA and either FilP or DivIVA. We surmise from these interactions that Scy, DivIVA and FilP may interact in the hyphal tip of *S.coelicolor*.

7 Purification of Coiled-coil Proteins

7.1.1 Introduction

As localisation studies and the bacterial two-hybrid system revealed intriguing results with Scy, FilP and DivIVA, we wanted to further study the proteins by purifying them. Protein expression from the host is quite often low yield, especially as *Streptomyces* growth in liquid culture is problematic. Therefore we wanted to overexpress and purify the proteins from the heterologous host *E.coli*. Making use of commonly used high expression systems and fast growth speed of *E.coli*.

7.1.2 Overexpression and purification of His-Scy

In order to perform *in vitro* biochemical experiments such as binding of Scy to other proteins, Scy protein needed to be overexpressed and purified in high quantities. Previously in the Kelemen lab the plasmids pET21a-scy and pET28a-scy (pGS2) were generated (Figure 211). These both were constructed using the Novagen expression vectors pET21a and pET28a. They contain origins of replication for high copy number propagation in *E. coli* cells. The plasmid pET28a-scy (pGS2) differs from pET21a-scy by encoding a 6xHis-tagged Scy rather than untagged Scy in pET21a. Expression of Scy or 6xHis-Scy are driven by T7 RNA polymerase dependent and IPTG inducible promoters, therefore, transformation of these vectors into an expression strain of *E. coli* containing T7 RNA polymerase driven by a *lacUV5* promoter, allows IPTG inducible expression of Scy or His-Scy proteins.

Previously in the Kelemen lab, pGS2 was used to overexpress and purify His-Scy by Ni-affinity chromatography using FPLC. A purification method was developed where cell extracts were generated using sonication of cells overexpressing His-Scy and were applied to HisTrap HP 1ml (GE Healthcare). HisScy then was eluted using a gradient of increasing imidazole concentration. However, it was found that His-Scy did not elute within a narrow range of imidazole concentration, instead His-Scy was spread over a large volume of eluent. In order to generate a concentrated His-Scy sample, we tested an altered method of purification. Plasmid pGS2 was transformed into *E. coli* BL21 (DE3) pLysS, this latter encoding T7 lysozyme, which is an inhibitor of T7 polymerase and therefore prevents leaky expression of proteins in the absence of IPTG . A freshly transformed single colony

was used to inoculate a 10ml starter culture. Then, 500µl was subcultured into 50ml LB and grown to an OD ~0.7. Where upon addition of 1mM IPTG was added to induce overproduction of His-Scy. The culture was then incubated at 37˚C shaking vigorously for 4 hours. At this point the culture was centrifuged and the pelleted cells were then resuspended in a low volume of phosphate/salt buffer with a low concentration (10mM) of imidazole. The cells were lysed using FastPrep (MP Biomedicals) by shaking at high speed with glass beads (<106µm). The remaining unlysed or insoluble cell fraction was centrifuged and the supernatant was filtered through a 0.2µm filter in preparation for running through an Amersham AKTA FRC FPLC machine. Affinity chromatography using a Nickel HisTrap HP 1ml (GE Healthcare) column was used to purify His-Scy. Histidine amino acids in proteins have affinity for nickel ions, and a patch of histidine such as in a 6xHis (now referred to as just His) tag provides a great enough affinity to be able to bind to nickel ions on a solid surface. If a His-tagged protein such as His-Scy in this experiment is available in high concentration in a cell extract, then by passing the cell extract through a nickel column this can selectively bind the His-tagged protein on the column. The remainder of the proteins in the cell extract will pass through the column and be discarded. Imidazole which is similar in structure to histidine, can be used to elute a His-tagged protein by raising the concentration of imidazole which will displace the bound His-tagged protein from the column.

Instead of the previously used gradient elution, a strategy using step elutions of imidazole was approached. Approximately 2-3ml of filtered cytoplasmic cell extract was loaded onto the column with the sample and loading buffer containing 10mM imidazole. Additional 15ml loading buffer was added for the initial displacement of non-binding proteins. In order to displace proteins with a weak affinity to the column, a wash with 20mM imidazole buffer was applied for 10ml. His-Scy protein would then be eluted from the column by increasing the concentration of imidazole to 250mM for 15ml. A final step was then performed by increasing the concentration of imidazole to 300mM for 10ml to elute any more tightly bound proteins. A routine 500mM imidazole wash was routinely performed post running a purification in order to clean the column of any remaining binding proteins and allowing columns to be reused.

During the FPLC run, the absorbance of the eluted samples was monitored at 280nm. Generally proteins absorb light at the wavelength of 280nm due to the presence of amino acids with aromatic rings. So an increasing absorbance should correlate with increasing amount of protein in solution. The FPLC readout for a His-Scy run can be seen in Figure

91. From the UV data we can see two main peaks that are of interest. The large peak in the sample load represents most of the cell's proteins, which did not have an affinity for the column, so that they ran straight through. There is a small rise in the 20mM imidazole wash which shows proteins with a lower affinity, eluting from the column. The modest peak seen in the step up to 250mM imidazole, should be proteins with a higher affinity for the column and presumably His-Scy. His-Scy has a low extinction coefficient for absorption at 280nm so will not be strongly detected, explaining the small peak (His-Scy = 12950 M^{-1} cm^{-1}, BSA = 62865 M^{-1} cm^{-1}).

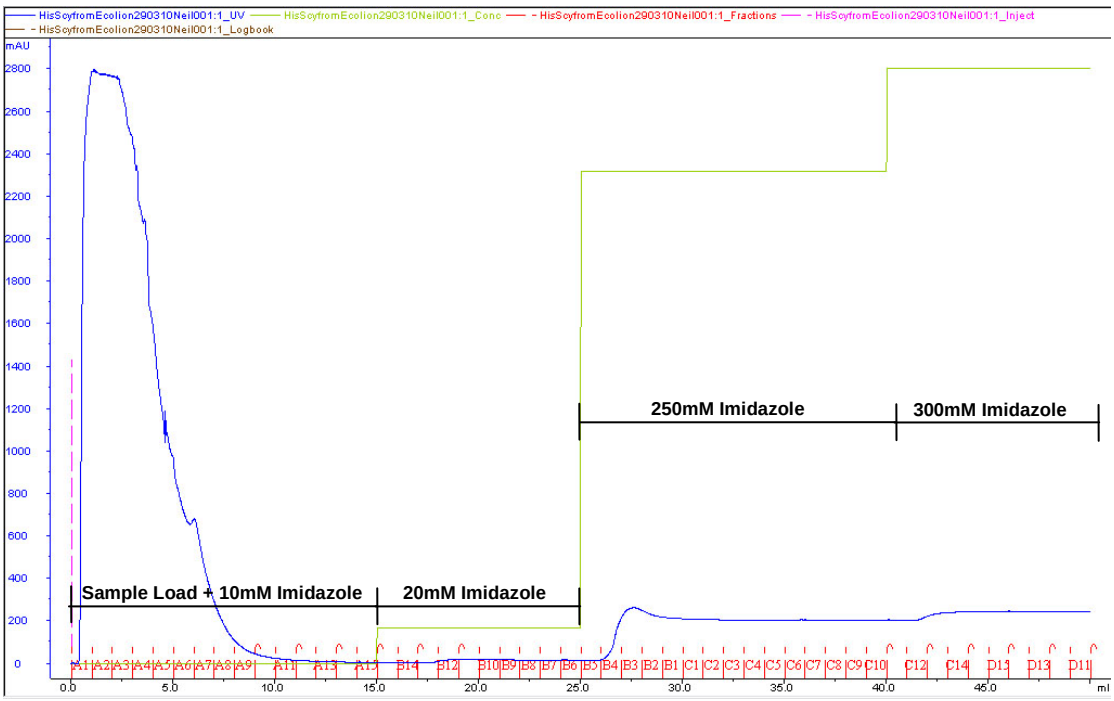

Figure 91: FPLC Chromatogram readout for purification of His-Scy using a step elution strategy. Absorbance data at 280nm of the different eluted samples. 0-15ml represents the addition of cell extract with 10mM imidazole buffer. 15-25ml represents an increase in buffer to 20mM imidazole. 25-40ml represents a step increase in buffer from 20mM to 250mM imidazole. 40-50ml is a final rise in Imidazole to 300mM. Blue is the absorbance data (mAU) at 280nm. Green represents the change in imidazole concentration. Red represents the fractions of eluted samples collected.

To attempt to visualise the proteins eluted from the column a selection of the fractions was used in Sodium dodecyl sulphate polyacrylamide gel electrophoresis (SDS-PAGE). The gel used was an 8% acrylamide gel, stained with Coomassie blue (Figure 92). It appears that the majority of bound His-Scy was eluted in samples B4 and B3 after the rise of imidazole concentration to 250mM. However, it is of note that a large amount of His-Scy appears not to have bound to the column by the prominent band corrersponding to His-Scy in the flowthrough sample A2.

Depending on the further use of His-Scy, the samples were dialysed against the appropriate buffers to remove the imidazole and for buffer exchange. Protein samples were quantified using the Bradford assay and were kept at -80^{o}C.

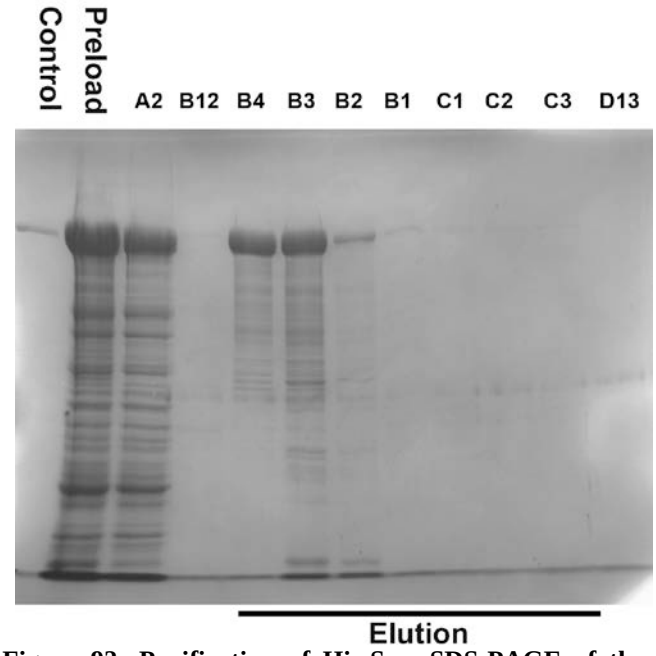

Figure 92: Purification of His-Scy. SDS-PAGE of the FPLC samples loaded onto an 8% acrylamide gel. The control is His-Scy purified previously from *E. coli.* Preload is an aliquot of the cell extract prior to loading onto the FPLC column. Lane notation corresponds with the fraction numbers in Figure 91. A2 is from the Flowthrough. B12 is from the wash. B3 to C3 are from the elution with a step increase to 250mM Imidazole. D13 is from an additional elutions at 300mM Imidazole. The gel was stained with Coomassie blue R250.

7.1.3 Overexpression and purification of His-FilP

To be able to carry out protein based experiments between Scy and FilP we had to overexpress and purify FilP protein. Therefore, we generated constructs of pET21a and pET28a containing *filP* (10.1.61). The pET21a construct containing *filP* would be able to express FilP with no tag, whereas the pET28a construct containing *filP* would be able to express a His-tagged version of FilP.

In order to overexpress His-tagged FilP, the plasmid pET28a-filP was transformed into *E. coli* BL21 (DE3) pLysS. His-FilP overexpressed at a very high level in *E. coli*, a large amount was in the soluble fraction as well as in the insoluble fraction. We purified His-FilP from the soluble fraction. A freshly transformed single colony was used to inoculate a 10ml starter culture. After overnight growth at 37˚C, 500µl was subcultured into 50ml LB and grown to an OD ~0.7 (~4 hours). Whereupon 1mM IPTG was added to induce overproduction of His-FilP. The culture was then incubated at 37˚C shaking vigorously for

4 hours. The pelleted cells were lysed using FastPrep and the cell debris and insoluble cell fraction was removed by centrifugation. The supernatant was filtered through a 0.2µm filter prior to loading the 2-3ml of extract onto the HisTrap HP 1ml (GE Healthcare) column of the FPLC AKTA machine.

Affinity chromatography was performed initially using a gradient elution with an increasing concentration of imidazole, as we were unaware of the imidazole concentration that would elute the highest proportion of His-FilP. After loading the sample, a further 15ml of loading buffer and 10ml of buffer containing 27.4mM imidazole was used to elute proteins with non-specific or weak binding. His-FilP protein was eluted from the column by increasing imidazole concentration over a gradient from 27.4mM to 300mM for 20ml. To ensure the buffer was kept at 300mM imidazole for long enough the concentration of imidazole was maintained at 300mM for a further ~6.2ml. Any tightly bound proteins were eluted with the buffer containing 500mM imidazole for ~20ml.

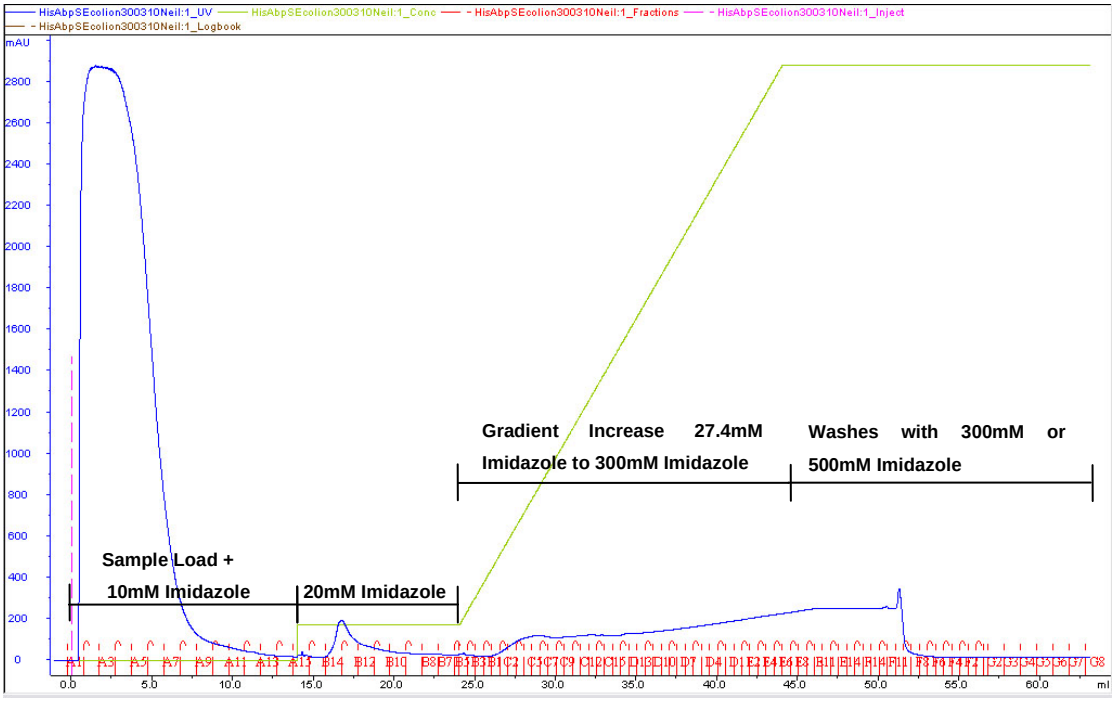

Figure 93: FPLC Chromatogram readout for purification of His-FilP using a gradient elution strategy. Absorbance data at 280nm of the different eluted samples. 0-15ml represents the addition of cell extract with 10mM imidazole buffer. 15-25ml represents an increase in buffer to 27.4mM imidazole. 25-45ml represents a gradient increase in buffer from 27.4mM to 300mM imidazole. 45-51.2ml represents a wash using 300mM Imidazole. 51.2-64ml represents a wash using 500mM Imidazole. Blue is the absorbance data (mAU) at 280nm. Green represents the change in imidazole concentration. Red represents the fractions of eluted samples collected.

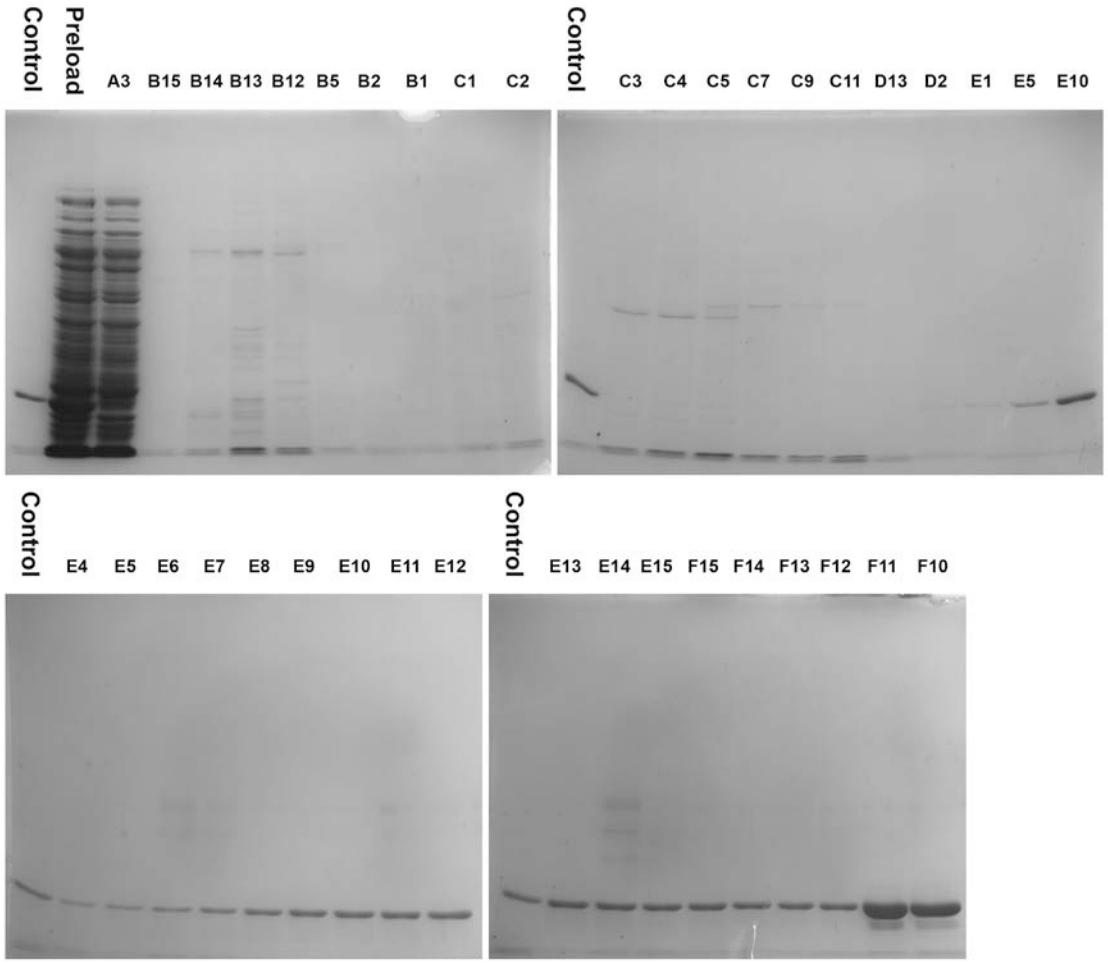

Figure 94: Purification of His-FilP. SDS-PAGE of the FPLC samples loaded onto 8% acrylamide gels. The control is His-FilP purified previously from *E. coli* via small scale isolation. Preload is an aliquot of the cell extract prior to loading onto the FPLC column. Lane notation corresponds with the fraction numbers in Figure 93. A3 is from the Flowthrough. B15 to B12 is from the wash. B5 to E5 are from the rising gradient of Imidazole to 500mM Imidazole. E6 to F12 represents elutions at 300mM Imidazole. F11 and F10 are elutions at 500mM Imidazole. The gel was stained with Coomassie blue R250.

The chromatogram of the purification (Figure 93) shows UV peaks of interest, the flowthrough peak, a prominent peak in the wash, followed by an absence of a prominent peak in the gradient elution and a sharp peak corresponding to when the imidazole concentration was raised to 500mM. To visualise the proteins eluted from the column a range of the fractions from the wash, gradient and high imidazole elution were analysed using 8% SDS acrylamide electrophoresis gels stained with Coomassie blue (Figure 94). In contrast to His-Scy, His-FilP was not visible in the flowthrough (A3) suggesting that all or most His-FilP of the cell extract bound to the Ni-column. Although there was a protein peak in the wash, this did not correspond to His-FilP (B14-B12). His-FilP appeared to elute over an extensive range of the gradient elution step from E5 toF10. When the imidazole concentration was raised to 500mM (F11 & F10), a large quantity of His-FilP eluted,

suggesting that although some His-FilP can elute at the lower ranges of imidazole concentration, to elute all of His-FilP, high concentration of imidazole is needed.

In order to elute His-FilP more efficiently, our strategy was to use a single step elution with a buffer containing 500mM imidazole. Cell lysate from cells overexpressing His-FilP were generated and loaded onto the His-Trap column as before. This was followed by washing steps performed as before. His-FilP was eluted from the column by increasing the concentration of imidazole to 500mM for 20ml.

The chromatogram of the purification (Figure 95) shows UV peaks of interest, the flowthrough peak, a peak in the wash, followed by a peak corresponding to when the imidazole concentration was raised to 500mM. Visualised on an 8% SDS acrylamide electrophoresis gel stained with Coomassie blue (Figure 96), His-FilP bound to the column strongly (A2), resisting elution in the wash (B13) and only eluting when the imidazole concentration was raised to 500mM imidazole (B4-C2).

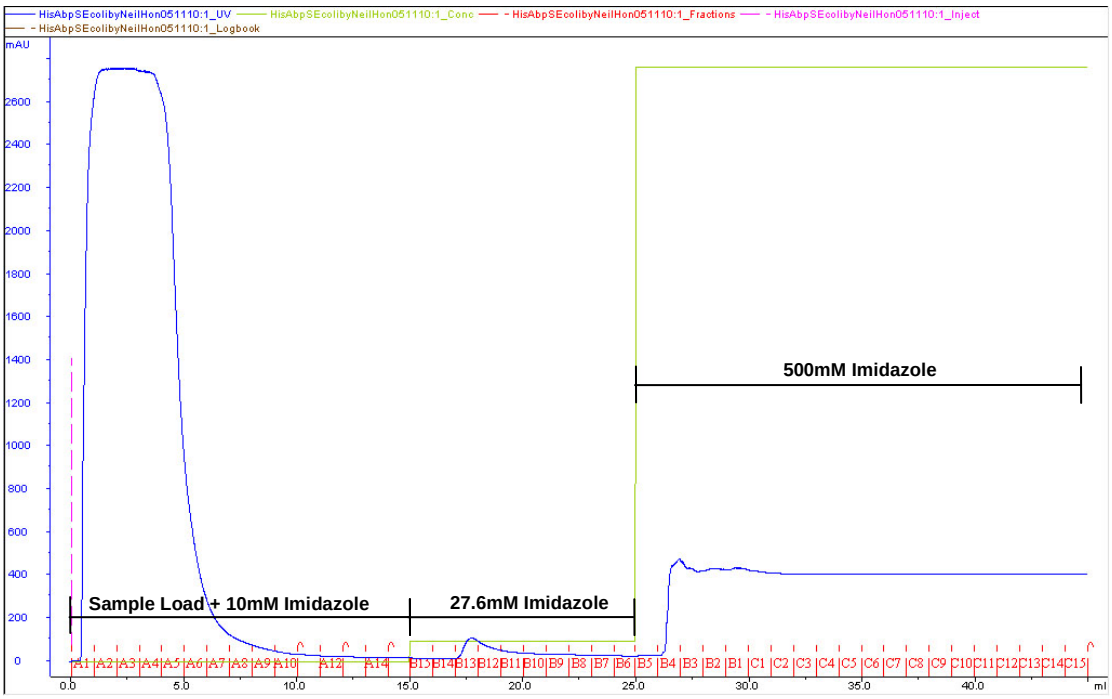

Figure 95: FPLC Chromatogram readout for purification of His-FilP using a step elution strategy. Absorbance data at 280nm of the different eluted samples. 0-15ml represents the addition of cell extract with 10mM imidazole buffer. 15-25ml represents an increase in buffer to 27.6mM imidazole. 25-45ml represents a step increase in buffer from 27.6mM to 500mM imidazole. Blue is the absorbance data (mAU) at 280nm. Green represents the change in imidazole concentration. Red represents the fractions of eluted samples collected.

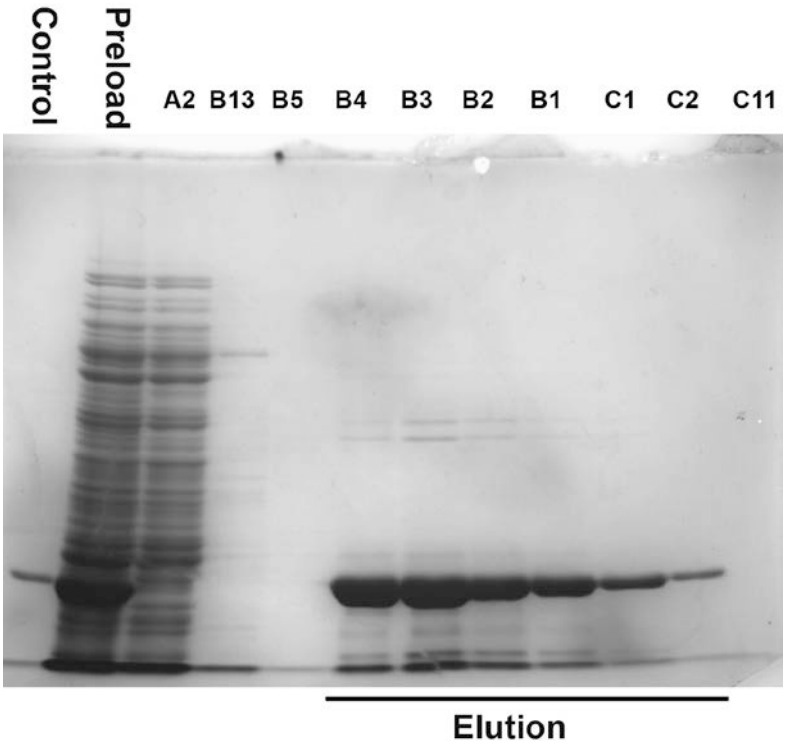

Figure 96: Purification of His-FilP. SDS-PAGE of the FPLC samples loaded onto an 8% acrylamide gel. The control is His-FilP purified previously from *E. coli.* Preload is an aliquot of the cell extract prior to loading onto the FPLC column. Lane notation corresponds with the fraction numbers in Figure 95. A2 is from the Flowthrough. B13 is from the wash. B5 to C11 are from the elution with a step increase to 500mM Imidazole. The gel was stained with Coomassie blue R250.

7.1.4 Overexpression and purification of His-DivIVA

In order to perform *in vitro* experiments with Scy and DivIVA (and possibly including FilP) we needed to overexpress and purify DivIVA protein. Therefore, we generated constructs of pET21a and pET28a containing *divIVA* (10.1.62). The pET21a construct is designed to be able to express DivIVA with no additional tag. Whereas the pET28a construct should express His-tagged DivIVA.

In order to overexpress His-tagged DivIVA, the plasmid pET28a-divIVA was transformed into *E. coli* BL21 (DE3) pLysS. It was quickly found that the majority of the overexpressed protein was in the insoluble fraction. Therefore, a strategy of lysing the cells with urea buffers was used in order to increase the amount of soluble protein.

A freshly transformed single colony was used to inoculate a 10ml starter culture. Then, 5ml was subcultured into 500ml LB and grown to an OD ~0.7, whereupon 1mM IPTG was added to induce overproduction of His-DivIVA.

The culture was then incubated at 37˚C shaking vigorously overnight. At this point the large volume of culture was centrifuged in 2 aliquots in an Avanti® J-26XP Beckman Coulter high speed centrifuge. The pelleted cells were then resuspended in 10ml of urea

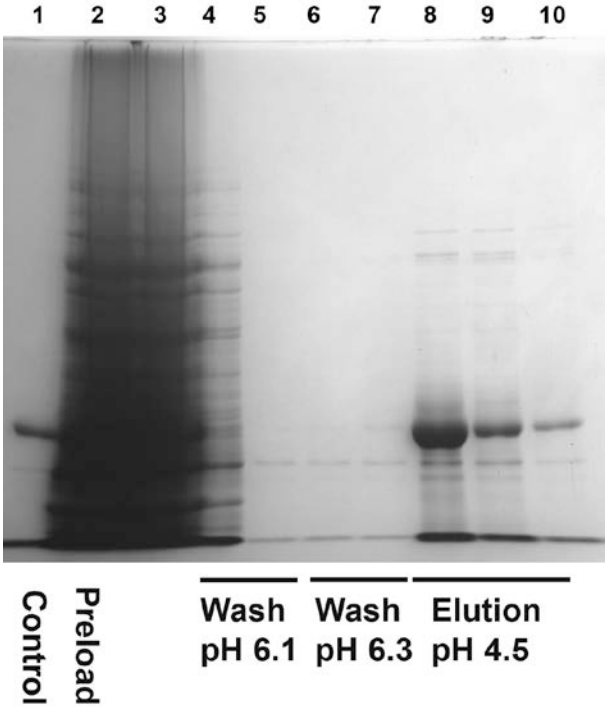

Figure 97: Purification of His-DivIVA. SDS-PAGE of the FPLC samples loaded onto an 8% acrylamide gel. The control is His-DivIVA purified previously from *E. coli* (Lane 1). Preload is an aliquot of the cell extract before loading on the Ni-NTA (Lane 2). Lane 3 is from the Flowthrough. Lane 4 and 5 are from the wash with Urea pH 6.1 buffer. Lane 6 and 7 are from the wash with Urea pH 6.3 buffer. Lane 8, 9 and 10 are from the elution with Urea pH 4.5 buffer. The gel was stained with Coomassie blue R250.

buffer. The resulting resuspension was then sonicated, lysing the cell material. The remaining unlysed or insoluble cell fraction was removed by centrifugation at high speed and aliquots of the supernatant were frozen. Small scale Ni-NTA columns (Qiagen) were used to purify DivIVA through step elutions. 600µl sample was loaded on the Ni-NTA column in a urea buffer pH 8.0 followed by washes with 2.4ml of urea buffer pH 6.3 and 1.8ml of urea buffer pH 6.1. His-DivIVA protein was then eluted from the column in a low volume of two 400µl with urea buffer pH 4.5. A final elution was carried out with a further 300µl of pH 4.5 urea buffer. Samples were visualised on 8% SDS acrylamide electrophoresis gels stained with Coomassie blue (Figure 97). Not clearly visible, but due to the high concentration of protein in the preload, the column was unable to support binding all His-DivIVA in the sample, however, this was fine as the desire was to saturate

the column. As can be seen in the elution fractions (Lane 8 & 9), His-DivIVA was bound to the column and eluted with urea buffer at low pH.

7.1.5 Overexpression and purification of His-DivIVA-C

As in the bacterial two-hybrid experiments the C-terminal domain of DivIVA interacted strongly with Scy, we also sought to overexpress and purify DivIVA-C by generating constructs of pET21a and pET28a containing *divIVA-C*. The pET21a construct containing *divIVA-C* to express DivIVA-C with no tag and the pET28a construct containing *divIVA-C* to express a His-tagged version of DivIVA-C.

In order to overexpress His-tagged DivIVA-C, the plasmid pET28a-divIVA-C was transformed into *E. coli* BL21 (DE3) pLysS. Soluble His-DivIVA-C was overexpressed at a very high level in *E. coli*. For large scale preparations, a freshly transformed single colony of *E. coli* BL21 (DE3) pLysS carrying pET28a-divIVA-C was used to inoculate a 10ml starter culture, which was subcultured into 50ml LB and grown to an OD ~0.7. 1mM IPTG was added to induce overproduction of His-DivIVA-C and the culture was incubated at 37˚C shaking vigorously for 4 hours. Cells were collected and lysed using FastPrep and the insoluble cell fraction was removed by centrifugation. The supernatant was filtered through a 0.2μm filter in preparation for an FPLC purification.

Affinity chromatography using an Amersham AKTA FRC FPLC machine and a Nickel HisTrap HP 1ml (GE Healthcare) column was used to purify His-DivIVA-C. Due to the success of step elution strategies for both His-Scy and His-FilP, for His-DivIVA-C we did not attempt a first gradient elution strategy and went straight to a strategy using step elutions of imidazole. As before, approximately 2-3ml of extract was loaded onto the column with the sample and loading buffer at 10mM imidazole. Washes with 15ml of loading buffer and 10ml of buffer with 27.6mM imidazole was applied. The elution was with 5ml of buffer with 300mM imidazole followed by 20ml of buffer with 500mM imidazole.

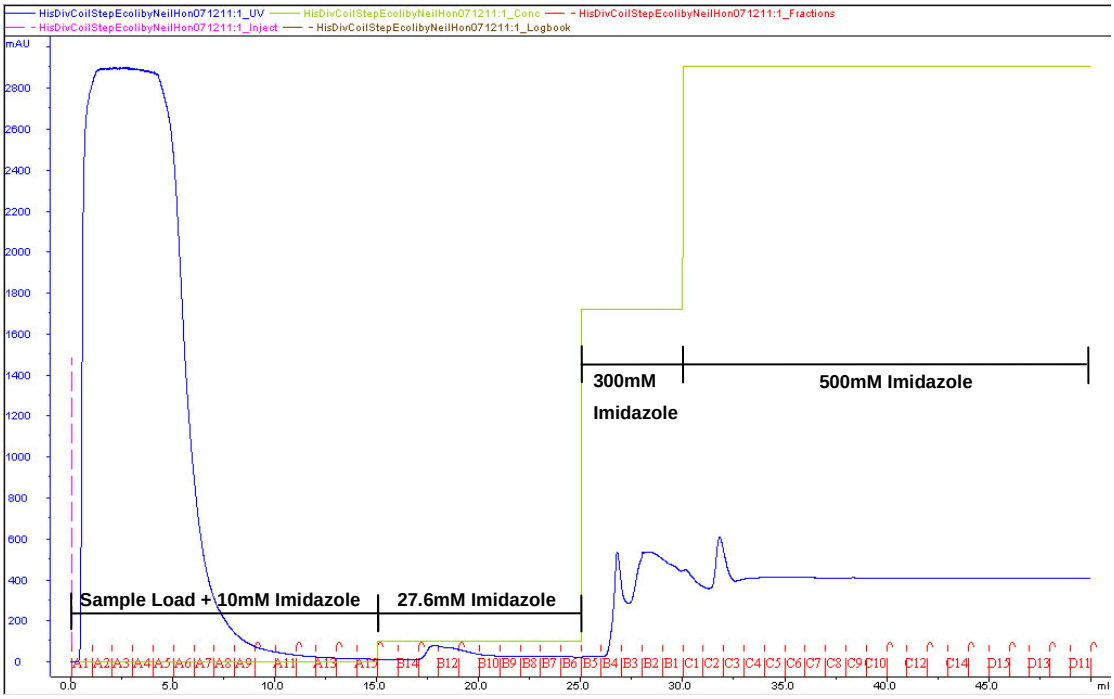

Figure 98: FPLC Chromatogram readout for purification of His-DivIVA-C using a step elution strategy. Absorbance data at 280nm of the different eluted samples. 0-15ml represents the addition of cell extract with 10mM imidazole buffer. 15-25ml represents an increase in buffer to 27.6mM imidazole. 25-30ml represents a step increase in buffer from 27.6mM to 300mM imidazole. 40-50ml is a final rise in Imidazole to 500mM. Blue is the absorbance data (mAU) at 280nm. Green represents the change in imidazole concentration. Red represents the fractions of eluted samples collected.

The chromatogram of the purification (Figure 98) shows UV peaks of interest, the flowthrough peak, a small peak in the wash, followed by a number of peaks corresponding to when the imidazole concentration was raised to 300mM and 500mM. The fractions were analysed on a 10% SDS acrylamide electrophoresis gel stained with Coomassie blue (Figure 99). His-DivIVA-C bound to the column strongly (A2) and resisted elution in the wash (B12). The initial peak in the chromatogram corresponding with sample B4, likely represents more contaminating protein eluting from the column. The majority of the elution of His-DivIVA-C coming in the later peak following the rise to 300mM imidazole and not clearly discriminated in the gel is the continued elution when imidazole concentration was raised to 500mM (B3-C3).

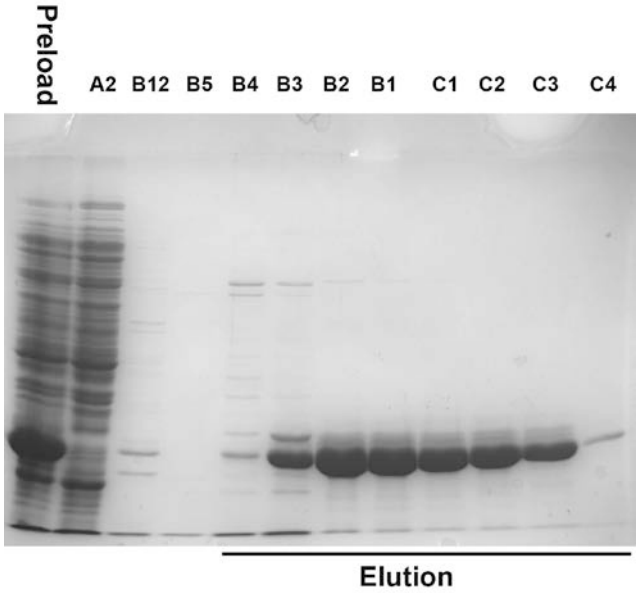

Figure 99: Purification of His-DivIVA-C. SDS-PAGE of the FPLC samples loaded onto a 10% acrylamide gel. Preload is an aliquot of the cell extract prior to loading onto the FPLC column. Lane notation corresponds with the fraction numbers in Figure 98. A2 is from the Flowthrough. B12 is from the wash. B5 to B1 are from the elution with a step increase to 300mM Imidazole. C1 to C4 are from the elution with a step increase to 500mM Imidazole. The gel was stained with Coomassie blue R250.

7.1.6 Summary

The proteins Scy, FilP and DivIVA as well as the C-terminal domain of DivIVA were all expressed and purified from *E.coli*. For Scy, FilP and DivIVA-C aqueous purification was achieved through an FPLC machine. For DivIVA urea purification was found to be most efficient. Availability of the proteins allows us to analyse them *in vitro* in downstream applications.

8 Protein Interactions Studies

8.1.1 Introduction

As the bacterial two-hybrid system revealed interactions between Scy, FilP and DivIVA, we wanted to confirm these interactions by using *in vitro* biochemical experiments. Therefore we performed pelleting ultracentrifugation assays with pairwise combinations of proteins. We also tried to use co-affinity pull down experiments between proteins. In order to verify that Scy and DivIVA were involved in the same *in vivo* complex in cells of *Streptomyces* we also wanted to overexpress Scy from *Streptomyces coelicolor* and pull down any interacting proteins, whereby we could use an anti-DivIVA antibody to detect the presence of DivIVA in elutions.

8.2 Pelleting ultracentrifugation assay of Coiled-coil proteins

To demonstrate direct interactions between Scy, DivIVA and FilP *in vitro*, purified proteins were analysed using a pelleting assay. The conditions that we used had previously been used to demonstrate an interaction between MreB and RodZ (van den Ent *et al.*, 2010).

This particular technique is of use for studying proteins that are able to form oligomeric structures, which can be separated by pelleting using ultracentrifugation The proteins purified in the previous chapter were dialysed against the buffer of 20mM Tris, 200mM NaCl, 10mM $MgCl_2$, pH 8.0 buffer. The concentrations of the proteins used were DivIVA, 3.073µM; Scy, 1.266µM and FilP, 6.718µM. Although initial attempts were made to perform pelleting assays at 1:1 molar ratio, we did have a problem of detecting DivIVA at µM concentrations. Therefore, without attempting 1:1 stochiometry the final protein concentrations in the pairwise mixes were the following: DivIVA, 1.5µM; Scy, 0.65µM and FilP, 3.3µM. For the ultracentrifugation assays the purified proteins were first incubated at 30°C for 20 minutes. They were then spun at 100,000rpm for 30 minutes at 4°C in a Beckman Optima TLX Ultracentrifuge using a Beckmann Coulter TLA 100 Fixed Angle Rotor. After ultracentrifugation both the pellet and the supernatant of the Scy, DivIVA, FilP, Scy-DivIVA, Scy-FilP and DivIVA-FilP mixtures were analysed on a 10% SDS Polyacrylamide gel (Figure 100). Scy and FilP formed higher order assemblies that were pelleted using ultracentrifugation. DivIVA, on the other hand, did not pellet under the

conditions we used. However, Scy pulled DivIVA to the pellet fraction which confirms the interaction between these two proteins. Similarly, FilP pulled DivIVA to the pellet fraction, also confirming their interaction *in vitro*. Both Scy and FilP were in the pellet fractions after ultracentrifugation and therefore this technique was unable to demonstrate a direct *in vitro* interaction between these two proteins.

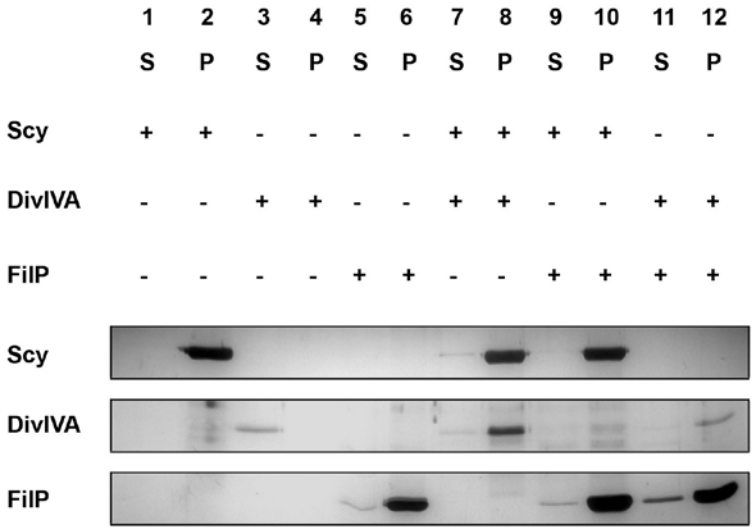

Figure 100: Pelleting Ultracentrifugation assay of Scy, DivIVA and FilP. SDS-PAGE of the Ultracentrifugation samples that were loaded onto a 10% acrylamide gel. Whereby; Scy was mixed with buffer (Lane 1 & 2), with DivIVA (Lane 7 & 8) or FilP (Lane 9 & 10). DivIVA was mixed with buffer (Lane 3 & 4) or with FilP (Lane 11 & 12). FilP was mixed with buffer (Lane 5 & 6). Samples were separated into supernatant (S) and pellet (P) fractions.

To further analyse the interaction between Scy and DivIVA we wanted to test direct interaction between Scy and the C-terminal domain of DivIVA. Both Scy and DivIVA-C were used in an ultacentrifugation assay after the proteins were dialysed against 20mM Tris, 200mM NaCl, 10mM $MgCl_2$, pH 8.0 buffer. The proteins used in the assay were DivIVA-C, 36.344µM (3µl used) and Scy, 0.747µM (25µl used). As before, the purified proteins were first incubated at 30°C for 20 minutes followed by centrifugation at 100000rpm for 30 minutes at 4°C in a Beckman Optima TLX Ultracentrifuge using a Beckmann Coulter TLA 100 Fixed Angle Rotor. After ultracentrifugation both the pellet and the supernatant fractions of Scy, DivIVA-C and a Scy-DivIVA-C mixture were analysed on a 10% SDS Polyacrylamide gel (Figure 101). Not surprisingly Scy pulled DivIVA-C to the pellet fraction which confirms that DivIVA-C is sufficient for interaction with Scy.

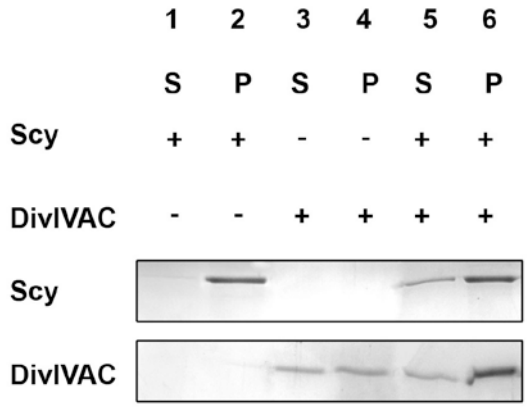

Figure 101: Pelleting Ultracentrifugation assay of Scy and DivIVA-C. SDS-PAGE of the Ultracentrifugation samples that were loaded onto a 10% acrylamide gel. Whereby; Scy was mixed with buffer (Lane 1 & 2) or with DivIVA-C (Lane 5 & 6). DivIVA-C was mixed with buffer (Lane 3 & 4). Samples were separated into supernatant (S) and pellet (P) fractions.

Previously it has been shown that DivIVA from *Bacillus subtilis* could bind to the membrane and pelleted during ultracentrifugation when mixed with with liposomes (Oliva *et al.*, 2010). We wanted to test whether *S. coelicolor* DivIVA, DivIVA-C and/or Scy would bind to liposomes *in vitro*. It was also of interest to see if Scy would complex with DivIVA and liposomes. It was previously shown that the C-terminus of DivIVA alone would not be able to bind to liposomes and that full length DivIVA is required (Oliva *et al.*, 2010). The concentrations of the proteins used were DivIVA; 3.073µM (20µl used), Scy; 1.099µM (20µl used) and DivIVA-C; 11.857µM (20µl used). The liposomes used in this experiment were prepared by resuspending phosphatidyl choline in the experimental buffer followed by sonication to aid liposome formation generating a non-homogenous range of liposomes. The proteins were mixed either with 15µl 1mg/ml liposomes and buffer or just buffer to a total of 55µl reactions. For the ultracentrifugation assay the purified proteins with and without liposomes were first incubated at 30°C for approximately an hour to stimulate interactions. They were then spun at a lower speed of 65000rpm for 12 minutes at 4°C in accordance with Oliva *et al.*, (2010) in a Beckman Optima TLX Ultracentrifuge using a Beckmann Coulter TLA 100 Fixed Angle Rotor. This time and speed was sufficient to pellet the liposomes. After ultracentrifugation Scy, DivIVA, DivIVA-C, Scy-DivIVA, Scy-DivIVA-C mixtures all with and without lipsomes were analysed on a 10% SDS Polyacrylamide gel (Figure 102). Without liposomes Scy did not enter the pellet, which was useful as at the higher rotation speeds Scy spun down in the pellet fraction and we wanted to assess Scy binding to the liposomes. Suprisingly we did not see DivIVA pellet with the liposomes. Nor did DivIVA-C or Scy, or any of the

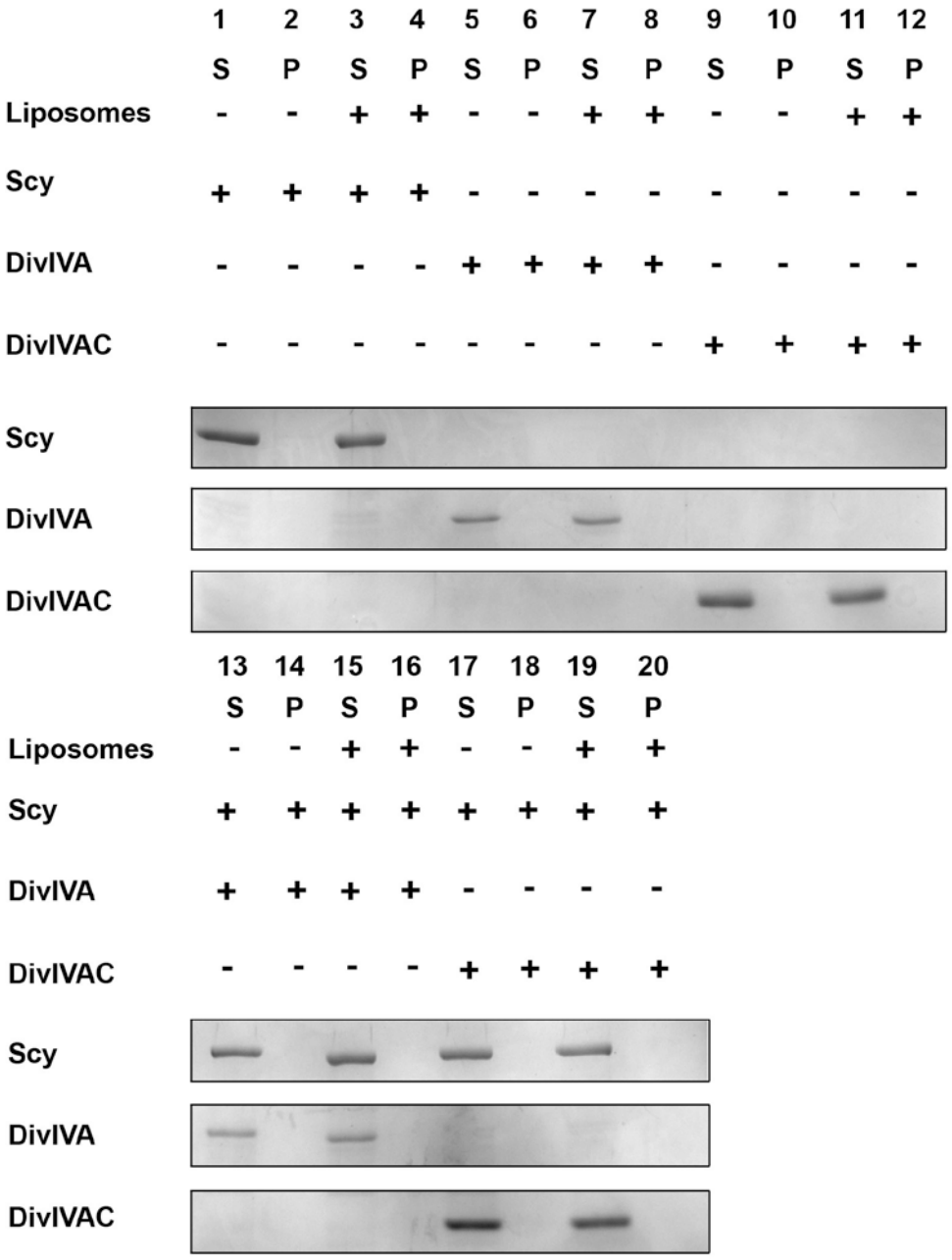

Figure 102: Pelleting Ultracentrifugation assay of Scy, DivIVA and DivIVA-C with Lipsomes. SDS-PAGE of the Ultracentrifugation samples that were loaded onto a 10% acrylamide gel. Samples with addition (+) of Liposomes or absence of Liposomes (-) are noted above image. Mixtures also included; Scy with buffer (Lane 1, 2, 3 & 4), with DivIVA (Lane 13, 14, 15 & 16) or with DivIVA-C (Lane 17, 18, 19 & 20). DivIVA with buffer (Lane 5, 6, 7 & 8). DivIVA-C with buffer (Lane 17, 18, 19 & 20). Samples were separated into supernatant (S) and pellet (P) fractions.

mixtures. This was unfortunate as we were expecting DivIVA to pellet in our similar conditions to Oliva *et al.*, (2010). However, the liposomes used by Oliva *et al.*, (2010) were from an *E. coli* extract so they may have been more like lipids encountered in a bacterial cell. Also, we tried extruding lipids of set sizes (0.2µm or 0.4µm) and this did not generate liposome interactions (data not shown), however, we did not have filters at our

disposal of the 1µm sizes that might reflect more the size of the bacterial cell diameter and the conditions used by Oliva *et al.,* (2010). It is worth noting as well that in accordance with a theory that DivIVA recognises negative membrane curvature (Lenarcic *et al.*, 2009; Ramamurthi, and Losick, 2009), binding of DivIVA to liposomes in this experiment would be primarily be on a membrane with positive curvature.

8.3 Co-Pull down of Coiled-coil proteins

Following two-hybrid analysis, to further characterise interactions between coiled-coil proteins, pull-down assays were performed. The general idea behind these types of experiments were that one protein of a pair would be able to bind to an affinity column, whilst the other would not have affinity to the column. However, if the two proteins were to interact then the protein without affinity for the column would be able to bind onto the column via interaction with the other partner (Brymora *et al.*, 2004; Vikis, and Guan, 2004). As previously shown, we generated overexpression construct for the production of both His-tagged and non-tagged Scy, DivIVA and FilP. These constructs enabled us to test pair-wise interactions using a His-tagged protein with a non-tagged potential partner. At this point let it be noted that these experiments are intended to compliment the bacterial two-hybrid experiments and any other experiments to detect protein-protein interactions. However, pull-down assays like any experimental technique have limitations (Mackay *et al.*, 2007; Wissmueller *et al.*, 2011). Therefore, whilst attempting these experiments we intended to use appropriate experimental controls.

8.3.1 Coaffinity of His-FilP and Scy

The strategy in this experiment was to bind His-FilP from a cell lysate onto the Ni-affinity column and then to be able to assess the co-purification of untagged Scy from a separate cell lysate. Firstly *E. coli* BL21 pLysS (DE3) carrying either pET28a-filP or pET21a-scy, were inoculated and 10ml subcultures were grown to an OD ~0.7. 1mM IPTG was added to induce overproduction at 37°C for 4 hours. Cells were collected and lysed using FastPrep and the insoluble cell fraction was removed by centrifugation. The supernatant containing His-FilP was applied onto the Ni-NTA column (600µl). Following washes twice with 600µl of buffer to remove unbound proteins, the supernatant containing untagged Scy was passed through the column (600µl). After further washes (four times

with 600µl of buffer), specifically bound proteins were eluted with 2X300µl of 500mM imidazole buffer. The fractions were analysed by SDS-PAGE (Figure 103A) confirming that in addition to His-FilP, Scy was detectable in the elution fractions. As we don't have Scy antibody, the presence of Scy was based on the high molecular weight band detectable in the elution fractions.

This experiment was repeated again but with the strategy to bind a His-FilP containing cell lysate onto the column and then to be able to assess the co-purification of untagged EGFP-Scy passed through in a separate cell lysate. The reason why we did this was because we did not have an antibody against Scy therefore wanted to tag Scy with a fluorescent tag we could monitor using semi-denaturing SDS-polyacrylamide gels. We generated pET21a-egfp-scy (10.1.64) to express non-tagged EGFP-Scy. In order to perform co-purification firstly *E. coli* BL21 pLysS (DE3) carrying either pET28a-filP or pET21a-egfp-scy, were inoculated and 10ml subcultures were grown to an OD ~0.7. 1mM IPTG was added to induce overproduction at 37°C for 4 hours. Cells were collected and lysed using FastPrep and the insoluble cell fraction was removed by centrifugation. The supernatant containing His-FilP was applied onto the Ni-NTA column (600µl). Following washes twice with 600µl of buffer to remove unbound proteins, the supernatant containing untagged EGFP-Scy was passed through the column (600µl). After further washes (four times with 600µl of buffer), specifically bound proteins were eluted with 2X300µl of 500mM imidazole buffer. Finally the fractions were analysed by SDS-PAGE without boiling the samples so to maintain the fluorescence of EGFP-Scy. After the electrophoresis the gel was scanned for fluorescence activity using a phosphoimager prior to staining with Coomassie (Figure 103B). As can be seen there was EGFP-Scy protein in the elution fractions, however, it was only detectable on the gel via its fluorescence. This is likely to occur because this construct perhaps does not express EGFP-Scy as well as untagged native Scy was expressed in *E. coli*. The detection of fluorescence was in this case stronger than by Coomassie staining.

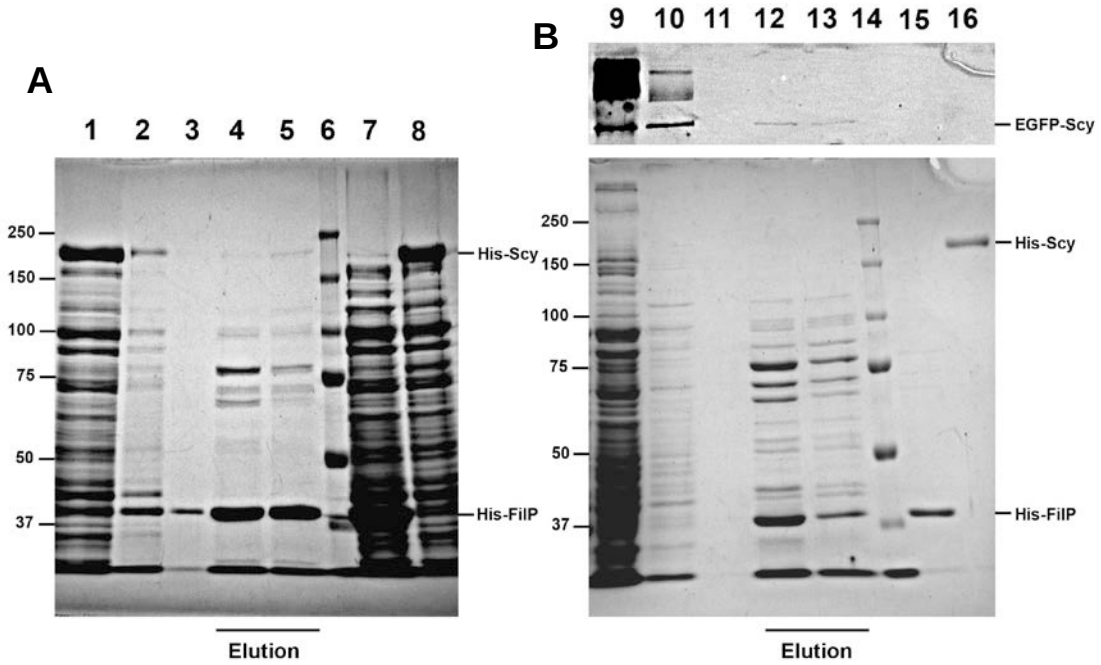

Figure 103: Pull Down Co-affinity of His-FilP and Scy or EGFP-Scy.

A) SDS-PAGE of the pull down co-affinity experiment testing His-FilP and Scy, samples loaded onto an 8% acrylamide gel. Scy supernatant flowthrough (Lane 1). After Scy addition, beginning wash (Lane 2). After Scy addition, finishing wash (Lane 3). His-FilP + Scy elution fractions (Lane 4&5). MW marker is a Biorad precision plus protein All Blue Standards sample (kDa sizes listed left, Lane 6). His-FilP preload (Lane 7). Scy preload (Lane 8).

B) SDS-PAGE of the pull down co-affinity experiment testing His-FilP and EGFP-Scy, samples loaded onto an 8% acrylamide gel. EGFP-Scy preload (Lane 9). After EGFP-Scy addition, beginning wash (Lane 10). After EGFP-Scy addition, finishing wash (Lane 11). His-FilP + EGFP-Scy elution fractions (Lane 12&13). MW marker is a Biorad precision plus protein All Blue Standards sample (kDa sizes listed left, Lane 14). His-FilP control (Lane 15). His-Scy control (Lane 16). The top panel is the part of the gel containing EGFP-Scy, excited at 488nm and the emission read at 532nm.

8.3.2 Coaffinity of His-DivIVA and Scy

The strategy in this experiment was to bind His-DivIVA onto the column and then to be able to assess the co-purification of untagged Scy passed through from a separate cell lysate. However, with this experiment because DivIVA was often in the insoluble fraction, we attempted a different strategy of purifying His-DivIVA under denaturing conditions (7.1.4) and loading on refolded (10.1.37) purified DivIVA protein. We needed a cell lysate of overexpressed untagged Scy, so *E. coli* BL21 pLysS (DE3) carrying pET21a-scy was grown in 10ml subcultures to an OD ~0.7. 1mM IPTG was added to induce overproduction at 37°C for 4 hours when the cells were collected and lysed using FastPrep. After centrifugation the supernatant was applied (600µl) onto the Ni-NTA column that was previously loaded with His-DivIVA (600µl). After several washes (four times with 600µl

of buffer) the column was eluted twice with 300µl of 500mM imidazole buffer and the fractions were analysed by SDS-PAGE (Figure 104A). Togerther with His-DivIVA, Scy is detectable in the elution fractions.

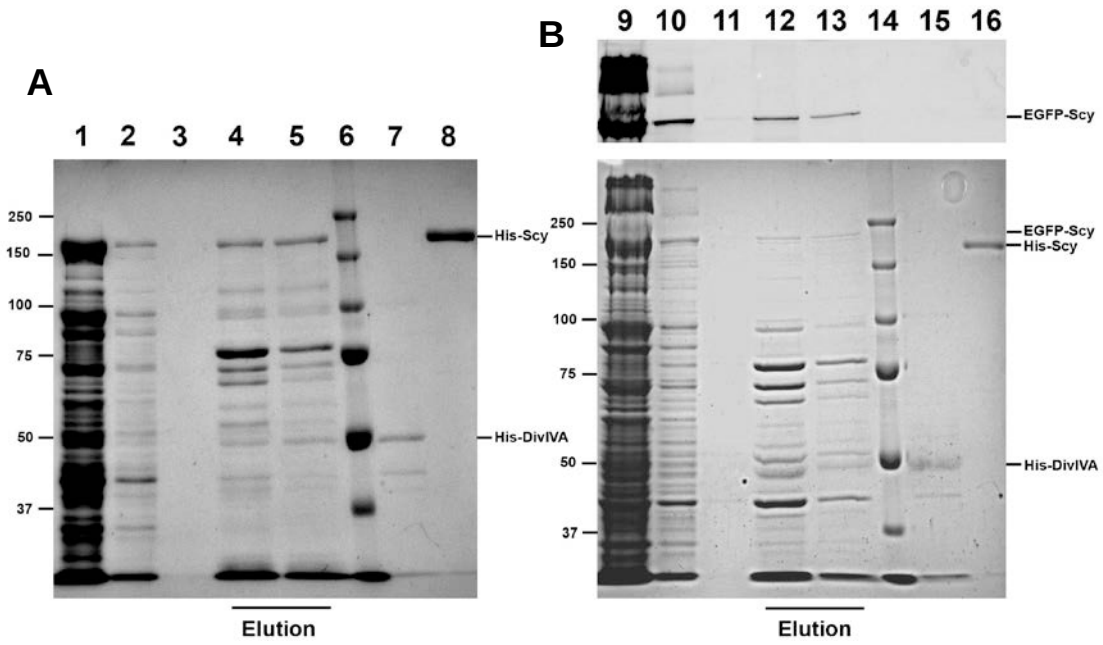

Figure 104: Pull Down Co-affinity of His-DivIVA and Scy or EGFP-Scy.

A) SDS-PAGE of the pull down co-affinity experiment testing His-DivIVA and Scy, samples loaded onto an 8% acrylamide gel. Scy supernatant flowthrough (Lane 1). After Scy addition, beginning wash (Lane 2). After Scy addition, finishing wash (Lane 3). His-DivIVA + Scy elution fractions (Lane 4&5). MW marker is a Biorad precision plus protein All Blue Standards sample (kDa sizes listed left, Lane 6). His-DivIVA preload (Lane 7). His-Scy control (Lane 8).

B) SDS-PAGE of the pull down co-affinity experiment testing His-DivIVA and EGFP-Scy, samples loaded onto an 8% acrylamide gel. EGFP-Scy supernatant flowthrough (Lane 9). After EGFP-Scy addition, beginning wash (Lane 10). After EGFP-Scy addition, finishing wash (Lane 11). His-DivIVA + EGFP-Scy elution fractions (Lane 12&13). MW marker is a Biorad precision plus protein All Blue Standards sample (kDa sizes listed left, Lane 14). His-DivIVA control (Lane 15). His-Scy control (Lane 16). The top panel is the part of the gel containing EGFP-Scy, excited at 488nm and the emission read at 532nm.

This experiment was repeated again but with the strategy to bind His-DivIVA onto the column and then to use untagged EGFP-Scy from cell exracts. Firstly *E. coli* BL21 pLysS (DE3) carrying pET21a-egfp-scy was cultured to an OD ~0.7, when 1mM IPTG was added to induce overproduction at 37°C for 4 hours. After collecting the cells, they were lysed using FastPrep and the insoluble fraction was removed by centrifugation. After equilibrating the Ni-NTA column with buffer, 600µl of His-DivIVA solution was passed through the column. Following washes (three times with 600µl of buffer) 600µl of untagged EGFP-Scy supernatant was passed through the column. Following further

washes, proteins were eluted with 2x300µl of 500mM imidazole buffer. Finally the fractions were analysed by SDS-PAGE without boiling the samples so to maintain the fluorescence of EGFP-Scy, which was detected by phophoimager prior to staining with Coomassie (Figure 104B). In addition to His-DivIVA, EGFP-Scy is detectable in the elution fractions on both the fluorescence scanned image and on the Coomassie stained gel.

8.3.3 Non-tagged Scy also has affinity to the nickel column

As a control experiment to those performed already we had to demonstrate that untagged Scy did not bind to a Ni-NTA column. To this effect, a cell lysate of overexpressed untagged Scy was generated as before using *E. coli* BL21 pLysS (DE3) carrying pET21a-scy. The cell lysate then was loaded onto the Ni-NTA column (600µl) directly and after several washes identical to those performed in the experiments using His-DivIVA or His-FilP. Bound samples were eluted twice with 300µl of 500mM imidazole buffer and the fractions were analysed by SDS-PAGE (Figure 105A). To our surprise, Scy protein was detectable in the elution fractions suggesting that non-tagged Scy had affinity to the Ni-NTA column used.

We also tested the possible binding of untagged EGFP-Scy to the Ni-NTA column. A cell lysate of overexpressed untagged EGFP-Scy was generated using *E. coli* BL21 pLysS (DE3) carrying pET21a-egfp-scy as before. Soluble cell extract was introduced to the Ni-NTA column (600µl) and after several washes identical to those perfomed in the previous experiments we eluted the bound proteins with 2x300µl of 500mM imidazole buffer. The fractions were analysed by SDS-PAGE without boiling the samples to maintain the fluorescence of EGFP-Scy. Fluorescence was detected by scanning the gel in a phosphoimager prior to staining with Coomassie (Figure 105B). Clearly, EGFP-Scy was detectable in the elution fractions of both the scanned image and the Coomassie stained gel.

These control experiments confirmed that both non-tagged Scy and non-tagged EGFP-Scy had some affinity to the columns we used. Therefore the appearance of Scy or EGFP-Scy in the elution fractions in Figure 103 and Figure 104 is not necessarily indicative of positive interaction between Scy and FilP or Scy and DivIVA.

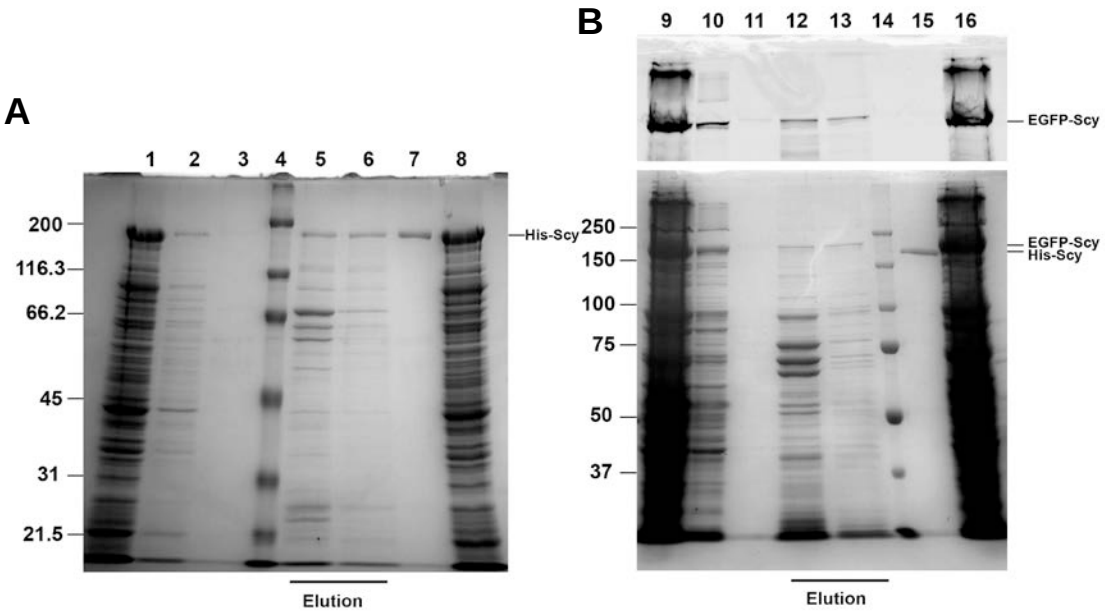

Figure 105: Pull down of Scy or EGFP-Scy control.

A) SDS-PAGE of the pull down experiment testing Scy, samples loaded onto a 10% acrylamide gel. Scy supernatant flowthrough (Lane 1). After Scy addition, beginning wash (Lane 2). After Scy addition, finishing wash (Lane 3). MW marker is a Biorad Prestained SDS-PAGE Standards Broad Range sample (kDa sizes listed left, Lane 4). Scy elution fractions (Lane 5&6). His-Scy control (Lane 7). Scy preload (Lane 8).

B) SDS-PAGE of the pull down experiment testing EGFP-Scy, samples loaded onto an 8% acrylamide gel. EGFP-Scy supernatant flowthrough (Lane 9). After EGFP-Scy addition, beginning wash (Lane 10). After EGFP-Scy addition, finishing wash (Lane 11). EGFP-Scy elution fractions (Lane 12&13). MW marker is a Biorad precision plus protein All Blue Standards sample (kDa sizes listed left, Lane 14). His-Scy control (Lane 15). EGFP-Scy preload (Lane 16). The top panel is the part of the gel containing EGFP-Scy, excited at 488nm and the emission read at 532nm.

8.3.4 Coaffinity of His-Scy and DivIVA

We tried to test the interaction between Scy and DivIVA using coaffinity so that His-Scy was loaded onto the Ni-NTA column and non-tagged DivIVA was tested for *in vitro* interaction.

In this experiment 200µl of already purified His-Scy was first loaded onto the Ni-NTA column. After three washes with the loading buffer we applied cell lysate generated from *E. coli* BL21 pLysS (DE3) carrying pET21a-divIVA overexpressing non-tagged DivIVA (600µl). Cell extract containing overproduced DivIVA was generated as before using the denaturing urea buffer and so it was dialysed against phosphate/salt buffer with 10 mM imidazole prior to applying it to the Ni-NTA column. After washes four times with 600µl of buffer to remove unbound proteins, bound proteins were eluted with 300µl of 500mM

imidazole buffer. The fractions were analysed by SDS-PAGE (Figure 106A). DivIVA was detectable in the elution fractions as assessed by comparisons with the molecular weight of previously purified His-DivIVA.

To perform the control experiment, we applied cell lysate containing overexpressed DivIVA onto the column in the absence of His-Scy. The cell lysate was generated in the same way as above and all steps were identical apart from that no His-Scy was loaded onto the Ni-NTA column. When the fractions were analysed by SDS-PAGE (Figure 106B), DivIVA could be detected in the elution samples suggesting that similarly to Scy, DivIVA also had affinity to the column used. This suggested that our strategy to confirm the direct interaction between Scy and DivIVA using affinity co-elution was not conclusive due to the fact that both Scy and DivIVA had affinity to the columns even in the absence of a His-tag.

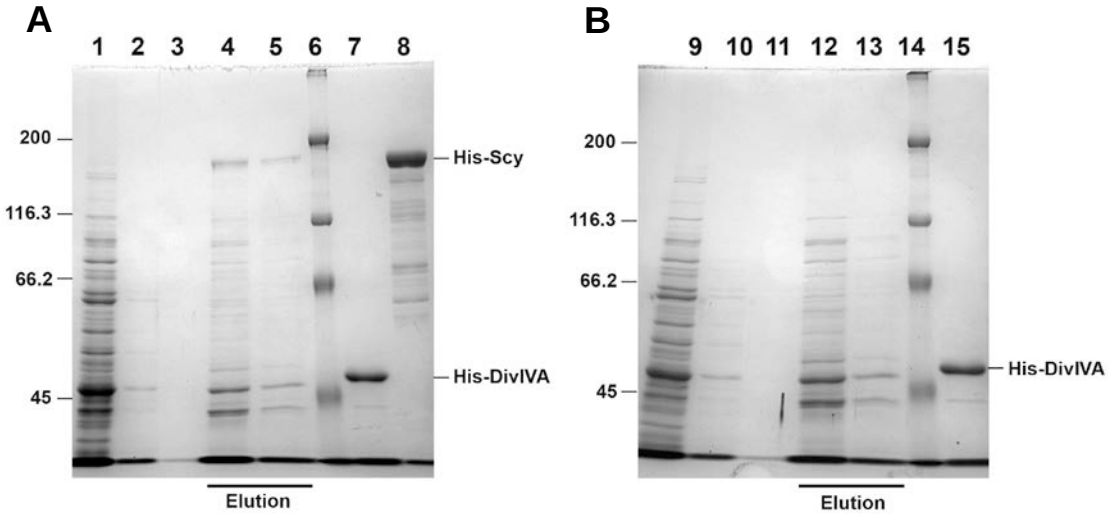

Figure 106: Pull Down Co-affinity of His-Scy and DivIVA or Pull down of DivIVA control.

A) SDS-PAGE of the pull down co-affinity experiment testing His-Scy and DivIVA, samples loaded onto an 8% acrylamide gel. DivIVA supernatant flowthrough (Lane 1). After DivIVA addition, beginning wash (Lane 2). After DivIVA addition, finishing wash (Lane 3). His-Scy + DivIVA elution fractions (Lane 4&5). MW marker is a Biorad Prestained SDS-PAGE Standards Broad Range sample (kDa sizes listed right, Lane 6). His-DivIVA control (Lane 7). His-Scy preload (Lane 8).

B) SDS-PAGE of the pull down experiment testing DivIVA, samples loaded onto an 8% acrylamide gel. DivIVA supernatant flowthrough (Lane 9). After DivIVA addition, beginning wash (Lane 10). After DivIVA addition, finishing wash (Lane 11). DivIVA elution fractions (Lane 12&13). MW marker is a Biorad Prestained SDS-PAGE Standards Broad Range sample (kDa sizes listed right, Lane 14). His-DivIVA control

8.3.5 Coaffinity of His-Scy and DivIVA-C

There was a strong interaction between the C-terminal domain of DivIVA, DivIVA-C and Scy when the bacterial two hybrid assay was used. Therefore we wanted to test whether we could demonstrate direct, *in vitro* interaction between these two proteins using affinity co-elution.

Purified His-Scy was first loaded onto the Ni-NTA column (200µl) followed by several washes as before. A Cell lysate was generated from *E. coli* BL21 pLysS (DE3) carrying pET21a-divIVA-C, where DivIVA-C was overproduced using the same non-denaturing conditions as was used for FilP or Scy production before. This cell lysate was then added to the Ni-NTA column (600µl) where His-Scy was immobilised. After four washes, the bound proteins were eluted with 2x300µl of 500mM imidazole buffer and the fractions were analysed by SDS-PAGE (Figure 107A). DivIVA-C protein was likely to be present in the elution fractions as it is comparable to a purified His-DivIVA-C control.

As a control, we tested whether the untagged DivIVA-C was binding to the Ni-NTA column in the absence of a His-tagged binding partner. So, cell lysate containing overexpressed DivIVA-C was loaded onto the column in the absence of His-Scy. Column fractions were collected as before and were analysed by SDS-PAGE (Figure 107B). There appears to be a band present in the elutions that corresponds to DivIVA-C. However, in elution lanes 4 and 12 there was indication of a greater amount of DivIVA-C in the elution when His-Scy was present than in the control. Therefore, this suggests that DivIVA-C have bound to Scy in this experiment. To verify the presence of DivIVA-C in the elution samples, we used a Western blot using an anti-DivIVA antibody. The samples from Figure 107 were used as well as the full length DivIVA experiment as a control (Figure 106), whereby they were separated on a 10% acrylamide gel. The gel was then used to blot onto a membrane. The blot was incubated first in primary antibody. The primary antibody used was an anti-DivIVA antibody raised in a rabbit (Wang *et al.*, 2009). The blot was then washed and incubated with the secondary antibody. The secondary antibody was Horseradish peroxidase-linked anti-rabbit IgG. As can be seen (Figure 107C) DivIVA-C was detectable in the presence of His-Scy but less so in the absence of His-Scy. However, for full length DivIVA, DivIVA was detectable both in the presence and absence of His-Scy. Suggesting that DivIVA-C was pulled down with His-Scy.

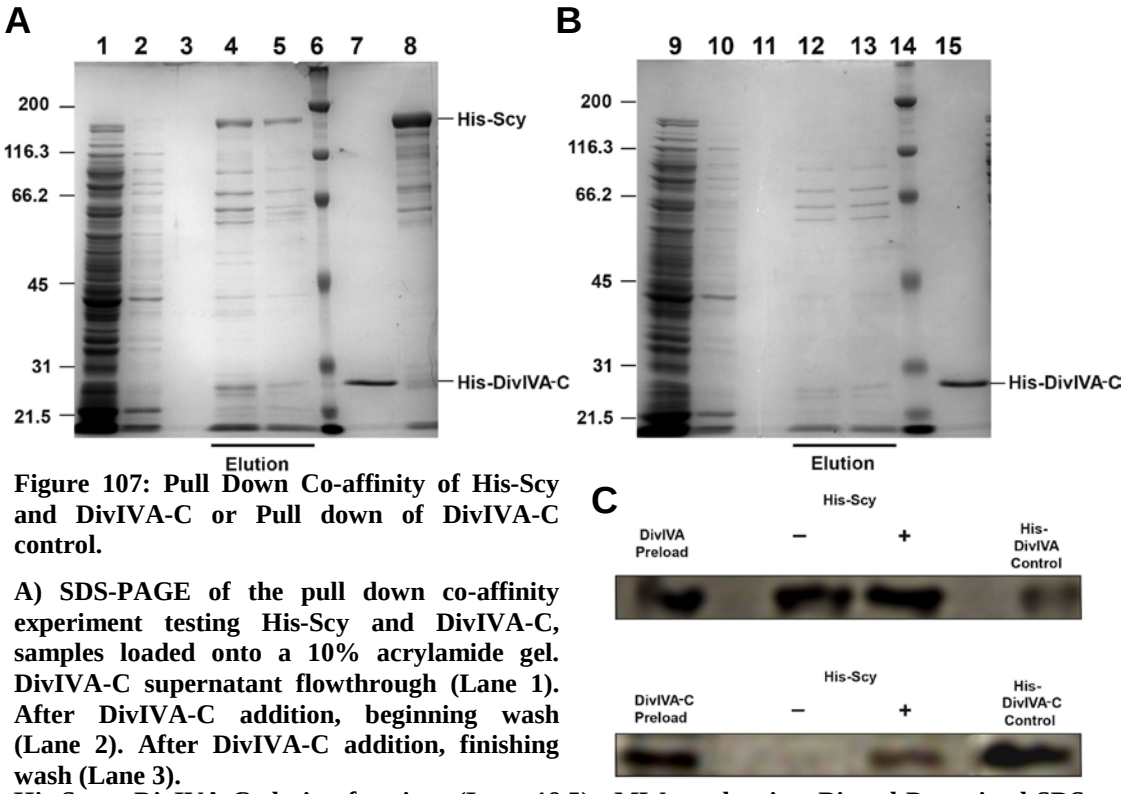

Figure 107: Pull Down Co-affinity of His-Scy and DivIVA-C or Pull down of DivIVA-C control.

A) SDS-PAGE of the pull down co-affinity experiment testing His-Scy and DivIVA-C, samples loaded onto a 10% acrylamide gel. DivIVA-C supernatant flowthrough (Lane 1). After DivIVA-C addition, beginning wash (Lane 2). After DivIVA-C addition, finishing wash (Lane 3). His-Scy + DivIVA-C elution fractions (Lane 4&5). MW marker is a Biorad Prestained SDS-PAGE Standards Broad Range sample (kDa sizes listed right, Lane 6). His-DivIVA-C control (Lane 7). His-Scy preload (Lane 8).

B) SDS-PAGE of the pull down experiment testing DivIVA-C, samples loaded onto a 10% acrylamide gel. DivIVA-C supernatant flowthrough (Lane 9). After DivIVA-C addition, beginning wash (Lane 10). After DivIVA-C addition, finishing wash (Lane 11). DivIVA-C elution fractions (Lane 12&13). MW marker is a Biorad Prestained SDS-PAGE Standards Broad Range sample (kDa sizes listed right, Lane 14). His-DivIVA-C control (Lane 15).

C) Western blot of the coaffinity samples for DivIVA (Figure 106) and DivIVA-C. Samples were loaded onto a 10% acrylamide gel and used in SDS-PAGE. The SDS-PAGE gel was then used in Western blotting with a primary anti-divIVA antibody and an anti-rabbit HRP-IgG secondary antibody. Peroxidase activity was measured by chemiluminescence and development on an X-ray film. His-Scy was either preloaded on the column (+) or not loaded as a control (-). The DivIVA samples correspond with Lane 4 (+) and Lane 12 (-) from Figure 106. The DivIVA-C samples correspond with Lane 4 (+) and Lane 12 (-) from Figure 107. Preload cell extract samples containing either DivIVA (Preload from experiment in Figure 106A) or DivIVA-C (Preload from experiment in Figure 107A) overexpressed were loaded as well as samples containing His-DivIVA (Lane 7, Figure 106A) or His-DivIVA-C (Lane 7, Figure 107A).

8.3.6 Coaffinity of His-Scy and FilP

Following on from the previous experience of both Scy and DivIVA binding to the Ni-affinity column in the absence of a His-tag, we tried to change the buffer conditions to reduce or eliminate the binding of the coiled-coil proteins to the column matrix. To test a possible interaction between Scy and FilP, we aimed to immobilise His-Scy to the Ni-NTA

column and test the binding of non-tagged FilP. We increased the imidazole concentration to 50 mM in the loading and wash buffers and we included 20 mM $MgCl_2$ in the buffers to reduce the weak ionic interactions.

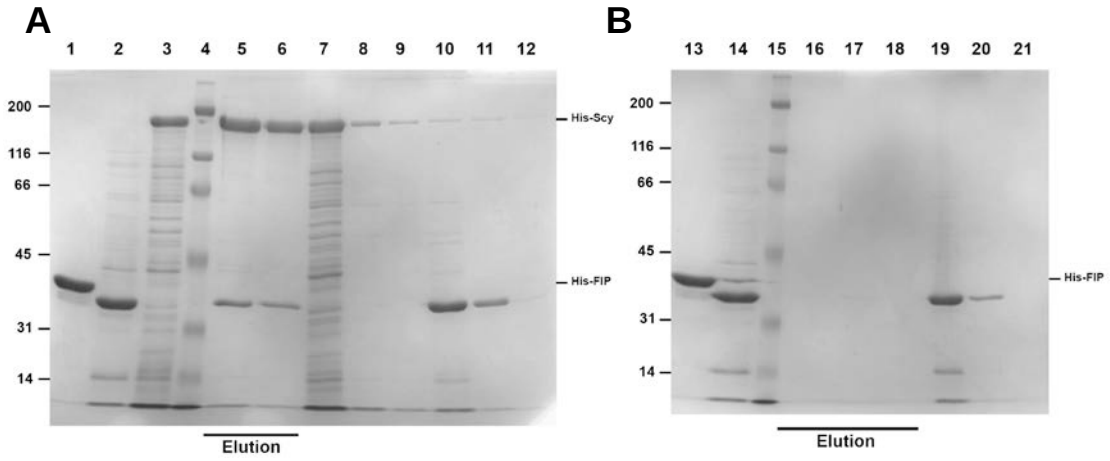

Figure 108: Pull Down Co-affinity of His-Scy and FilP or Pull down of FilP control.

A) SDS-PAGE of the pull down co-affinity experiment testing His-Scy and FilP, samples loaded onto a 10% acrylamide gel. His-FilP control (Lane 1). FilP preload (Lane 2). His-Scy preload (Lane 3). MW marker is a Biorad Prestained SDS-PAGE Standards Broad Range sample (kDa sizes listed left, Lane 4). His-Scy + FilP elution fractions (Lane 5&6). His-Scy flowthrough (Lane 7). After His-Scy addition, beginning wash (Lane 8). After His-Scy addition, finishing wash (Lane 9). FilP supernatant flowthrough (Lane 10). After FilP addition, beginning wash (Lane 11). After FilP addition, finishing wash (Lane 12).

B) SDS-PAGE of the pull down experiment testing FilP, samples loaded onto a 10% acrylamide gel. His-FilP control (Lane 13). FilP preload (Lane 14). MW marker is a Biorad Prestained SDS-PAGE Standards Broad Range sample (kDa sizes listed left, Lane 15). FilP elution fractions (Lane 16,17&18). His-FilP, flowthrough (Lane 19). After FilP addition, beginning wash (Lane 20). After FilP addition, finishing wash (Lane 21).

Purified His-Scy was immobilised to the column (500µl of diluted sample) and cell lysate from *E. coli* BL21 pLysS (DE3) carrying pET21a-filP overexpressing non-tagged FilP was passed through the column (450µl). After washes elution samples were taken using 2x300µl of 500mM imidazole buffer. The fractions were analysed by SDS-PAGE and FilP was clearly detectable in the elution samples (Figure 108A). As a control, cell extract containing overexpressed non-tagged FilP was applied to the Ni-NTA column (450µl) and the washes and elution was performed as before. The fractions were analysed by SDS-PAGE. There was no or negligible FilP in the elution fractions (Figure 108B). This suggested that the changes in the buffer conditions applied eliminated the binding of FilP to the column without a His-tag. Therefore, the presence of FilP in the elution samples where the column was pre-loaded with His-Scy suggest *in vitro* interaction between Scy and FilP.

8.4 Pull down of Scy from *S. coelicolor*

8.4.1 Scy overexpression and purification from S. coelicolor

In order to overexpress Scy in *S. coelicolor* we used the plasmid pCJW93-Scy (Figure 204), previously generated by the Kelemen lab. The *scy* gene is driven by the P_{tipA} promoter that is a thiostrepton inducible promoter. In pCJW93 preceding the *Nde*I site of the polylinker region there is a His-tag sequence, allowing the production of a His-Scy fusion protein. The plasmid also contains a thiostrepton resistance gene (*tsr*), an apramycin resistance gene (*aac(3)IV*) and the replication origin *oriV* from the vector pIJ6021 (Takano *et al.*, 1995) allowing high copy replication in *Streptomyces*.

Introduction of the plasmid into *Streptomyces* was through *E. coli* ET12567/pUZ8002 generating *S.coelicolor* M145/pK48. We needed a large stock of spores from this strain in order to inoculate liquid cultures. 50µl of an M145/pCJW93-Scy spore stock (~$5x10^9$ spores/ml) was used to inoculate 50ml TSB-PEG medium containing apramycin for the selection of the plasmid. The culture was grown at 30°C, shaking at 310rpm for 24 hours generating the starter culture for our experiment. 2ml of this culture was then used to inoculate a new 50ml TSB-PEG medium. The culture was grown at 30°C, shaking at 310rpm in the presence of apramycin for 13.5 hours. At this point the cells were considered to be in the exponential growth phase. Thiostrepton (20µg/ml) was added to induce the *tipA* promoter in pCJW93, thereby to overexpress Scy and the culture was grown for a further 5 hours. Cells were collected by centrifugation and were washed with 10mM imidazole buffer A. In our initial trial experiments cells were lysed by using FastPrep, that breaks the cells by vigorous shaking in the presence of glass particles (<100µm). However, we found that more reproducible and complete lysis was achieved by using sonication of the cells. Sonication disrupts the cell membrane and wall to release protein. Fractions were separated by centrifugation and the supernatant was filtered and used in an FPLC-purification.

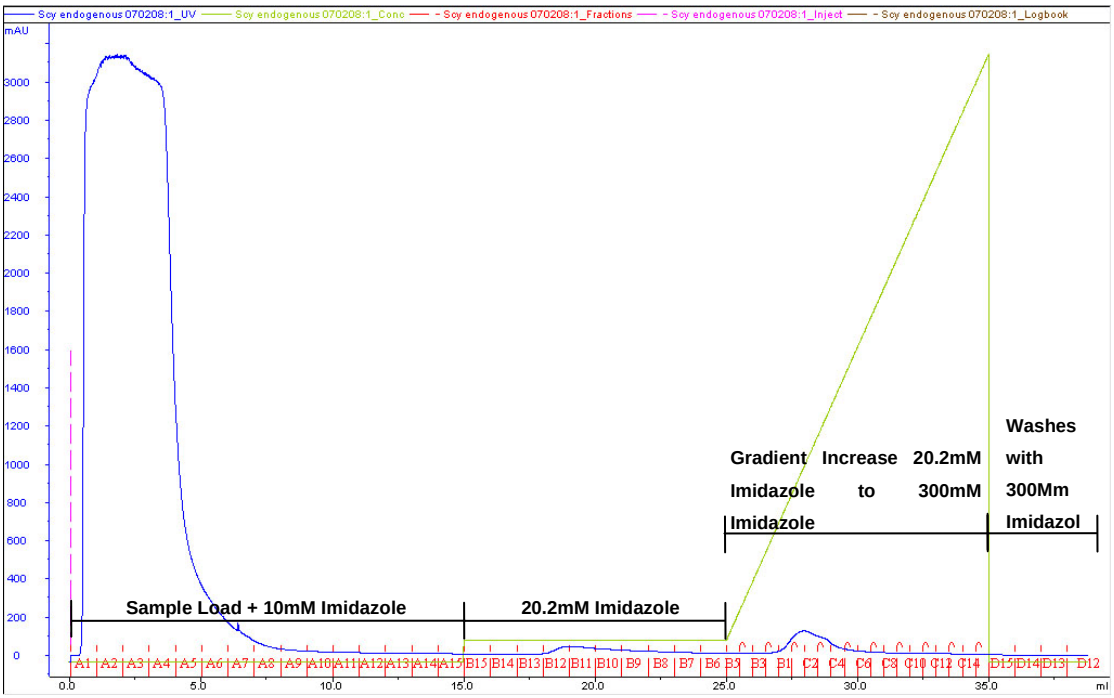

Figure 109: FPLC Chromatogram readout for purification of His-Scy from *S. coelicolor* using a gradient elution strategy. Absorbance data at 280nm of the different eluted samples. 0-15ml represents the addition of cell extract with 10mM imidazole buffer. 15-25ml represents an increase in buffer to 20.2mM imidazole. 25-35ml represents a gradient increase in buffer from 20.2mM to 300mM imidazole. Blue is the absorbance data (mAU) at 280nm. Green represents the change in imidazole concentration. Red represents the fractions of eluted samples collected.

A

Nickel HisTrap HP 1ml (GE Healthcare) column was used with an Amersham AKTA FRC FPLC machine for affinity chromatography. Approximately 2-3ml of extract was loaded onto the column with 10mM imidazole buffer A, the combined flow running to 15ml. A 10ml wash was carried out whereby the imidazole concentration was raised to 20.2mM. A gradient of rising imidazole concentration was then applied, from 25ml to 35ml the concentration increased from 20.2mM to 300mM. The absorbance of the eluted liquids at 280nm was monitored and plotted against the fraction numbers (Figure 109). From the UV data we can see three peaks that are of interest. The large peak in the sample load represents most of the cell's proteins, which did not have an affinity for the column, so that they ran straight through. The peak in the 20.2mM imidazole shows proteins with a lower affinity, eluting from the column during the wash step. Whereas the large peak seen in the rising gradient at approximately 102.8mM imidazole concentration, should be proteins with a higher affinity for the column. His-Scy was expected in this latter samples.

Selected samples were analysed using 8% SDS-PAGE stained with Biosafe G250 Coomassie blue (Figure 110).

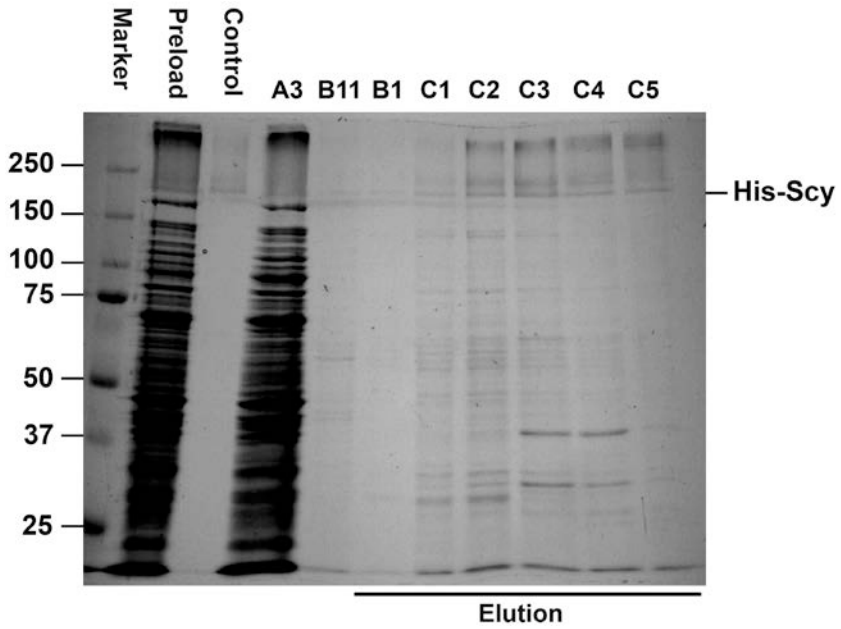

Figure 110: SDS-PAGE of the FPLC samples loaded onto an 8% acrylamide gel. MW marker is a Biorad precision plus protein standard sample (kDa sizes listed left). Preload is an aliquot of the cell extract prior to loading onto the FPLC column. The control is His-Scy purified from *E. coli*. Lane notation corresponds with the fraction numbers in Figure 109. A3 is from the flowthrough. B11 is from the wash. B1 to C5 are from the rising gradient of imidazole to 300mM imidazole. The gel was stained with Biosafe G250 Coomassie blue.

The predicted size of Scy from StrepDB (StrepDB, strepdb.streptomyces.org.uk/) is 146.4 kDa. However, the size of our induced Scy is likely to be slightly bigger due to the His tag. The control of Scy appears to have a band between the size markers 250 kDa and 150kDa and this band is visible in the elution samples C1-C5. The gel appears to indicate that a small amount of Scy came off the column in the 20.2mM imidazole wash (B11). However, most of the Scy appears to have eluted in fractions C1-C5. There are many other bands that are present in C1-C5. The identity of these is unknown and the explanation for their presence could be that either the purification procedure was not efficient or that they are in fact proteins that have eluted at the same time as Scy and they are potentially proteins that formed a complex with Scy.

8.4.2 Crosslinking Scy in vivo

To identify *S. coelicolor* proteins that might interact with Scy at the growing hyphal tip, we could analyse the previous samples where proteins that co-eluted with His-Scy could potentially be Scy partners. However, this assumed that the Scy-partner interaction survived the conditions used for cell lysis and affinity purification. To attempt to purify something that interacts with Scy *in vivo* but with an affinity too low to allow co-purification in FPLC, we decided to use a reversible chemical crosslinker to fix the Scy-partner interactions throughout the purification procedure.

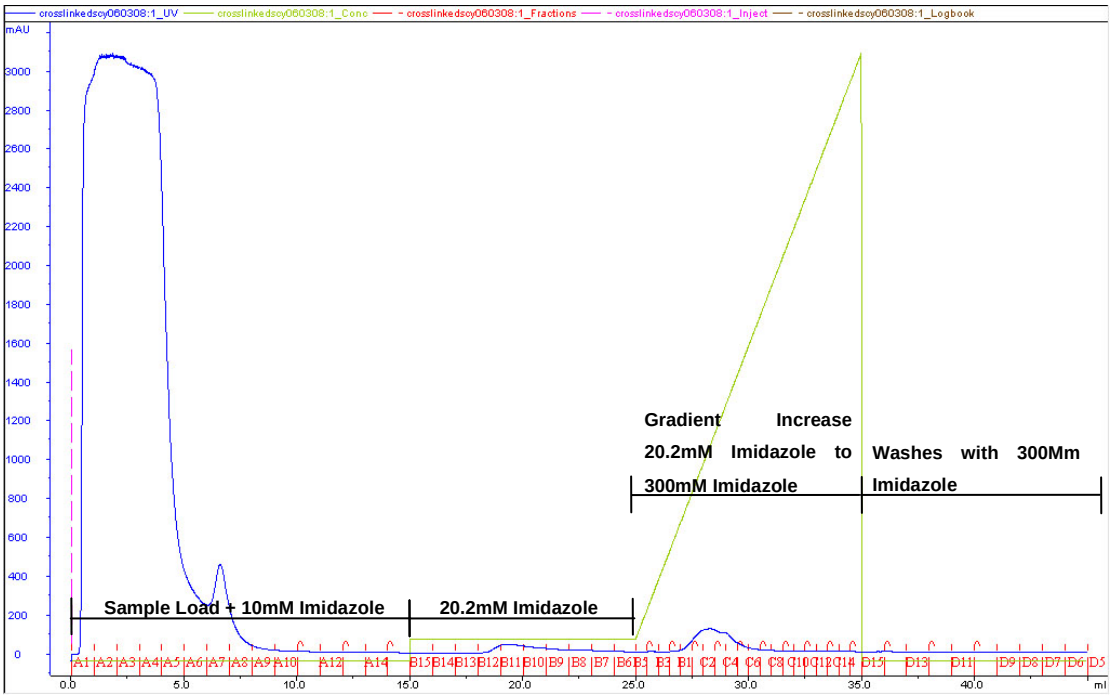

Figure 111: FPLC Chromatogram readout for purification of crosslinked His-Scy using a gradient elution strategy. Absorbance data at 280nm of the different eluted samples. 0-15ml represents the addition of cell extract with 5mM imidazole buffer. 15-25ml represents an increase in buffer to 15.3mM imidazole. 25-35ml represents a gradient increase in buffer from 15.3mM to 300mM imidazole. Blue is the absorbance data (mAU) at 280nm. Green represents the change in imidazole concentration. Red represents the fractions of eluted samples collected.

Two sets of cultures were grown so that one set could later be chemically crosslinked and one set left uncrosslinked. In this experiment the culture conditions used were slightly different, these changes were mostly to attempt to increase the yield of Scy protein by preventing aggregations of cells that could be inaccessible to thiostrepton. For each 50ml TSB-PEG medium, 60µl of an M145/pCJW93-scy spore stock was introduced after inducing germination in 500µl 2xYT at 50°C for 10 minutes. The conical flask also

contained a metal coil to break apart cell aggregates. The cultures were grown at 30°C, with vigorous shaking at 310rpm maintaining apramycin selection for 21.5 hours. Thiostrepton (20μg/ml) was used to induce the TipA promoter in pCJW93, thereby to overexpress His-Scy and the culture was grown for further 5 hours.

Cells were collected by centrifugation and washed with a buffer 50mM NaH_2PO_4,50mM NaCl, pH 9. To chemically crosslink Scy with its potential partners we used the chemical Dimethyl 3,3'-dithiobispropionimidate (DTBP; Sigma). This chemical reacts with amine groups, due to its structure it bifunctionally reacts linking neighbouring amine group side chains to each other. The spacer arm length of DTBP is 11.9 Å (8 atoms). DTBP is a reversible crosslinker, as reducing agents such as DTT or βmercapto-ethanol will abolish the disulfide groups within the crosslinker and therefore liberate the interacting partner proteins. To cells removed from the culture that we wanted to crosslink, we added DTBP at a concentration of 20mM in a phosphate buffer at pH 9. Cells were incubated for 30 minutes with the crosslinker and finally 100mM Tris pH 8 was added to stop the reaction and scavenge of any unused DTBP. Tris having an amine group would sequester any unused DTBP. Alternatively for the culture set that was not to be crosslinked, the DTBP and Tris steps were omitted and the cells were washed in 10mM imidazole buffer A. DTBP crosslinked cells were also washed in 10mM imidazole buffer A so that the cells were kept in similar solutions. Both the crosslinked and the non-crosslinked cells were then lysed by sonication as before.

FPLC was used to purify His-Scy as before, apart from the 5mM imidazole in the loading buffer and the 15.3mM imidazole in the washes. A gradient of rising imidazole concentration was then applied, from 25ml to 35ml where the concentration increased from 15.3mM to 300mM. The FPLC readout for the crosslinked sample is shown in Figure 111, whereas the FPLC readout for the non-crosslinked sample can be seen in Figure 114.

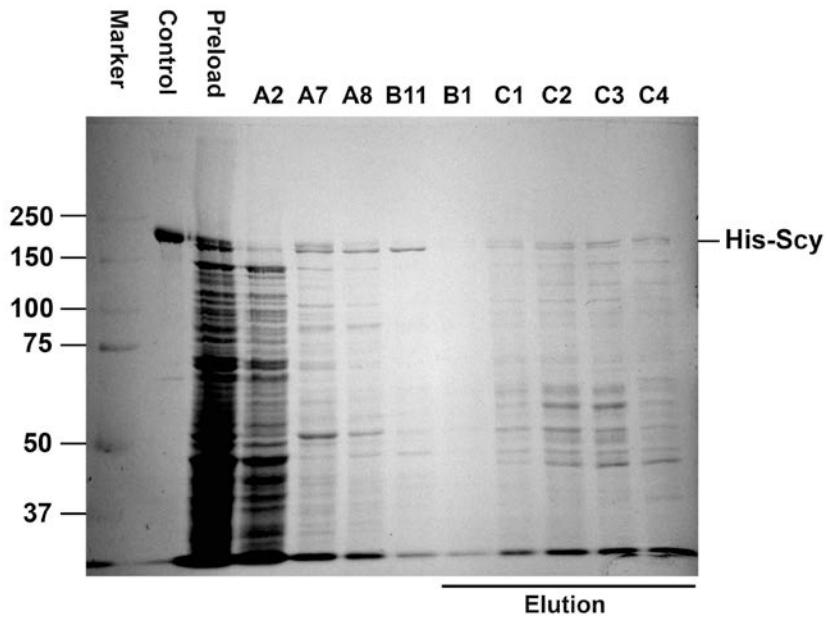

Figure 112: SDS-PAGE of the reduced crosslinked FPLC samples loaded onto an 8% acrylamide gel. Using reducing conditions of incubation with 100mM DTT and 4x loading dye with β-mercaptoethanol. MW marker is a Biorad precision plus protein standard sample (kDa sizes listed left). The control is His-Scy purified from *E. coli*. Preload is an aliquot of the cell extract prior to loading onto the FPLC column. Lane notation corresponds with the fraction numbers in Figure 111. A2 is from the flowthrough. A7 and A8 are from the peak following addition on the column. B11 is from the wash. B1 to C4 are from the rising gradient of imidazole to 300mM imidazole. The gel was stained with Biosafe G250 Coomassie blue.

For the crosslinked samples a number of the fractions corresponding to the positions of the 280nm absorbance peaks were analysed using SDS-PAGE. Two sets of aliquots of the crosslinked samples were taken, one set was treated with dithiothreitol (DTT) at 37°C for 30 minutes prior to loading using a dye containing β-mercaptoethanol. The other set was not treated with DTT and was loaded with 4x loading dye that did not include β-mercaptoethanol. The samples were then analysed on separate gels (Figure 112 and Figure 113). Dithiothreitol and β-mercaptoethanol are chemical agents that can reduce the disulphide bonds of the DTBP crosslinker and therefore separate the proteins that were crosslinked.

Fractions of the non-crosslinked samples were also analysed using SDS-PAGE, 8% (Figure 115) or 12% (Figure 116). These samples were also treated with DTT and the loading dye used did contain β-mercaptoethanol.

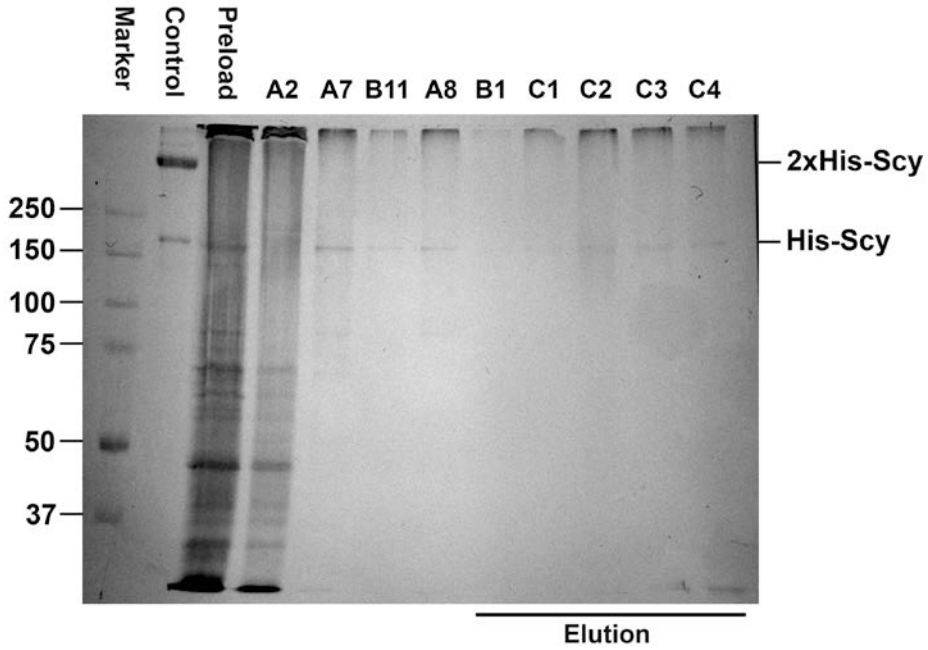

Figure 113: SDS-PAGE of the unreduced crosslinked FPLC samples loaded onto an 8% acrylamide gel. Samples were loaded using loading dye without β-mercaptoethanol. MW marker is a Biorad precision plus protein standard sample (kDa sizes listed left). The control is His-Scy purified from *E. coli*. Preload is an aliquot of the cell extract prior to loading onto the FPLC column. Lane notation corresponds with the fraction numbers in Figure 111. A2 is from the flowthrough. A7 and A8 are from the peak following addition on the column. B11 is from the wash. B1 to C4 are from the rising gradient of imidazole to 300mM imidazole. The gel was stained with Biosafe G250 Coomassie blue.

A comparison of the FPLC UV absorption readouts for the crosslinked and the non-crosslinked samples shows some similarities and some differences. Both FPLC readouts have a large peak in the sample load, which represents most of the cell's proteins, which did not have an affinity for the column, so that they passed straight through. The crosslinked sample contains another peak shortly after the majority of proteins have run through. These being in the A7 and A8 fraction positions. This is an unusual peak that is not present in the non-crosslinked sample. It is currently unknown why this peak is present. Though it could be hypothesised that the His-tag which is present on the N-terminal amine end of the protein could be crosslinked and behaves differently, however, it is unlikely that this is the case for this peak as a similar peak had been produced from a non-crosslinked Scy sample (data not shown). The crosslinked sample has an extremely visible peak in the 15.3mM imidazole wash, whereas there is a small rise in the non-crosslinked sample during the 15.3mM imidazole wash, which can only be seen clearly by zooming in on the image. The peak in the wash is likely to represent proteins with a weaker affinity for the column. It is perhaps a little unexpected that the wash for the crosslinked sample appears to have eluted more protein. The crosslinked sample if successfully crosslinked, then we

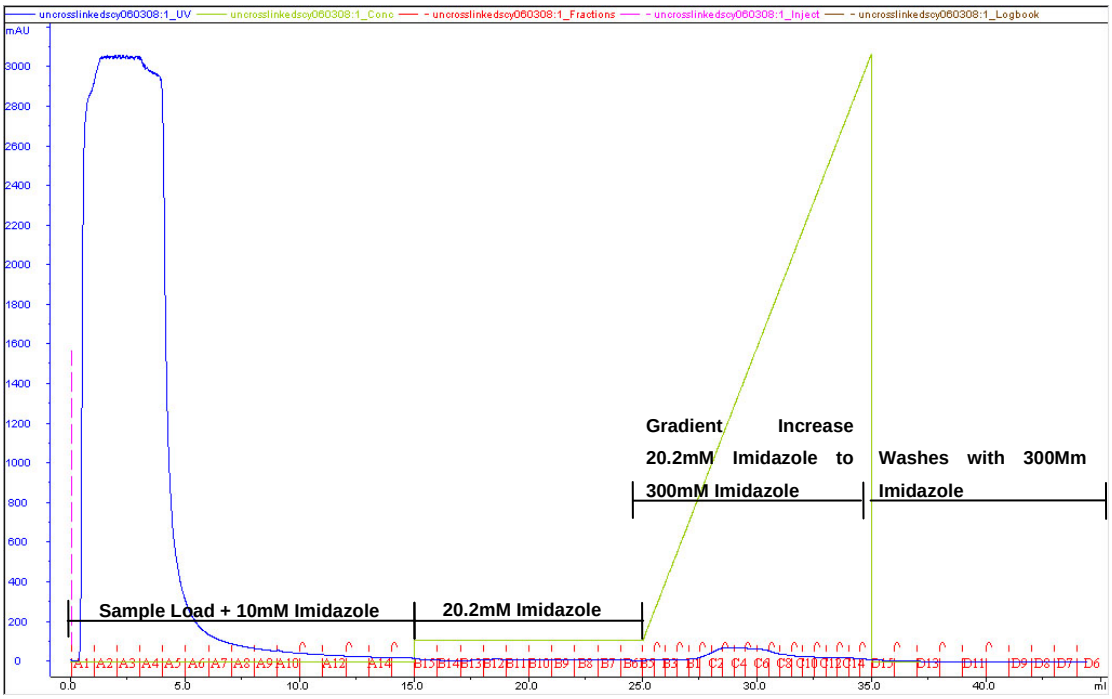

Figure 114: FPLC Chromatogram readout for purification of non-crosslinked His-Scy using a gradient elution strategy. Absorbance data at 280nm of the different eluted samples from a non-crosslinked sample. 0-15ml represents the addition of cell extract with 5mM imidazole buffer. 15-25ml represents an increase in buffer to 15.3mM imidazole. 25-35ml represents a gradient increase in buffer from 15.3mM to 300mM imidazole. Blue is the absorbance data (mAU) at 280nm. Green represents the change in imidazole concentration. Red represents the fractions of eluted samples collected.

would expect any Scy partner proteins to be crosslinked and bound tightly to Scy. Both the crosslinked and the non-crosslinked samples have a peak in the imidazole gradient which likely represents imidazole displacing histidine residues. The non-crosslinked peak coincides with 107mM imidazole, however, it appears to be a broad peak around this concentration of imidazole. Whereas the crosslinked sample has a peak at 97mM imidazole. However, as the peaks for both are broad the difference in imidazole concentration is unlikely to be significant. The gel images of the FPLC-eluted samples show interesting results. A direct comparison of both the non-crosslinked and the crosslinked samples on an 8% acylamide gel (Figure 115 and Figure 112 respectively) shows differences between the two samples. The control on both forms a distinctive band between the 150 and 250kDa markers. The peak in the load in the crosslinked samples (fractions A7 and A8) appears to contain Scy eluting at an earlier stage than expected. There are also a number of other bands present, these could be explained as proteins co-eluting with Scy or could just be the remaining samples that were in the tail end of the large load peak. The fraction (B12) in the non-crosslinked sample does not appear to have

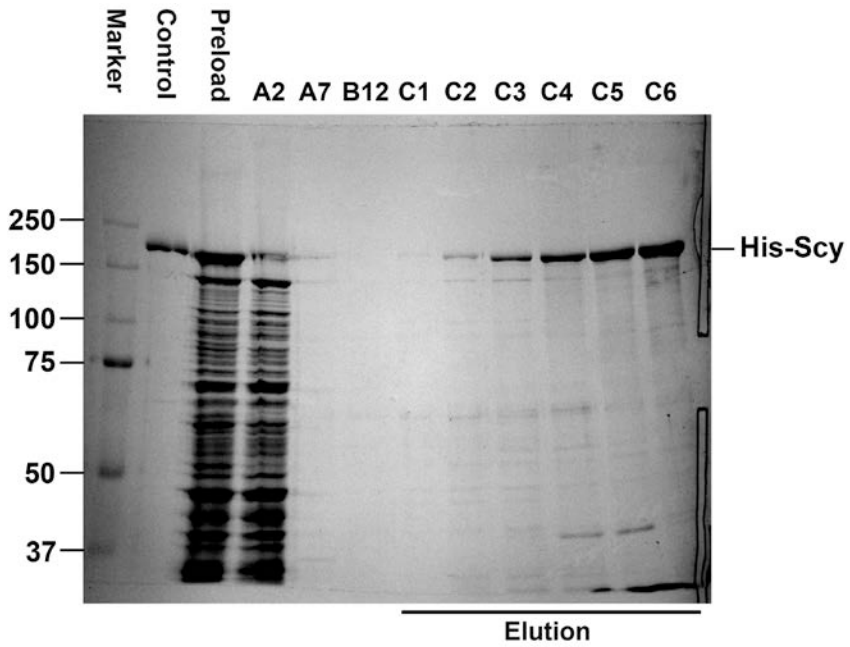

Figure 115: SDS-PAGE of the non-crosslinked FPLC samples loaded onto an 8% acrylamide gel. Using reducing conditions of incubation with 100mM DTT and 4x loading dye with β-mercaptoethanol. MW marker is a Biorad precision plus protein standard sample (kDa sizes listed left). The control is His-Scy purified from *E. coli*. Preload is an aliquot of the cell extract prior to loading onto the FPLC column. Lane notation corresponds with the fraction numbers in Figure 114. A2 is from the flowthrough. A7 is from after addition on the column. B12 is from the wash. C1 to C6 are from the rising gradient of imidazole to 300mM imidazole. The gel was stained with Biosafe G250 Coomassie blue.

any strong bands. Whereas the wash fraction (B11) in the crosslinked sample does appear to have Scy and some lower weight bands that could be co-eluting proteins. Both the imidazole gradient washes for the crosslinked (fractions C1,C2,C3,C4) and non-crosslinked (fractions C2,C3,C4,C5) samples appear to have eluted Scy. The non-crosslinked Scy elution appears to be more concentrated; however, a certain amount of Scy appears to have been lost in the load peak of the crosslinked sample. Interestingly there appears to be a larger number of bands in the crosslinked imidazole gradient elutions (fractions C1,C2,C3,C4) than the non-crosslinked imidazole gradient elutions (fractions C2,C3,C4,C5). We predict a number of these bands are due to the crosslinking enabling a number of *in vivo* Scy interacting proteins to have a high enough affinity for Scy that they are present in the high imidazole elutions, whereas in the non-crosslinked samples these have probably not bound with Scy/associated complexes in the column.

Analysing the non-reducing gel of the crosslinked samples (Figure 113) confirms that the crosslinking has been successful. All of the samples appear to have the presence of a supershifted band, which is much bigger than the 250kDa size marker. It is likely that these are crosslinked proteins that are unable to travel far on a gel as their combined weights

make them too heavy. However, there is a blurring effect, which can probably be explained as being due to the variation in sizes created in crosslinking proteins. The crosslinked elutions appear to have many more proteins than the non-crosslinked, the high number of proteins means that the crosslinked proteins probably would not create very defined bands on a non-reduced gel. For example if there had been 2 proteins as well as Scy, the different variations of crosslinking would probably create a fair number of bands. The fact that so many proteins are pulled out through crosslinking suggests that Scy could possibly interact with a large number of different proteins *in vivo*. It's also interesting to note that the Scy control forms 2 distinct bands in the crosslinked non-reduced sample. The distance migrated of the higher molecular weight band was used to calculate an approximate size of this band of 270kDa, which is consistent with the size of a Scy dimer. It was previously unknown how Scy assembles *in vivo*, but this strongly hints that it forms at least dimeric multimers. The amino acid sequence of Scy has one cysteine residue. Due to the two bands on the SDS-PAGE, it is likely one band represents dimers of Scy linked by a disulphide bond, whereas the other band likely represents single, fully reduced Scy.

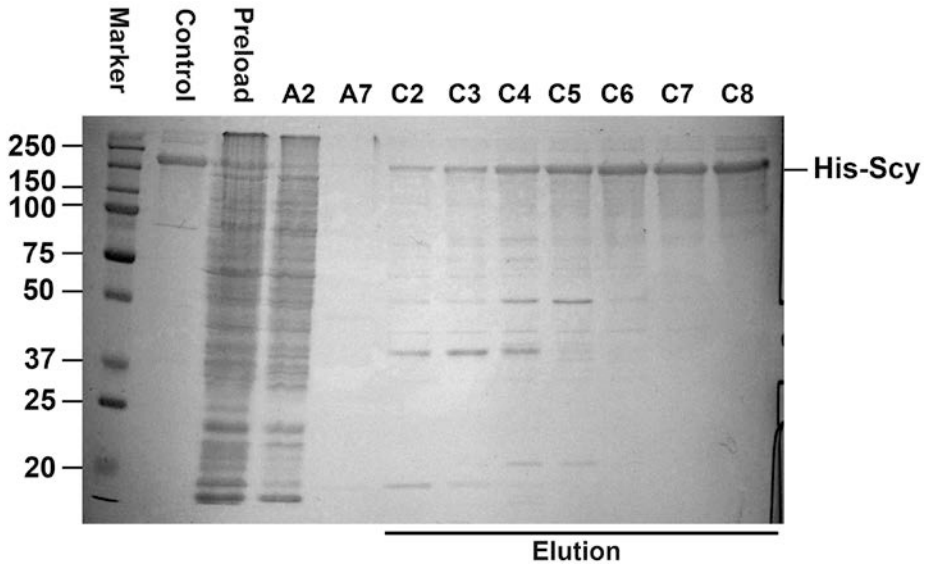

Figure 116: SDS-PAGE of the non-crosslinked FPLC samples loaded onto a 12% acrylamide gel. Using reducing conditions of incubation with 100mM DTT and 4x loading dye with β-mercaptoethanol. MW marker is a Biorad precision plus protein standard sample (kDa sizes listed left). The control is His-Scy purified from *E. coli*. Preload is an aliquot of the cell extract prior to loading onto the FPLC column. Lane notation corresponds with the fraction numbers in Figure 114. A2 is from the flowthrough. A7 is from after addition on the column. B12 is from the wash. C2 to C8 are from the rising gradient of imidazole to 300mM imidazole. The gel was stained with Biosafe G250 Coomassie blue.

The reason that the non-crosslinked samples were analysed on both a 12% acrylamide and an 8% acrylamide gel, is that we wanted visualise some proteins at lower molecular

weights. There do appear to be some extra bands at the lower molecular weights that are not visible on the 8% acrylamide gels. The non-crosslinked samples appear to have a number of candidate bands that would be interesting to identify. The crosslinked sample also contains a number of additional bands that would also be interesting to identify.

8.4.3 Western blot analysis of pulled-down proteins

To confirm that His-Scy was being purified by FPLC we used a Western blot. A selection of the elution and wash fractions from the non-crosslinked protein samples from Figure 114 were first separated on an 8% acrylamide gel. The proteins were then blotted onto a membrane, which was incubated first with the primary antibody, an anti-His antibody raised in a mouse. The blot was then quickly washed and incubated with the secondary antibody, an anti-mouse heavy chain antibody raised in a goat. This antibody was an LI-COR IRdye 800CW antibody labelled with a fluorophore that is excited by light at 780nm. The blot was visualised with an Odyssey Infrared Imaging System. This system uses two colour detection where the blot is viewed with the fluorescent channels 680nm and 780nm. The Odyssey software generated an image with 780nm emission seen as green and 680nm emission as red (Figure 117). A quantitative measurement of the relative intensities of the bands to the control is shown in Figure 118. This shows that the greatest amount of signal measured was in the C5 and C4 samples, which corroborates the stained SDS-PAGE gel (Figure 115) where C5 and C4 appear to have the most eluted His-Scy, suggesting the visible higher molecular weight band in both gels is the same.

It can be seen that there are bands from the Western blot that are visible in the co-elutions (Figure 117). These are comparable in size to the control of Scy that was purified from *E. coli*. It is the His-tag in which the primary antibody is specific for, so it can definitely be said that the protein that can be seen on the Western blot is a His fusion, or just has a large number of histidine residue repeats. However, it is likely that it is His-Scy in the elutions due to the positions of the bands. The preload sample does not have a visible band. There must be His-Scy in the preload as this is the same cell extract just taken before FPLC. So it is likely that the lack of appearance of a band is due to the Scy being in a much less concentrated form and therefore the fluorescence is not strong enough to be visible. There

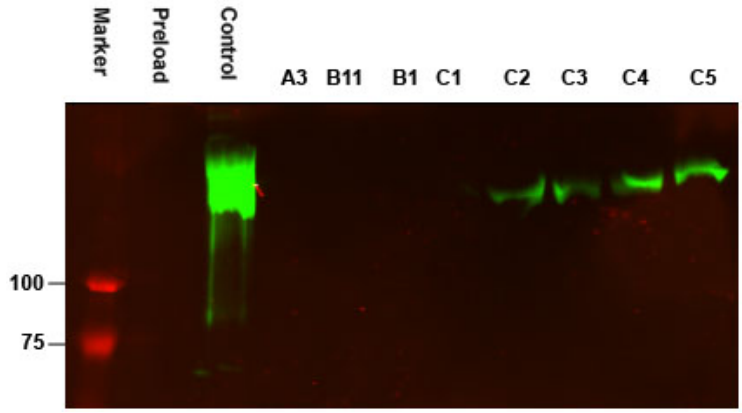

Figure 117: Western blot of the FPLC samples from Figure 114. Samples were loaded onto an 8% acrylamide gel and used in SDS-PAGE. The SDS-PAGE gel was then used in Western blotting with a primary anti-His antibody and an LI-COR IRdye 800CW anti-mouse secondary antibody. Fluorescence was measured after excitation at 780nm (Green) and 680nm (Red). MW marker is a Biorad Prestained SDS-PAGE Broad Range standard (kDa sizes listed left). Preload is an aliquot of the cell extract prior to loading onto the FPLC column. The control is His-Scy purified from *E. coli.*

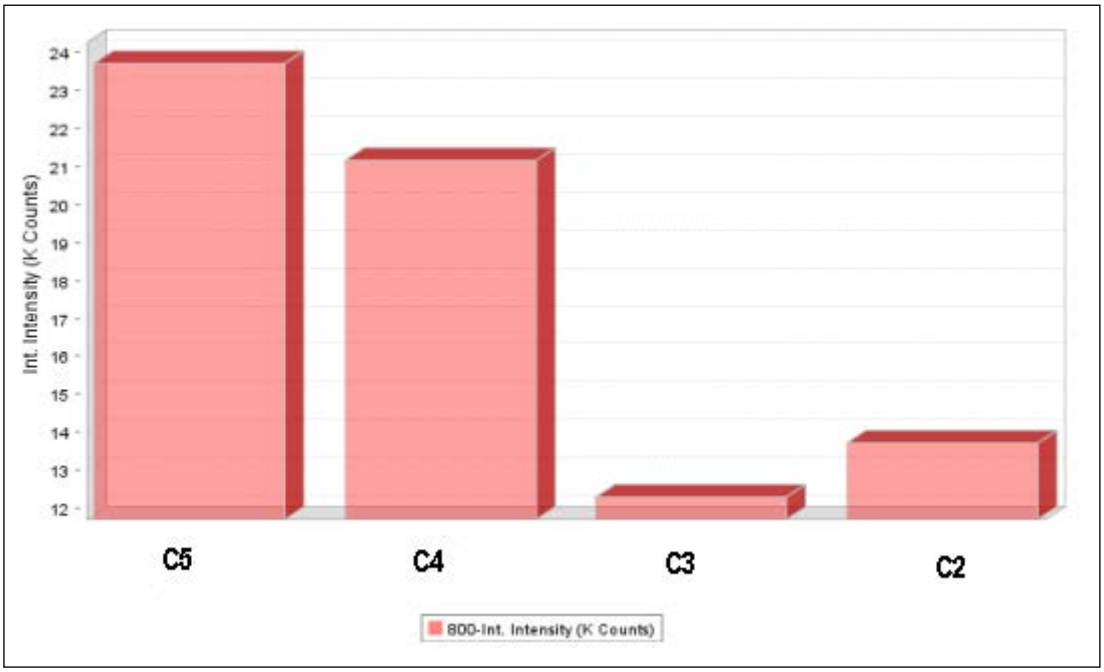

Figure 118: Quantitative measurement of fluorescence intensity at 780nm wavelength excitation, measured using an Infrared Odyssey imaging system. Fluorescence was measured from bands of samples from the Western Blot in Figure 117.

is also no band in the 20.2mM imidazole, which we said that there was a faint band in the SDS-PAGE (Figure 115). This could be due to the fluorescence being too low to detect. Alternatively a hypothesis is that the Scy in the 20.2mM imidazole wash is the endogenous Scy. For this hypothesis to be true Scy would have to be forming multimers *in vivo*, so therefore we might expect that His-Scy would co-elute some endogenous Scy. We might also expect this to be true for the samples that aren't the wash and this cannot be ruled out

for these samples as well. For a number of the SDS-PAGE gels there does appear to be a doublet of bands in the position of Scy that could represent both purified His-Scy and co-purified endogenous Scy.

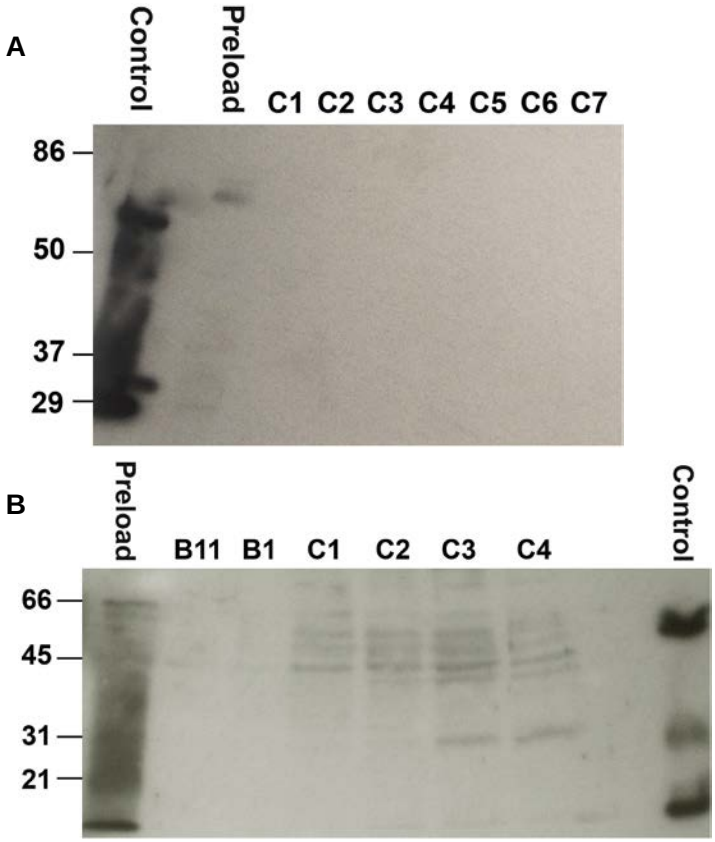

Figure 119: Western blot analysis of His-Scy non-crosslinked and crosslinked samples to detect DivIVA co-purification.

Western blot of the FPLC non-crosslinked samples from Figure 114 (A) and the FPLC crosslinked samples from Figure 111 (B). Samples were loaded onto a 10% acrylamide gel and used in SDS-PAGE. The SDS-PAGE gel was then used in Western blotting with a primary anti-divIVA antibody and an anti-rabbit HRP-IgG secondary antibody. Peroxidase activity was measured by chemiluminescence and development on an X-ray film. MW marker is Biorad Prestained SDS-PAGE Broad Range standard (kDa sizes listed left). Preload is an aliquot of the cell extract prior to loading onto the FPLC column. The control is His-DivIVA purified from *E. coli*.

To check if DivIVA was being co-purified with His-Scy in the FPLC we used a Western blot using an anti-DivIVA antibody. The non-crosslinked protein samples from FPLC in Figure 114 were used as well as the crosslinked samples from Figure 111. Whereby they were separated on a 10% acrylamide gel. The gel was then used to blot onto a membrane. The blot was incubated first in primary antibody. The primary antibody used was an anti-DivIVA antibody raised in a rabbit (Wang *et al.*, 2009). The blot was then washed and incubated with the secondary antibody. The secondary antibody was Horseradish

peroxidase-linked anti-rabbit IgG. No relevant bands were detected in the elution samples of the Western blot of the non-crosslinked samples (Figure 119A). Whereas for the Western blot of the crosslinked samples, there were several bands present that may correspond with DivIVA, potentially modified DivIVA or degradation products of DivIVA (Figure 119B). Therefore, suggesting that DivIVA was co-purified with His-Scy from the Ni-NTA column. Therefore, in amongst the potential complex formed by crosslinking Scy, DivIVA is a member.

8.4.4 Summary

Use of a pelleting assay allowed us to monitor pelleting of DivIVA with either Scy or FilP under the conditions tested. Suggesting an *in vitro* interaction between DivIVA and Scy and between DivIVA and FilP. DivIVA-C was also able to pellet with Scy suggesting an interaction. Scy, DivIVA or DivIVA-C were unable to pellet with lipids in the conditions tested. However more experiments should be performed to verify if these proteins interact with the lipid membrane and perhaps use the membrane as a cue for localisation. In co-pull down experiments we were able to demonstrate an interaction between Scy and FilP, as well as an interaction between Scy and DivIVA-C, however this experimental technique had many technical problems that prevented us from dissecting all combinations of proteins. Scy pulled down from cells of *S.coelicolor* also pulled down other proteins and reaction of these with anti-DivIVA antibody suggests that Scy and DivIVA are members of the same complex in the *in vivo* environment of *S.coelicolor*.

9 Discussion

The bacterial cytoskeleton is a somewhat novel concept. Central to the emergence of this field was the discovery of eukaryotic cytoskeletal homologues in prokaryotes. This has led to the conclusion that cytoskeletal proteins were present in the last common universal ancestor (Faguy, and Doolittle, 1998; van den Ent *et al.*, 2001). It might also be expected that since the divergence from the last common ancestor that bacteria would have evolved their own specialised cytoskeletal proteins or evolved to have very different cytoskeletal proteins. As far as we are aware, a long repetitive non-heptad coiled-coil containing protein that may be considered directly homologous to Scy is unique to filamentous actinomycetes. The filamentous actinomycetes have quite unique development and morphological states. It is not suprising then that a unique cytoskeleton and cell shape determining factors might be needed for actinomycete development. Therefore, mutating the gene encoding a possible cytoskeletal protein such as Scy in *S. coelicolor* might be thought to affect morphology. As such we found that mutating *scy* and/or *filP* appears to affect the morphology and growth of *S. coelicolor*. Mutations in these genes have been assessed in this report and together with work here and by others in the Kelemen lab it is now known that a double mutant can also be tolerated. The ability to complement the *scy* mutant using a copy of *scy* added *in trans* suggests that the *scy* mutant phenotype is due to the absence of this gene. The *filP* mutant was not complemented here, but had been complemented by Bagchi *et al.,* (2008). Due to the similarity of our strain microscopically to their strain it is likely that they are genetically similar. Creating a *scy-filP* double mutant dispels a potential theory that the two genes act in a functionally redundant manner in a process that is essential for *Streptomyces* development, in which both cannot be tolerated being lost. However, it is likely that these two genes are involved in similar functions though maybe to a certain extent mutually exclusive as they have non-identical phenotypes (and localise differently). In terms of the effect on growth, it appears that *scy* deletion is more detrimental than *filP* deletion, as the hyphae are far more distorted. This may suggest that perhaps Scy has a more important role in the development of *S. coelicolor*. It is possible that the proteins encoded by *scy* and *filP* function in a similar process during development, to which Scy has a more dominant role.

The phenotypic consequences of the genetic alterations created in the mutants has been assessed both macroscopically and microscopically on SFM media and initially only macroscopically on CM, MMM and MMG. At certain time points macroscopically the *scy*

and *scy-filP* double knockout mutant strains are reminiscent of *bld* or *whi* mutants. However, the *scy* and *scy-filP* double knockout mutant strains are more likely just delayed in growth, as their appearance on confluent plates for spore preparation, where they had been grown for longer, appeared to be grey. They formed spores enabling us to prepare spore preparations, so they are not *whi* mutants (and therefore neither are they *bld*). Across rich media and minimal media they were delayed in aerial hyphae production, so this indicates an overall delay as opposed to defects associated with *bld* genes, SapB or the chaplins. The microscopic observations made here suggest that the *scy* mutant and the *scy-filP* double mutant produce less spores than the M145 wild-type. An attempt to quantify the *scy* mutant spore production in comparison to M145 was attempted, to which the result suggests that in the same time period the *scy* mutant produces less spores. It seems possible that this may be manifested by the production of less aerial hyphae by the substrate vegetative hyphae. As well as shorter aerial hyphae. It is currently not thought that *scy* mutants produce large numbers of non-viable spores. However, the irregularities in the resulting septum positioning and spore shapes would be thought to produce non-viable spores and how this is circumvented is unknown. It is possible that the *scy* mutant still maintains correct chromosome segregation and spore wall formation. Whereby the spores would be irregular in shape but the normal mechanisms of development for the segregation and compaction of DNA as well as the spore wall formation are able to compensate for shape irregularities. Possibly by more active ParA (Jakimowicz unpublished), ParA in *B. subtilis* was found to alter the initiation of DNA replication (Lee, and Grossman, 2006; Murray, and Errington, 2008) and perhaps a *scy* mutant replicated the DNA more often and so this ensures that each spore will contain at least a single viable chromosome. It would also be interesting to perform experiments to determine if the spores formed from the *scy* mutant are less resistant to extreme environmental conditions than the wild-type spores. The localisation of developmental proteins FtsZ and ParB was perturbed in a *scy* background, suggesting defects associated with cell division. Presumably ParB mislocalisation provides an insight into the chromosome segregation defects seen microscopically in a *scy* mutant. It is possible that FtsZ mislocalisation could cause aerial hyphae branching seen in a *scy* mutant, as in *E. coli* FtsZ mislocalisation facilitates branching (Potluri *et al.*, 2012). However, aerial hyphae branching could also be brought on before this by mislocalisation of DivIVA/cell wall synthesis placement. There are different experiments that could be performed to analyse the phenotype of the different mutants. Perhaps it would be interesting to change the carbon substrate to avicel, as FilP

was suggested to be an Avicel-binding protein in *S. reticuli* (Walter *et al.*, 1998). It would be interesting to see if the mutants are effected when grown on a substrate such as lignocellulose, as this is a carbon substrate that is commonly in high amounts in the natural soil environment of *S. coelicolor* (Kieser *et al.*, 2000).

It was previously reported that the *filP* mutant, had less rigid hyphae and so could be involved with cell wall integrity (Bagchi *et al.*, 2008). Based on the hyphal width irregularities, apical branching and possible greater number of branch points, the knotted aerial branches, "wriggly" hyphae (which at some level is shared with the *filP* mutant) and abnormal aerial hyphae, it is very likely that the Scy protein has a function involved with cell wall integrity. This is likely to be some form of cytoskeletal protein role associated with hyphal tip growth as this is where *Streptomyces* hyphae extend (Flärdh, 2003b). Based on the knowledge of FilP and the *scy* mutant phenotype, we thought Scy could be involved in tip formation, with a function involved with the protein DivIVA. It is interesting to know that a *scy* mutant has an effect on the placement of DivIVA or the cell wall synthesis machinery (marked by Van-Fl), consistent with the defects in apical growth. However, the mutant observations were not enough evidence alone for this and we wanted to be able to localise Scy to determine if it had a direct effect, rather than a secondary effect on transcription of a direct player or on the nucleoid (that may impart information to the tip).

FilP has previously been localised by Bagchi *et al.,* (2008). It was informative to localise Scy and place this protein in the context of *S. coelicolor* development. This project aimed to create translation fusions of *egfp* and *mCherry* to *scy*. Based on the knockout phenotype of a *scy* mutant and as well as its putative novel coiled-coil containing amino acid sequence it was of significant interest to determine its subcellular localisation. At this time it appears that Scy localises to the hyphal tips of *S. coelicolor*, as well as at future branch positions and sites of the germinating spores. As the hyphal tips are the main site of cell wall growth this could mean that Scy functions at the hyphal tip in a process related to new cell wall insertion. It is currently unclear as to the most suitable way to study Scy localisation, as we tried translational fusions but have not tried immunolocalisation. Already informative are the N-terminal fusions to Scy of the reporter proteins EGFP and mCherry. These appear to be partially functional as they are able to complement a *scy* mutant. However, they appear to also have abnormalities that are not seen in the wild-type strain. Perhaps reflected by the fact that Scy is an important protein for apical growth. Also attempted were fusions of the reporters EGFP and mCherry to the C-terminus of the Scy

protein. EGFP fused to the C-terminus of Scy was also able to complement a *scy* mutant. This strain is lacking intensive study but it could have the advantage of being more natively functional than an N-terminal fusion. However, this advantage appears to come with the disadvantage that the fluorescence signal appears to be relatively weaker. It was reassuring that it also localised to the hyphal tip of *S. coelicolor*, increasing the evidence that this is the location of Scy in the *in vivo* environment of *Streptomyces*. Also, the C-terminal mCherry fusion directly fused with no linker, also generated a tip localised signal. However, it was also seen that a C-terminal fusion of Scy to mCherry when separated with a linker was not visible. Perhaps this is indicative of a proteolytic event or that the construct is simply translated incorrectly as only a free mCherry protein due to a large number of methionine codons encoded at the junction between Scy and mCherry. This as well as being able to fully complement a translational fusion could help underline problems with using fluorescent proteins as reporters in *Streptomyces*. As Scy is possibly a filamentous protein we were unsure of the effects on polymerisation or folding of the protein in the presence of the fluorescent protein tag. It is already known that in many cases fluorescent protein tags have a degenerative effect on the normal functioning of the protein (Westphal *et al.*, 1997; Deibler *et al.*, 2011; Ballestrem *et al.*, 1998; Wu *et al.*, 2009; Flärdh, 2003a; Bagchi *et al.*, 2008; Charbon *et al.*, 2011; Hamoen *et al.*, 2006). However, this represents a limitation in molecular and cellular biology techniques. The nature of protein folding into separate domain structures provides a good chance that a given fusion protein will behave with some similarity to the native scenario. Also, due to the possibility of the different domains of Scy being responsible for localisation of the protein, it was sought to attach a fluorescent fusion to both ends separately. Hopefully attaching a tag to either end would allow optimisation of localisation in order to find the most suitable reporter system of Scy localisation. It is often seen that different domains of a protein are responsible for quite different functions, so as well as localising Scy we wanted to determine which domain of Scy may be the most important for its localisation. Therefore, we attempted to localise Scy in the case of having truncations of the protein. The experiments here suggest that the Scy C-terminal domain containing the novel coiled-coil repeat could be more important than the N-terminal domain in the localisation of Scy to the hyphal tips. This is interesting as it has previously been suggested that the localisation of DivIVA to negative membrane curvature was via its N-terminal domain (Lenarcic *et al.*, 2009). Although more recently the crystal structure for *Bacillus subtilis* DivIVA has been solved (Oliva *et al.*, 2010) and it was suggested that if DivIVA is able to

recognize membrane curvature that the C-terminal domain of DivIVA would probably also be important. It is not known if Scy recognizes membrane curvature, or even if it directly interacts with the membrane. However, due to the large size of Scy and especially the length of the C-terminal domain that this part of Scy could possibly be able to detect the curvature of the membrane in a bacterial cell. It cannot be ruled out that the N-terminal of Scy is not involved in the localisation of the protein as the configuration of EGFP to the N-terminal part of the N-terminal domain could prevent it being able to localise. Therefore, we thought it would be a good idea to attach the EGFP fusion to the C-terminal side of the N-terminal domain of Scy. However, this also did not localise, but it could be with such a small domain that a larger fusion protein affects normal folding/functioning.

Scy appears to co-localise with the apical growth controlling protein DivIVA and the cell wall machinery as highlighted by fluorescent vancomycin staining. As DivIVA was shown to localise to future branch point positions prior to formation of the branch (Hempel *et al.*, 2008), this would suggest that Scy is also localised to sites destined to be branches. We were unable to discriminate a difference in the localisation pattern of Scy and DivIVA, which it would be interesting to know if one protein was first to recruit the other or if perhaps they are both initially recruited by another factor, for example SsgA in a germinating spore (Noens *et al.*, 2007). It was interesting to test the localisation of FilP, where we found that there were some links to the hyphal tip. As the *scy* mutant was altered in phenotype with aspects that indicated it had a role in apical growth we decided to monitor DivIVA-EGFP both in a *scy* mutant and in a Scy overexpression strain. We found that DivIVA was mislocalised in a *scy* mutant sometimes forming multiple foci that were less restricted to the hyphal tip dome. It would be interesting to know if DivIVA was mislocalised due to a direct interaction with Scy or by the indirect effect of the phenotypic abnormalities of a *scy* mutant. As DivIVA is likely the apical growth factor making direct contact with the cell wall machinery it seems more likely that Scy may have a direct influence on DivIVA positioning. When Scy was overexpressed we found that it was capable of forming multiple new branches via recruitment of DivIVA/and or the cell wall synthetic machinery or other factors. This suggesting that Scy does have a direct role in the placement of new branch sites when overproduced.

Here Scy localisation was monitored when DivIVA was depleted or overexpressed. Unfortunately it is not possible to study Scy localisation in the complete absence of DivIVA, as *divIVA* is an essential gene (Flärdh, 2003a). In the event of DivIVA depletion Scy localisation did not appear to be perturbed and Scy remained at polar sites. DivIVA

can be seen to disperse from the hyphal tip in a *scy* mutant. However, it seems that Scy does not exhibit this behaviour when DivIVA is depleted. It could be that this reflects that it is not possible to truly remove the protein DivIVA from the hyphal tips in this system. It could also be suggestive that in an intimate relationship between Scy and DivIVA that Scy restricts DivIVA to the hyphal tip dome but that DivIVA does not necessarily restrict Scy to the hyphal tip dome. DivIVA targeting to the hyphal tips presumably does not depend on Scy by the fact it finds its way to this environment in a *scy* mutant (although is still disturbed). DivIVA from *Bacillus subtilis* has also been suggested to have the ability to determine localisation dependent on the geometrical cue of negative membrane curvature (Ramamurthi, and Losick, 2009; Lenarcic *et al.*, 2009). Suggesting it localises by its own right. Scy possibly also localises independently of DivIVA and hence this could be why Scy is still positioned at the hyphal tips when the expression of DivIVA is depleted. When DivIVA was overexpressed, it was found that existing hyphal tips swelled and new branch sites were generated, consistent with previous observations (Flärdh, 2003a; Hempel *et al.*, 2008). We found that the ballooning tips and the new branches recruited Scy. This suggests that DivIVA directly recruited Scy or indirectly through other factors, be it other proteins, morphological changes of cell shape and/or more active cell wall growth. This was similar to the reciprocal effects of overproducing Scy and recruiting DiviVA to new sites. However, DivIVA overproduction resulted in swelling of hyphal tips suggesting excessive active growth and possible lysis, whereas Scy overproduction did not result in the same effect. Suggesting that Scy may only have an effect in placement of sites of active growth and not necessarily the amount of active growth.

As the evidence up to that point suggested that Scy might have a biological role involved in apical growth it was also interesting to test if there is a biochemical interaction between Scy and FilP/DivIVA. Also, the nature of the proteins consisting heavily of coiled coils might also mean that they have possible binding interfaces. Using the bacterial two-hybrid technique we looked at interactions between the proteins Scy, DivIVA and FilP. We found an indication of a positive reaction between all three proteins, backing up the idea that they might form part of a TIPOC. Subsequently we were interested in which part of Scy was responsible for interaction with DivIVA. It was found that the C-terminus and not the N-terminus was more responsible for the interaction. It was also found that the C-terminus of DivIVA was responsible for its interaction with Scy. This is interesting as it was found that the protein domain of Scy containing the novel 51-mer repeat sequence appears to be important for directing Scy to the hyphal tips. DivIVA could have some similarities with

Scy suggested by the C-terminal coiled-coil of DivIVA possibly containing a small stretch of the 51-mer repeat found in the C-terminal domain of Scy (Walshaw *et al.*, 2010). However, if DivIVA has this type of repeat sequence it is hard to predict based on the repeat containing sequence being quite short, it could equally be true that it contains irregularities in heptad repeats that are not truly reflective of it being a 51-mer repeat.

Sequences of *divIVA* and *filP* have been cloned into plasmids for heterologous overproduction in *E. coli*. Along with Scy vectors already available in the Kelemen lab this means that Scy, DivIVA and FilP protein can be purified from *E. coli* and therefore be used for Biochemical studies relating to possible interactions, filament dynamics or molecular structure. The *egfp* fusions to *scy* have also been cloned in plasmids for heterologous overproduction in *E. coli* for studies where a reporter tag to Scy might be useful. We attempted to perform a number of *in vitro* based techniques to confirm interactions seen in the two-hybrid experiments. The co-affinity technique hinted that there may have been an interaction between DivIVA-C and Scy and between FilP and Scy. Though we had to perform much optimisation of this technique it did give us information and suggested that the interactions might rely quite heavily on the conditions. Pelleting assays performed with Ultracentrifugation also suggested that Scy and DivIVA interacted, as well as FilP and DivIVA, but for technical reasons we could not identify any interaction between Scy and FilP. To test if Scy interacted with the membrane we also span Scy down in pelleting assays with liposomes. Though we could not detect any pelleted Scy interacting with liposomes, we also did not detect DivIVA spinning down with the liposomes so this might suggest that there was a problem with the technique, the conditions or the protein preparations.

One of the aims of this report were to overexpress and purify Scy, in which using affinity chromatography could co-purify a number of potential *in vivo* partner proteins from *S. coelicolor*. This appears to have been achieved quite successfully, with His-Scy protein successfully expressed and purified from *S. coelicolor* carrying pCJW93-scy. The Western blot carried out with an anti-His antibody confirms His-Scy was indeed expressed and purified, by the presence of a His positive band. In these sets of experiments His-Scy was not actually purified completely, as in a large number of elutions there are other bands that are not Scy. In fact some of the Scy that we can see in the SDS-PAGE could also be endogenous Scy that has co-purified with His-Scy. Low purity was actually in accordance with the design of this experiment, as our actual intention was to attempt to purify proteins that interact with Scy *in vivo*, rather than to isolate pure His-Scy protein. It seems likely

that we have some candidate bands of proteins that co-eluted with His-Scy due to their ability to bind Scy. It also seems reasonably likely that we have some candidate proteins that we crosslinked in an *in vivo* environment with Scy. Due to time restrictions matrix-assisted laser desorption/ionisation with time of flight analysers (MALDI-TOF) mass spectrometry analysis could not be performed on these proteins. MALDI-TOF analysis would allow peptide fingerprinting and we would therefore be able to identify the proteins that we isolated in this experiment. Any proteins that are identified at a later point from this experiment or a similarly designed experiment could be potential Scy partner proteins, although not necessarily making a direct contact with Scy but perhaps being present in the same molecular complex. The possibility, however, that some of the proteins eluted in their own right due to affinity towards the column cannot be easily ruled out. It is interesting that bands were identified in the anti-DivIVA Western blot and that these bands were only present in the crosslinked samples.

The co-affinity experiment also raised a number of questions about the biochemistry of the Scy protein and its formation *in vivo*. As can be seen from analysing any cytoskeletal protein, it can generally have the potential to form multimers, as well as to form complexes with other proteins that regulate or contribute to its function. Scy could infact form multimers with other Scy proteins. This could be an explanation for what could be endogenous Scy purified with His-Scy from *S.coelicolor* through pull down, that is it could have co-purified due to its ability to bind His-Scy in the column. Scy also binds Scy in the BTH experiments suggesting multimer formation. An extremely real possibility for the biochemical associations of Scy is that two Scy molecules are joined by a single disulphide bond between two cysteine residues making a functional dimer. If Scy is anything like the coiled-coil M proteins of *Streptococcus* or eukaryotic Tropomyosin, it is interesting to note that these proteins also form dimers of α-helical coiled-coils (Phillips *et al.*, 1981; Perry, 2001). Streptococcal M proteins and Tropomyosin dimers associate along the hydrophobic backbone of the helix. In a tropomyosin dimer there is a cysteine on both helices, Cys-190, which together form a disulphide bond crosslink (Brown *et al.*, 2005). This disulphide bond does not disturb the phase of the coiled-coil. Perhaps a crosslink between Scy dimers could reinforce dimersitation.

To increase the evidence that we are looking for to determine if Scy does actually interact with other proteins, more experiments could be attempted in the future and possibly including Biophysical techniques. Experiments that could be useful are Surface Plasmon Resonance or Thermophoresis (Willander, and Al-Hilli, 2009; Jerabek-Willemsen *et al.*,

2011). These techniques can quantitatively determine the affinity of two proteins towards each other. Though they are not direct evidence of their interaction *in vivo* only *in vitro*. The bacterial two-hybrid experiments using Scy as bait could also yield potential protein:protein interactions of Scy if a library was screened, to find new binding partners. It would also be desirable to attempt to have a more *in vivo* experiment, possibly using the pull down technique whereby crosslinking of Scy is attempted before the cells are disrupted, where Scy may be more in its natural state. However, a more truely *in vivo* technique that could be attempted is Fluorescence Resonance Energy Transfer; however, this needs ideal partner pairs of fluorescence tags and also relies on the tags being in close enough proximity upon protein:protein binding to allow fluorescence transfer.

The results collected here as well as the conclusions drawn in (Holmes *et al.*, 2013), have led us to propose that polarised growth in *S. coelicolor* occurs via a complex assembly of proteins named the Tip Organising Centre (TIPOC). The TIPOC contains the two proteins Scy and DivIVA (Figure 120). As shown here Scy co-localises with DivIVA at these centres of activity, seemingly controlling apical growth. Scy co-localisation with DivIVA at the hyphal tips is interesting as not only are both of these proteins possibly intimately coupled with directing the cell wall machinery, but they are both coiled-coil proteins. It remains to be seen if the similar pattern of localisation of Scy and DivIVA reflect their similarities as proteins. The precise roles of these proteins are still open to investigation. However, they appear to form some form of dynamic complex that is capable of directing the synthesis of new cell wall material. The model shown in Figure 120 places DivIVA at the inner side of the membrane based on the observations of localisation of DivIVA in *B. subtilis* (Lenarcic *et al.*, 2009; Ramamurthi, and Losick, 2009). Possibly Scy forms a structure behind DivIVA; however, equally likely is that they occupy a similar position in the extreme of the hyphal tip. However, as in a *scy* mutant DivIVA disperses from the hyphal tip dome, it has been suggested that Scy restricts DivIVA to the end of the tip dome. As Scy is a long protein with a predicted length of 190nm, which coincidently is compatible with the radius of the hyphal tip, then it could be that Scy forms a structure such as that seen in Figure 120 forming ‘spokes’. As the C-terminus of Scy appears to be more important for localisation, then perhaps it contacts the membrane. Possibly with the N-terminal domain facilitating higher order structure formation with other Scy molecules.

Figure 120: A Potential Model of the TIPOC in a growing hyphal tip of *Streptomyces coelicolor*. Shown as Green dots are the accumulating cell wall precursors. Shown in red is DivIVA which is believed to make contact with the inner side of the membrane possibly localised via negative membrane curvature. Shown in Blue is Scy which has a predicted length of 190nm and could form a structure that helps to stabilise DivIVA and the hyphal tip dome. Figure from (Kelemen unpublished).

It is also sensible to consider some of the other proteins that may form part of the TIPOC (Figure 121). In this complex governining apical growth is also FilP; however, its role is also currently unknown, though a *filP* mutant was shown to have reduced hyphal rigidity suggesting it may influence the positioning of the cell wall. DivIVA was shown previously to interact with CslA, a cellulose synthase like protein that was found to be responsible for production of cellulose like beta-glucan-containing polysaccharides at the hyphal tip (Xu *et al.*, 2008), suggesting that its possible DivIVA directed functioning may contribute to apical growth. Among TIPOC it is likely that there exists PBPs, as presumably these would be needed to synthesize extension of the cell wall at the hyphal tip. This is backed up by staining with Van-Fl marking the hyphal tips of *S. coelicolor* (Daniel, and Errington, 2003). Presumably DivIVA makes contact with a PBP as in *M. Tuberculosis* the DivIVA homologue interacts with a PBP (Mukherjee *et al.*, 2009). However, we cannot rule out that perhaps Scy might make direct contact with a PBP or might affect a factor, be it DivIVA or another protein, that might make contact with a PBP. This is also backed up by the result that Scy co-localises with Van-Fl staining. Conjugation machinery may also be part of TIPOC as it has been shown that the protein TraB is localised to the hyphal tip (Reuther *et al.*, 2006). TIPOC may also include links to the machinery associated with chromosome segregation/separation and cell division. This would include the protein ParA

which we have shown in BTH here interacts with Scy and is the feature of current study (Jakimowicz unpublished). ParB has also been shown to interact with DivIVA (Donovan *et al.*, 2012). Presumably their already established localisations at times associated with the hyphal tip would also backup inclusion of both ParA and ParB into TIPOC (Jakimowicz *et al.*, 2005a; Jakimowicz *et al.*, 2007). Presumably TIPOC has some function in conveying signals onto the ParAB machinery to coordinate cessation of growth with subsequent DNA segregation associated with sporulation in the aerial hyphae. Presumably this is why we see that ParB-EGFP foci are no longer regularly arrayed in the aerial hyphae of a *scy* mutant and the DNA appears to be unevenly segregated into future spore compartments. In the aerial hyphae of a *scy* mutant we also monitored that FtsZ was mislocalised, correlating the effect seen of having irregular placement of the sporulation septa in the *scy* mutant. The protein SsgA which along with SsgB is directly involved in placing the FtsZ ring (Willemse *et al.*, 2011a), is at times localised to the hyphal tip (Noens *et al.*, 2007), perhaps suggesting that it is part of TIPOC and can then affect SsgB and downstream from SsgB, FtsZ. However, as far as we know at the moment, no interaction partners have been found for SsgA/SsgB/FtsZ amongst the other members of TIPOC. It has recently been shown that DivIVA is phosphorylated by AfsK, AfsK has also been shown to localise to the hyphal tips (Hempel *et al.*, 2012) and is also a member of TIPOC. Phosphorylation of DivIVA may result in redistribution of DivIVA out of the TIPOC.

A possible mechanism of the interplay between Scy and DivIVA is shown in Figure 122. It was suggested that negative curvature was a cue for DivIVA localisation (Lenarcic *et al.*, 2009; Ramamurthi, and Losick, 2009), whether this is geometrical sensing or recognition of specific lipic moieties at this location (Huang *et al.*, 2006) e.g. cardiolipin (Jyothikumar *et al.*, 2012). It was reported that branch points mediated by formation of DivIVA were normally generated at the convex side of hyphal curvatures (Hempel *et al.*, 2008), which incidentally generate negative membrane curvature possibly recruiting DivIVA. However, *S. coelicolor* with its long filamentous cells that typically curve and undulate has many sites that exhibit negative curvature but don't lead to the formation of branches. Therefore, a mechanism of controlling DivIVA mediated branch formation must exist. Due to the affects of a *scy* mutant on hyphal branching and Scy overexpression on hyphal branching, a possible model can be proposed whereby Scy regulates DivIVA formation by sequestering DivIVA assemblies and preventing DivIVA formation at too many locations.

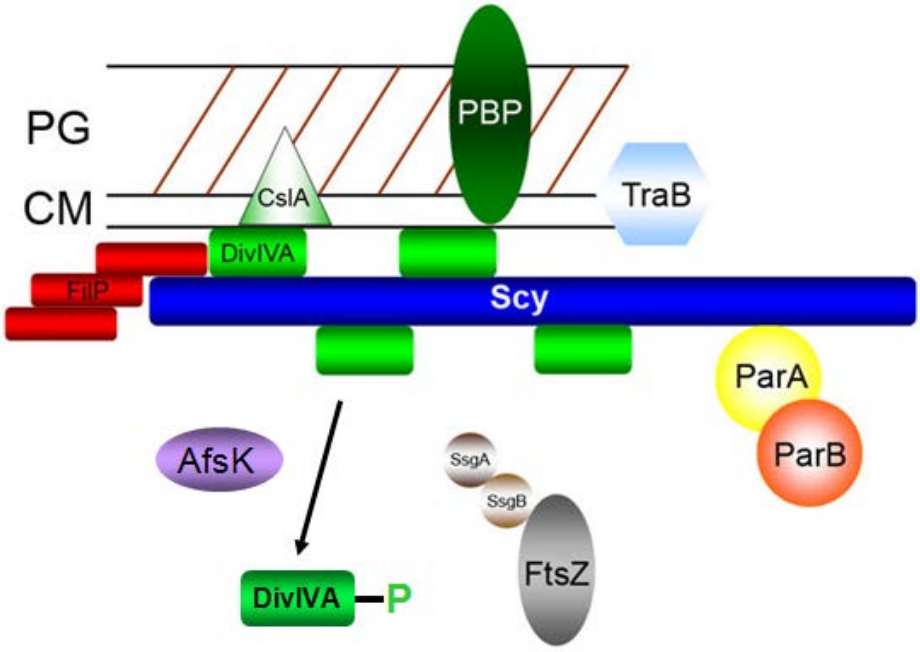

Figure 121: The *Streptomyces* Tip Organising Centre for the selection, establishment and maintenance of polarised hyphal extension. The machinery of the Tip organising centre presumably makes connections both to the Peptodoglycan (PG) cell wall and the Cell Membrane (CM). Figure from (Holmes *et al.*, 2013).

Thus, a possible scenario is that there are many sites of high DivIVA affinity via geometrical or compositional cues, but normally not all of these sites would lead to active cell wall growth as DivIVA might be sequestered to a select number of sites. However, as was seen in the *scy* mutant where there is no Scy, there leads to greater numbers of DivIVA foci and active cell wall synthesis, this would be a scenario where DivIVA is not sequestered to any sites. At high DivIVA levels, when Scy is at wild-type levels and therefore limited to the amount of DivIVA, the excessive branching is caused by occupancy of DivIVA at all possible locations. It is then possible that the high abundance of DivIVA at all sites then results in excessive recruitment of cell wall synthesis machinery, resulting in the ballooning tips seen when DivIVA is overexpressed. Alternatively when Scy is overexpressed and DivIVA is at wild-type levels the result is that DivIVA is shared between excessive amounts of Scy, therefore resulting in branching at more sites. However, assuming that DivIVA is responsible for the active recruitment of the cell wall synthesis machinery this would suggest that the lack of excessive DivIVA means that these branches do not balloon like those seen for DivIVA overexpression. However, instead they cause branches off from newly formed branches referred to as “hook on hook”, where DiviVA is shared unevenly between splitting assemblies and therefore abortive branches can form where the recruitment of the cell wall synthesis

machinery becomes limiting (Holmes *et al.*, 2013). In the case of a wild-type scenario of normal levels of DivIVA and Scy, Scy assemblies would not be present at all possible sites which could attract DivIVA, DivIVA would be sequestered by Scy, meaning not all of the possible sites would lead to positioning of active cell wall growth. Instead a refined system would exist where branch sites are less frequent as occurs in the wild-type scenario.

Another important factor for controlling the localisation of DivIVA is AfsK (Hempel *et al.*, 2012). As suggested by Hempel *et al.*, (2012), AfsK phosphorylates DivIVA and controls the *in vivo* dynamics of DivIVA. This would be by a mechanism in which DivIVA phosphorylation would promote disassembly of DivIVA foci at an already established hyphal tip. We believe that this could be important for regulation of DivIVA and TIPOC and may well impart a mechanism for feedback to the TIPOC when cell wall synthesis stalls at the hyphal tips, for example under conditions of nutritional starvation or when the tip hits an impassable object. As far as we know there is no reason why our proposed models of DivIVA and TIPOC control should be in objection with those of Hempel *et al.*, (2012), perhaps Scy control of DivIVA is more linked to fine control of branch positioning, whereas AfsK phosphorylation of DivIVA is more associated with feedback to the cell wall synthesis machinery. Branching undoubtly is a complex biological process and it would seem necessary to have multiple methods of regulation, hence by Scy, phosphorylation of DivIVA or any currently unknown mechanism. However, it should be pointed out that the theory that DivIVA in a wild-type cell operates by tip focused splitting as deduced by the same authors (Richards *et al.*, 2012) is controversial. The only piece of evidence for this theory are time-lapse images of DivIVA-EGFP where DivIVA-EGFP foci were seen to split from the growing tip and led to formation of new branches. The evidence is also based on a DivIVA-EGFP fusion which is not regarded as strictly functional as is the native protein, and is viewed in the hyphae in addition with the native DivIVA possibly causing problems with dosage of DivIVA (Flärdh, 2003a). The authors of (Richards *et al.*, 2012) though admitting that spontaneous formation of new branches could occur in synteny with tip focused splitting, are generally dismissive of spontaneous branch formation being a major form of mechanism for branching. However, it has long been known that new branch formation can occur at great distances behind the actively growing hyphal tip, presumably too far away for DivIVA shedding to be considered seriously in these cases. According to data collected by Richard Leggett in the Kelemen lab it has also been seen that branching occurs most often further behind the existing hyphal tip, where it would be more feasible for *de novo* formation of a TIPOC, rather than DivIVA from split

foci waiting in a latent form for a considerable amount of time without stimulating new branch formation. Spontaneous nucleation by DivIVA recruitment to sites of possible correct geometrical curvature or other cues would be more feasible based on the idea of DivIVA being a landmark protein that can localise presumably without the presence of an existing DivIVA foci. Spontaneous nucleation must occur for germination of spores to begin, as it is considered at this time that there is no DivIVA foci already present, other proteins such as SsgA may become important at this point (Noens *et al.*, 2007).

Due to the complex developmental cycle and filamentous mycelial growth of the streptomycetes, there is much ongoing research into the role of cytoskeletal proteins in *Streptomyces coelicolor*. A number of the proteins already studied appear to show novel differences to their equivalent counterparts in other prokaryotic models. This makes *S. coelcolor* a particularly interesting organism to work on, as well as it being the model organism for studies of polarised filamentous growth in bacteria. To which there is an expanding understanding and interest as more factors of a TIPOC are isolated. It is interesting to note how factors in the TIPOC such as Scy, DivIVA and FilP are made up of coiled-coils. This system does show some similarities with polarised growth observed in fungi where coiled-coil proteins have been shown in some cases to be important in directing polarised growth (Zizlsperger *et al.*, 2008; Zizlsperger, and Keating, 2010; Valtz, and Herskowitz, 1996). As well as coiled-coil proteins involved in other bacterial polarisation systems such as RsmP that together with DivIVA control polarised growth in *C. glutamicum* (Fiuza *et al.*, 2010). Cyanobacteria use a coiled-coil protein SepJ that marks polar sites required for acquisition of multicellular filaments (Mariscal *et al.*, 2011). *C. crescentus* also uses coiled-coil proteins for polar functions with the birth scar protein TipN (Lam *et al.*, 2006) and proteins involved in directing the formation of polar organelles (Obuchowski, and Jacobs-Wagner, 2008; Lawler *et al.*, 2006). Together these observations suggest that mechanisms of coiled-coil based polarisation systems have been highly advantageous for cell shape determination and cell processes widespread in microbial life.

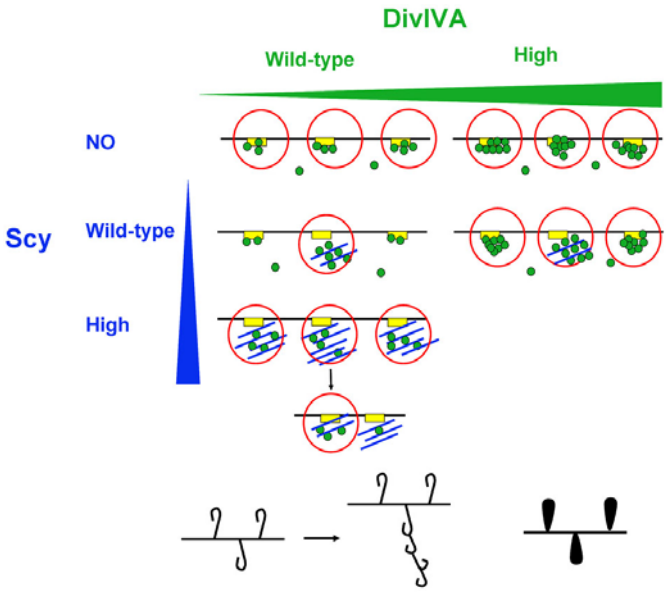

Figure 122: Scy is a molecular assembler of new polarity centres.

Scy (blue rods) and DivIVA (green circles) are key components of the emerging polarity centres at sites that are marked by geometrical or compositional cues (yellow boxes) of the hyphal wall (black lines). Due to the lack of selectivity of DivIVA to the marked sites, DivIVA initiates new tip formation (red circles) indiscriminately when DivIVA levels reach a certain threshold. Scy, the molecular scaffold protein controls the number of polarity centres by its propensity for self-assembly and by sequestering DivIVA. The "hook on hook" growth pattern of Scy overproduction (bottom left and centre), where there is not enough DivIVA/cell wall synthesis machinery to support active growth at all branches so some branches abort. The ballooning tips of DivIVA overproduction (bottom right) are also shown where cell wall synthesis machinery is recruited excessively, causing branches to bulge. Figure from (Kelemen unpublished).

10 Materials and methods

10.1.1 Bacterial strains and plasmids

The strains of *E. coli* used in this study are listed in Table 12. The stains of *Streptomyces* used in this study are listed in Table 13. The plasmids and cosmids used in this study are listed in Table 15.

Table 12: *E. coli* strains used in this study.

Strain	Genotype	Reference or source
DH5α	F$^-$λ$^-$, *endA1, glnV44, thi-1, recA1, relA1, gyrA96, deoR, nupG, Φ80dlacZ*Δ*M15,* Δ(*lacZYA-argF*)*U169, hsdR17*(r_K^- m_K^+)	(Hanahan, 1983)
BW25113	λ$^-$, Δ(*araD-araB*)*567,* Δ*lacZ4787*(*::rrnB-4*), *lacIp-4000*($lacI^Q$), *rpoS369*(*Am*), *rph-1,* Δ(*rhaD-rhaB*)*568, hsdR514*	(Datsenko, and Wanner, 2000)
BL21 (DE3) pLysS	F$^-$, *dcm, ompT, lon, hsdS*$_B$(r_B^- m_B^-), *gal,* λ (DE3), pLysS(cm^R)	(Studier, and Moffatt, 1986)
ET12567	*dam dcm hsdS*	(MacNeil *et al.*, 1992)
BTH101	F$^-$, *cya-99, araD139, galE15, galK16, rpsL1* (*Str* ^{r}), *hsdR2, mcrA1, mcrB1*	(Karimova *et al.*, 2000)

Table 13: *Streptomyces* strains used in this study.

Strain	Genotype	Reference or source
M145	SCP1$^-$ SCP2$^-$ Pgl+	(Hopwood *et al.*, 1985)
scy::aac(3)IV	M145 *scy::aac(3)IV*	This work
filP::aac(3)IV	M145 *filP::aac(3)IV*	This work
scy-filP::aac(3)IV	M145 *scy-filP::aac(3)IV*	This work

scy	M145 *scy*::*scar*	Kelemen Lab, University of East Anglia
filP	M145 *filP::scar*	Kelemen Lab, University of East Anglia
scy-filP	M145 *scy-filP::scar*	Kelemen Lab, University of East Anglia
K110	Δ*scy(*Δ28-381aa)::*apr* derivative of M145	Kelemen Lab, University of East Anglia
K114	M145 $attB_{pSAM2}$*::*pKF58 [*tipAp-divIVASC*]	(Flärdh, 2003b)
K115	M145 *ΔdivIVA::*Ω*aacC4* $attB_{pSAM2}$*::*pKF58[*tipAp-divIVASC*]	(Flärdh, 2003b)
J3310	M145 *parB-egfp*	(Jakimowicz *et al.*, 2005a)
J3310/*scy::aac(3)IV*	J3310 *scy::aac(3)IV*	This work

Table 14: Oligonucleotide sequences

Primer	5'-3' Sequence
scy Fwd	GAAGATTTGCGACCAGGGGACGGATGGGACCGCGCAGTGATTCCGGGGATCCGTCGACC
scy Rev	AAAGATCTCCAGCAGACACCCAAACCGCCCCGAACGCTATGTAGGCTGGAGCTGCTTC
filP Fwd	CTATCACCTCACCCGGTCTCTTTCGACAGGAACCCCATGATTCCGGGGATCCGTCGACC
filP Rev	CCCCCGCGCAGCCGAAACCGCCCGGGCGCAAGGGCGTCATGTAGGCTGGAGCTGCTTC
ScyUP	AGGGGCCGGTAGGGTTGGGTGC
ScyDOWN	CTTGGAGATGCGTTCGTCCACC
FilPUP	GAGGCGCTGGAGTCGTTCGAGG
FilPDOWN	GAGGAAGCCCGTGATGATGCCG
Apra5'reverse	GGCGGGATGCGAAGAATGCG
Apra3'forward	CGCACCTGGCGGTGCTCAACG
Linker1	CTAGACTGATGTACAACGGCGGCGGCGGCGG
Linker2	TACCGCCGCCGCCGCCGTTGTACATCAGT
scyprom3-Nde	ACCGCCATATGCGCGGTCCCATCCGTCCC
scyprom4-Bam	CTGGAGGATCCCGTACGCGTTCTGTACGACGAGC

scyKpn2	CGCGTTGCGCAGCAACTGCTCG
EGFPLinker1	GATCCTCTAGACATATGGGCGGCGGCGGCGG
EGFPLinker2	TACCGCCGCCGCCGCCCATATGTCTAGAG
scy-Nde	GATACCATATGGCCGTCTGACGACTTGCCACCC
scy-Bam	GATACGGATCCGCCGAGCAGCTGGTCTCGGACG
Bsrg-Kpn Linker 1	GTACAACCTCGAGGGCGGCGGCGGCGGCGGGTAC
Bsrg-Kpn Linker 2	CCGCCGCCGCCGCCGCCCTCGAGGTT
Kpn-Eco Linker 1	CAGTAGTAGGATATCAAGCTTG
Kpn-Eco Linker 2	AATTCAAGCTTGATATCCTACTACTGGTAC
THAbpS_F	GGATCATCTAGAGCATATGAGCGACACTTCCCCCTACG
THAbpS_R	GGATCAGAATTCTCAGCGGGACTGCTGGGCCG
AbpS_Nde_Cterm	GGATCACATATGGCGGGACTGCTGGGCCGGGACC
scyNde1	ACCGCCATATGCGGGGCTACGAGAGCCAGGAGC
ScyN_FPrev	CATGCGCATATGCTGGTACCCGATGTCGCCGC
THDiv_F	GGATCATCTAGAGCATATGCCGTTGACCCCCGAGGACG
THDiv_R	GGATCAGAATTCTCAGTTGTCGTCCTCGTCGATCAGGAACC
DivN_STOPEco	CATGCGAATTCTAGCCGCCGGGGCCGCCCTGACC
DivN_RevNdeEco	CATGCGAATTCTGCATATGGCCGCCGGGGCCGCCCTGACC
DivCC51_ForwXbaNde	GGATCAGTCTAGAGCATATGGGCGACAGTGCCGCCCGCGTGC
DivCC51_STOPEco	CATGCGGAATTCTAGCGCAGGTCCTCGACCTTGCG
DivcoilF/PET	GGATCACATATGGGCCCCGGCGGCGACAGTGC
div_nde	GATACCATATGGTTGTCGTCCTCGTCGATCAGG
THDiv_coilR	GGATCAGAATTCGAGTTGTCGTCCTCGTCGATCAGG
EGFPseq	GGGTCTTGTAGTTGCCGTCG
mCherryseq	CGTACATGAACTGAGGGGAC
mCherryseq2	GAGCCGTACATGAACTGAGG
pET28a(+)-1	ATCCGGATATAGTTCCTCCTTTCAG
pET28a(+)-2	CCGATCTTCCCCATCGGTGATGTCG
pUC18 Direct	CGCCAGGGTTTTCCCAGTCACGACG
pUC18 Reverse	TTTACACATTTATGCTTCCGGCTCG
TH Scy F4	CGCGAGGAGGCCGAGCGCAC
TH Scy R4	CCGTCTGACGACTTGCCAC
THScy_T18	CGGATGTACTGGAAACGGTG
FP-BsrGI	TTACTTGTACAGCTCGTCCATGCCGAGAG
FP-Nde	CGTAACATATGGTGAGCAAGGGCGAGGAGC

Tfd	GATTTTCAACGTGAAAAAATTATTA

Table 15: Plasmid/Cosmid DNA used in this study.

Plasmid	Genotype	Reference or source
pIJ773	*aac(3)IV oriT bla*	(Gust *et al*., 2002)
pIJ790	*araC-*P_{araB}*, γ, β, exo, cat, repA101ts, oriR101*	(Gust *et al*., 2002)
pUZ8002	RK2 derivative with a mutation in *oriT*	(Kieser *et al*., 2000)
St8F4	Supercos-1 Cosmid with a 33.9Kbp chromosomal fragment with *scy* and *filP*.	Redenbach *et al.*, 1996
St8F4/*scy::aac(3)IV*	Cosmid St8F4 with *scy::aac(3)IV* allele	This Work
St8F4/*filP::aac(3)IV*	Cosmid St8F4 with *filP::aac(3)IV* allele	This Work
St8F4/*scy-filP::aac(3)IV*	Cosmid St8F4 with *scy-filP::aac(3)IV* allele	This Work
St8F4/*scy::scar*	Cosmid St8F4 with *scy::scar* allele	Kelemen Lab, University of East Anglia
St8F4/*filP::scar*	Cosmid St8F4 with *filP::scar* allele	Kelemen Lab, University of East Anglia
St8F4/*scy-filP::scar*	Cosmid St8F4 with *scy-filP::scar* allele	Kelemen Lab, University of East Anglia
pIJ8660	*ori* pUC18, *aac(3)IV*, *oriT* RK2, *int ΦC31*, *attP*, Promoterless *egfp*	(Sun *et al.*, 1999)
pIJ8660-Pscy-scy	Plasmid pIJ8660 with *Pscy-scy*	Kelemen Lab, University of East Anglia
pIJ8660-Pscy	Plasmid pIJ8660 with *Pscy*	This Work
pCJW93-egfp-scy	Plasmid pCJW93 with *egfp-scy*	Kelemen Lab, University of East Anglia
pIJ8660-Pscy-egfp-scy (pK56)	Plasmid pIJ8660 with *Pscy-egfp-scy*	This Work

pIJ6902-mCherry-scy	Plasmid pIJ6902 with *mCherry-scy*	Kelemen Lab, University of East Anglia
pIJ8660-Pscy-mCherry-scy (pK57)	Plasmid pIJ8660 with *Pscy-mCherry-scy*	This Work
pIJ8668	*ori* pUC18, *aac(3)IV*, *oriT* RK2, Promoterless *egfp*	(Sun *et al.*, 1999)
pAZ1	A pIJ8668 derivative containing the EGFP linker formed by EGFPLinker1 and EGFPLinker2	Kelemen Lab, University of East Anglia
pUC18	*ori* pBR322, *rep* (pMB1), *lacZ*, *bla*	Genscript
pUC18-scyCterm	Plasmid pUC18 with the PCR product of the last 1000bp of *scy*	This Work
pAZ1-scyCterm-egfp	Plasmid pIJ8668 with the PCR product of the last 1000bp of *scy* fused to *egfp*	This Work
pIJ8660-scyCterm-egfp	Plasmid pIJ8660 with the PCR product of the last 1000bp of *scy* fused to *egfp*	This Work
pIJ8660-Pscy-scy-egfp	Plasmid pIJ8660 with *Pscy-scy-egfp*	This Work
pIJ8660-PnepA-nepA-mCherry	Plasmid pIJ8660 with *PnepA-nepA-mCherry*	Kelemen Lab, University of East Anglia
pIJ8660-scyCterm-mCherry	Plasmid pIJ8660 with the PCR product of the last 1000bp of *scy* fused to *mCherry*	This Work
pIJ8660-Pscy-scy-mCherry	Plasmid pIJ8660 with *Pscy-scy-mCherry*	This Work
pIJ8660-scyCterm-Δlink-mCherry	Plasmid pIJ8660 with *scyCterm-mCherry* and	This Work

	with no glycine linker.	
pIJ8660-Pscy-scy-Δlink-mCherry	Plasmid pIJ8660 with *Pscy-scy-mCherry* and with no glycine linker.	This Work
pKF59	pEGFP-1 derivative with *divIVA* promoter and gene cloned upstream of *egfp*.	(Flärdh, 2003a)
pMS82	*ori* pUC18, *hyg*, *oriT* RK2, *int ΦBT1*, *attP*	(Gregory *et al.*, 2003)
pMS82-Pscy-mCherry-scy (pK66)	Plasmid pMS82 with *Pscy-mCherry-scy*	This Work
pIJ8660-Pscy-egfp-scy-C	Derivative of pIJ8660-Pscy-egfp-scy with the N-terminal domain removed	This Work
pIJ8660-Pscy-egfp-scy-N	Derivative of pIJ8660-*Pscy-egfp-scy* with the C-terminal domain removed.	This Work
pIJ8660-Pscy-scy-N-egfp	Derivative of pIJ8660-Pscy-scy-egfp with the C-terminal domain removed.	This Work
pGEM-T Easy	*ori* pBR322, *f1 ori*, *lacZ*, *bla*	Promega
pGEM-T Easy-filP	pGEM-T Easy with *filP*	This Work
pAZ1-filP-egfp	Plasmid pIJ8668 with *filP-egfp*	This Work
pUC8.9-scy	Plasmid pUC18 with the 8.9Kbp *Eco*RI fragment with *scy* and *filP* from St8F4	Kelemen Lab, University of East Anglia
pUC18-PfilP	Plasmid pUC18 with the 2.1Kbp *Bam*HI fragment with *scyCterm* and *filPNterm* from St8F4	This work
pAZ1-PfilP-filP-egfp	Plasmid pIJ8668 with *PfilP-filP-egfp*	This Work
pIJ8660-PfilP-filP-egfp	Plasmid pIJ8660 with	This Work

	PfilP-filP-egfp	
pIJ8660-PfilP-filP-mCherry	Plasmid pIJ8660 with *PfilP-filP-mCherry*	This Work
pIJ8660-PfilP-filP-Δlink-mCherry	Plasmid pIJ8660 with *PfilP-filP-mCherry* with no linker.	This Work
pUT18C	pUC19 derivative with T18 domain upstream of MCS.	(Karimova *et al.*, 2000)
pKT25	pSU40 derivative with T25 domain upstream of MCS.	(Karimova *et al.*, 2000)
pUT18C-zip	pUT18C with leucine zipper	(Karimova *et al.*, 2000)
pKT25-zip	pKT25 with leucine zipper	(Karimova *et al.*, 2000)
pUT18C-scy	pUT18C with *scy*	(Walshaw *et al.*, 2010)
pUT18C-scy-N	pUT18C with *scy-N*	(Walshaw *et al.*, 2010)
pUT18C-scy-C	pUT18C with *scy-C*	(Walshaw *et al.*, 2010)
pKT25-scy	pKT25 with *scy*	(Walshaw *et al.*, 2010)
pKT25-scy-N	pKT25 with *scy-N*	(Walshaw *et al.*, 2010)
pKT25-scy-C	pKT25 with *scy-C*	(Walshaw *et al.*, 2010)
pUT18C-filP	pUT18C with *filP*	Kelemen Lab, University of East Anglia
pKT25-filP	pKT25 with *filP*	Kelemen Lab, University of East Anglia
pUT18C-divIVA	pUT18C with *divIVA*	This Work
pKT25-divIVA	pKT25 with *divIVA*	This Work
pUT18C-divIVA-N	pUT18C with *divIVA-N*	This Work
pKT25-divIVA-N	pKT25 with *divIVA-N*	This Work
pUT18C-divIVA-C	pUT18C with *divIVA-C*	Kelemen Lab, University of East Anglia
pKT25-divIVA-C	pKT25 with *divIVA-N*	This Work
pKT25-parA	pKT25 with *parA*	(Jakimowicz *et al.*, 2007)
pET21a	*ori* pBR322, T7 Promoter, *lacI*, *bla*, *ori* f1	Novagen

pET28a	*ori* pBR322, T7 Promoter, His•Tag coding sequence, *lacI*, *kan*, *ori* f1	Novagen
pET21a-divIVA	Plasmid pET21a with *divIVA*	This Work
pET28a-divIVA	pET28a with *divIVA* generating His-divIVA fusion	This Work
pET21a-filP	Plasmid pET21a with *filP*	This Work
pET28a-filP	pET28a with *filP* generating His-FilP fusion	This Work
pGEM-T Easy-divIVA-C	pGEM-T Easy with *divIVA-C*	This Work
pET21a-divIVA-C	Plasmid pET21a with *divIVA-C*	This Work
pET28a-divIVA-C	pET28a with *divIVA-C* generating His-DivIVA-C fusion	This Work
pET21a-egfp-scy	Plasmid pET21a with *egfp-scy*	This Work
pET28a-egfp-scy	Plasmid pET28a with *egfp-scy* generating His-EGFP-Scy fusion	This Work

10.1.2 Solid media

The agar used is Formedium(TM) agar made by Formedium Ltd.

SFM or alternatively referred to as MS medium (Hobbs *et al.*, 1989)-
This medium was used to grow *Streptomyces* strains and for phenotypic analysis of *Streptomyces* strains.

Mannitol	30g
Soya Flour	30g
Tap Water	1500ml
Agar	30g

6g of soya flour and 6g of agar was deposited in five 500ml Duran Bottles. Mannitol was dissolved in tap water, then 300ml was poured into each bottle. The media was then autoclaved twice.

Lennox Broth (LB) Agar (Kieser *et al.*, 2000)-

This medium was used for growing *E. coli* and for Spore titrations of *Streptomyces* strains.

Agar	16g
Tryptone	16g
Yeast Extract	8g
NaCl	8g
Glucose	1.6g
dH_2O	up to 1600ml

4g of agar was deposited in four 500ml Duran Bottles. The other ingredients were dissolved in dH_20, then 400ml was poured into each bottle and the media was autoclaved.

Minimal Medium Mannitol (MMM) (Kieser *et al.*, 2000)-

This Medium was used for phenotypic analysis of *Streptomyces* strains.

Agar	16g
L-asparagine	0.8g
K_2HPO_4	0.8g
$MgSO_4.7H_20$	0.32g
$FeSO_4.7H_2O$	0.016g
Mannitol	8.0g
dH_2O	up to 1600ml

4g of agar was deposited in four 500ml Duran Bottles. The other ingredients were dissolved in dH_20, adjusted to pH 7.0-7.2 with orthophosphoric acid then 400ml was poured into each bottle and the media was autoclaved.

Complete Medium (CM), modified from Kieser *et al.*, (2000)-

This Medium was used for phenotypic analysis of *Streptomyces* strains.

Agar	5g
K_2HPO_4	2.5g
NaCl	0.25g
$MgSO_4.7H_20$	0.25g

Peptone	1.0g
Yeast Extract	0.5g
Casamino Acids	0.75g
Glucose	12.5g
dH_2O	up to 1600ml

2.5g of agar was deposited in two 500ml Duran Bottles. The other ingredients were dissolved in dH_20, adjusted to pH 7.0-7.2 with orthophosphoric acid then 250ml was poured into each bottle and the media was autoclaved.

Minimal Medium Glucose (MMG), change from Mannitol in MMM to Glucose–
This Medium was used for phenotypic analysis of *Streptomyces* strains.

Agar	24g
L-asparagine	0.6g
K_2HPO_4	0.6g
$MgSO_4.7H_20$	0.24g
$FeSO_4.7H_2O$	0.012g
Mannitol	12g
dH_2O	up to 1200ml

3g of agar was deposited in four 500ml Duran Bottles. The other ingredients were dissolved in dH_20, adjusted to pH 7.0-7.2 with orthophosphoric acid then 300ml was poured into each bottle and the media was autoclaved.

10.1.3 Liquid Media

Lennox Broth (LB) (Kieser *et al.*, 2000)-
Used for growing *E. coli*.

Tryptone	10g
Yeast Extract	5g
NaCl	5g
Glucose	1g
dH_20	up to 1000ml

The mixture was dispensed in either 10ml or 50ml volumes and then autoclaved.

SOB (Gust *et al.*, 2002)-

Used to grow *E. coli* BW25113/ pIJ790, with the addition of L-arabinose allows efficient PCR targeting of *S. coelicolor* cosmids.

Tryptone	10g
Yeast Extract	2.5g
NaCl (5M)	1ml
KCl	0.093g
$MgCl_2$ (1M)	5ml
$MgSO_4$	1.23g
dH_2O	up to 500ml

The mixture was dispensed in 10ml volumes and then autoclaved.

2X YT (Kieser *et al.*, 2000)-

Used for inducing germination of *Streptomyces* spores prior to conjugation.

Bactotryptone	16g
Yeast Extract	10g
NaCl	5g
dH_2O	up to 1000ml

The mixture was dispensed in 10ml volumes and then autoclaved.

Tryptone Soya Broth (TSB) and Polyethylene Glycol (PEG) (Kieser *et al.*, 2000)-

Used for overexpression of His-Scy in *S. coelicolor*, PEG is used as a dispersing agent.

TSB	7.5g
PEG	12.5g
dH_20	up to 250ml

The mixture was dispensed in 50ml volumes and then autoclaved.

10.1.4 Antibiotic concentrations

Table 16: Antibiotic concentrations used in this study.

Antibiotic	Stock (mg/ml)	*Streptomyces* (final concentration μg/ml) SFM	*E. coli* (final concentration μg/ml) LB
Ampicillin	100	-	100

Apramycin	100	50	50
Chloramphenicol	25	-	25
Hygromycin	50	50	50
Kanamycin	100	50	50
Spectionomycin	100	50	100
Thiostrepton	50	0.1-20	-
Nalidixic Acid	25	25	-
Bacitracin	50	50	-

10.1.5 Solutions and buffers

10x DNA loading dye (100 ml)- 50 ml 100% Glycerol; 10 ml 0.5 M EDTA pH8.0; 5 ml 1 M Tris pH7.4; 35 ml dH_20; Autoclave; 0.005 g Xylene Cyanol; 0.05 g Bromophenol Blue.

4x Protein loading dye (10 ml)- 2 ml 1 M Tris pH6.8, 4 ml 100% Glycerol, 2 ml β Mercaptoethanol, 0.8 g SDS, 40mg Bromophenol Blue, 1.5 ml dH_2O.

10x SDS-PAGE running buffer (1 L)- 144 g Glycine, 30 g Tris, 10g SDS, 1 L dH_2O.

50x TAE pH7.5 (2 L)- 484.4g Tris, 164.08g Sodium Acetate, 74.4g EDTA, up to 1L dH_2O.

Tris-magnesium buffer- 20mM Tris pH 8, 10mM $MgCl_2$

Phosphate buffer- 50mM Na_2HPO_4, 50mM NaCl pH 8.0

Tris-NaCl buffer- 20mM Tris, 200mM NaCl, pH 8.0

10.1.6 Agarose gel electrophoresis of DNA

DNA was subjected to electrophoresis on agarose gels after addition of 1/10 volume of 10x loading dye. Agarose gels were prepared (with the addion of 0.5 μg/ml ethidium bromide to stain the gel) and run submerged with 1xTAE buffer. Routinely, 0.7% gels were used,

although >0.7-1% gels were used for analysis of smaller fragments. Gels were photographed with UV light illumination using a BioRad transilluminator.

10.1.7 PCR for generation of cloning sequences

All PCR reactions were performed using a BioRAD DNA Engine® Peltier Thermal Cycler. PCR reactions for cloning fragments were a 50µl total volume or for colony PCR were prepared in master mix and aliquoted to 10µl volumes. The PCR mixes generally consisted of; Promega Go Taq Polymerase Buffer (1x), dNTPs (0.25mM), $MgCl_2$ (2.5mM), dimethyl sulphoxide (5%), upstream primer (1pmol), downstream primer (1pmol), template DNA or cells from a colony and Promega Go Taq Polymerase (1.25u).

For cloning purposes or colony PCR screening, the following PCR cycle conditions were used, with variable annealing temperatures, extension times and cycles:

1. Denaturation 96ºC, 5 minutes.
2. Deanturation 92ºC, 1 minutes.
3. Primer Annealing xºC, 30 seconds. } repeat cycles
4. Extension 72ºC, x seconds.
5. Final Extension, 72ºC, 5 minutes.
6. Cool down 20˚C, 5 minutes.

Generally for colony PCR screening 30 cycles were performed and for generating cloning fragments this was lowered to 25 cycles to lower the chances of mutations. Typically extension times were designed for 30 seconds per 500bp of the expected fragment size. Annealing temperature was normally 55°C; however, this would routinely have been optimised for each PCR.

For PCR amplification of the *aac(3)IV* cassette in the mutant generation the program was edited to include to different cycles so that the conditions used were:

1. Denaturation 94ºC, 2 minutes.
2. Deanturation 94ºC, 45 seconds.
3. Primer Annealing 50ºC, 45 seconds. } 10 cycles
4. Extension 72ºC, 90 seconds.
5. Denaturation 94ºC, 45 seconds.
6. Primer Annealing, 55ºC, 45 seconds. } 15 cycles.
7. Extension, 72ºC, 90 seconds.

8. Final Extension, 72ºC, 5 minutes.

PCR products were analsed by agarose electrophoresis gel (10.1.6). The bands containing the knockout disruption cassettes were excised and then purified by use of the QIAquick PCR purification kit protocol from the QIAquick Spin Handbook (QIAGEN, 2006). This protocol uses a QIAquick column with a Silica membrane for binding of DNA in high salt buffer and elution with low salt buffer or water.

10.1.8 Klenow treatment of PCR products

For generation of blunt ended PCR fragments; following the PCR, 46µl of the fragment formed was incubated at 37˚C with 2 units of Roche Klenow Enzyme for 15 minutes at 37˚C. Klenow or the large fragment of DNA polymerase as it is also known, has 3' → 5' exonuclease activity useful for removing poly-A overhangs generated during PCR. This was followed by addition of 1/10 volume of 10x loading dye. Then, incubation at 65˚C for 5 minutes. The DNA was then loaded onto an agarose gel and analysed by electrophoresis.

10.1.9 Restriction digest

Restriction digests for preparation of DNA fragments were a 200µl total volume consisting of; miniprep DNA or PCR DNA (passed through a G75 sephadex column prior to digestion), Restriction Digestion Buffer (1x) and Restriction Enzyme (15U). Commonly restriction enzymes were sourced from F. Hoffmann-La Roche Ltd and New England Biolabs (UK) Ltd. Where recommended from the enzyme supplier restriction digests also contained BSA protein. Restriction digests were incubated at 37˚C for 4-5 hours. This was followed by addition of 1/10 volume of 10x loading dye. Then, incubation at 65˚C for 5 minutes. They were then loaded onto an agarose gel and separated by electrophoresis.

Restriction digests for analysis of plasmids were a 20µl total volume consisting of; miniprep DNA, Restriction Digestion Buffer (1x) and Restriction Enzyme (5U). Commonly restriction enzymes were sourced from F. Hoffmann-La Roche Ltd and New England Biolabs (UK) Ltd. Where recommended from the enzyme supplier restriction digests also contained BSA protein. Restriction digests were incubated at 37˚C for 1.5-3 hours. This was followed by addition of 1/10 volume of 10x loading dye. Then, incubation at 65˚C for 5 minutes. They were then loaded onto an agarose gel and analysed using electrophoresis.

10.1.10 Isolation of DNA fragments from agarose

Digested DNA was analysed by agarose electrophoresis gels. The bands containing the fragments were visualized using long-wavelength UV light (310 nm) and excised with a razor blade. DNA was then purified by use of the Qiagen QIAquick Gel Extraction kit protocol from the QIAquick Spin Handbook (QIAGEN, 2006). This protocol uses a QIAquick column with a Silica membrane for binding of DNA in high salt buffer and elution with low salt buffer or in this case water.

10.1.11 Annealing of oligonucleotides prior to ligation

To anneal oligonucleotides, 9 µl of each oligonucleotide with a concentration of 50 pmol/µl was mixed and incubated at 100ºC for 5 minutes. Followed by cooling quickly on ice. Then, 2 µl of 10x SB Buffer was added, followed by gentle vortexing and incubation for 15 minutes at 37ºC. An aliquot of 2 µl was added to the appropriate ligation mixture.
10x SB buffer- 600 mM NaCl, 100 mM Tris, pH 7.6.

10.1.12 Ligation of DNA fragments

A molar ratio of approximately 3:1 of linearised insert to vector DNA fragments were set up and mixed into a final volume of 13µl, made up to the final volume with analytical grade H_20. The mixture was vortexed and incubated for 2 minutes at 65ºC. The mix was cooled on ice prior to the addition of 1.5µl of 10x ligation buffer and 0.5µl 3U/µl T4 DNA ligase from Promega. The mixture was incubated overnight on ice in a 4ºC temperature controlled room.

10.1.13 Transformation of competent E. coli cells by electroporation

A single colony of the appropriate *E. coli* strain was used to inoculate 10ml of LB supplemented with the appropriate antibiotics. This culture was then grown overnight at either 30˚C or 37˚C, shaking 270rpm. The overnight culture was diluted 100-fold and used to inoculate a fresh media (usually either 10ml or 50ml). The subculture was incubated at either 30˚C or 37˚C, shaking 270rpm, to an OD_{600} of ~0.7. The culture was then

centrifuged and the cell pellet was collected. The cells were then washed two times with ice cold 10% glycerol and resuspended to a final volume of ~100-250µl in 10% glycerol. For introduction of linear DNA, plasmid or cosmid DNA, 50µl of *E. coli* cell suspension was mixed with 1-3µl of the DNA. Alternatively for introduction of ligation mix, the ligation mix was first desalted through a G-75 Sephadex column, 50µl of *E. coli* cell suspension was mixed with 5µl of the desalted ligation mix. Following mixture of cells and DNA, electroporation was then quickly carried out in a 0.2cm ice cold electroporation cuvette using a BioRad Gene Pulser II set to: 200Ω, 25µF and 2.5kV. 1ml of ice cold LB was added to shocked cells and subsequently they were incubated for approximately an hour at either 30˚C or 37˚C. The transformed cells were plated out onto LB agar plates containing the appropriate antibiotics and incubated at either 30˚C or 37˚C. (Modified from Gust *et al.*, (2002))

10.1.14 Transformation of competent E. coli cells by chemical competence

A single colony of the appropriate *E. coli* strain was used to inoculate 10ml of LB supplemented with the appropriate antibiotics. This culture was then grown overnight at either 30˚C or 37˚C, shaking 270rpm. The overnight culture was diluted 100-fold and used to inoculate a fresh media (usually either 10ml or 50ml). The subculture was incubated at either 30˚C or 37˚C, shaking 270rpm, to an OD_{600} of ~0.4-0.6. The culture was then centrifuged and the cell pellet was collected. The cells were then washed 1 times with 10mM NaCl solution. The resulting cell pellet was then resuspended in 30mM $CaCl_2$, 10mM $RbCl_2$ solution. The cells were then incubated on ice for 30-60minutes. The cells were then collected by centrifugation and resuspended to a final volume of ~100-250µl in 30mM $CaCl_2$, 10mM $RbCl_2$ solution. For introduction of linear DNA, plasmid or cosmid DNA, 50µl of *E. coli* cell suspension was mixed with 1-3µl of the DNA. The mixture was then incubated on ice for 30 minutes. Followed by a heat shock with an incubation at 42˚C for 1 minute. A cold shock of 5 minutes on ice was followed. 500µl of LB was added to the shocked cells and subsequently they were incubated for approximately an hour at either 30˚C or 37˚C. The transformed cells were plated out onto LB agar plates containing the appropriate antibiotics and incubated at either 30˚C or 37˚C.

10.1.15 Isolation of plasmid DNA from E. coli

The following method is a modification of a method described by (Ish-Horowicz, and Burke, 1981). A smaller scale miniprep used 3ml total of cells, whereas a large scale maxiprep used 50ml of cells. The cells were grown overnight at 37˚C, shaking (200rpm) in either 10ml or 50ml of LB, inoculated with a single colony. Cells were harvested by centrifugation and resuspended in either 100µl or 1ml of ice cold solution I (50mM Tris/HCl pH8 + 10mM EDTA). The resuspended cells were then gently mixed with either 200µl or 2ml of solution II (200mM NaOH + 1% SDS) and incubated on ice for 5 minutes. 150µl or 1.5ml of solution III (5M Potassium Acetate pH5.5) was added, mixed vigorously and left on ice for 10 minutes. The mixture was centrifuged for 5 minutes and the supernatant was extracted with an equal volume of phenol:chloroform (1:1,v/v). 3µg/ml RNase was added and the nucleic acid solution was incubated at 37˚C for approximately 40-60 minutes. The nucleic acid was then extracted from the RNase with an equal volume of phenol:chloroform (1:1,v/v). The nucleic acid was precipated by adding an equal volume of isopropanol. The nucleic acid was separated by centrifugation, washed in 70% (v/v) ethanol, dried and redissolved in dH_20.

10.1.16 Sequencing ready reactions

All sequencing ready reactions were performed using a BioRAD DNA Engine® Peltier Thermal Cycler. Sequencing reactions were carried out using a BigDye® Terminator v3.1 Cycle Sequencing Kit, Applied Biosystems. Reactions were a 10µl total volume generally consisted of; dimethyl sulphoxide (5%), primer (0.5pmol), template DNA, Sequencing Buffer (1x), 1µl HBD (Makes final concentration = 25mM Tris pH 9.0, 1mM $MgCl_2$) and 1µl Big Dye v3.1. The following cycle program was used;

1. Denaturation 96ºC, 5 minutes.
2. Deanturation 96ºC, 16 seconds.
3. Primer Annealing 50ºC, 10 seconds.
4. Extension 60ºC, 4 minutes.

} 25 cycles

5. Cool down 20˚C, 5 minutes.

Products were then sent to Genome Enterprise Limited (The Genome Analysis Centre, Norwich Research Park, Norwich, NR4 7UH, UK) for sequencing.

10.1.17 Disruption of S. coelicolor cosmid DNA

Cosmid DNA was transformed into *E. coli* BW25113/pIJ790. A single colony of *E. coli* BW25113/pIJ790 carrying the cosmid was grown up in 10ml LB in the presence of chloramphenicol and kanamycin at 30ºC overnight. This was used to inoculate 10ml SOB containing the same antibiotics and L-arabinose (10mM), the inducer of the lambda Red recombinase genes. Competent cells were generated after 5 hours growth and disruption cassettes were introduced by transformation using electroporation. Successful recombinants were selected on LB plates containing apramycin at 37ºC. Single colonies that grew after 1 day were inoculated in 10ml LB cultures overnight at 37ºC, in the presence of apramycin and kanamycin and cosmids were isolated. To obtain homogenous cosmid DNA, cosmid DNA was then transformed by electroporation into *E. coli* strain DH5α and DNA was then isolated from a single colony of the transformants.

10.1.18 Generating a spore stock of S. coelicolor

To generate a concentrated stock of *S. coelicolor* spores a single colony was resuspended in dH_2O and spread onto an SFM plate with any appropriate antibiotics. The plate was incubated at 30°C for about 5 days or until confluent lawns of grey spores were visible. Spores were harvested in 5ml of sterile H_2O with a sterile cotton bud. The collected spores were then centrifuged for 5 minutes at 4,500rpm and the supernatant discarded. The pellet was resuspended in 20% glycerol and stored at -20ºC. The viable spore concentration was determined by plating out a dilution series on LB agar plates.

10.1.19 Conjugation into S. coelicolor

E. coli ET12567/pUZ8002 was used for conjugation of *oriT* containing vectors to *S. coelicolor*. The strain *E. coli* ET12567/pUZ8002 was always grown in the presence of kanamycin which maintains pUZ8002 and chloramphenicol where resistance is carried for chromosomally. *E. coli* ET12567/pUZ8002 was used in the transformation procedure with the desired cosmids/plasmids for the conjugation. Single colonies of *E. coli* ET12567/pUZ8002 carrying the conjugation vectors were grown up overnight in 10ml LB containing kanamycin, chloramphenicol and the antibiotic needed to select for the cosmid/plasmid of interest. Growth was carried out at 37˚C, shaking 270rpm. The

overnight culure was diluted 100-fold into a fresh 10ml LB plus the same antibiotics. The subculture was incubated at 37˚C, shaking 270rpm, to an OD_{600} of ~0.4-0.6. The cells were then washed 2 times with ice cold LB and resuspended to a final volume of ~1-2.5ml. Simultaneously, approximately 10^8 of the desired *Streptomyces* spores were activated for germination by heating at 50˚C for 10 minutes in 500µl of 2xYT and then cooled shortly on ice. A 500µl volume of the donor *E. coli* cell suspension was then mixed with the recipent *Streptomyces* spore solution. Following centrifugation, the *E. coli*/*Streptomyces* mix was used to make 4 serial 10x dilutions. 100µl of each serial dilution was plated on SFM (For knockout generation; with 3 repeats for each dilution). Plates were incubated at 30ºC overnight. After 1 nights incubation (~14-18 hours) each of the plates were overlaid with nalidixic acid and the antibiotic needed to select for the cosmid/plasmid of interest. The plates were then allowed to grow for about 4-7 days at 30ºC. In the case of knockout generation the exconjugants were subject to replica plating to test for those with single or double crossovers. Whereas for integrative vectors the exconjugants were directly picked and streaked for single colonies on SFM plates plus nalidixic acid and the antibiotic needed to select for the cosmid/plasmid of interest. Followed by setting up of a confluent plate for spore preparation, usually grown on SFM plates with the antibiotic needed to select for the cosmid/plasmid of interest and omitting nalidixic acid.

10.1.20 Replica plating

To isolate double crossover apramycin marked mutants, the conjugation plates were replica plated. This involved using a sterile velveteen cloth to transfer spores from the SFM plate onto an LB agar plate plus kanamycin and nalidixic acid. Followed by another transfer of the remaining spores on the cloth onto an LB agar plate plus apramycin and nalidixic acid. The LB agar plates were incubated at 30ºC for 2 days. Potential double crossover colonies that were missing from the kanamycin plates but present on the apramycin plates were then isolated from the original SFM plate and spread for single colonies onto SFM plates plus apramycin and nalidixic acid. These plates were then grown at 30ºC for about 5 days, followed by another round of replica plating to confirm the identity of double crossovers. Successful doublecrossover colonies were then used to spread for setting up of a confluent plate for spore preparation.

10.1.21 Chromosomal DNA extraction from S. coelicolor

In order to generate Chromosomal DNA the spores of different strains were grown on a cellophane surface on LB solid medium plus Glycine (0.5%). In the range of 10^7 Spores of the desired strain were added to two plates per strain and spread across the total area of the cellophane. The plates were incubated at 30˚C for 48 hours. After which cell material was scraped off the surface of the cellophane and added to tubes containing ~100µl volume of 425-600 micron acid washed glass beads, combining the two plates of each strain to one tube. Then, 500µl of Tris-EDTA Buffer was added to each tube (10mM Tris/HCl pH 8, 50mM $EDTA_)$. The cells underwent one 20 second blast with a FastPrep®-24 Tissue and Cell Homogenizer machine (MP Biomedicals) set at 4 m/s. Following this the cell material was more dispersed and 60µl of Lysozyme (100mg/ml stock) was added, the samples were then incubated on ice for 10 minutes and 37˚C for 10-30 minutes. 100µl of 10% SDS was added and the cell lysis solution incubated at 60˚C for approximately 20 minutes. The supernatant from the cell lysates was extracted with an equal volume of phenol:chloroform (1:1,v/v). The nucleic acid was then further cleaned with two extractions with equal volumes of chloroform. The nucleic acid was precipated by adding an equal volume of 100% (v/v) ethanol. The precipitated DNA was fished out with a glass rod, washed in 100% (v/v) ethanol, then 70% (v/v) ethanol, then 100% (v/v) ethanol, air dried and redissolved in 200-400µl dH_20.

10.1.22 Coverslip microscopy setup

Microscopic analysis of different strains involved growing *S. coelicolor* between the angle of a coverslip and nutrient agar medium (Figure 123). Spores of the desired strain were spread into confluent patches on SFM medium (plus any antibiotics). A glass coverslip 22x22mm with a thickness of 0.13-0.17mm was inserted at approximately 45˚ to the medium. The plates were incubated at 30˚C for 2-4 days to which at varying times coverslips were removed and stained for microscopic analysis.

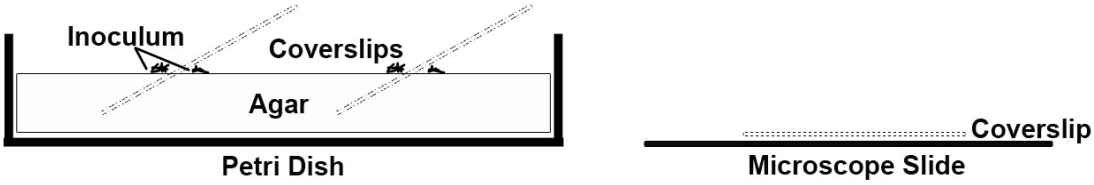

Figure 123: Plate Setup for growth of *Streptomyces* inbetween the angle of a coverslip inserted into agar media in a petri dish. Following growth of *Streptomyces* the coverslip was removed and either stained or directly placed face down between a microscope slide and a coverslip.

10.1.23 Propidium Iodide and Wheat Germ Agglutinin-Alexa488 staining of coverslip samples

Removed coverslips were fixed with 100% methanol for 1 minute. Sterile H_2O was used to wash the coverslips, followed by application of WGA Alexa Fluor® 488 conjugate (50µg/ml) and propidium iodide (25µg/ml) to each coverslip on the growth line. The samples were incubated for 30 minutes under dark conditions. After which the dyes were removed with dH_2O and the slides were mounted onto microscope slides (76 x 26mm (thickness 1.0 – 1.2mm).

10.1.24 Cellophane microscopy setup

Microscopic analysis of different strains involved growing *S. coelicolor* on a cellophane surface on SFM solid medium (Figure 124). Spores of the desired strain were diluted to ~4x 10^5 spores per plate, induced for germination at 50˚C for 10 minutes and sonicated 2 x 15 seconds in order to disperse the spores. The dilution was then spread across the surface of a cellophane ontop of SFM medium (plus relevant antibiotics). The plates were incubated at 30˚C for 14-16 hours. After which 1cm^2 squares of cellophane were cut with a razor blade and mounted onto microscope slides with 20% glycerol. Samples were sealed with Coverslips 22x22mm with a thickness of 0.13-0.17mm on a microscope slide (76 x 26mm (thickness 1.0 – 1.2mm). Alternatively cellophanes were stained.

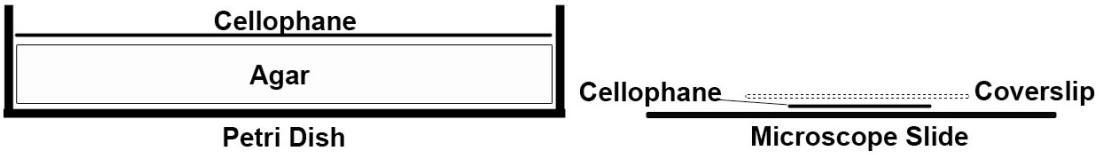

Figure 124: Plate Setup for growth of *Streptomyces* ontop of a cellophane placed above agar media in a petri dish. Following growth of *Streptomyces* the cellophane was cut and either stained or directly placed face up between a microscope slide and a coverslip.

10.1.25 Propidium Iodide, Wheat Germ Agglutinin-Alexa488 and/or Fluorescent Vancomycin staining of cellophane samples

Cellophane squares were placed onto pre-cut filter paper with cell material facing upwards. Cellophanes were fixed by soaking ~300µl of 100% methanol for 1 minute. Sterile H_2O, 500µl was used to wash the cellophanes, 15µl of WGA Alexa Fluor® 488 conjugate (50µg/ml) and propidium iodide (25µg/ml) droplets were placed onto a solid surface. Cellophanes were then placed onto droplet (cell material facing upwards still). The samples were incubated for 30 minutes under dark conditions. After which the dyes were removed with dH_2O. The cellophanes were then mounted with 20% glycerol onto microscope slides.

For staining with fluorescent vancomycin, cellophane samples prior to collection were simply incubated with 10µl droplets of 1 µg/ml BODIPY FL vancomycin (Molecular Probes) and 1 µg/ml unlabelled vancomycin (Sigma) placed ontop of the sample for 5 minutes, in dark conditions. Samples were then collected and either directly mounted onto microscope slides or were stained with propidium iodide as mentioned above.

10.1.26 Microscopy

Samples were visualised by using an Axioplan 2 Imaging E (Carl Zeiss) Universal microscope with an An AxioCamMR camera. Using a Plan Apochromat 100x/1.40 Oil (440780) objective. Filters used were FS 38 GFP and FS 45 TxR. Alternatively samples were visualised by using a Leica TCS SP2 [Leica Microsytems CMA GmbH, Wetzlar, Germany] laser-scanning confocal microscope.

10.1.27 Overexpression and depletion experiments

For overexpression experiments strains were grown on cellophanes on SFM medium (plus any relevant antibiotics), usually with an overnight growth of 14-18 hours. Then, the cellophane was transferred to a fresh SFM plate containing either thiostrepton (20µg/ml) or the control which had no thiostrepton (also with relevant antibiotics and possibly plus or minus bacitracin 50µg/ml). The plates were then grown for a further 1-5 hours. Cellophane samples were then used for microscopy or generation of cell extracts.
For K115 based depletion experiments strains were grown on cellophanes on SFM (plus any relevant antibiotics) plus 0.1µg/ml of thiostrepton, usually with an overnight growth of 14-18 hours.Then, the cellophane was transferred to a fresh SFM plate containing either no thiostrepton for the depleted sample or 0.1µg/ml thiostrepton for the control sample (also with relevant antibiotics). The plates were then grown for a further 1-5 hours. Cellophane samples were then used for microscopy or generation of cell extracts.

10.1.28 Generating cell extracts of Streptomyces fluorescent fusion samples

In order to monitor the fluorescence signal of the fusion proteins the spores of different strains were grown on a cellophane surface on SFM solid medium plus relevant antibiotics. In the range of 10^7 Spores of the desired strain were added to 2-3 plates per strain and spread across the total area of the cellophane. The plates were incubated at 30˚C for 14-18 hours. After which, cellophanes had enough cell material to be directly collected or cellophanes may have been moved onto different plates depending on the experimental setup (e.g. with or without thiostrepton). When samples were collected cell material was scraped off the surface of the cellophane and added to tubes containing ~100µl volume of <106 micron acid washed glass beads, combining multiple plates of each strain to one tube. Then, 100-200µl of Tris-Mg Buffer was added to each tube (20mM Tris pH 8, 10mM $MgCl_{2)}$. The cells underwent five 30 second blasts with a FastPrep®-24 Tissue and Cell Homogenizer machine (MP Biomedicals) set at 6.5 m/s. The cells were centrifuged for 30 seconds at a low speed of 2,000rpm and the supernatant transferred to new tubes. The supernatant was further centrifuged at high speed at 13,000 rpm for 15 minutes, after which the supernatant was added to new tubes leaving a pellet fraction which was resuspended in 100µl of Tris-Mg Buffer.

10.1.29 Bacterial two-hybrid assay

The bacterial two-hybrid assay was performed by cotransforming the *E. coli* strain BTH101 with pUT18C vectors encoding relevant T18 domain fusion proteins together with pKT25 vectors encoding relevant T25 domain fusion proteins. Cotransformant strains were grown on LB solid medium omitting glucose. The medium contained the antibiotics ampicilin and kanamycin. The medium was supplemented with 0.5 mM of IPTG allowing induction of the *lac* promoter and expression of the fusion protein. The medium was also supplemented with 40 μg/ml X-gal, to allow for visualisation of a positive interaction through the increased activity of β-galactosidase. The plates were imaged at growth after 1, 2 and 3 days at 30ºC and the appearance of blue colonies was looked for.

10.1.30 Overexpression of proteins from E. coli

The strain BL21 pLysS (DE3) will enable high levels of protein expression as the pET21a or pET28a vectors put the cloned in gene under the control of a T7 promoter. BL21 pLysS (DE3) can express T7 RNA polymerase via the lac UV5 promoter which is IPTG inducible. A freshly transformed single colony was routinely used to inoculate a 10ml starter culture that would be grown overnight at 37˚C shaking rigorously (270rpm). Then, 100µl or 500µl was subcultured into 10ml or 50ml LB, respectively. The cultures were then grown usually at 37˚C shaking rigorously (270rpm) to an OD ~0.7. Whereupon addition of 1mM IPTG was added to induce overproduction of the desired protein. The culture was then continued specifically at 37˚C shaking rigorously for 4 hours or overnight. At this point the culture was centrifuged and the cells pelleted and lysed freshly or resuspended in the desired buffer and frozen -80°C using liquid N_2.

10.1.31 E. coli cell lysis procedure

For 50ml/10ml overnight or 4 hour cultures, culture material was centrifuged at 5000rpm for 5 minutes at 4°C, the supernatant discarded and the cells resuspended in 5ml/800µl of appropriate buffer. For lysis 800-1000µl of resuspended pellets were placed in screw cap tubes containing ~0.1ml acid washed glass beads (<106µm) and fast prepped for three x 30 second bursts at 6.5m/s, with 5 minute rests in between, using a FastPrep®-24 Tissue and Cell Homogenizer machine (MP Biomedicals). Cells were centrifuged at 2000rpm for 30

seconds at room temperature and the cell material was removed from the beads pellet and added to new tubes. Cell material was commonly centrifuged 13000rpm for 15-20 minutes at 4°C to pellet unlysed cells and the insoluble fraction. The supernatant was added to new tubes and then used directly for downstream applications.

For large scale 500ml cultures of His-DivIVA expressing cells. The large volume of culture was centrifuged in two 250ml aliquots added to Nalgene centrifuge canisters and centrifuged at 7000rpm for 15 minutes at 4°C in an Avanti® J-26XP Beckman Coulter centrifuge with a Beckman JLA 16.250 J-lite® Series Rotor (no. 06U 3339). The supernatant was removed and each pellet was initially resuspended in 5ml of NP1-10 lysis buffer, the pellets were then combined in one canister and made up to a total volume of 125ml with NP1-10 lysis buffer. Centrifugation was repeated at 7000rpm for 15 minutes at 4°C. The supernatant was removed and the single pellet was resuspended in 10ml of urea buffer 8.0. The sample was then sonicated for 10 x 10 seconds, with 1 minute pauses on ice inbetween. The lysed cell suspension was then added to a 50ml Nalgene centrifuge canister and centrifuged at 14000rpm for 20 minutes at 4°C in an Avanti® J-26XP Beckman Coulter centrifuge with a Beckman JA-25.50 Rotor (no. 07E 321). The resulting supernatant was removed and aliquoted, aliquots were frozen with liquid N_2 and stored -80°C.

10.1.32 Overexpression of His-Scy from S. coelicolor

Scy was overexpressed from *S.coelicolor* from TSB-PEG liquid cultures. There are two methods either with an initial culture in TSB-PEG or with an initial germination of spores in 2xYT, to attempt to prepare the cells for exponential growth.

For two sets of TSB-PEG cultures the following was carried out in sterile conditions. The 50ml TSB-PEG culture (containing apramycin) was inoculated with 50µl of spore stock of M145/pCJW93-scy. The culture was then incubated at 30°C for 24 hours, shaking at 310 rpm. 2ml of this culture was transferred into a new 50ml TSB-PEG liquid culture containing apramycin. The subculure was then incubated at 30°C for 16 hours, shaking at 310 rpm. After 16 hours 10 µg/ml of thiostrepton was added to the culture for induction or Scy expression. Incubation resumed at the previous conditions for 5 hours.

Alternatively to pre-germinate the spores the procedure is as followed, in sterile conditions. 500µl of 2 YT was added to a screw cap tube. 60µl of spore prep was also added to the tube. The spore solution was vortexed to mix and then incubated at 50ºC for 10 minutes.

The sample was then cooled on ice. The spore solution were then transferred to a 50ml coiled TSB-PEG flask (containing apramycin). The flask was incubated at 30ºC, 310rpm for 21 hours. Then thiostrepton (20μg/ml) was added to the culture. The flask was then incubated at 30ºC, 310rpm for 5 hours.

10.1.33 Preparing a cell extract from S. coelicolor

Buffer A = 50mM NaH_2PO_4 + 500mM NaCl + 10mM Imidazole, pH 8.0.

For protein extraction by sonication the following was performed, the sample was kept on ice in between steps. The culture was added to a 50ml centrifuge tube. The cell suspension was centrifuged at 4500rpm for 5 minutes. The supernatant was discarded. The pellet was resuspended in 40ml of Buffer A. The sample was centrifuged at 4500rpm for 5 minutes. The supernatant was again discarded. The pellet was resuspended in 40ml of Buffer A. The resuspended samples was centrifuged again at 4500rpm for 5 minutes. The supernatant was again discarded. A 5ml Buffer A + protease inhibitor solution was made (4.6ml of Buffer A, 0.2ml of 100mM Pefabloc SC inhibitor, 0.2ml Pefabloc SC protector). 1ml of buffer plus protease inhibitor was added to pellet. Sample vortexed to mix. The cell suspension was sonicated for 30 seconds. Another 1ml of buffer plus protease inhibitor was added, then the sample was sonicated two x 30 seconds. Another 1ml of buffer plus protease inhibitor was added, then the sample was sonicated three x 30 seconds. The sample was centrifuged for 1 minute, 4500rpm. The sample was again sonicated for two x 30 seconds, aiming at the pellet generated by centrifuging. The sample was centrifuged at 5000rpm for 5 minutes. The supernatant was transferred to multiple eppendorf tubes. The sample was centrifuged 13,000rpm for 20 minutes. The supernatants were combined from the eppendorfs upon being transferred into a new tube. The supernatant was then used for purification by FPLC.

10.1.34 FPLC HisTrap nickel affinity chromatography

Buffer A = 50mM NaH_2PO_4 + 500mM NaCl + 10mM Imidazole, pH 8.0.
Buffer B = 50mM NaH_2PO_4 + 500mM NaCl + 300mM Imidazole, pH 8.0
Buffer C = 50mM NaH_2PO_4 + 500mM NaCl + 500mM Imidazole, pH 8.0

From an *E. coli* or *S. coelicolor* cell lysate carrying overexpressed His-tagged protein, the supernatant was passed through a 0.2 µm filter before being loaded onto a HisTrap HP 1 ml (GE Healthcare) column on an Amersham AKTA FRC FPLC machine. Affinity chromatography was then used to purify His-tagged proteins normally through either step elutions or gradient elutions whereby the initial flowthrough was added at 5-10mM imidazole concentration, at a flow speed of 0.2ml/minute. The column was washed with a 20-30mM imidazole concentration and an increased flow speed of 0.5ml/minute to remove any unbound protein. The bound His-tagged protein was then eluted from the column by increasing the concentration of imidazole and reducing the flow speed back to 0.2ml/minute. In step elutions this was to either 300mM or 500mM imidazole. Alternatively gradient elutions were used where the gradient was slowly increased from the wash concentration to either 300mM or 500mM imidazole. The column was also usually further washed in 500mM imidazole Buffer C following purification. Fractions containing the His-tagged protein were identified using SDS-PAGE.

10.1.35 Ni-NTA column affinity purification of His-DivIVA with denaturing conditions

Urea buffer 8.0 = 7M Urea, 0.1M Na_2HPO_4, 0.01M Tris-Cl, pH 8.0
Urea buffer 6.3 = 8M Urea, 0.1M Na_2HPO_4, 0.01M Tris-Cl, pH 6.3
Urea buffer 6.1 = 8M Urea, 0.1M Na_2HPO_4, 0.01M Tris-Cl, pH 6.1
Urea buffer 4.5 = 8M Urea, 0.1M Na_2HPO_4, 0.01M Tris-Cl, pH 4.5

To equilibrate the Qiagen Ni-NTA spin column, 600µl of urea buffer pH 8.0 was added and centrifuged 3100rpm for 2 minutes at room temperature with the lid open. The flow through was discarded and 600µl of the BL21 pET28a-divIVA supernatant sample from cell lysis was added to the column, 10.5µl supernatant was held back to be used as a preload sample. The column was incubated at room temperature for 1 minute and centrifuged 1400rpm for 5 minutes at room temperature with the lid closed. The flow through was collected. The column was washed four times with 600µl of urea buffer pH 6.3, each time by centrifuging 3100rpm for 2 minutes at room temperature with the lid open. The flow through was collected after each wash (W1-W4). The column was then washed three times with 600µl of urea buffer pH 6.1 by centrifuging 3100rpm for 2 minutes at room temperature with the lid open. Flow through was collected after each wash (W5-7). The protein was eluted from the column two times with 400µl of urea buffer pH

4.5, following each addition the column was incubated at room temperature for 1 minute. The column was centrifuged 1400rpm for 3minutes at room temperature with the lid closed. Flow through samples were collected (E1-E2). Protein was eluted further with 300µl of urea buffer pH 4.5 by centrifuging 3100rpm, 2 minutes, room temperature with the lid open and flow through was collected (E3).

10.1.36 Ni-NTA column co-affinity purification

Samples of His tagged or non-tagged proteins were prepared in varying ways (mentioned in results). His-tagged protein samples were applied to the column in such a way as to then provide the non-tagged protein samples to test their ability to bind. To equilibrate the Qiagen Ni-NTA spin column, 600µl of NP1-10 lysis buffer was added and centrifuged 3100rpm for 2 minutes at room temperature with the lid open. The flow through was discarded and the His-tagged protein sample was added to the column, 30µl supernatant was held back to be used as a preload sample. The column was incubated at room temperature for 1 minute and centrifuged 1400rpm for 5 minutes at room temperature with the lid closed. The flow through was collected. The column was washed two-three times with 600µl of NP1-10 lysis buffer, each time by centrifuging 3100rpm for 2 minutes at room temperature with the lid open. The flow through was collected after each wash (W1, W2...W3). Then, the non-tagged protein sample was added to the column, 30µl supernatant was held back to be used as a preload sample. The column was incubated at room temperature for 1 minute and centrifuged 1400rpm for 5 minutes at room temperature with the lid closed. The flow through was collected. The column was washed three-four times with 600µl of NP1-10 lysis buffer, each time by centrifuging 3100rpm for 2 minutes at room temperature with the lid open. The flow through was collected after each wash (W3/W4, W5...W6...W7). The bound protein was then eluted from the column two-three times with 300µl of NP1-500 elution buffer, following each addition the column was incubated at room temperature for 1 minute. The column was centrifuged 1400rpm for 3 minutes at room temperature with the lid closed. Flow through samples were collected (E1, E2...E3). In control experiment cases where no His-tagged protein was used, the His-tagged protein binding step was missed out and instead the non-tagged protein was added directly onto the column. The buffers used were;

Phosphate buffer = 50mM Na_2HPO_4 + 50mM NaCl pH 8.0

NP1-10 lysis buffer = 50mM Na_2HPO_4 + 300mM NaCl + 10mM Imidazole, pH 8.0

NP1-500 elution buffer = 50mM Na_2HPO_4 + 300mM NaCl + 500mM Imidazole, pH 8.0

For the optimised His-Scy plus non-tagged FilP experiment the buffers used were;
Loading/Wash buffer = 50mM Na_2HPO_4 + 300mM NaCl + 50mM Imidazole + 20mM MgCl2, pH 8.0
Elution buffer = 50mM Na_2HPO_4 + 300mM NaCl + 500mM Imidazole + 20mM MgCl2, pH 8.0

10.1.37 Protein sample buffer exchange

To exchange buffers protein samples were placed in 2ml screw cap tubes and sealed with a porous membrane. They were then placed in a floater and inverted against the buffer of choice for a period of 2-4 days with the buffer being changed 2-3 times. The membrane used was Spectrum (R) Spectra/Por (R) Molecularporous membrane tubing, 3 membrane. It has an MWCO (Molecular Weight Cut Off) of 3500 Daltons.

10.1.38 Protein concentration determination

In the range of 10-15µl of Protein sample was made up to 1000µl with dH_20 and the addition of 200µl of Bio-Rad Protein Assay. After mixing and 5 minutes incubation at room temperature, the absorbance was determined at 595nm in a Spectrophotometer (Hitachi U-1100). This was then compared with a standard line of BSA concentrations 0-15µg/ml and an estimate of the concentration of protein in the sample was calculated and/or the molar concentration of purified protein was estimated.

10.1.39 SDS-Polyacrylamide Gel Electrophoresis (SDS-PAGE)

Fluorescent protein cell extracts samples were treated in conditions that were able to semi-denature proteins. This included using protein loading dye (diluted to 1x) including SDS and β-mercaptoethanol. In order to maintain the conformation of the fluorescent proteins and therefore their fluorescent activity, samples were not boiled prior to loading. For full denaturing gels proteins were mixed with protein loading dye (diluted to 1x) including SDS and β-mercaptoethanol, then boiled at 100˚C for 5minutes prior to loading.

For full reducing conditions needed to reduce disulphide bonds in a DTBP crosslink, the samples were incubated with 100mM DTT at 37ºC for 20 minutes. Then, addition of protein loading dye (diluted to 1x) including β-mercaptoethanol and boiling at 100ºC for 5 minutes were used.

For nonreducing conditions in order to maintain disulphide bonds such as in DTBP crosslinks, protein loading dye (diluted to 1x) that does not include β-mercaptoethanol was used and the DTT step omitted. Samples were still boiled at 100ºC for 5 minutes.

Table 17: Recipe of an 8% Acrylamide Resolving Gel used in this study.

Compound	Stock Concentration	Volume used	Final Concentration
Acrylamide	30%	2.66ml	8%
Tris pH8.8	1.5M	2.5ml	0.375M
SDS	10%	0.1ml	0.1%
Freshly made APS	25%	0.04ml	0.1%
TEMED	>99%	0.006ml	~0.04%
dH_20		4.634ml	

Table 18: Recipe of a 3.75% Acrylamide Stacking Gel used in this study.

Compound	Stock Concentration	Volume used	Final Concentration
Acrylamide	30%	0.5ml	3.75%
Tris pH6.8	1M	0.5ml	0.125M
SDS	10%	0.04ml	0.1%
Freshly made APS	25%	0.016ml	0.1%
TEMED	>99%	0.004ml	~0.04%
dH_20		3ml	

SDS-Polyacrylamide gels were made using a higher percentage acrylamide resolving layer (8% recipe shown in Table 17) and a 3.75% acrylamide stacking layer (Table 18). For higher percentage gels the amount of acrylamide and dH_20 were adjusted. Gels were placed in a tank containing 1% SDS running buffer. Samples were loaded and the gel run at 200 Volts, for 45-60 minutes depending on the running distance desired. For visualisation of fluorescent proteins, following running, the gels were immediately transferred to a BioRAD Molecular Imager FX. For visualisation of mCherry proteins, gels were excited with 532nm and the emission read at 555nm. For visualisation of EGFP proteins, a BioRAD external laser attached to the BioRAD Molecular Imager FX was used to excite the fluorophore at 488nm and the emission was then read at 532nm. Subsequently

gels were fixed by incubating in fixing solution (10% methanol, 7% acetic acid) for 1 hour with gentle agitation. Then, gels were stained with Colloidal Coomassie blue R250 for a minimum of 1 hour with gentle agitation. Gels were destained by boiling in dH_20. The gels were then viewed with white light illumination using a BioRad transilluminator.

10.1.40 Western blotting

Prior to performing a Western Blot samples were separated on SDS-PAGE gels (in some cases the samples used were treated differently either with/without DTT, but were treated with β-mercaptoethanol). After the gels had been removed from the tank. Per gel 2 thick pieces of filter paper (Bio-Rad Extra Thick Blot Paper, Protean® XL Size, Catlog No. 1703969) were cut to a size of 9.1cm x 6.5cm. A PVDF membrane (Membrane; HybondTM-P Protein Transfer, PVDF Transfer Membrane, Amersham Pharmacia Biotech, Version RPNF L/98/03) was cut to the same size and soaked in 100% methanol for 30 minutes coinciding with the end of the running of the SDS-PAGE gel. The membrane was then placed in transfer buffer (Transfer buffer = 20% Methanol, 3.03% Tris, 14.4% Glycine) for 30 minutes. The gel was simultaneously equilibrated in transfer buffer at the same time as the membrane, in a separate container. After 25 minutes the filter paper was placed in transfer buffer for the remaining 5 minutes. The filter paper, membrane and gel on the apparatus were then arranged from bottom to top; Anode, layer of filter paper, acrylamide gel, membrane and remaining layer of filter paper. Air bubbles were rolled out prior to the cathode being placed. The transfer was run at 10-15 volts for 1 hour. The membrane was then carefully removed from the Transblot and placed in blocking solution for 2 hours, rocking at room temperature. The membrane was then washed with TBST. The membrane was then placed in blocking solution with the addition of the primary antibody and incubated in the cold overnight, rocking gently. The membrane was then washed 3 times for 5 minutes each at room temperature in TBS + 0.1% Tween-20 with gentle rocking. The membrane was then incubated in TBST solution + secondary antibody at room temperature with gentle rocking for a minimum of 2 hours (this incubation was performed with protection from light if necessary). The membrane was then washed 3 times for atleast 10 minutes each at room temperature in TBS + 0.1% Tween-20 with gentle rocking (plus protection from light if necessary). (For Odyssey the TBS + 0.1% Tween-20 was removed and the membrane was further washed 2 times for 5 minutes each at room temperature in TBS (without Tween-20)). The membrane was then

used for detection either through scanning on an Odyssey Infrared Imaging System or though X-ray film developing. Developing was carried out in Dark conditions. Whereby 10ml of Solution A was mixed with 10ml of Solution B. Approximately half was added to the membrane. The membrane was then incubated for 2 minutes at room temperature, manually shaking. The solution was then poured away, the dry membrane was wrapped tightly in cling film and placed in an autorad cassette, where the probed membrane was exposed to an X-ray film (Fuji film Super RX NIF blue), the X-ray radiograph film was then developed using a Konika SRX-101A Photon Imaging System.

Western Blot solutions;

Transfer Buffer- Tris 25mM, Glycine 150mM, 10% methanol

TBS- 10mM Tris-HCl, 150mM NaCl, pH 7.5

TBST- TBS with 0.1% Tween-20, pH 7.5

Blocking Buffer- TBST with 4% milk

Luminol- 0.44g Luminol in 10ml DMSO. Store 110µl aliquots -20˚C.

Coumaric Acid- 0.15g in 10ml DMSO. Store 60µl aliquots -20˚C.

Solution A- 1ml Tris-HCl pH8.5, 45µl Coumaric Acid, 110µl Luminol, 8845µl dH_20

Solution B- 1ml Tris-HCl pH8.5, 6µl 30% Hydrogen Peroxide, 8996µl dH_20

For anti-DivIVA experiments the primary antibody was a 1:5000 dilution of anti-DivIVA (Wang *et al.*, 2009) and the secondary antibody was a 1:5000 dilution of Horseradish peroxidase-linked anti-rabbit IgG (Gift from the Munsterberg Lab).

The Odyssey system uses two colour detection where the blot is viewed with the fluorescent channels 680nm and 780nm. Odyssey Blocking solution was used instead of TBST with milk powder. The Odyssey Western blot was performed using a primary antibody that was anti-his and raised in a mouse (added as 20ml Odyssey Blocking solution + 1/3000 primary antibody (6.6µl) + 0.1% Tween20 (20µl)). The secondary

antibody was Goat raised anti-mouse heavy chain from LI-COR (IRDye 800CW) (added as 17ml Odyssey Blocking Solution + 1/15000 secondary antibody (1.1µl) + 0.1% Tween20 (20µl)).

10.1.41 Ultracentrifugation protein pellet assays

Protein preparations were prepared in a 20mM Tris, 200mM Salt, 10mM $MgCl_2$, pH 8.0 buffer, were mixed as according to experimental design. The proteins were incubated at 30˚C for 15 minutes. They were then transferred to Polycarbonate Beckmann Centrifuge tubes 5/16 x 13/16 inches (7 x 20mm). They were then centrifuged at 100,000rpm in a Beckman Optima TLX Ultracentrifuge using a Beckmann Coulter TLA 100 Fixed Angle Rotor for 30 minutes at 4˚C. The supernatant fractions were immediately removed from the tubes. The pellet fractions were left to redissolve in the tubes and were manually pipetted up and down and transferred to eppendorf tubes. The samples were then run on SDS-PAGE gels in order to visualise the abundance of each protein in the pellet or the supernatant fraction.

10.1.42 Strategy of PCR targeting of scy, filP and scy-filP

To create knockouts of *scy*, *filP* and generate a *scy-filP* double knockout mutation, the REDIRECT© PCR-targeting system was applied (Gust *et al.*, 2002). Using *S. coelicolor* chromosomal DNA carried on supercos-1 cosmids, the targeted gene is replaced with a resistance cassette generated by PCR using oligonucleotides with 39nt homology extensions. The cosmid carrying the target gene is mutagenised in *E. coli* expressing a phage lambda Red recombinase (λ RED)(Datsenko, and Wanner, 2000). This recombinase increases homologous recombination of linear fragments, in this case between the target gene and the homologous ends of the PCR-generated resistance cassette. The apramycin resistance cassette (*aac(3)IV*) was the template for the production of a linear PCR product that due to the incorporated homology extensions on the oligonucleotides can undergo recombination with the flanking sequences to *scy*, *filP* or *scy-filP* (Figure 125A). The disruption cassette also includes *oriT* from RK2 (Pansegrau *et al.*, 1994) that allows the PCR targeted cosmid to be moved into *S. coelicolor* via conjugation from *E. coli*. The disruption cassette also carries FLP recognition target sequences (FRT) that at a later point can be used for removal of the intervening sequences with an FLP-recombinase. The

design and positioning of primers flanking either the *scy* gene or the *filP* gene are shown in Figure 125B. Primers scy Fwd and scy Rev were used for the *scy* mutant, primers filP Fwd and filP Rev for the *filP* mutant and the primers scy Fwd and filP Rev for the *scy-filP* double mutant. The predicted result of recombination for each mutant scenario is shown in Figure 125.

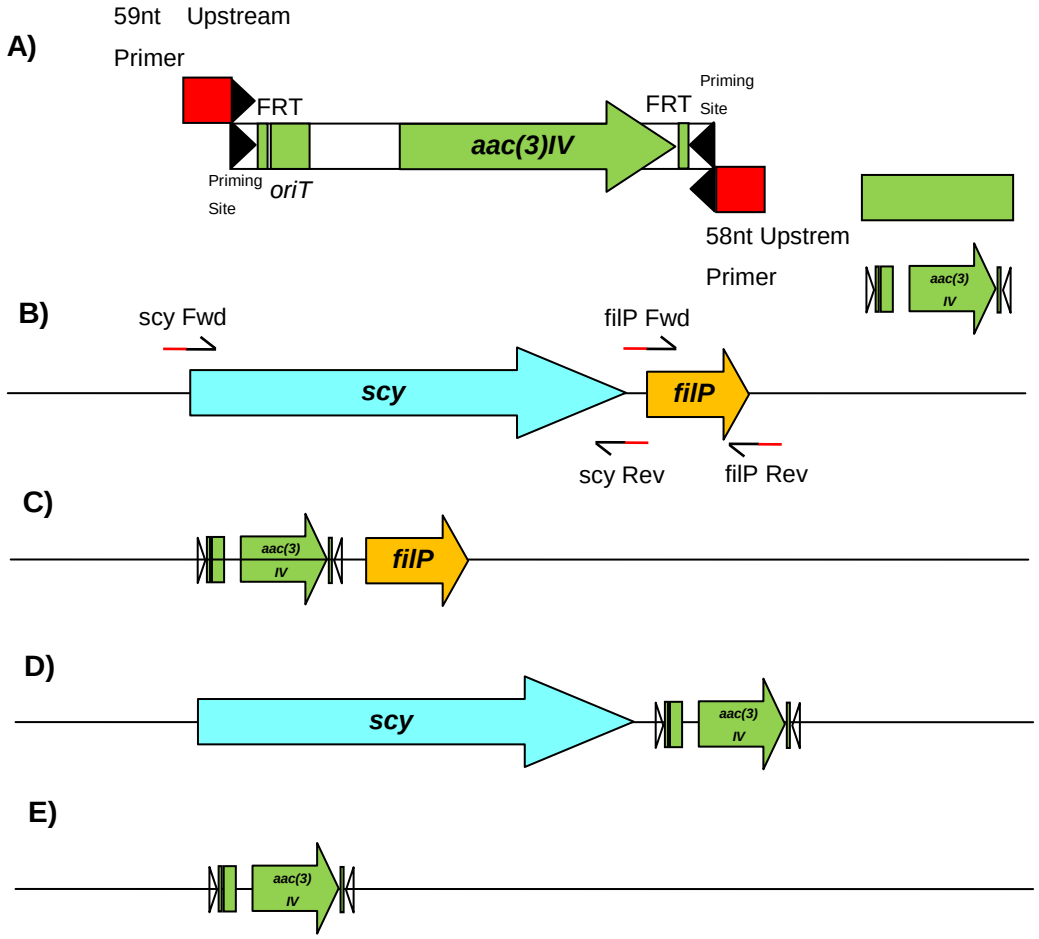

Figure 125: The strategy for knockout generation of *scy*, *filP* and *scy-filP*. (A) Primers were designed for the ampilification of an apramycin resistance (*aac(3)IV*) cassette from pIJ773. The primers were designed to anneal to 19 or 20 nucleotides (indicated in black) of the disruption cassette and 39 nucleotides that are homologous to the flanking regions around *scy* and *filP* (red). The cassette also contains FLP recognition target sequences (FRT) that can be used for FLP-mediated excision and *oriT* from RK2. (B) The wild-type locus of *scy* and *filP* on St8F4 cosmid. The position of the primers used in the PCR shown. The predicted scenario for mutants for *scy* (C) using scy Fwd and scy Rev. For a *filP* mutant (D) with filP Fwd and filP Rev. For a *scy-filP* mutant (E) with scy Fwd and filP Rev.

10.1.43 PCR of scy, filP and scy-filP disruption cassettes

To generate the knockout cassettes the PCR reaction was carried out using the template of the ~1.3Kb *Eco*RI-*Hind*III fragment of pIJ773 (Gust *et al.*, 2003) carrying the apramycin resistance cassette. For the *scy* knockout cassette the primers scy Fwd and scy Rev were used. For the *filP* knockout cassette the primers filP Fwd and filP Rev were used. For the *scy-filP* knockout cassette the primers scy Fwd and filP Rev were used. The PCR was performed so that there were 10 cycles with an annealing temperature of 50°C and 15 cycles with an annealing temperature of 55°C. This was done as the initial template DNA would only have 19 or 20nt for the primers to anneal to. In later steps when earlier products act as the template and the oligos will be able to anneal along the full length (58-59nt) higher annealing temperature is used. The PCR product was analysed using a 0.7% agarose gel (Figure 126). The apramycin cassette is 1382bp long, the primers add another 39bps to either side of the cassette making it 1460bps long. The main PCR product (Figure 126) is in the region of 1400bps long, so this indicates that the PCR reaction was successful. The PCR products were then purified using a QIAquick PCR purification kit.

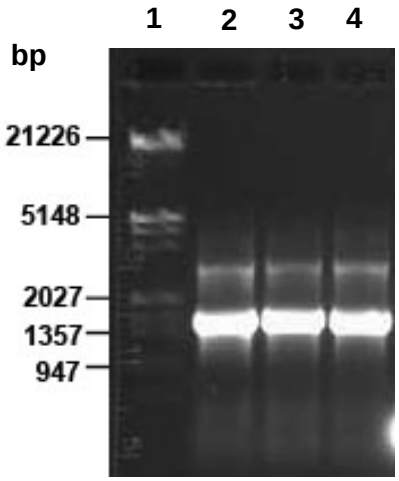

Figure 126: Analysis of the disruption cassettes generated by PCR. The PCR products were loaded onto a 0.7% agarose gel and used in electrophoresis. The PCR products generated were the *scy* mutant cassette (Lane 2), the *filP* mutant cassette (Lane 3) and the *scy-filP* mutant cassette (Lane 4). The DNA size marker is Lambda *Hind*III/*Eco*RI (Lane 1).

10.1.44 Targeting of the St8F4 cosmid

The *S. coelicolor* genome was sequenced from a set of ordered Supercos-1 clones containing ~37.5kb chromosomal fragments (Redenbach *et al.*, 1996). The cosmid St8F4 contains a 33.9kbp fragment of *S.coelicolor* chromosomal DNA, which carries the genes *scy* and *filP* in their native genetic arrangement. The cosmid also encodes the neomycin resistance gene (*neo*^{r}) which also confers resistance to kanamycin. Preliminary to the PCR targeting, St8F4 was transformed into *E. coli* BW25113 carrying pIJ790. The pIJ790

plasmid carries the lambda Red recombinase genes *gam*, *bet* and *exo* under the L-arabinose inducible promoter $Para_{BAD}$. The plasmid carries the selectable marker *cat*, the chloramphenicol resistance gene. The plasmid also has a temperature sensitive replicon, repA101ts so in order to maintain the plasmid, cells were grown at 30˚C. *E. coli* BW25113/pIJ790 carrying St8F4, expressing the lambda Red recombinase genes were made competent and the appropriate PCR cassette was introduced using electroporation. Introduction of the disruption cassette in a strain expressing *gam*, *bet* and *exo* should enable homologous recombination between the ~39nt ends of the linear PCR cassette and the appropriate sites on the cosmid DNA. Successful recombinational events were selected on plates containing apramycin. Growth at 37ºC was to insure loss of pIJ790 as further recombinational events are undesirable. Around 20-50 colonies grew successfully after 1 day for each of the disruption cassettes. Cosmid DNA was isolated from four colonies for each of the three sets of knockouts. As the recombinational event targets only a proportion of the multicopy cosmid in the *E.coli* BW25113/pIJ790 cells. In order to thoroughly purify cosmids carrying the mutant alleles the cosmids from *E. coli* BW25113 were further transformed into *E. coli* DH5α and clones with the mutant alleles were reselected using apramycin. Cosmid DNA then purified from DH5α was used as samples in the subsequent experiments. For analysis *Eco*RI and *Pst*I restriction digestions were performed to confirm that the cosmids carried the correct mutations (Figure 127).

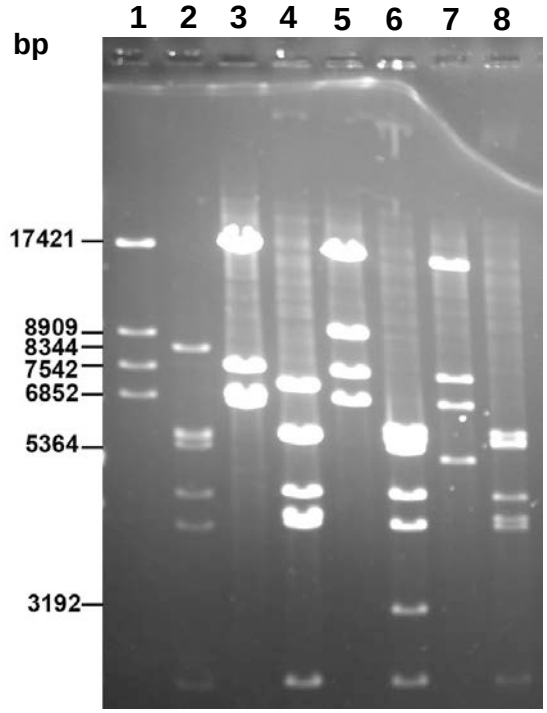

Figure 127: Confirmation of the mutant alleles generated. *Eco*RI (Lanes 1, 3, 5 & 7) and *Pst*I (Lanes 2, 4, 6 & 8) restriction digests of each cosmid were analysed on a 0.7% agarose gel. The following cosmids were tested St8F4 (Lanes 1 & 2), St8F4/*scy::aac(3)IV* (Lanes 3 & 4), St8F4/*filP::aac(3)IV* (Lanes 5 & 6) and St8F4/*scy-filP::aac(3)IV* (Lanes 7 & 8).

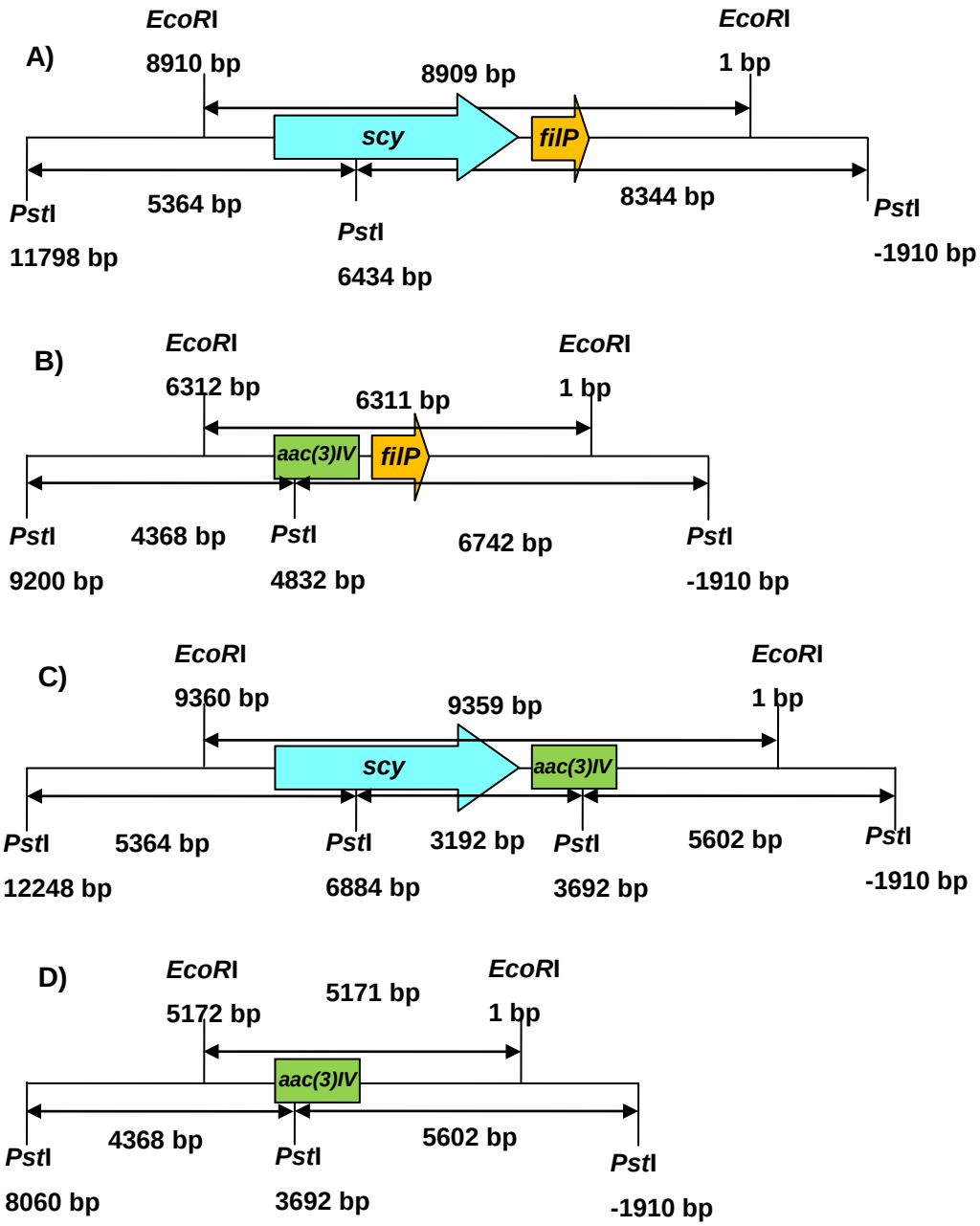

Figure 128: A) Restriction patterns for *Eco*RI and *Pst*I on the relevant sections of (A) the St8F4 cosmid, (B) the cosmid with *scy::aac(3)IV*, (C) the cosmid with *filP::aac(3)IV* and (D) the cosmid with the cosmid with *scy-filP::aac(3)IV*. The numbers at restriction sites were a calculated with 1bp being the 1st nucleotide of the *S. coelicolor* chromosomal DNA insert in St8F4.

The expected sizes of the DNA fragments after for *Eco*RI and *Pst*I restriction digestions of the cosmid DNA, in the region of the *scy* and *filP* genes, is shown in Figure 128. The *Eco*RI digestion shows a reduction in the size of the *Eco*RI fragment containing the *scy/filP* alleles for both the St8F4/*scy::aac(3)IV* and the St8F4/*scy-filP::aac(3)IV* knockout cosmids. For the St8F4/*filP::aac(3)IV* cosmid the small change in size of the *Eco*RI fragment from the wild-type is not detectable, in order to confirm this disruption cosmid the *Pst*I digest is more diagnostic. For St8F4/*filP::aac(3)IV* cosmid it appears that the 8344bp wild-type fragment in St8F4 has been replaced by two fragments of the expected size ranges of 5602bp and 3192bp. The comparison of the restriction patterns of the generated cosmids and the sizes, expected from the genome sequence data confirms that the disruption cassettes have been successfully introduced to the St8F4 cosmid and we successfully generated the mutant alleles in *E. coli*.

10.1.45 Introduction of the knockout cosmids into S. coelicolor

Streptomyces can not readily be transformed by electroporation, protoplast transformation can be used, however, conjugation is much more efficient (Matsushima *et al.*, 1994). Due to *S. coelicolor's* intrinsic methyl-specific restriction endonuclease system a non-methylating strain such as *E. coli* ET12567 (MacNeil *et al.*, 1992) is needed for successful passage of the DNA from *E. coli* to *Streptomyces* via conjugation. For conjugation *E. coli* ET12567 must also contain a plasmid, pUZ8002, which can mobilise vectors containing *oriT in trans*. Each of the mutant cosmids generated were moved first into *E. coli* ET12567/pUZ8002 cells. To select for transformants containing the disruption cosmid, cells were grown on plates also containing apramycin. Then from *E. coli* ET12567/pUZ8002 the cosmids were mobilised into *S. coelicolor* M145 by conjugation. The exconjugants were selected using apramycin (for the mutant cosmid) and nalidixic acid (for the elimination of *E. coli*).

The cosmid used cannot replicate in *S. coelicolor*, therefore the only way possible to generate an apramycin resistant colony is by the cosmid undergoing homologous recombination with the chromosomal DNA. However, this can result in two outcomes, a single recombination event can result in the incorporation of the whole cosmid DNA carrying the mutant allele into the chromosome maintaining an intact copy of the gene as well as the apramycin cassette; whereas, a second recombination event on the adjacent side of the apramycin cassette will result in the replacement of the gene with the apramycin

cassette which will be now positioned at the locus of the knocked out gene. As the cosmid also carries a *neo* gene outside of the *S. coelicolor* DNA sequences, a single crossover colony will produce kanamycin resistant colonies whereas a double crossover will generate kanamycin sensitive colonies. Therefore, plates carrying the exconjugants were replica plated onto LB medium containing kanamycin and apramycin, respectively. The medium also contained nalidixic acid to prevent the growth of *E. coli*. These plates were grown at 30°C for 2 days. Colonies that grew on apramycin plates but failed to grow on kanamycin plates were of interest as these were the colonies where double crossovers had occurred.

After replica plating we identified 3 *scy::aac(3)IV* mutants, 3 *filP::aac(3)IV* mutants and 3 *scy-filP::aac(3)IV* double mutants. Each colony was streaked onto SFM plates containing apramycin and nalidixic acid. These were incubated for 5 days at 30°C, then were replica plated again to confirm that they were kanamycin sensitive and apramycin resistant. A number of the plates contained heterogenous looking populations that were heterogenous in sensitivity to kanamycin. This can be explained by the ease of contamination with spores of single crossover strains. One *filP::aac(3)IV* knockout was confirmed to be false. However, all the others appeared to have likely double crossovers that were apramycin resistant and kanamycin sensitive. From the SFM plates that were screened with replica plating, a single colony was picked and used to make spore preparations, this enabled the strains to be stored at -20°C.

Introduction of the apramycin cassette to a gene can result in polar effects on downstream genes. The *aac(3)IV* marked cosmids were then used by the Kelemen lab (M. Gillespie) so that taking advantage of the FLP recognition target sequences, FLP recombinase was used to remove the apramycin cassette from the disruption cosmids. This generated an 81bp fragment encoding a 28 amino-acid “scar”. The removal of the apramycin cassette also removed *oriT* that is required for conjugation. The *aac(3)IV* cassette and *oriT* was reintroduced into the cosmid by replacing the ampicillin resistance gene. The resulting cosmids carrying the unmarked mutant alleles were then introduced into the *aac(3)IV* marked *Streptomyces* strains, whereby the flanking sequences to the “scar” could undergo recombination and double crossover events lead to an unmarked knockout mutant where the previous *aac(3)IV* cassette was “flipped” out. This generated a non-polar mutation and enabled further use of apramycin resistance for future knockouts or genetic alterations. The unmarked and “non-polar” mutants which are used for phenotypic studies are hence forth designated *scy* (K112), *filP*, and *scy-filP*.

10.1.46 Generation of a Scy N-terminal EGFP translational fusion

To establish the localisation of Scy we aimed to generate an N-terminal translational EGFP-Scy fusion. However, an *egfp-scy* fusion had previously been generated in the plasmid pCJW93-egfp-scy (Hunter and Kelemen unpublished)(Figure 129). This is a derivative of the multicopy vector pCJW93 (Wilkinson *et al.*, 2002) whereby an *egfp-scy* fusion is driven by the thiostrepton inducible promoter *PtipA* (Murakami *et al.*, 1989). The fusion sequence was constructed so that the 3' end of the *egfp* sequence lacks a stop codon and reads into a linker with the amino acid sequence Tyr-Asn-Gly-Gly-Gly-Gly-Gly in frame to the 5' of *scy*, whereby the first codon of *scy* has been swapped from GTG to ATG (Figure 129B). As this fusion is driven by a thiostrepton inducible promoter in a high copy number vector we decided that it would be more suitable to study the localisation of Scy when a single copy of *egfp-scy* was driven by its native promoter sequence.

To deliver this construct we chose an integrative plasmid pIJ8660 (Sun *et al.*, 1999) which as discussed earlier is able to be passeged into *Streptomyces* species through conjugation from *E. coli ET* 12567/pUZ8002 via *oriT*. The strategy was to PCR amplify the *scy* promoter sequence, cloning this into pIJ8660.The *egfp-scy* fusion would then be moved downstream of the *scy* promoter allowing it to be under the direct transcriptional regulation of the *scy* promoter. The *scy* promoter sequence was amplified from *S. coelicolor* M145 chromosomal DNA using the oligonucleotides scyprom3-Nde and scyprom4-Bam generating a 385bp product that contained the whole intergenic region between *scy* and *sco5398*. This PCR product was then treated with the Klenow fragment of DNA polymerase to generate blunt ends and the fragment was cloned into the *Eco*RV site of vector pIJ8660 (Figure 130). The DNA fragments used in the ligation to generate pIJ8660-Pscy can be seen in Figure 131B. After ligation of the fragments the ligation mixture was used for transformation of *E. coli* strain DH5α. The transformants were screened with colony PCR (Figure 131D) to find potential clones where the fragment containing the *scy* promoter was cloned in the correct direction to *egfp*, positive colonies were predicted to produce a ~750bp product. Plasmid DNA was then isolated from positive colonies, isolated DNA was confirmed by restriction digestion (Figure 131C) to liberate a small *Bgl*II fragment approximately 422bp in size. Sequencing was also used to verify that the *scy* promoter had indeed been cloned into pIJ8660. Therefore, confirming the product generated was the plasmid pIJ8660-Pscy, with the *scy* promoter upstream of *egfp*.

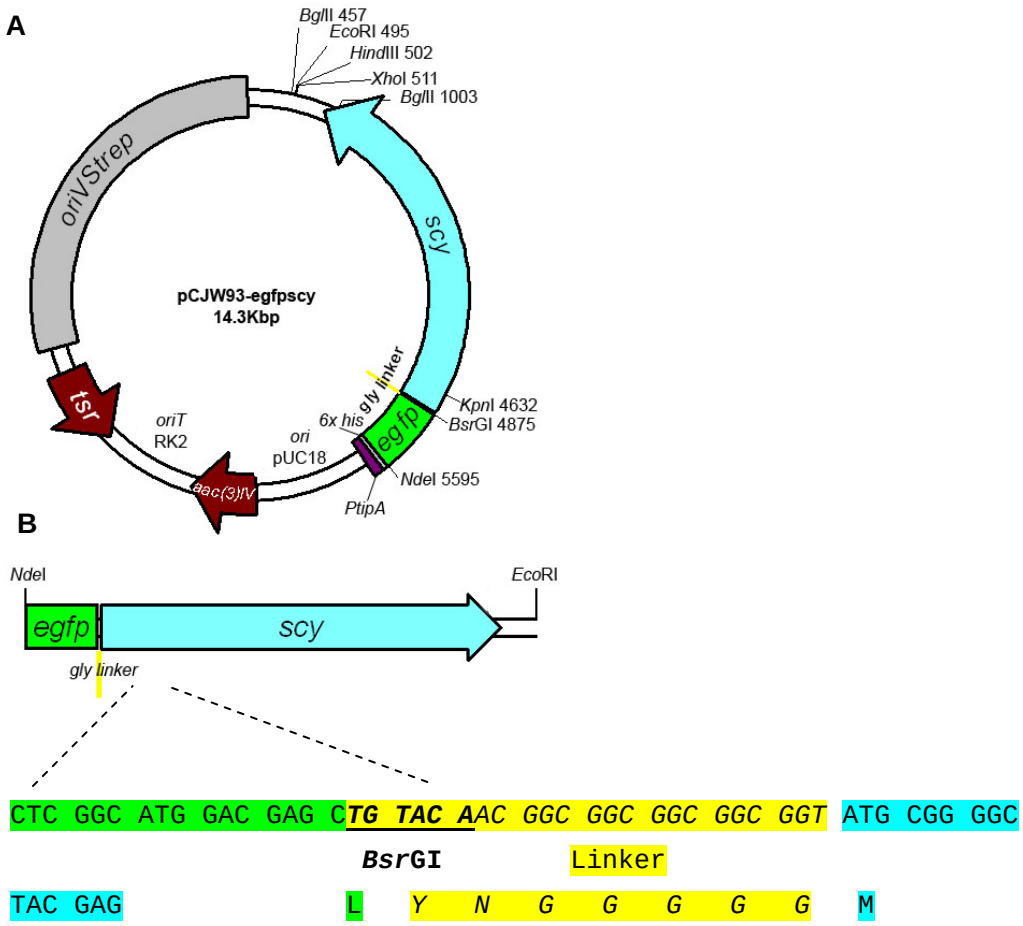

Figure 129: pCJW93-egfp-scy encodes an EGFP-Scy fusion driven by a thiostrepton inducible promoter in a multicopy plasmid.

A) The map of pCJW93-egfp-scy including restriction sites, antibiotic resistance genes, origins of replication and an inducible promoter sequence.

B) Sequence of the junctions between *egfp* and *scy*. The *egfp-scy* junction contains a glycine linker originally generated by annealing the oligonucleotides Linker 1 and Linker 2 (highlighted yellow/italics). Restriction site sequences are bold and underlined. The *scy* sequences are highlighted light blue and *egfp* is highlighted green.

An *Nde*I site corresponding with the translational start point of *egfp* and an *Eco*RI site at the end of the open reading frame of *scy* were used as restriction sites to lift the *egfp-scy* 5.1kb fragment from pCJW93-egfp-scy into the same sites in pIJ8660-Pscy (Figure 130). The DNA fragments used in the ligation can be seen in Figure 132B & C. After ligation of the fragments the ligation mixture was used for transformation of *E. coli* strain DH5α. The transformants were screened with colony PCR (Figure 132E) to find potential clones where the fragment containing *egfp-scy* was cloned downstream to the *scy* promoter, positive colonies were predicted to produce a ~750bp product. The primers used, however, would not be able to differentiate between clones with *egfp-scy* or just *egfp* as was found in pIJ8660-Pscy, though it is assumed that the digestion of pIJ8660-Pscy was complete and

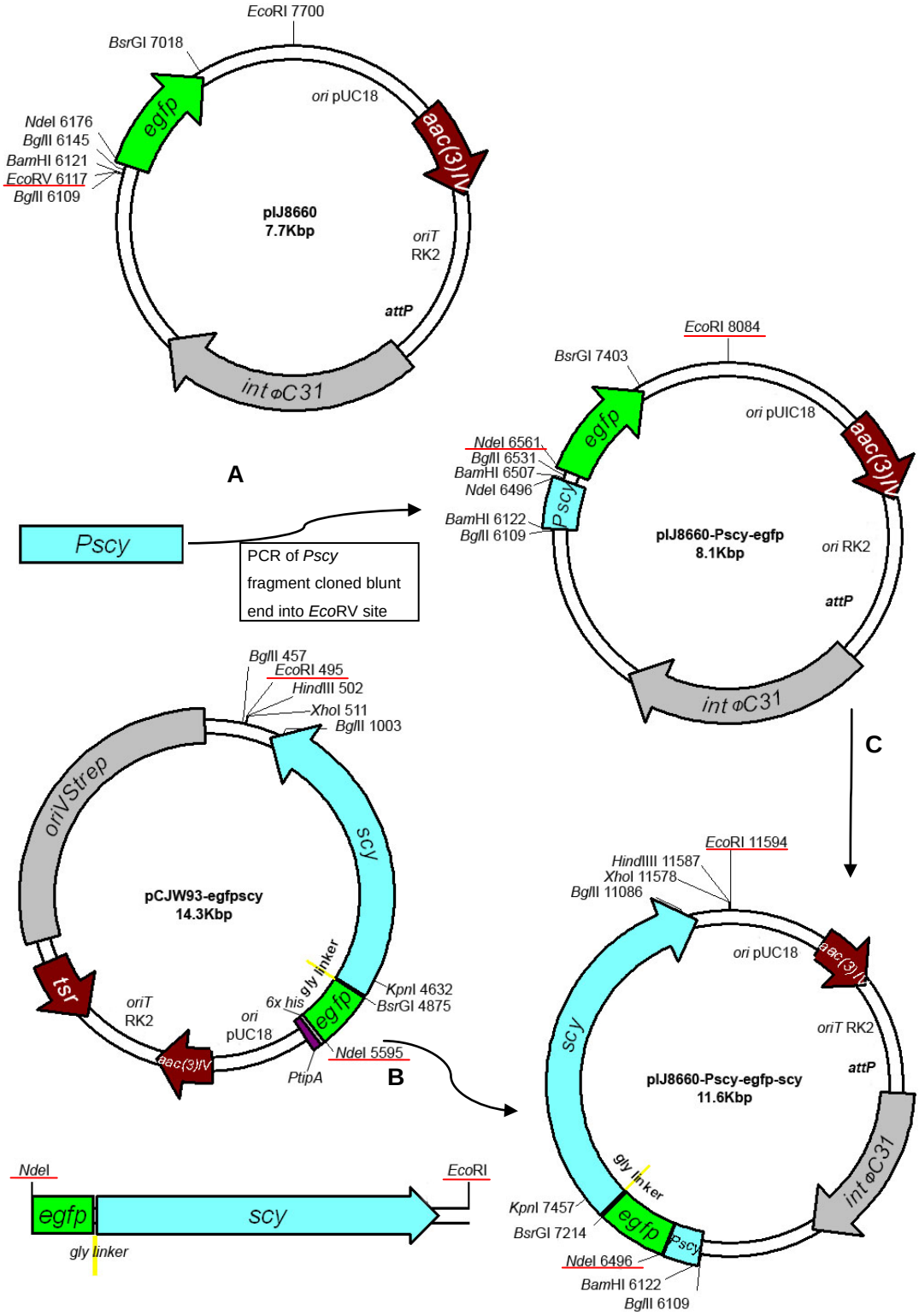

Figure 130: Generation of pIJ8660-Pscy and pIJ8660-Pscy-egfp-scy.

A) pIJ8660-Pscy is a pIJ8660 derivative containing a *Pscy* PCR fragment cloned blunt end into the *Eco*RV. B) An *egfp-scy* fragment was liberated using *Nde*I and *Eco*RI from pCJW93-egfp-scy. C) Using the enzymes *Nde*I and *Eco*RI pIJ8660-Pscy was digested and the *egfp-scy* fragment cloned so that it was put under the direction of the *Pscy* fragment. The restriction sites used in the cloning are underlined in red.

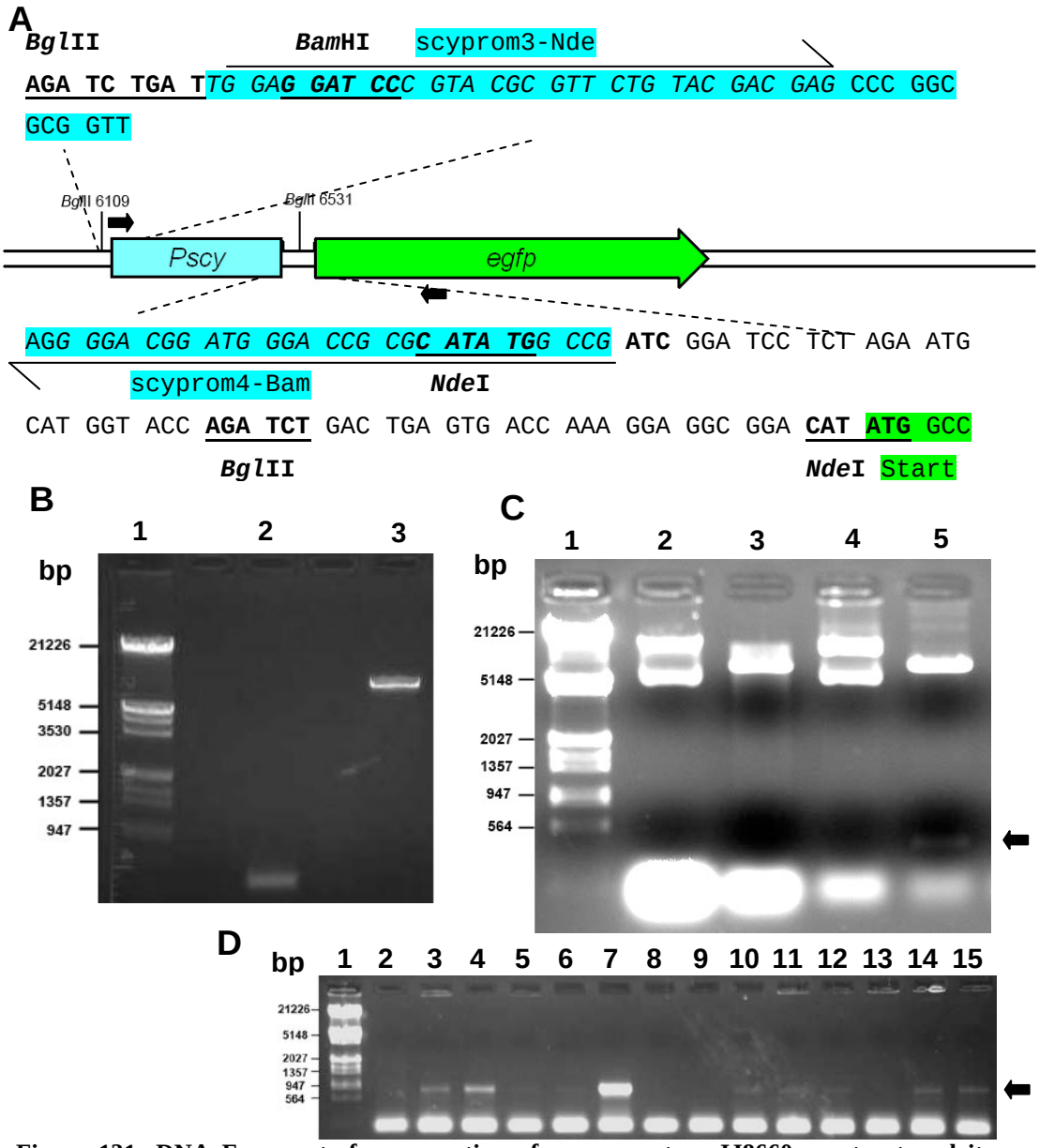

Figure 131: DNA Fragments for generation of *scy* promoter pIJ8660 construct and its confirmation by restriction digests.

A) pIJ8660-Pscy. Sequence of the junctions between the blunt ended PCR product of the *scy* promoter cloned into the *Eco*RV site of pIJ8660. Restriction site sequences are bold and underlined. Primer sequences are marked in italics and with arrows. The *Pscy* sequences are highlighted light blue and *egfp* is highlighted green. Primers for colony PCR are marked (black arrows).

B) The gel isolated fragments used for construction of pIJ8660-Pscy were analysed on a 0.7% agarose gel. The fragments used were the Klenow treated PCR fragment containing *Pscy* (Lane 2) and an EcoRV fragment of pIJ8660 (Lane 3). The DNA size marker is Lambda *Hind*III/*Eco*RI (Lane 1).

C) The plasmids pIJ8660 (Lanes 2 & 3) and the plasmid pIJ8660-Pscy (Lanes 4 & 5) were analysed on a 1% agarose gel. Undigested samples (Lanes 2 & 4) were run together with samples digested with *Bgl*II (Lanes 3 & 5). The arrow indicates the 422bp fragment carrying the *scy* promoter. The DNA size marker is Lambda *Hind*III/*Eco*RI (Lane 1).

D) Candidate colonies were screened with colony PCR using scyprom4-Bam (Upstream) and EGFPseq (downstream) primers and PCR products were analysed on a 1% agarose gel. The plasmid pIJ8660 was used as a control template (Lane 2). Candidate colonies are shown Lanes 3-15. The arrow indicates the ~750bp PCR product expected. The DNA size marker is Lambda *Hind*III/*Eco*RI (Lane 1).

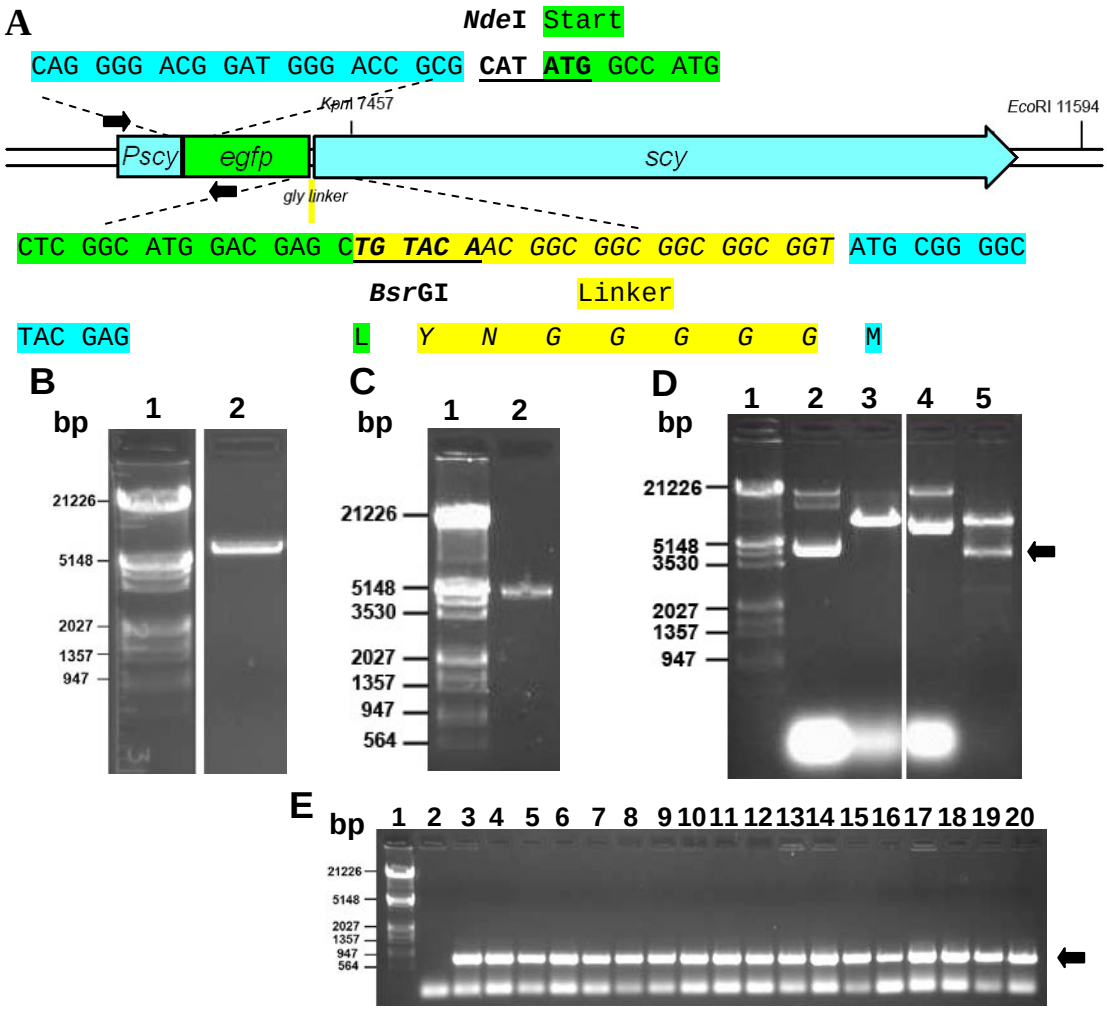

Figure 132: DNA Fragments for generation of an EGFP-Scy fusion construct and its confirmation by restriction digests.

A) pIJ8660-Pscy-egfp-scy. Sequence of the junctions between the *scy* promoter, *egfp* and *scy*. The *egfp-scy* junction contains a glycine linker originally generated by annealing the oligonucleotides Linker 1 and Linker 2 (highlighted yellow/italics). Restriction site sequences are bold and underlined. The *Pscy* and *scy* sequences are highlighted light blue and *egfp* is highlighted green. Primers for colony PCR are marked (black arrows).

B) The gel isolated *Nde*I/*Eco*RI fragment of pIJ8660-Pscy used for construction of pIJ8660-Pscy-egfp-scy was analysed on a 0.7% agarose gel (Lane 2). The DNA size marker is Lambda *Hind*III/*Eco*RI (Lane 1).

C) The gel isolated *Nde*I/*Eco*RI fragment containing *egfp-scy* used for construction of pIJ8660-Pscy-egfp-scy was analysed on a 0.7% agarose gel (Lane 2). The DNA size marker is Lambda *Hind*III/*Eco*RI (Lane 1).

D) The plasmids pIJ8660-Pscy (Lanes 2 & 3) and the plasmid pIJ8660-Pscy-egfp-scy (Lanes 4 & 5) were analysed on a 0.7% agarose gel. Undigested samples (Lanes 2 & 4) were run together with samples digested with *Kpn*I and *Eco*RI (Lanes 3 & 5). The arrow indicates the 4137bp fragment carrying part of *scy*. The DNA size marker is Lambda *Hind*III/*Eco*RI (Lane 1).

E) Candidate colonies were screened with colony PCR using scyprom4-Bam (Upstream) and EGFPseq (downstream) primers and PCR products were analysed on a 0.7% agarose gel. Candidate colonies are shown Lanes 2-20. The arrow indicates the ~750bp PCR product expected. The DNA size marker is Lambda *Hind*III/*Eco*RI (Lane 1).

the PCR was able to differentiate between possible ligation of the vector fragments with and without the fragment containing *egfp-scy*. Plasmid DNA was then isolated from positive colonies, isolated DNA was confirmed by restriction digestion (Figure 132D) to liberate a large *Kpn*I/*Eco*RI fragment approximately 4137bp in size containing the C-terminal of *scy*. Sequencing was also used to verify the junctions between the *scy* promoter and between *egfp* and *scy*. Thus, confirming the generation of pIJ8660-Pscy-egfp-scy (pK56) with the *egfp-scy* fusion sequence directly regulated under the native *scy* promoter sequence.

10.1.47 Generation of a Scy N-terminal mCherry translational fusion

To establish the localisation of Scy with a different fluorescent tag, with a different tag it was sought to generate an N-terminal fusion of *scy* to *mCherry*, similar to the construct pIJ8660-Pscy-egfp-scy (pK56). An *mCherry-scy* fusion had previously been generated in the vector pIJ6902-mCherry-scy (Gillespie and Kelemen unpublished)(Figure 133). This is a derivative of the integrative vector pIJ6902 (Huang *et al.*, 2005) whereby an *mCherry-scy* fusion is driven by the thiostrepton inducible promoter *PtipA* (Murakami *et al.*, 1989). The *mCherry* fusion sequence was generated by simply replacing the *egfp* in the *egfp-scy* fusion from pCJW93-egfp-scy sequence with *mCherry* using the restriction enzymes *Nde*I and *Bsr*GI. This means that the 3' end of the *mCherry* sequence lacks a stop codon and reads into a linker with the amino acid sequence Tyr-Asn-Gly-Gly-Gly-Gly-Gly in frame to the 5' of *scy* similarly starting with an ATG codon instead of a GTG (Figure 133B). The vector pIJ6902 due to the *Φ*C31 attP and integrase found on this plasmid, it is only contained as a single copy on the chromosome. However, the *mCherry-scy* fusion in pIJ6902-mCherry-scy is driven by a thiostrepton inducible promoter, so we decided that it would be more suitable to study the localisation of Scy when *mCherry-scy* was driven by its native promoter sequence.

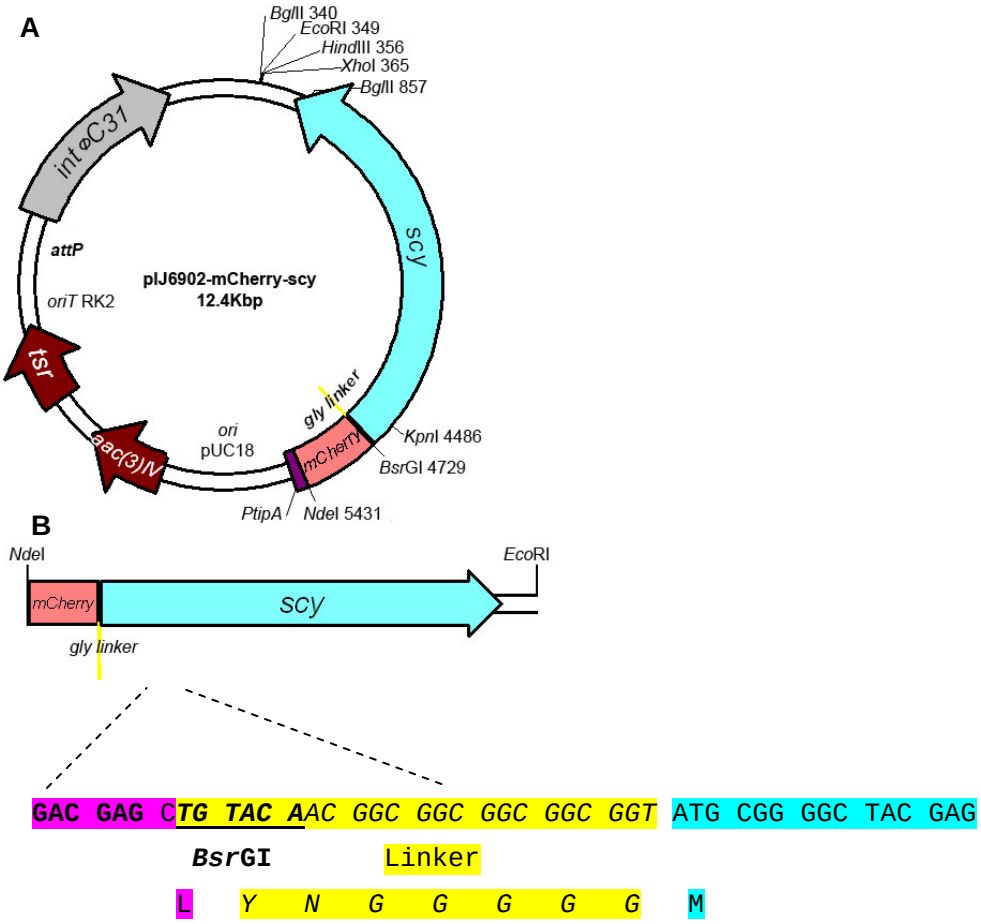

Figure 133: pIJ6902-mCherry-scy encodes an *mCherry-scy* fusion driven by a thiostrepton inducible promoter in a multicopy plasmid.

A) The map of pIJ6902-mCherry-scy including restriction sites, antibiotic resistance genes, origins of replication and an inducible promoter sequence.

B) Sequence of the junctions between *mCherry* and *scy*. The *mCherry-scy* junction contains a glycine linker originally generated by annealing the oligonucleotides Linker 1 and Linker 2 (highlighted yellow/italics). Restriction site sequences are bold and underlined. The *scy* sequences are highlighted light blue and *mCherry* is highlighted pink.

To generate an N-terminal *mCherry* fusion to *scy* driven by the native *scy* promoter we choose a strategy to move a fragment containing *mCherry-scy* to our previously generated pIJ8660-Pscy plasmid. Similarly to *egfp-scy* an *Nde*I site at the start of *mCherry* and an *Eco*RI site at the end of *scy* were used as restriction sites to lift the 5.1kb fragment containing the *mCherry-scy* sequence into the same sites in pIJ8660-Pscy (Figure 134). The DNA fragments used in the ligation can be seen in Figure 135B. After ligation of the fragments the ligation mixture was used for transformation of *E. coli* strain DH5α. The transformants were screened with colony PCR (Figure 135D) to find potential clones where the fragment containing *mCherry-scy* was cloned downstream to the *scy* promoter, positive colonies were predicted to produce a ~1300bp product. Plasmid DNA was then

isolated from positive colonies, isolated DNA was confirmed by restriction digestion (Figure 135C) to liberate a large *Kpn*I/*Eco*RI fragment approximately 4137bp in size containing the C-terminal of *scy*. Sequencing was also used to verify the junctions between the *scy* promoter and between *mCherry* and *scy*. Thus, confirming the generation of pIJ8660-Pscy-mCherry-scy (pK57) with the *mCherry-scy* fusion sequence directly regulated under the native *scy* promoter sequence.

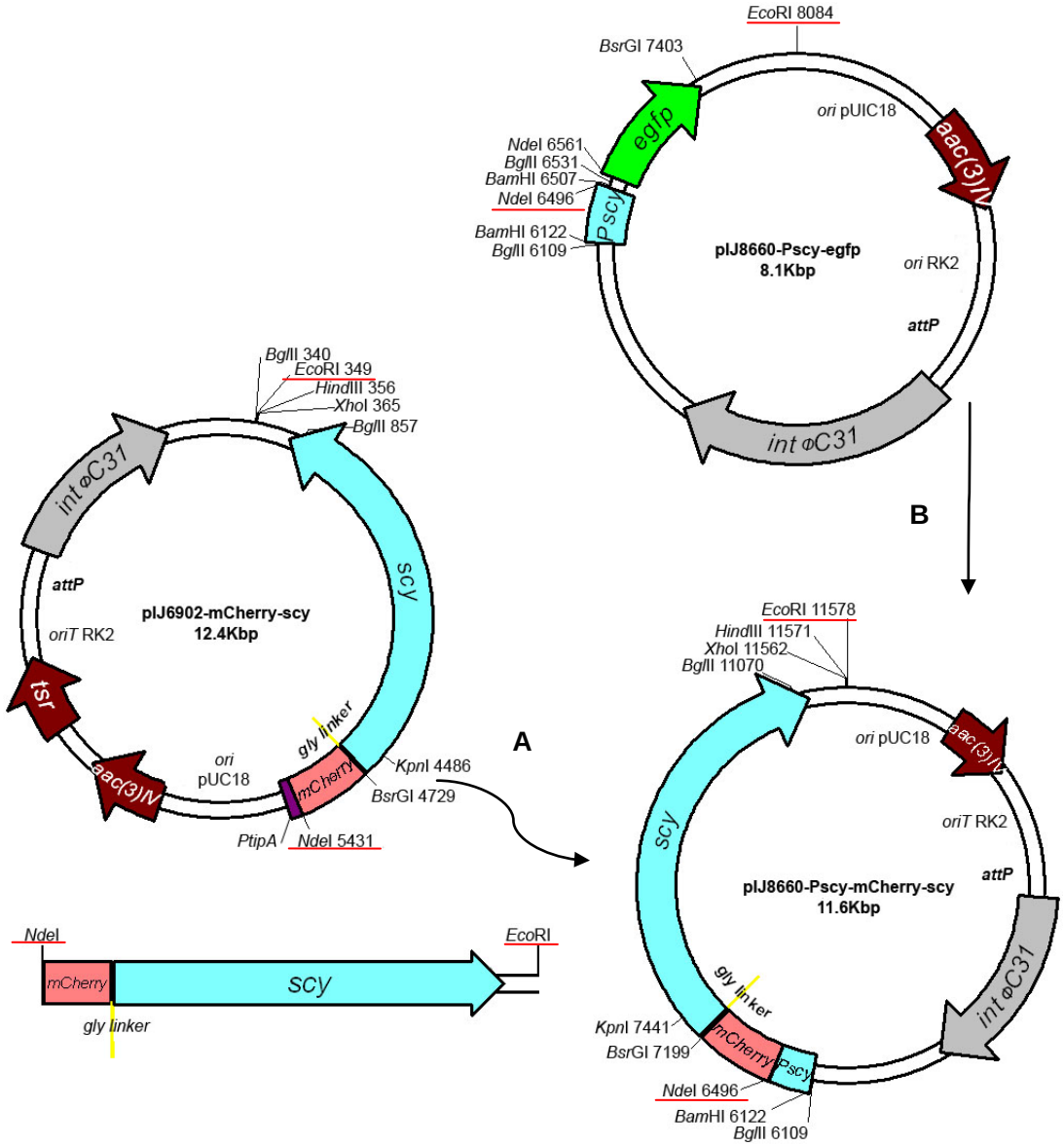

Figure 134: Generation of pIJ8660-Pscy-mCherry-scy.

pIJ8660-Pscy-mCherry-scy is a derivative of pIJ8660-Pscy. A) An *mCherry-scy* fragment was liberated using *Nde*I and *Eco*RI from pIJ6902-mCherry-scy. B) Using the enzymes *Nde*I and *Eco*RI pIJ8660-Pscy was digested and the *mCherry-scy* fragment cloned so that it was put under the direction of the *Pscy* fragment. The restriction sites used in the cloning are underlined in red.

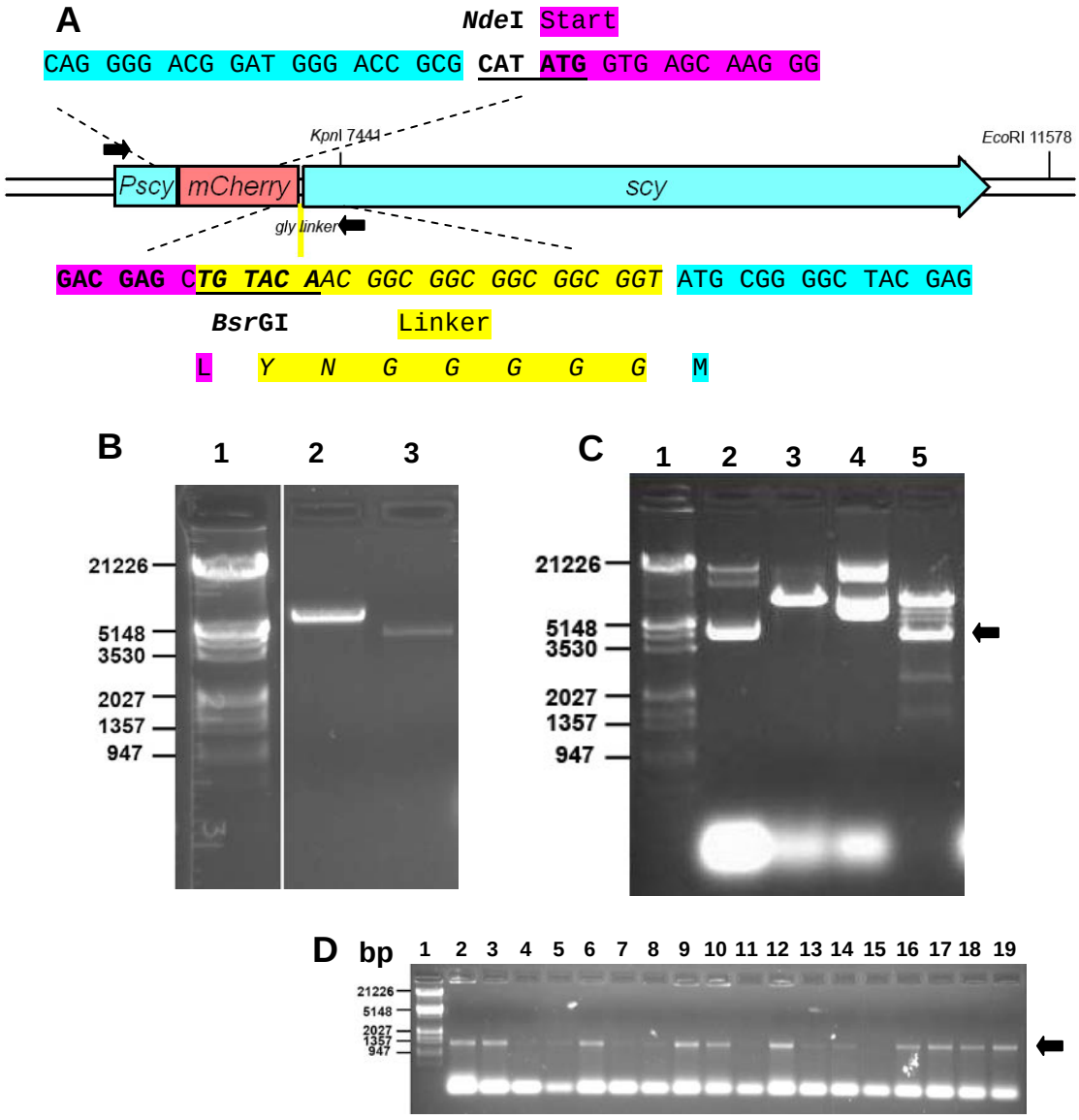

Figure 135: DNA Fragments for generation of an mCherry-Scy fusion construct and its confirmation by restriction digests.

A) pIJ8660-Pscy-mCherry-scy. Sequence of the junctions between the *scy* promoter, *mCherry* and *scy*. The mCherry-scy junction contains a glycine linker originally generated by annealing the oligonucleotides Linker 1 and Linker 2 (highlighted yellow/italics). Restriction site sequences are bold and underlined. The *Pscy* and *scy* sequences are highlighted light blue and *mCherry* is highlighted pink. Primers for colony PCR are marked (black arrows).

B) The gel isolated fragments used for construction of pIJ8660-Pscy-mCherry-scy were analysed on a 0.7% agarose gel. The fragments used were an *Nde*I/*Eco*RI fragment of pIJ8660-Pscy (Lane 2) and an *Nde*I/*Eco*RI fragment containing *mCherry-scy* (Lane 3). The DNA size marker is Lambda *Hind*III/*Eco*RI (Lane 1).

C) The plasmids pIJ8660-Pscy (Lanes 2 & 3) and the plasmid pIJ8660-Pscy-mCherry-scy (Lanes 4 & 5) were analysed on a 0.7% agarose gel. Undigested samples (Lanes 2 & 4) were run together with samples digested with *Kpn*I and *Eco*RI (Lanes 3 & 5). The arrow indicates the 4137bp fragment carrying part of *scy*. The DNA size marker is Lambda *Hind*III/*Eco*RI (Lane 1).

D) Candidate colonies were screened with colony PCR using scyprom4-Bam (Upstream) and scyKpn2 (downstream) primers and PCR products were analysed on a 1% agarose gel. Candidate colonies are shown Lanes 2-19. The arrow indicates the ~1300bp PCR product expected. The DNA size marker is Lambda *Hind*III/*Eco*RI (Lane 1).

10.1.48 Generation of a Scy C-terminal EGFP translational fusion

To further verify the localisation of Scy we aimed to generate a C-terminal translational Scy-EGFP fusion. In order to be able to do this we needed to use an already generated vector, pAZ1 (Kelemen Lab, University of East Anglia)(Figure 136). The vector

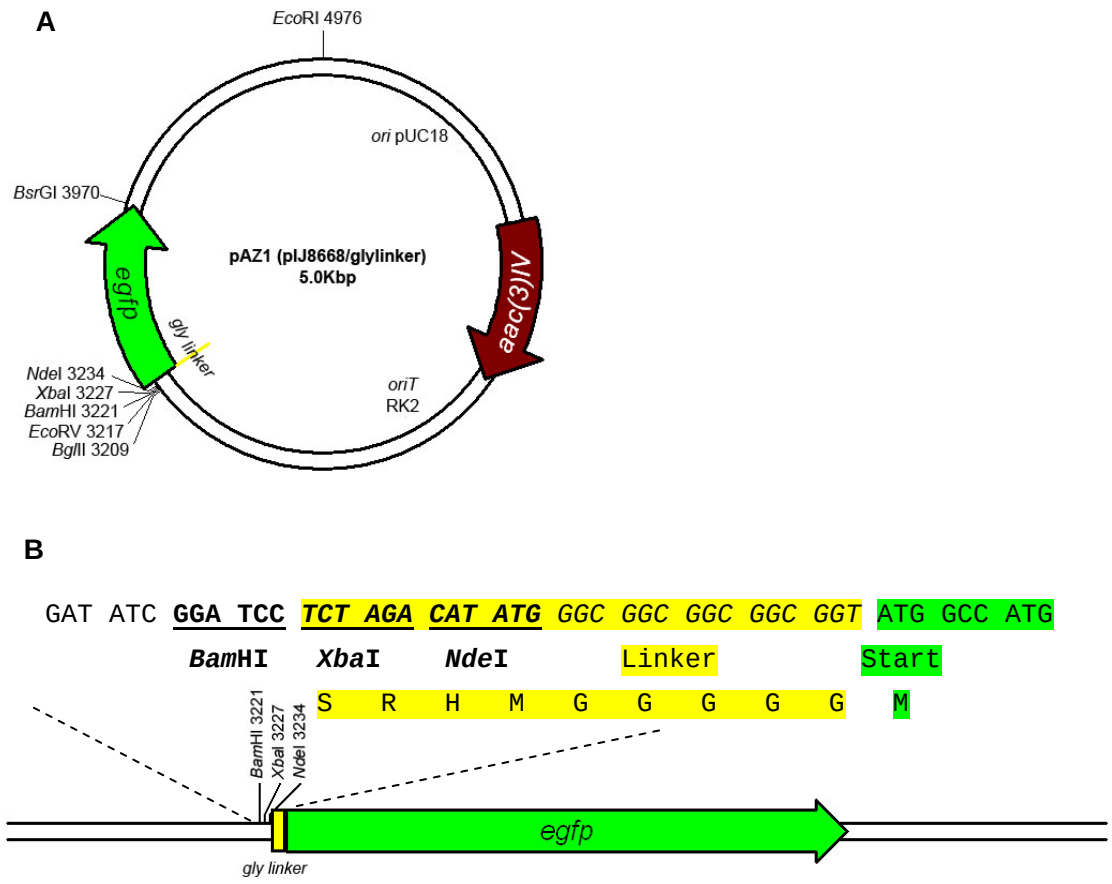

Figure 136: pAZ1 is a vector with egfp downstream of a multiple cloning site and a glycine linker.

A) The map of pAZ1 including restriction sites, antibiotic resistance genes, origins of replication and a glycine linker.

B) Sequence of the linker and *egfp* in pAZ1. The glycine linker was originally generated by annealing the oligonucleotides EGFPLinker1 and EGFPLinker2 (highlighted yellow/italics). Restriction site sequences are bold and underlined. The *egfp* sequence is highlighted green.

pAZ1 is a derivative of pIJ8668 (Sun *et al.*, 1999) containing a linker made by annealing EGFPLinker1 and EGFPLinker2 and placing these between the *Bam*HI and *Nde*I sites of *egfp* in pIJ8668. This linker deleted the *NdeI* site of *egfp* and adds an additional *NdeI* site

followed by a linker encoding the amino acid sequence Ser-Arg-His-Met-Gly-Gly-Gly-Gly-Gly in frame to the 5' of *egfp* (Figure 136B). Thus, meaning that pAZ1 is ideal for generating C-terminal fusions to EGFP. The strategy to be able to generate a Scy C-terminal fusion to EGFP was obviously complicated by the need to remove the stop codon of *scy* so that it would be able to read into *egfp*. So to be able to remove the stop codon from *scy*, it was planned to PCR amplify the end of *scy* removing the stop codon and cloning it into pAZ1. To generate a full length *scy-egfp* fragment, the C-terminal *scy* fragment fused to *egfp* would be lifted to pIJ8660, therefore allowing the use in a vector able to integrate into the *S. coelicolor* chromosome. Then, the remainder of *scy* and the *scy* promoter could be subcloned upstream of the fragment in pIJ8660, making a full length fusion with the means to be driven by the native promoter.

It was aimed that the last 1001bp of *scy* would be amplified using the primers scy-Bam and scy-Nde. The primer scy-Nde would anneal to the C-terminal of *scy* and remove the stop codon and add an *NdeI* site making it possible to fuse *scy* in frame to *egfp* in the vector pAZ1. The primer scy-Bam introduces a *BamHI* site so that the PCR product could be digested with *Bam*HI and *Nde*I for directional cloning (Figure 139). The template used was a *scy* linear fragment from pCJW93-egfp-scy (Figure 132C). For efficient screening for the detection of mutations the PCR product was first cloned via *Bam*HI and *Nde*I into pUC18, facilitating blue/white selection for plasmids carrying inserts (Figure 137A & Figure 138). After ligation of the fragments the ligation mixture was used for transformation of *E. coli* strain DH5α. Plasmids from successful white colonies were screened with colony PCR (Figure 138D) to find potential clones where the a fragment containing *scyCterm* was cloned into pUC18, positive colonies were predicted to produce a ~1000bp product. Plasmid DNA was then isolated from positive colonies, isolated DNA was confirmed by restriction digest (Figure 138C) to liberate a small *Bam*HI/*Nde*I fragment, yet it appeared at this stage that it might be slightly smaller than the ~1000bp predicted product. Several candidate clones were analysed by sequencing from the multiple cloning site of pUC18 using the pUC18 reverse primer. However, it was continuously found that there was a large deletion of part of the sequence and also point mutations (Figure 137B), these observations are not abnormal as generating PCR products of GC rich sequences such as those in *S. coelicolor* is technically challenging. Not shown here, but the Kelemen lab has had numerous attempts of PCR with High Fidelity Taq Polymerases. As well the PCR shown here was also tried with Roche Applied Science Expand High Fidelity Taq Polymerase (Cat. No. 11 732 641 001), use of High Fidelity Taq also generated mutations in this

A

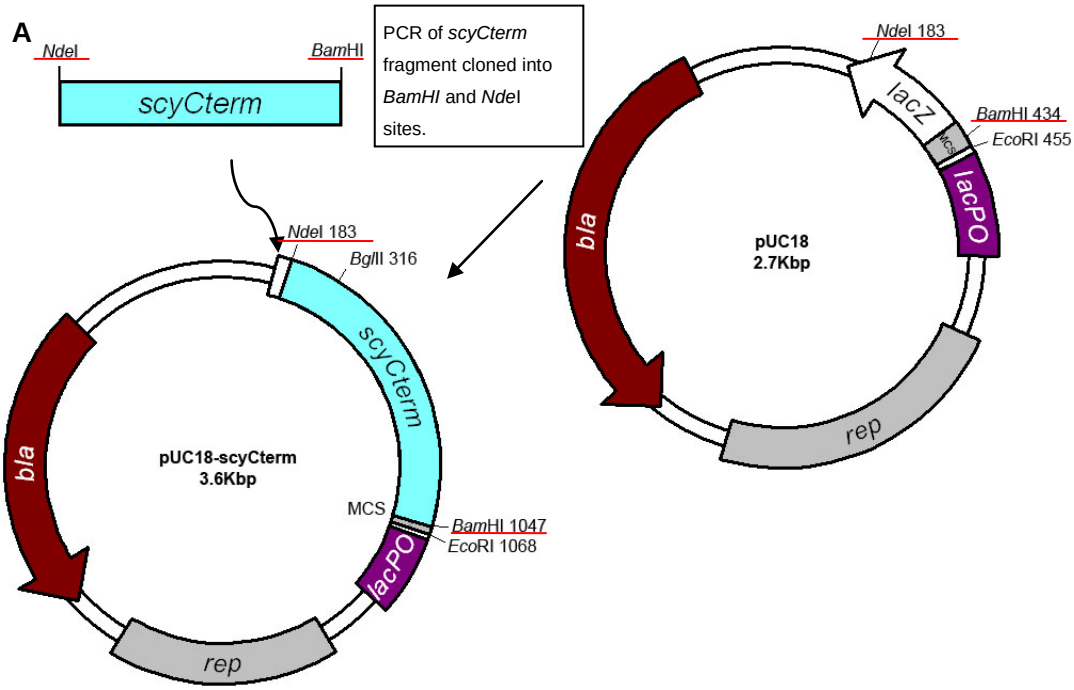

B

***Bam*HI** scy-Bam Deletion

GGATCC*GCCAGCAGCTGGTCTCGGACG*GCACCGGGGAGGCGGAGCGGCT→GCGGGCCGAGG

CCGCCGACACCGTCGGCTCCGCGCAGCAGCACGCCGAGCAGGTCGACACGCTCATCACGGAG

ACCGCCGCCGAGGCCGACAAGCTGCTCACCGAGGCTCAGCAGCAGGCCCAGAAGACCACCGC

GGACGCCGAGTCGCAGGTCGACACGATGGTCGGCGCGGCCCGCTCGGAGGCCGACCGGATCG

TCCAGGAGGCGACGGTCGAGGGCAACACCCGGGTGGAGAAGGCCCGTACGGACGCGGACGAG

CTGCTGGTCGGCGCCCGCCGGGACGCGACCGCCATAAGGGAGCGCGCGGAGGAGCTGCGCGA

GCGGCTCACCTCCGAGATCGAGGAGCTGCACGAGCGGGCCCGCCGCGAGGCCGCCGAGACGA

TGAAGTCGGCCGGCGACCGCTGCGACGCGCTCATCAAGGCCGCCGAGGAGCAGCTCGCCAAG

GCGGAGGCGAAGGCGAAGGAGCTGGTGTCGGAGGCCAACTCCGAGGCCGGCAAGGTGCGCAT

CGCCGCCGTCAAGAAGGCCGAGGGGCTGCTCAAGGAGGCCGAGCAGAAGAAGGCCACCCTGG

TCCGCGAGGCCGAGGAGCTGAAGGCCGAGGCGGTCCGCGAGGCCCGGGCCACGGTCGACGAG

GGCAAGCGCGAGCTGGAGGTGCTGGTCCGGCGCCGCGAGGACATCAACGCGG**AGATCT**CCCG

***Bgl*II**

GGTCCAGGACGTGCTGGAGGCGCTGGAGTCGTTCGAGGCGCCCGGGGGTGCGAAGGACAACG

GGGTGAAGGCCGGAGCGACGGTGGGCGCCCCACGTTC*GGGTGGCAAGTCGTCAGACGGC****CAT***

scy-Nde ***Nde*I**

ATG

Figure 137: Generation of pUC18-scyCterm

A) pUC18-scyCterm is a derivative of pUC18 containing the 864bp *scyCterm* PCR product cloned using *Bam*HI and *Nde*I. The restriction sites used in the cloning are underlined in red.

B) The sequence of the 864bp *scyCterm* PCR product generated using the primers scy-Nde and scy-Bam. Primer sequences are marked in italics and with arrows. Restriction site sequences are bold and underlined. The *scyCterm* sequences are highlighted light blue. "→" marks a deletion produced during the PCR.

sequence (~2/1000 bases) as well as others attempted in the Kelemen lab. Suggesting that even High Fidelity Taq polymerases can also have problems with the integrity with high percentage GC sequences. However, despite the mutations found with Go Taq® Polymerase, in the identified clone shown there is a *Bgl*II site at the end of *scy* and the C-terminal sequence to this site had no mutations (Figure 137B) making the selected clone useful for later steps of cloning.

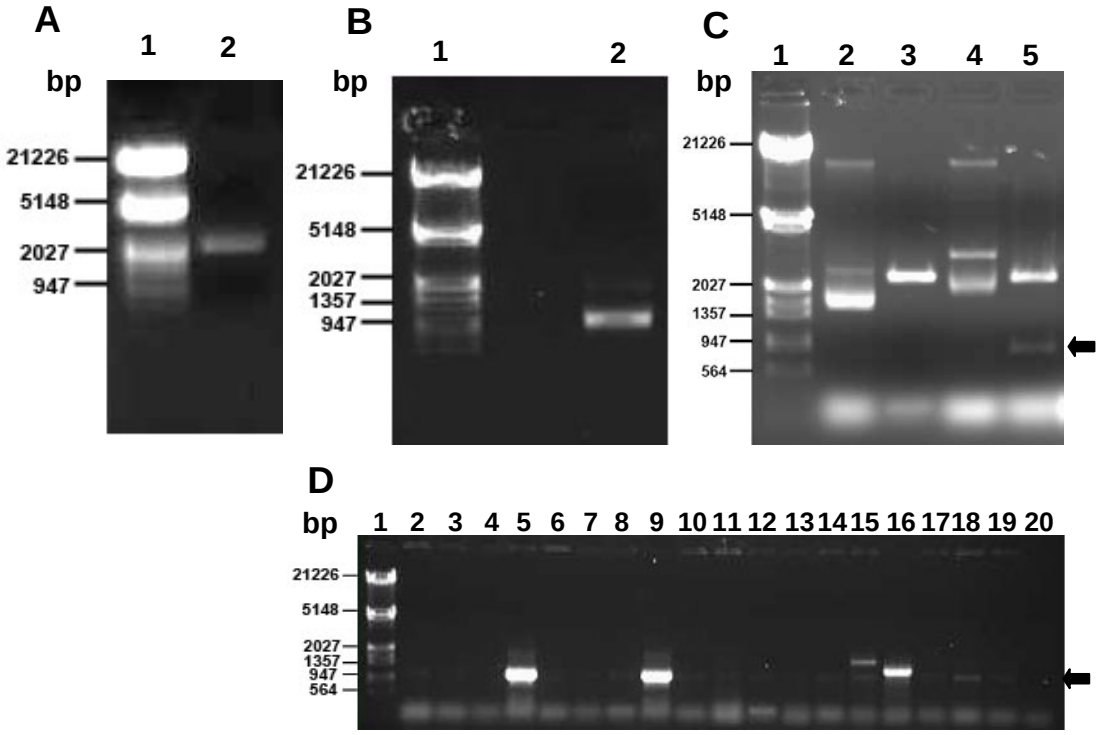

Figure 138: DNA Fragments for generation of the 864bp *scyCterm* pUC18 construct and its confirmation by restriction digests.

A) The gel isolated fragment *Bam*HI/*Nde*I fragment of pUC18 used for construction of pUC18-scyCterm was analysed on a 0.7% agarose gel (Lane 2). The DNA size marker is Lambda *Hind*III/*Eco*RI (Lane 1).

B) The gel isolated *Bam*HI/NdeI fragment of a *scyCterm* PCR product used for construction of pUC18-scyCterm was analysed on a 0.7% agarose gel (Lane 2). The DNA size marker is Lambda *Hind*III/*Eco*RI (Lane 1).

C) The plasmids pUC18 (Lanes 2 & 3) and the plasmid pUC18-scyCterm (Lanes 4 & 5) were analysed on a 0.7% agarose gel. Undigested samples (Lanes 2 & 4) were run together with samples digested with *Bam*HI and *Nde*I (Lanes 3 & 5). The arrow indicates the ~1000bp (post sequencing size ~864bp) fragment carrying the PCR amplified *scyCterm*. The DNA size marker is Lambda *Hind*III/*Eco*RI (Lane 1).

D) Candidate colonies were screened with colony PCR using pUC18 Reverse (upstream) and scy-Nde (downstream) primers and PCR products were analysed on a 0.7% agarose gel. Candidate colonies are shown Lanes 2-19. The arrow indicates the ~1000bp (post sequencing size ~989bp) PCR product expected. A blue negative colony was also included (Lane 20). The DNA size marker is Lambda *Hind*III/*Eco*RI (Lane 1).

Following the *scy* C-terminal fragment was cloned from the pUC18-scyCterm into pAZ1 using *Bam*HI and *Nde*I (Figure 139 & Figure 140). After ligation of the fragments the ligation mixture was used for transformation of *E. coli* strain DH5α. The transformants were screened with colony PCR (Figure 140E) to find potential clones which could generate an ~1220bp PCR product of *scyCterm* joined to *egfp*. Plasmid DNA was then isolated from potential clones, isolated DNA was confirmed by restriction digestion (Figure 140D) to liberate a small *Bam*HI/*Nde*I fragment in the 864bp expected from the sequenced pUC18-scyCterm clone. Sequencing was also used to verify the junctions between *scyCterm* and *egfp*. Thus, confirming the generation of pAZ1-scyCterm-egfp with the *scyCterm* in the same reading frame to *egfp* (Figure 140A).

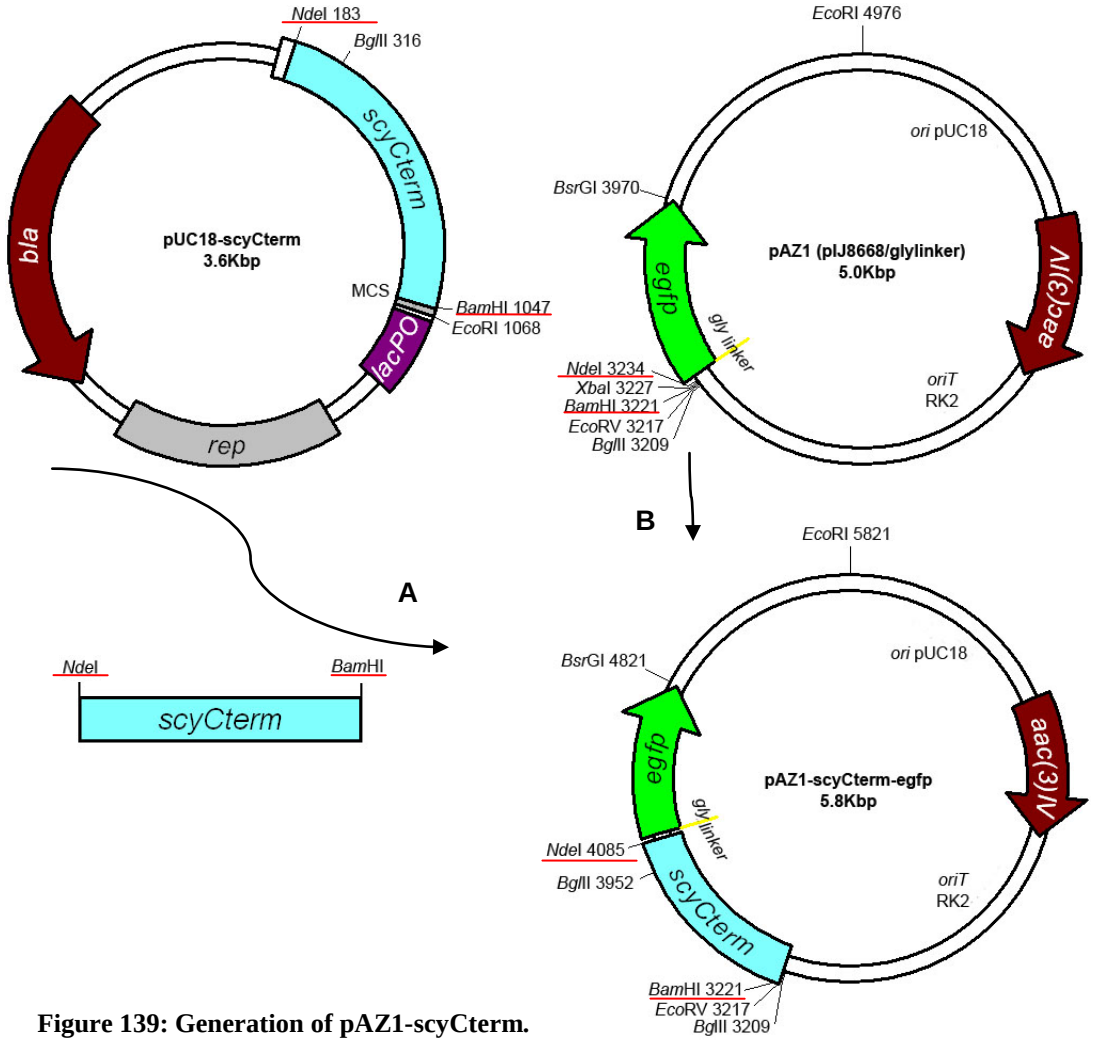

Figure 139: Generation of pAZ1-scyCterm.

pAZ1-scyCterm is a derivative of pAZ1. A) The *scyCterm* fragment was liberated using *Bam*HI and *Nde*I from pUC18-scyCterm. B) Using the enzymes *Bam*HI and *Nde*I pAZ1 was digested and the *scyCterm* fragment was cloned so that *scyCterm* was in frame with *egfp*. The restriction sites used in the cloning are underlined in red.

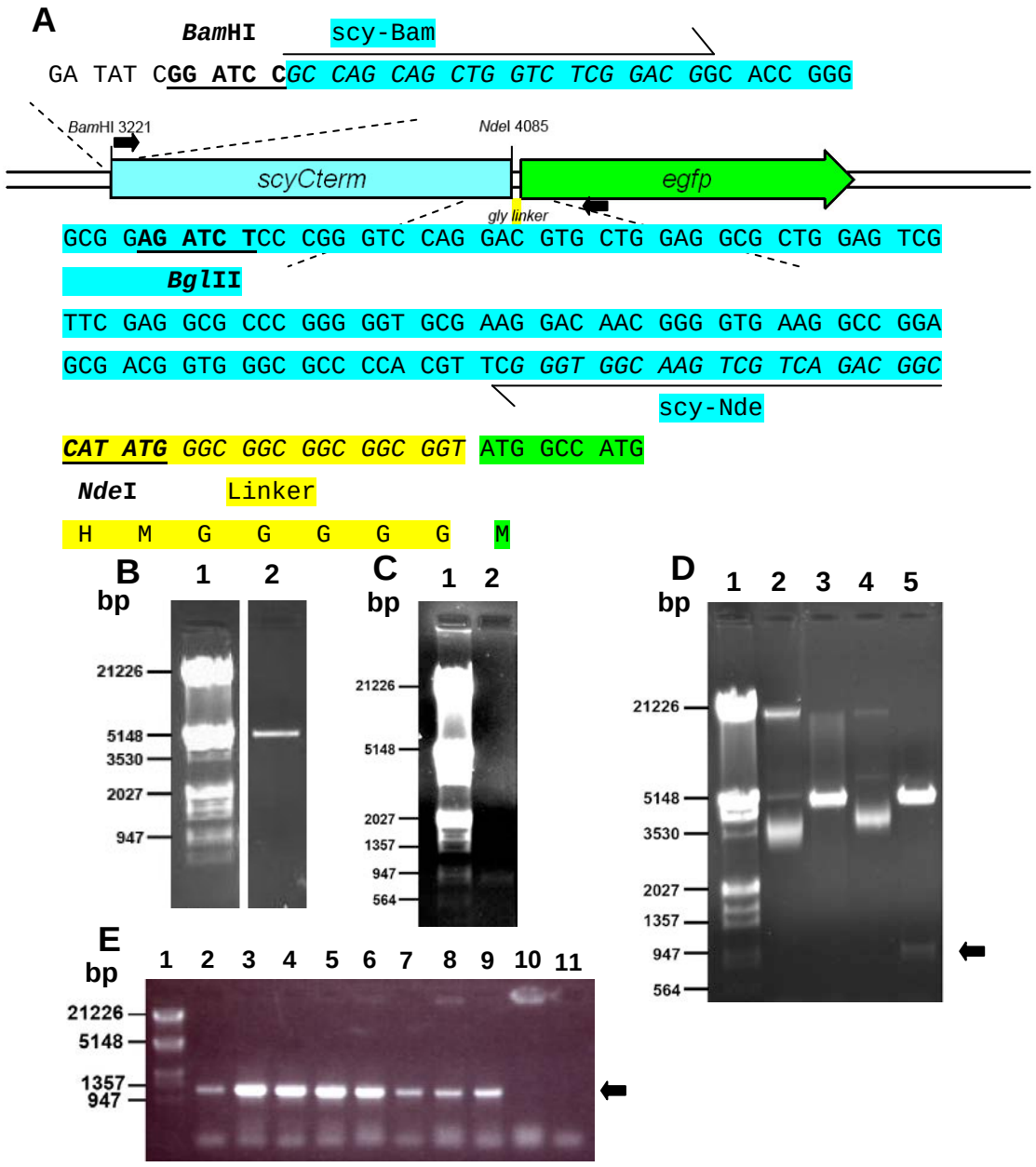

Figure 140: DNA Fragments for generation of a scyCterm containing pAZ1 consrtuct and its confirmation by restriction digests.

A) pAZ1-scyCterm-egfp. Sequence of the junctions formed between the multiple cloning site, the *scyCterm* fragment and *egfp*. The *scy-egfp* junction contains a glycine linker (highlighted yellow/italics). Restriction site sequences are bold and underlined. Primer sequences are marked in italics and with arrows. The *scyCterm* sequences are highlighted light blue and *egfp* is highlighted green. Primers for colony PCR are marked (black arrows).

B) The gel isolated *Bam*HI/*Nde*I fragment of pAZ1 used for construction of pAZ1-scyCterm was analysed on a 0.7% agarose gel (Lane 2). The DNA size marker is Lambda *Hind*III/*Eco*RI (Lane 1).

C) The gel isolated *Bam*HI/*Nde*I fragment containing *scyCterm* used for construction of pAZ1-scyCterm was analysed on a 0.7% agarose gel (Lane 2). The DNA size marker is Lambda *Hind*III/*Eco*RI (Lane 1).

D) The plasmids pAZ1 (Lanes 2 & 3) and the plasmid pAZ1-scyCterm (Lanes 4 & 5) were analysed on a 0.7% agarose gel. Undigested samples (Lanes 2 & 4) were run together with samples digested with *Bam*HI and *Nde*I (Lanes 3 & 5). The arrow indicates the 864bp fragment carrying part of *scyCterm*. The DNA size marker is Lambda *Hind*III/*Eco*RI (Lane 1).

E) Candidate colonies were screened with colony PCR using scy-Bam (upstream) and EGFPseq (downstream) primers and PCR products were analysed on a 0.7% agarose gel. Candidate colonies are shown Lanes 2-10. The arrow indicates the ~1220bp PCR product expected. The plasmids pAZ1 (Lane 11) was used as a control template. The DNA size marker is Lambda *Hind*III/*Eco*RI (Lane 1).

In order to move the fusion to a vector that will integrate into the *S. coelicolor* chromosome at high efficiency, we moved the *scyCterm-egfp* fragment to pIJ8660 using *Bam*HI and *Eco*RI (Figure 141 & Figure 142). After ligation of the fragments the ligation mixture was used for transformation of *E. coli* strain DH5α. The transformants were screened with colony PCR (Figure 142C) to find potential clones which carried the *scyCterm* fragment, positive colonies were predicted to produce a ~864bp product. Plasmid DNA was then isolated from positive colonies, isolated DNA was confirmed by restriction digestion (Figure 142B) to liberate a *Bam*HI/*Eco*RI fragment approximately 2600bp in size containing *scyCterm-egfp*. Thus, confirming the generation of pIJ8660-scyCterm-egfp.

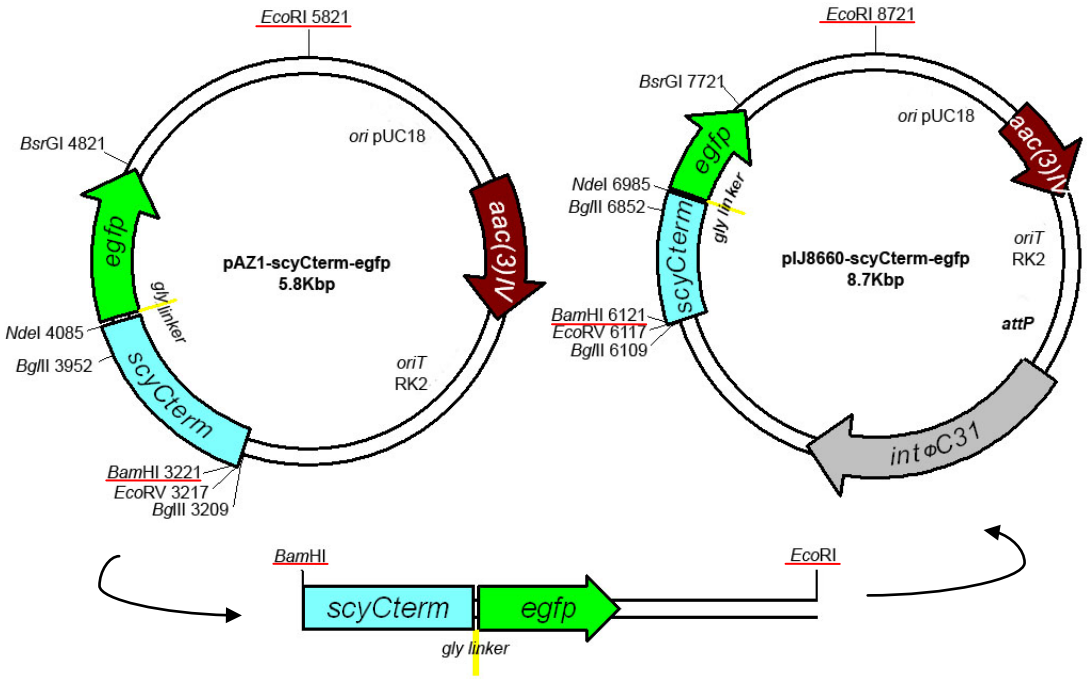

Figure 141: Generation of pIJ8660-scyCterm-egfp.

pIJ8660-scyCterm is a derivate of pIJ8660. The *scyCterm-egfp* fragment was liberated using *Bam*HI and *Eco*RI from pAZ1-scyCterm. Using the enzymes *Bam*HI and *Eco*RI pIJ8660 was digested and the *scyCterm-egfp* fragment cloned in. The restriction sites used in the cloning are underlined in red.

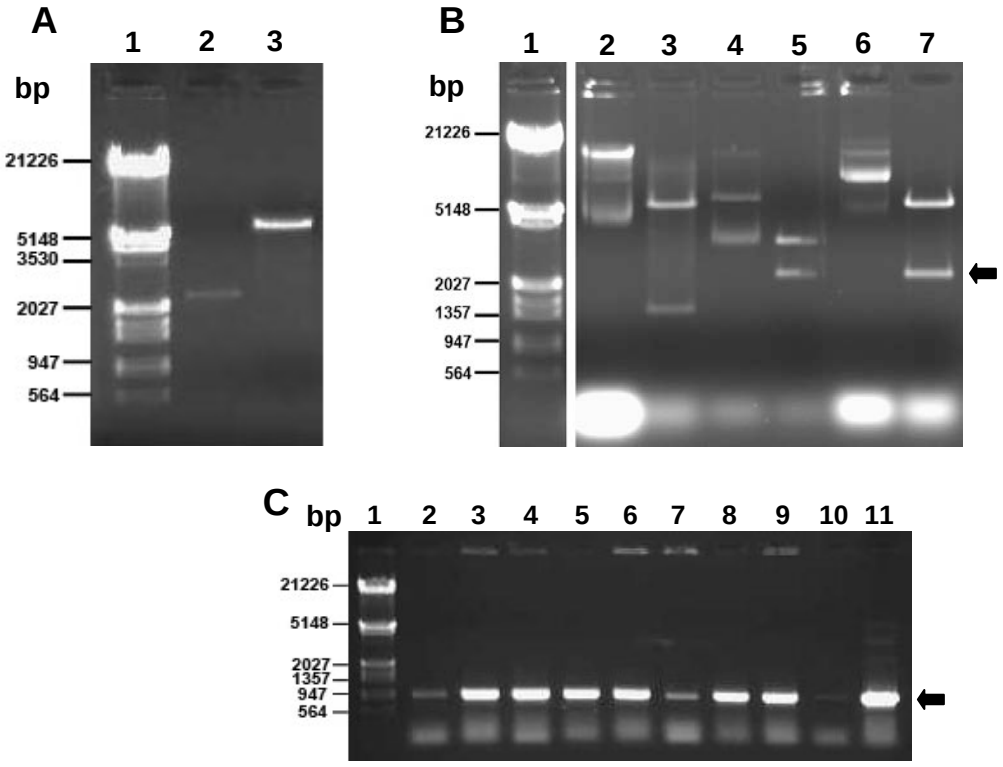

Figure 142: DNA Fragments for generation of a *scyCterm-egfp* containing pIJ8660 consrtuct and its confirmation by restriction digests.

A) The gel isolated fragments used for construction of pIJ8660-scyCterm-egfp were analysed on a 0.7% agarose gel. The fragments used were the *Bam*HI/*Eco*RI fragment containing *scyCterm-egfp* from pAZ1-scyCterm (Lane 2) and a *Bam*HI/*Eco*RI fragment of pIJ8660 (Lane 3). The DNA size marker is Lambda *Hind*III/*Eco*RI (Lane 1).

B) The plasmids pIJ8660 (Lanes 2 & 3), pAZ1-scyCterm-egfp (Lanes 4 & 5) and the plasmid pIJ8660-scyCterm-egfp (Lanes 6 & 7) were analysed on a 0.7% agarose gel. Undigested samples (Lanes 2, 4 & 6) were run together with samples digested with *Bam*HI/*Eco*RI (Lanes 3, 5 & 7). The arrow indicates the 2600bp fragment containing scyCterm-egfp. The DNA size marker is Lambda *Hind*III/*Eco*RI (Lane 1).

C) Candidate colonies were screened with colony PCR using scy-Bam (upstream) and scy-Nde (downstream) primers and PCR products were analysed on a 0.7% agarose gel. Candidate colonies are shown Lanes 2-9. The arrow indicates the ~864 bp PCR product expected. The plasmids pIJ8660 (Lane 10) and pAZ1-scyCterm-egfp (Lane 11) were used as control templates. The DNA size marker is Lambda *Hind*III/*Eco*RI (Lane 1).

The plasmid pIJ8660-Pscy-scy (used in 2.1.7) was used to generate the final construct of pIJ8660-Pscy-scy-egfp. The plasmid pIJ8660-Pscy-scy contains the promoter sequence of *scy* that was generated above as well as the full length sequence of *scy* that is identical to the chromosomal sequence except for exchange of a GTG start codon for ATG caused by the *Psy-scy* junction having a CATATG *Nde*I site insert. The use of an alternative start codon was not shown to have a significant effect when complementing the *scy* mutant (Figure 40 & Figure 41). A 4.2kb *Bgl*II fragment of pIJ8660-Pscy-scy was moved into pIJ8660-scyCterm-egfp using the same enzyme (Figure 143 & Figure 144). Replacing the

part of the *scy* C-terminal fragment containing mutations. After ligation of the fragments the ligation mixture was used for transformation of *E. coli* strain DH5α. The transformants were screened with colony PCR (Figure 144D) to find potential clones which now carried the 364bp *Pscy* sequence and hence the *Pscy-scy* containing fragment. Plasmid DNA was then isolated from positive colonies, isolated DNA was confirmed by restriction digestion (Figure 144C) to liberate a *Bgl*II fragment approximately 4236bp in size containing *Pscy-scy*. Thus, generating the construct pIJ8660-Pscy-scy-egfp, which carries the *scy* promoter followed by the full length of *scy* in frame to *egfp* (Figure 144A). The plasmid was confirmed by sequencing to verify the junctions between the *scy* promoter and between *scy* and *egfp*.

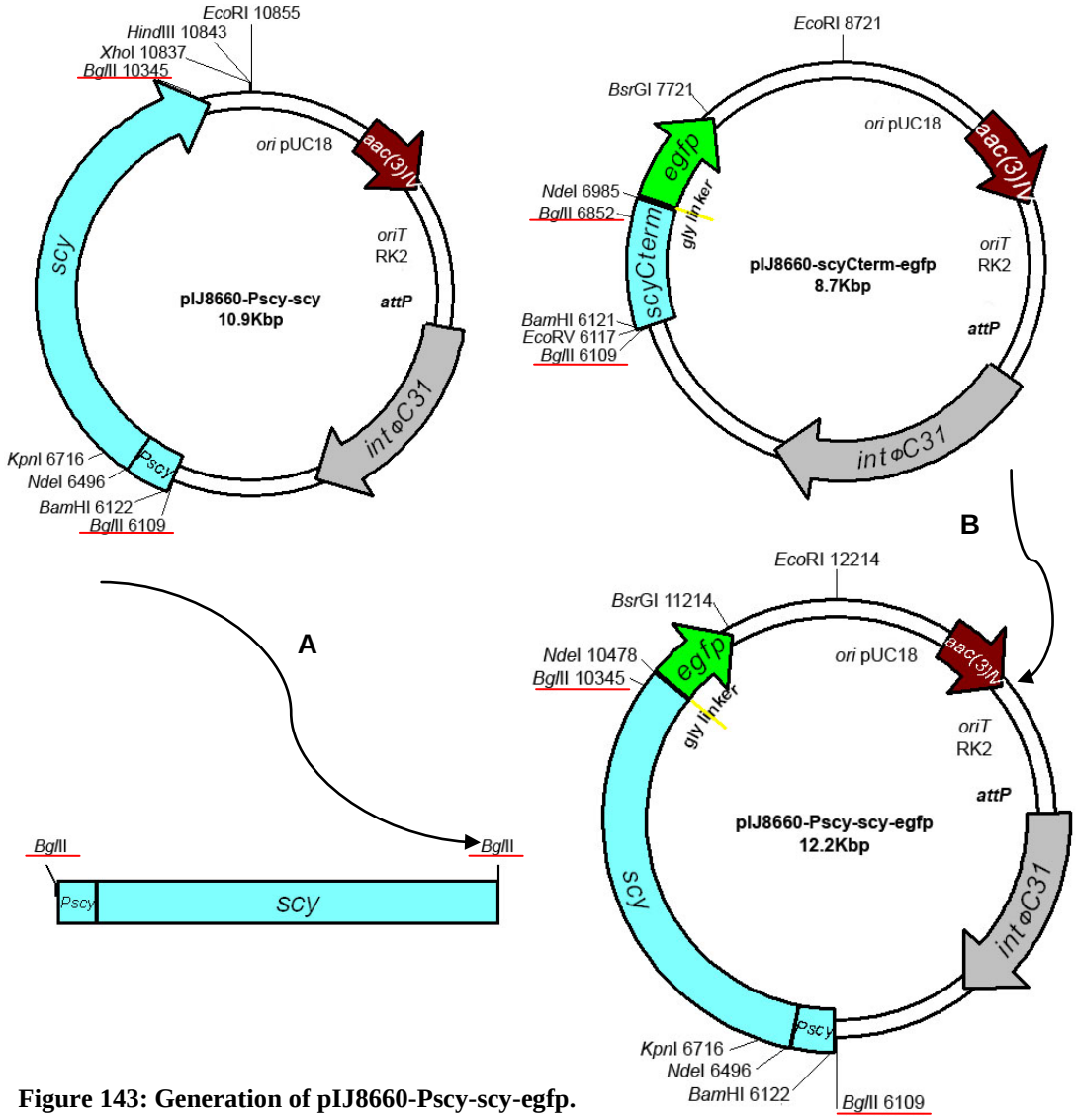

Figure 143: Generation of pIJ8660-Pscy-scy-egfp.

pIJ8660-Pscy-scy-egfp is a derivative of pIJ8660-scyCterm-egfp. A) A *Pscy-scy* BglII fragment was liberated from pIJ8660-Pscy-scy using *Bgl*II. B) Using *Bgl*II, pIJ8660-scyCterm-egfp was digested and the small fragment replaced with the *Pscy-scy* BglII fragment resulting in a *scy-egfp* fusion under the direction of *Pscy*. The restriction sites used in the cloning are underlined in red.

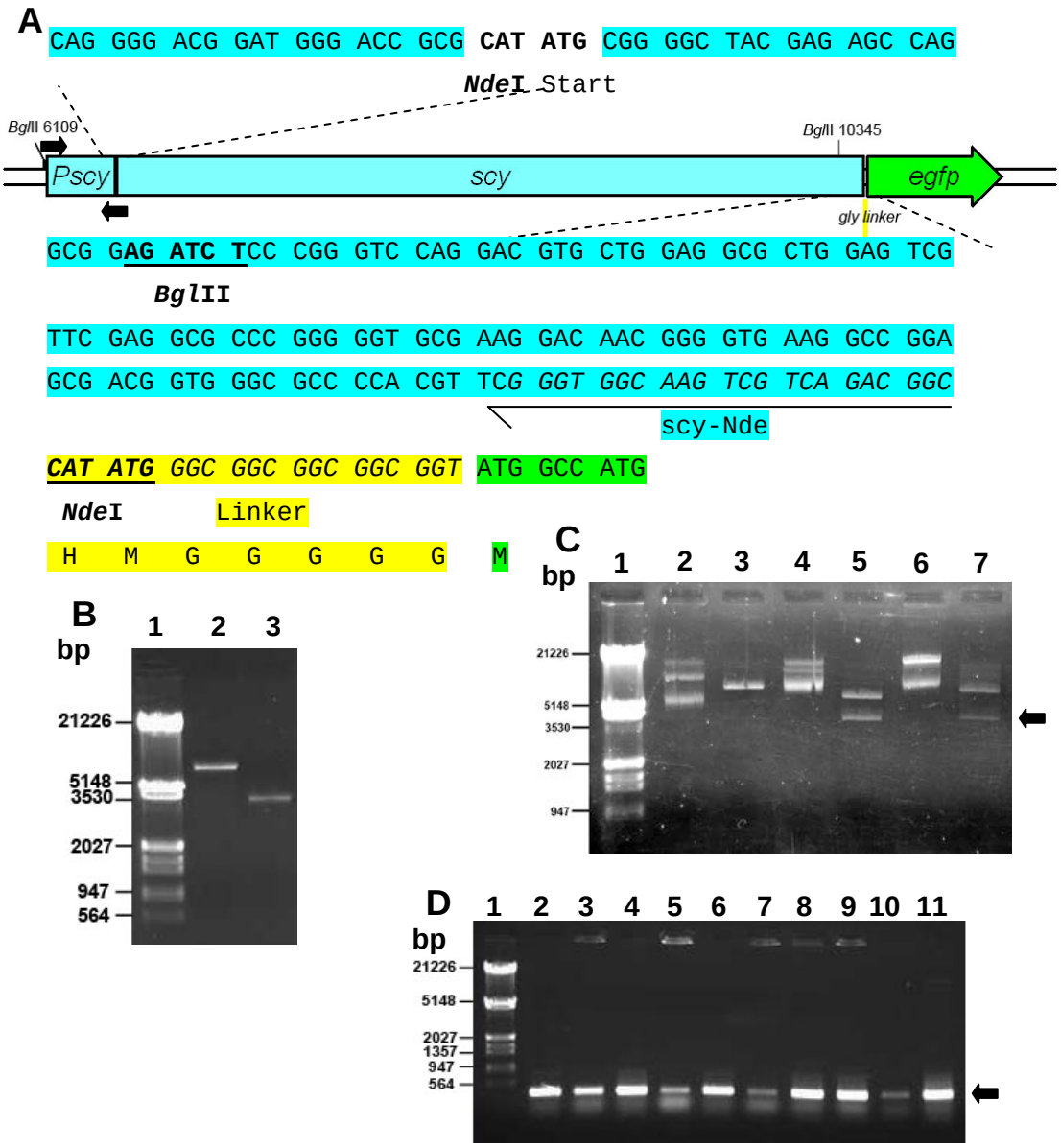

Figure 144: DNA Fragments for generation of pIJ8660-Pscy-scy-egfp and its confirmation by restriction digests.

A) pIJ8660-Pscy-scy-egfp. Sequence of the junctions between the promoter and the open reading frame, as well as the *scyCterm* fragment and *egfp*. The *scy-egfp* junction contains the glycine linker from pAZ1 (highlighted yellow/italics). Restriction site sequences are bold and underlined. Primer sequences are marked in italics and with arrows. The *Pscy* and *scy* sequences are highlighted light blue and *egfp* is highlighted green. Primers for colony PCR are marked (black arrows).

B) The gel isolated fragments used for construction of pIJ8660-Pscy-scy-egfp were analysed on a 0.7% agarose gel. The fragments used were a *Bgl*II fragment of pIJ8660-scyCterm-egfp (Lane 2) and a *Bgl*II containing *Pscy-scy* from pIJ8660-Pscy-scy (Lane 3). The DNA size marker is Lambda *Hind*III/*Eco*RI (Lane 1).

C) The plasmids pIJ8660-scyCterm-egfp (Lanes 2 & 3), pIJ8660-Pscy-scy (Lanes 4 & 5) and the plasmid pIJ8660-Pscy-scy-egfp (Lanes 6 & 7) were analysed on a 0.7% agarose gel. Undigested samples (Lanes 2, 4 & 6) were run together with samples digested with *Bgl*II (Lanes 3, 5 & 7). The arrow indicates the 4236bp fragment containing *Pscy-scy*. The DNA size marker is Lambda *Hind*III/*Eco*RI (Lane 1).

D) Candidate colonies were screened with colony PCR using scyprom4-Bam (upstream) and scyprom3-Nde (downstream) primers and PCR products were analysed on a 0.7% agarose gel. Candidate colonies are shown Lanes 2-9. The arrow indicates the ~364 bp PCR product expected. The plasmids pIJ8660-scyCterm-egfp (Lane 10) and pIJ8660-Pscy-scy (Lane 11) were used as control templates. The DNA size marker is Lambda *Hind*III/*Eco*RI (Lane 1).

10.1.49 Generation of a Scy C-terminal mCherry translational fusion

To further assess the localisation of Scy with a C-terminal fluorescent fusion a Scy-mCherry C-terminal fusion was constructed. We did not have an mCherry version of pIJ8660 or pAZ1

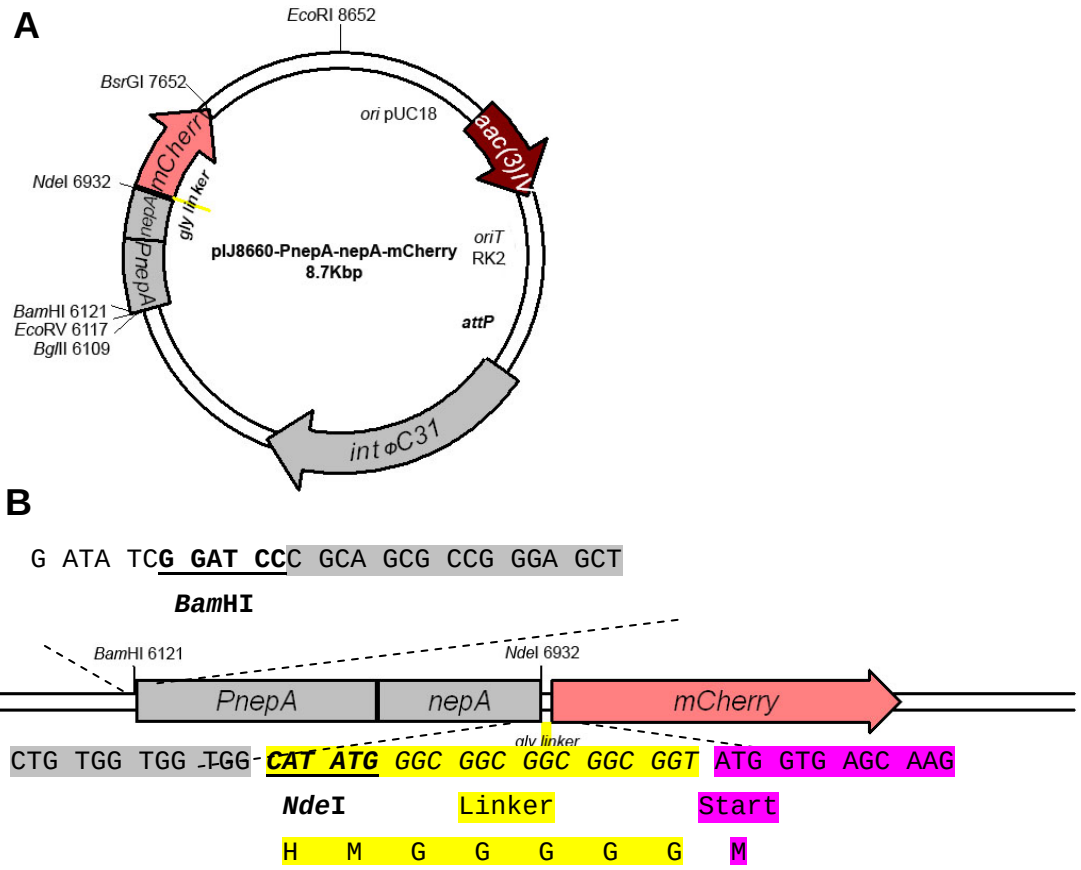

Figure 145: pIJ8660-PnepA-nepA-mCherry is a plasmid with *mCherry* downstream of a glycine linker. Replacement of the *PnepA-nepA* sequence allows the formation of a desired C-terminal mCherry fusion.

A) The map of pIJ8660-PnepA-nepA-mCherry including restriction sites, antibiotic resistance genes, origins of replication and a glycine linker.

B) pIJ8660-PnepA-nepA-mCherry. Sequence of the upstream region to *PnepA* and the sequence of *nepA* followed by a linker and *mCherry*. The glycine linker was originally generated by annealing the oligonucleotides EGFPLinker1 and EGFPLinker2 similar to pAZ1 (highlighted yellow/italics). Restriction site sequences are bold and underlined. The *mCherry* sequence is highlighted pink.

so we made use of a plasmid that was generated to express a C-terminal mCherry fusion of NepA (Winter and Kelemen, unpublished). The plasmid pIJ8660-PnepA-nepA-mCherry (Figure 146), contains the gene *nepA* (Dalton *et al.*, 2007) fused to *mCherry* driven by its native promoter. The linker between *nepA* and *mCherry* is similar to the linker used in the

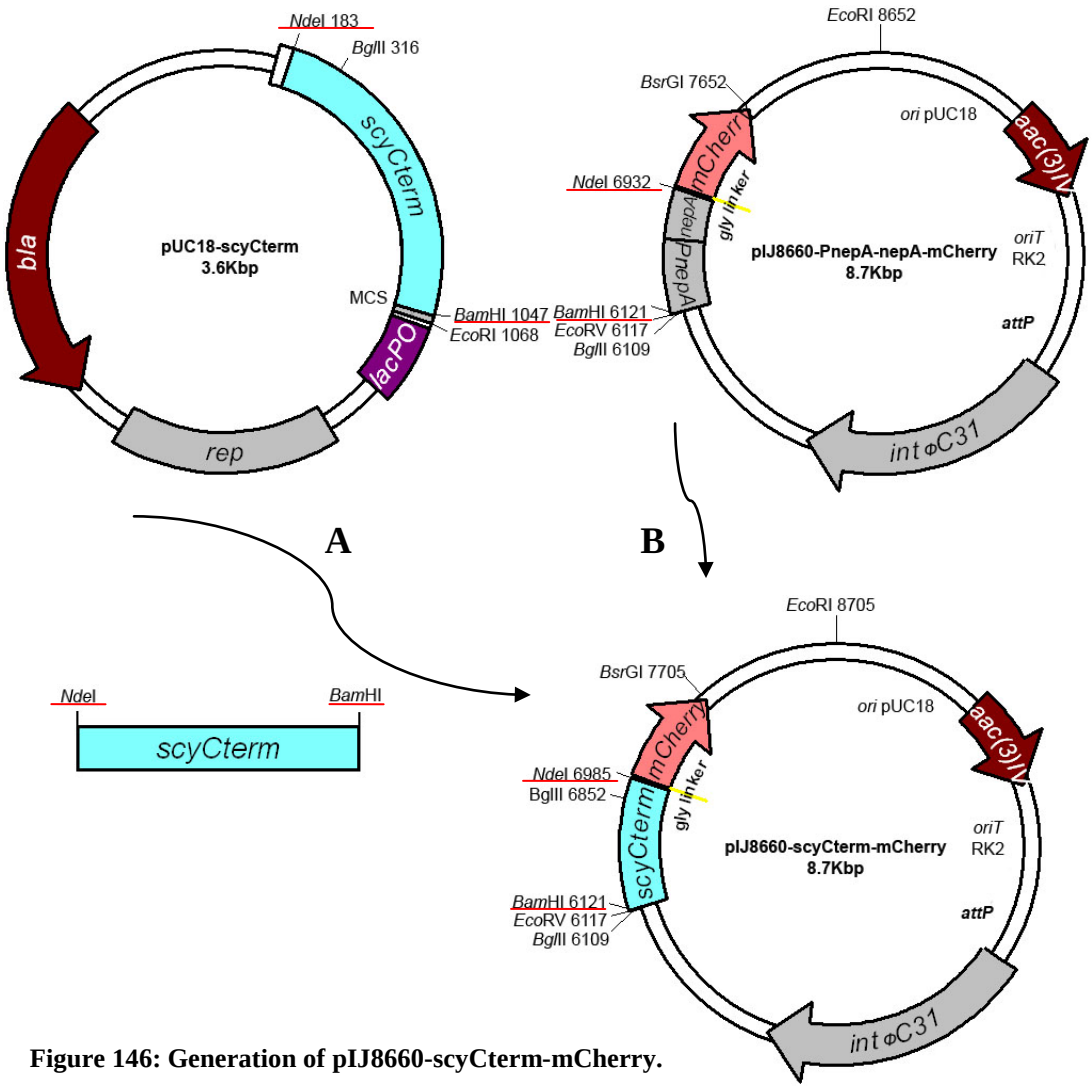

Figure 146: Generation of pIJ8660-scyCterm-mCherry.

pIJ8660-scyCterm-mCherry is derivative of pIJ8660-PnepA-nepA-mCherry. A) The *scyCterm* fragment was liberated using *Bam*HI and *Nde*I from pUC18-scyCterm. B) Using the enzymes *Bam*HI and *Nde*I pIJ8660-PnepA-nepA-mCherry was digested and the *PnepA-nepA* fragment replaced with *scyCterm* fragment, so that *scyCterm* sequence was in frame with *mCherry*. The restriction sites used in the cloning are underlined in red.

plasmid pIJ8660-Pscy-scy-egfp (Figure 146A). However, in this case there is the *NdeI* site followed by the linker encoding His-Met-Gly-Gly-Gly-Gly-Gly that reads in frame to *mCherry* (Figure 146B). In order to generate C-terminal mCherry fusions the desired gene would have to be cloned upstream of the *Nde*I site. Unfortunately we could not lift the entire *scy* gene together with its promoter from pIJ8660-Pscy-scy-egfp, but instead we had to repeat the strategy used for the generation of the Scy-EGFP fusion. Whereby the small *scyCterm* fragment would replace *PnepA-nepA*, and then finally the large *Pscy-scy* fragment would be used to generate the full length fusion. Therefore, the *scyCterm* fragment was cloned from pUC18-scyCterm into pIJ8660-PnepA-nepA-mCherry using *Bam*HI and *Nde*I, replacing the *PnepA-nepA* sequence with the *scyCterm* fragment (Figure 146 & Figure 147). After ligation of the fragments the ligation mixture was used for

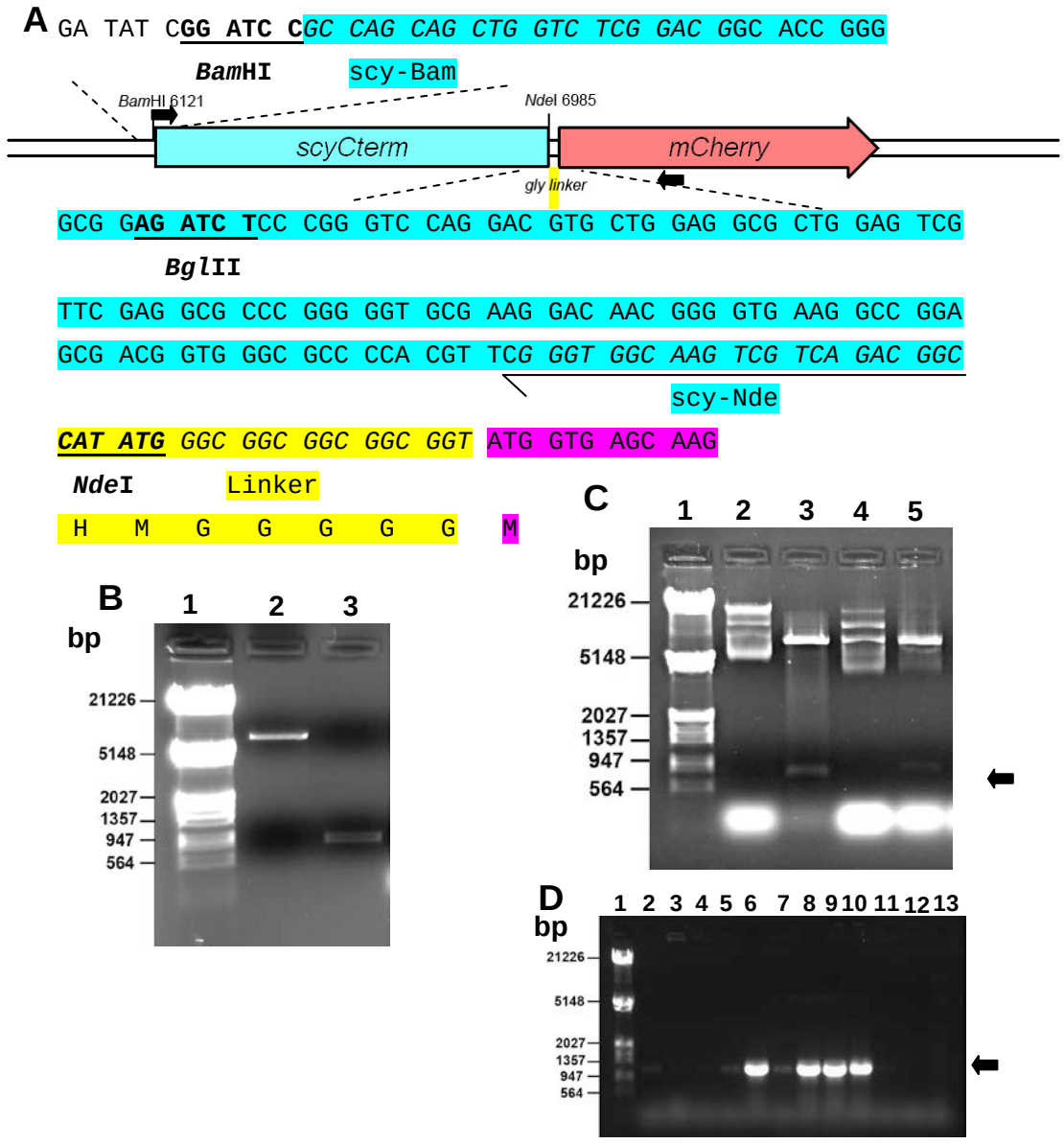

Figure 147: DNA Fragments for generation of a *scyCterm-mCherry* fusion and its confirmation by restriction digests.

A) pIJ8660-scyCterm-mCherry. Sequence of the junctions between the multiple cloning site, the *scyCterm* fragment and *mCherry*. The *scy-mCherry* junction contains a glycine linker (highlighted yellow/italics). Restriction site sequences are bold and underlined. The *scyCterm* sequences are highlighted light blue and *mCherry* is highlighted pink. Primers for colony PCR are marked (black arrows).

B) The gel isolated fragments used for construction of pIJ8660-scyCterm-mCherry were analysed on a 0.7% agarose gel. The fragments used were a *Bam*HI/*Nde*I fragment of pIJ8660-PnepA-nepA-mCherry (Lane 2) and a *Bam*HI/*Nde*I fragment containing *scyCterm* (Lane 3). The DNA size marker is Lambda *Hind*III/*Eco*RI (Lane 1).

C) The plasmids pIJ8660-PnepA-nepA-mCherry (Lanes 2 & 3) and the plasmid pIJ8660-scyCterm-mCherry (Lanes 4 & 5) were analysed on a 0.7% agarose gel. Undigested samples (Lanes 2 & 4) were run together with samples digested with *BamH*I and *Nde*I (Lanes 3 & 5). The arrow indicates the 864bp fragment carrying part of *scyCterm*. The DNA size marker is Lambda *Hind*III/*Eco*RI (Lane 1).

D) Candidate colonies were screened with colony PCR using scy-Bam (upstream) and mCherryseq (downstream) primers and PCR products were analysed on a 0.7% agarose gel. Candidate colonies are shown Lanes 2-12. The arrow indicates the ~1100bp PCR product expected. The plasmids pIJ8660-PnepA-nepA-mCherry was used as a control template (Lane 13). The DNA size marker is Lambda *Hind*III/*Eco*RI (Lane 1).

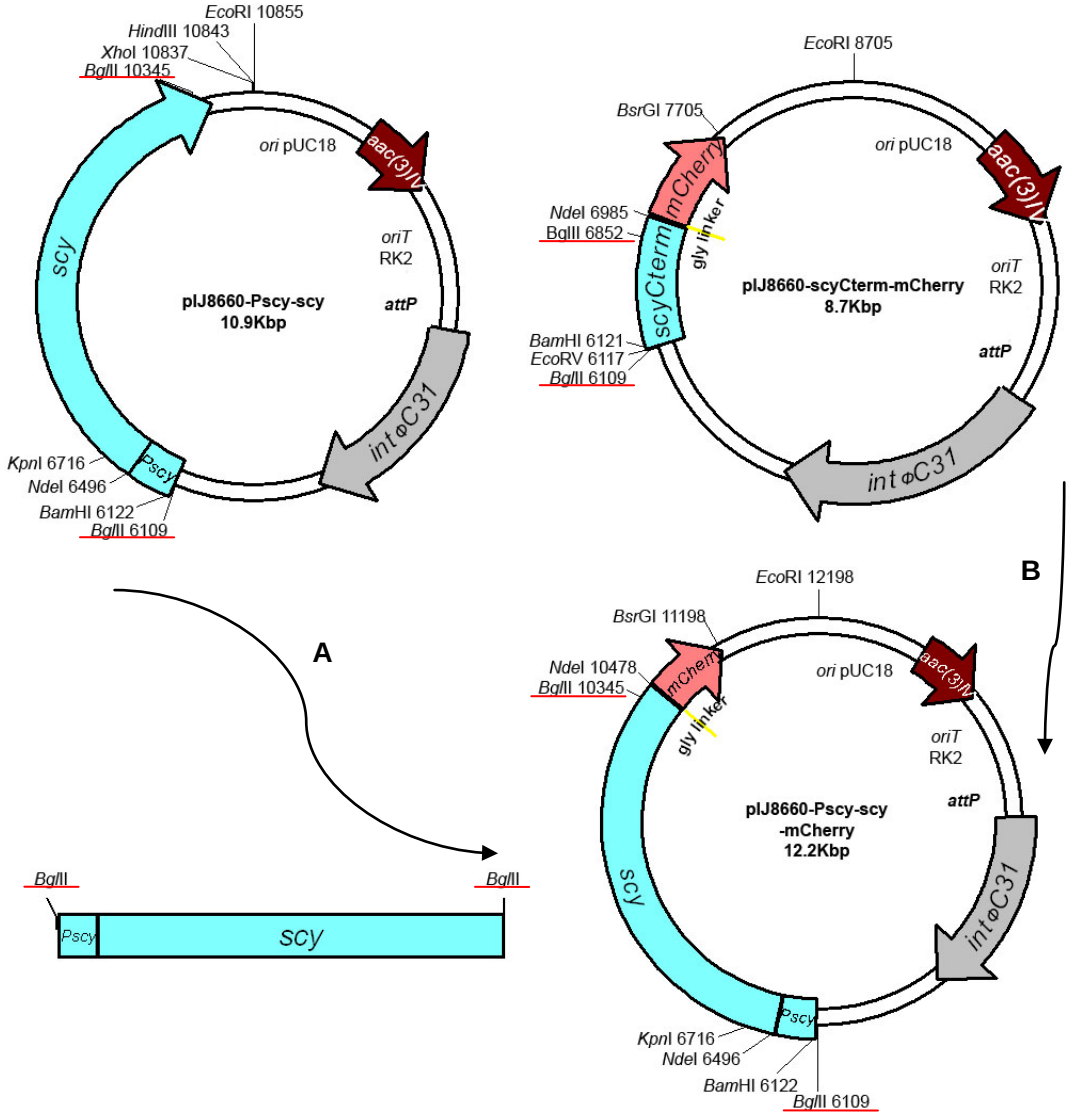

Figure 148: Generation of pIJ8660-Pscy-scy-mCherry.

pIJ8660-Pscy-scy-mCherry is a derivative of pIJ8660-scyCterm-mCherry. A) A *Pscy-scy* BglII fragment was liberated from pIJ8660-Pscy-scy using *Bgl*II. B) Using *Bgl*II, pIJ8660-scyCterm-mCherry was digested and the small fragment replaced with the *Pscy-scy* BglII fragment resulting in a *scy-mCherry* fusion under the direction of *Pscy*. The restriction sites used in the cloning are underlined in red.

transformation of *E. coli* strain DH5α. The transformants were screened with colony PCR (Figure 147) to find potential clones carrying ~1100bp PCR product generated from the *scyCterm-mCherry* sequence. Plasmid DNA was then isolated from positive colonies, isolated DNA was confirmed by restriction digestion (Figure 147C) to liberate a ~864bp *Bam*HI/*Nde*I fragment containing *scyCterm*. Thus, confirming the generation of the plasmid pIJ8660-scyCterm-mCherry.

To generate the full length *scy* fusion to *mCherry*, a 4.2kb *Bgl*II fragment from pIJ8660-Pscy-scy was moved into pIJ8660-scyCterm-mCherry (Figure 148 & Figure 149). After

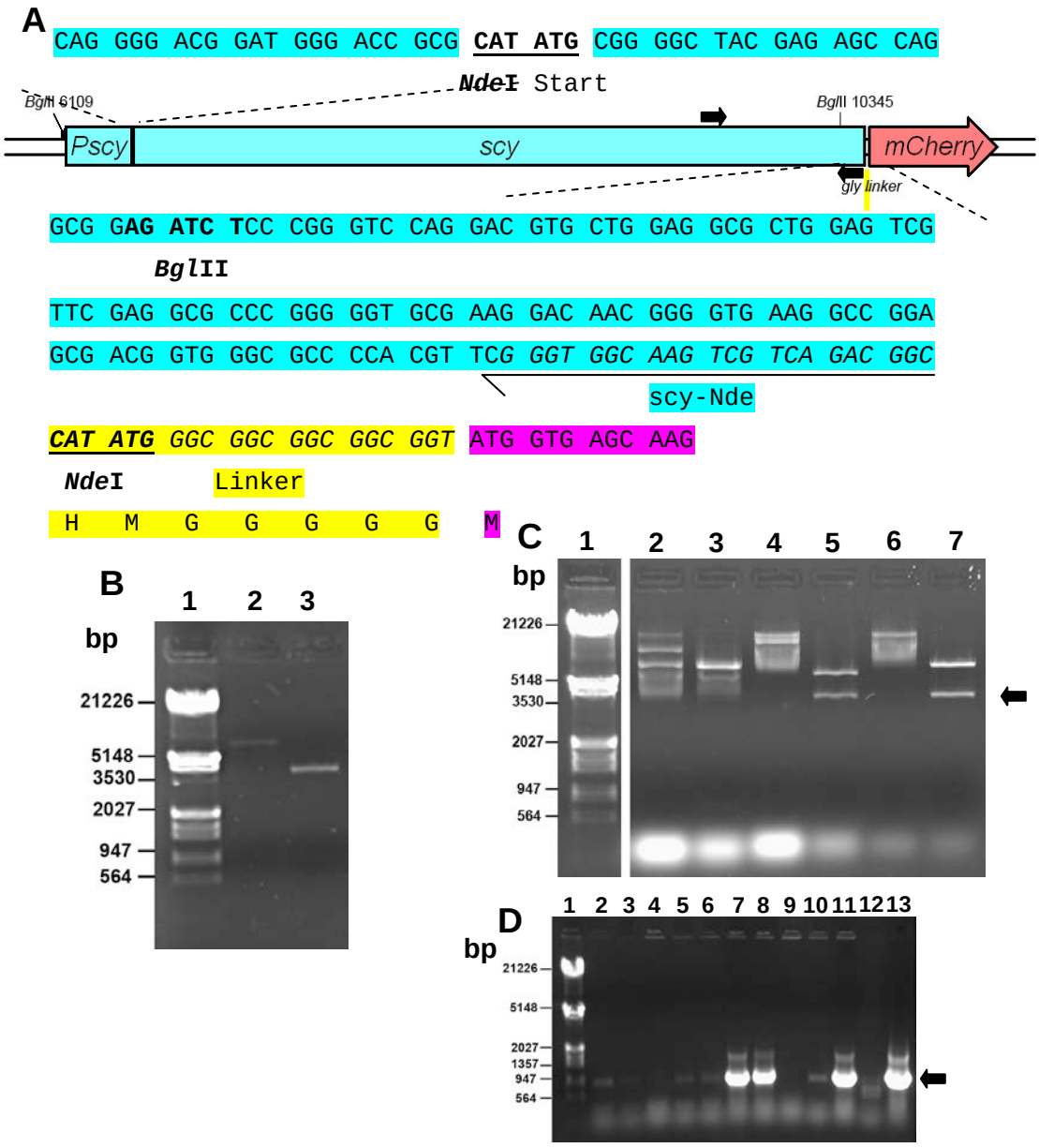

Figure 149: DNA Fragments for generation of a Scy-mCherry fusion and its confirmation by restriction digests.

A) pIJ8660-Pscy-scy-mCherry. Sequence of the junctions between the *scy* promoter, *scy* and *mCherry*. The *scy-mCherry* junction contains a glycine linker (highlighted yellow/italics). Restriction site sequences are bold and underlined. The *Pscy* and *scy* sequences are highlighted light blue and *mCherry* is highlighted pink. Primers for colony PCR are marked (black arrows).

B) The gel isolated fragments used for construction of pIJ8660-Pscy-scy-mCherry were analysed on a 0.7% agarose gel. The fragments used were a *Bgl*II fragment of pIJ8660-scyCterm-mCherry (Lane 2) and a *Bgl*II fragment containing *Pscy-scy* (Lane 3). The DNA size marker is Lambda *Hind*III/*Eco*RI (Lane 1).

C) The plasmids pIJ8660-scyCterm-mCherry (Lanes 2 & 3), pIJ8660-Pscy-scy (Lanes 4 & 5) and the plasmid pIJ8660-Pscy-scy-mCherry (Lanes 6 & 7) were analysed on a 0.7% agarose gel. Undigested samples (Lanes 2, 4 & 6) were run together with samples digested with *Bgl*II (Lanes 3, 5 & 7). The arrow indicates the 4236bp fragment containing *Pscy-scy*. The DNA size marker is Lambda *Hind*III/*Eco*RI (Lane 1).

D) Candidate colonies were screened with colony PCR using TH Scy F4 (upstream) and TH Scy R4 (downstream) primers and PCR products were analysed on a 0.7% agarose gel. Candidate colonies are shown Lanes 2-11. The arrow indicates the ~835bp PCR product expected. The plasmids pIJ8660-scyCterm-mCherry (Lane 12) and pIJ8660-Pscy-scy-egfp (Lane 13) were used as control templates. The DNA size marker is Lambda *Hind*III/*Eco*RI (Lane 1).

ligation of the fragments the ligation mixture was used for transformation of *E. coli* strain DH5α. The transformants were screened with colony PCR (Figure 149D) to find potential clones which now produced a ~835bp PCR product that can only be generated from the full length *scy* fragment and not the smaller *scyCterm* fragment. Plasmid DNA was then isolated from positive colonies, isolated DNA was confirmed by restriction digestion (Figure 149C) to liberate a fragment approximately 4236bp in size containing *Pscy-scy*. Confirming the generation of the plasmid pIJ8660-Pscy-scy-mCherry, carrying the *scy* promoter followed by the full length of *scy* in frame with the linker and *mCherry* (Figure 149A). pIJ8660-Pscy-scy-mCherry was also sequenced to analyse the junctions between the *scy* promoter and *scy* and between *scy* and *mCherry*.

10.1.50 Generation of a Scy-Δlink-mCherry construct

As the plasmid pIJ8660-Pscy-scy-mCherry did not give a definitive signal, we aimed to remove the His-Met-Gly-Gly-Gly-Gly-Gly linker. We could not simply replace the linkered *mCherry* fragment with *mCherry* due to the multiple *Nde*I sites. Instead we used a strategy similar to the other *scy* C-terminal fusions whereby we used the intermediate pIJ8660-scyCterm-egfp, replaced the *egfp* with non-linkered *mCherry* and then added in the large *Pscy-scy* fragment later. The *egfp* intermediate construct was used instead of the linkered *mCherry* to ensure that the linker was replaced by the distinguishable change of *egfp* to *mCherry*. The plasmid pBluescript-mCherry (gift from David Widdick) carries the *mCherry* gene and was used to remove an *Nde*I-*Bsr*GI fragment containing the *mCherry* gene. The *Nde*I-*Bsr*GI *mCherry* fragment was used to replace the *egfp* gene in the plasmid

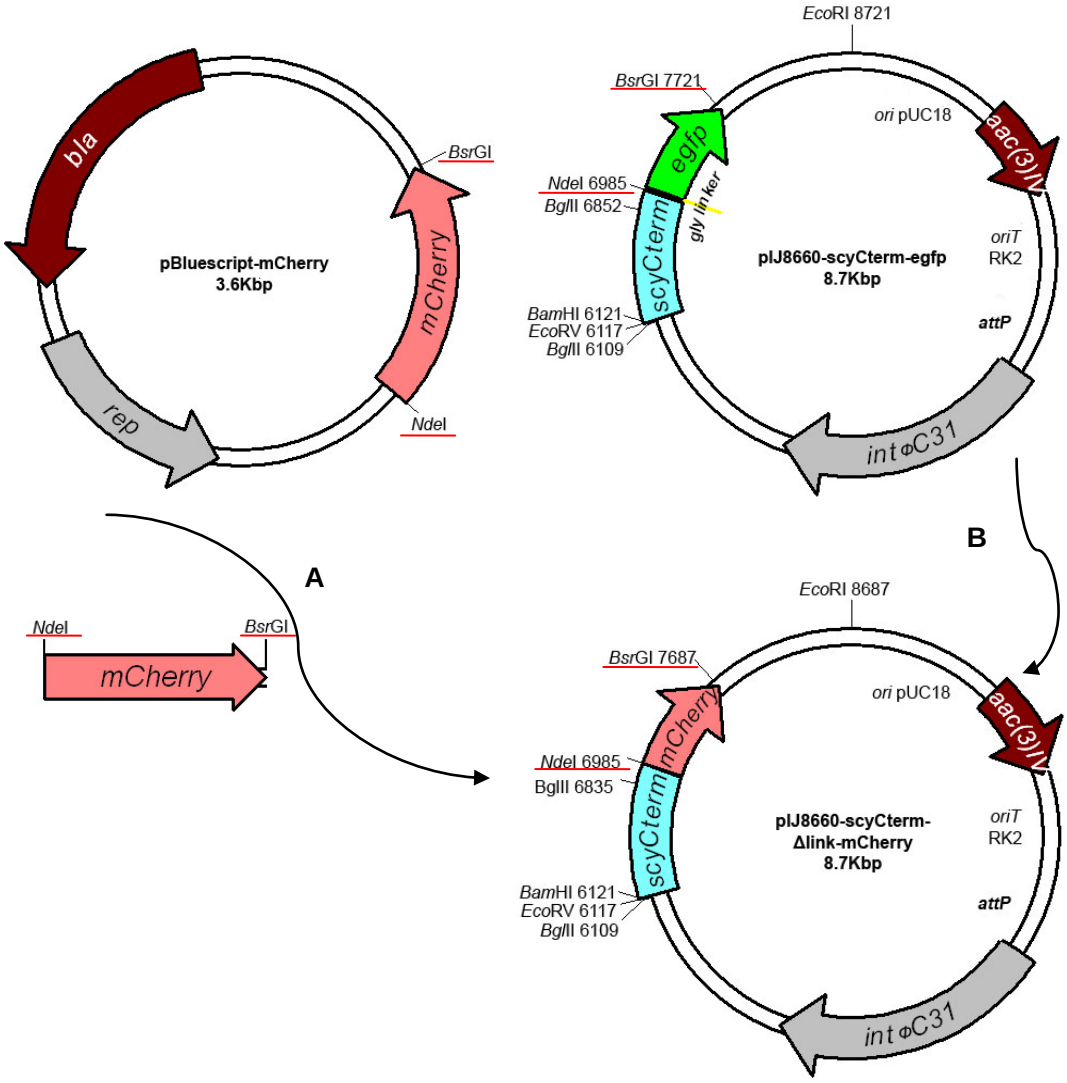

Figure 150: Generation of pIJ8660-scyCterm-Δlink-mCherry.

pIJ8660-scyCterm-Δlink-mCherry is a derivative of pIJ8660-scyCterm-egfp. A) An mCherry fragment was liberated from pBluescripty-mCherry using *Nde*I and *Bsr*GI. B) Using the enzymes *Nde*I and *Bsr*GI, pIJ8660-scyCterm-egfp was digested and *egfp* replaced with *mCherry*, so that that *scyCterm* sequence was in frame with *mCherry* and the glycine linker abolished. The restriction sites used in the cloning are underlined in red.

pIJ8660-scyCterm-egfp (Figure 150 & Figure 151). After ligation of the fragments the ligation mixture was used for transformation of *E. coli* strain DH5α. The transformants were screened with colony PCR (Figure 151E) to find potential clones which would now carry a *scyCterm-mCherry* fusion that would generate a ~1100bp PCR product, where *egfp-scy* should not generate a PCR product with the primers used. Plasmid DNA was then isolated from positive colonies, isolated DNA was confirmed by restriction digestion (Figure 151C) to liberate a 726bp fragment containing *scyCterm*. The plasmid DNA was

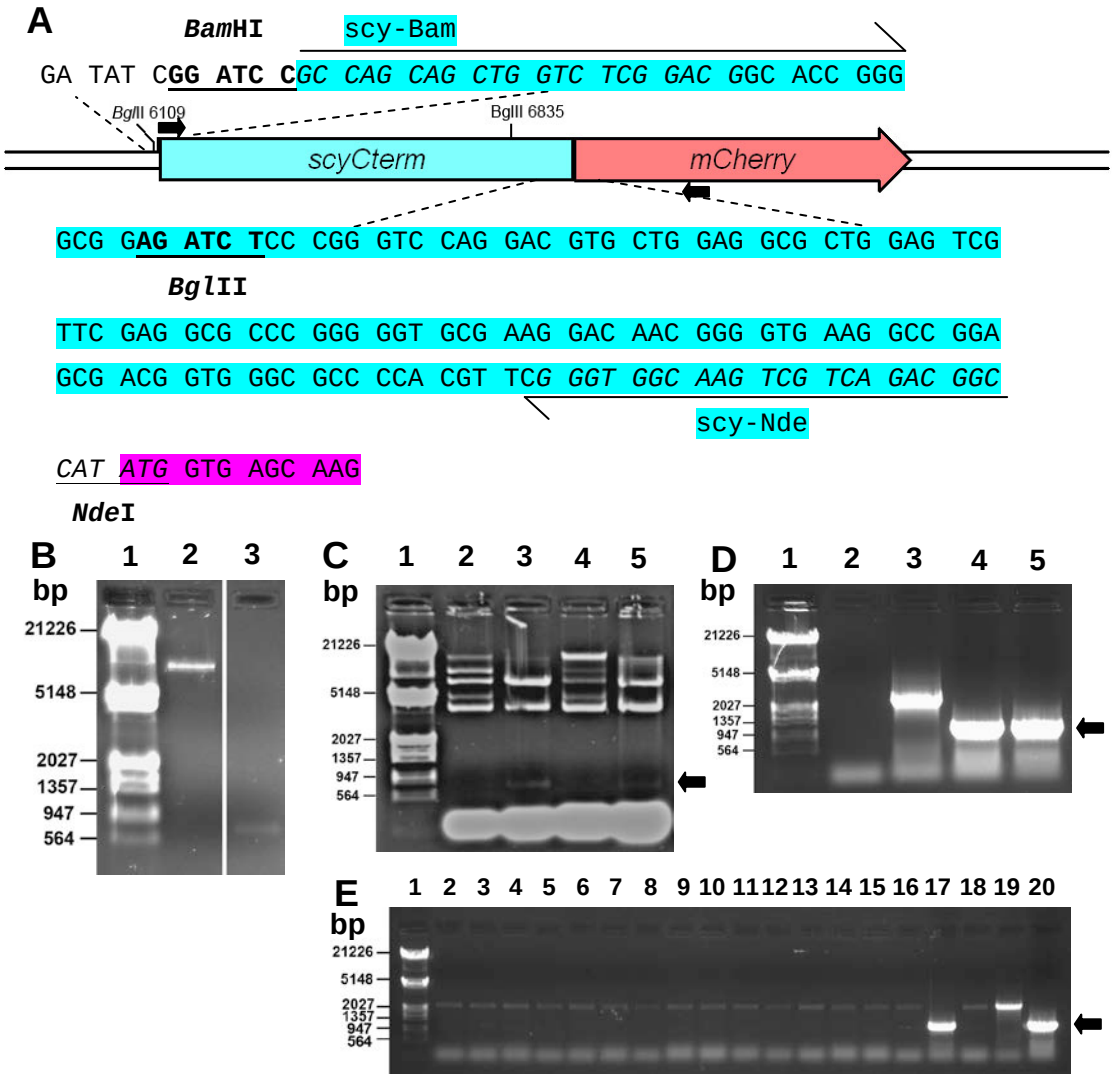

Figure 151: DNA Fragments for generation of pIJ8660-scyCterm-Δlink-mCherry and its confirmation.

A) pIJ8660-scyCterm-Δlink-mCherry. Sequence of the junctions between the multiple cloning site, the *scyCterm* fragment and *mCherry*. The *scy-mCherry* junction lacks a linker with *scy* reading directly into *mCherry*. Restriction site sequences are bold and underlined. Primer sequences are marked in italics and with arrows. The *Pscy* and *scy* sequences are highlighted light blue and *mCherry* is highlighted pink. Primers for colony PCR are marked (black arrows).

B) The gel isolated fragments used for construction of pIJ8660-scyCterm-Δlink-mCherry were analysed on a 0.8% agarose gel. The fragments used were a *Bsr*GI/*Nde*I fragment of pIJ8660-scyCterm-egfp (Lane 2) and a *Bsr*GI/*Nde*I fragement containing *mCherry* (Lane 3). The DNA size marker is Lambda *Hind*III/*Eco*RI (Lane 1).

C) The plasmids pIJ8660-scycterm-mCherry (Lanes 2 & 3) and the plasmid pIJ8660-scyCterm-Δlink-mCherry (Lanes 4 & 5) were analysed on a 0.7% agarose gel. Undigested samples (Lanes 2 & 4) were run together with samples digested with *Bgl*II (Lanes 3 & 5). The arrow indicates the 726bp fragment carrying part of *scyCterm*. The DNA size marker is Lambda *Hind*III/*Eco*RI (Lane 1).

D) The plasmids were confirmed by PCR using ScyBam and mCherryseq primers, products were analysed an on a 0.7% agarose gel. The templates used were the plasmids pIJ8660-scyCterm-egfp (Lane 3), pIJ8660-scyCterm-Δlink-mCherry (Lane 4), pIJ8660-scyCterm-mCherry (Lane 5) and a PCR mix only control (Lane 2). The DNA size marker is Lambda *Hind*III/*Eco*RI (Lane 1).

E) Candidate colonies were screened with colony PCR using scy-Bam (upstream) and mCherryseq (downstream) primers and PCR products were analysed on a 0.7% agarose gel. Candidate colonies are shown Lanes 2-18. The arrow indicates the ~1100bp PCR product expected. The plasmids pIJ8660-scyCterm-egfp (Lane 19) and pIJ8660-scyCterm-mCherry (Lane 20) were used as control templates. The DNA size marker is Lambda *Hind*III/*Eco*RI (Lane 1).

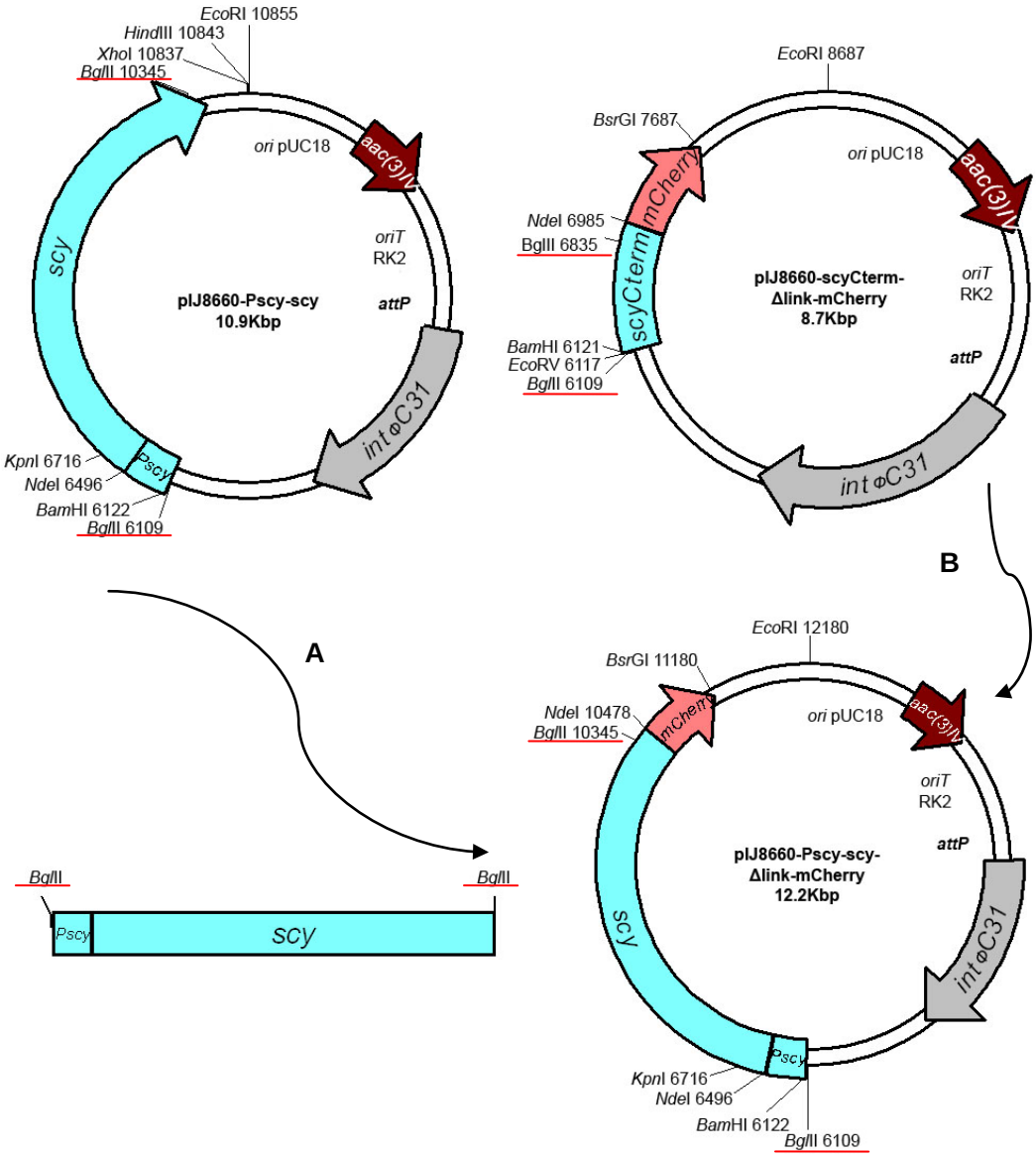

Figure 152: Generation of pIJ8660-Pscy-scy-Δlink-mCherry.

pIJ8660-Pscy-scy-Δlink-mCherry is a derivative of pIJ8660-scyCterm-Δlink-mCherry. A) A *Pscy-scy* BglII fragment was liberated from pIJ8660-Pscy-scy using *Bgl*II. B) Using *Bgl*II, pIJ8660-scyCterm-Δlink-mCherry was digested and the small fragment replaced with the *Pscy-scy* BglII fragment resulting in a *scy-mCherry* fusion with no glycine linker under the direction of *Pscy*. The restriction sites used in the cloning are underlined in red.

used as template DNA in a repeat PCR experiment (Figure 151D) to check that the *scyCterm-mCherry* specific ~1100bp PCR product could be generated, the control template of pIJ8660-scyCterm-egfp could not generate the correct sized product, whereas the non-linkered and linkered *mCherry* intermediate constructs could. Thus, confirming the generation of plasmid pIJ8660-scyCterm-Δlink-mCherry whereby a non-linkered *mCherry* sequence is fused to a *scyCterm* fragment (Figure 151A).

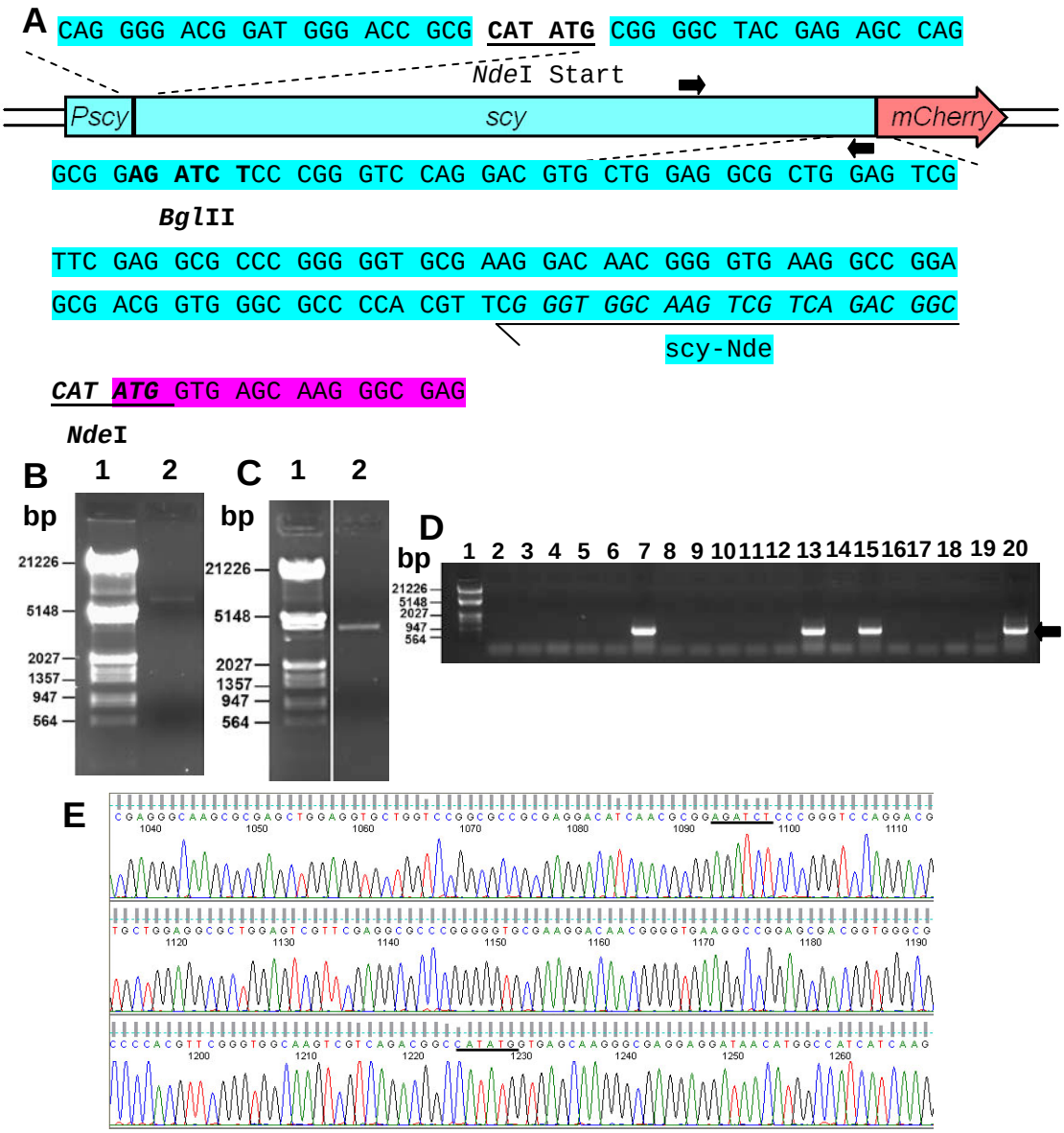

Figure 153: DNA Fragments for generation of pIJ8660-Pscy-scy-Δlink-mCherry and sequencing of subsequent pIJ8660-Pscy-scy-Δlink-mCherry clone.

A) Sequence of joins in the construct pIJ8660-Pscy-scy-Δlink-mCherry. The *scy-mCherry* junction lacks a linker with *scy* reading directly into *mCherry*. Restriction site sequences are bold and underlined. The *Pscy* and *scy* sequences are highlighted light blue and *mCherry* is highlighted pink. Primers for colony PCR are marked (black arrows).

B) The gel isolated *Bgl*II fragment of pIJ8660-scyCterm-Δlink-mCherry used for construction of pIJ8660-Pscy-scy-Δlink-mCherry was analysed on a 0.7% agarose gel (Lane 2). The DNA size marker is Lambda *Hind*III/*Eco*RI (Lane 1).

C) The gel isolated *Bgl*II fragment containing *Pscy-scy* used for construction of pIJ8660-Pscy-scy-Δlink-mCherry was analysed on a 0.7% agarose gel (Lane 2). The DNA size marker is Lambda *Hind*III/*Eco*RI (Lane 1).

D) Candidate colonies were screened with colony PCR using TH Scy F4 (upstream) and TH Scy R4 (downstream) primers and PCR products were analysed on a 1% agarose gel. Candidate colonies are shown Lanes 2-18. The arrow indicates the ~835bp PCR product expected. The plasmids pIJ8660-scyCterm-mCherry (no link) (Lane 19) and pIJ8660-Pscy-scy-egfp (Lane 20) were used as control templates. The DNA size marker is Lambda *Hind*III/*Eco*RI (Lane 1).

E) Sequencing chromatogram showing the reverse complement of pIJ8660-Pscy-scy-mCherry (no link) sequenced with the mCherryseq primer. Underlined sequences are *Bgl*II or *Nde*I restriction sites.

To generate the full length *scy* fusion to a non-linkered *mCherry*, a 4.2kb *Bgl*II fragment from pIJ8660-Pscy-scy was moved into pIJ8660-scyCterm-Δlink-mCherry (Figure 152 & Figure 153). After ligation of the fragments the ligation mixture was used for transformation of *E. coli* strain DH5α. The transformants were screened with colony PCR (Figure 153D) to find potential clones which now produced a ~835bp PCR product that can only be generated from the full length *scy* fragment and not the smaller *scyCterm* fragment. Plasmid DNA was then isolated from positive colonies and was sequenced to verify that there was no glycine linkered between the sequence of *scy* and *mCherry* (Figure 153E). Thus, confirming the generation of the plasmid pIJ8660-Pscy-scy-Δlink-mCherry, with the *scy* promoter followed by the full length of *scy* in frame to *mCherry* with no glycine linker (Figure 153).

10.1.51 Generation of an EGFP-Scy-C translational fusion

To determine if the C-terminal domain alone was important for localisation we generated an *egfp* fusion to DNA encoding the Scy-C domain. To be able to do this it was aimed to use the full length N-terminal EGFP fusion construct pIJ8660-Pscy-egfp-scy (pK56). For the *egfp-scy-C* fusion the aim was that a linker would be inserted between the *egfp* and the beginning of the *scy-C* sequence replacing the sequence of *scy-N*. A *Kpn*I site is located in the *scy* gene and marks the border between the sequences encoding the heptad coiled-coil N-terminal domain and the non-heptad coiled-coil C-terminal domain of the Scy protein. To remove the N-terminal domain and place the C-terminal domain in frame with *egfp*, a linker was designed to be inserted inbetween the *Bsr*GI and the *Kpn*I sites of pIJ8660-Pscy-egfp-scy (pK56) (Figure 154A). This linker consisted of two primers, Bsrg-Kpn Linker 1 and Bsrg-Kpn Linker 2 annealed to one another generating protruding *Kpn*I and *Bsr*GI ends. The primers were designed that the linker also contained an *Xba*I site, which would enable the identification of the successful constructs correctly. Also, the triplets encoding the amino acid sequence of the linker were designed according to the *Streptomyces* codon preference. Insertion of this linker between the *Bsr*GI and the *Kpn*I sites of pIJ8660-Pscy-egfp-scy (pK56) removed the sequence encoding the N-terminal domain and generated a fusion whereby *egfp* reads in frame to sequence encoding the C-

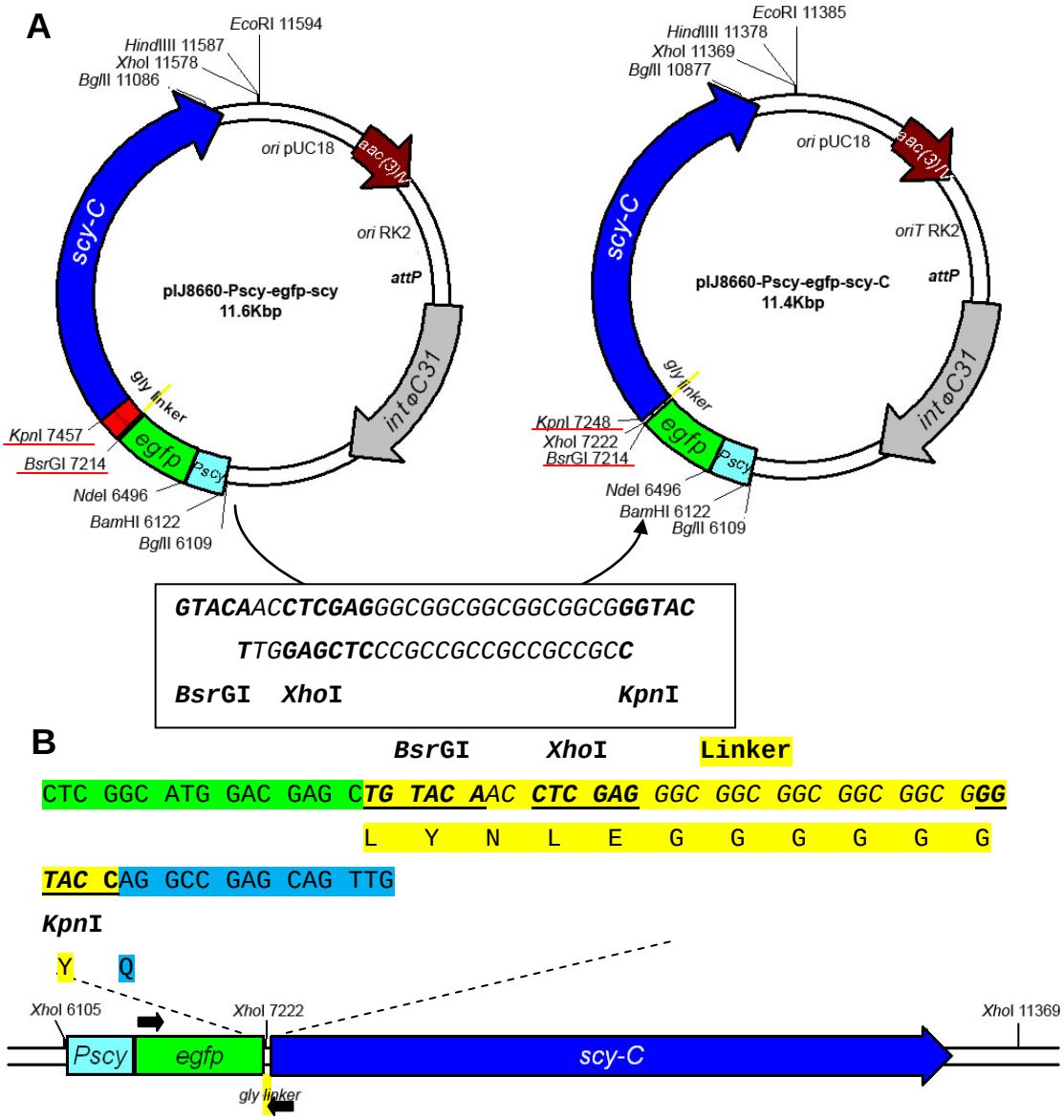

Figure 154: Generation of pIJ8660-Pscy-egfp-scy-C.

A) pIJ8660-Pscy-egfp-scy-C is a pIJ8660-Pscy-egfp-scy derivative with a linker inserted between the *Bsr*GI and *Kpn*I site removing the *scy-N* terminal domain and placing the *scy-C* terminal domain in frame with *egfp*. The restriction sites used in the cloning are underlined in red.

B) Sequence of the junctions in the construct pIJ8660-Pscy-egfp-scy-C. The *egfp-scy-C* junction contains a glycine linker (highlighted yellow/italics). Restriction site sequences are bold and underlined. The *scy-C* sequence is highlighted blue and *egfp* is highlighted green. Primers for colony PCR are marked (black arrows).

terminal domain via a sequence encoding a penta-glycine linker (Figure 154B). The vector DNA fragment used in the ligation can be seen in (Figure 156A). Annealing of the primers for the linker directly preceded ligation of vector fragment and the linker, the ligation mixture was then used for transformation of *E. coli* strain DH5α. The transformants were

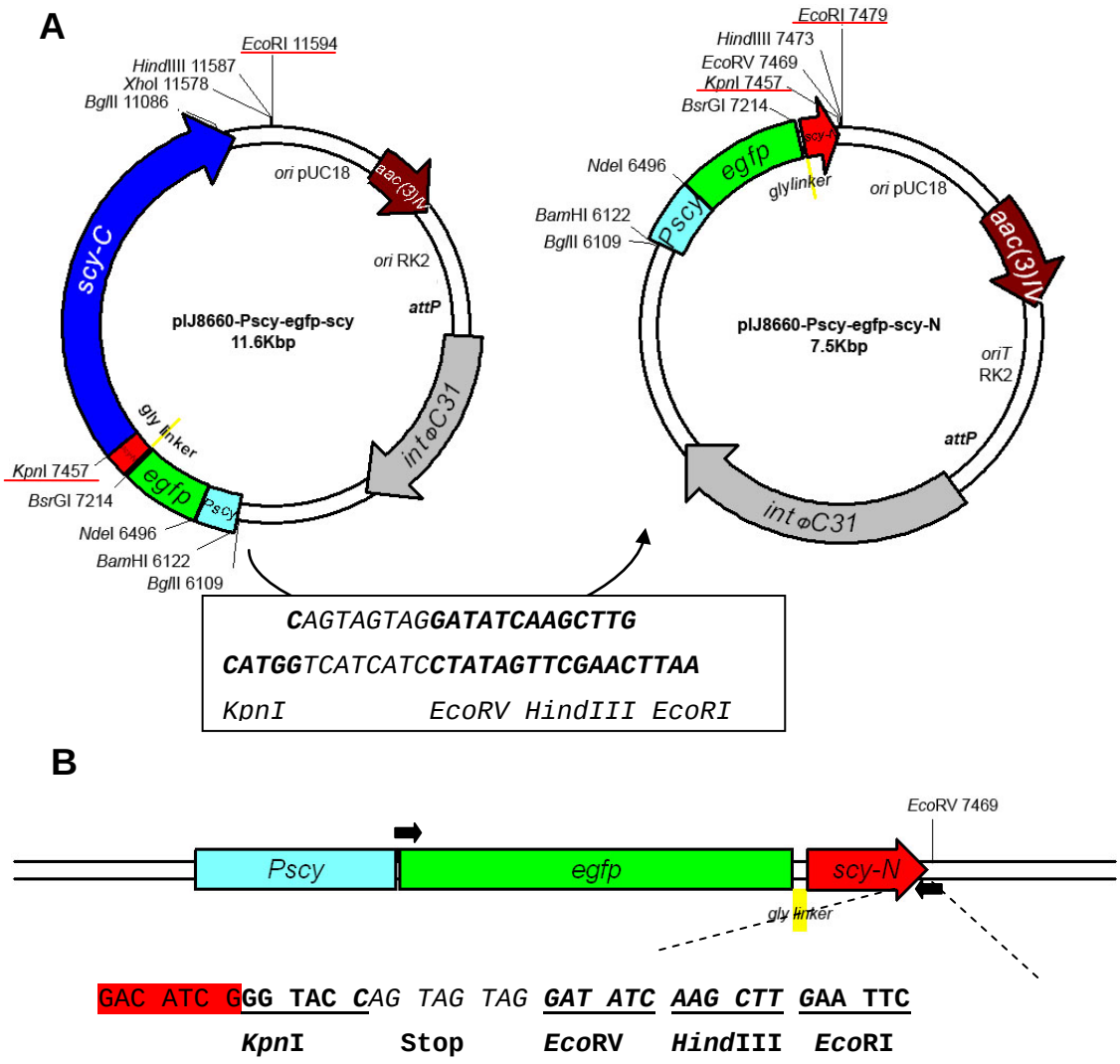

Figure 155: Generation of pIJ8660-Pscy-egfp-scy-N.

A) pIJ8660-Pscy-egfp-scy-N is a pIJ8660-Pscy-egfp-scy derivative with a linker inserted between *Kpn*I EcoRI site removing the *scy-C* terminal domain and placing a stop codon following *scy-N*. The restriction sites used in the cloning are underlined in red.

B) Sequence of the junctions in the construct pIJ8660-Pscy-egfp-scy-N. The *scy-N* sequence ends with a stop codon introduced from the linker. Restriction site sequences are bold and underlined. The *scy-N* sequence is highlighted red. Primers for colony PCR are marked (black arrows).

screened with colony PCR (Figure 156C) to find potential clones which now generated a ~748bp PCR product. Plasmid DNA was then isolated from positive colonies, isolated DNA was confirmed by restriction digestion (Figure 156B) with *Xho*I to generate a different pattern including the generation of a short 1117bp fragment and a longer 4147bp fragment not present in pIJ8660-Pscy-egfp-scy. The junction between *egfp* and *scy-C* was also sequenced to verify that a single linker had been added. Thus, confirming the generation of pIJ8660-Pscy-egfp-scy-C.

10.1.52 Generation of an EGFP-Scy-N translation fusion

To be able to establish if the N-terminal domain of Scy was able to localise in the absence of the C-terminal domain, an *egfp-scy-N* fusion was constructed. The strategy was to use the full length *egfp-scy* construct and to remove the sequence encoding the C-terminal domain and add a stop codon following the sequence encoding the N-terminal domain. Therefore, a linker was designed to be inserted inbetween the *Kpn*I and the *Eco*RI sites of pIJ8660-Pscy-egfp-scy (pK56) (Figure 155A). The linker design involved annealing of the Kpn-Eco Linker 1 and Kpn-Eco Linker 2 primers which created overhangs corresponding to *Kpn*I and *Eco*RI restriction sites. The linker was designed that it contained the restriction sites *Eco*RV and *Hind*III which enabled the identification of the successful clones. Insertion of this linker between the *Kpn*I and the *Eco*RI sites of pIJ8660-Pscy-egfp-scy (pK56) would remove the C-terminal domain and placed a stop codon following the N-terminal domain (Figure 155B). The vector DNA fragment used in the ligation can be seen in (Figure 156A). The Kpn-Eco Linker 1 and Kpn-Eco Linker 2 were annealed to one another directly preceding ligation of vector fragment and the linker, the ligation mixture was then used for transformation of *E. coli* strain DH5α. The transformants were screened with colony PCR (Figure 156D) to find potential clones which now produced a ~985bp PCR product. Plasmid DNA was then isolated from positive colonies, isolated DNA was confirmed by restriction digestion (Figure 156B) with *Eco*RV which would only be present in the linker and thus a single band confirmed the incorporation of the linker. The junction between *scy-N* and the vector was also sequenced to verify that the linker had been added in the intended way. Thus, confirming the generation of pIJ8660-Pscy-egfp-scy-N.

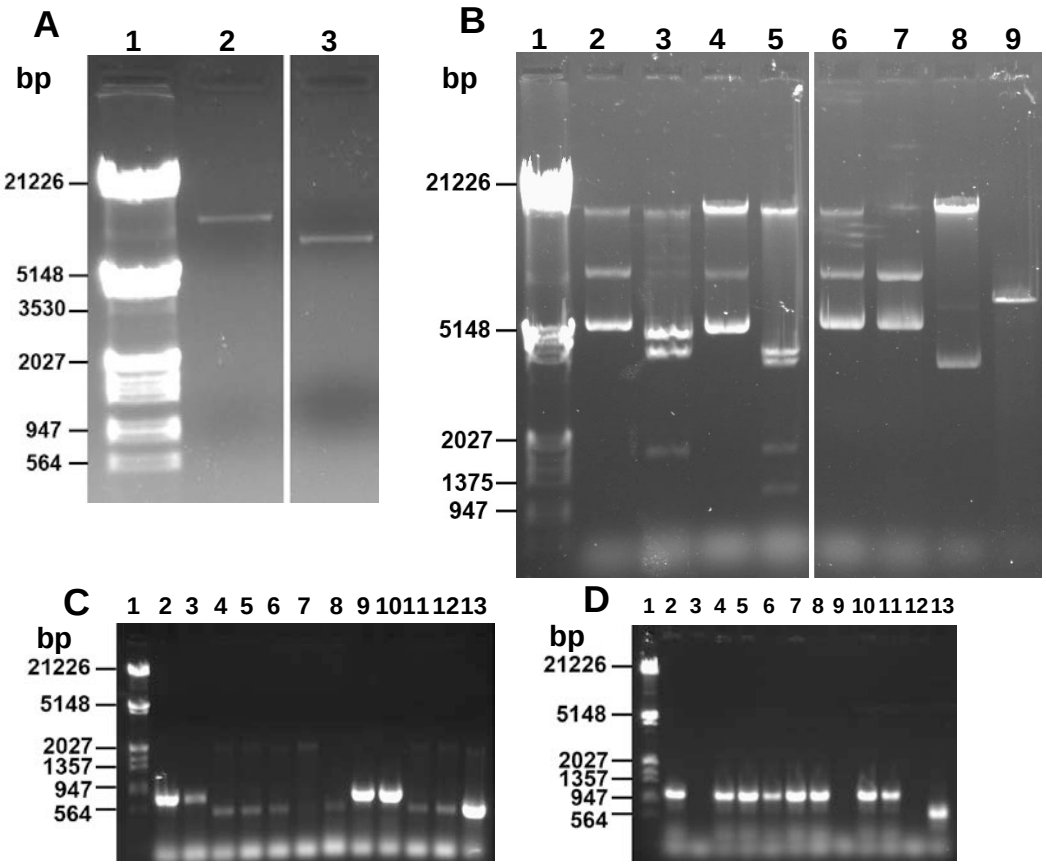

Figure 156: DNA Fragments for generation of pIJ8660-Pscy-egfp-scy-C and pIJ8660-Pscy-egfp-scy-N, as well as Digestion of subsequent pIJ8660-Pscy-egfp-scy-C and pIJ8660-Pscy-egfp-scy-N clones.

A) The gel isolated fragments used for construction of pIJ8660-Pscy-egfp-scy-C and pIJ8660-Pscy-egfp-scy-N were analysed on a 0.7% agarose gel. The fragments used were a *Bsr*GI/*Kpn*I fragment of pIJ8660-Pscy-egfp-scy (Lane 2) and a *Kpn*I/*Eco*RI fragment of pIJ8660-Pscy-egfp-scy (Lane 3). The DNA size marker is Lambda *Hind*III/*Eco*RI (Lane 1).

B) The plasmids pIJ8660-Pscy-egfp-scy (Lanes 2, 3, 6 & 7), pIJ8660-Pscy-egfp-scy-C (Lanes 4 & 5) and the plasmid pIJ8660-Pscy-egfp-scy-N (Lanes 8 & 9) were analysed on a 0.7% agarose gel. Undigested samples (Lanes 2, 4, 6 & 8) were run together with samples digested with *Xho*I (Lanes 3 & 5) or *Eco*RV (Lanes 7 & 9). The DNA size marker is Lambda *Hind*III/*Eco*RI (Lane 1)

C) Candidate colonies carrying pIJ8660-Pscy-egfp-scy-C were screened with colony PCR using FP-Nde (upstream) and Bsrg-Kpn Linker 2 (downstream) primers and PCR products were analysed on a 0.7% agarose gel. Candidate colonies are shown Lanes 2-12. The arrow indicates the ~748bp PCR product expected. The plasmid pIJ8660-Pscy-egfp-scy (Lane 13) was used as a control template. The DNA size marker is Lambda *Hind*III/*Eco*RI (Lane 1).

D) Candidate colonies carrying pIJ8660-Pscy-egfp-scy-N were screened with colony PCR using FP-Nde (upstream) and Kpn-Eco Linker 2 (downstream) primers and PCR products were analysed on a 0.7% agarose gel. Candidate colonies are shown Lanes 2-12. The arrow indicates the ~985bp PCR product expected. The plasmid pIJ8660-Pscy-egfp-scy (Lane 13) was used as a control template. The DNA size marker is Lambda *Hind*III/*Eco*RI (Lane 1).

10.1.53 Generation of a Scy-N-EGFP translational fusion

To be able to generate a fusion of *scy-N-egfp* we needed to use pIJ8660-Pscy-scy-egfp, but due to there being two *Nde*I sites we were not able to simply insert a linker to replace *scy-C*. Instead due to the small size of the sequence encoding the N-terminal domain we decided to PCR amplify an *Nde*I fragment that could replace the full length *Nde*I fragment.

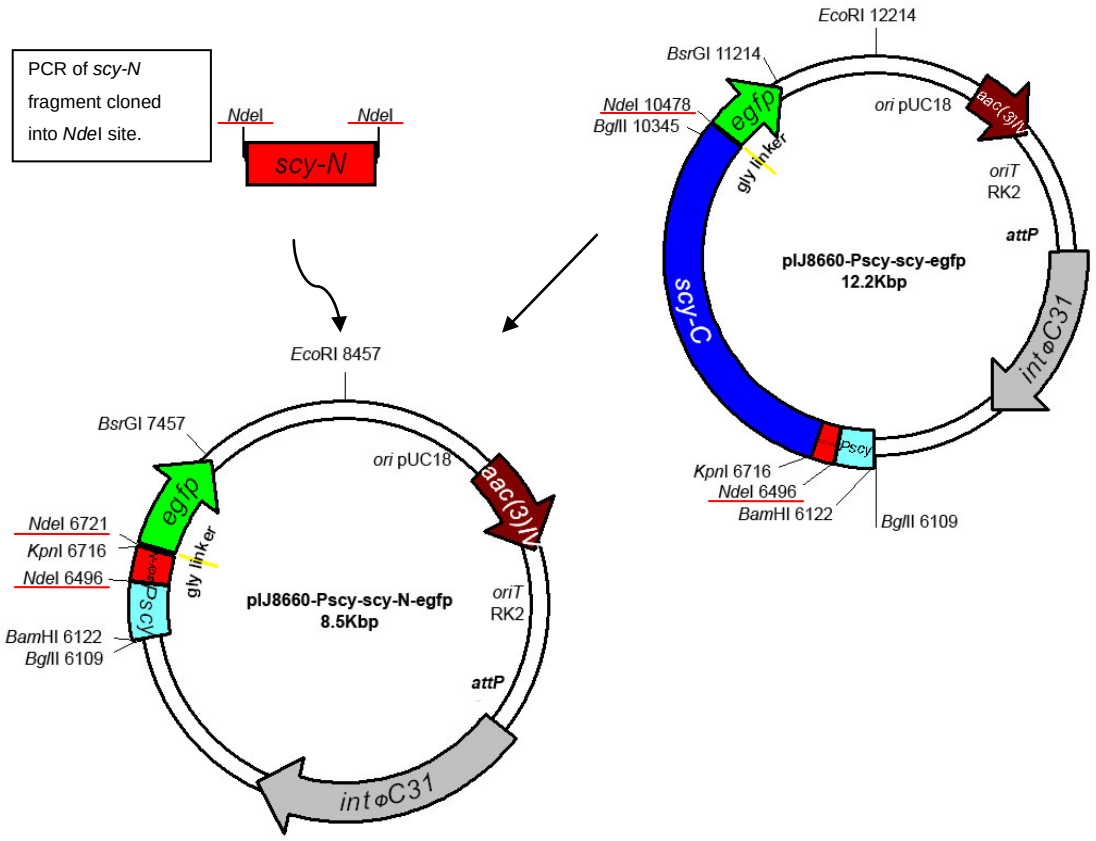

Figure 157: Generation of pIJ8660-Pscy-scy-N-egfp.

pIJ8660-Pscy-scy-N-egfp is a derivative of pIJ8660-Pscy-scy-egfp. A *scy-N* fragment was amplified using PCR and digested using *Nde*I. Using *Nde*I pIJ8660-Pscy-scy-egfp was digested and the full length *scy* fragment replaced with the *scy-N* fragment in frame with *egfp*. The restriction sites used in the cloning are underlined in red.

A fragment encoding the Scy-N domain was amplified using the St8F4 cosmid as a template for PCR using the oligonucleotides scyNde1 and ScyN_FPrev. The oligonucleotides introduced *Nde*I restriction sites at both ends of the PCR product, when digested with *Nde*I this should leave an approximately 225bp product. The plasmid pIJ8660-Pscy-scy-egfp was also digested with *Nde*I so that the full length *scy* fragment was dropped out. Upon ligation the loss of the full length *scy* fragment should result in replacement with the *scy-N* PCR fragment (Figure 157 & Figure 158). After ligation of the

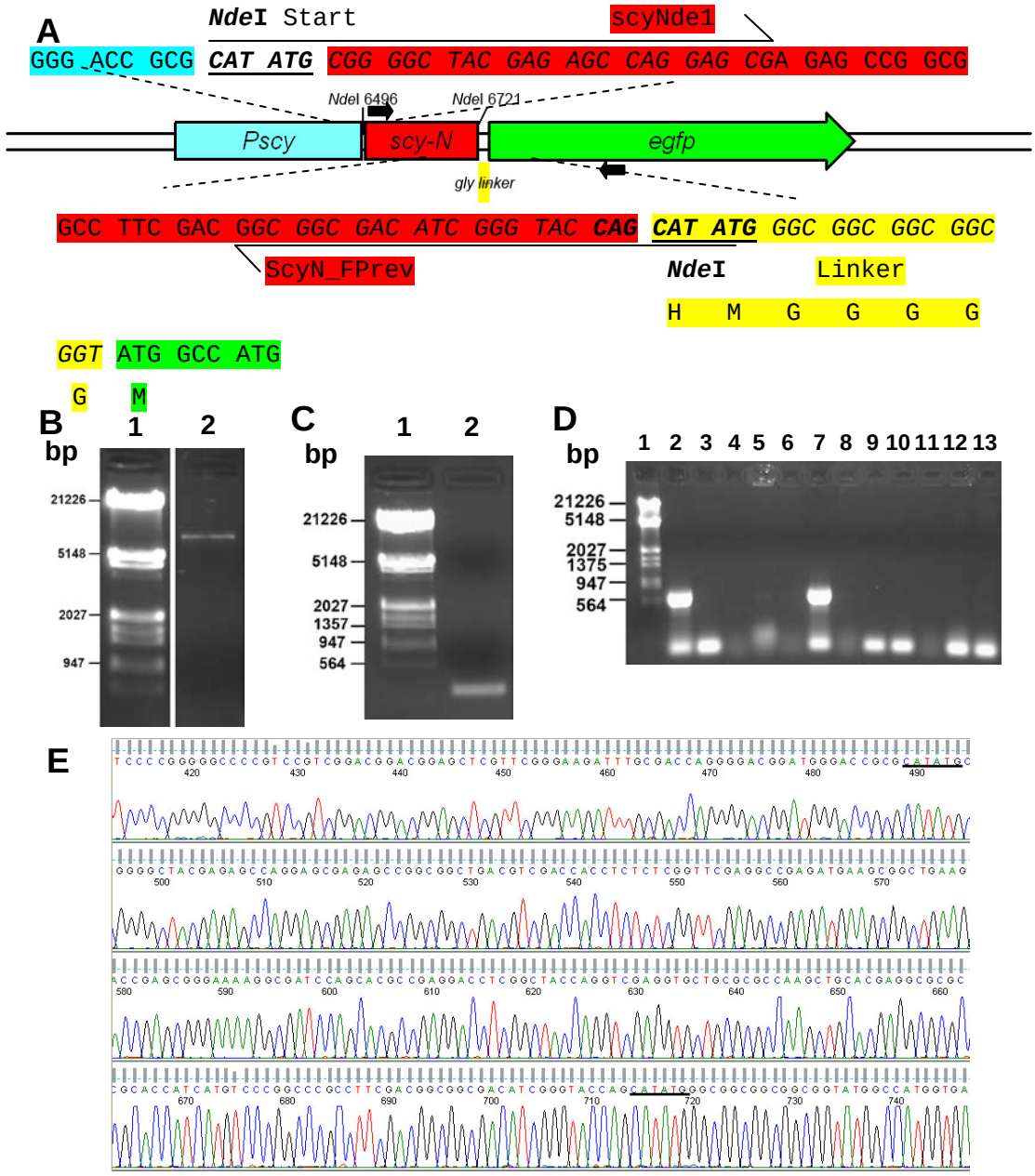

Figure 158: DNA Fragments for generation of pIJ8660-Pscy-scy-N-EGFP and sequencing of subsequent pIJ8660-Pscy-scy-N-EGFP clone.

A) Sequence of joins in the construct pIJ8660-Pscy-scy-N-EGFP. Sequence of the junctions between the promoter and the open reading frame, as well as the *scy-N* fragment and *egfp*. The *scy-N-egfp* junction contains a glycine linker (highlighted yellow/italics). Restriction site sequences are bold and underlined. Primer sequences are marked in italics and with arrows. The *Pscy* sequence is highlighted light blue, the *scy-N* sequence is highlighted red and *egfp* is highlighted green. Primers for colony PCR are marked (black arrows).

B) Gel isolated fragment of pIJ8660-Pscy-scy-egfp (*Nde*I) used for construction of pIJ8660-Pscy-scy-N-EGFP run on a 0.85% agarose gel. The lanes were loaded as follows: 1) ladder; 2) pIJ8660-Pscy-scy-egfp *Nde*I digested.

C) Gel isolated fragment of *scy-N* PCR product (*Nde*I) used for construction of pIJ8660-Pscy-scy-N-EGFP run on a 0.85% agarose gel. The lanes were loaded as follows: 1) ladder; 2) scy-N PCR product *Nde*I digested.

D) Candidate colonies were screened with colony PCR using scyNde1 (upstream) and EGFPseq (downstream) primers and PCR products were analysed on a 1% agarose gel. Candidate colonies are shown Lanes 2-12. The arrow indicates the ~586bp PCR product expected. The plasmid pIJ8660-Pscy-scy-egfp (Lane 13) was used as a control template. The DNA size marker is Lambda *Hind*III/*Eco*RI (Lane 1).

E) Sequencing chromatogram showing the reverse complement of pIJ8660-Pscy-scy-N-egfp sequenced with the EGFPseq primer. Underlined sequences are *Nde*I restriction sites.

fragments the ligation mixture was used for transformation of *E. coli* strain DH5α. The transformants were screened with colony PCR (Figure 158D) to find potential clones which now produced a ~586bp PCR product that can only be generated from the *scy-N* fragment being in close proximity to *egfp*. Plasmid DNA was then isolated from positive colonies, isolated DNA was confirmed by sequencing (Figure 158E) to contain the *scy-N* fragment. Thus, confirming the generation of the plasmid pIJ8660-Pscy-scy-N-egfp, with the *scy-N* domain in frame to *egfp* fused at the C-terminus (Figure 158A).

10.1.54 Generation of pMS82 construct containing Pscy-mCherry-scy

In order to visualise Scy localisation in a variety of alternative genetic backgrounds, pMS82 was an ideal candidate in which it was aimed to directly move a fragment containing *Pscy-mCherry-scy* into pMS82 (Figure 159). From pIJ8660-Pscy-mCherry-scy

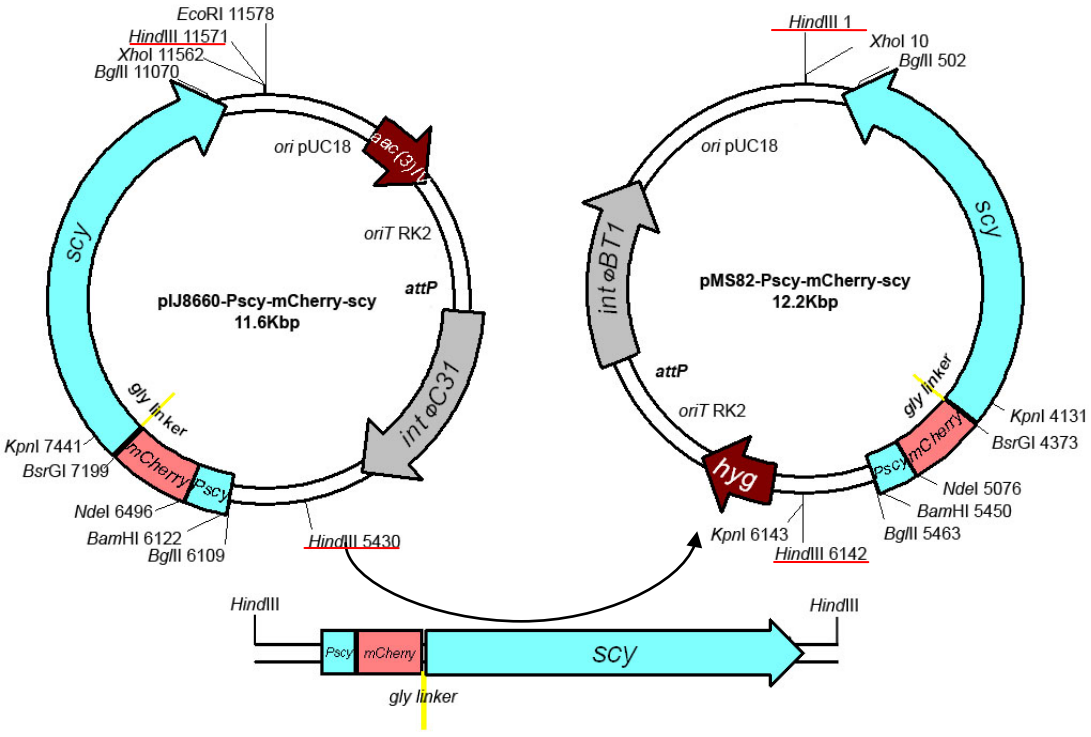

Figure 159: Generation of pMS82-Pscy-mCherry-scy.

pMS82-Pscy-mCherry-scy is a derivative of pMS82. A *Pscy-mCherry-scy* fragment was liberated using *Hind*III from pIJ8660-Pscy-mCherry-scy and cloned into the *Hind*III site of pMS82. The restriction sites used in the cloning are underlined in red.

(pK57) a 6.1kb *Hind*III fragment was excised and cloned into the *Hind*III site of pMS82 (Figure 160). After ligation of the fragments and transformation of *E. coli* strain DH5α, the transformants were screened with colony PCR (Figure 160D) where positive clones were

predicted to produce a ~385bp product of the *scy* promoter. Potential clones were confirmed by restriction digestion to contain the *Pscy-mCherry-scy* fragment (Figure 160C), thus, generating pMS82-Pscy-mCherry-scy (pK66) which carries an alternative resistance cassette and integrates into an alternative site in the *S. coelicolor* genome in comparison to pIJ8660.

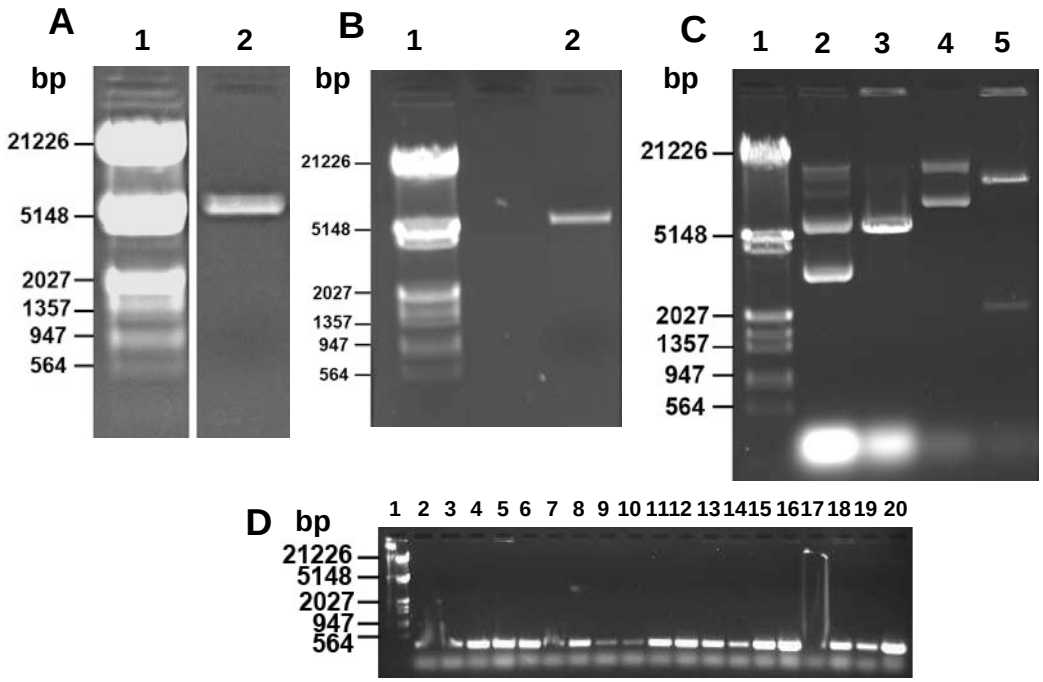

Figure 160: DNA Fragments for generation of pMS82-Pscy-mCherry-scy and Digestion of subsequent pMS82-Pscy-mCherry-scy clone.

A) The gel isolated *Hind*III fragment of pMS82 used for construction of pMS82-Pscy-mCherry-scy was analysed on a 0.7% agarose gel (Lane 2). The DNA size marker is Lambda *Hind*III/*Eco*RI (Lane 1).

B) The gel isolated *Hind*III fragment containing *Pscy-mCherry-scy* used for construction of pMS82-Pscy-mCherry-scy was analysed on a 0.7% agarose gel (Lane 2). The DNA size marker is Lambda *Hind*III/*Eco*RI (Lane 1).

C) The plasmids pMS82 (Lanes 2 & 3) and the plasmid pMS82-Pscy-mCherry-scy (Lanes 4 & 5) were analysed on a 0.7% agarose gel. Undigested samples (Lanes 2 & 4) were run together with samples digested with *Kpn*I (Lanes 3 & 5). The DNA size marker is Lambda *Hind*III/*Eco*RI (Lane 1).

D) Candidate colonies were screened with colony PCR using scyprom4-Bam (upstream) and scyprom3-Nde (downstream) primers and PCR products were analysed on a 1% agarose gel. Candidate colonies are shown Lanes 2-19. The arrow indicates the ~385bp PCR product expected. The plasmid pIJ8660-Pscy-mCherry-scy (Lane 20) was used as a control template. The DNA size marker is Lambda *Hind*III/*Eco*RI (Lane 1).

10.1.55 Generation of a FilP-EGFP translational fusion

We generated a *filP-egfp* fusion in order to investigate the localisation of FilP in *Streptomyces*. The strategy for generating a *filP-egfp* fusion was to PCR amplify the whole of *filP* lacking a stop codon and clone an *Nde*I fragment into pAZ1. Then, to this *filP-egfp*

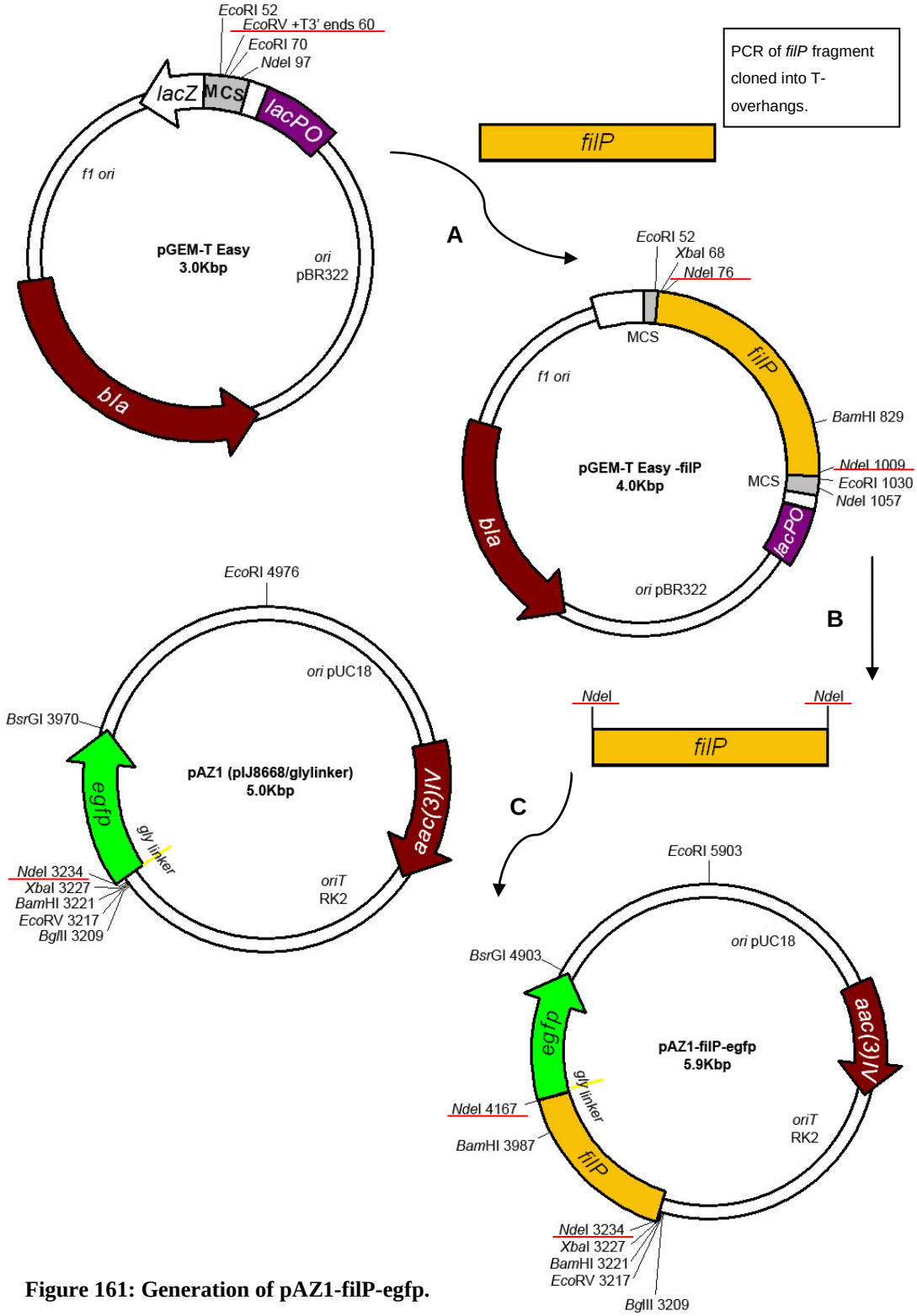

Figure 161: Generation of pAZ1-filP-egfp.

pAZ1-filP-egfp is a derivative of pAZ1 containing a *filP* fragment. A) A *filP* PCR fragment was cloned into the multiple cloning site of pGEM-T Easy, which is designed with T overhangs for easy incorporation of a Taq polymerase generated PCR product. B) The *filP* *Nde*I fragment was liberated from pGEM-T Easy-filP. C) Using *Nde*I, pAZ1 was digested and the *filP* fragment cloned so that *filP* was in frame with *egfp*. The restriction sites used in the cloning are underlined in red.

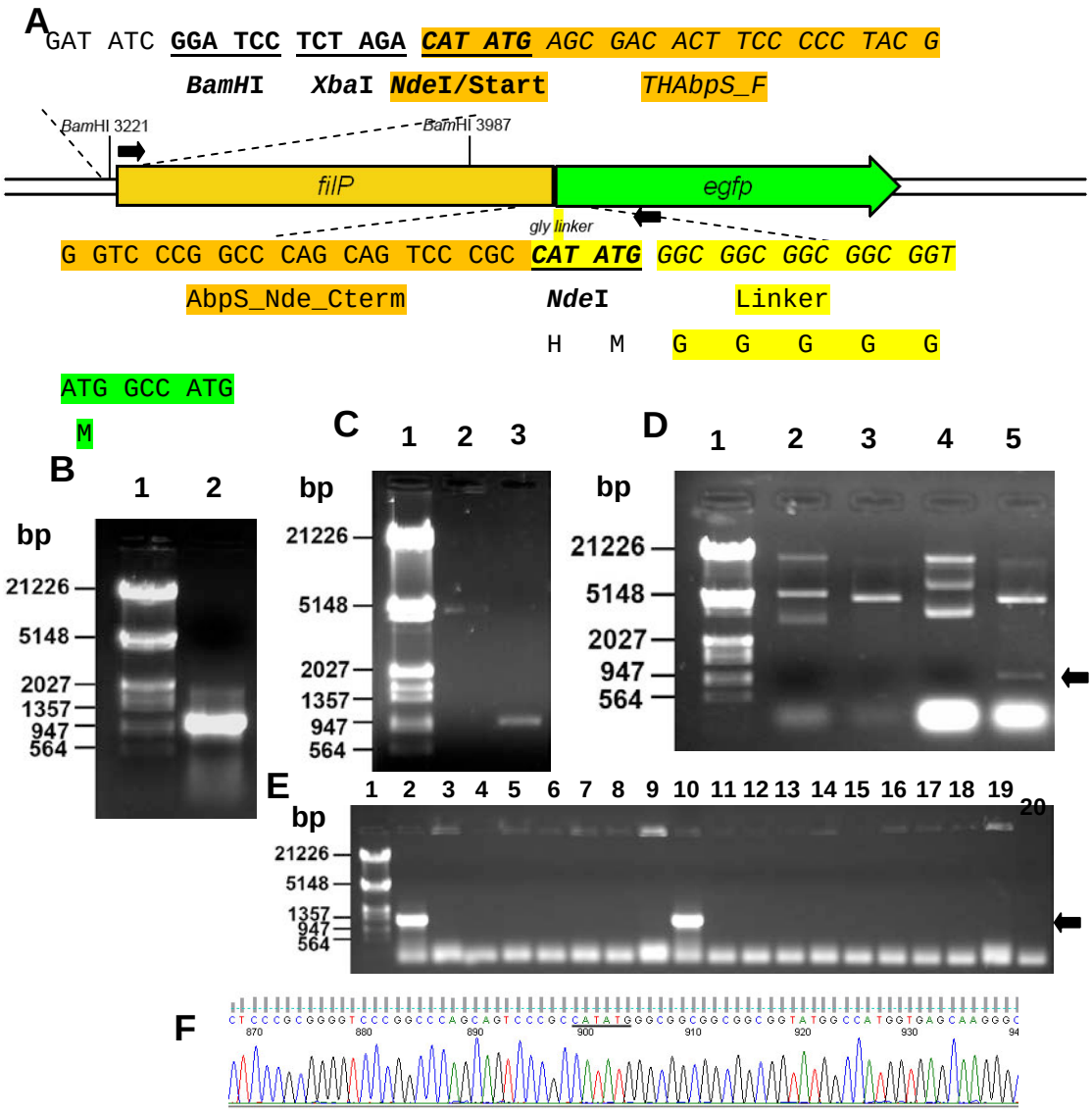

Figure 162: DNA Fragments for generation of FilP-EGFP fusion in pAZ1 and its confirmation by restriction digests.

A) pAZ1-filP-egfp. Sequence of the junctions between the multiple cloning site, the *filP* fragment and *egfp*. The *filP-egfp* junction contains a glycine linker (highlighted yellow/italics). Restriction site sequences are bold and underlined. Primer sequences are marked in italics and with arrows. The *filP* sequences are highlighted orange and *egfp* is highlighted green. Primers for colony PCR are marked (black arrows).

B) The PCR product generated from using the primers THAbpS_F and AbpS_Nde_Cterm was analysed on a 0.7% agarose gel (Lane 2). The DNA size marker is Lambda *Hind*III/*Eco*RI (Lane 1).

C) The gel isolated fragments used for construction of pAZ1-filP-egfp were analysed on a 0.7% agarose gel. The fragments used were the *Nde*I fragment of pAZ1 (Lane 2) and the NdeI fragment of the PCR of *filP* (Lane 3). The DNA size marker is Lambda *Hind*III/*Eco*RI (Lane 1).

D) The plasmids pAZ1 (Lanes 2 & 3) and the plasmid pAZ1-filP-egfp (Lanes 4 & 5) were analysed on a 0.7% agarose gel. Undigested samples (Lanes 2 & 4) were run together with samples digested with *Nde*I (Lanes 3 & 5). The arrow indicates the 933bp fragment carrying *filP*. The DNA size marker is Lambda *Hind*III/*Eco*RI (Lane 1).

E) Candidate colonies were screened with colony PCR using THAbpS_F (upstream) and EGFPseq (downstream) primers and PCR products were analysed on a 0.7% agarose gel. Candidate colonies are shown Lanes 2-19. The arrow indicates the ~1302bp PCR product expected. The plasmid pAZ1 (Lane 20) was used as control templates. The DNA size marker is Lambda *Hind*III/*Eco*RI (Lane 1).

F) Sequencing chromatogram showing the reverse complement of pAZ1-filP-egfp sequenced with the EGFPseq primer, shown is *filP* in frame to *egfp*, revealing that the NdeI fragment was cloned in the correct orientation.

pAZ1 construct the aim would be to clone in a 2.1 Kbp *Bam*HI fragment originating from the cosmid St8F4. This fragment would contain the upstream region to *filP* including the intergenic region between *scy* and *filP*, as well as containing the last ~1000bp of the *scyCterm*. Therefore, hopefully ensuring that if the *filP* promoter extends into the *scy* open reading frame that it will be present in the construct. Lastly the whole of the fusion construct was intended to be moved to pIJ8660 as this vector can integrate at a specific site in the *S. coelicolor* chromosome at high efficiency.

Firstly a *filP* fragment was generated by PCR using the primers THAbpS_F and AbpS_Nde_Cterm. The primer AbpS_Nde_Cterm binds to the 3' end of *filP* and would remove the stop codon and add an *NdeI* site making it possible to fuse *filP* in frame to *egfp* in the vector pAZ1. THAbpS_F anneals to the 5' end of the *filP* gene and introduces another *Nde*I site allowing cloning (Figure 161). The template used was the St8F4 cosmid which contains a fragment of the *S. coelicolor* chromosome with *scy* and *filP* genes encoded. For efficient cloning and screening the PCR fragment containing *filP* was first moved into the commercial vector pGEM-T Easy. The vector pGEM-T Easy is of use for cloning PCR products as it is distributed as a linearised fragment with single 3' thymidines at both ends. A PCR product generated with Go Taq® Polymerase will generate 3' adenines at both ends which will be complementary to the thymidine overhangs on pGEM-T Easy. The vector pGEM-T Easy also facilitates blue/white selection for plasmids carrying inserts. Therefore, the PCR product of *filP* was moved directly into pGEM-T Easy without digestion. An aliquot of the PCR product used in the ligation can be seen in Figure 162B. After ligation of the PCR product and linearised pGEM-T Easy, the ligation mixture was used for transformation of *E. coli* strain DH5α. Plasmids from successful white colonies were then confirmed by sequencing the entire insert. We found a clone that contained the correct insert of *filP* with no mutations. Therefore, this clone was used further downstream.

The *filP* fragment was then lifted with *Nde*I and moved into the vector pAZ1 to make a *filP-egfp* fusion (Figure 162). After ligation of the fragments the ligation mixture was used for transformation of *E. coli* strain DH5α. The transformants were screened with colony PCR (Figure 162E) to find potential clones which now produced a ~1302bp PCR product that can only be generated by a *filP-egfp* fusion. Plasmid DNA was then isolated from positive colonies, isolated DNA was confirmed by restriction digestion (Figure 162D) to liberate a ~933bp fragment containing *filP*. Therefore, confirming the generation of pAZ1-filP-egfp with a *filP-egfp* fusion.

In order to then be able to express *filP* we wanted to move a *filP* promoter fragment upstream of the *filP-egfp* fusion generated in pAZ1. To do this we wanted to utilise a plasmid pUC8.9-scy which contains an 8.9Kbp fragment from the St8F4 cosmid encoding both *scy* and *filP*. Conveniently there is a *Bam*HI site located in the C-terminus of *scy* and then there is not another *Bam*HI site until the coding sequence of *filP*. This *Bam*HI fragment 2.1Kbp in length was the desired fragment needed to obtain the *filP* promoter. This 2.1Kbp fragment was first cloned into the vector pUC18 (Figure 163 & Figure 164) to verify that it was infact the intended fragment from pUC8.9-scy. After ligation and transformation of *E. coli* strain DH5α. The transformants were screened with colony PCR (Figure 164D) to find potential clones which now produced a ~1269bp PCR product that can only be generated from the 2.1Kbp fragment in pUC18. Plasmid DNA was then isolated from positive colonies, isolated DNA was confirmed by restriction digestion (Figure 164C) to liberate a ~2.1Kbp fragment. Furthermore plasmid DNA was sequenced to verify that the correct fragment was cloned into pUC18. Therefore, confirming the generation of pUC18-PfilP.

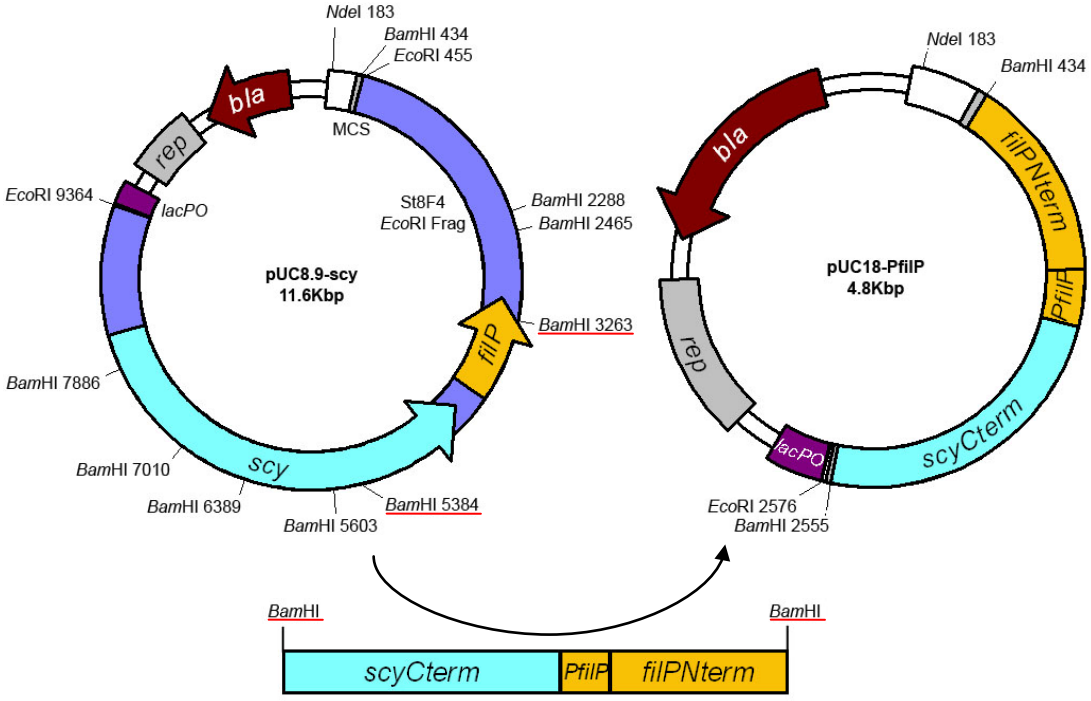

Figure 163: pUC18-PfilP is a derivate of pUC8.9-scy. The *PfilP* fragment was liberated using *Bam*HI from pUC8.9-scy. Using *Bam*HI pUC18 was digested and the *PfilP* fragment cloned in. The restriction sites used in the cloning are underlined in red.

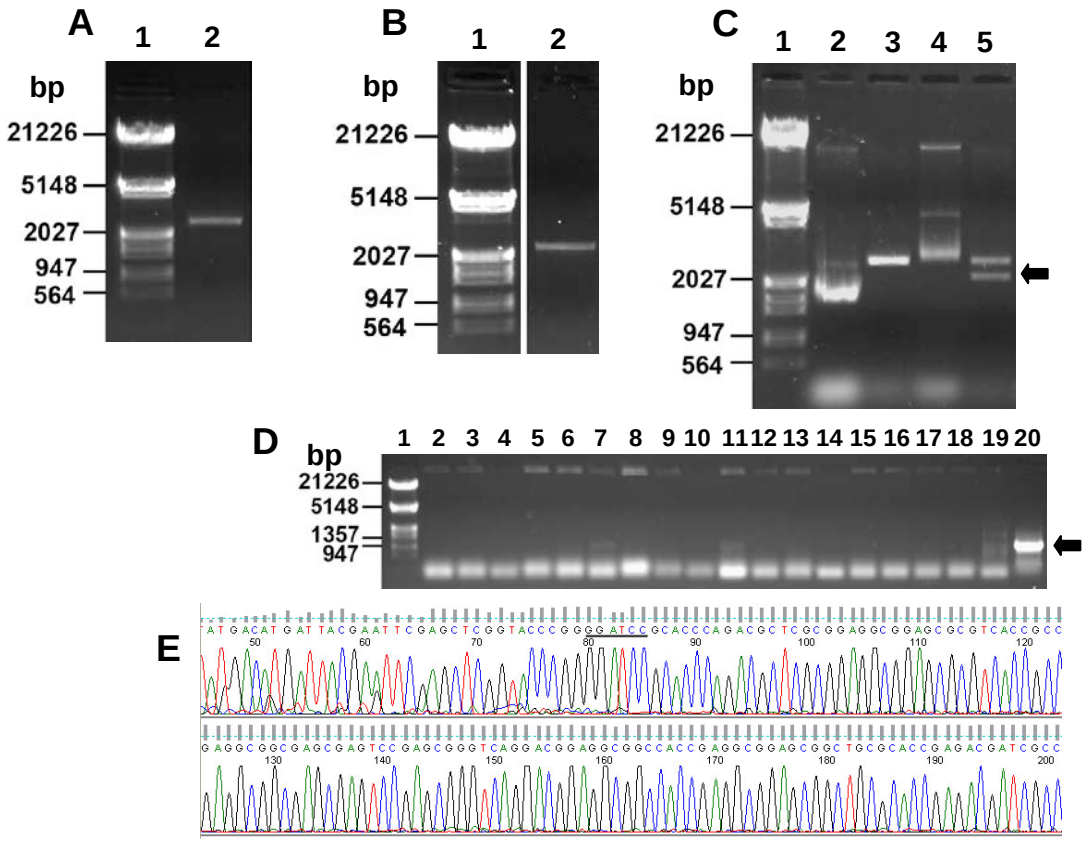

Figure 164: DNA Fragments for generation of a *PfilP* containing pUC18 construct and its confirmation by restriction digest.

A) The gel isolated *Bam*HI fragment of pUC18 used for construction of pUC18-PfilP was analysed on a 0.7% agarose gel (Lane 2). The DNA size marker is Lambda *Hind*III/*Eco*RI (Lane 1).

B) The gel isolated *Bam*HI fragment containing *PfilP* used for construction of pUC18-PfilP was analysed on a 0.7% agarose gel (Lane 2). The DNA size marker is Lambda *Hind*III/*Eco*RI (Lane 1).

C) The plasmids pUC18 (Lanes 2 & 3) and the plasmid pUC18-PfilP (Lanes 4 & 5) were analysed on a 0.7% agarose gel. Undigested samples (Lanes 2 & 4) were run together with samples digested with *Bam*HI (Lanes 3 & 5). The arrow indicates the ~2121bp fragment carrying *scyCterm-PfilP-filP*. The DNA size marker is Lambda *Hind*III/*Eco*RI (Lane 1).

D) Candidate colonies were screened with colony PCR using pUC18 Reverse (upstream) and TH Scy R4 (downstream) primers and PCR products were analysed on a 0.7% agarose gel. Candidate colonies are shown Lanes 2-18. The arrow indicates the ~1269bp PCR product expected. The plasmids pUC18 (Lane 19) and pUC18-scyCterm (Lane 20) were used as control templates.The DNA size marker is Lambda *Hind*III/*Eco*RI (Lane 1).

E) Sequencing chromatogram showing of pUC18-PfilP sequenced with the pUC18 reverse primer, shown is the *Bam*HI site leading into *scyCterm*, revealing that the correct *Bam*HI fragment was cloned in. Underlined sequence is a *Bam*HI restriction site.

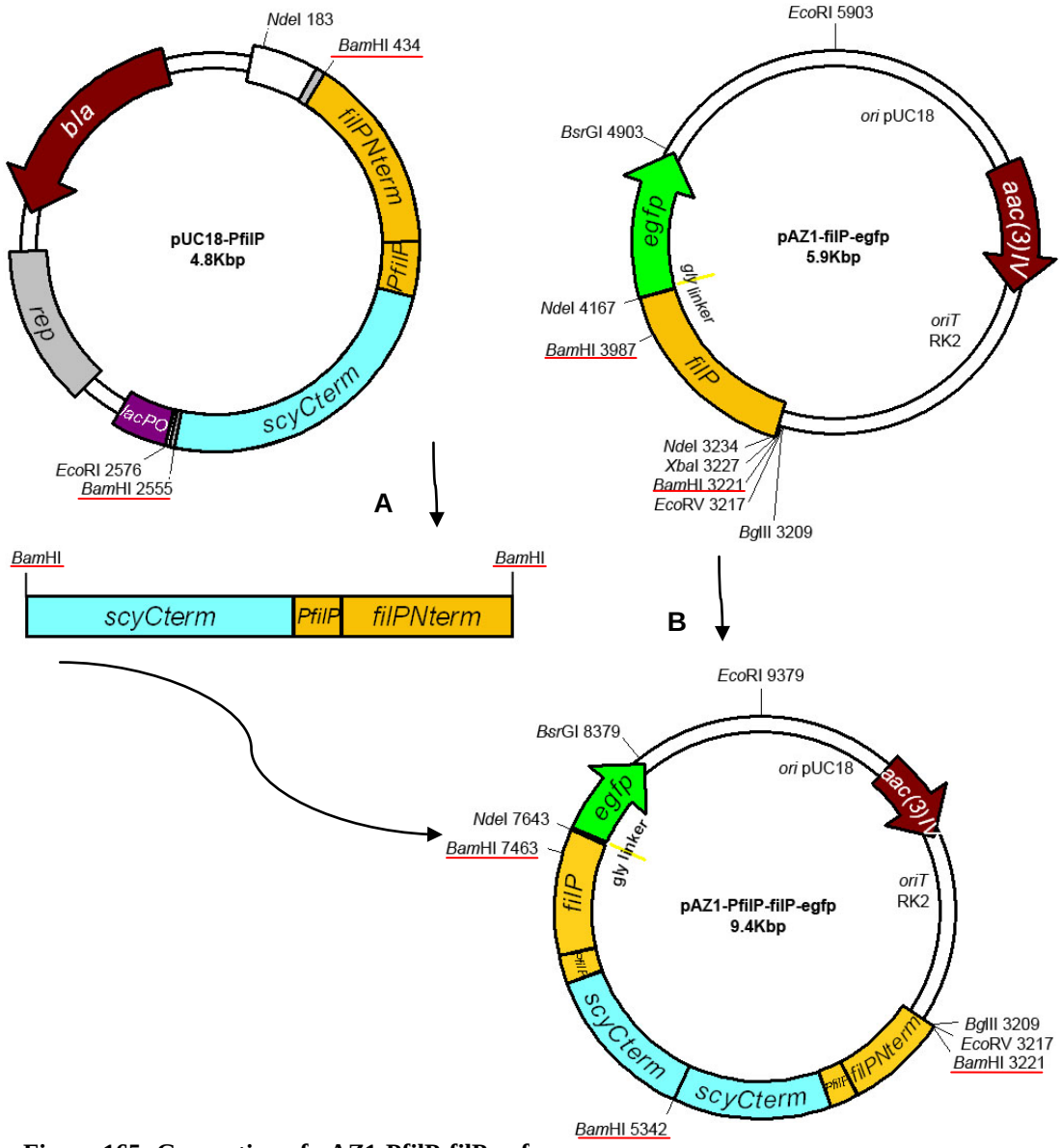

Figure 165: Generation of pAZ1-PfilP-filP-egfp.

pAZ1-PfilP-filP-egfp is a derivative of pAZ1-filP-egfp. A) The *PfilP* *Bam*HI fragment was liberated from pUC18-PfilP. B) Using *Bam*HI, pAZ1-filP-egfp was digested and the *PfilP* fragment cloned so that *filP-egfp* could then be driven by the *filP* promoter. The restriction sites used in the cloning are underlined in red.

We then wanted to move the 2.1Kbp fragment containing *PfilP* from pUC18-PfilP and clone it into the *Bam*HI sites in pAZ1-filP-egfp (Figure 165 & Figure 166). After ligation and transformation of *E. coli* strain DH5α. The transformants were screened with colony PCR (Figure 166E) to find potential clones which now produced a ~1309bp (1159bp for *scyCterm* +150bp for *Tfd*) PCR product that can be generated using the Tfd primer located upstream in pAZ1 and TH Scy R4 downstream in the 2.1Kbp fragment. We found a positive colony that carried a PCR product of the correct site. Plasmid DNA was then isolated from the positive colony, isolated DNA was confirmed by restriction digestion (Figure 166D) to liberate a ~2.1Kbp fragment. However, despite these confirmations that

this was the correct construct we later learned from downstream cloning that this construct had two *Bam*HI 2.1Kbp fragments cloned in, this was indistinguishable in the *Bam*HI restriction digestion. We are unsure of how the PCR product was generated.

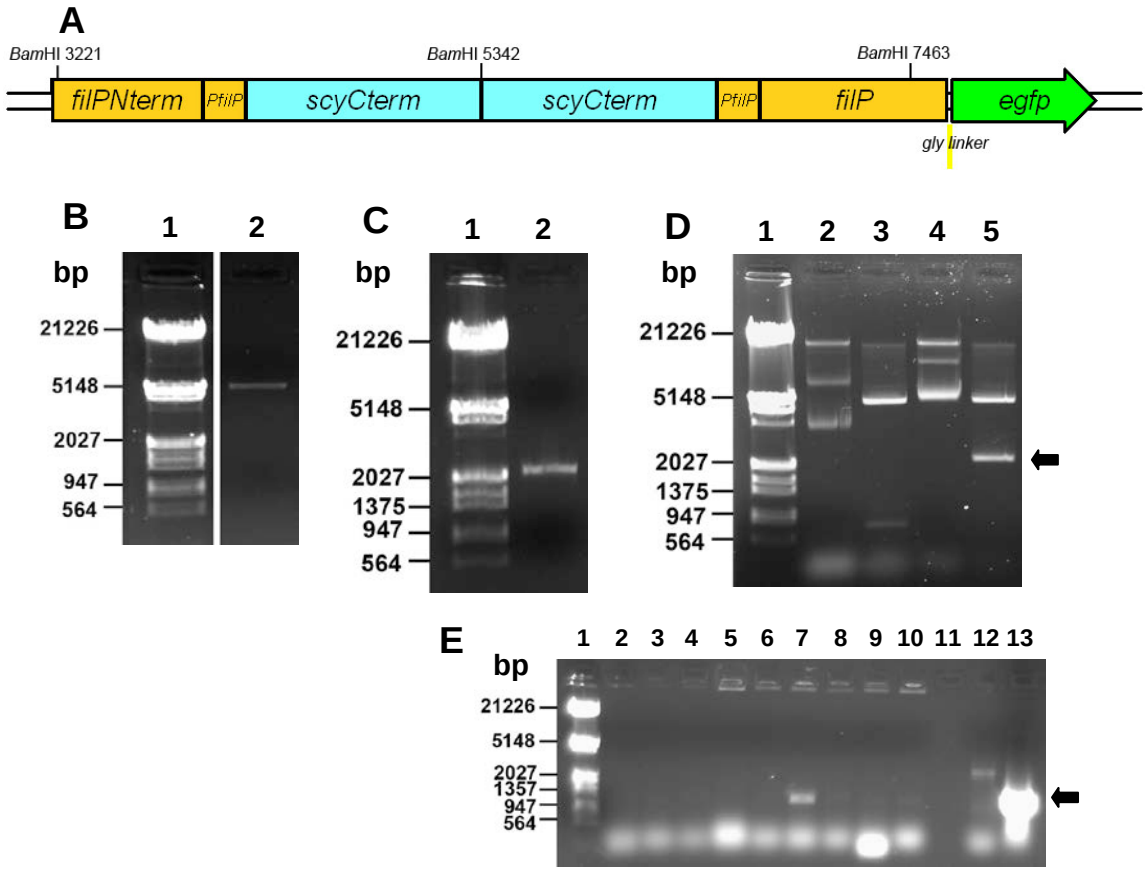

Figure 166: DNA Fragments for generation of a promoter containing FilP-EGFP fusion in pAZ1 and its confirmation by restriction digests.

A) Arrangement of fragments and *Bam*HI sites in the construct pAZ1-PfilP-filP-egfp.

B) The gel isolated fragment *Bam*HI fragment of pAZ1-filP-egfp used for construction of pAZ1-PfilP-filP-egfp was analysed on a 0.7% agarose gel (Lane 2). The DNA size marker is Lambda *Hind*III/*Eco*RI (Lane 1).

C) The gel isolated *Bam*HI fragment containing *PfilP* used for construction of pAZ1-PfilP-filP-egfp was analysed on a 0.7% agarose gel (Lane 2). The DNA size marker is Lambda *Hind*III/*Eco*RI (Lane 1).

D) The plasmids pAZ1-filP-egfp (Lanes 2 & 3) and the plasmid pAZ1-PfilP-filP-egfp (Lanes 4 & 5) were analysed on a 0.7% agarose gel. Undigested samples (Lanes 2 & 4) were run together with samples digested with *Bam*HI (Lanes 3 & 5). The arrow indicates the ~2121bp fragment carrying *scyCterm-PfilP-filP*. The DNA size marker is Lambda *Hind*III/*Eco*RI (Lane 1).

E) Candidate colonies were screened with colony PCR using Tfd (upstream) and TH Scy R4 (downstream) primers and PCR products were analysed on a 0.7% agarose gel. Candidate colonies are shown Lanes 2-10. The arrow indicates the ~1309bp (1159bp for *scyCterm* + 150bp for tfd)bp PCR product expected. The plasmids pAZ1-filP-egfp (Lane 11) and pIJ8660-scyCterm-egfp (Lane 12) were used as control templates.The DNA size marker is Lambda *Hind*III/*Eco*RI (Lane 1).

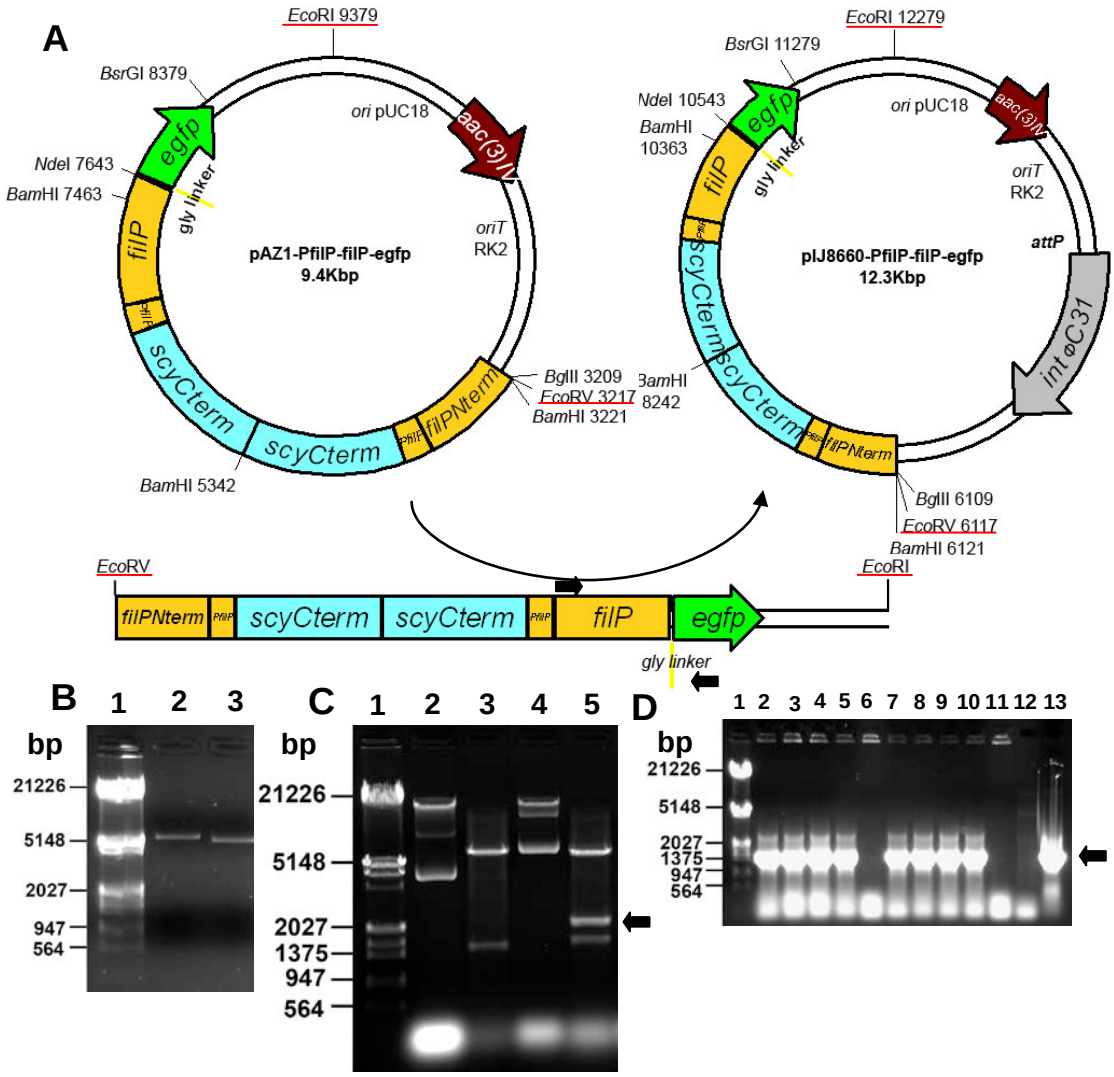

Figure 167: DNA Fragments for generation of pIJ8660-PfilP-filP-egfp and its confirmation by restriction digest.

A) Generation of pIJ8660-PfilP-filP-egfp. Plasmid pIJ8660-PfilP-filP-egfp is a derivative of pIJ8660. A *PfilP-filP-egfp* fragment was liberated using *Eco*RI and *Eco*RV from pAZ1-PfilP-filP-egfp and cloned into the same sites of pIJ8660. Primers for colony PCR are marked (black arrows). The restriction sites used in the cloning are underlined in red.

B) The gel isolated fragments used for construction of pIJ8660-PfilP-filP-egfp were analysed on a 0.7% agarose gel. The fragments used were the *Eco*RI/*Eco*RV fragment of pIJ8660 (Lane 2) and an *Eco*RI/*Eco*RV fragment containing *PfilP-filP-egfp* (Lane 3). The DNA size marker is Lambda *Hind*III/*Eco*RI (Lane 1).

C) The plasmids pIJ8660 (Lanes 2 & 3) and the plasmid pIJ8660-PfilP-filP-egfp (Lanes 4 & 5) were analysed on a 0.7% agarose gel. Undigested samples (Lanes 2 & 4) were run together with samples digested with *Bam*HI and *Eco*RI (Lanes 3 & 5). The arrow indicates the ~2121bp fragment carrying *scyCterm-PfilP-filP*. The DNA size marker is Lambda *Hind*III/*Eco*RI (Lane 1).

D) Candidate colonies were screened with colony PCR using THAbpS_F (upstream) and EGFPseq (downstream) primers and PCR products were analysed on a 0.7% agarose gel. Candidate colonies are shown Lanes 2-11. The arrow indicates the ~1302bp PCR product expected. The plasmids pIJ8660 (Lane 12) and pAZ1-PfilP-filP-egfp (Lane 13) were used as control templates.The DNA size marker is Lambda *Hind*III/*Eco*RI (Lane 1).

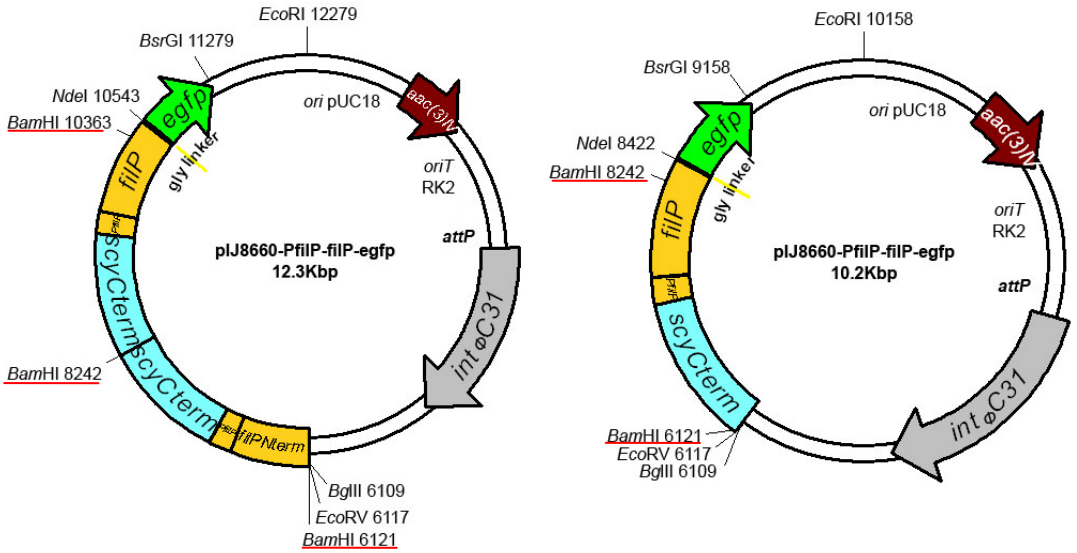

Figure 168: Generation of pIJ8660-PfilP-filP-egfp. Plasmid pIJ8660-PfilP-filP-egfp was corrected by liberating the two *scyCterm-PfilP-filPNterm* fragments using a *Bam*HI digestion and cloning back in a single *scyCterm-PfilP-filPNterm Bam*HI fragment. The restriction sites used in the cloning are underlined in red.

As the intention was to generate the *filP-egfp* fusion in pIJ8660 a vector that will integrate into the *S. coelicolor* chromosome at high efficiency, we aimed to move the *filP* Promoter sequence plus the *filP-egfp* fusion as one fragment with *EcoRV* and *Eco*RI to pIJ8660 (Figure 167). It was here that we detected that this fragment was too large (Figure 167B), hinting at multiple fragments. After ligation of the large fragment with a pIJ8660 fragment, the ligation mixture was used for transformation of *E. coli* strain DH5α. The transformants were screened with colony PCR (Figure 167D) to find potential clones with a *filP-egfp* fusion, positive colonies were predicted to produce a ~1302bp product. Plasmid DNA was then isolated from positive colonies, isolated DNA was confirmed by restriction digestion (Figure 167C), however, here it appears that the 2.1Kbp fragment is too bright for a single copy. As we then realised that there were two *Bam*HI promoter fragments they were both excised and only one cloned back in (Figure 168 & Figure 169). After ligation of the fragments the ligation mixture was used for transformation of *E. coli* strain DH5α. The transformants were screened with colony PCR (Figure 169E) to produce a ~961bp product that can only be generated upon the re-generation of a *filP-egfp* fusion to ensure directional cloning. Plasmid DNA was then isolated from positive colonies, restriction digests (Figure 169D) were then performed to verify that there was only one 2.1Kbp *Bam*HI fragment in the new clone. Thus, confirming the generation of a correct pIJ8660-PfilP-filP-egfp construct.

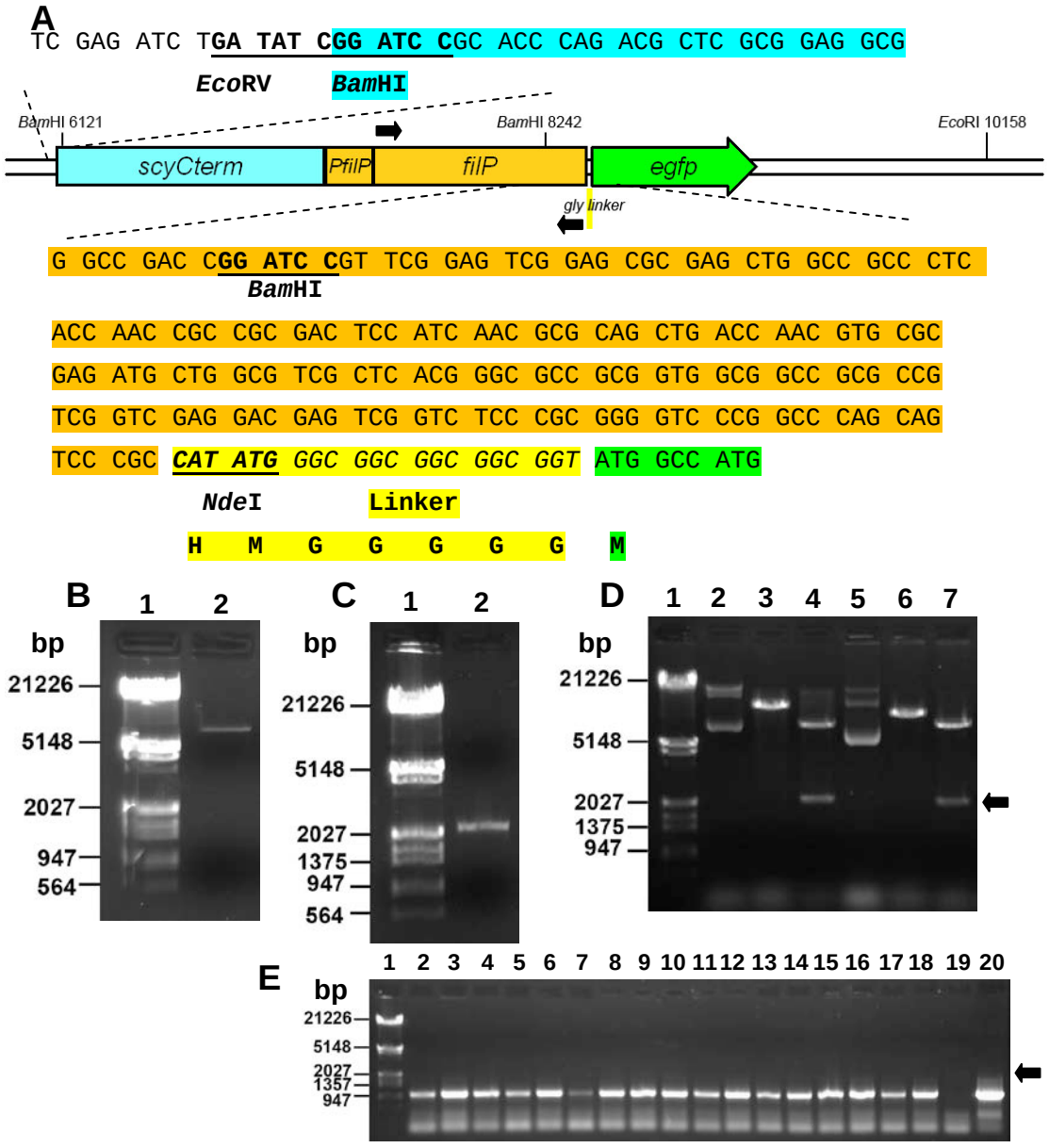

Figure 169: DNA Fragments for generation of correct pIJ8660-PfilP-filP-egfp and its confirmation by restriction digest.

A) pIJ8660-PfilP-filP-egfp. Sequence of the junctions between pIJ8660 and *scyCterm* and *filP* and *egfp*. The *filP-egfp* junction contains a glycine linker (highlighted yellow/italics). Restriction site sequences are bold and underlined. The *scy* sequences are highlighted light blue, *filP* is highlighted orange and *egfp* is highlighted green. Primers for colony PCR are marked (black arrows).

B) The gel isolated *Bam*HI vector fragment of pIJ8660-PfilP-filP-egfp used for construction of the correct pIJ8660-PfilP-filP-egfp was analysed on a 0.7% agarose gel (Lane 2). The DNA size marker is Lambda *Hind*III/*Eco*RI (Lane 1).

C) The gel isolated *Bam*HI fragment containing *PfilP* from pUC18-PfilP used for construction of the correct pIJ8660-PfilP-filP-egfp was analysed on a 0.7% agarose gel (Lane 2). The DNA size marker is Lambda *Hind*III/*Eco*RI (Lane 1).

D) The plasmids pIJ8660-PfilP-filP-egfp (incorrect version) (Lanes 2, 3 & 4) and the plasmid pIJ8660-PfilP-filP-egfp (correct version)(Lanes 5, 6 & 7) were analysed on a 0.7% agarose gel. Undigested samples (Lanes 2 & 5) were run together with samples digested with *Eco*RI (Lanes 3 & 6) or BamHI (Lanes 4 & 7). The arrow indicates the ~2121bp fragment. The DNA size marker is Lambda *Hind*III/*Eco*RI (Lane 1).

E) Candidate colonies were screened with colony PCR using THAbpS_F (upstream) and THAbpS_R (downstream) primers and PCR products were analysed on a 0.7% agarose gel. Candidate colonies are shown Lanes 2-18. The arrow indicates the ~961bp PCR product expected. The plasmids pIJ8660 (Lane 19) and pIJ8660-PfilP-filP-egfp (incorrect version) (Lane 20) were used as control templates.The DNA size marker is Lambda *Hind*III/*Eco*RI (Lane 1).

10.1.56 Generation of a FilP-mCherry translational fusion

For assessing the localisation of FilP with a different fusion we aimed to generate a FilP-mCherry construct. The strategy to do this was to isolate an *mCherry* containing fragment from pIJ8660-PnepA-nepA-mCherry and swap *egfp* in the pIJ8660-PfilP-filP-egfp construct.

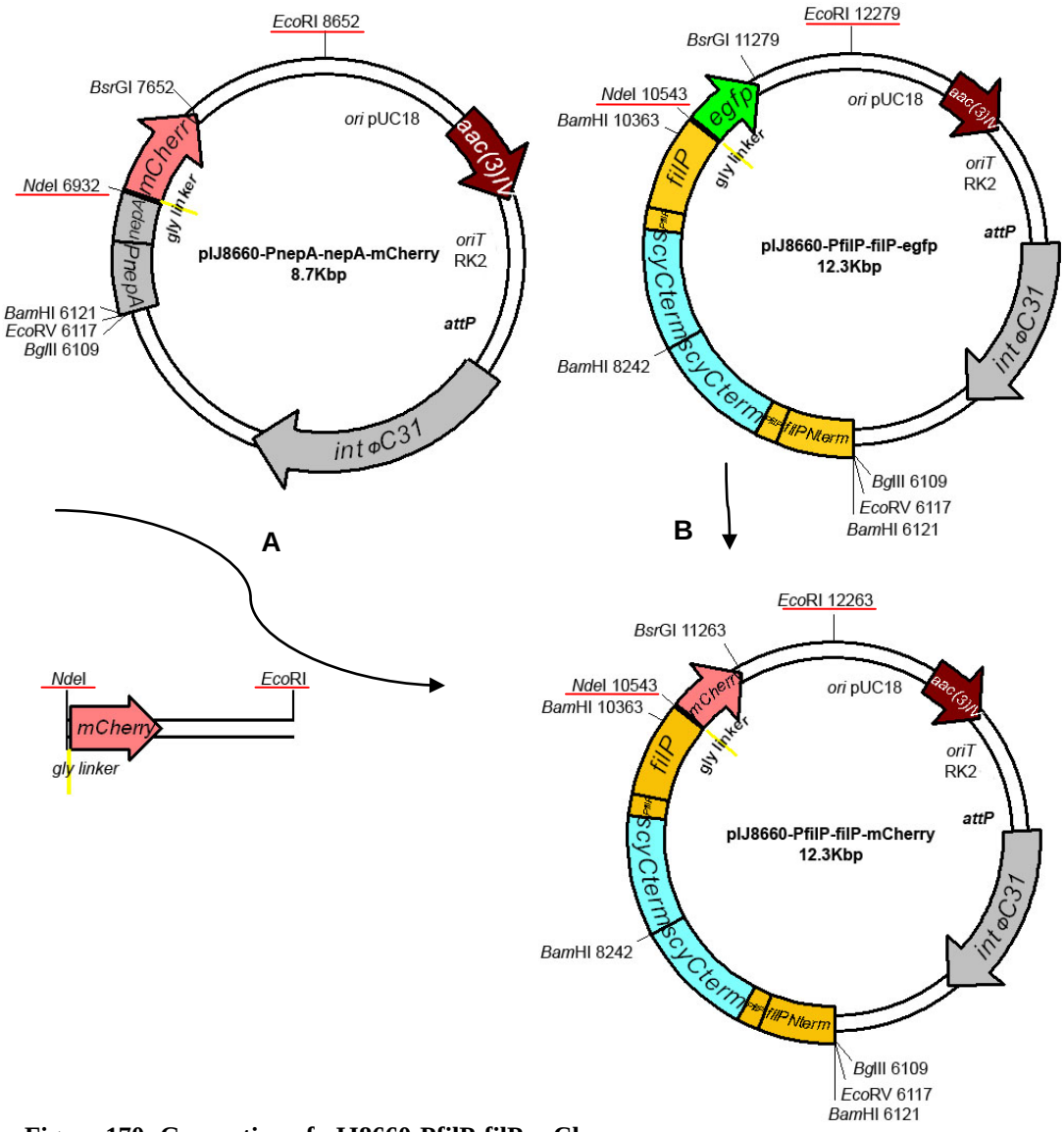

Figure 170: Generation of pIJ8660-PfilP-filP-mCherry.

pIJ8660-PfilP-filP-mCherry is a derivative of pIJ8660-PfilP-filP-egfp. A) The *mCherry* *Nde*I/*Eco*RI fragment was liberated from pIJ8660-PnepA-nepA-mCherry. B) Using *Nde*I and *Eco*RI, pIJ8660-PfilP-filP-egfp was digested and the *mCherry* fragment cloned so that *egfp* was replaced by *mCherry* placed in frame with *filP*. The restriction sites used in the cloning are underlined in red.

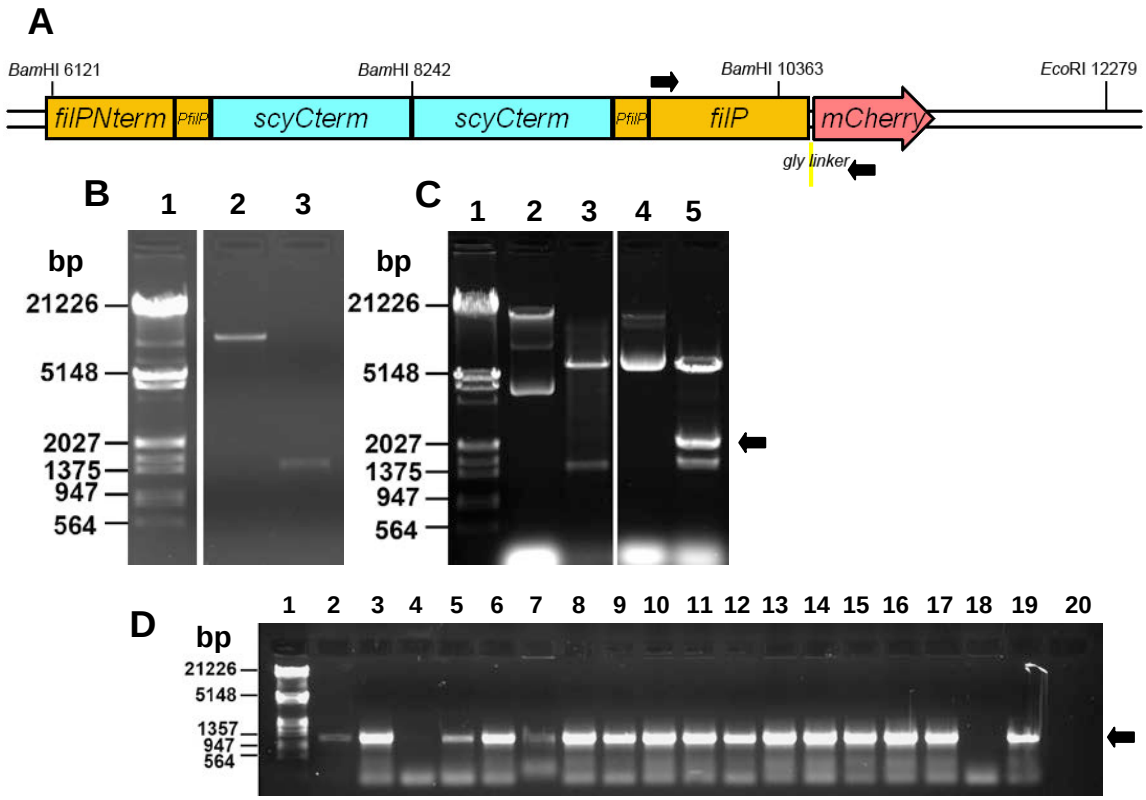

Figure 171: DNA Fragments for generation of pIJ8660-PfilP-filP-mCherry and its confirmation by restriction digest.

A) Arrangement of fragments and restriction sites in the construct pIJ8660-PfilP-filP-mCherry. Primers for colony PCR are marked (black arrows).

B) The gel isolated fragments used for construction of pIJ8660-PfilP-filP-mCherry were analysed on a 0.7% agarose gel. The fragments used were the *Nde*I/*Eco*RI fragment of pIJ8660-PfilP-filP-egfp (Lane 2) and an *Nde*I/*Eco*RI fragment containing *mCherry* (Lane 3). The DNA size marker is Lambda *Hind*III/*Eco*RI (Lane 1).

C) The plasmids pIJ8660 (Lanes 2 & 3) and the plasmid pIJ8660-PfilP-filP-mCherry (Lanes 4 & 5) were analysed on a 0.7% agarose gel. Undigested samples (Lanes 2 & 4) were run together with samples digested with *Bam*HI and *Eco*RI (Lanes 3 & 5). The arrow indicates the ~2121bp fragment carrying *scyCterm-PfilP-filP*. The DNA size marker is Lambda *Hind*III/*Eco*RI (Lane 1).

D) Candidate colonies were screened with colony PCR using THAbpS_F (upstream) and mCherryseq (downstream) primers and PCR products were analysed on a 0.7% agarose gel. Candidate colonies are shown Lanes 2-19. The arrow indicates the ~1184bp PCR product expected. The plasmid pIJ8660-PfilP-filP-egfp (Lane 20) was used as a control template. The DNA size marker is Lambda *Hind*III/*Eco*RI (Lane 1).

At the time in the project this was approached it was unclear that there was a problem with the initial pIJ8660-PfilP-filP-egfp construct with two 2.1Kbp *Bam*HI fragments. From the vector pIJ8660-PnepA-nepA-mCherry an *Nde*I-*Eco*RI fragment containing a polyglycine linkered mCherry fragment was generated. The precursor construct of pIJ8660-PfilP-filP-egfp (with two 2.1Kbp *Bam*HI fragments) was then opened up with *Nde*I-*Eco*RI and the polyglycine linkered mCherry fragment was used to replace the polyglycine linkered EGFP fragment (Figure 170 & Figure 171). After ligation of the fragments the ligation and

transformation, the transformants were screened with colony PCR (Figure 171D) to find potential clones with a *filP-mCherry* fusion using an *mCherry* specific downstream primer, positives would generate a PCR product with the predicted size of ~1184bp. Plasmid DNA was then isolated from positive colonies, isolated DNA was confirmed by restriction digestion (Figure 171C), however, here it appears that the 2.1Kbp fragment is too bright for a single copy. As we then realised that there were two *Bam*HI promoter fragments they were both excised and only one cloned back in (Figure 172 & Figure 173). After ligation of the fragments the ligation mixture was used for transformation, the transformants were screened with colony PCR (Figure 173E) to produce a ~961bp product that can only be generated upon the re-generation of a *filP-mCherry* fusion to ensure directional cloning. Plasmid DNA was then isolated from positive colonies, restriction digests (Figure 173D) were then performed to verify that there was only one 2.1Kbp *Bam*HI fragment in the new clone. Thus, confirming the generation of a correct pIJ8660-PfilP-filP-mCherry construct.

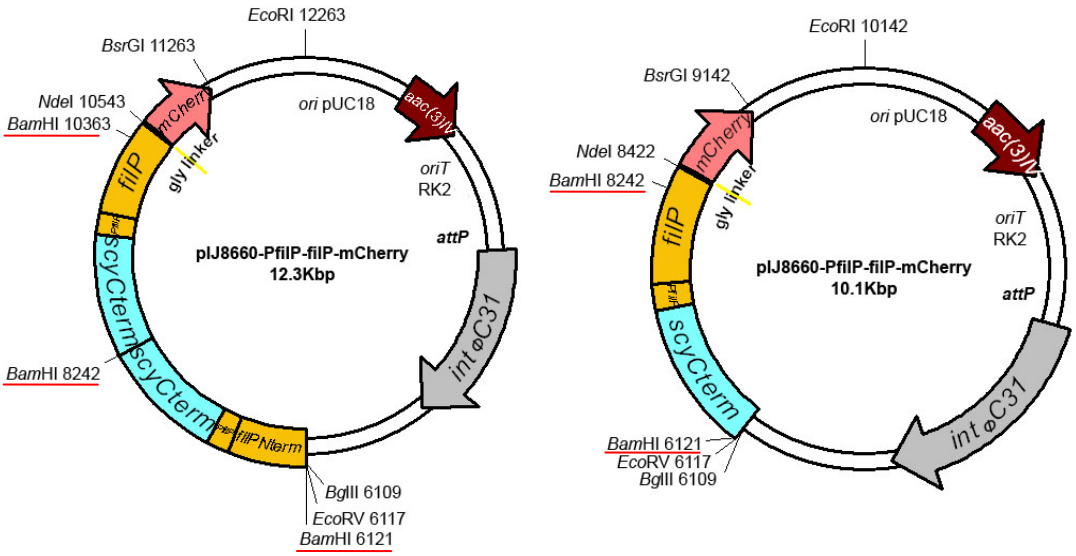

Figure 172: Generation of pIJ8660-PfilP-filP-mCherry. Plasmid pIJ8660-PfilP-filP-mCherry was corrected by liberating the two *scyCterm-PfilP-filPNterm* fragments using a *Bam*HI digestion and cloning back in a single *scyCterm-PfilP-filPNterm* *Bam*HI fragment. The restriction sites used in the cloning are underlined in red.

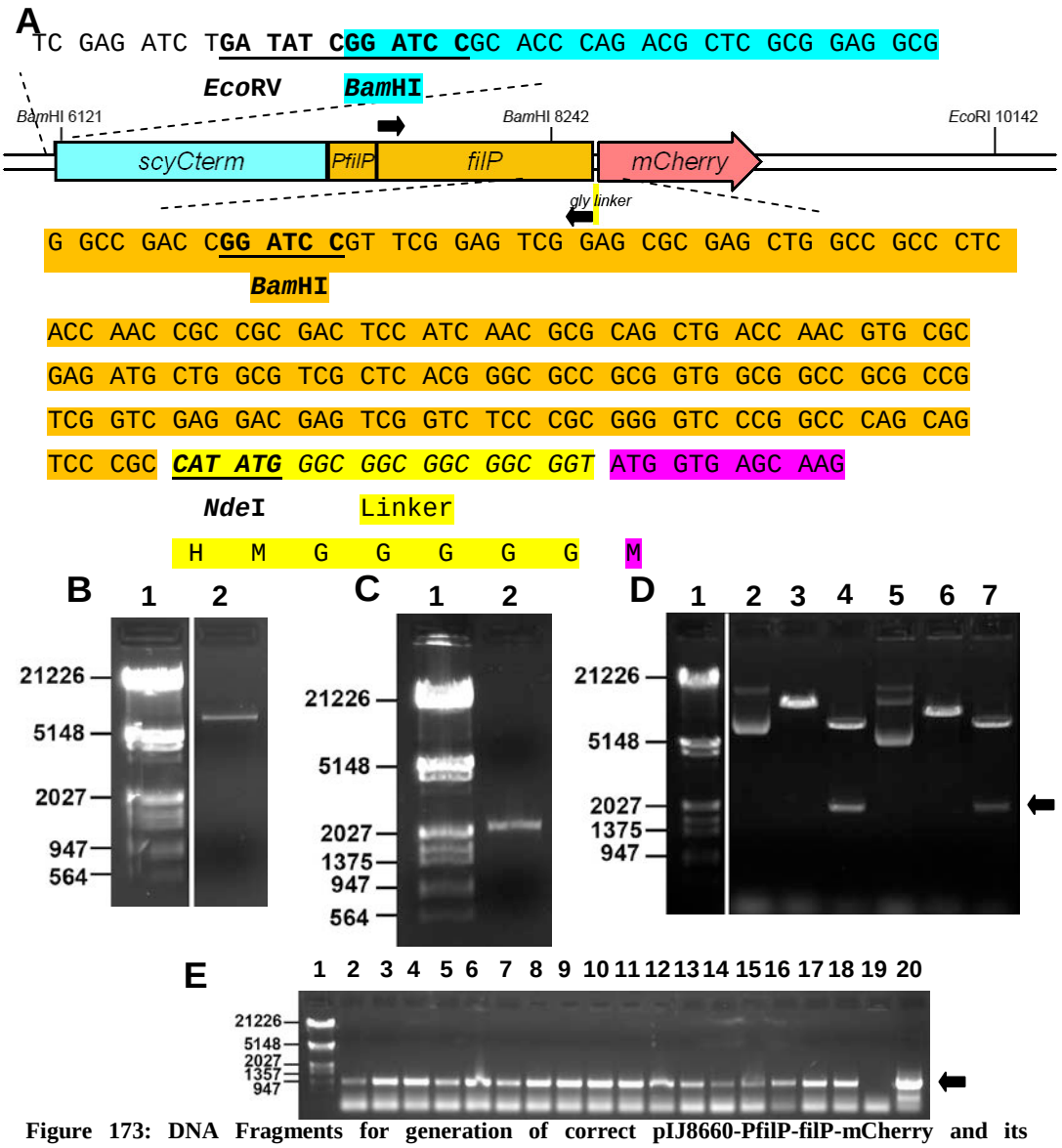

Figure 173: DNA Fragments for generation of correct pIJ8660-PfilP-filP-mCherry and its confirmation by restriction digest.

A) pIJ8660-PfilP-filP-mCherry. Sequence of the junctions between pIJ8660 and *scyCterm* and *filP* and *mCherry*. The *filP-mCherry* junction contains a glycine linker (highlighted yellow/italics). Restriction site sequences are bold and underlined. The *scy* sequences are highlighted light blue, *filP* is highlighted orange and *mCherry* is highlighted pink. Primers for colony PCR are marked (black arrows).

B) The gel isolated *Bam*HI fragment of pIJ8660-PfilP-filP-mCherry used for construction of the correct pIJ8660-PfilP-filP-mCherry was analysed on a 0.7% agarose gel (Lane 2). The DNA size marker is Lambda *Hind*III/*Eco*RI (Lane 1).

C) The gel isolated *Bam*HI fragment containing *PfilP* from pUC18-PfilP used for construction of the correct pIJ8660-PfilP-filP-mCherry was analysed on a 0.7% agarose gel (Lane 2). The DNA size marker is Lambda *Hind*III/*Eco*RI (Lane 1).

D) The plasmids pIJ8660-PfilP-filP-mCherry (incorrect version) (Lanes 2, 3 & 4) and the plasmid pIJ8660-PfilP-filP-mCherry (correct version)(Lanes 5, 6 & 7) were analysed on a 0.7% agarose gel. Undigested samples (Lanes 2 & 5) were run together with samples digested with *Eco*RI (Lanes 3 & 6) or BamHI (Lanes 4 & 7). The arrow indicates the ~2121bp fragment. The DNA size marker is Lambda *Hind*III/*Eco*RI (Lane 1).

E) Candidate colonies were screened with colony PCR using THAbpS_F (upstream) and THAbpS_R (downstream) primers and PCR products were analysed on a 0.7% agarose gel. Candidate colonies are shown Lanes 2-18. The arrow indicates the ~961bp PCR product expected. The plasmids pIJ8660 (Lane 19) and pIJ8660-PfilP-filP-egfp (incorrect version) (Lane 20) were used as control templates.The DNA size marker is Lambda *Hind*III/*Eco*RI (Lane 1).

10.1.57 Generation of a FilP-Δlink-mCherry construct

For assessing the localisation of FilP-mCherry with no poly glycine linker we aimed to construct a pIJ8660 plasmid carrying a non-linkered *filP-mCherry* fusion. The strategy was that from the plasmid pIJ88660-Pscy-scy-Δlink-mCherry a fragment containing *mCherry* would be used to swap around the linkered *egfp* sequence in pIJ8660-PfilP-filP-egfp (Figure 174), as the *mCherry* fragment has no linker it would generate a fusion lacking a linker between *filP* and *mCherry*. The plasmid pIJ8660-PfilP-filP-egfp was used instead of the already generated *mCherry* version so that we could easily screen for the swap of egfp at the same time as ensuring a product with no linker was generated when the *mCherry* containing fragment was inserted. An *Nde*I-*Bsr*GI fragment containing *mCherry* was liberated from pBluescript-mCherry. The plasmid pIJ8660-PfilP-filP-egfp was digested with *Nde*I-*Bsr*GI to remove the polyglycine linkered EGFP fragment. After ligation of the fragments the ligation mixture was used for transformation of *E. coli* strain DH5α. The transformants were screened with colony PCR (Figure 175C) to find potential clones able to produce a ~1166bp product that can only be generated with a *filP-mCherry* fusion, using an *mCherry* specific downstream primer. Plasmid DNA was then isolated from positive colonies and was confirmed by sequencing to have a *filP-mCherry* fusion lacking a linker where instead *filP* reads directly into *mCherry*. Thus, confirming the generation of a pIJ8660-PfilP-filP-Δlink-mCherry construct.

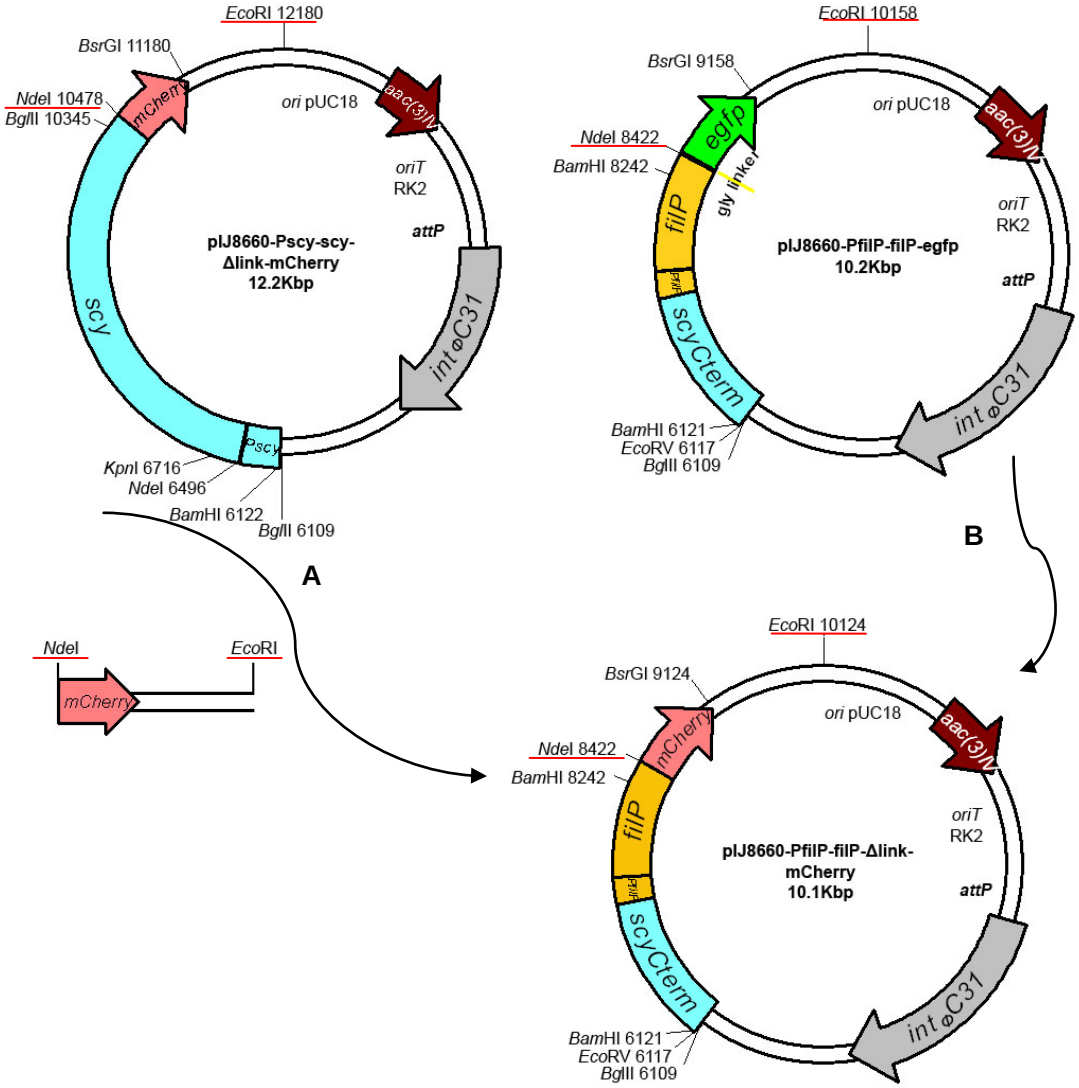

Figure 174: Generation of pIJ8660-PfilP-filP-Δlink-mCherry.

pIJ8660-PfilP-filP-Δlink-mCherry is a derivative of pIJ8660-PfilP-filP-egfp. A) The *mCherry* *Nde*I/*Eco*RI fragment was liberated from pIJ8660-Pscy-scy-Δlink-mCherry. B) Using *Nde*I and *Eco*RI, pIJ8660-PfilP-filP-egfp was digested and the *mCherry* fragment cloned so that *egfp* was replaced by *mCherry* placed in frame with *filP* with no linker. The restriction sites used in the cloning are underlined in red.

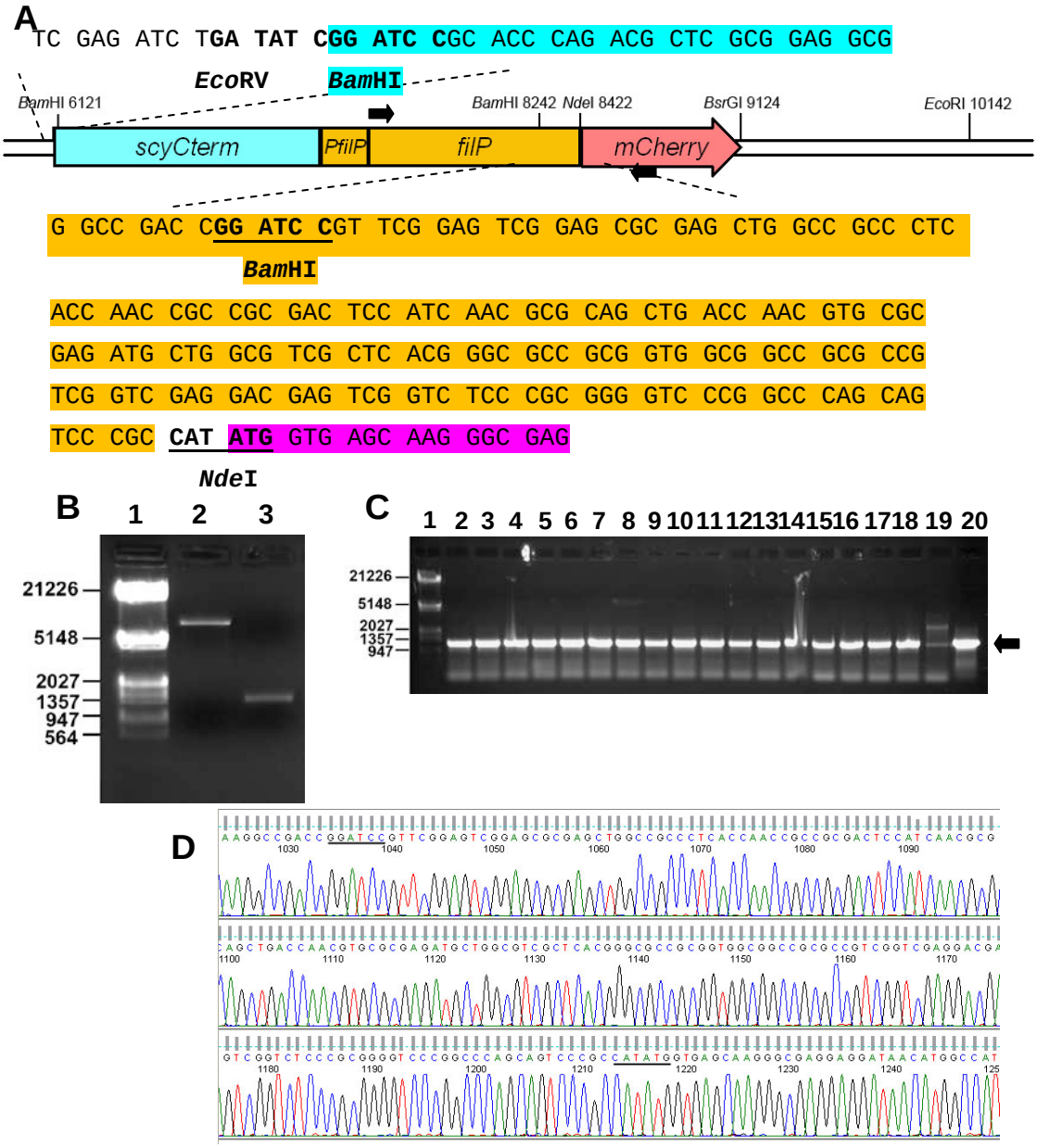

Figure 175: DNA Fragments for generation of pIJ8660-PfilP-filP-Δlink-mCherry and digestion of subsequent pIJ8660-PfilP-filP-Δlink-mCherry clone.

A) pIJ8660-PfilP-filP-Δlink-mCherry. Sequence of the junctions between pIJ8660 and *scyCterm* and *filP* and *mCherry*. The *filP-mCherry* junction lacks a linker with *filP* reading directly into *mCherry*. Restriction site sequences are bold and underlined. The *scy* sequences are highlighted light blue, *filP* is highlighted orange and *mCherry* is highlighted pink. Primers for colony PCR are marked (black arrows).

B) The gel isolated fragments used for construction of pIJ8660-PfilP-filP-Δlink-mCherry were analysed on a 0.7% agarose gel. The fragments used were the *Nde*I/*Eco*RI fragment of pIJ8660-PfilP-filP-egfp (Lane 2) and the *Nde*I/*Eco*RI fragment containing *mCherry* (no link) (Lane 3). The DNA size marker is Lambda *Hind*III/*Eco*RI (Lane 1).

C) Candidate colonies were screened with colony PCR using THAbpS_F (upstream) and mCherryseq (downstream) primers and PCR products were analysed on a 0.7% agarose gel. Candidate colonies are shown Lanes 2-18. The arrow indicates the ~1166bp PCR product expected. The plasmids pIJ8660-PfilP-filP-egfp (Lane 19) and pIJ8660-PfilP-filP-mCherry (Lane 20) were used as control templates. The DNA size marker is Lambda *Hind*III/*Eco*RI (Lane 1).

D) Sequencing chromatogram showing the reverse complement of pIJ8660-PfilP-filP-Δlink-mCherry sequenced with the mCherryseq primer. Underlined sequences are *Bam*HI or *Nde*I restriction sites.

10.1.58 Generation of DivIVA bacterial two-hybrid constructs

In order to test the interactions of DivIVA in the Bacterial two-hybrid system we aimed to clone *divIVA* into pUT18C and pKT25 to generate DNA encoding T18-DivIVA or T25-DivIVA with T18 or T25 at the N-terminal of DivIVA, respectively. The strategy to generate these fusions was to PCR amplify the whole of *divIVA* and firstly clone it into pUT18C, which is a high copy number plasmid, aiding cloning. Then, subclone the *divIVA* fragment from pUT18C into pKT25 (Figure 176 & Figure 177). The *divIVA* fragment was generated by PCR using the primers THDiv_F and THDiv_R. The PCR product was then digested with *Xba*I and *Eco*RI and cloned into the same sites in pUT18C (Figure 178). After ligation of the fragments the ligation mixture was used for transformation of *E. coli* strain DH5α. The transformants were screened with colony PCR (Figure 178C) to find potential clones which could generate a ~1219bp PCR product that carries *divIVA*. Plasmid DNA was then isolated from positive colonies, isolated DNA was confirmed by restriction digestion (Figure 178B) to liberate a ~1207bp fragment containing *divIVA*. Candidate clones were picked and the *divIVA* insert sequenced from two directions. Despite several candidates carrying in the range of 2-3 single base pair mutations, one clone was sequenced and contained the expected sequence of *divIVA*. Therefore, confirming this clone as the plasmid pUT18C-divIVA, encoding DivIVA fused to the C-terminus of the T18 adenylate cyclase domain.

For reciprocal tests from the lower copy BTH plasmid pKT25, the insert from pUT18C-divIVA was also cloned into pKT25 using *Xba*I and *Eco*RI (Figure 179). After ligation of the fragments the ligation mixture was used for transformation of *E. coli* strain DH5α. The transformants were screened with colony PCR (Figure 179C) to find potential clones which now carried template for a ~630bp PCR product of the C-terminal sequence of *divIVA*. Plasmid DNA was then isolated from positive colonies, and was confirmed by restriction digestion (Figure 179B) to liberate a ~1207bp fragment containing the full length of *divIVA*. Thus, confirming the generation of the plasmid pKT25-divIVA, encoding DivIVA fused to the C-terminus of the T25 adenylate cyclase domain.

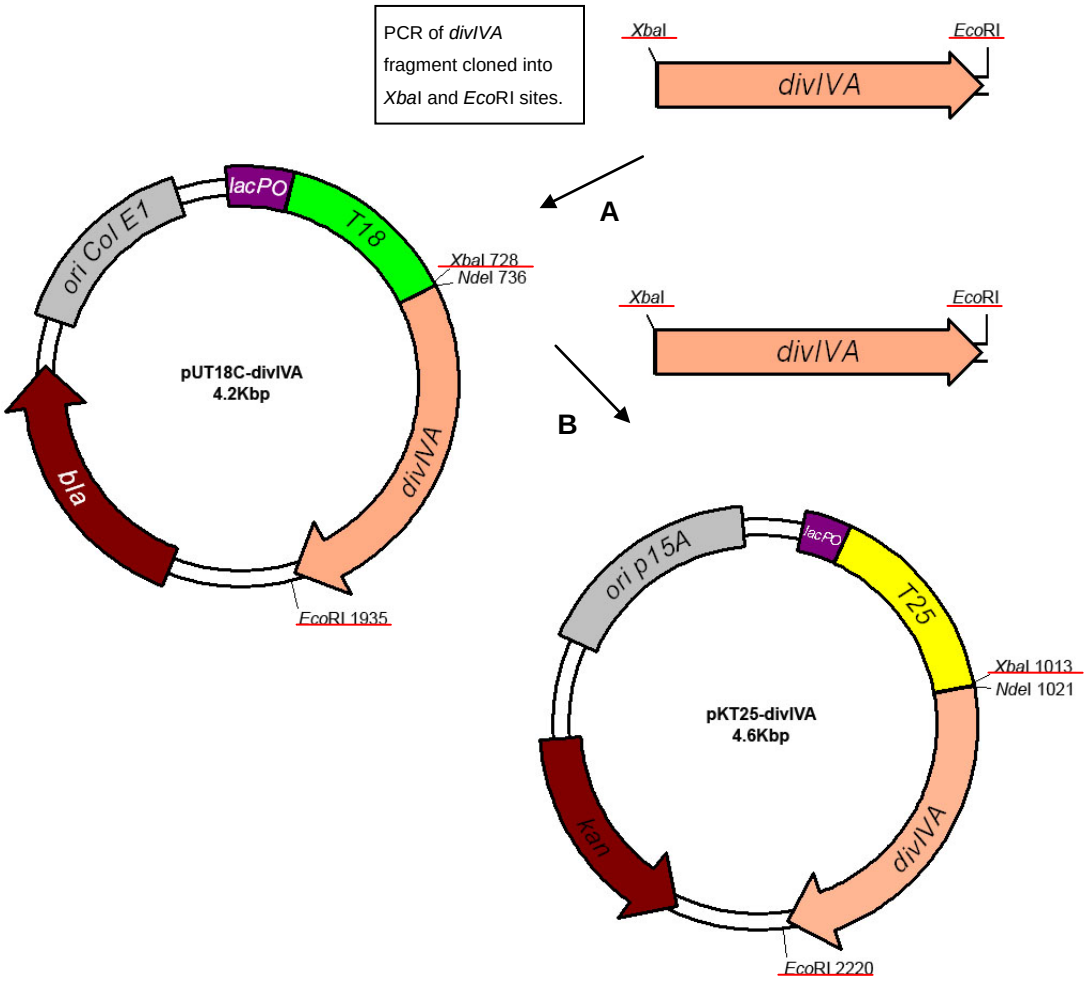

Figure 176: Generation of pUT18C-divIVA and pKT25-divIVA.

A) pUT18C-divIVA is a pUT18C derivative containing a *divIVA* PCR fragment cloned in via *Xba*I and *Eco*RI. B) The *divIVA* fragment was then liberated using *Xba*I and *Eco*RI from pUT18C-divIVA and cloned into pKT25 to generate pKT25-divIVA. Both pUT18C-divIVA and pKT25-divIVA have DNA encoding either the adenylate cyclase domain T18 or T25, respectively, reading inframe to *divIVA*. The restriction sites used in the cloning are underlined in red.

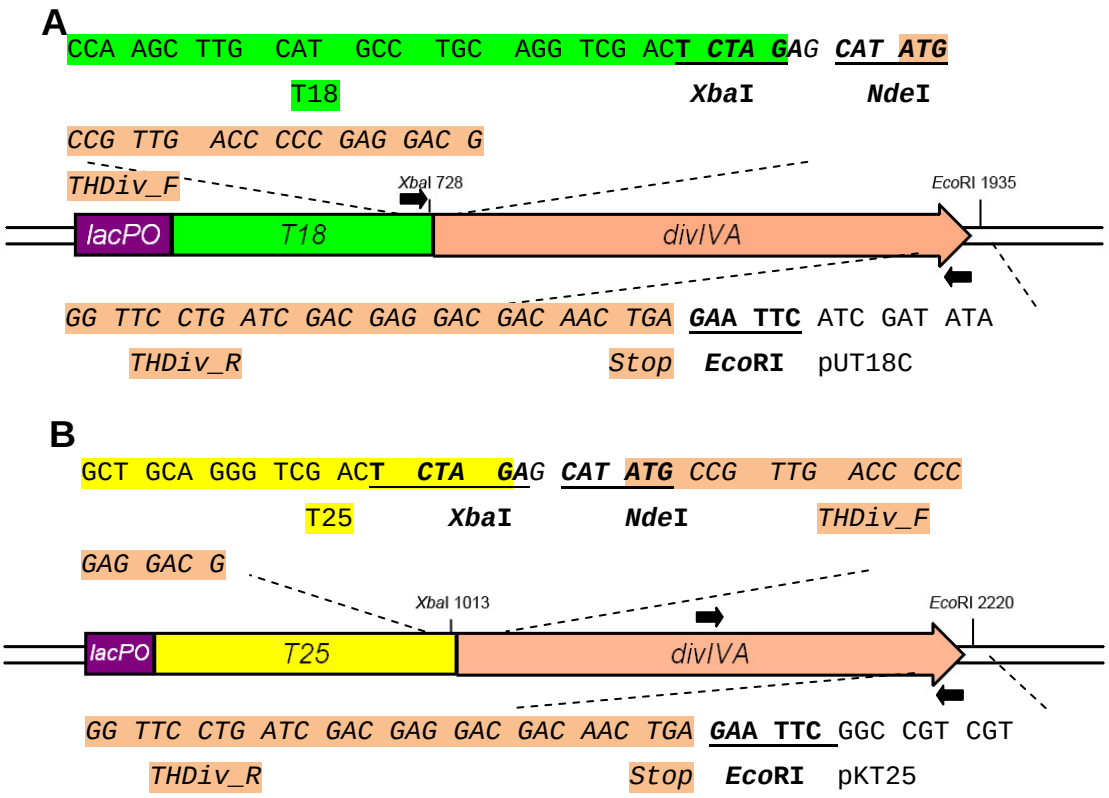

Figure 177: Sequence of joins formed in the constructs pUT18C-divIVA and pKT25-divIVA.

A) Sequence of junctions in the construct pUT18C-divIVA. The cloned in *divIVA* fragment is fused to DNA encoding the C-terminus of T18 and under the direction of a lactose inducible promoter. Restriction site sequences are bold and underlined. The *divIVA* sequences are highlighted salmon pink and *T18* is highlighted green. Primers for colony PCR are marked (black arrows).

B) Sequence of junctions in the construct pKT25-divIVA. The cloned in *divIVA* fragment is fused DNA encoding the C-terminus of T25 and under the direction of a lactose inducible promoter. Restriction site sequences are bold and underlined. The *divIVA* sequences are highlighted salmon pink and *T25* is highlighted yellow. Primers for colony PCR are marked (black arrows).

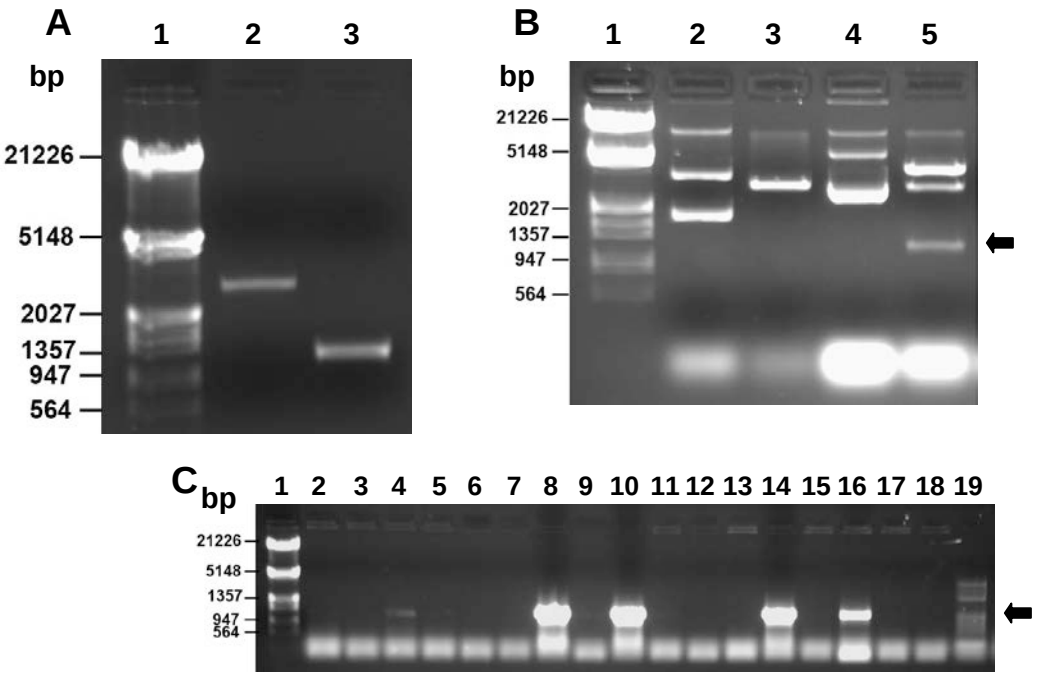

Figure 178: DNA Fragments for generation of a *divIVA* pUT18C construct and its confirmation by restriction digests.

A) The gel isolated fragments used for construction of pUT18C-divIVA were analysed on a 0.7% agarose gel. The fragments used were the *Xba*I/*Eco*RI fragment of pUT18C (Lane 2) and the *Xba*I/*Eco*RI fragment of a *divIVA* PCR product (Lane 3). The DNA size marker is Lambda *Hind*III/*Eco*RI (Lane 1).

B) The plasmids pUT18C (Lanes 2 & 3) and the plasmid pUT18C-divIVA (Lanes 4 & 5) were analysed on a 1% agarose gel. Undigested samples (Lanes 2 & 4) were run together with samples digested with *Xba*I and *Eco*RI (Lanes 3 & 5). The arrow indicates the ~1207bp fragment carrying the PCR amplified *divIVA*. The DNA size marker is Lambda *Hind*III/*Eco*RI (Lane 1).

C) Candidate colonies were screened with colony PCR using THScy_T18 (upstream) and TH DivIVA R (downstream) primers and PCR products were analysed on a 0.7% agarose gel. Candidate colonies are shown Lanes 2-18. The arrow indicates the ~1219bp PCR product expected. The plasmid pUT18C-filP was used as a control template (Lane 19).The DNA size marker is Lambda *Hind*III/*Eco*RI (Lane 1).

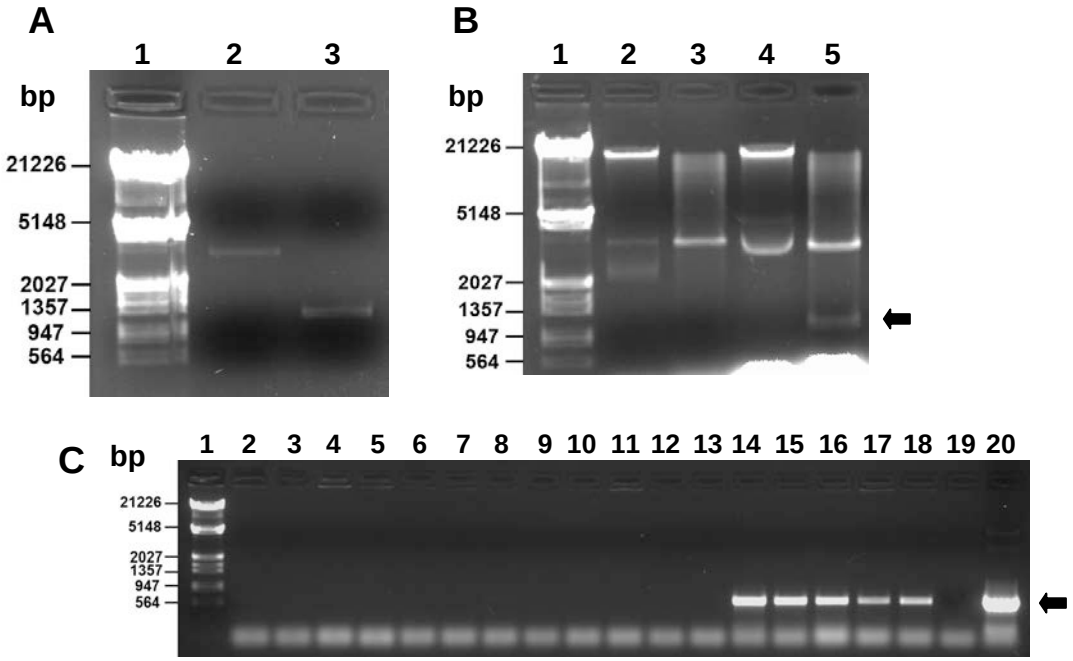

Figure 179: DNA Fragments for generation of a *divIVA* pKT25 construct and its confirmation by restriction digests.

A) The gel isolated fragments used for construction of pKT25-divIVA were analysed on a 0.7% agarose gel. The fragments used were the *Xba*I/*Eco*RI fragment of pKT25 (Lane 2) and the *Xba*I/*Eco*RI fragment of *divIVA* (Lane 3). The DNA size marker is Lambda *Hind*III/*Eco*RI (Lane 1).

B) The plasmids pKT25 (Lanes 2 & 3) and the plasmid pKT25-divIVA (Lanes 4 & 5) were analysed on a 0.7% agarose gel. Undigested samples (Lanes 2 & 4) were run together with samples digested with *Xba*I and *Eco*RI (Lanes 3 & 5). The arrow indicates the ~1207bp fragment carrying the PCR amplified *divIVA*. The DNA size marker is Lambda *Hind*III/*Eco*RI (Lane 1).

C) Candidate colonies were screened with colony PCR using DivcoilF/PET (upstream) and THDiv_R (downstream) primers and PCR products were analysed on a 1% agarose gel. Candidate colonies are shown Lanes 2-18. The arrow indicates the ~630bp PCR product expected. The plasmids pKT25 (Lane 19) and pUT18C-divIVA (Lane 20) were used as control templates. The DNA size marker is Lambda *Hind*III/*Eco*RI (Lane 1).

10.1.59 Generation of DivIVA-N bacterial two-hybrid constructs

In order to test the interactions of the N-terminal domain of DivIVA in the Bacterial two-hybrid system it was aimed to clone a *divIVA-N* encoding fragment into pUT18C and pKT25. This would generate T18-DivIVA-N and T25-DivIVA-N, N-terminal fusions of the DivIVA-N domain to T18 or T25, respectively. The strategy to generate these fusions was to PCR amplify just the N-terminal fragment of *divIVA* and firstly clone it into pUT18C, then subclone this into pKT25 (Figure 180 & Figure 181). A *divIVA-N* fragment was generated by PCR using the primers THDiv_F and DivN_STOPEco. The PCR product

was then digested with *Xba*I and *Eco*RI and cloned into the same sites in pUT18C (Figure 182). The ligation mixture was used to transform *E. coli* strain DH5α. The transformants

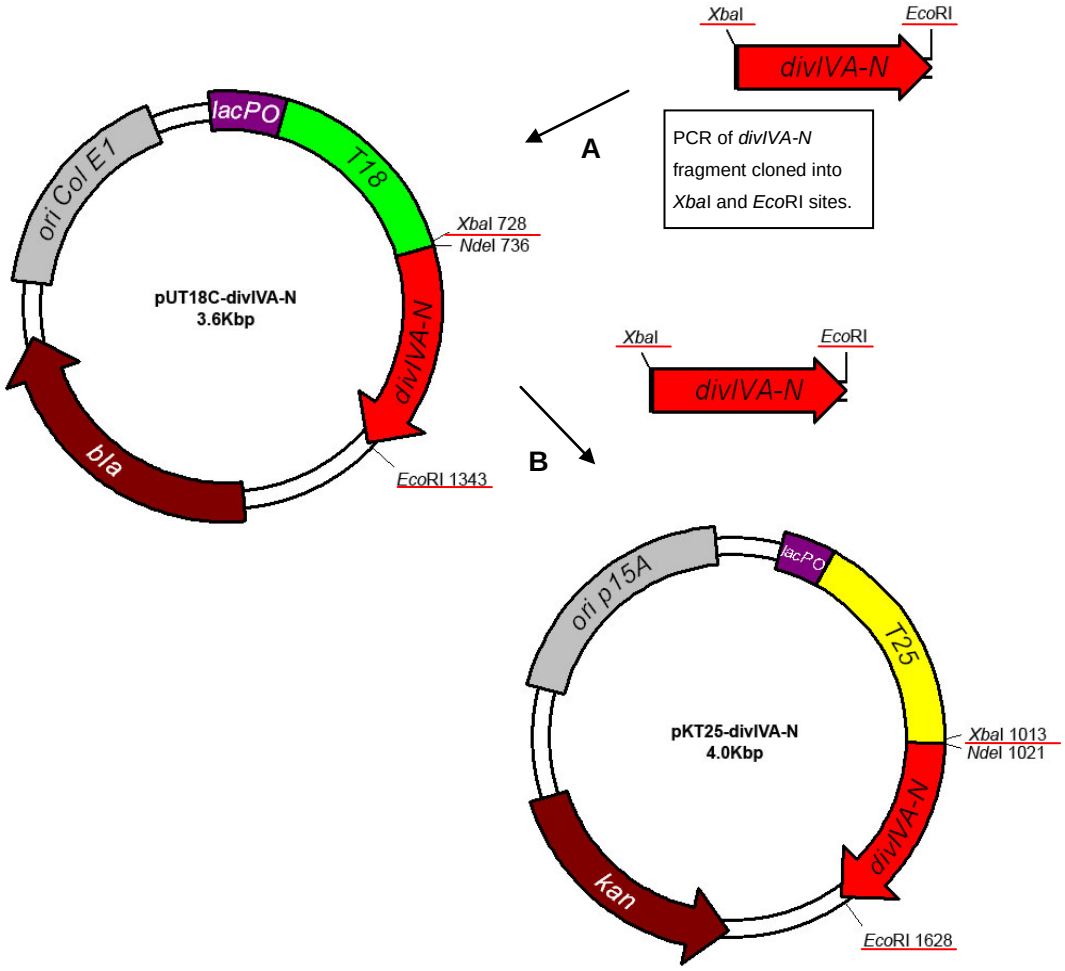

Figure 180: Generation of pUT18C-divIVA-N and pKT25-divIVA-N.

A) pUT18C-divIVA-N is a pUT18 derivative containing a *divIVA-N* PCR fragment cloned in via *Xba*I and *Eco*RI. B) The *divIVA-N* fragment was then liberated using *Xba*I and *Eco*RI from pUT18C-divIVA-N and cloned into pKT25 to generate pKT25-divIVA-N. Both pUT18C-divIVA-N and pKT25-divIVA-N have DNA encoding either the adenylate cyclase domain T18 or T25, respectively, reading inframe to *divIVA-N*. The restriction sites used in the cloning are underlined in red.

were screened with colony PCR (Figure 182D) to find potential clones which could generate a ~632bp PCR product that carries *divIVA-N*. Plasmid DNA was then isolated from positive colonies, and was confirmed by restriction digestion (Figure 182C) to liberate a ~615bp fragment containing *divIVA-N*. Candidate clones were picked and the *divIVA-N* insert sequenced. A clone was found that had the expected sequence of *divIVA-N*. Thus, confirming this clone as the plasmid pUT18C-divIVA-N, with *divIVA-N* fused to the C-terminus of the T18 adenylate cyclase domain.

For reciprocal tests from the lower copy BTH plasmid pKT25, the insert was also moved into pKT25 using *Xba*I and *Eco*RI (Figure 183). After ligation of the fragments the ligation

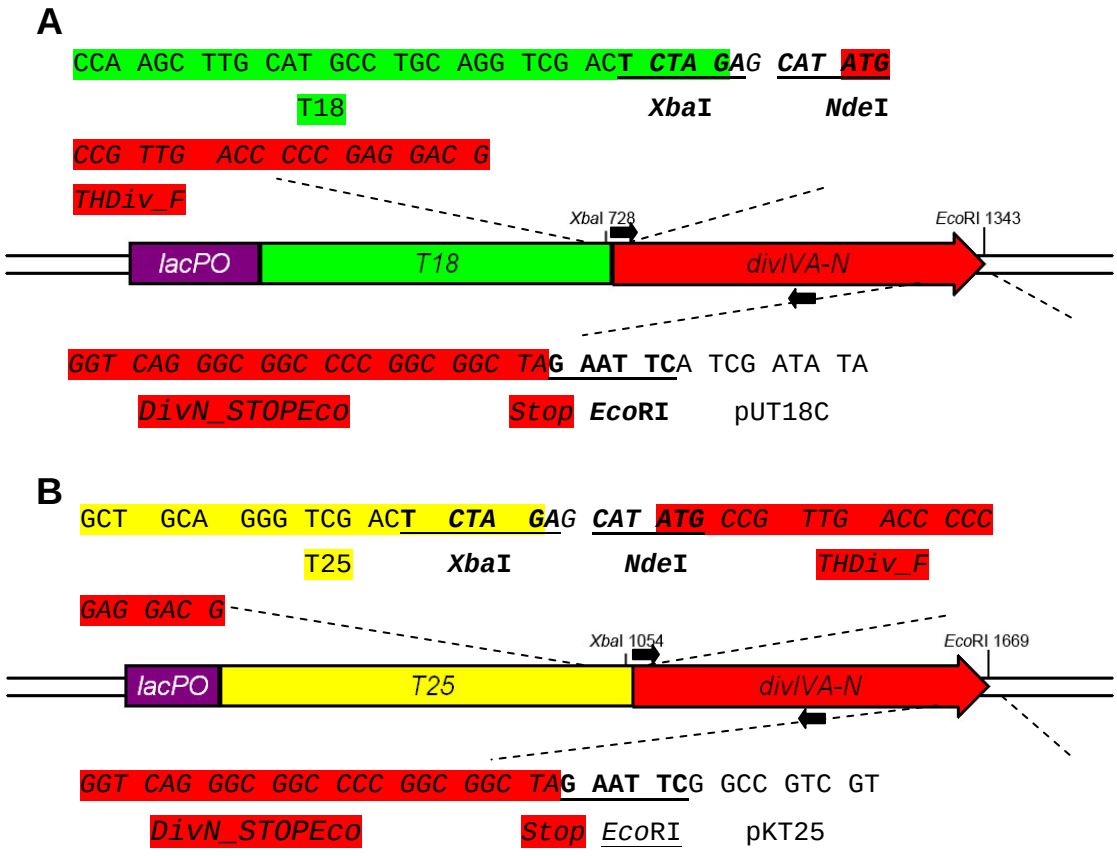

Figure 181: Sequence of joins formed in the constructs pUT18C-DivIVA-N and pKT25-DivIVA-N.

A) Sequence of junctions in the construct pUT18C-divIVA-N. The cloned in *divIVA-N* fragment is fused to DNA encoding the C-terminus of T18 and under the direction of a lactose inducible promoter. Restriction site sequences are bold and underlined. The *divIVA-N* sequences are highlighted red and *T18* is highlighted green. Primers for colony PCR are marked (black arrows).

B) Sequence of junctions in the construct pKT25-divIVA-N. The cloned in *divIVA-N* fragment is fused to DNA encoding the C-terminus of T25 and under the direction of a lactose inducible promoter. Restriction site sequences are bold and underlined. The *divIVA-N* sequences are highlighted red and *T25* is highlighted yellow. Primers for colony PCR are marked (black arrows).

mixture was used for transformation of *E. coli* strain DH5α. The transformants were screened with colony PCR (Figure 183D) to find potential clones which could generate a ~632bp PCR product that carries *divIVA-N*. Plasmid DNA was then isolated from positive colonies, and was confirmed by restriction digestion (Figure 183C) to liberate a ~615bp fragment containing *divIVA-N*. Therefore, confirming the generation of the plasmid

pKT25-divIVA-N, with *divIVA-N* fused to DNA encoding the C-terminus of the T25 adenylate cyclase domain.

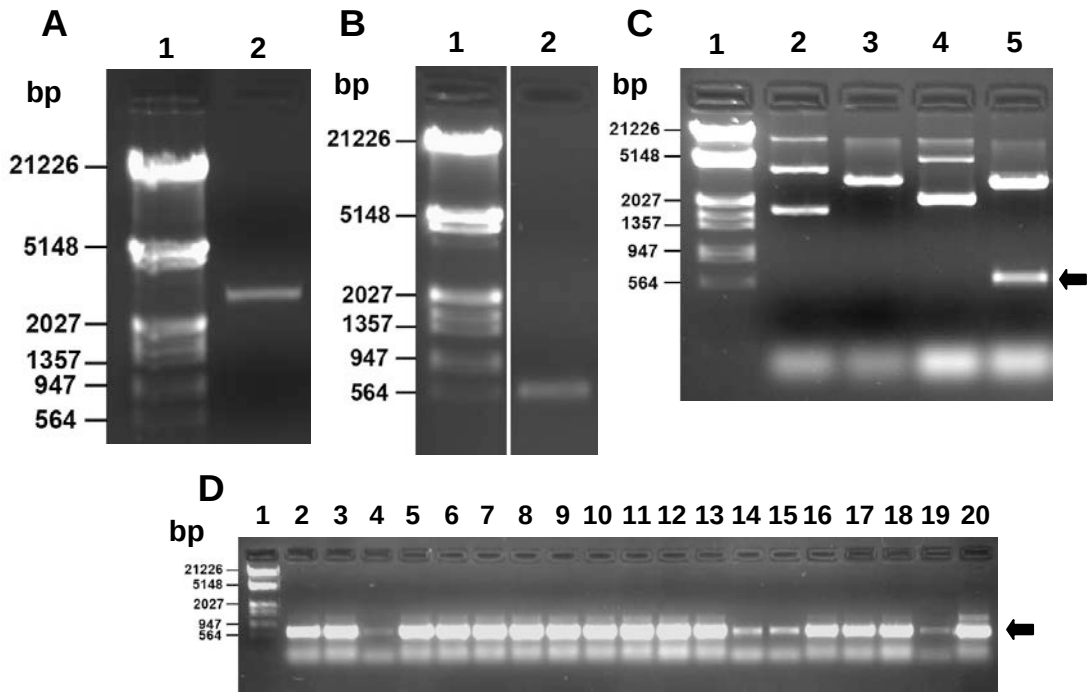

Figure 182: DNA Fragments for generation of a *divIVA-N* pUT18C construct and its confirmation by restriction digests.

A) The gel isolated *Xba*I/*Eco*RI fragment of pUT18C used for construction of pUT18C-divIVA-N was analysed on a 1% agarose gel (Lane 2). The DNA size marker is Lambda *Hind*III/*Eco*RI (Lane 1).

B) The gel isolated *Xba*I/*Eco*RI fragment of the PCR product containing *divIVA-N* used for construction of pUT18C-divIVA-N was analysed on a 0.85% agarose gel (Lane 2). The DNA size marker is Lambda *Hind*III/*Eco*RI (Lane 1).

C) The plasmids pUT18C (Lanes 2 & 3) and the plasmid pUT18C-divIVA-N (Lanes 4 & 5) were analysed on a 1% agarose gel. Undigested samples (Lanes 2 & 4) were run together with samples digested with *Xba*I and *Eco*RI (Lanes 3 & 5). The arrow indicates the ~615bp fragment carrying the PCR amplified *divIVA-N*. The DNA size marker is Lambda *Hind*III/*Eco*RI (Lane 1).

D) Candidate colonies were screened with colony PCR using THDiv_F (upstream) and DivN_STOPEco (downstream) primers and PCR products were analysed on a 1% agarose gel. Candidate colonies are shown Lanes 2-18. The arrow indicates the ~632bp PCR product expected. The plasmids pUT18C (Lane 19) and pET28a-DivIVA-EGFP (Lane 20) were used as control templates. The DNA size marker is Lambda *Hind*III/*Eco*RI (Lane 1).

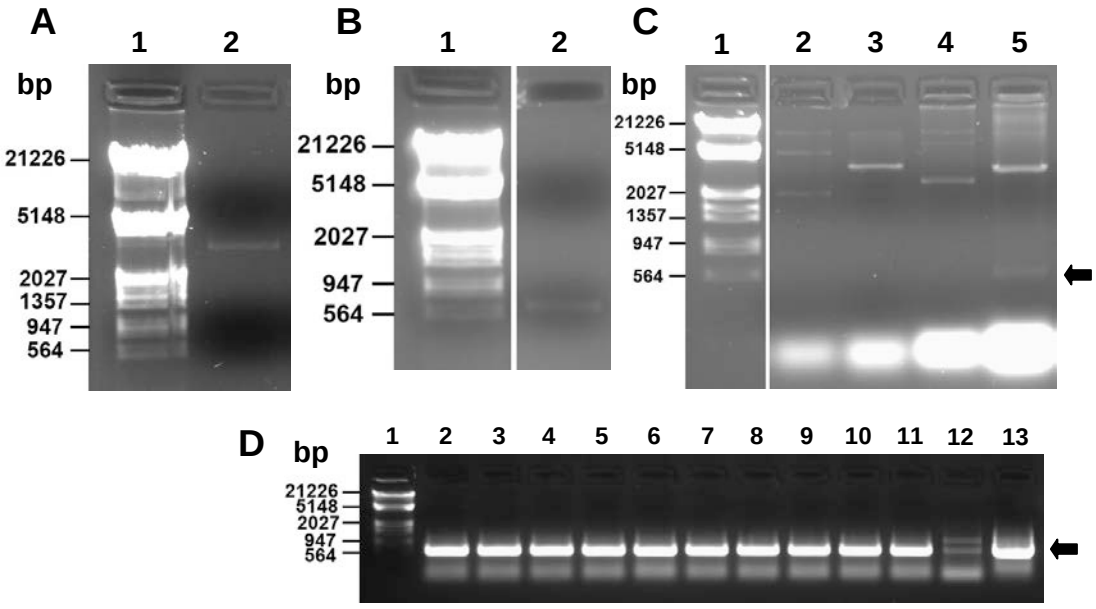

Figure 183: DNA Fragments for generation of a *divIVA-N* pKT25 construct and its confirmation by restriction digests.

A) The gel isolated *Xba*I/*Eco*RI fragment of pKT25 used for construction of pKT25-divIVA-N was analysed on a 0.7% agarose gel (Lane 2). The DNA size marker is Lambda *Hind*III/*Eco*RI (Lane 1).

B) The gel isolated *Xba*I/*Eco*RI fragment containing *divIVA-N* used for construction of pKT25-divIVA-N was analysed on a 0.85% agarose gel (Lane 2). The DNA size marker is Lambda *Hind*III/*Eco*RI (Lane 1).

C) The plasmids pKT25 (Lanes 2 & 3) and the plasmid pKT25-divIVA-N (Lanes 4 & 5) were analysed on a 1% agarose gel. Undigested samples (Lanes 2 & 4) were run together with samples digested with *Xba*I and *Eco*RI (Lanes 3 & 5). The arrow indicates the ~615bp fragment carrying *divIVA-N*. The DNA size marker is Lambda *Hind*III/*Eco*RI (Lane 1).

D) Candidate colonies were screened with colony PCR using THDiv_F (upstream) and DivN_STOPEco (downstream) primers and PCR products were analysed on a 1% agarose gel. Candidate colonies are shown Lanes 2-11. The arrow indicates the ~632bp PCR product expected. The plasmids pKT25 (Lane 12) and pUT18C-divIVA-N (Lane 13) were used as control templates. The DNA size marker is Lambda *Hind*III/*Eco*RI (Lane 1).

10.1.60 Generation of a DivIVA-C pKT25 construct

The construct pUT18C-divIVA-C had already been made (Kelemen lab, unpublished). Therefore, in order for reciprocal tests from the lower copy BTH plasmid pKT25, we aimed to move a *divIVA-C* fragment from pUT18C-divIVA-C. From the vector pUT18C-divIVA-C, using *Xba*I and *Eco*RI the sequence containing *divIVA-C* was inserted into the same sites of pKT25 (Figure 184 and Figure 185). After ligation and transformation of *E. coli*, the transformants were screened with colony PCR (Figure 185E) to find potential

clones which now generated a ~630bp PCR product that carries *divIVA-C*. Plasmid DNA was then isolated from positive colonies, and was confirmed by restriction digestion (Figure 185D) to liberate a ~612bp fragment containing *divIVA-C*. The product generated was the plasmid pKT25-divIVA-C, with *divIVA-C* fused to the C-terminus of the T25 adenylate cyclase domain.

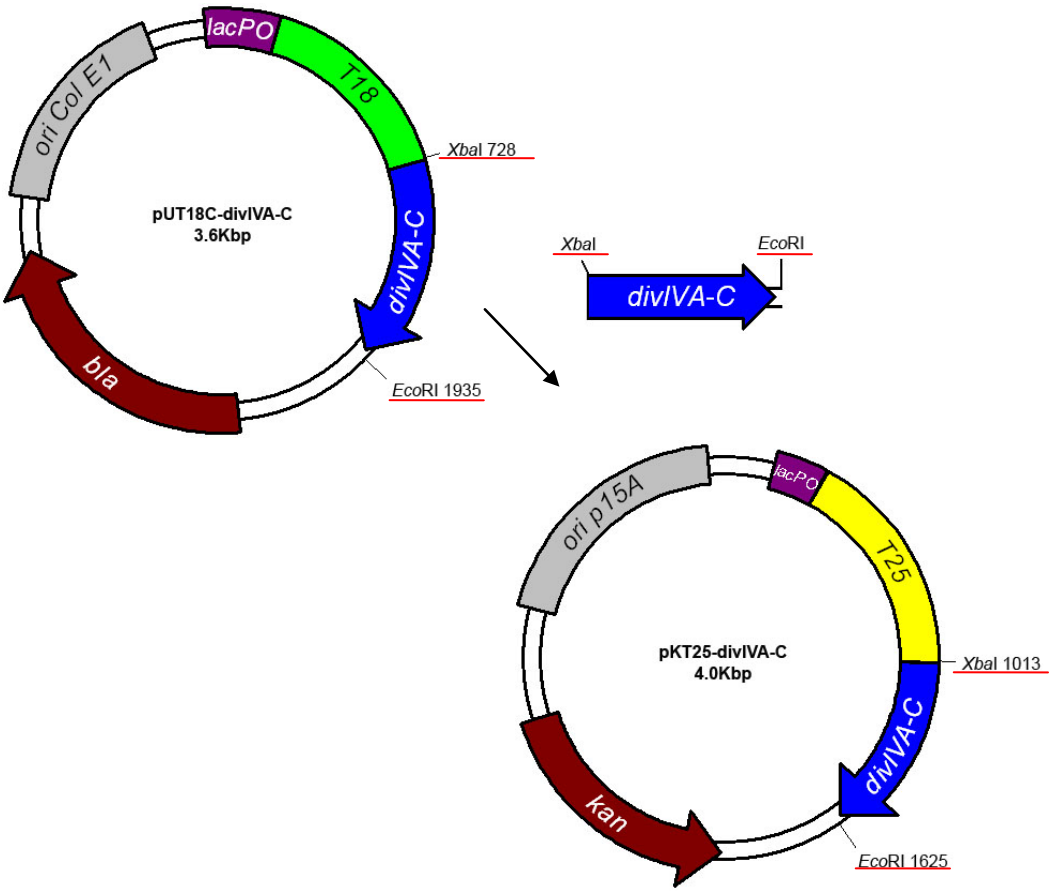

Figure 184: Generation of pKT25-divIVA-C.

pKT25-divIVA-C is a derivative of pKT25. A *divIVA-C* fragment was liberated using *Xba*I and *Eco*RI from pUT18C-divIVA-C. Using the enzymes *Xba*I and *Eco*RI pKT25 was digested and the *divIVA-C* fragment cloned so that DNA encoding the adenylate cyclase domain T25 reads inframe to *divIVA-C*. The restriction sites used in the cloning are underlined in red.

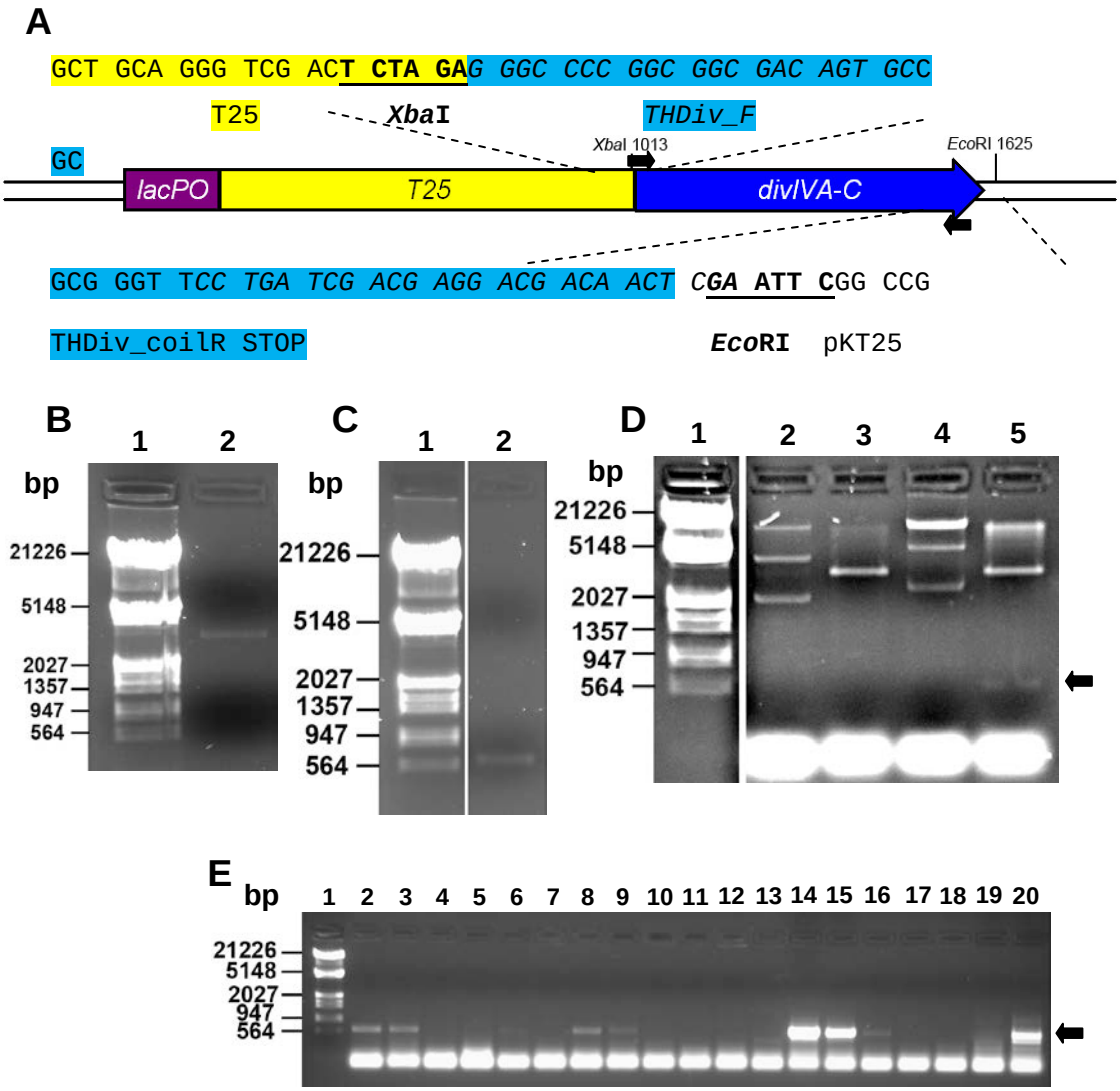

Figure 185: DNA Fragments for generation of a *divIVA-C* pKT25 construct and its confirmation by restriction digests.

A) Sequence of junctions in the construct pKT25-divIVA-C. The cloned in *divIVA-C* fragment is fused to DNA encoding the C-terminus of T25 and under the direction of a lactose inducible promoter. Restriction site sequences are bold and underlined. The *divIVA-C* sequences are highlighted blue and *T25* is highlighted yellow. Primers for colony PCR are marked (black arrows).

B) The gel isolated *Xba*I/*Eco*RI fragment of pKT25 used for construction of pKT25-divIVA-N was analysed on a 0.7% agarose gel (Lane 2). The DNA size marker is Lambda *Hind*III/*Eco*RI (Lane 1).

C) The gel isolated *Xba*I/*Eco*RI fragment containing *divIVA-C* used for construction of pKT25-divIVA-C was analysed on a 0.7% agarose gel (Lane 2). The DNA size marker is Lambda *Hind*III/*Eco*RI (Lane 1).

D) The plasmids pKT25 (Lanes 2 & 3) and the plasmid pKT25-divIVA-C (Lanes 4 & 5) were analysed on a 1% agarose gel. Undigested samples (Lanes 2 & 4) were run together with samples digested with *Xba*I and *Eco*RI (Lanes 3 & 5). The arrow indicates the ~612bp fragment carrying *divIVA-C*. The DNA size marker is Lambda *Hind*III/*Eco*RI (Lane 1).

E) Candidate colonies were screened with colony PCR using DivcoilF/PET (upstream) and THDiv_R (downstream) primers and PCR products were analysed on a 1% agarose gel. Candidate colonies are shown Lanes 2-18. The arrow indicates the ~630bp PCR product expected. The plasmids pKT25 (Lane 19) and pKT25-divIVA (Lane 20) were used as control templates. The DNA size marker is Lambda *Hind*III/*Eco*RI (Lane 1).

10.1.61 Generation of FilP overexpression constructs

To be able to overexpress and purify FilP protein, we sought to generate constructs of pET21a and pET28a containing *filP*. The easiest strategy to be able to do this was to make use of the two-hybrid construct pUT18C-filP, where we could lift a fragment from and

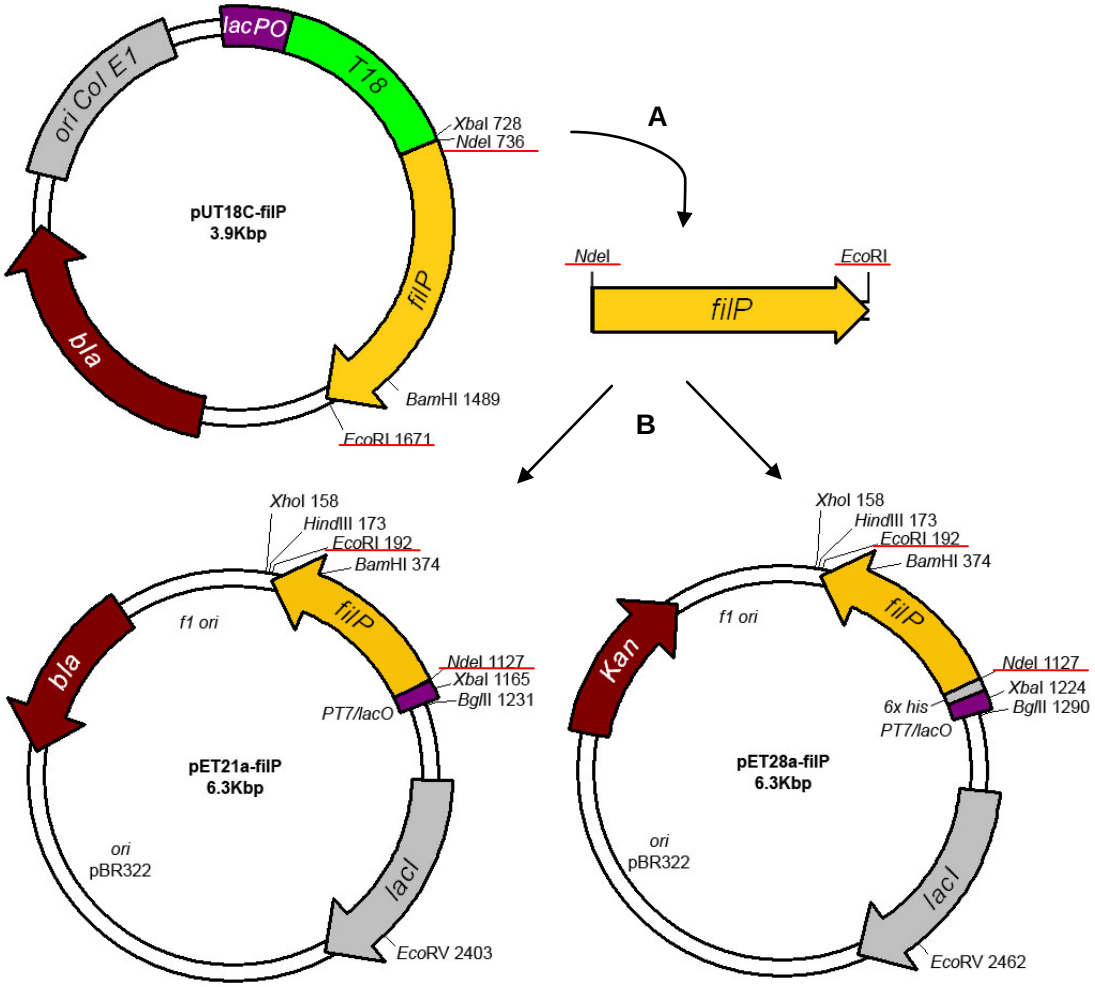

Figure 186: Generation of pET21a-filP and pET28a-filP.

pET21a-filP and pET28a-filP are derivatives of pET21a and pET28a, respectively. A) A *filP* fragment was liberated from pUT18C-filP using *Nde*I and *Eco*RI. B) Using *Nde*I and *Eco*RI, pET21a and pET28a were digested and the *filP* fragment was cloned. The restriction sites used in the cloning are underlined in red.

clone it directly into either pET21a or pET28a (Figure 186 & Figure 187). From pUT18C-filP an *Nde*I-*Eco*RI fragment was moved into pET21a (Figure 188). After ligation of the appropriate fragments the ligation mixture was used for transformation of *E. coli* strain DH5α. The transformants were screened with colony PCR (Figure 188C) to find potential clones which could generate a ~961bp PCR product that carries *filP*. Plasmid DNA was

then isolated from positive colonies, isolated DNA was confirmed by restriction digestion (Figure 188B) to liberate a ~973bp fragment containing *filP*, confirming the generation of pET21a-filP with the *filP* gene under the direction of a T7 RNA polymerase regulated

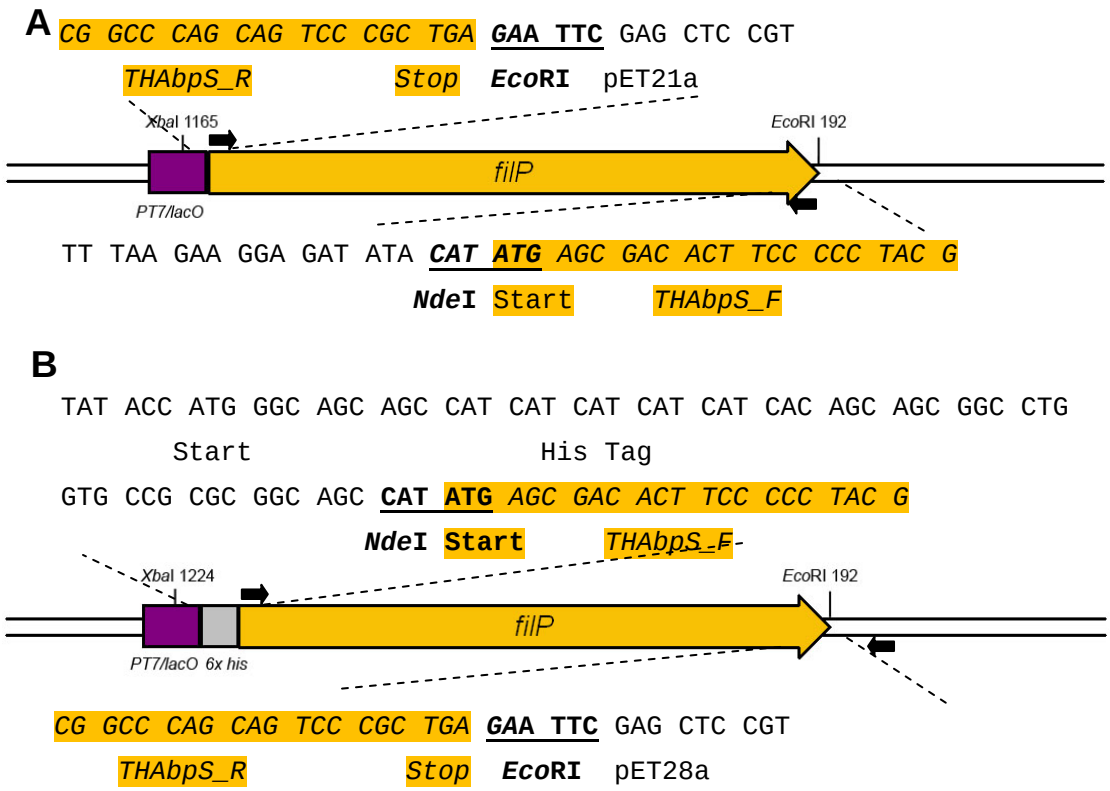

Figure 187: Sequences of the junctions in the constructs pET21a-FilP and pET28a-FilP

A) Sequence of junctions in the construct pET21a-filP. The cloned in *filP* gene is under the direction of a T7 RNA polymerase dependent/lactose inducible promoter. Restriction site sequences are bold and underlined. The *filP* sequences are highlighted orange. Primers for colony PCR are marked (black arrows).

B) Sequence of junctions in the construct pET28a-filP. The cloned in *filP* gene is fused to an N-terminal 6xhis encoding sequence under the direction of a T7 RNA polymerase dependent/lactose inducible promoter. Restriction site sequences are bold and underlined. The *filP* sequences are highlighted orange. Primers for colony PCR are marked (black arrows).

promoter. For overexpression of His-tagged FilP, the same *Nde*I-*Eco*RI fragment containing *filP* was moved into pET28a (Figure 189). After ligation and transformation of *E. coli* DH5α, the transformants were screened with colony PCR (Figure 189D) to find potential clones which could generate a ~1146bp PCR product that carries *filP*. Plasmid DNA was then isolated from positive colonies, isolated DNA was confirmed by restriction digestion (Figure 189C) to liberate a ~1032bp fragment containing *filP*. Therefore, confirming the generation of pET28a-filP, with the *filP* gene fused to a DNA encoding a

6xHis tag at the N-terminus under the direction of a T7 RNA polymerase regulated promoter.

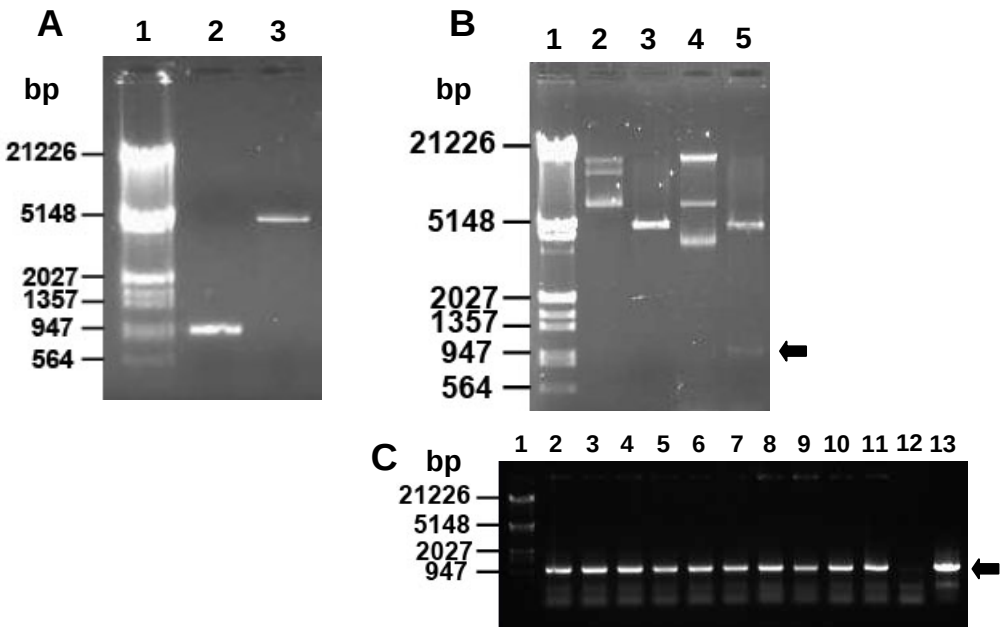

Figure 188: DNA Fragments for generation of a *filP* containing pET21a consrtuct and its confirmation by restriction digests.

A) The gel isolated fragments used for construction of pET21a-filP were analysed on a 0.7% agarose gel. The fragments used were the *Nde*I/*Eco*RI fragment of a filP (Lane 2) and the *Nde*I/*Eco*RI fragment of pET21a (Lane 3). The DNA size marker is Lambda *Hind*III/*Eco*RI (Lane 1).

B) The plasmids pET21a (Lanes 2 & 3) and the plasmid pET21a-filP (Lanes 4 & 5) were analysed on a 0.7% agarose gel. Undigested samples (Lanes 2 & 4) were run together with samples digested with *Xba*I and *Eco*RI (Lanes 3 & 5). The arrow indicates the ~973bp fragment carrying *filP*. The DNA size marker is Lambda *Hind*III/*Eco*RI (Lane 1).

C) Candidate colonies were screened with colony PCR using THAbpS_F (upstream) and THAbpS_R (downstream) primers and PCR products were analysed on a 0.7% agarose gel. Candidate colonies are shown Lanes 2-11. The arrow indicates the ~961bp PCR product expected. The plasmids pET21a (Lane 12) and pUT18C-filP (Lane 13) were used as control templates. The DNA size marker is Lambda *Hind*III/*Eco*RI (Lane 1).

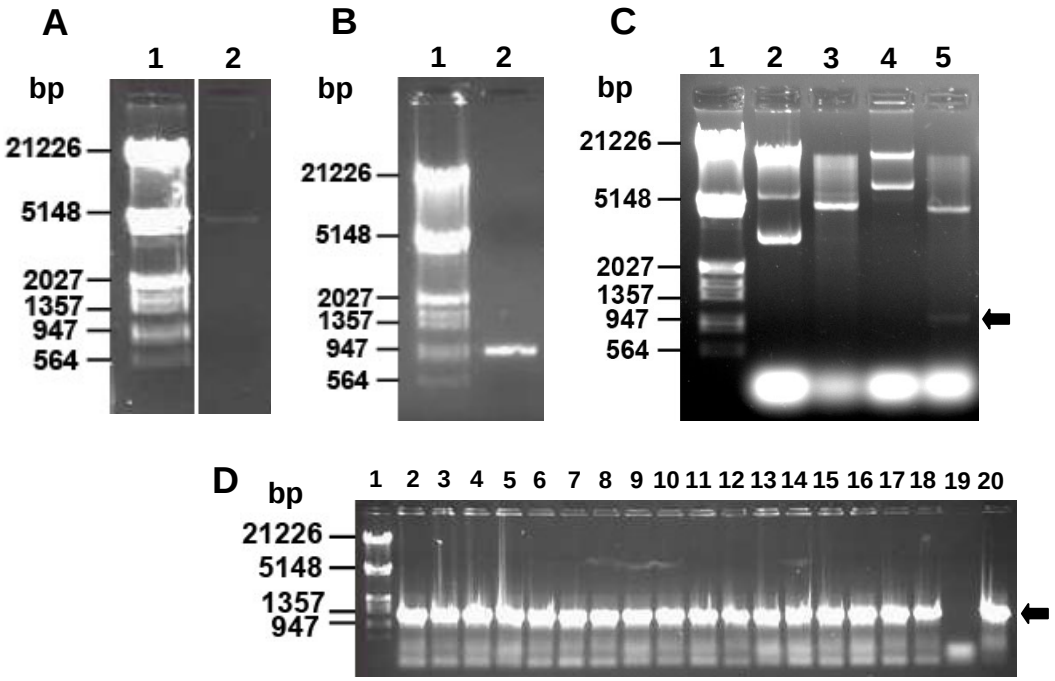

Figure 189: DNA Fragments for generation of a *filP* containing pET28a consrtuct and its confirmation by restriction digests.

A) The gel isolated *Nde*I/*Eco*RI fragment of pET28a used for construction of pET28a-filP was analysed on a 0.7% agarose gel (Lane 2). The DNA size marker is Lambda *Hind*III/*Eco*RI (Lane 1).

B) The gel isolated *Nde*I/*Eco*RI fragment containing *filP* used for construction of pET28a-filP was analysed on a 0.7% agarose gel (Lane 2). The DNA size marker is Lambda *Hind*III/*Eco*RI (Lane 1).

C) The plasmids pET28a (Lanes 2 & 3) and the plasmid pET28a-filP (Lanes 4 & 5) were analysed on a 0.7% agarose gel. Undigested samples (Lanes 2 & 4) were run together with samples digested with *Xba*I and *Eco*RI (Lanes 3 & 5). The arrow indicates the ~1032bp fragment carrying *filP*. The DNA size marker is Lambda *Hind*III/*Eco*RI (Lane 1).

D) Candidate colonies were screened with colony PCR using THAbpS_F (upstream) and pET28a(+)-1 (downstream) primers and PCR products were analysed on a 0.7% agarose gel. Candidate colonies are shown Lanes 2-18. The arrow indicates the ~1146bp PCR product expected. The plasmids pET28a (Lane 19) and pET21a-filP (Lane 20) were used as control templates. The DNA size marker is Lambda *Hind*III/*Eco*RI (Lane 1).

10.1.62 Generation of DivIVA overexpression constructs

In order to overexpress and purify DivIVA protein, we sought to generate constructs of pET21a and pET28a expressing DivIVA. A similar strategy was designed to that of the FilP overexpression constructs, whereby we could make use of the two hybrid construct pUT18C-divIVA, where we could lift a fragment from and clone it directly into either pET21a or pET28a (Figure 190 & Figure 191). From pUT18C-divIVA an *Nde*I-*Eco*RI fragment was moved into pET21a (Figure 192). After ligation and transformation of *E. coli*

DH5α, the transformants were screened with colony PCR (Figure 192D) to find potential clones which could generate a ~1410bp PCR product that carries *divIVA*. Plasmid DNA was then isolated from positive colonies, isolated DNA was confirmed by restriction

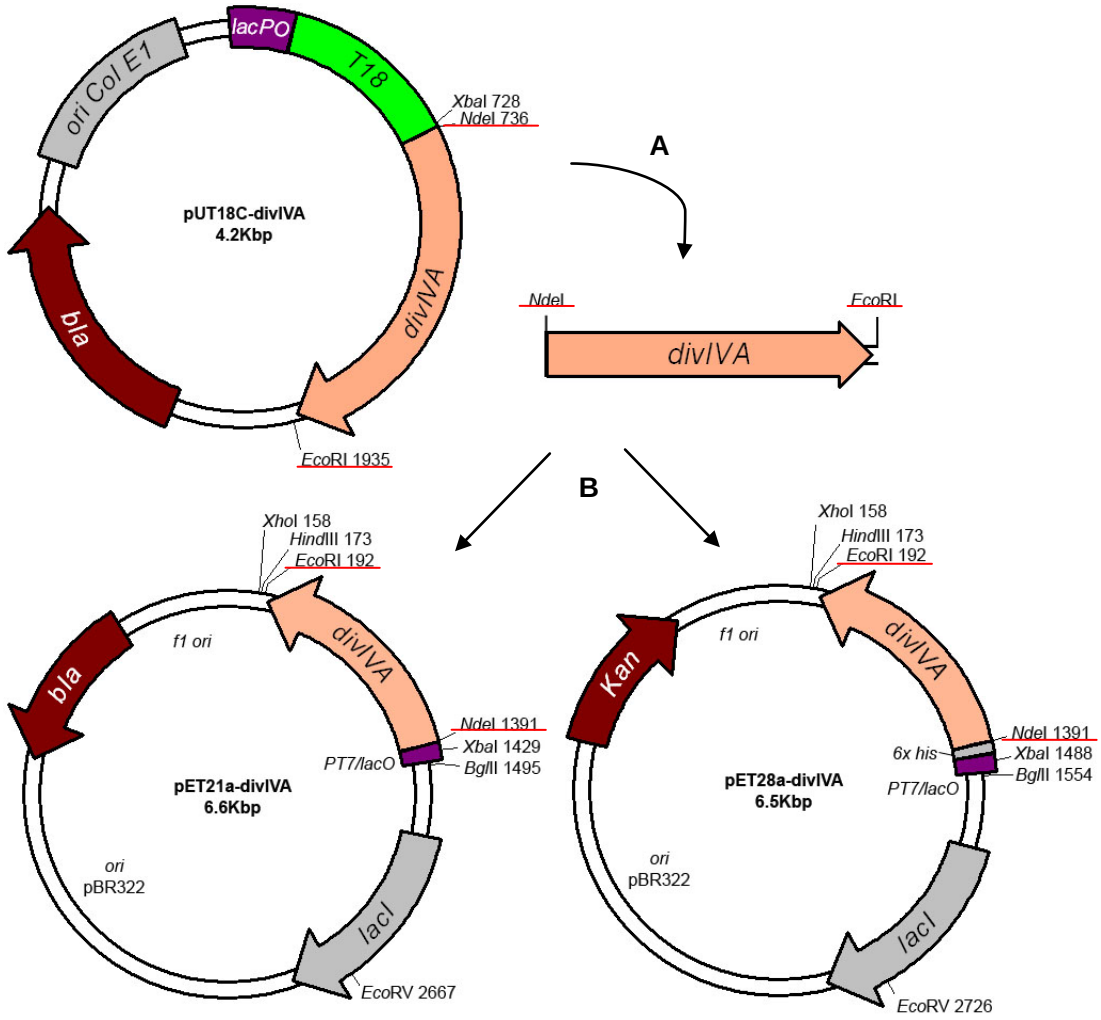

Figure 190: Generation of pET21a-divIVA and pET28a-divIVA.

pET21a-divIVA and pET28a-divIVA are derivatives of pET21a and pET28a, respectively. A) A *divIVA* fragment was liberated from pUT18C-divIVA using *Nde*I and *Eco*RI. B) Using *Nde*I and *Eco*RI, pET21a and pET28a were digested and the *divIVA* fragment was cloned. The restriction sites used in the cloning are underlined in red.

digestion (Figure 192C) to liberate a ~1199bp fragment containing *divIVA*, confirming the generation of pET21a-divIVA with the *divIVA* gene with no tag under the direction of a T7 RNA polymerase regulated promoter. For overexpression and purification of His-tagged DivIVA, the same *Nde*I-*Eco*RI fragment containing *divIVA* was moved into pET28a (Figure 193). After ligation of the fragments the ligation mixture was used for transformation of *E. coli* strain DH5α. The transformants were screened with colony PCR (Figure 193D) to find potential clones which could generate a ~1410bp PCR product that carries *divIVA*. Plasmid DNA was then isolated from positive colonies, isolated DNA was

confirmed by restriction digestion (Figure 193C) to liberate a ~1199bp fragment containing *divIVA*. Therefore, confirming the generation of pET28a-divIVA, with the *divIVA* gene fused to DNA encoding a 6xHis tag at the N-terminus under the direction of a T7 RNA polymerase regulated promoter.

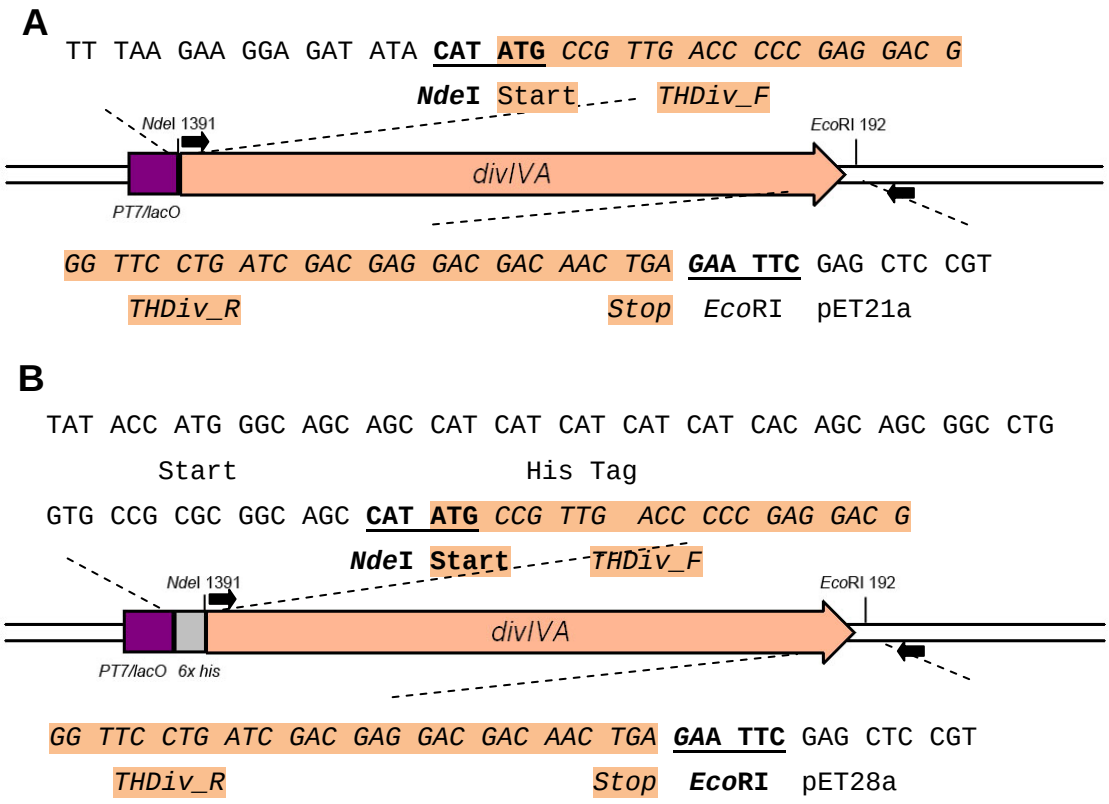

Figure 191: Sequences of the junctions in the constructs pET21a-DivIVA and pET28a-DivIVA

A) Sequence of junctions in the construct pET21a-divIVA. The cloned in *divIVA* gene is under the direction of a T7 RNA polymerase dependent/lactose inducible promoter. Restriction site sequences are bold and underlined. The *divIVA* sequences are highlighted salmon pink. Primers for colony PCR are marked (black arrows).

B) Sequence of junctions in the construct pET28a-divIVA. The cloned in *divIVA* gene is fused to an N-terminal 6xhis encoding sequence under the direction of a T7 RNA polymerase dependent/lactose inducible promoter. Restriction site sequences are bold and underlined. The *divIVA* sequences are highlighted salmon pink. Primers for colony PCR are marked (black arrows).

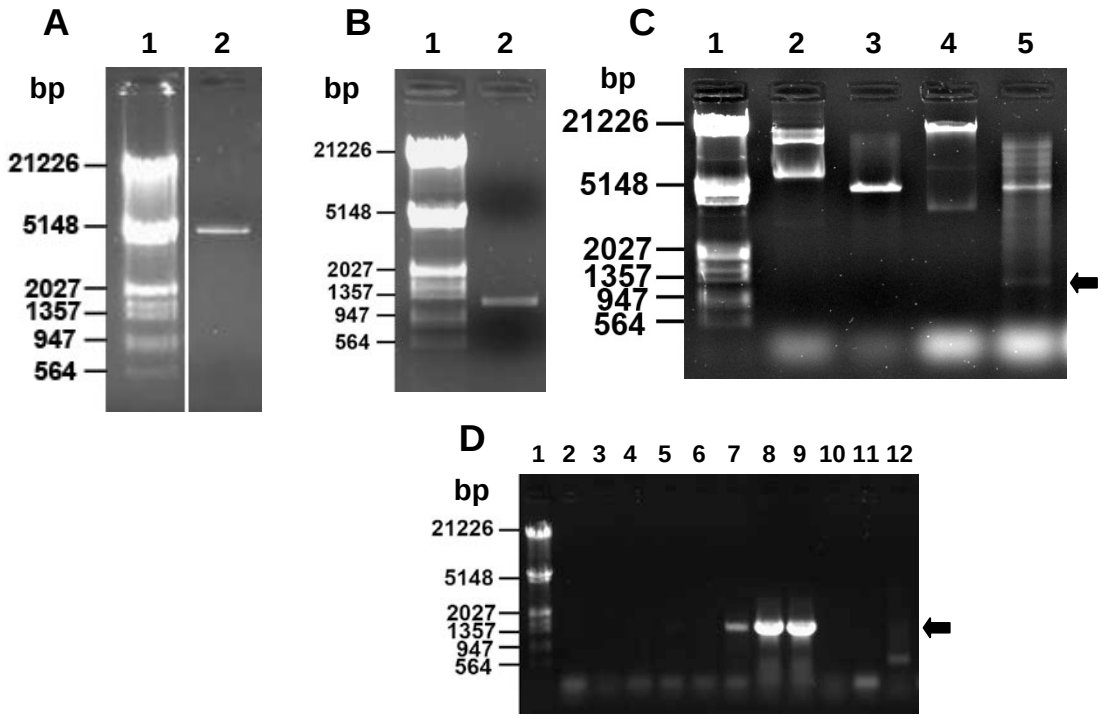

Figure 192: DNA Fragments for generation of a *divIVA* containing pET21a consrtuct and its confirmation by restriction digests.

A) The gel isolated *Nde*I/*Eco*RI fragment of pET21a used for construction of pET21a-divIVA was analysed on a 0.7% agarose gel (Lane 2). The DNA size marker is Lambda *Hind*III/*Eco*RI (Lane 1).

B) The gel isolated *Nde*I/*Eco*RI fragment containing *divIVA* used for construction of pET21a-divIVA was analysed on a 0.7% agarose gel (Lane 2). The DNA size marker is Lambda *Hind*III/*Eco*RI (Lane 1).

C) The plasmids pET21a (Lanes 2 & 3) and the plasmid pET21a-divIVA (Lanes 4 & 5) were analysed on a 0.7% agarose gel. Undigested samples (Lanes 2 & 4) were run together with samples digested with *Nde*I and *Eco*RI (Lanes 3 & 5). The arrow indicates the ~1199bp fragment carrying *divIVA*. The DNA size marker is Lambda *Hind*III/*Eco*RI (Lane 1).

D) Candidate colonies were screened with colony PCR using THDiv_F (upstream) and pET28a(+)-1 (downstream) primers and PCR products were analysed on a 0.7% agarose gel. Candidate colonies are shown Lanes 2-11. The arrow indicates the ~1410bp PCR product expected. The plasmid pET21a (Lane 12) was used as a control template. The DNA size marker is Lambda *Hind*III/*Eco*RI (Lane 1).

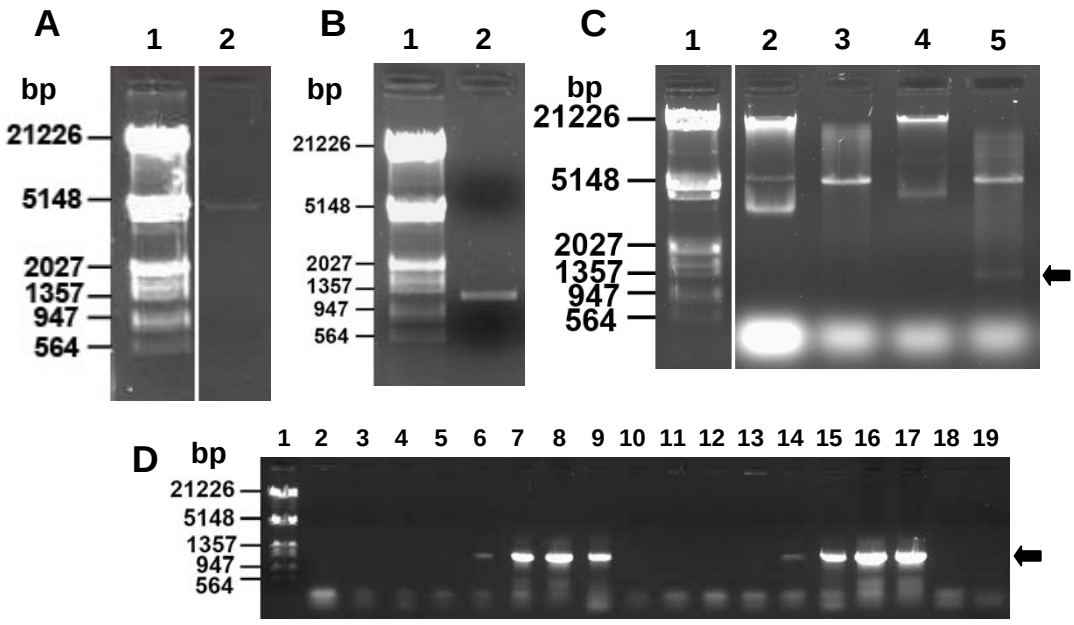

Figure 193: DNA Fragments for generation of a *divIVA* containing pET28a consrtuct and its confirmation by restriction digests.

A) The gel isolated *Nde*I/*Eco*RI fragment of pET28a used for construction of pET28a-divIVA was analysed on a 0.7% agarose gel (Lane 2). The DNA size marker is Lambda *Hind*III/*Eco*RI (Lane 1).

B) The gel isolated *Nde*I/*Eco*RI fragment containing *divIVA* used for construction of pET28a-divIVA was analysed on a 0.7% agarose gel (Lane 2). The DNA size marker is Lambda *Hind*III/*Eco*RI (Lane 1).

C) The plasmids pET28a (Lanes 2 & 3) and the plasmid pET28a-divIVA (Lanes 4 & 5) were analysed on a 0.7% agarose gel. Undigested samples (Lanes 2 & 4) were run together with samples digested with *Nde*I and *Eco*RI (Lanes 3 & 5). The arrow indicates the ~1199bp fragment carrying *divIVA*. The DNA size marker is Lambda *Hind*III/*Eco*RI (Lane 1).

D) Candidate colonies were screened with colony PCR using THDiv_F (upstream) and pET28a(+)-1 (downstream) primers and PCR products were analysed on a 0.7% agarose gel. Candidate colonies are shown Lanes 2-18. The arrow indicates the ~1410bp PCR product expected. The plasmid pET28a (Lane 19) was used as a control template. The DNA size marker is Lambda *Hind*III/*Eco*RI (Lane 1).

10.1.63 Generation of DivIVA-C overexpression constructs

We sought to overexpress and purify DivIVA-C by generating constructs of pET21a and pET28a containing *divIVA-C*. However, the complication with generating these constructs was that we could not employ the same strategy as used for the other pET21a and pET28a constructs generated for overproducing either DivIVA or FilP because the pUT18C-divIVA-C construct that was previously generated, did not include an *Nde*I site at the start of the *divIVA-C* insert. So we aimed to generate a *divIVA-C* fragment

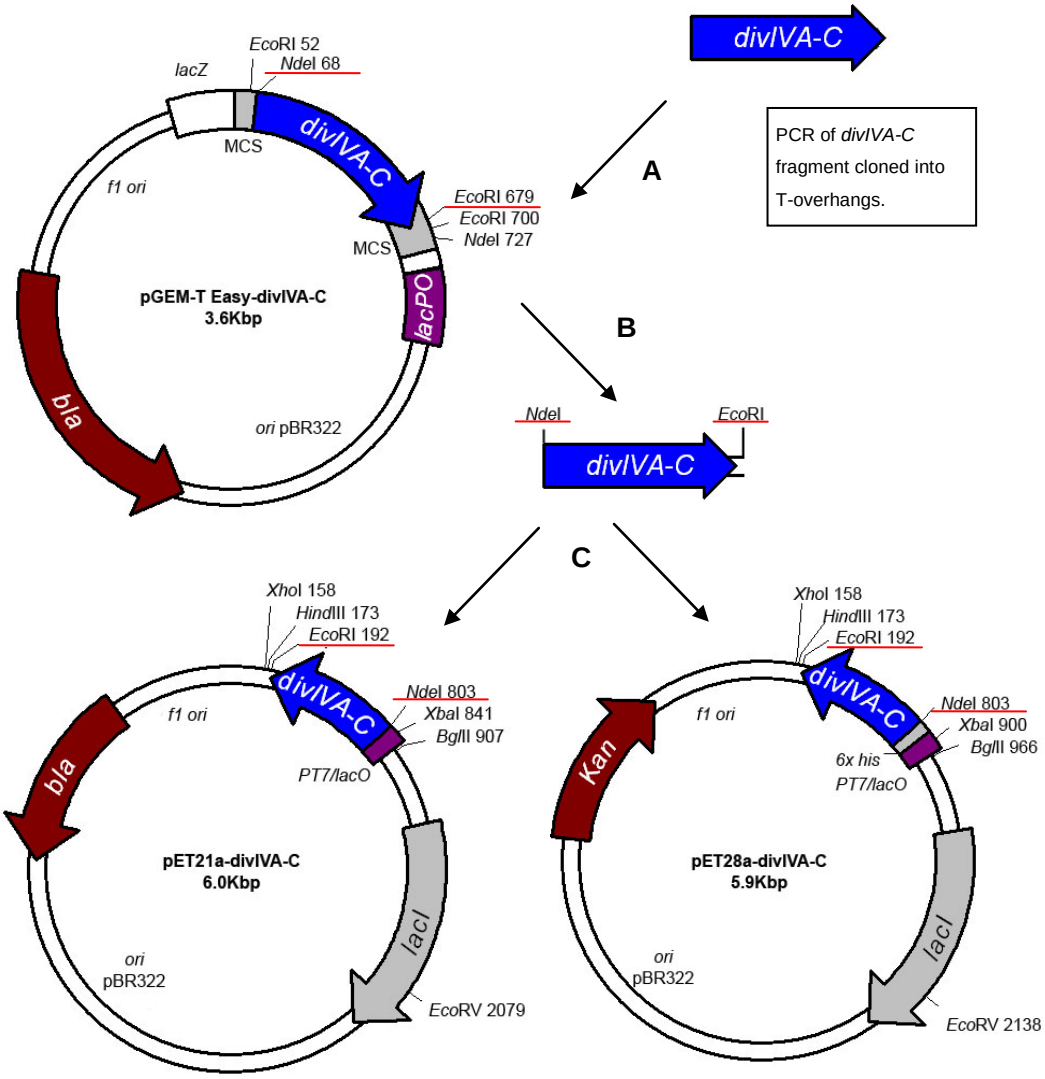

Figure 194: Generation of pGEM-T Easy-divIVA-C, pET21a-divIVA-C and pET28a-divIVA-C.

A) pGEM-T Easy-divIVA-C is a derivative of pGEM-T Easy containing the *divIVA-C* PCR product cloned into the multiple cloning site which is designed with T overhangs for easy incorporation of a Taq polymerase generated PCR product. pET21a-divIVA-C and pET28a-divIVA-C are derivatives of pET21a and pET28a, respectively. B) A *divIVA-C* fragment was liberated from pGEM-T Easy-divIVA-C using *Nde*I and *Eco*RI. C) Using *Nde*I and *Eco*RI, pET21a and pET28a were digested and the *divIVA-C* fragment was cloned. The restriction sites used in the cloning are underlined in red.

with the desired *Nde*I and *Eco*RI restriction sites by PCR amplification. As inserting this fragment directly into pET21a or pET28a might prove problematic, we used the commercial vector pGEM-T Easy. Where we would then be able to move the *divIVA-C* fragment later into pET21a or pET28a (Figure 194 & Figure 195). The vector pGEM-T Easy is useful for cloning PCR products directly as it is a linearised fragment with single 3' thymidines at both ends. A PCR product generated with Go Taq® Polymerase will

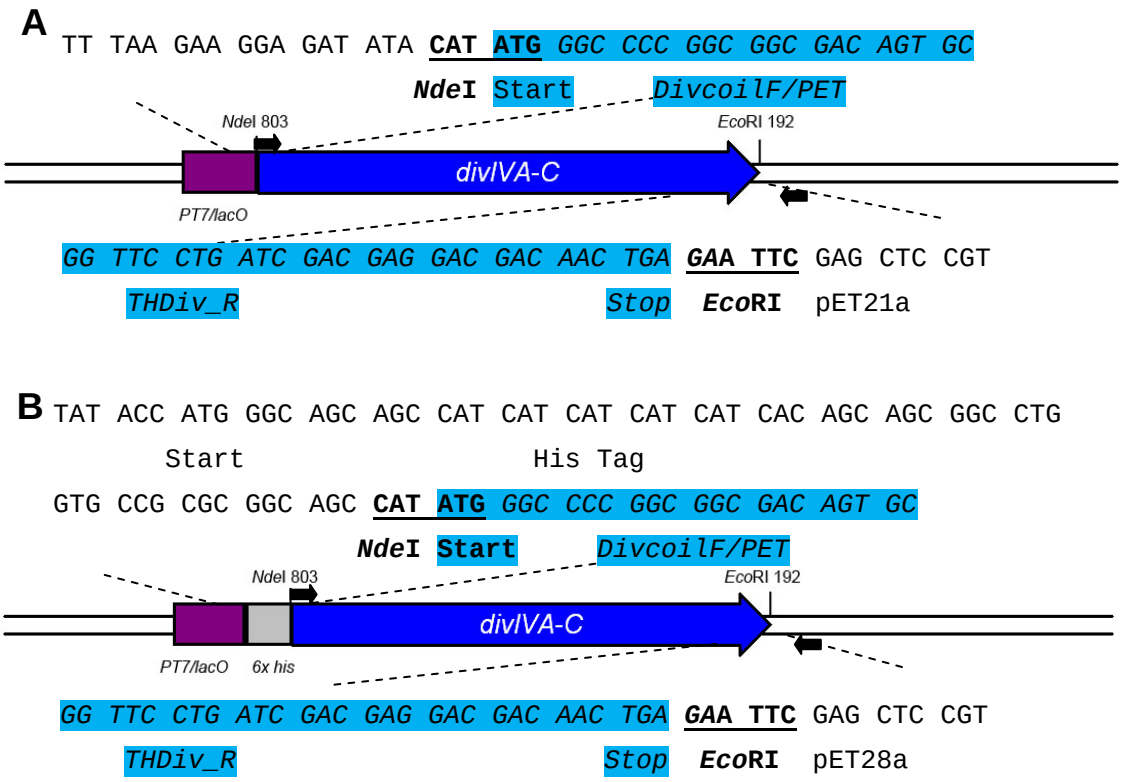

Figure 195: Sequences of the junctions in the constructs pET21a-DivIVA-C and pET28a-DivIVA-C.

A) Sequence of junctions in the construct pET21a-divIVA-C. The cloned in *divIVA-C* fragment is under the direction of a T7 RNA polymerase dependent/lactose inducible promoter. Restriction site sequences are bold and underlined. The *divIVA-C* sequences are highlighted blue. Primers for colony PCR are marked (black arrows).

B) Sequence of junctions in the construct pET28a-divIVA-C. The cloned in *divIVA-C* fragment is fused to an N-terminal 6xhis encoding sequence under the direction of a T7 RNA polymerase dependent/lactose inducible promoter. Restriction site sequences are bold and underlined. The *divIVA-C* sequences are highlighted blue. Primers for colony PCR are marked (black arrows).

generate 3' adenines at both ends which will be complementary to the thymidine overhangs on pGEM-T Easy. The vector pGEM-T Easy also facilitates blue/white selection for plasmids carrying inserts. The *divIVA-C* fragment was generated by PCR using the primers DivcoilF/PET and THDiv_R (Figure 196A) and cloned into the commercial vector pGEM-T Easy. After transformation, the white colonies were further screened using colony PCR (Figure 196B) to find potential clones which could generate a ~630bp PCR product that carries *divIVA-C*. There were numerous colonies that generated the expected

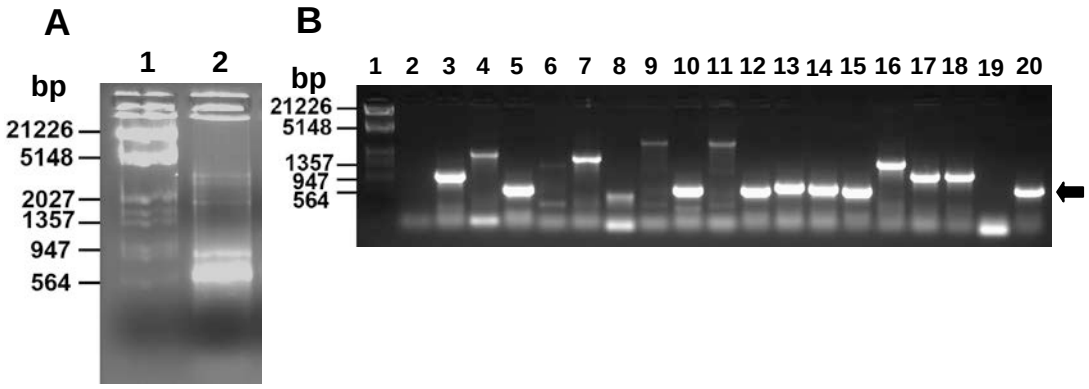

Figure 196: PCR of a *divIVA-C* fragment and its identification in the vector pGEM-T Easy.

A) The DivIVA-C PCR product used for construction of pET28a-divIVA-C was analysed on a 1% agarose gel (Lane 2). The DNA size marker is Lambda *Hind*III/*Eco*RI (Lane 1).

B) Candidate colonies were screened with colony PCR using TH DivCoil F PET (upstream) and TH DivIVA R (downstream) primers and PCR products were analysed on a 1% agarose gel. Candidate colonies are shown Lanes 2-18. The arrow indicates the ~630bp PCR product expected. A blue negative colony was also included (Lane 19). The plasmid pET28a-divIVA (Lane 20) was used as a control template. The DNA size marker is Lambda *Hind*III/*Eco*RI (Lane 1).

PCR product, although there were also colonies with larger PCR inserts likely corresponding to insertion of incorrect PCR products (Figure 196A). Analysing the plasmids with the correct insert size using sequencing, we identified a clone that contained the correct insert of *divIVA-C* with no mutations.

Therefore, this clone was used as the source of the *divIVA-C* fragment, which was then lifted with *Nde*I and *Eco*RI and was cloned into pET21a (Figure 197). After ligation and transformation, transformants were screened with colony PCR (Figure 197D) to find potential clones which could generate a ~815bp PCR product that carries *divIVA-C*. Plasmid DNA was then isolated from positive colonies and was confirmed by restriction digestion (Figure 197C) to liberate a ~611bp fragment containing *divIVA-C*, verifying the generation of pET21a-divIVA-C carrying *divIVA-C* sequence with no tag under the direction of a T7 RNA polymerase regulated promoter.

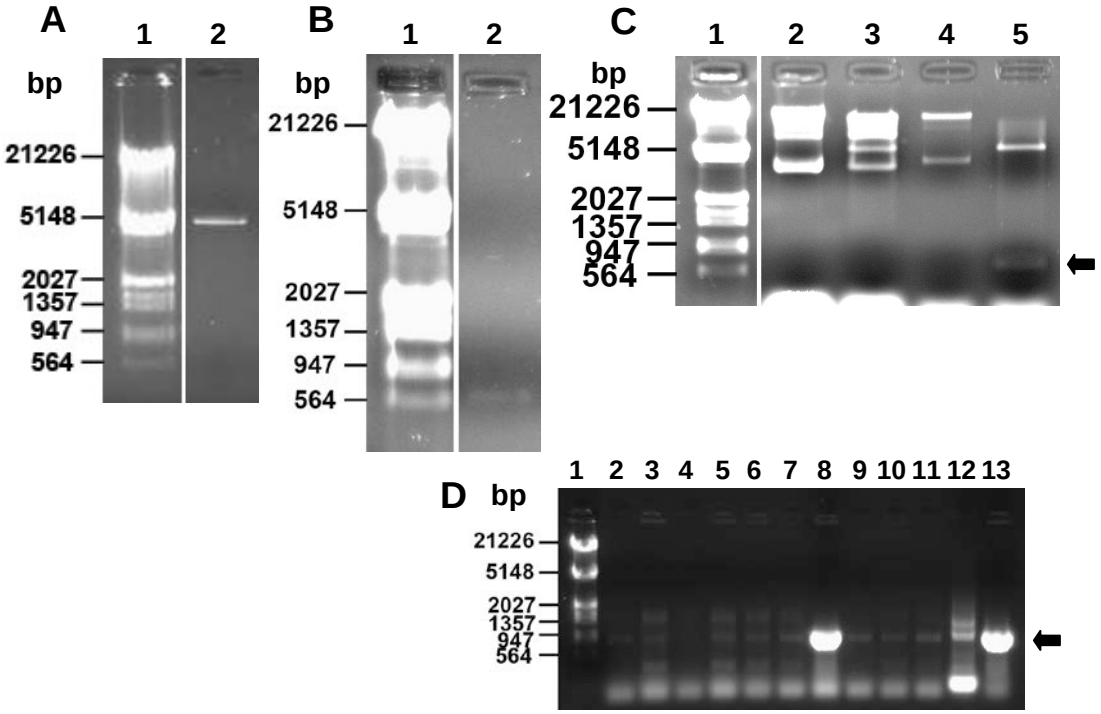

Figure 197: DNA Fragments for generation of a *divIVA-C* containing pET21a consrtuct and its confirmation by restriction digests.

A) The gel isolated *Nde*I/*Eco*RI fragment of pET21a used for construction of pET21a-divIVA-C was analysed on a 0.7% agarose gel (Lane 2). The DNA size marker is Lambda *Hind*III/*Eco*RI (Lane 1).

B) The gel isolated *Nde*I/*Eco*RI fragment containing *divIVA-C* used for construction of pET21a-divIVA-C was analysed on a 0.8% agarose gel (Lane 2). The DNA size marker is Lambda *Hind*III/*Eco*RI (Lane 1).

C) The plasmids pET28a (Lanes 2 & 3) and the plasmid pET21a-divIVA-C (Lanes 4 & 5) were analysed on a 1% agarose gel. Undigested samples (Lanes 2 & 4) were run together with samples digested with *Nde*I and *Eco*RI (Lanes 3 & 5). The arrow indicates the ~611bp fragment carrying *divIVA-C*. The DNA size marker is Lambda *Hind*III/*Eco*RI (Lane 1).

D) Candidate colonies were screened with colony PCR using DivcoilF/PET (upstream) and pET28a(+)-1 (downstream) primers and PCR products were analysed on a 1% agarose gel. Candidate colonies are shown Lanes 2-11. The arrow indicates the ~815bp PCR product expected. The plasmids pET21a (Lane 12) and pET28a-divIVA (Lane 13) were used as control templates. The DNA size marker is Lambda *Hind*III/*Eco*RI (Lane 1).

For overexpression and purification of His-tagged DivIVA-C, the same *Nde*I-*Eco*RI fragment containing *divIVA-C* was moved into pET28a (Figure 198). The transformants were screened with colony PCR (Figure 198D) to find clones which could generate a ~815bp PCR product that carries *divIVA-C*. Plasmid DNA was then isolated from positive colonies and was confirmed by restriction digestion (Figure 198C) to liberate a ~611bp fragment containing *divIVA-C* verifying the generation of pET28a-divIVA-C.

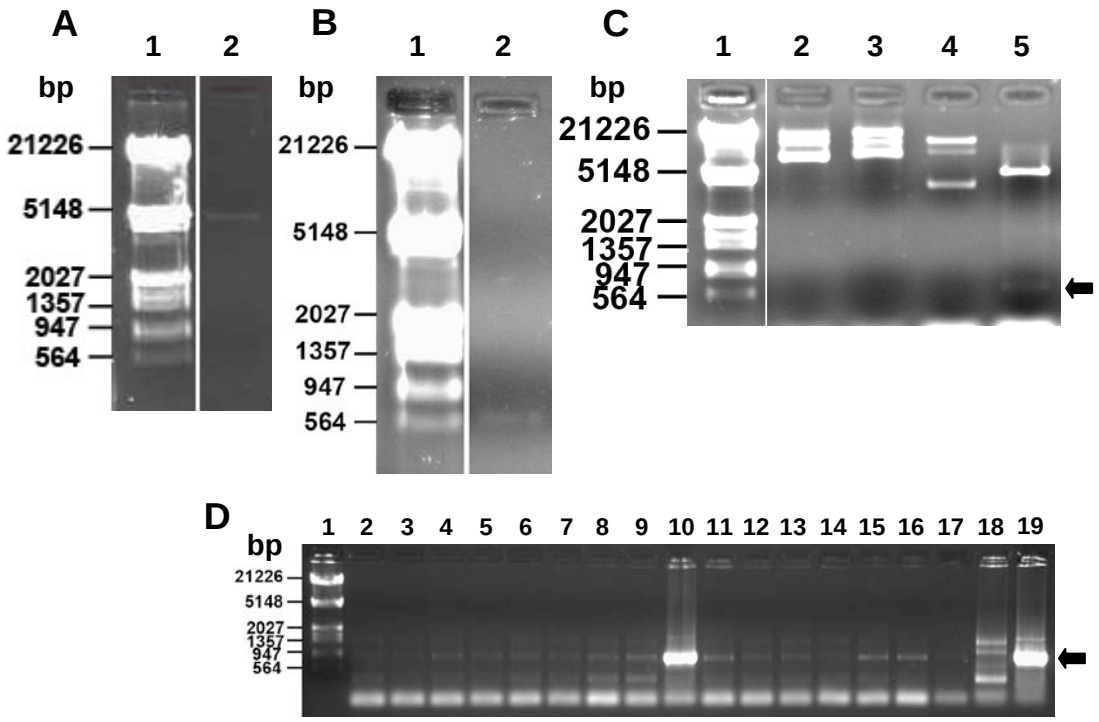

Figure 198: DNA Fragments for generation of a *divIVA-C* containing pET28a consrtuct and its confirmation by restriction digests.

The gel isolated *Nde*I/*Eco*RI fragment of pET28a used for construction of pET28a-divIVA-C was analysed on a 0.7% agarose gel (Lane 2). The DNA size marker is Lambda *Hind*III/*Eco*RI (Lane 1).

The gel isolated *Nde*I/*Eco*RI fragment containing *divIVA-C* used for construction of pET28a-divIVA-C was analysed on a 0.8% agarose gel (Lane 2). The DNA size marker is Lambda *Hind*III/*Eco*RI (Lane 1).

The plasmids pET28a (Lanes 2 & 3) and the plasmid pET28a-divIVA-C (Lanes 4 & 5) were analysed on a 1% agarose gel. Undigested samples (Lanes 2 & 4) were run together with samples digested with *Nde*I and *Eco*RI (Lanes 3 & 5). The arrow indicates the ~611bp fragment carrying *divIVA-C*. The DNA size marker is Lambda *Hind*III/*Eco*RI (Lane 1).

Candidate colonies were screened with colony PCR using DivcoilF/PET (upstream) and pET28a(+)-1 (downstream) primers and PCR products were analysed on a 1% agarose gel. Candidate colonies are shown Lanes 2-17. The arrow indicates the ~815bp PCR product expected. The plasmids pET28a (Lane 18) and pET28a-divIVA (Lane 19) were used as control templates. The DNA size marker is Lambda *Hind*III/*Eco*RI (Lane 1).

10.1.64 Generation of EGFP-Scy overexpression constructs

As we had no antibody against Scy, we wanted to be able to overexpress Scy with a protein tag that we could monitor. The strategy to make EGFP-Scy expression constructs was to move an *Nde*I-*Eco*RI fragment carrying *egfp-scy* from pCJW93-egfp-scy (Hunter and Kelemen unpublished) and clone it directly into either pET21a or pET28a (Figure 199 & Figure 200). This should then result in the pET21a construct expressing EGFP-Scy with no extra tag. Whereas the pET28a construct containing *egfp-scy* would express a His-tagged

version of EGFP-Scy. From pCJW93-egfp-scy an *Nde*I and *Eco*RI fragment containing *egfp-scy* was inserted into the same sites of pET21a (Figure 201). After ligation and transformation the transformants were screened with colony PCR (Figure 201D) to find potential clones which now produced a ~1411bp PCR product generated from the C-terminal of Scy inserted into pET21a. Plasmid DNA was then isolated from positive colonies and was confirmed by restriction digestion (Figure 201C) to liberate a ~4137bp fragment containing the C-terminal end of *scy*. This verified the generation of pET21a-egfp-scy, with *egfp-scy* with no tag under the direction of a T7 RNA polymerase regulated promoter.

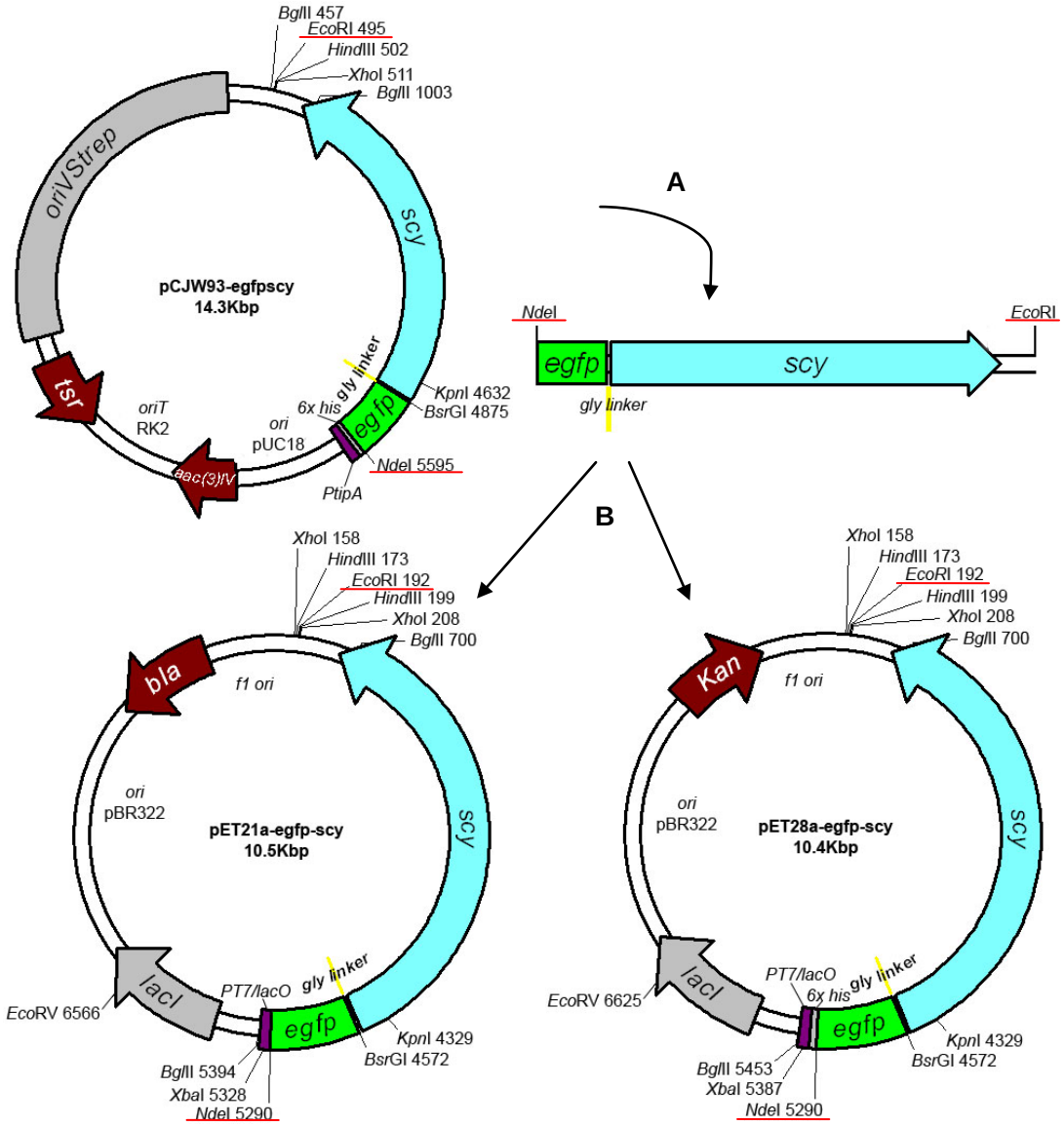

Figure 199: Generation of pET21a-egfp-scy and pET28a-egfp-scy.

pET21a-egfp-scy and pET28a-egfp-scy are derivatives of pET21a and pET28a, respectively. A) An *egfp-scy* fragment was liberated from pCJW93-egfp-scy using *Nde*I and *Eco*RI. B) Using *Nde*I and *Eco*RI, pET21a and pET28a were digested and the *egfp-scy* fragment was cloned. The restriction sites used in the cloning are underlined in red.

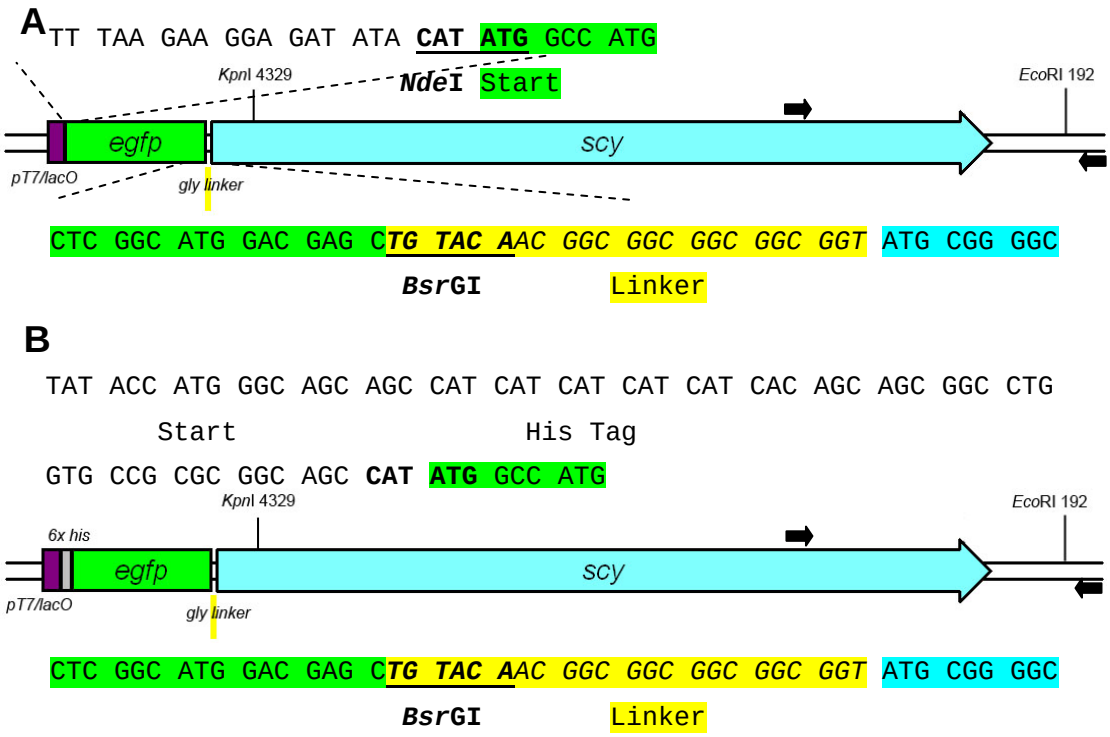

Figure 200: Sequences of joins in the constructs pET21a-egfp-scy and pET28a-egfp-scy.

A) Sequence of junctions in the construct pET21a-egfp-scy. The cloned in *egfp-scy* fragment is under the direction of a T7 RNA polymerase dependent/lactose inducible promoter. Restriction site sequences are bold and underlined. The *egfp-scy* junction contains a glycine linker (highlighted yellow/italics). The *scy* sequences are highlighted light blue and *egfp* is highlighted green. Primers for colony PCR are marked (black arrows).

B) Sequence of junctions in the construct pET28a-egfp-scy. The cloned in *egfp-scy* fragment is fused to an N-terminal 6xhis encoding sequence under the direction of a T7 RNA polymerase dependent/lactose inducible promoter. Restriction site sequences are bold and underlined. The *egfp-scy* junction contains a glycine linker (highlighted yellow/italics). The *scy* sequences are highlighted light blue and *egfp* is highlighted green. Primers for colony PCR are marked (black arrows).

For overexpression of His-tagged EGFP-Scy, the same *Nde*I-*Eco*RI fragment containing *egfp-scy* was inserted into the *Nde*I-*Eco*RI sites of pET28a (Figure 202). The transformants were screened with colony PCR (Figure 202D) to find potential clones which now produced a ~1411bp PCR product that can be generated from the C-terminal part of *scy* inserted into pET28a. Plasmid DNA was then isolated from positive colonies and was

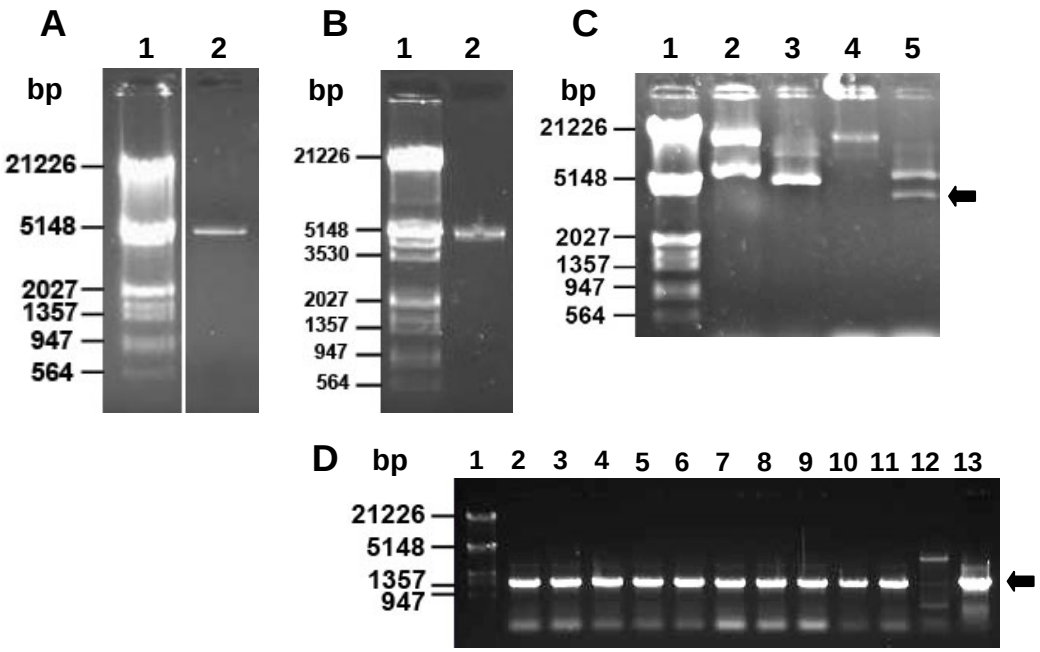

Figure 201: DNA Fragments for generation of an *egfp-scy* containing pET21a consrtuct and its confirmation by restriction digests.

A) The gel isolated *Nde*I/*Eco*RI fragment of pET21a used for construction of pET21a-divIVA-C was analysed on a 0.7% agarose gel (Lane 2). The DNA size marker is Lambda *Hind*III/*Eco*RI (Lane 1).

B) The gel isolated *Nde*I/*Eco*RI fragment containing egfp-scy used for construction of pIJ8660-Pscy-egfp-scy was analysed on a 0.7% agarose gel (Lane 2). The DNA size marker is Lambda *Hind*III/*Eco*RI (Lane 1).

C) The plasmids pET21a (Lanes 2 & 3) and the plasmid pET21a-egfp-scy (Lanes 4 & 5) were analysed on a 0.7% agarose gel. Undigested samples (Lanes 2 & 4) were run together with samples digested with *Kpn*I and *Eco*RI (Lanes 3 & 5). The arrow indicates the ~4137bp fragment carrying part of *scy*. The DNA size marker is Lambda *Hind*III/*Eco*RI (Lane 1).

D) Candidate colonies were screened with colony PCR using TH Scy F4 (upstream) and pET28a(+)-1 (downstream) primers and PCR products were analysed on a 0.7% agarose gel. Candidate colonies are shown Lanes 2-11. The arrow indicates the ~1411bp PCR product expected. The plasmids pET21a (Lane 12) and pET21a-scy (Lane 13) were used as control templates. The DNA size marker is Lambda *Hind*III/*Eco*RI (Lane 1).

confirmed by restriction digestion (Figure 202C) to liberate a ~4137bp fragment containing the C-terminal end of *scy*. This verified the construction of plasmid pET28a-egfp-scy, with *egfp-scy* downstream of DNA encoding a 6xHis tag under the direction of a T7 RNA polymerase regulated promoter.

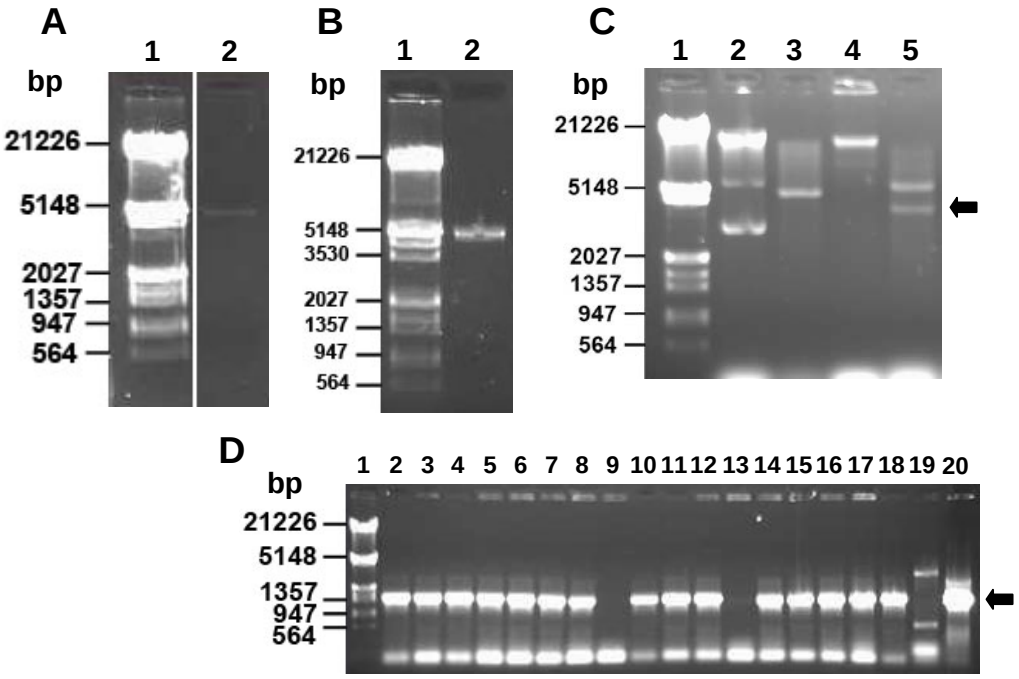

Figure 202: DNA Fragments for generation of an *egfp-scy* containing pET28a consrtuct and its confirmation by restriction digests.

A) The gel isolated *Nde*I/*Eco*RI fragment of pET28a used for construction of pET28a-divIVA-C was analysed on a 0.7% agarose gel (Lane 2). The DNA size marker is Lambda *Hind*III/*Eco*RI (Lane 1).

B) The gel isolated *Nde*I/*Eco*RI fragment containing egfp-scy used for construction of pIJ8660-Pscy-egfp-scy was analysed on a 0.7% agarose gel (Lane 2). The DNA size marker is Lambda *Hind*III/*Eco*RI (Lane 1).

C) The plasmids pET28a (Lanes 2 & 3) and the plasmid pET28a-egfp-scy (Lanes 4 & 5) were analysed on a 0.7% agarose gel. Undigested samples (Lanes 2 & 4) were run together with samples digested with *Kpn*I and *Eco*RI (Lanes 3 & 5). The arrow indicates the ~4137bp fragment carrying part of *scy*. The DNA size marker is Lambda *Hind*III/*Eco*RI (Lane 1).

D) Candidate colonies were screened with colony PCR using TH Scy F4 (upstream) and pET28a(+)-1 (downstream) primers and PCR products were analysed on a 0.7% agarose gel. Candidate colonies are shown Lanes 2-18. The arrow indicates the ~1411bp PCR product expected. The plasmids pET28a (Lane 12) and pET21a-scy (Lane 13) were used as control templates. The DNA size marker is Lambda *Hind*III/*Eco*RI (Lane 1).

References

Abhayawardhane, Y., and Stewart, G.C. (1995) *Bacillus subtilis* possesses a second determinant with extensive sequence similarity to the *Escherichia coli mreB* morphogene. *J Bacteriol* 177: 765-773.

Adler, H.I., Fisher, W.D., Cohen, A., and Hardigree, A.A. (1967) Miniature *Escherichia coli* cells deficient in DNA. *Proc Natl Acad Sci U S A* 57: 321-326.

Ainsa, J.A., Bird, N., Ryding, N.J., Findlay, K.C., and Chater, K.F. (2010) The complex *whiJ* locus mediates environmentally sensitive repression of development of *Streptomyces coelicolor* A3(2). *Antonie Van Leeuwenhoek* 98: 225-236.

Ainsa, J.A., Parry, H.D., and Chater, K.F. (1999) A response regulator-like protein that functions at an intermediate stage of sporulation in *Streptomyces coelicolor* A3(2). *Mol Microbiol* 34: 607-619.

Ainsa, J.A., Ryding, N.J., Hartley, N., Findlay, K.C., Bruton, C.J., and Chater, K.F. (2000) WhiA, a protein of unknown function conserved among gram-positive bacteria, is essential for sporulation in *Streptomyces coelicolor* A3(2). *J Bacteriol* 182: 5470-5478.

Alam, M.S., Garg, S.K., and Agrawal, P. (2007) Molecular function of WhiB4/Rv3681c of *Mycobacterium tuberculosis* H37Rv: a [4Fe-4S] cluster co-ordinating protein disulphide reductase. *Mol Microbiol* 63: 1414-1431.

Allen, A.K., Neuberger, A., and Sharon, N. (1973) The purification, composition and specificity of wheat-germ agglutinin. *Biochem J* 131: 155-162.

Alyahya, S.A., Alexander, R., Costa, T., Henriques, A.O., Emonet, T., and Jacobs-Wagner, C. (2009) RodZ, a component of the bacterial core morphogenic apparatus. *Proc Natl Acad Sci U S A* 106: 1239-1244.

Anderson, A.S., and Wellington, E.M. (2001) The taxonomy of *Streptomyces* and related genera. *Int J Syst Evol Microbiol* 51: 797-814.

Arndt-Jovin, D.J., and Jovin, T.M. (1989) Fluorescence labeling and microscopy of DNA. *Methods Cell Biol* 30: 417-448.

Ausmees, N., Kuhn, J.R., and Jacobs-Wagner, C. (2003) The bacterial cytoskeleton: an intermediate filament-like function in cell shape. *Cell* 115: 705-713.

Aussel, L., Barre, F.X., Aroyo, M., Stasiak, A., Stasiak, A.Z., and Sherratt, D. (2002) FtsK Is a DNA motor protein that activates chromosome dimer resolution by switching the catalytic state of the XerC and XerD recombinases. *Cell* 108: 195-205.

Aylett, C.H., Wang, Q., Michie, K.A., Amos, L.A., and Löwe, J. (2010) Filament structure of bacterial tubulin homologue TubZ. *Proc Natl Acad Sci U S A* 107: 19766-19771.

Bagchi, S., Tomenius, H., Belova, L.M., and Ausmees, N. (2008) Intermediate filament-like proteins in bacteria and a cytoskeletal function in *Streptomyces*. *Mol Microbiol* 70: 1037-1050.

Baird, G.S., Zacharias, D.A., and Tsien, R.Y. (2000) Biochemistry, mutagenesis, and oligomerization of DsRed, a red fluorescent protein from coral. *Proc Natl Acad Sci U S A* 97: 11984-11989.

Ball Jr, A.R., and Yokomori, K. (2001) The structural maintenance of chromosomes (SMC) family of proteins in mammals. *Chromosome Res* 9: 85-96.

Ballestrem, C., Wehrle-Haller, B., and Imhof, B.A. (1998) Actin dynamics in living mammalian cells. *J Cell Sci* 111 (Pt 12): 1649-1658.

Barilla, D., Rosenberg, M.F., Nobbmann, U., and Hayes, F. (2005) Bacterial DNA segregation dynamics mediated by the polymerizing protein ParF. *EMBO J* 24: 1453-1464.

Bartolome, B., Jubete, Y., Martinez, E., and de la Cruz, F. (1991) Construction and properties of a family of pACYC184-derived cloning vectors compatible with pBR322 and its derivatives. *Gene* 102: 75-78.

Bath, J., Wu, L.J., Errington, J., and Wang, J.C. (2000) Role of *Bacillus subtilis* SpoIIIE in DNA transport across the mother cell-prespore division septum. *Science* 290: 995-997.

Beall, B., and Lutkenhaus, J. (1989) Nucleotide sequence and insertional inactivation of a *Bacillus subtilis* gene that affects cell division, sporulation, and temperature sensitivity. *J Bacteriol* 171: 6821-6834.

Beilharz, K., Novakova, L., Fadda, D., Branny, P., Massidda, O., and Veening, J.W. (2012) Control of cell division in *Streptococcus pneumoniae* by the conserved Ser/Thr protein kinase StkP. *Proc Natl Acad Sci U S A* 109: E905-913.

Ben-Yehuda, S., and Losick, R. (2002) Asymmetric cell division in *B. subtilis* involves a spiral-like intermediate of the cytokinetic protein FtsZ. *Cell* 109: 257-266.

Bendezu, F.O., Hale, C.A., Bernhardt, T.G., and de Boer, P.A. (2009) RodZ (YfgA) is required for proper assembly of the MreB actin cytoskeleton and cell shape in *E. coli*. *EMBO J* 28: 193-204.

Bentley, S.D., Chater, K.F., Cerdeno-Tarraga, A.M., Challis, G.L., Thomson, N.R., James, K.D., Harris, D.E., Quail, M.A., Kieser, H., Harper, D., Bateman, A., Brown, S., Chandra, G., Chen, C.W., Collins, M., Cronin, A., Fraser, A., Goble, A., Hidalgo, J., Hornsby, T., Howarth, S., Huang, C.H., Kieser, T., Larke, L., Murphy, L., Oliver, K., O'Neil, S., Rabbinowitsch, E., Rajandream, M.A., Rutherford, K., Rutter, S., Seeger, K., Saunders, D., Sharp, S., Squares, R., Squares, S., Taylor, K., Warren, T., Wietzorrek, A., Woodward, J., Barrell, B.G., Parkhill, J., and Hopwood, D.A. (2002) Complete genome sequence of the model actinomycete *Streptomyces coelicolor* A3(2). *Nature* 417: 141-147.

Bernhardt, T.G., and de Boer, P.A. (2003) The *Escherichia coli* amidase AmiC is a periplasmic septal ring component exported via the twin-arginine transport pathway. *Mol Microbiol* 48: 1171-1182.

Bi, E.F., and Lutkenhaus, J. (1991) FtsZ ring structure associated with division in *Escherichia coli*. *Nature* 354: 161-164.

Bibb, M.J. (2005) Regulation of secondary metabolism in streptomycetes. *Curr Opin Microbiol* 8: 208-215.

Bibb, M.J., Domonkos, A., Chandra, G., and Buttner, M.J. (2012) Expression of the chaplin and rodlin hydrophobic sheath proteins in *Streptomyces venezuelae* is controlled by sigma(BldN) and a cognate anti-sigma factor, RsbN. *Mol Microbiol* 84: 1033-1049.

Bibb, M.J., Molle, V., and Buttner, M.J. (2000) Sigma(BldN), an extracytoplasmic function RNA polymerase sigma factor required for aerial mycelium formation in *Streptomyces coelicolor* A3(2). *J Bacteriol* 182: 4606-4616.

Bignell, D.R., Warawa, J.L., Strap, J.L., Chater, K.F., and Leskiw, B.K. (2000) Study of the *bldG* locus suggests that an anti-anti-sigma factor and an anti-sigma factor may be involved in *Streptomyces coelicolor* antibiotic production and sporulation. *Microbiology* 146 (Pt 9): 2161-2173.

Blumberg, P.M., and Strominger, J.L. (1974) Interaction of penicillin with the bacterial cell: penicillin-binding proteins and penicillin-sensitive enzymes. *Bacteriol Rev* 38: 291-335.

Bork, P., Sander, C., and Valencia, A. (1992) An ATPase domain common to prokaryotic cell cycle proteins, sugar kinases, actin, and hsp70 heat shock proteins. *Proc Natl Acad Sci U S A* 89: 7290-7294.

Bowman, G.R., Comolli, L.R., Gaietta, G.M., Fero, M., Hong, S.H., Jones, Y., Lee, J.H., Downing, K.H., Ellisman, M.H., McAdams, H.H., and Shapiro, L. (2010) *Caulobacter* PopZ forms a polar subdomain dictating sequential changes in pole composition and function. *Mol Microbiol* 76: 173-189.

Bowman, G.R., Comolli, L.R., Zhu, J., Eckart, M., Koenig, M., Downing, K.H., Moerner, W.E., Earnest, T., and Shapiro, L. (2008) A polymeric protein anchors the chromosomal origin/ParB complex at a bacterial cell pole. *Cell* 134: 945-955.

Boylan, S.A., Redfield, A.R., Brody, M.S., and Price, C.W. (1993) Stress-induced activation of the sigma B transcription factor of *Bacillus subtilis*. *J Bacteriol* 175: 7931-7937.

Bramhill, D., and Thompson, C.M. (1994) GTP-dependent polymerization of *Escherichia coli* FtsZ protein to form tubules. *Proc Natl Acad Sci U S A* 91: 5813-5817.

Bramkamp, M., Emmins, R., Weston, L., Donovan, C., Daniel, R.A., and Errington, J. (2008) A novel component of the division-site selection system of Bacillus subtilis and a new mode of action for the division inhibitor MinCD. *Mol Microbiol* 70: 1556-1569.

Breier, A.M., and Grossman, A.D. (2007) Whole-genome analysis of the chromosome partitioning and sporulation protein Spo0J (ParB) reveals spreading and origin-distal sites on the *Bacillus subtilis* chromosome. *Mol Microbiol* 64: 703-718.

Brown, J.H., Zhou, Z., Reshetnikova, L., Robinson, H., Yammani, R.D., Tobacman, L.S., and Cohen, C. (2005) Structure of the mid-region of tropomyosin: bending and binding sites for actin. *Proc Natl Acad Sci U S A* 102: 18878-18883.

Brown, P.J., de Pedro, M.A., Kysela, D.T., Van der Henst, C., Kim, J., De Bolle, X., Fuqua, C., and Brun, Y.V. (2012) Polar growth in the Alphaproteobacterial order Rhizobiales. *Proc Natl Acad Sci U S A* 109: 1697-1701.

Brown, P.J., Kysela, D.T., and Brun, Y.V. (2011) Polarity and the diversity of growth mechanisms in bacteria. *Semin Cell Dev Biol* 22: 790-798.

Brymora, A., Valova, V.A., and Robinson, P.J. (2004) Protein-protein interactions identified by pull-down experiments and mass spectrometry. *Curr Protoc Cell Biol* Chapter 17: Unit 17 15.

Burger, A., Sichler, K., Kelemen, G., Buttner, M., and Wohlleben, W. (2000) Identification and characterization of the *mre* gene region of *Streptomyces coelicolor* A3(2). *Mol Gen Genet* 263: 1053-1060.

Cabeen, M.T., Charbon, G., Vollmer, W., Born, P., Ausmees, N., Weibel, D.B., and Jacobs-Wagner, C. (2009) Bacterial cell curvature through mechanical control of cell growth. *EMBO J* 28: 1208-1219.

Cabeen, M.T., and Jacobs-Wagner, C. (2005) Bacterial cell shape. *Nat Rev Microbiol* 3: 601-610.

Campbell, R.E., Tour, O., Palmer, A.E., Steinbach, P.A., Baird, G.S., Zacharias, D.A., and Tsien, R.Y. (2002) A monomeric red fluorescent protein. *Proc Natl Acad Sci U S A* 99: 7877-7882.

Cane, D.E., He, X., Kobayashi, S., Omura, S., and Ikeda, H. (2006) Geosmin biosynthesis in *Streptomyces avermitilis*. Molecular cloning, expression, and mechanistic study of the germacradienol/geosmin synthase. *J Antibiot (Tokyo)* 59: 471-479.

Capstick, D.S., Willey, J.M., Buttner, M.J., and Elliot, M.A. (2007) SapB and the chaplins: connections between morphogenetic proteins in *Streptomyces coelicolor*. *Mol Microbiol* 64: 602-613.

Carballido-Lopez, R. (2006a) The bacterial actin-like cytoskeleton. *Microbiol Mol Biol Rev* 70: 888-909.

Carballido-Lopez, R. (2006b) Orchestrating bacterial cell morphogenesis. *Mol Microbiol* 60: 815-819.

Carballido-Lopez, R., and Errington, J. (2003) A dynamic bacterial cytoskeleton. *Trends Cell Biol* 13: 577-583.

Cha, J.H., and Stewart, G.C. (1997) The *divIVA* minicell locus of *Bacillus subtilis*. *J Bacteriol* 179: 1671-1683.

Charbon, G., Brustad, E., Scott, K.A., Wang, J., Lobner-Olesen, A., Schultz, P.G., Jacobs-Wagner, C., and Chapman, E. (2011) Subcellular protein localization by using a genetically encoded fluorescent amino acid. *Chembiochem* 12: 1818-1821.

Charbon, G., Cabeen, M.T., and Jacobs-Wagner, C. (2009) Bacterial intermediate filaments: in vivo assembly, organization, and dynamics of crescentin. *Genes Dev* 23: 1131-1144.

Chater, K.F. (1972) A morphological and genetic mapping study of white colony mutants of *Streptomyces coelicolor*. *J Gen Microbiol* 72: 9-28.

Chater, K.F. (1975) Construction and phenotypes of double sporulation deficient mutants in *Streptomyces coelicolor* A3(2). *J Gen Microbiol* 87: 312-325.

Chater, K.F. (1993) Genetics of differentiation in *Streptomyces*. *Annu Rev Microbiol* 47: 685-713.

Chater, K.F. (2001) Regulation of sporulation in *Streptomyces coelicolor* A3(2): a checkpoint multiplex? *Curr Opin Microbiol* 4: 667-673.

Chater, K.F. (2006) *Streptomyces* inside-out: a new perspective on the bacteria that provide us with antibiotics. *Philos Trans R Soc Lond B Biol Sci* 361: 761-768.

Chater, K.F., Bruton, C.J., Plaskitt, K.A., Buttner, M.J., Mendez, C., and Helmann, J.D. (1989) The developmental fate of *S. coelicolor* hyphae depends upon a gene product homologous with the motility sigma factor of *B. subtilis*. *Cell* 59: 133-143.

Chater, K.F., and Chandra, G. (2006) The evolution of development in *Streptomyces* analysed by genome comparisons. *FEMS Microbiol Rev* 30: 651-672.

Chater, K.F., and Chandra, G. (2008) The use of the rare UUA codon to define "expression space" for genes involved in secondary metabolism, development and environmental adaptation in *Streptomyces*. *J Microbiol* 46: 1-11.

Chauhan, A., Lofton, H., Maloney, E., Moore, J., Fol, M., Madiraju, M.V., and Rajagopalan, M. (2006) Interference of *Mycobacterium tuberculosis* cell division by Rv2719c, a cell wall hydrolase. *Mol Microbiol* 62: 132-147.

Claessen, D., Emmins, R., Hamoen, L.W., Daniel, R.A., Errington, J., and Edwards, D.H. (2008) Control of the cell elongation-division cycle by shuttling of PBP1 protein in Bacillus subtilis. *Mol Microbiol* 68: 1029-1046.

Claessen, D., Rink, R., de Jong, W., Siebring, J., de Vreugd, P., Boersma, F.G., Dijkhuizen, L., and Wosten, H.A. (2003) A novel class of secreted hydrophobic proteins is involved in aerial hyphae formation in *Streptomyces coelicolor* by forming amyloid-like fibrils. *Genes Dev* 17: 1714-1726.

Claessen, D., Stokroos, I., Deelstra, H.J., Penninga, N.A., Bormann, C., Salas, J.A., Dijkhuizen, L., and Wosten, H.A. (2004) The formation of the rodlet layer of

streptomycetes is the result of the interplay between rodlins and chaplins. *Mol Microbiol* 53: 433-443.

Claessen, D., Wosten, H.A., van Keulen, G., Faber, O.G., Alves, A.M., Meijer, W.G., and Dijkhuizen, L. (2002) Two novel homologous proteins of *Streptomyces coelicolor* and *Streptomyces lividans* are involved in the formation of the rodlet layer and mediate attachment to a hydrophobic surface. *Mol Microbiol* 44: 1483-1492.

Crack, J.C., den Hengst, C.D., Jakimowicz, P., Subramanian, S., Johnson, M.K., Buttner, M.J., Thomson, A.J., and Le Brun, N.E. (2009) Characterization of [4Fe-4S]-containing and cluster-free forms of *Streptomyces* WhiD. *Biochemistry* 48: 12252-12264.

Cuylen, S., Metz, J., and Haering, C.H. (2011) Condensin structures chromosomal DNA through topological links. *Nat Struct Mol Biol* 18: 894-901.

Dajkovic, A., Lan, G., Sun, S.X., Wirtz, D., and Lutkenhaus, J. (2008) MinC spatially controls bacterial cytokinesis by antagonizing the scaffolding function of FtsZ. *Curr Biol* 18: 235-244.

Dalton, K.A., Thibessard, A., Hunter, J.I., and Kelemen, G.H. (2007) A novel compartment, the 'subapical stem' of the aerial hyphae, is the location of a sigN-dependent, developmentally distinct transcription in *Streptomyces coelicolor*. *Mol Microbiol* 64: 719-737.

Daniel, R.A., and Errington, J. (2003) Control of cell morphogenesis in bacteria: two distinct ways to make a rod-shaped cell. *Cell* 113: 767-776.

Danilova, O., Reyes-Lamothe, R., Pinskaya, M., Sherratt, D., and Possoz, C. (2007) MukB colocalizes with the *oriC* region and is required for organization of the two *Escherichia coli* chromosome arms into separate cell halves. *Mol Microbiol* 65: 1485-1492.

Datsenko, K.A., and Wanner, B.L. (2000) One-step inactivation of chromosomal genes in *Escherichia coli* K-12 using PCR products. *Proc Natl Acad Sci U S A* 97: 6640-6645.

Davis, M.A., Martin, K.A., and Austin, S.J. (1992) Biochemical activities of the ParA partition protein of the P1 plasmid. *Mol Microbiol* 6: 1141-1147.

Davis, N.K., and Chater, K.F. (1990) Spore colour in *Streptomyces coelicolor* A3(2) involves the developmentally regulated synthesis of a compound biosynthetically related to polyketide antibiotics. *Mol Microbiol* 4: 1679-1691.

Davis, N.K., and Chater, K.F. (1992) The *Streptomyces coelicolor whiB* gene encodes a small transcription factor-like protein dispensable for growth but essential for sporulation. *Mol Gen Genet* 232: 351-358.

De Pedro, M.A., Schwarz, H., and Koch, A.L. (2003) Patchiness of murein insertion into the sidewall of *Escherichia coli*. *Microbiology* 149: 1753-1761.

Dedrick, R.M., Wildschutte, H., and McCormick, J.R. (2009) Genetic interactions of *smc*, *ftsK*, and *parB* genes in *Streptomyces coelicolor* and their developmental genome segregation phenotypes. *J Bacteriol* 191: 320-332.

Deibler, M., Spatz, J.P., and Kemkemer, R. (2011) Actin fusion proteins alter the dynamics of mechanically induced cytoskeleton rearrangement. *PLoS One* 6: e22941.

den Hengst, C.D., and Buttner, M.J. (2008) Redox control in actinobacteria. *Biochim Biophys Acta* 1780: 1201-1216.

den Hengst, C.D., Tran, N.T., Bibb, M.J., Chandra, G., Leskiw, B.K., and Buttner, M.J. (2010) Genes essential for morphological development and antibiotic production in *Streptomyces coelicolor* are targets of BldD during vegetative growth. *Mol Microbiol* 78: 361-379.

Derman, A.I., Becker, E.C., Truong, B.D., Fujioka, A., Tucey, T.M., Erb, M.L., Patterson, P.C., and Pogliano, J. (2009) Phylogenetic analysis identifies many uncharacterized actin-like proteins (Alps) in bacteria: regulated polymerization, dynamic instability and treadmilling in Alp7A. *Mol Microbiol* 73: 534-552.

Desai, A., and Mitchison, T.J. (1997) Microtubule polymerization dynamics. *Annu Rev Cell Dev Biol* 13: 83-117.

Ditkowski, B., Troc, P., Ginda, K., Donczew, M., Chater, K.F., Zakrzewska-Czerwinska, J., and Jakimowicz, D. (2010) The actinobacterial signature protein ParJ (SCO1662) regulates ParA polymerization and affects chromosome segregation and cell division during *Streptomyces* sporulation. *Mol Microbiol* 78: 1403-1415.

Divakaruni, A.V., Baida, C., White, C.L., and Gober, J.W. (2007) The cell shape proteins MreB and MreC control cell morphogenesis by positioning cell wall synthetic complexes. *Mol Microbiol* 66: 174-188.

Doi, M., Wachi, M., Ishino, F., Tomioka, S., Ito, M., Sakagami, Y., Suzuki, A., and Matsuhashi, M. (1988) Determinations of the DNA sequence of the *mreB* gene and of the gene products of the *mre* region that function in formation of the rod shape of *Escherichia coli* cells. *J Bacteriol* 170: 4619-4624.

Dominguez-Escobar, J., Chastanet, A., Crevenna, A.H., Fromion, V., Wedlich-Soldner, R., and Carballido-Lopez, R. (2011) Processive movement of MreB-associated cell wall biosynthetic complexes in bacteria. *Science* 333: 225-228.

Donovan, C., Sieger, B., Kramer, R., and Bramkamp, M. (2012) A synthetic *Escherichia coli* system identifies a conserved origin tethering factor in Actinobacteria. *Mol Microbiol* 84: 105-116.

Duong, A., Capstick, D.S., Di Berardo, C., Findlay, K.C., Hesketh, A., Hong, H.J., and Elliot, M.A. (2012) Aerial development in *Streptomyces coelicolor* requires sortase activity. *Mol Microbiol* 83: 992-1005.

Dye, N.A., Pincus, Z., Theriot, J.A., Shapiro, L., and Gitai, Z. (2005) Two independent spiral structures control cell shape in *Caulobacter*. *Proc Natl Acad Sci U S A* 102: 18608-18613.

Ebersbach, G., Briegel, A., Jensen, G.J., and Jacobs-Wagner, C. (2008) A self-associating protein critical for chromosome attachment, division, and polar organization in *Caulobacter*. *Cell* 134: 956-968.

Ebersbach, G., and Gerdes, K. (2001) The double *par* locus of virulence factor pB171: DNA segregation is correlated with oscillation of ParA. *Proc Natl Acad Sci U S A* 98: 15078-15083.

Ebersbach, G., and Gerdes, K. (2004) Bacterial mitosis: partitioning protein ParA oscillates in spiral-shaped structures and positions plasmids at mid-cell. *Mol Microbiol* 52: 385-398.

Eccleston, M., Ali, R.A., Seyler, R., Westpheling, J., and Nodwell, J. (2002) Structural and genetic analysis of the BldB protein of *Streptomyces coelicolor*. *J Bacteriol* 184: 4270-4276.

Eccleston, M., Willems, A., Beveridge, A., and Nodwell, J.R. (2006) Critical residues and novel effects of overexpression of the *Streptomyces coelicolor* developmental protein BldB: evidence for a critical interacting partner. *J Bacteriol* 188: 8189-8195.

Edwards, D.H., and Errington, J. (1997) The *Bacillus subtilis* DivIVA protein targets to the division septum and controls the site specificity of cell division. *Mol Microbiol* 24: 905-915.

Edwards, D.H., Thomaides, H.B., and Errington, J. (2000) Promiscuous targeting of *Bacillus subtilis* cell division protein DivIVA to division sites in *Escherichia coli* and fission yeast. *EMBO J* 19: 2719-2727.

Elliot, M., Damji, F., Passantino, R., Chater, K., and Leskiw, B. (1998) The *bldD* gene of *Streptomyces coelicolor* A3(2): a regulatory gene involved in morphogenesis and antibiotic production. *J Bacteriol* 180: 1549-1555.

Elliot, M.A., Bibb, M.J., Buttner, M.J., and Leskiw, B.K. (2001) BldD is a direct regulator of key developmental genes in *Streptomyces coelicolor* A3(2). *Mol Microbiol* 40: 257-269.

Elliot, M.A., Karoonuthaisiri, N., Huang, J., Bibb, M.J., Cohen, S.N., Kao, C.M., and Buttner, M.J. (2003) The chaplins: a family of hydrophobic cell-surface proteins involved in aerial mycelium formation in *Streptomyces coelicolor*. *Genes Dev* 17: 1727-1740.

Erickson, H.P. (1997) FtsZ, a tubulin homologue in prokaryote cell division. *Trends Cell Biol* 7: 362-367.

Erickson, H.P. (1998) Atomic structures of tubulin and FtsZ. *Trends Cell Biol* 8: 133-137.

Erickson, H.P. (2000) Dynamin and FtsZ. Missing links in mitochondrial and bacterial division. *J Cell Biol* 148: 1103-1105.

Erickson, H.P., Taylor, D.W., Taylor, K.A., and Bramhill, D. (1996) Bacterial cell division protein FtsZ assembles into protofilament sheets and minirings, structural homologs of tubulin polymers. *Proc Natl Acad Sci U S A* 93: 519-523.

Errington, J. (2003) Dynamic proteins and a cytoskeleton in bacteria. ***Nat Cell Biol*** **5: 175-178.**

Errington, J., Daniel, R.A., and Scheffers, D.J. (2003) Cytokinesis in bacteria. ***Microbiol Mol Biol Rev*** **67: 52-65, table of contents.**

Fadda, D., Santona, A., D'Ulisse, V., Ghelardini, P., Ennas, M.G., Whalen, M.B., and Massidda, O. (2007) ***Streptococcus pneumoniae*** **DivIVA: localization and interactions in a MinCD-free context.** ***J Bacteriol*** **189: 1288-1298.**

Faguy, D.M., and Doolittle, W.F. (1998) Cytoskeletal proteins: the evolution of cell division. ***Curr Biol*** **8: R338-341.**

Feitelson, J.S., Malpartida, F., and Hopwood, D.A. (1985) Genetic and biochemical characterization of the ***red*** **gene cluster of** ***Streptomyces coelicolor*** **A3(2).** ***J Gen Microbiol*** **131: 2431-2441.**

Figge, R.M., Divakaruni, A.V., and Gober, J.W. (2004) MreB, the cell shape-determining bacterial actin homologue, co-ordinates cell wall morphogenesis in ***Caulobacter crescentus*****.** ***Mol Microbiol*** **51: 1321-1332.**

Figge, R.M., Easter, J., and Gober, J.W. (2003) Productive interaction between the chromosome partitioning proteins, ParA and ParB, is required for the progression of the cell cycle in ***Caulobacter crescentus*****.** ***Mol Microbiol*** **47: 1225-1237.**

Fiuza, M., Letek, M., Leiba, J., Villadangos, A.F., Vaquera, J., Zanella-Cleon, I., Mateos, L.M., Molle, V., and Gil, J.A. (2010) Phosphorylation of a novel cytoskeletal protein (RsmP) regulates rod-shaped morphology in ***Corynebacterium glutamicum*****.** ***J Biol Chem*** **285: 29387-29397.**

Flärdh, K. (2003a) Essential role of DivIVA in polar growth and morphogenesis in ***Streptomyces coelicolor*** **A3(2).** ***Mol Microbiol*** **49: 1523-1536.**

Flärdh, K. (2003b) Growth polarity and cell division in ***Streptomyces*****.** ***Curr Opin Microbiol*** **6: 564-571.**

Flärdh, K., and Buttner, M.J. (2009) ***Streptomyces*** **morphogenetics: dissecting differentiation in a filamentous bacterium.** ***Nat Rev Microbiol*** **7: 36-49.**

Flärdh, K., Findlay, K.C., and Chater, K.F. (1999) Association of early sporulation genes with suggested developmental decision points in ***Streptomyces coelicolor*** **A3(2).** ***Microbiology*** **145 (Pt 9): 2229-2243.**

Flärdh, K., Leibovitz, E., Buttner, M.J., and Chater, K.F. (2000) Generation of a non-sporulating strain of ***Streptomyces coelicolor*** **A3(2) by the manipulation of a developmentally controlled** ***ftsZ*** **promoter.** ***Mol Microbiol*** **38: 737-749.**

Fleurie, A., Cluzel, C., Guiral, S., Freton, C., Galisson, F., Zanella-Cleon, I., Di Guilmi, A.M., and Grangeasse, C. (2012) Mutational dissection of the S/T-kinase StkP reveals crucial roles in cell division of ***Streptococcus pneumoniae*****.** ***Mol Microbiol*** **83: 746-758.**

Galli, E., and Gerdes, K. (2012) FtsZ-ZapA-ZapB interactome of *Escherichia coli*. *J Bacteriol* 194: 292-302.

Garner, E.C., Bernard, R., Wang, W., Zhuang, X., Rudner, D.Z., and Mitchison, T. (2011) Coupled, circumferential motions of the cell wall synthesis machinery and MreB filaments in *B. subtilis*. *Science* 333: 222-225.

Garner, E.C., Campbell, C.S., and Mullins, R.D. (2004) Dynamic instability in a DNA-segregating prokaryotic actin homolog. *Science* 306: 1021-1025.

Garner, E.C., Campbell, C.S., Weibel, D.B., and Mullins, R.D. (2007) Reconstitution of DNA segregation driven by assembly of a prokaryotic actin homolog. *Science* 315: 1270-1274.

Gehring, A.M., Nodwell, J.R., Beverley, S.M., and Losick, R. (2000) Genomewide insertional mutagenesis in *Streptomyces coelicolor* reveals additional genes involved in morphological differentiation. *Proc Natl Acad Sci U S A* 97: 9642-9647.

Gerber, N.N., and Lechevalier, H.A. (1965) Geosmin, an earthly-smelling substance isolated from actinomycetes. *Appl Microbiol* 13: 935-938.

Giepmans, B.N., Adams, S.R., Ellisman, M.H., and Tsien, R.Y. (2006) The fluorescent toolbox for assessing protein location and function. *Science* 312: 217-224.

Gitai, Z., Dye, N., and Shapiro, L. (2004) An actin-like gene can determine cell polarity in bacteria. *Proc Natl Acad Sci U S A* 101: 8643-8648.

Goodson, H.V., and Hawse, W.F. (2002) Molecular evolution of the actin family. *J Cell Sci* 115: 2619-2622.

Grantcharova, N., Lustig, U., and Flardh, K. (2005) Dynamics of FtsZ assembly during sporulation in *Streptomyces coelicolor* A3(2). *J Bacteriol* 187: 3227-3237.

Grantcharova, N., Ubhayasekera, W., Mowbray, S.L., McCormick, J.R., and Flardh, K. (2003) A missense mutation in *ftsZ* differentially affects vegetative and developmentally controlled cell division in *Streptomyces coelicolor* A3(2). *Mol Microbiol* 47: 645-656.

Graumann, P.L., Losick, R., and Strunnikov, A.V. (1998) Subcellular localization of *Bacillus subtilis* SMC, a protein involved in chromosome condensation and segregation. *J Bacteriol* 180: 5749-5755.

Gregory, M.A., Till, R., and Smith, M.C. (2003) Integration site for *Streptomyces* phage phiBT1 and development of site-specific integrating vectors. *J Bacteriol* 185: 5320-5323.

Gross, L.A., Baird, G.S., Hoffman, R.C., Baldridge, K.K., and Tsien, R.Y. (2000) The structure of the chromophore within DsRed, a red fluorescent protein from coral. *Proc Natl Acad Sci U S A* 97: 11990-11995.

Gruber, S., and Errington, J. (2009) Recruitment of condensin to replication origin regions by ParB/SpoOJ promotes chromosome segregation in *B. subtilis*. *Cell* 137: 685-696.

Gueiros-Filho, F.J., and Losick, R. (2002) A widely conserved bacterial cell division protein that promotes assembly of the tubulin-like protein FtsZ. *Genes Dev* 16: 2544-2556.

Gust, B., Challis, G.L., Fowler, K., Kieser, T., and Chater, K.F. (2003) PCR-targeted *Streptomyces* gene replacement identifies a protein domain needed for biosynthesis of the sesquiterpene soil odor geosmin. *Proc Natl Acad Sci U S A* 100: 1541-1546.

Gust, B., Kieser T, and K, C. (2002) PCR-targeting system in *Streptomyces coelicolor*. In.: John Innes Centre, pp.

Guzman, L.M., Barondess, J.J., and Beckwith, J. (1992) FtsL, an essential cytoplasmic membrane protein involved in cell division in *Escherichia coli*. *J Bacteriol* 174: 7716-7728.

Hale, C.A., Meinhardt, H., and de Boer, P.A. (2001) Dynamic localization cycle of the cell division regulator MinE in *Escherichia coli*. *EMBO J* 20: 1563-1572.

Hale, C.A., Rhee, A.C., and de Boer, P.A. (2000) ZipA-induced bundling of FtsZ polymers mediated by an interaction between C-terminal domains. *J Bacteriol* 182: 5153-5166.

Hale, C.A., Shiomi, D., Liu, B., Bernhardt, T.G., Margolin, W., Niki, H., and de Boer, P.A. (2011) Identification of *Escherichia coli* ZapC (YcbW) as a component of the division apparatus that binds and bundles FtsZ polymers. *J Bacteriol* 193: 1393-1404.

Hamoen, L.W., Meile, J.C., de Jong, W., Noirot, P., and Errington, J. (2006) SepF, a novel FtsZ-interacting protein required for a late step in cell division. *Mol Microbiol* 59: 989-999.

Hanahan, D. (1983) Studies on transformation of *Escherichia coli* with plasmids. *J Mol Biol* 166: 557-580.

Harris, S.D. (2008) Branching of fungal hyphae: regulation, mechanisms and comparison with other branching systems. *Mycologia* 100: 823-832.

Harry, E.J. (2001) Bacterial cell division: regulating Z-ring formation. *Mol Microbiol* 40: 795-803.

Hayama, R., and Marians, K.J. (2010) Physical and functional interaction between the condensin MukB and the decatenase topoisomerase IV in *Escherichia coli*. *Proc Natl Acad Sci U S A* 107: 18826-18831.

Heichlinger, A., Ammelburg, M., Kleinschnitz, E.M., Latus, A., Maldener, I., Flardh, K., Wohlleben, W., and Muth, G. (2011) The MreB-like protein Mbl of *Streptomyces coelicolor* A3(2) depends on MreB for proper localization and contributes to spore wall synthesis. *J Bacteriol* 193: 1533-1542.

Heidrich, C., Templin, M.F., Ursinus, A., Merdanovic, M., Berger, J., Schwarz, H., de Pedro, M.A., and Holtje, J.V. (2001) Involvement of N-acetylmuramyl-L-alanine amidases in cell separation and antibiotic-induced autolysis of *Escherichia coli*. *Mol Microbiol* 41: 167-178.

Hempel, A.M., Cantlay, S., Molle, V., Wang, S.B., Naldrett, M.J., Parker, J.L., Richards, D.M., Jung, Y.G., Buttner, M.J., and Flardh, K. (2012) The Ser/Thr protein kinase AfsK regulates polar growth and hyphal branching in the filamentous bacteria *Streptomyces*. *Proc Natl Acad Sci U S A* 109: E2371-2379.

Hempel, A.M., Wang, S.B., Letek, M., Gil, J.A., and Flardh, K. (2008) Assemblies of DivIVA mark sites for hyphal branching and can establish new zones of cell wall growth in *Streptomyces coelicolor*. *J Bacteriol* 190: 7579-7583.

Hesketh, A., Bucca, G., Laing, E., Flett, F., Hotchkiss, G., Smith, C.P., and Chater, K.F. (2007) New pleiotropic effects of eliminating a rare tRNA from *Streptomyces coelicolor*, revealed by combined proteomic and transcriptomic analysis of liquid cultures. *BMC Genomics* 8: 261.

Hesketh, A.R., Chandra, G., Shaw, A.D., Rowland, J.J., Kell, D.B., Bibb, M.J., and Chater, K.F. (2002) Primary and secondary metabolism, and post-translational protein modifications, as portrayed by proteomic analysis of *Streptomyces coelicolor*. *Mol Microbiol* 46: 917-932.

Hirano, M., and Hirano, T. (1998) ATP-dependent aggregation of single-stranded DNA by a bacterial SMC homodimer. *EMBO J* 17: 7139-7148.

Hirano, S., Kato, J.Y., Ohnishi, Y., and Horinouchi, S. (2006) Control of the *Streptomyces* Subtilisin inhibitor gene by AdpA in the A-factor regulatory cascade in *Streptomyces griseus*. *J Bacteriol* 188: 6207-6216.

Hirsch, P. (1974) Budding bacteria. *Annu Rev Microbiol* 28: 391-444.

Hobbs, G., Frazer, C.M., Gardner, D.C.J., Cullum, J.A., and Oliver, S.G. (1989) Dispersed growth of *Streptomyces* in liquid culture. *Applied Microbiology and Biotechnology* 31: 272-277.

Holmes, N.A., Walshaw, J., Leggett, R.M., Thibessard, A., Dalton, K.A., Gillespie, M.D., Hemmings, A.M., Gust, B., and Kelemen, G.H. (2013) Coiled-coil protein Scy is a key component of a multiprotein assembly controlling polarized growth in *Streptomyces*. *Proc Natl Acad Sci U S A* 110: E397-406.

Hopwood, D.A., Bibb, M., Chater, K., T, K., Bruton, C.J., Kieser, H., Lydiate, D.J., Smith, C.P., Ward, J.M., and Schrempf, H. (1985) *Genetic Manipulation of Streptomyces. A Laboratory Manual*. John Innes Foundation, Norwich.

Hopwood, D.A., and Glauert, A.M. (1961) Electron microscope observations on the surface structures of *Streptomyces violaceoruber*. *J Gen Microbiol* 26: 325-330.

Huang, J., Shi, J., Molle, V., Sohlberg, B., Weaver, D., Bibb, M.J., Karoonuthaisiri, N., Lih, C.J., Kao, C.M., Buttner, M.J., and Cohen, S.N. (2005) Cross-regulation among disparate antibiotic biosynthetic pathways of *Streptomyces coelicolor*. *Mol Microbiol* 58: 1276-1287.

Huang, K.C., Mukhopadhyay, R., and Wingreen, N.S. (2006) A curvature-mediated mechanism for localization of lipids to bacterial poles. *PLoS Comput Biol* 2: e151.

Hunt, A.C., Servin-Gonzalez, L., Kelemen, G.H., and Buttner, M.J. (2005) The *bldC* developmental locus of *Streptomyces coelicolor* encodes a member of a family of small DNA-binding proteins related to the DNA-binding domains of the MerR family. *J Bacteriol* 187: 716-728.

Ingerson-Mahar, M., Briegel, A., Werner, J.N., Jensen, G.J., and Gitai, Z. (2010) The metabolic enzyme CTP synthase forms cytoskeletal filaments. *Nat Cell Biol* 12: 739-746.

Ingerson-Mahar, M., and Gitai, Z. (2012) A growing family: the expanding universe of the bacterial cytoskeleton. *FEMS Microbiol Rev* 36: 256-266.

Ish-Horowicz, D., and Burke, J.F. (1981) Rapid and efficient cosmid cloning. *Nucleic Acids Res* 9: 2989-2998.

Jakimowicz, D., Chater, K., and Zakrzewska-Czerwinska, J. (2002) The ParB protein of *Streptomyces coelicolor* A3(2) recognizes a cluster of *parS* sequences within the origin-proximal region of the linear chromosome. *Mol Microbiol* 45: 1365-1377.

Jakimowicz, D., Gust, B., Zakrzewska-Czerwinska, J., and Chater, K.F. (2005a) Developmental-stage-specific assembly of ParB complexes in *Streptomyces coelicolor* hyphae. *J Bacteriol* 187: 3572-3580.

Jakimowicz, D., Mouz, S., Zakrzewska-Czerwinska, J., and Chater, K.F. (2006) Developmental control of a *parAB* promoter leads to formation of sporulation-associated ParB complexes in *Streptomyces coelicolor*. *J Bacteriol* 188: 1710-1720.

Jakimowicz, D., and van Wezel, G.P. (2012) Cell division and DNA segregation in *Streptomyces*: how to build a septum in the middle of nowhere? *Mol Microbiol* 85: 393-404.

Jakimowicz, D., Zydek, P., Kois, A., Zakrzewska-Czerwinska, J., and Chater, K.F. (2007) Alignment of multiple chromosomes along helical ParA scaffolding in sporulating *Streptomyces* hyphae. *Mol Microbiol* 65: 625-641.

Jakimowicz, P., Cheesman, M.R., Bishai, W.R., Chater, K.F., Thomson, A.J., and Buttner, M.J. (2005b) Evidence that the *Streptomyces* developmental protein WhiD, a member of the WhiB family, binds a [4Fe-4S] cluster. *J Biol Chem* 280: 8309-8315.

Jensen, R.B., and Gerdes, K. (1997) Partitioning of plasmid R1. The ParM protein exhibits ATPase activity and interacts with the centromere-like ParR-*parC* complex. *J Mol Biol* 269: 505-513.

Jensen, R.B., and Gerdes, K. (1999) Mechanism of DNA segregation in prokaryotes: ParM partitioning protein of plasmid R1 co-localizes with its replicon during the cell cycle. *EMBO J* 18: 4076-4084.

Jensen, R.B., and Shapiro, L. (1999) The *Caulobacter crescentus smc* gene is required for cell cycle progression and chromosome segregation. *Proc Natl Acad Sci U S A* 96: 10661-10666.

Jerabek-Willemsen, M., Wienken, C.J., Braun, D., Baaske, P., and Duhr, S. (2011) Molecular interaction studies using microscale thermophoresis. *Assay Drug Dev Technol* 9: 342-353.

Jimenez, M., Martos, A., Vicente, M., and Rivas, G. (2011) Reconstitution and organization of *Escherichia coli* proto-ring elements (FtsZ and FtsA) inside giant unilamellar vesicles obtained from bacterial inner membranes. *J Biol Chem* 286: 11236-11241.

Jones, L.J., Carballido-Lopez, R., and Errington, J. (2001) Control of cell shape in bacteria: helical, actin-like filaments in *Bacillus subtilis*. *Cell* 104: 913-922.

Jyothikumar, V., Klanbut, K., Tiong, J., Roxburgh, J.S., Hunter, I.S., Smith, T.K., and Herron, P.R. (2012) Cardiolipin synthase is required for *Streptomyces coelicolor* morphogenesis. *Mol Microbiol* 84: 181-197.

Jyothikumar, V., Tilley, E.J., Wali, R., and Herron, P.R. (2008) Time-lapse microscopy of *Streptomyces coelicolor* growth and sporulation. *Appl Environ Microbiol* 74: 6774-6781.

Kaiser, B.K., Clifton, M.C., Shen, B.W., and Stoddard, B.L. (2009) The structure of a bacterial DUF199/WhiA protein: domestication of an invasive endonuclease. *Structure* 17: 1368-1376.

Kaiser, B.K., and Stoddard, B.L. (2011) DNA recognition and transcriptional regulation by the WhiA sporulation factor. *Sci Rep* 1: 156.

Kang, C.M., Abbott, D.W., Park, S.T., Dascher, C.C., Cantley, L.C., and Husson, R.N. (2005) The *Mycobacterium tuberculosis* serine/threonine kinases PknA and PknB: substrate identification and regulation of cell shape. *Genes Dev* 19: 1692-1704.

Kang, C.M., Nyayapathy, S., Lee, J.Y., Suh, J.W., and Husson, R.N. (2008) Wag31, a homologue of the cell division protein DivIVA, regulates growth, morphology and polar cell wall synthesis in mycobacteria. *Microbiology* 154: 725-735.

Karimova, G., Pidoux, J., Ullmann, A., and Ladant, D. (1998) A bacterial two-hybrid system based on a reconstituted signal transduction pathway. *Proc Natl Acad Sci U S A* 95: 5752-5756.

Karimova, G., Ullmann, A., and Ladant, D. (2000) A bacterial two-hybrid system that exploits a cAMP signaling cascade in *Escherichia coli*. *Methods Enzymol* 328: 59-73.

Kato, J.Y., Chi, W.J., Ohnishi, Y., Hong, S.K., and Horinouchi, S. (2005) Transcriptional control by A-factor of two trypsin genes in *Streptomyces griseus*. *J Bacteriol* 187: 286-295.

Kato, J.Y., Suzuki, A., Yamazaki, H., Ohnishi, Y., and Horinouchi, S. (2002) Control by A-factor of a metalloendopeptidase gene involved in aerial mycelium formation in *Streptomyces griseus*. *J Bacteriol* 184: 6016-6025.

Kawai, F., Shoda, M., Harashima, R., Sadaie, Y., Hara, H., and Matsumoto, K. (2004) Cardiolipin domains in *Bacillus subtilis* marburg membranes. *J Bacteriol* 186: 1475-1483.

Kawamoto, S., Watanabe, H., Hesketh, A., Ensign, J.C., and Ochi, K. (1997) Expression analysis of the *ssgA* gene product, associated with sporulation and cell division in *Streptomyces griseus*. *Microbiology* 143 (Pt 4): 1077-1086.

Keijser, B.J., Noens, E.E., Kraal, B., Koerten, H.K., and van Wezel, G.P. (2003) The *Streptomyces coelicolor ssgB* gene is required for early stages of sporulation. *FEMS Microbiol Lett* 225: 59-67.

Keijser, B.J., van Wezel, G.P., Canters, G.W., Kieser, T., and Vijgenboom, E. (2000) The ram-dependence of *Streptomyces lividans* differentiation is bypassed by copper. *J Mol Microbiol Biotechnol* 2: 565-574.

Kelemen, G.H., Brian, P., Flardh, K., Chamberlin, L., Chater, K.F., and Buttner, M.J. (1998) Developmental regulation of transcription of *whiE*, a locus specifying the polyketide spore pigment in *Streptomyces coelicolor* A3 (2). *J Bacteriol* 180: 2515-2521.

Kelemen, G.H., Brown, G.L., Kormanec, J., Potuckova, L., Chater, K.F., and Buttner, M.J. (1996) The positions of the sigma-factor genes, *whiG* and *sigF*, in the hierarchy controlling the development of spore chains in the aerial hyphae of *Streptomyces coelicolor* A3(2). *Mol Microbiol* 21: 593-603.

Kelemen, G.H., and Buttner, M.J. (1998) Initiation of aerial mycelium formation in *Streptomyces*. *Curr Opin Microbiol* 1: 656-662.

Kelemen, G.H., Viollier, P.H., Tenor, J., Marri, L., Buttner, M.J., and Thompson, C.J. (2001) A connection between stress and development in the multicellular prokaryote *Streptomyces coelicolor* A3(2). *Mol Microbiol* 40: 804-814.

Kiekebusch, D., Michie, K.A., Essen, L.O., Löwe, J., and Thanbichler, M. (2012) Localized dimerization and nucleoid binding drive gradient formation by the bacterial cell division inhibitor MipZ. *Mol Cell* 46: 245-259.

Kieser, T., Bibb, M., Buttner, M., Chater, K., and Hopwood, D.A. (2000) *Practical Streptomyces Genetics*. The John Innes Foundation.

Kim, D.W., Chater, K., Lee, K.J., and Hesketh, A. (2005) Changes in the extracellular proteome caused by the absence of the *bldA* gene product, a developmentally significant tRNA, reveal a new target for the pleiotropic regulator AdpA in *Streptomyces coelicolor*. *J Bacteriol* 187: 2957-2966.

Kim, H.J., Calcutt, M.J., Schmidt, F.J., and Chater, K.F. (2000) Partitioning of the linear chromosome during sporulation of *Streptomyces coelicolor* A3(2) involves an *oriC*-linked *parAB* locus. *J Bacteriol* 182: 1313-1320.

Kleinschnitz, E.M., Heichlinger, A., Schirner, K., Winkler, J., Latus, A., Maldener, I., Wohlleben, W., and Muth, G. (2011) Proteins encoded by the *mre* gene cluster in *Streptomyces coelicolor* A3(2) cooperate in spore wall synthesis. *Mol Microbiol* 79: 1367-1379.

Koch, A.L. (2000) The bacterium's way for safe enlargement and division. *Appl Environ Microbiol* 66: 3657-3663.

Kodani, S., Hudson, M.E., Durrant, M.C., Buttner, M.J., Nodwell, J.R., and Willey, J.M. (2004) The SapB morphogen is a lantibiotic-like peptide derived from the product of the developmental gene *ramS* in *Streptomyces coelicolor*. *Proc Natl Acad Sci U S A* 101: 11448-11453.

Kois, A., Swiatek, M., Jakimowicz, D., and Zakrzewska-Czerwinska, J. (2009) SMC-protein-dependent chromosome condensation during aerial hyphal development in *Streptomyces*. *J Bacteriol*.

Komeili, A., Li, Z., Newman, D.K., and Jensen, G.J. (2006) Magnetosomes are cell membrane invaginations organized by the actin-like protein MamK. *Science* 311: 242-245.

Koonin, E.V. (1993) A superfamily of ATPases with diverse functions containing either classical or deviant ATP-binding motif. *J Mol Biol* 229: 1165-1174.

Kormanec, J., and Sevcikova, B. (2002) The stress-response sigma factor sigma(H) controls the expression of *ssgB*, a homologue of the sporulation-specific cell division gene *ssgA*, in *Streptomyces coelicolor* A3(2). *Mol Genet Genomics* 267: 536-543.

Korn, E.D., Carlier, M.F., and Pantaloni, D. (1987) Actin polymerization and ATP hydrolysis. *Science* 238: 638-644.

Kruse, T., Bork-Jensen, J., and Gerdes, K. (2005) The morphogenetic MreBCD proteins of *Escherichia coli* form an essential membrane-bound complex. *Mol Microbiol* 55: 78-89.

Kruse, T., Moller-Jensen, J., Lobner-Olesen, A., and Gerdes, K. (2003) Dysfunctional MreB inhibits chromosome segregation in *Escherichia coli*. *EMBO J* 22: 5283-5292.

Lam, H., Schofield, W.B., and Jacobs-Wagner, C. (2006) A landmark protein essential for establishing and perpetuating the polarity of a bacterial cell. *Cell* 124: 1011-1023.

Larsen, R.A., Cusumano, C., Fujioka, A., Lim-Fong, G., Patterson, P., and Pogliano, J. (2007) Treadmilling of a prokaryotic tubulin-like protein, TubZ, required for plasmid stability in *Bacillus thuringiensis*. *Genes Dev* 21: 1340-1352.

Lawler, M.L., Larson, D.E., Hinz, A.J., Klein, D., and Brun, Y.V. (2006) Dissection of functional domains of the polar localization factor PodJ in *Caulobacter crescentus*. *Mol Microbiol* 59: 301-316.

Lawlor, E.J., Baylis, H.A., and Chater, K.F. (1987) Pleiotropic morphological and antibiotic deficiencies result from mutations in a gene encoding a tRNA-like product in *Streptomyces coelicolor* A3(2). *Genes Dev* 1: 1305-1310.

Leaver, M., and Errington, J. (2005) Roles for MreC and MreD proteins in helical growth of the cylindrical cell wall in *Bacillus subtilis*. *Mol Microbiol* 57: 1196-1209.

Lederberg, J. (1956) Bacterial Protoplasts Induced by Penicillin. *Proc Natl Acad Sci U S A* 42: 574-577.

Lee, P.S., and Grossman, A.D. (2006) The chromosome partitioning proteins Soj (ParA) and Spo0J (ParB) contribute to accurate chromosome partitioning, separation of replicated sister origins, and regulation of replication initiation in *Bacillus subtilis*. *Mol Microbiol* 60: 853-869.

Lee, S., and Price, C.W. (1993) The *minCD* locus of *Bacillus subtilis* lacks the *minE* determinant that provides topological specificity to cell division. *Mol Microbiol* 7: 601-610.

Lenarcic, R., Halbedel, S., Visser, L., Shaw, M., Wu, L.J., Errington, J., Marenduzzo, D., and Hamoen, L.W. (2009) Localisation of DivIVA by targeting to negatively curved membranes. *EMBO J* 28: 2272-2282.

Leonard, T.A., Butler, P.J., and Löwe, J. (2005) Bacterial chromosome segregation: structure and DNA binding of the Soj dimer--a conserved biological switch. *EMBO J* 24: 270-282.

Leskiw, B.K., Mah, R., Lawlor, E.J., and Chater, K.F. (1993) Accumulation of *bldA*-specified tRNA is temporally regulated in *Streptomyces coelicolor* A3(2). *J Bacteriol* 175: 1995-2005.

Letek, M., Fiuza, M., Ordonez, E., Villadangos, A.F., Flardh, K., Mateos, L.M., and Gil, J.A. (2009) DivIVA uses an N-terminal conserved region and two coiled-coil domains to localize and sustain the polar growth in *Corynebacterium glutamicum*. *FEMS Microbiol Lett* 297: 110-116.

Letek, M., Ordonez, E., Vaquera, J., Margolin, W., Flardh, K., Mateos, L.M., and Gil, J.A. (2008) DivIVA is required for polar growth in the MreB-lacking rod-shaped actinomycete *Corynebacterium glutamicum*. *J Bacteriol* 190: 3283-3292.

Levin, P.A., Kurtser, I.G., and Grossman, A.D. (1999) Identification and characterization of a negative regulator of FtsZ ring formation in *Bacillus subtilis*. *Proc Natl Acad Sci U S A* 96: 9642-9647.

Levin, P.A., and Losick, R. (1994) Characterization of a cell division gene from *Bacillus subtilis* that is required for vegetative and sporulation septum formation. *J Bacteriol* 176: 1451-1459.

Levin, P.A., Margolis, P.S., Setlow, P., Losick, R., and Sun, D. (1992) Identification of *Bacillus subtilis* genes for septum placement and shape determination. *J Bacteriol* 174: 6717-6728.

Li, W., Wu, J., Tao, W., Zhao, C., Wang, Y., He, X., Chandra, G., Zhou, X., Deng, Z., Chater, K.F., and Tao, M. (2007a) A genetic and bioinformatic analysis of *Streptomyces coelicolor* genes containing TTA codons, possible targets for regulation by a developmentally significant tRNA. *FEMS Microbiol Lett* 266: 20-28.

Li, Y., Stewart, N.K., Berger, A.J., Vos, S., Schoeffler, A.J., Berger, J.M., Chait, B.T., and Oakley, M.G. (2010) *Escherichia coli* condensin MukB stimulates topoisomerase IV activity by a direct physical interaction. *Proc Natl Acad Sci U S A* 107: 18832-18837.

Li, Z., Trimble, M.J., Brun, Y.V., and Jensen, G.J. (2007b) The structure of FtsZ filaments in vivo suggests a force-generating role in cell division. ***EMBO J*** **26: 4694-4708.**

Lin, D.C., and Grossman, A.D. (1998) Identification and characterization of a bacterial chromosome partitioning site. ***Cell*** **92: 675-685.**

Lindow, J.C., Britton, R.A., and Grossman, A.D. (2002a) Structural maintenance of chromosomes protein of ***Bacillus subtilis*** **affects supercoiling** ***in vivo*****.** ***J Bacteriol*** **184: 5317-5322.**

Lindow, J.C., Kuwano, M., Moriya, S., and Grossman, A.D. (2002b) Subcellular localization of the ***Bacillus subtilis*** **structural maintenance of chromosomes (SMC) protein.** ***Mol Microbiol*** **46: 997-1009.**

Liu, Z., Mukherjee, A., and Lutkenhaus, J. (1999) Recruitment of ZipA to the division site by interaction with FtsZ. ***Mol Microbiol*** **31: 1853-1861.**

Low, H.H., Moncrieffe, M.C., and Löwe, J. (2004) The crystal structure of ZapA and its modulation of FtsZ polymerisation. ***J Mol Biol*** **341: 839-852.**

Lutkenhaus, J. (1993) FtsZ ring in bacterial cytokinesis. ***Mol Microbiol*** **9: 403-409.**

Lutkenhaus, J., and Addinall, S.G. (1997) Bacterial cell division and the Z ring. ***Annu Rev Biochem*** **66: 93-116.**

Ma, H., and Kendall, K. (1994) Cloning and analysis of a gene cluster from ***Streptomyces coelicolor*** **that causes accelerated aerial mycelium formation in** ***Streptomyces lividans*****.** ***J Bacteriol*** **176: 3800-3811.**

Mackay, J.P., Sunde, M., Lowry, J.A., Crossley, M., and Matthews, J.M. (2007) Protein interactions: is seeing believing? ***Trends Biochem Sci*** **32: 530-531.**

MacNeil, D.J., Gewain, K.M., Ruby, C.L., Dezeny, G., Gibbons, P.H., and MacNeil, T. (1992) Analysis of ***Streptomyces avermitilis*** **genes required for avermectin biosynthesis utilizing a novel integration vector.** ***Gene*** **111: 61-68.**

Makarova, K.S., and Koonin, E.V. (2010) Two new families of the FtsZ-tubulin protein superfamily implicated in membrane remodeling in diverse bacteria and archaea. ***Biol Direct*** **5: 33.**

Mandic-Mulec, I., Doukhan, L., and Smith, I. (1995) The ***Bacillus subtilis*** **SinR protein is a repressor of the key sporulation gene** ***spo0A*****.** ***J Bacteriol*** **177: 4619-4627.**

Manteca, A., Ye, J., Sanchez, J., and Jensen, O.N. (2011) Phosphoproteome analysis of ***Streptomyces*** **development reveals extensive protein phosphorylation accompanying bacterial differentiation.** ***J Proteome Res*** **10: 5481-5492.**

Margolin, W. (2000) Themes and variations in prokaryotic cell division. ***FEMS Microbiol Rev*** **24: 531-548.**

Margolin, W. (2001) Spatial regulation of cytokinesis in bacteria. ***Curr Opin Microbiol*** **4: 647-652.**

Margolin, W. (2003) Bacterial shape: growing off this mortal coil. *Curr Biol* 13: R705-707.

Margolis, P.S., Driks, A., and Losick, R. (1993) Sporulation gene *spoIIB* from *Bacillus subtilis*. *J Bacteriol* 175: 528-540.

Mariscal, V., Herrero, A., Nenninger, A., Mullineaux, C.W., and Flores, E. (2011) Functional dissection of the three-domain SepJ protein joining the cells in cyanobacterial trichomes. *Mol Microbiol* 79: 1077-1088.

Mason, J.M., and Arndt, K.M. (2004) Coiled coil domains: stability, specificity, and biological implications. *Chembiochem* 5: 170-176.

Matsushima, P., Broughton, M.C., Turner, J.R., and Baltz, R.H. (1994) Conjugal transfer of cosmid DNA from *Escherichia coli* to *Saccharopolyspora spinosa*: effects of chromosomal insertions on macrolide A83543 production. *Gene* 146: 39-45.

Mattei, P.J., Neves, D., and Dessen, A. (2010) Bridging cell wall biosynthesis and bacterial morphogenesis. *Curr Opin Struct Biol* 20: 749-755.

Matz, M.V., Fradkov, A.F., Labas, Y.A., Savitsky, A.P., Zaraisky, A.G., Markelov, M.L., and Lukyanov, S.A. (1999) Fluorescent proteins from nonbioluminescent Anthozoa species. *Nat Biotechnol* 17: 969-973.

Mazza, P., Noens, E.E., Schirner, K., Grantcharova, N., Mommaas, A.M., Koerten, H.K., Muth, G., Flardh, K., van Wezel, G.P., and Wohlleben, W. (2006) MreB of *Streptomyces coelicolor* is not essential for vegetative growth but is required for the integrity of aerial hyphae and spores. *Mol Microbiol* 60: 838-852.

McCormick, J.R., Su, E.P., Driks, A., and Losick, R. (1994) Growth and viability of *Streptomyces coelicolor* mutant for the cell division gene *ftsZ*. *Mol Microbiol* 14: 243-254.

McVittie, A. (1974) Ultrastructural studies on sporulation in wild-type and white colony mutants of *Streptomyces coelicolor*. *J Gen Microbiol* 81: 291-302.

Melby, T.E., Ciampaglio, C.N., Briscoe, G., and Erickson, H.P. (1998) The symmetrical structure of structural maintenance of chromosomes (SMC) and MukB proteins: long, antiparallel coiled coils, folded at a flexible hinge. *J Cell Biol* 142: 1595-1604.

Merrick, M.J. (1976) A morphological and genetic mapping study of bald colony mutants of *Streptomyces coelicolor*. *J Gen Microbiol* 96: 299-315.

Michie, K.A., and Löwe, J. (2006) Dynamic filaments of the bacterial cytoskeleton. *Annu Rev Biochem* 75: 467-492.

Michie, K.A., Monahan, L.G., Beech, P.L., and Harry, E.J. (2006) Trapping of a spiral-like intermediate of the bacterial cytokinetic protein FtsZ. *J Bacteriol* 188: 1680-1690.

Mileykovskaya, E., and Dowhan, W. (2000) Visualization of phospholipid domains in *Escherichia coli* by using the cardiolipin-specific fluorescent dye 10-N-nonyl acridine orange. *J Bacteriol* 182: 1172-1175.

Mohammadi, T., van Dam, V., Sijbrandi, R., Vernet, T., Zapun, A., Bouhss, A., Diepeveen-de Bruin, M., Nguyen-Disteche, M., de Kruijff, B., and Breukink, E. (2011) Identification of FtsW as a transporter of lipid-linked cell wall precursors across the membrane. *EMBO J* 30: 1425-1432.

Molle, V., and Buttner, M.J. (2000) Different alleles of the response regulator gene *bldM* arrest *Streptomyces coelicolor* development at distinct stages. *Mol Microbiol* 36: 1265-1278.

Molle, V., Palframan, W.J., Findlay, K.C., and Buttner, M.J. (2000) WhiD and WhiB, homologous proteins required for different stages of sporulation in *Streptomyces coelicolor* A3(2). *J Bacteriol* 182: 1286-1295.

Moller-Jensen, J., Borch, J., Dam, M., Jensen, R.B., Roepstorff, P., and Gerdes, K. (2003) Bacterial mitosis: ParM of plasmid R1 moves plasmid DNA by an actin-like insertional polymerization mechanism. *Mol Cell* 12: 1477-1487.

Moller-Jensen, J., Jensen, R.B., Löwe, J., and Gerdes, K. (2002) Prokaryotic DNA segregation by an actin-like filament. *EMBO J* 21: 3119-3127.

Mori, H., Mori, Y., Ichinose, C., Niki, H., Ogura, T., Kato, A., and Hiraga, S. (1989) Purification and characterization of SopA and SopB proteins essential for F plasmid partitioning. *J Biol Chem* 264: 15535-15541.

Moriya, S., Tsujikawa, E., Hassan, A.K., Asai, K., Kodama, T., and Ogasawara, N. (1998) A *Bacillus subtilis* gene-encoding protein homologous to eukaryotic SMC motor protein is necessary for chromosome partition. *Mol Microbiol* 29: 179-187.

Muchova, K., Kutejova, E., Scott, D.J., Brannigan, J.A., Lewis, R.J., Wilkinson, A.J., and Barak, I. (2002) Oligomerization of the *Bacillus subtilis* division protein DivIVA. *Microbiology* 148: 807-813.

Mukherjee, A., and Lutkenhaus, J. (1998) Dynamic assembly of FtsZ regulated by GTP hydrolysis. *EMBO J* 17: 462-469.

Mukherjee, P., Sureka, K., Datta, P., Hossain, T., Barik, S., Das, K.P., Kundu, M., and Basu, J. (2009) Novel role of Wag31 in protection of mycobacteria under oxidative stress. *Mol Microbiol* 73: 103-119.

Muller, P., Ewers, C., Bertsche, U., Anstett, M., Kallis, T., Breukink, E., Fraipont, C., Terrak, M., Nguyen-Disteche, M., and Vollmer, W. (2007) The essential cell division protein FtsN interacts with the murein (peptidoglycan) synthase PBP1B in *Escherichia coli*. *J Biol Chem* 282: 36394-36402.

Murakami, T., Holt, T.G., and Thompson, C.J. (1989) Thiostrepton-induced gene expression in *Streptomyces lividans*. *J Bacteriol* 171: 1459-1466.

Murray, H., and Errington, J. (2008) Dynamic control of the DNA replication initiation protein DnaA by Soj/ParA. *Cell* 135: 74-84.

Nelson, D.E., and Young, K.D. (2000) Penicillin binding protein 5 affects cell diameter, contour, and morphology of *Escherichia coli*. *J Bacteriol* 182: 1714-1721.

Nguyen, K.T., Willey, J.M., Nguyen, L.D., Nguyen, L.T., Viollier, P.H., and Thompson, C.J. (2002) A central regulator of morphological differentiation in the multicellular bacterium *Streptomyces coelicolor*. *Mol Microbiol* 46: 1223-1238.

Nguyen, L., Scherr, N., Gatfield, J., Walburger, A., Pieters, J., and Thompson, C.J. (2007) Antigen 84, an effector of pleiomorphism in *Mycobacterium smegmatis*. *J Bacteriol* 189: 7896-7910.

Ni, L., Xu, W., Kumaraswami, M., and Schumacher, M.A. (2010) Plasmid protein TubR uses a distinct mode of HTH-DNA binding and recruits the prokaryotic tubulin homolog TubZ to effect DNA partition. *Proc Natl Acad Sci U S A* 107: 11763-11768.

Niki, H., Jaffe, A., Imamura, R., Ogura, T., and Hiraga, S. (1991) The new gene *mukB* codes for a 177 kd protein with coiled-coil domains involved in chromosome partitioning of *E. coli*. *EMBO J* 10: 183-193.

Nodwell, J.R., and Losick, R. (1998) Purification of an extracellular signaling molecule involved in production of aerial mycelium by *Streptomyces coelicolor*. *J Bacteriol* 180: 1334-1337.

Nodwell, J.R., McGovern, K., and Losick, R. (1996) An oligopeptide permease responsible for the import of an extracellular signal governing aerial mycelium formation in *Streptomyces coelicolor*. *Mol Microbiol* 22: 881-893.

Noens, E.E., Mersinias, V., Traag, B.A., Smith, C.P., Koerten, H.K., and van Wezel, G.P. (2005) SsgA-like proteins determine the fate of peptidoglycan during sporulation of *Streptomyces coelicolor*. *Mol Microbiol* 58: 929-944.

Noens, E.E., Mersinias, V., Willemse, J., Traag, B.A., Laing, E., Chater, K.F., Smith, C.P., Koerten, H.K., and van Wezel, G.P. (2007) Loss of the controlled localization of growth stage-specific cell-wall synthesis pleiotropically affects developmental gene expression in an *ssgA* mutant of *Streptomyces coelicolor*. *Molecular microbiology* 64: 1244-1259.

Nogales, E., Downing, K.H., Amos, L.A., and Löwe, J. (1998) Tubulin and FtsZ form a distinct family of GTPases. *Nat Struct Biol* 5: 451-458.

O'Connor, T.J., Kanellis, P., and Nodwell, J.R. (2002) The *ramC* gene is required for morphogenesis in *Streptomyces coelicolor* and expressed in a cell type-specific manner under the direct control of RamR. *Mol Microbiol* 45: 45-57.

Obuchowski, P.L., and Jacobs-Wagner, C. (2008) PflI, a protein involved in flagellar positioning in *Caulobacter crescentus*. *J Bacteriol* 190: 1718-1729.

Ohashi, T., Hale, C.A., de Boer, P.A., and Erickson, H.P. (2002) Structural evidence that the P/Q domain of ZipA is an unstructured, flexible tether between the membrane and the C-terminal FtsZ-binding domain. *J Bacteriol* 184: 4313-4315.

Ohnishi, Y., Kameyama, S., Onaka, H., and Horinouchi, S. (1999) The A-factor regulatory cascade leading to streptomycin biosynthesis in *Streptomyces griseus* : identification of a target gene of the A-factor receptor. *Mol Microbiol* 34: 102-111.

Ohnishi, Y., Yamazaki, H., Kato, J.Y., Tomono, A., and Horinouchi, S. (2005) AdpA, a central transcriptional regulator in the A-factor regulatory cascade that leads to morphological development and secondary metabolism in *Streptomyces griseus*. *Biosci Biotechnol Biochem* 69: 431-439.

Oliva, M.A., Halbedel, S., Freund, S.M., Dutow, P., Leonard, T.A., Veprintsev, D.B., Hamoen, L.W., and Löwe, J. (2010) Features critical for membrane binding revealed by DivIVA crystal structure. *EMBO J* 29: 1988-2001.

Osawa, M., Anderson, D.E., and Erickson, H.P. (2008) Reconstitution of contractile FtsZ rings in liposomes. *Science* 320: 792-794.

Owen, D.M., Magenau, A., Williamson, D., and Gaus, K. (2012) The lipid raft hypothesis revisited - New insights on raft composition and function from super-resolution fluorescence microscopy. *Bioessays*.

Pansegrau, W., Lanka, E., Barth, P.T., Figurski, D.H., Guiney, D.G., Haas, D., Helinski, D.R., Schwab, H., Stanisich, V.A., and Thomas, C.M. (1994) Complete nucleotide sequence of Birmingham IncP alpha plasmids. Compilation and comparative analysis. *J Mol Biol* 239: 623-663.

Patrick, J.E., and Kearns, D.B. (2008) MinJ (YvjD) is a topological determinant of cell division in Bacillus subtilis. *Mol Microbiol* 70: 1166-1179.

Perry, S.E., and Edwards, D.H. (2004) Identification of a polar targeting determinant for *Bacillus subtilis* DivIVA. *Mol Microbiol* 54: 1237-1249.

Perry, S.V. (2001) Vertebrate tropomyosin: distribution, properties and function. *J Muscle Res Cell Motil* 22: 5-49.

Petit, J.M., Maftah, A., Ratinaud, M.H., and Julien, R. (1992) 10N-nonyl acridine orange interacts with cardiolipin and allows the quantification of this phospholipid in isolated mitochondria. *Eur J Biochem* 209: 267-273.

Phillips, G.N., Jr., Flicker, P.F., Cohen, C., Manjula, B.N., and Fischetti, V.A. (1981) *Streptococcal* M protein: alpha-helical coiled-coil structure and arrangement on the cell surface. *Proc Natl Acad Sci U S A* 78: 4689-4693.

Pichoff, S., and Lutkenhaus, J. (2002) Unique and overlapping roles for ZipA and FtsA in septal ring assembly in *Escherichia coli*. *EMBO J* 21: 685-693.

Pogliano, K., Hofmeister, A.E., and Losick, R. (1997) Disappearance of the sigma E transcription factor from the forespore and the SpoIIE phosphatase from the mother cell contributes to establishment of cell-specific gene expression during sporulation in *Bacillus subtilis*. *J Bacteriol* 179: 3331-3341.

Pope, M.K., Green, B., and Westpheling, J. (1998) The *bldB* gene encodes a small protein required for morphogenesis, antibiotic production, and catabolite control in *Streptomyces coelicolor*. *J Bacteriol* 180: 1556-1562.

Potluri, L.P., de Pedro, M.A., and Young, K.D. (2012) *Escherichia coli* low-molecular-weight penicillin-binding proteins help orient septal FtsZ, and their absence leads to asymmetric cell division and branching. *Molecular microbiology* 84: 203-224.

Potuckova, L., Kelemen, G.H., Findlay, K.C., Lonetto, M.A., Buttner, M.J., and Kormanec, J. (1995) A new RNA polymerase sigma factor, sigma F, is required for the late stages of morphological differentiation in *Streptomyces* spp. *Mol Microbiol* 17: 37-48.

QIAGEN (2006) QIAquick® Spin Handbook. In., pp.

Ramamurthi, K.S., and Losick, R. (2009) Negative membrane curvature as a cue for subcellular localization of a bacterial protein. *Proc Natl Acad Sci U S A* 106: 13541-13545.

Ramos, A., Honrubia, M.P., Valbuena, N., Vaquera, J., Mateos, L.M., and Gil, J.A. (2003) Involvement of DivIVA in the morphology of the rod-shaped actinomycete *Brevibacterium lactofermentum*. *Microbiology* 149: 3531-3542.

Raskin, D.M., and de Boer, P.A. (1997) The MinE ring: an FtsZ-independent cell structure required for selection of the correct division site in *E. coli*. *Cell* 91: 685-694.

Raskin, D.M., and de Boer, P.A. (1999) Rapid pole-to-pole oscillation of a protein required for directing division to the middle of *Escherichia coli*. *Proc Natl Acad Sci U S A* 96: 4971-4976.

Redenbach, M., Kieser, H.M., Denapaite, D., Eichner, A., Cullum, J., Kinashi, H., and Hopwood, D.A. (1996) A set of ordered cosmids and a detailed genetic and physical map for the 8 Mb *Streptomyces coelicolor* A3(2) chromosome. *Mol Microbiol* 21: 77-96.

Renner, L.D., and Weibel, D.B. (2011) Cardiolipin microdomains localize to negatively curved regions of *Escherichia coli* membranes. *Proc Natl Acad Sci U S A* 108: 6264-6269.

Reuther, J., Gekeler, C., Tiffert, Y., Wohlleben, W., and Muth, G. (2006) Unique conjugation mechanism in mycelial streptomycetes: a DNA-binding ATPase translocates unprocessed plasmid DNA at the hyphal tip. *Molecular microbiology* 61: 436-446.

Richards, D.M., Hempel, A.M., Flardh, K., Buttner, M.J., and Howard, M. (2012) Mechanistic basis of branch-site selection in filamentous bacteria. *PLoS Comput Biol* 8: e1002423.

Roeben, A., Kofler, C., Nagy, I., Nickell, S., Hartl, F.U., and Bracher, A. (2006) Crystal structure of an archaeal actin homolog. *J Mol Biol* 358: 145-156.

Romberg, L., and Levin, P.A. (2003) Assembly dynamics of the bacterial cell division protein FTSZ: poised at the edge of stability. *Annu Rev Microbiol* 57: 125-154.

Rudd, B.A., and Hopwood, D.A. (1979) Genetics of actinorhodin biosynthesis by *Streptomyces coelicolor* A3(2). *J Gen Microbiol* 114: 35-43.

Ryding, N.J., Bibb, M.J., Molle, V., Findlay, K.C., Chater, K.F., and Buttner, M.J. (1999) New sporulation loci in *Streptomyces coelicolor* A3(2). *J Bacteriol* 181: 5419-5425.

Ryding, N.J., Kelemen, G.H., Whatling, C.A., Flardh, K., Buttner, M.J., and Chater, K.F. (1998) A developmentally regulated gene encoding a repressor-like protein is essential for sporulation in *Streptomyces coelicolor* A3(2). *Mol Microbiol* 29: 343-357.

Sawyer, E.B., Claessen, D., Haas, M., Hurgobin, B., and Gras, S.L. (2011) The assembly of individual chaplin peptides from *Streptomyces coelicolor* into functional amyloid fibrils. *PLoS One* 6: e18839.

Schlochtermeier, A., Niemeyer, F., and Schrempf, H. (1992a) Biochemical and Electron Microscopic Studies of the *Streptomyces reticuli* Cellulase (Avicelase) in Its Mycelium-Associated and Extracellular Forms. *Appl Environ Microbiol* 58: 3240-3248.

Schlochtermeier, A., Walter, S., Schroder, J., Moorman, M., and Schrempf, H. (1992b) The gene encoding the cellulase (Avicelase) Cel1 from *Streptomyces reticuli* and analysis of protein domains. *Mol Microbiol* 6: 3611-3621.

Schofield, W.B., Lim, H.C., and Jacobs-Wagner, C. (2010) Cell cycle coordination and regulation of bacterial chromosome segregation dynamics by polarly localized proteins. *EMBO J* 29: 3068-3081.

Schwedock, J., McCormick, J.R., Angert, E.R., Nodwell, J.R., and Losick, R. (1997) Assembly of the cell division protein FtsZ into ladder-like structures in the aerial hyphae of *Streptomyces coelicolor*. *Mol Microbiol* 25: 847-858.

Sevcikova, B., and Kormanec, J. (2003) The *ssgB* gene, encoding a member of the regulon of stress-response sigma factor sigmaH, is essential for aerial mycelium septation in *Streptomyces coelicolor* A3(2). *Arch Microbiol* 180: 380-384.

Sevcikova, B., Rezuchova, B., Homerova, D., and Kormanec, J. (2010) The anti-anti-sigma factor BldG is involved in activation of the stress response sigma factor sigma(H) in *Streptomyces coelicolor* A3(2). *J Bacteriol* 192: 5674-5681.

Shaevitz, J.W., and Gitai, Z. (2010) The structure and function of bacterial actin homologs. *Cold Spring Harb Perspect Biol* 2: a000364.

Shapiro, L., McAdams, H.H., and Losick, R. (2002) Generating and exploiting polarity in bacteria. *Science* 298: 1942-1946.

Sharpe, M.E., and Errington, J. (1996) The *Bacillus subtilis soj-spo0J* locus is required for a centromere-like function involved in prespore chromosome partitioning. *Mol Microbiol* 21: 501-509.

Shih, Y.L., Le, T., and Rothfield, L. (2003) Division site selection in *Escherichia coli* involves dynamic redistribution of Min proteins within coiled structures that extend between the two cell poles. *Proc Natl Acad Sci U S A* 100: 7865-7870.

Shih, Y.L., and Rothfield, L. (2006) The bacterial cytoskeleton. *Microbiol Mol Biol Rev* 70: 729-754.

Shiomi, D., Sakai, M., and Niki, H. (2008) Determination of bacterial rod shape by a novel cytoskeletal membrane protein. ***EMBO J*** **27: 3081-3091.**

Singh, A., Guidry, L., Narasimhulu, K.V., Mai, D., Trombley, J., Redding, K.E., Giles, G.I., Lancaster, J.R., Jr., and Steyn, A.J. (2007) ***Mycobacterium tuberculosis*** **WhiB3 responds to O2 and nitric oxide via its [4Fe-4S] cluster and is essential for nutrient starvation survival.** ***Proc Natl Acad Sci U S A*** **104: 11562-11567.**

Soliveri, J.A., Gomez, J., Bishai, W.R., and Chater, K.F. (2000) Multiple paralogous genes related to the ***Streptomyces coelicolor*** **developmental regulatory gene** ***whiB*** **are present in** ***Streptomyces*** **and other actinomycetes.** ***Microbiology*** **146 (Pt 2): 333-343.**

Soppa, J. (2001) Prokaryotic structural maintenance of chromosomes (SMC) proteins: distribution, phylogeny, and comparison with MukBs and additional prokaryotic and eukaryotic coiled-coil proteins. ***Gene*** **278: 253-264.**

Spratt, B.G. (1975) Distinct penicillin binding proteins involved in the division, elongation, and shape of ***Escherichia coli*** **K12.** ***Proc Natl Acad Sci U S A*** **72: 2999-3003.**

Spratt, B.G. (1977) Temperature-sensitive cell division mutants of ***Escherichia coli*** **with thermolabile penicillin-binding proteins.** ***J Bacteriol*** **131: 293-305.**

Stahlberg, H., Kutejova, E., Muchova, K., Gregorini, M., Lustig, A., Muller, S.A., Olivieri, V., Engel, A., Wilkinson, A.J., and Barak, I. (2004) Oligomeric structure of the ***Bacillus subtilis*** **cell division protein DivIVA determined by transmission electron microscopy.** ***Mol Microbiol*** **52: 1281-1290.**

Steinert, P.M., and Roop, D.R. (1988) Molecular and cellular biology of intermediate filaments. ***Annu Rev Biochem*** **57: 593-625.**

Stone, K.J., and Strominger, J.L. (1971) Mechanism of action of bacitracin: complexation with metal ion and C 55 -isoprenyl pyrophosphate. ***Proc Natl Acad Sci U S A*** **68: 3223-3227.**

Strelkov, S.V., Herrmann, H., and Aebi, U. (2003) Molecular architecture of intermediate filaments. ***Bioessays*** **25: 243-251.**

StrepDB (strepdb.streptomyces.org.uk/) The ***Streptomyces coelicolor*** **genome annotation server. In.: John Innes Centre, pp.**

Stricker, J., Maddox, P., Salmon, E.D., and Erickson, H.P. (2002) Rapid assembly dynamics of the ***Escherichia coli*** **FtsZ-ring demonstrated by fluorescence recovery after photobleaching.** ***Proc Natl Acad Sci U S A*** **99: 3171-3175.**

Strunnikov, A.V., and Jessberger, R. (1999) Structural maintenance of chromosomes (SMC) proteins: conserved molecular properties for multiple biological functions. ***Eur J Biochem*** **263: 6-13.**

Studier, F.W., and Moffatt, B.A. (1986) Use of bacteriophage T7 RNA polymerase to direct selective high-level expression of cloned genes. ***J Mol Biol*** **189: 113-130.**

Sun, J., Kelemen, G.H., Fernandez-Abalos, J.M., and Bibb, M.J. (1999) Green fluorescent protein as a reporter for spatial and temporal gene expression in *Streptomyces coelicolor* A3(2). *Microbiology* 145 (Pt 9): 2221-2227.

Sun, Q., and Margolin, W. (1998) FtsZ dynamics during the division cycle of live *Escherichia coli* cells. *J Bacteriol* 180: 2050-2056.

Swulius, M.T., Chen, S., Jane Ding, H., Li, Z., Briegel, A., Pilhofer, M., Tocheva, E.I., Lybarger, S.R., Johnson, T.L., Sandkvist, M., and Jensen, G.J. (2011) Long helical filaments are not seen encircling cells in electron cryotomograms of rod-shaped bacteria. *Biochem Biophys Res Commun* 407: 650-655.

Szardenings, F., Guymer, D., and Gerdes, K. (2011) ParA ATPases can move and position DNA and subcellular structures. *Curr Opin Microbiol* 14: 712-718.

Szwedziak, P., Wang, Q., Freund, S.M., and Löwe, J. (2012) FtsA forms actin-like protofilaments. *EMBO J* 31: 2249-2260.

Takano, E., Tao, M., Long, F., Bibb, M.J., Wang, L., Li, W., Buttner, M.J., Deng, Z.X., and Chater, K.F. (2003) A rare leucine codon in *adpA* is implicated in the morphological defect of *bldA* mutants of *Streptomyces coelicolor*. *Mol Microbiol* 50: 475-486.

Takano, E., White, J., Thompson, C.J., and Bibb, M.J. (1995) Construction of thiostrepton-inducible, high-copy-number expression vectors for use in *Streptomyces* spp. *Gene* 166: 133-137.

Thanbichler, M., and Shapiro, L. (2006) MipZ, a spatial regulator coordinating chromosome segregation with cell division in *Caulobacter*. *Cell* 126: 147-162.

Thomaides, H.B., Freeman, M., El Karoui, M., and Errington, J. (2001) Division site selection protein DivIVA of *Bacillus subtilis* has a second distinct function in chromosome segregation during sporulation. *Genes Dev* 15: 1662-1673.

Tian, Y., Fowler, K., Findlay, K., Tan, H., and Chater, K.F. (2007) An unusual response regulator influences sporulation at early and late stages in *Streptomyces coelicolor*. *J Bacteriol* 189: 2873-2885.

Tillotson, R.D., Wosten, H.A., Richter, M., and Willey, J.M. (1998) A surface active protein involved in aerial hyphae formation in the filamentous fungus *Schizophillum commune* restores the capacity of a bald mutant of the filamentous bacterium *Streptomyces coelicolor* to erect aerial structures. *Mol Microbiol* 30: 595-602.

Tomono, A., Tsai, Y., Ohnishi, Y., and Horinouchi, S. (2005) Three chymotrypsin genes are members of the AdpA regulon in the A-factor regulatory cascade in *Streptomyces griseus*. *J Bacteriol* 187: 6341-6353.

Touzain, F., Schbath, S., Debled-Rennesson, I., Aigle, B., Kucherov, G., and Leblond, P. (2008) SIGffRid: a tool to search for sigma factor binding sites in bacterial genomes using comparative approach and biologically driven statistics. *BMC Bioinformatics* 9: 73.

Traag, B.A., and van Wezel, G.P. (2008) The SsgA-like proteins in actinomycetes: small proteins up to a big task. ***Antonie Van Leeuwenhoek*** **94: 85-97.**

Tsien, R.Y. (1998) The green fluorescent protein. ***Annu Rev Biochem*** **67: 509-544.**

Typas, A., Banzhaf, M., Gross, C.A., and Vollmer, W. (2011) From the regulation of peptidoglycan synthesis to bacterial growth and morphology. ***Nat Rev Microbiol*** **10: 123-136.**

Ueda, K., Takano, H., Nishimoto, M., Inaba, H., and Beppu, T. (2005) Dual transcriptional control of ***amfTSBA*****, which regulates the onset of cellular differentiation in** ***Streptomyces griseus*****.** ***J Bacteriol*** **187: 135-142.**

Ursinus, A., van den Ent, F., Brechtel, S., de Pedro, M., Holtje, J.V., Löwe, J., and Vollmer, W. (2004) Murein (peptidoglycan) binding property of the essential cell division protein FtsN from ***Escherichia coli*****.** ***J Bacteriol*** **186: 6728-6737.**

Valtz, N., and Herskowitz, I. (1996) Pea2 protein of yeast is localized to sites of polarized growth and is required for efficient mating and bipolar budding. ***J Cell Biol*** **135: 725-739.**

van den Ent, F., Amos, L.A., and Löwe, J. (2001) Prokaryotic origin of the actin cytoskeleton. ***Nature*** **413: 39-44.**

van den Ent, F., Johnson, C.M., Persons, L., de Boer, P., and Löwe, J. (2010) Bacterial actin MreB assembles in complex with cell shape protein RodZ. ***EMBO J*** **29: 1081-1090.**

van den Ent, F., and Löwe, J. (2000) Crystal structure of the cell division protein FtsA from ***Thermotoga maritima*****.** ***EMBO J*** **19: 5300-5307.**

van den Ent, F., Moller-Jensen, J., Amos, L.A., Gerdes, K., and Löwe, J. (2002) F-actin-like filaments formed by plasmid segregation protein ParM. ***EMBO J*** **21: 6935-6943.**

van den Ent, F., Vinkenvleugel, T.M., Ind, A., West, P., Veprintsev, D., Nanninga, N., den Blaauwen, T., and Löwe, J. (2008) Structural and mutational analysis of the cell division protein FtsQ. ***Mol Microbiol*** **68: 110-123.**

van Teeffelen, S., Wang, S., Furchtgott, L., Huang, K.C., Wingreen, N.S., Shaevitz, J.W., and Gitai, Z. (2011) The bacterial actin MreB rotates, and rotation depends on cell-wall assembly. ***Proc Natl Acad Sci U S A*** **108: 15822-15827.**

van Wezel, G.P., van der Meulen, J., Kawamoto, S., Luiten, R.G., Koerten, H.K., and Kraal, B. (2000) ***ssgA*** **is essential for sporulation of** ***Streptomyces coelicolor*** **A3(2) and affects hyphal development by stimulating septum formation.** ***J Bacteriol*** **182: 5653-5662.**

Varley, A.W., and Stewart, G.C. (1992) The ***divIVB*** **region of the** ***Bacillus subtilis*** **chromosome encodes homologs of** ***Escherichia coli*** **septum placement (*minCD*) and cell shape (*mreBCD*) determinants.** ***J Bacteriol*** **174: 6729-6742.**

Vikis, H.G., and Guan, K.L. (2004) Glutathione-S-transferase-fusion based assays for studying protein-protein interactions. *Methods Mol Biol* 261: 175-186.

Vitha, S., McAndrew, R.S., and Osteryoung, K.W. (2001) FtsZ ring formation at the chloroplast division site in plants. *J Cell Biol* 153: 111-120.

Volff, J.N., and Altenbuchner, J. (1998) Genetic instability of the *Streptomyces* chromosome. *Mol Microbiol* 27: 239-246.

Wachi, M., Doi, M., Tamaki, S., Park, W., Nakajima-Iijima, S., and Matsuhashi, M. (1987) Mutant isolation and molecular cloning of *mre* genes, which determine cell shape, sensitivity to mecillinam, and amount of penicillin-binding proteins in *Escherichia coli*. *J Bacteriol* 169: 4935-4940.

Wagner, J.K., Galvani, C.D., and Brun, Y.V. (2005) *Caulobacter crescentus* requires RodA and MreB for stalk synthesis and prevention of ectopic pole formation. *J Bacteriol* 187: 544-553.

Waksman, S.A., Reilly, H.C., and Johnstone, D.B. (1946) Isolation of Streptomycin-producing Strains of *Streptomyces griseus*. *J Bacteriol* 52: 393-397.

Walshaw, J., Gillespie, M.D., and Kelemen, G.H. (2010) A novel coiled-coil repeat variant in a class of bacterial cytoskeletal proteins. *J Struct Biol* 170: 202-215.

Walter, S., Rohde, M., Machner, M., and Schrempf, H. (1999) Electron microscopy studies of cell-wall-anchored cellulose (Avicel)-binding protein (AbpS) from *Streptomyces reticuli*. *Appl Environ Microbiol* 65: 886-892.

Walter, S., and Schrempf, H. (2003) Oligomerization, membrane anchoring, and cellulose-binding characteristics of AbpS, a receptor-like *Streptomyces* protein. *J Biol Chem* 278: 26639-26647.

Walter, S., Wellmann, E., and Schrempf, H. (1998) The cell wall-anchored *Streptomyces reticuli* avicel-binding protein (AbpS) and its gene. *J Bacteriol* 180: 1647-1654.

Wang, L., Yu, Y., He, X., Zhou, X., Deng, Z., Chater, K.F., and Tao, M. (2007) Role of an FtsK-like protein in genetic stability in *Streptomyces coelicolor* A3(2). *J Bacteriol* 189: 2310-2318.

Wang, S.B., Cantlay, S., Nordberg, N., Letek, M., Gil, J.A., and Flärdh, K. (2009) Domains involved in the *in vivo* function and oligomerization of apical growth determinant DivIVA in *Streptomyces coelicolor*. *FEMS Microbiol Lett* 297: 101-109.

Wang, X., and Lutkenhaus, J. (1996) FtsZ ring: the eubacterial division apparatus conserved in archaebacteria. *Mol Microbiol* 21: 313-319.

Waring, M.J. (1965) Complex formation between ethidium bromide and nucleic acids. *J Mol Biol* 13: 269-282.

Weidel, W., and Pelzer, H. (1964) Bagshaped Macromolecules--a New Outlook on Bacterial Cell Walls. *Adv Enzymol Relat Areas Mol Biol* 26: 193-232.

Westphal, M., Jungbluth, A., Heidecker, M., Muhlbauer, B., Heizer, C., Schwartz, J.M., Marriott, G., and Gerisch, G. (1997) Microfilament dynamics during cell movement and chemotaxis monitored using a GFP-actin fusion protein. *Curr Biol* 7: 176-183.

Wheeler, R.T., Gober, J.W., and Shapiro, L. (1998) Protein localization during the *Caulobacter crescentus* cell cycle. *Curr Opin Microbiol* 1: 636-642.

White, C.L., Kitich, A., and Gober, J.W. (2010) Positioning cell wall synthetic complexes by the bacterial morphogenetic proteins MreB and MreD. *Mol Microbiol* 76: 616-633.

Wilkinson, C.J., Hughes-Thomas, Z.A., Martin, C.J., Bohm, I., Mironenko, T., Deacon, M., Wheatcroft, M., Wirtz, G., Staunton, J., and Leadlay, P.F. (2002) Increasing the efficiency of heterologous promoters in actinomycetes. *J Mol Microbiol Biotechnol* 4: 417-426.

Willander, M., and Al-Hilli, S. (2009) Analysis of biomolecules using surface plasmons. *Methods Mol Biol* 544: 201-229.

Willemse, J., Borst, J.W., de Waal, E., Bisseling, T., and van Wezel, G.P. (2011a) Positive control of cell division: FtsZ is recruited by SsgB during sporulation of *Streptomyces*. *Genes Dev* 25: 89-99.

Willemse, J., Mommaas, A.M., and van Wezel, G.P. (2011b) Constitutive expression of *ftsZ* overrides the *whi* developmental genes to initiate sporulation of *Streptomyces coelicolor*. *Antonie Van Leeuwenhoek*.

Willey, J., Santamaria, R., Guijarro, J., Geistlich, M., and Losick, R. (1991) Extracellular complementation of a developmental mutation implicates a small sporulation protein in aerial mycelium formation by *S. coelicolor*. *Cell* 65: 641-650.

Willey, J., Schwedock, J., and Losick, R. (1993) Multiple extracellular signals govern the production of a morphogenetic protein involved in aerial mycelium formation by *Streptomyces coelicolor*. *Genes Dev* 7: 895-903.

Wissmueller, S., Font, J., Liew, C.W., Cram, E., Schroeder, T., Turner, J., Crossley, M., Mackay, J.P., and Matthews, J.M. (2011) Protein-protein interactions: analysis of a false positive GST pulldown result. *Proteins* 79: 2365-2371.

Wright, C.S. (1984) Structural comparison of the two distinct sugar binding sites in wheat germ agglutinin isolectin II. *J Mol Biol* 178: 91-104.

Wright, L.F., and Hopwood, D.A. (1976) Actinorhodin is a chromosomally-determined antibiotic in *Streptomyces coelicolor* A3(2). *J Gen Microbiol* 96: 289-297.

Wu, L.J., and Errington, J. (2003) RacA and the Soj-Spo0J system combine to effect polar chromosome segregation in sporulating *Bacillus subtilis*. *Mol Microbiol* 49: 1463-1475.

Wu, L.J., and Errington, J. (2011) Nucleoid occlusion and bacterial cell division. *Nat Rev Microbiol* 10: 8-12.

Wu, L.J., Ishikawa, S., Kawai, Y., Oshima, T., Ogasawara, N., and Errington, J. (2009) Noc protein binds to specific DNA sequences to coordinate cell division with chromosome segregation. *EMBO J* 28: 1940-1952.

Xiang, X., and Plamann, M. (2003) Cytoskeleton and motor proteins in filamentous fungi. *Curr Opin Microbiol* 6: 628-633.

Xu, H., Chater, K.F., Deng, Z., and Tao, M. (2008) A cellulose synthase-like protein involved in hyphal tip growth and morphological differentiation in *Streptomyces*. *J Bacteriol* 190: 4971-4978.

Xu, Q., Traag, B.A., Willemse, J., McMullan, D., Miller, M.D., Elsliger, M.A., Abdubek, P., Astakhova, T., Axelrod, H.L., Bakolitsa, C., Carlton, D., Chen, C., Chiu, H.J., Chruszcz, M., Clayton, T., Das, D., Deller, M.C., Duan, L., Ellrott, K., Ernst, D., Farr, C.L., Feuerhelm, J., Grant, J.C., Grzechnik, A., Grzechnik, S.K., Han, G.W., Jaroszewski, L., Jin, K.K., Klock, H.E., Knuth, M.W., Kozbial, P., Krishna, S.S., Kumar, A., Marciano, D., Minor, W., Mommaas, A.M., Morse, A.T., Nigoghossian, E., Nopakun, A., Okach, L., Oommachen, S., Paulsen, J., Puckett, C., Reyes, R., Rife, C.L., Sefcovic, N., Tien, H.J., Trame, C.B., van den Bedem, H., Wang, S., Weekes, D., Hodgson, K.O., Wooley, J., Deacon, A.M., Godzik, A., Lesley, S.A., Wilson, I.A., and van Wezel, G.P. (2009) Structural and functional characterizations of SsgB, a conserved activator of developmental cell division in morphologically complex actinomycetes. *J Biol Chem* 284: 25268-25279.

Xu, W., Huang, J., Lin, R., Shi, J., and Cohen, S.N. (2010) Regulation of morphological differentiation in *S. coelicolor* by RNase III (AbsB) cleavage of mRNA encoding the AdpA transcription factor. *Mol Microbiol* 75: 781-791.

Yamanaka, K., Mitani, T., Feng, J., Ogura, T., Niki, H., and Hiraga, S. (1994) Two mutant alleles of *mukB*, a gene essential for chromosome partition in *Escherichia coli*. *FEMS Microbiol Lett* 123: 27-31.

Yamazaki, H., Ohnishi, Y., and Horinouchi, S. (2000) An A-factor-dependent extracytoplasmic function sigma factor (sigma(AdsA)) that is essential for morphological development in *Streptomyces griseus*. *J Bacteriol* 182: 4596-4605.

Yamazaki, H., Takano, Y., Ohnishi, Y., and Horinouchi, S. (2003) *amfR*, an essential gene for aerial mycelium formation, is a member of the AdpA regulon in the A-factor regulatory cascade in *Streptomyces griseus*. *Mol Microbiol* 50: 1173-1187.

Yamazaki, H., Tomono, A., Ohnishi, Y., and Horinouchi, S. (2004) DNA-binding specificity of AdpA, a transcriptional activator in the A-factor regulatory cascade in *Streptomyces griseus*. *Mol Microbiol* 53: 555-572.

Yanisch-Perron, C., Vieira, J., and Messing, J. (1985) Improved M13 phage cloning vectors and host strains: nucleotide sequences of the M13mp18 and pUC19 vectors. *Gene* 33: 103-119.

Yu, X.C., and Margolin, W. (1999) FtsZ ring clusters in *min* and partition mutants: role of both the Min system and the nucleoid in regulating FtsZ ring localization. *Mol Microbiol* 32: 315-326.

Zhang, G., Gurtu, V., and Kain, S.R. (1996) An enhanced green fluorescent protein allows sensitive detection of gene transfer in mammalian cells. *Biochem Biophys Res Commun* 227: 707-711.

Zizlsperger, N., and Keating, A.E. (2010) Specific coiled-coil interactions contribute to a global model of the structure of the spindle pole body. *J Struct Biol* 170: 246-256.

Zizlsperger, N., Malashkevich, V.N., Pillay, S., and Keating, A.E. (2008) Analysis of coiled-coil interactions between core proteins of the spindle pole body. *Biochemistry* 47: 11858-11868.

11 Appendix

11.1 Subcellular localisation of proteins using the reporter proteins EGFP and mCherry

Subcellular localisation of a protein is often important for dissecting the role of the protein in the developmental biology of the organism. The two main cell biology methods for establishing the subcellular localisation of a protein are immunolocalisation and localisation via a fluorescent tag (Giepmans *et al.*, 2006). Each method has its advantages and disadvantages. Immunolocalisation is an important technique that can specifically recognize a protein, but requires fixation and permeabilization. This leads to death of the cell and potentially to artificial affects caused by the fixation. One of the most used fluorescent tags is the Green Fluorescent Protein and its derivatives. Green Fluorescent Protein (GFP) is a bioluminescent protein first isolated from the Jellyfish *Aequorea victoria* (Tsien, 1998). GFP has since been developed through mutations to enhanced Green Fluorescent Protein (EGFP), which is 35 times brighter than the wild-type protein (Zhang *et al.*, 1996). The coding sequence of *egfp* contains more than 190 silent nucleotide changes that were intended for expression of *egfp* in eukaryotic organisms. However, these changes were also beneficial for expression of *egfp* in *S. coelicolor* as it reduced the usage of rare codons useful for expression of a heterologous gene. This has resulted in the utilisation of EGFP as a reporter for gene expression and protein localisation in *S. coelicolor* (Sun *et al.*, 1999). Fusing of a gene and EGFP so that they are translated as a single protein can, however, have detrimental effects on proteins folding and behaviour of the protein *in vivo*.

Similar to GFP is DsRed isolated from a Coral *Discosoma sp* (Matz *et al.*, 1999; Baird *et al.*, 2000). The chromophore of DsRed is subtly different to that of GFP resulting in a shift in the maxima of excitation, its emission is shifted to the red part of the spectrum (Gross *et al.*, 2000). Similarly to GFP, DsRed has since been optimised, in this case a significant change altering the ability of the protein to form tetramers, by generation of a monomeric form of the protein (Campbell *et al.*, 2002). The current form of Red Fluorescent protein that has been seen to be developed as a tool in *Streptomyces* research (Flärdh, and Buttner, 2009) is the monomeric Cherry (mCherry) that we sought to use here. The use of mCherry

in *S. coelicolor* possesses several advantages to EGFP including that there is less auto-fluorescence in the excitation and emission range of mCherry than there is for EGFP.

11.2 Complementation with EGFP fusions

To further assess the functioning of the various Scy fusions to EGFP. The strains *scy*/pIJ8660-Pscy-efgp-scy, *scy*/pIJ8660-Pscy-scy-egfp, *scy*/pIJ8660-Pscy-efgp-scy-C, *scy*/pIJ8660-Pscy-efgp-scy-N and *scy*/pIJ8660-Pscy-scy-N-egfp were grown on SFM

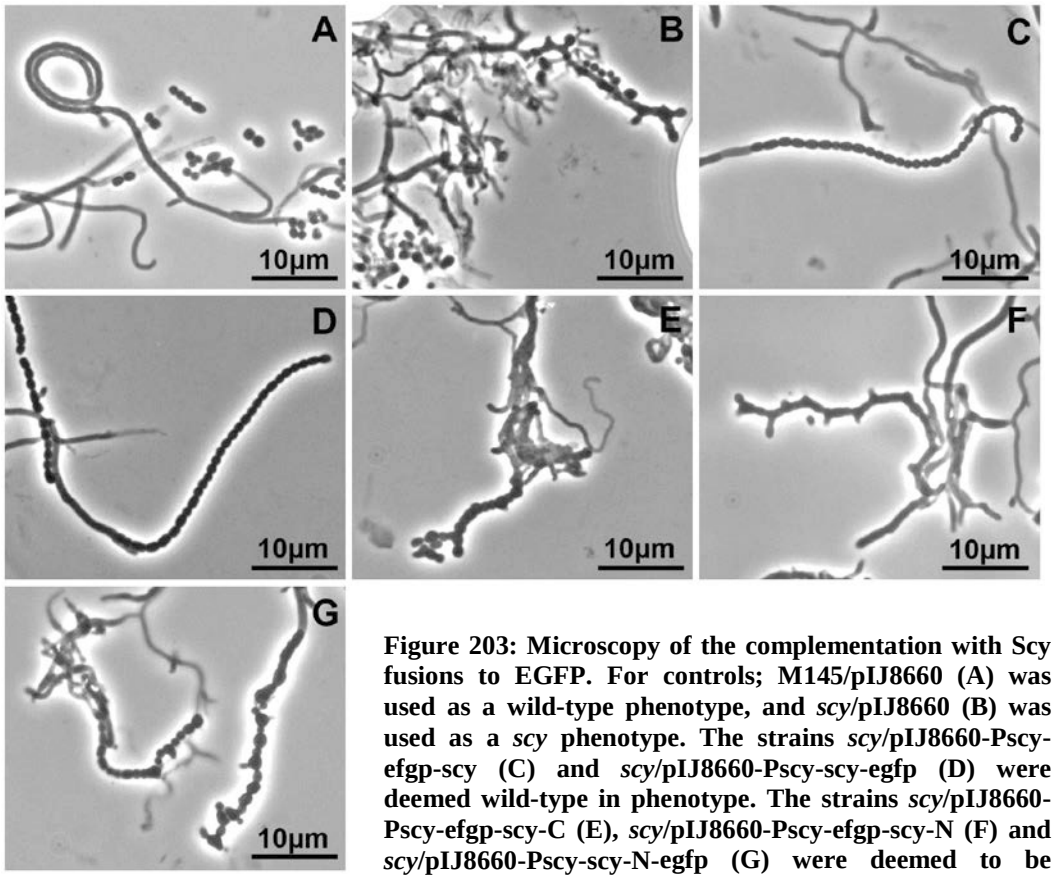

Figure 203: Microscopy of the complementation with Scy fusions to EGFP. For controls; M145/pIJ8660 (A) was used as a wild-type phenotype, and *scy*/pIJ8660 (B) was used as a *scy* phenotype. The strains *scy*/pIJ8660-Pscy-efgp-scy (C) and *scy*/pIJ8660-Pscy-scy-egfp (D) were deemed wild-type in phenotype. The strains *scy*/pIJ8660-Pscy-efgp-scy-C (E), *scy*/pIJ8660-Pscy-efgp-scy-N (F) and *scy*/pIJ8660-Pscy-scy-N-egfp (G) were deemed to be similar to a *scy* phenotype suggesting that these fusions don't complement. Samples were grown for 3 days on SFM agar plates alongside coverslips. Images were taken using phase contrast. Scale bars are shown.

alongside coverslips (as shown in Figure 203). M145/pIJ8660 and *scy*/pIJ8660 were also grown as control strains in order to deem a phenotype as complemented or more similer to the *scy* mutant. Time points of 3 days were observed, in order to catch the part of the developmental cycle that would produce spore forming aerial hyphae. In this experiment we considered these as a good marker of a wild-type phenotype or *scy* phenotype, due to the very obvious phenotype associated with the aerial hyphae of a *scy* mutant (Chapter 2).

We found that both the full length N and C terminal fusions of Scy to EGFP were able to complement the *scy* mutant. As we had shown that the full length N-terminal could complement the aerial hyphae phenotype already (3.2.1), then this shows that the full length C-terminal is able to do the same. However we found that none of the truncated forms of Scy bound to EGFP were able to complement the phenotype of the aerial hyphae. This is of interest as the Scy-C domain fused to EGFP was able to localise to hyphal tips (Figure 52), however the lack of complementation suggests that the Scy-N is also necessary for the biological function of Scy. As the Scy-N fusions did not localise to the hyphal tips (Figure 52 & Figure 54) we were not surprised to find that neither of the Scy-N fusions were able to complement the *scy* mutant.

11.3 Additional constructs

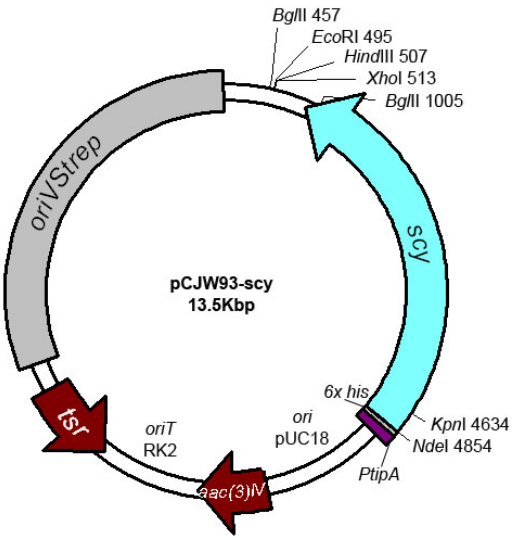

Figure 204: The scy overexpression vector pCJW93-Scy.

The vector pCJW93-scy is a high copy non-integrative plasmid carrying *scy* under the *tipA* promoter and a fusion to an N-terminal 6xHis tag. *oriT* enables conjugation from *E.coli* to *S. coelicolor*. Apramycin and thiostrepton resistance are also encoded by the plasmid.

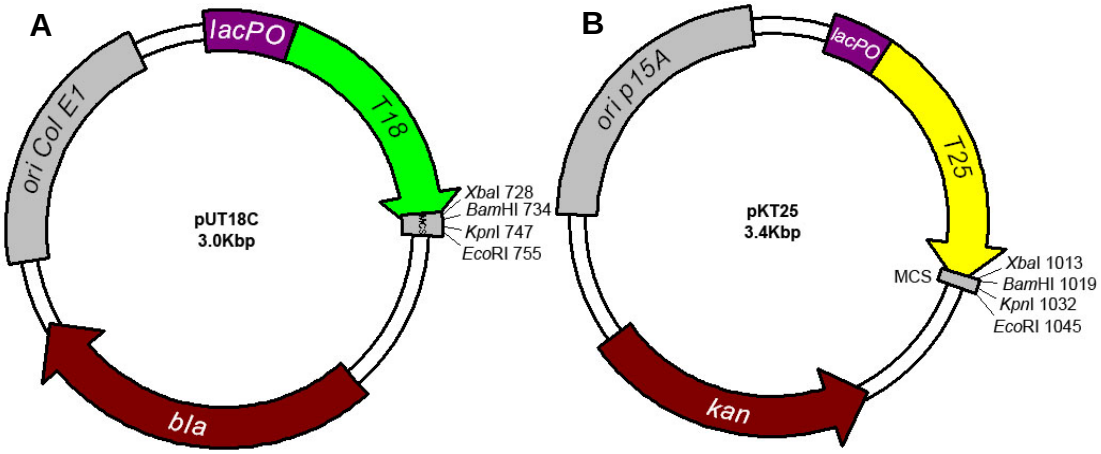

Figure 205: The BACTH vectors pUT18C and pKT25.

A) The vector pUT18C contains DNA encoding the T18 domain of CyaA with a C-terminal multiple cloning site, allowing the cloning of fragments to generate T18 C-terminal fusions. This vector is a high copy number plasmid and can be selected for ampicillin resistance.

B) The vector pKT25 contains DNA encoding the T25 domain of CyaA with a C-terminal multiple cloning site, allowing the cloning of fragments to generate T25 C-terminal fusions. This vector is a lower copy number plasmid and can be selected for kanamycin resistance.

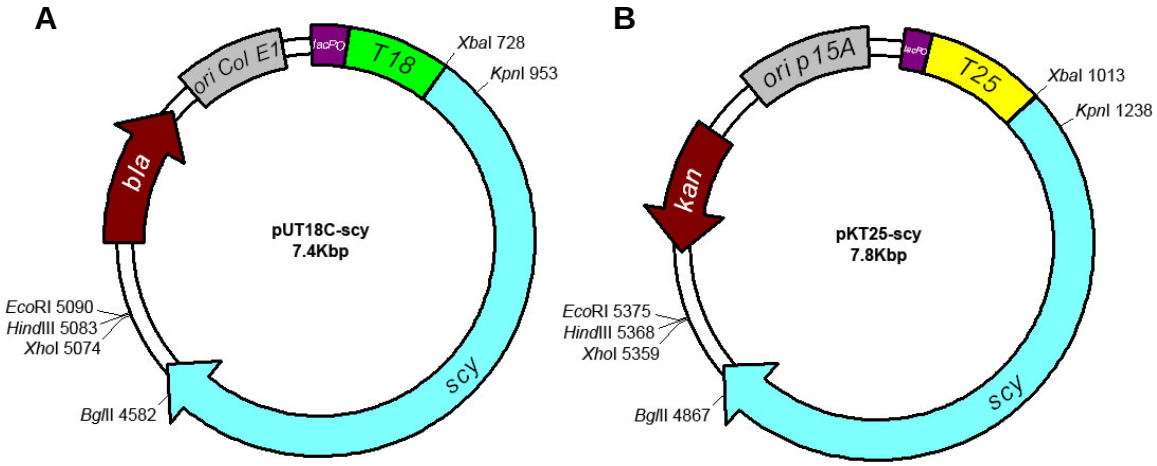

Figure 206: The Scy bacterial two-hybrid constructs.

A) pUT18C-scy is a derivative of pUT18C. A *scy* fragment was cloned into the *Xba*I and *Eco*RI sites so that the adenylate cyclase domain T18 read inframe to *scy*.

B) pKT25-scy is a derivative of pKT25. A *scy* fragment was cloned into the *Xba*I and *Eco*RI sites so that the adenylate cyclase domain T25 read inframe to *scy*.

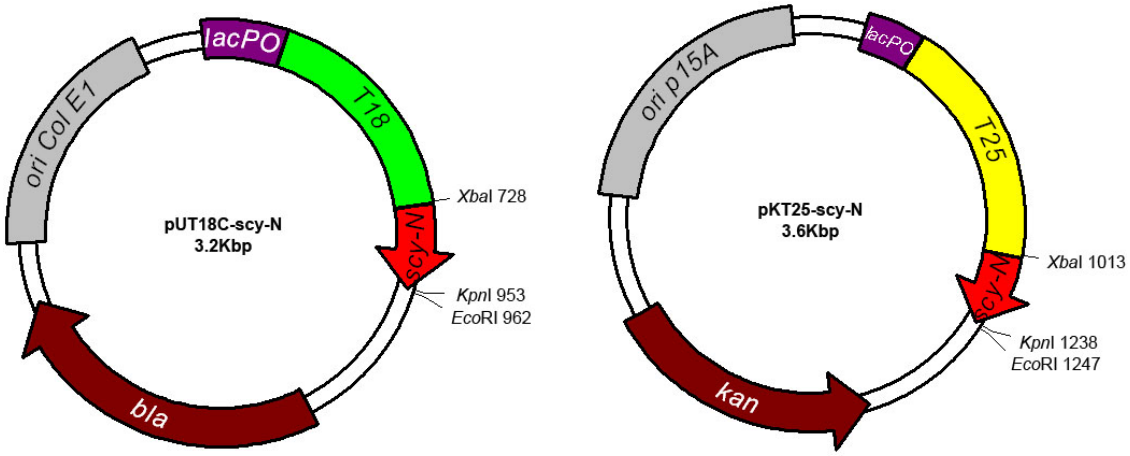

Figure 207: The Scy-N bacterial two-hybrid constructs.

A) pUT18C-scy-N is a derivative of pUT18C. A *scy-N* fragment was cloned into the *Xba*I and *Eco*RI sites so that the adenylate cyclase domain T18 read inframe to *scy-N*.

B) pKT25-scy-N is a derivative of pKT25. A *scy-N* fragment was cloned into the *Xba*I and *Eco*RI sites so that the adenylate cyclase domain T25 read inframe to *scy-N*.

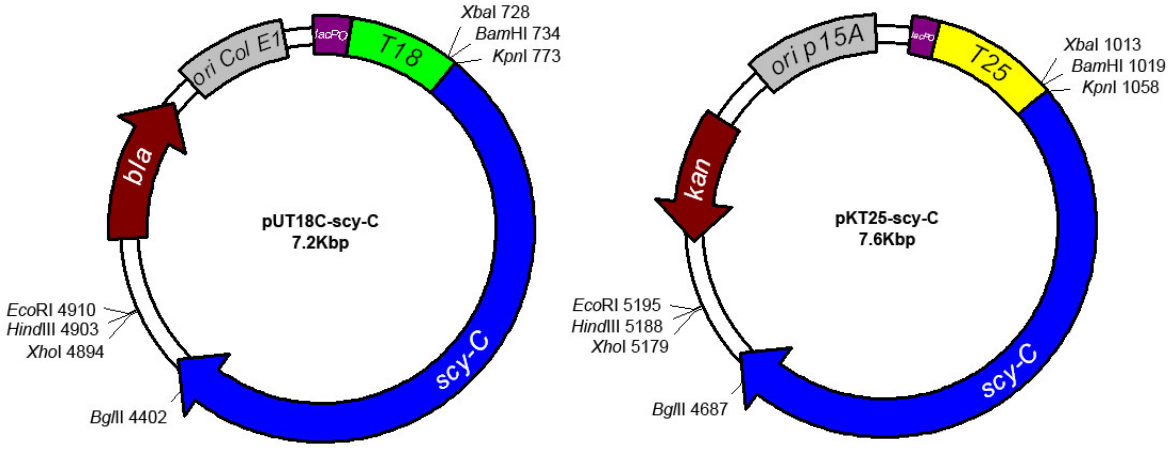

Figure 208: The Scy-C bacterial two-hybrid constructs.

A) pUT18C-scy-C is a derivative of pUT18C. A *scy-C* fragment was cloned into the *Kpn*I and *Eco*RI sites with a linker that placed the adenylate cyclase domain T18 read inframe to *scy-C*.

B) pKT25-scy-C is a derivative of pKT25. A *scy-C* fragment was cloned into the *Kpn*I and *Eco*RI sites with a linker that placed the adenylate cyclase domain T25 read inframe to *scy-C*.

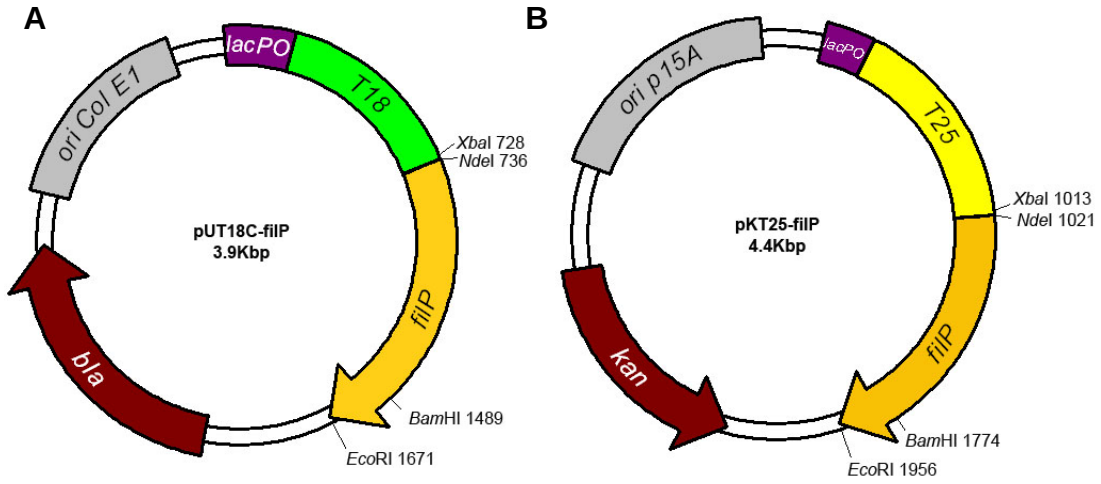

Figure 209: The FilP bacterial two-hybrid constructs.

A) pUT18C-filP is a derivative of pUT18C. A *filP* fragment was cloned into the *Xba*I and *Eco*RI sites so that the adenylate cyclase domain T18 read inframe to *filP*.

B) pKT25-filP is a derivative of pKT25. A *filP* fragment was cloned into the *Xba*I and *Eco*RI sites so that the adenylate cyclase domain T25 read inframe to *filP*.

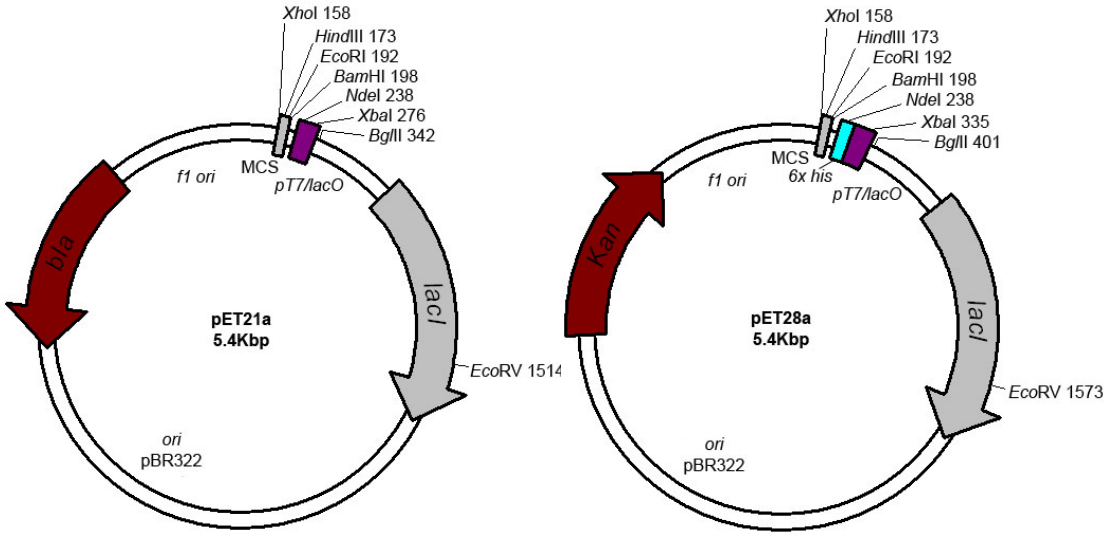

Figure 210: The Novagen vectors pET21a and pET28a.

A) The plasmid pET21a contains a T7 RNA polymerase dependent/lactose inducible promoter with a downstream multiple cloning site allowing cloning of fragments. Inducible expression can be driven by IPTG addition in an appropriate *E.coli* host. The Lac repressor is encoded by *lacI* and Ampicillin resistance is also encoded by the plasmid (*bla*).

B) The plasmid pET28a contains a T7 RNA polymerase dependent/lactose inducible promoter with DNA downstream encoding a *6xhis* tag with a multiple cloning site allowing cloning of fragments to generate a His tagged fusion protein. Inducible expression can be driven by IPTG addition in an appropriate *E.coli* host. The Lac repressor is encoded by *lacI* and Kanamycin resistance is also encoded by the plasmid (*kan*).

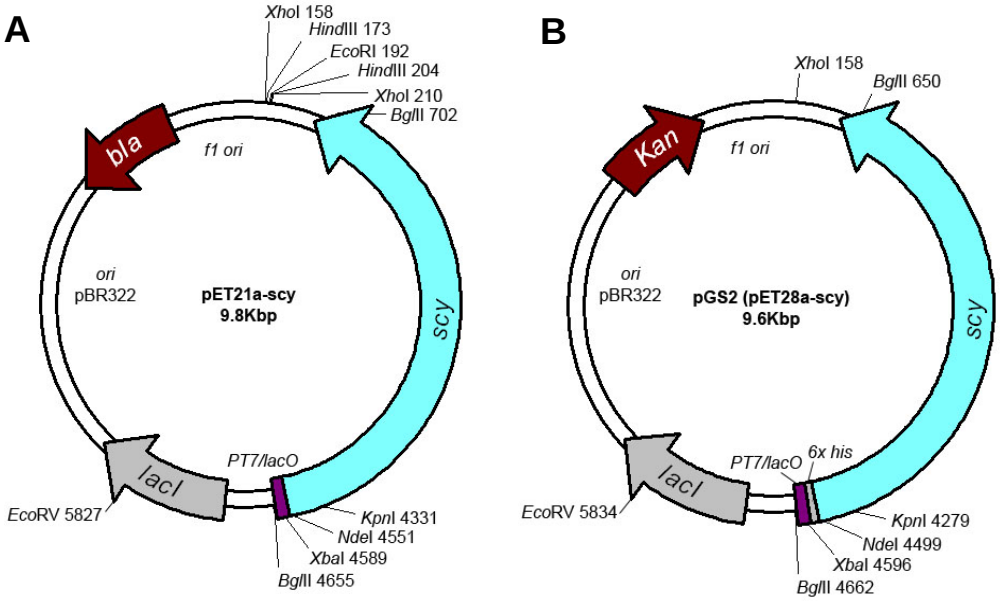

Figure 211: The Scy overexpression plasmids pET21a-scy and pET28a-scy (pGS2).

A) The plasmid pET21a-scy contains *scy* driven by a T7 RNA polymerase dependent/lactose inducible promoter in the high copy vector pET21a. Inducible *scy* expression can be driven by IPTG addition in an appropriate *E.coli* host. The Lac repressor is encoded by *lacI* and ampicillin resistance is also encoded by the plasmid (*bla*).

B) The plasmid pET28a-scy (pGS2) contains a *6xhis-scy* fusion driven by a T7 RNA polymerase dependent/lactose inducible promoter in the high copy vector pET28a. Inducible *scy* expression can be driven by IPTG addition in an appropriate *E.coli* host. The Lac repressor is encoded by *lacI* and kanamycin resistance is also encoded by the plasmid (*kan*).